

## **Library Declaration Form**



University of Otago Library

Author's full name and year of birth: Simon Thomas Kelly,  
(for cataloguing purposes) 24 February 1992

Title of thesis: A Bioinformatics Approach to Synthetic Lethal Interactions in Breast Cancer with Gene Expression Data

Degree: Doctor of Philosophy

Department: Department of Biochemistry

Permanent Address: 710 Cumberland Street, Dunedin, NZ

I agree that this thesis may be consulted for research and study purposes and that reasonable quotation may be made from it, provided that proper acknowledgement of its use is made.

I consent to this thesis being copied in part or in whole for

- i) a library
- ii) an individual

at the discretion of the University of Otago.

Signature:

Date:

A Bioinformatics Approach to  
Synthetic Lethal Interactions in  
Breast Cancer with Gene  
Expression Data

S. Thomas Kelly

a thesis submitted for the degree of  
Doctor of Philosophy  
at the University of Otago, Dunedin,  
New Zealand.

21 June 2017

## Abstract

### Background

Synthetic lethal genetic interactions are re-emerging in the post-genomics era due to their potential for use in precision medicine against cancers. Synthetic lethal drug design exploits the functional redundancy of genes disrupted in cancers (including tumour suppressors) to develop specific treatments against them. *CDH1*, which encodes [E-cadherin](#), is a tumour suppressor gene with loss of function in breast and stomach cancers. Experimental screens have identified candidate synthetic lethal interactions for drug target triage, which can be further supported with bioinformatics analysis. Furthermore, gene expression data enables investigation of synthetic lethal pathways and graph structure of synthetic lethal genes within them.

### Approach

A computational methodology, the Synthetic Lethal Prediction Tool ([SLIPT](#)) has been developed to detect synthetic lethal interactions in gene expression data. This methodology was demonstrated on interactions with *CDH1* in breast and stomach cancer data from The Cancer Genome Atlas ([TCGA](#)) project. Synthetic lethal genes and pathways were further investigated with unsupervised clustering, gene set over-representation analysis, metagenes, and permutation resampling. In particular, analyses focused on comparing [SLIPT](#) gene candidates to an experimental [siRNA](#) screen Telford *et al.* (2015). Network analysis methods were applied to the most supported pathways to test for pathway structure among between synthetic lethal candidates. Simulation and modelling was used to assess the statistical

performance of **SLIPT**, including simulated data with correlation structures derived from graph structures.

## Findings

Many candidate synthetic lethal partners of *CDH1* were detected in both **TCGA** breast cancer. These genes clustered into several distinct groups, with distinct biological functions and elevated expression in different clinical subtypes. While the number of genes detected by both approaches was not significant, these contained significantly enriched pathways. In particular,  $G_{\alpha i}$  signalling, cytoplasmic microfibres, and extracellular fibrin clotting were robustly supported by both approaches, which is consistent with the known cytoskeletal and cell signalling roles of **E-cadherin** and validation of **GPCR** pathways performed by **Telford et al.** (2015). Many of these pathways were replicated in stomach cancer data. The pathways supported only by **SLIPT** included regulation of immune signalling and translational elongation which were not expected to be detected in an isogenic cell line model but are still candidates for further investigation.

Synthetic lethal candidates detected by **SLIPT** and **siRNA** were compared within graph structures of the candidate synthetic lethal pathways. These genes did not differ with respect to network metrics of importance or connectivity in the pathway. There was little support, across pathways, that **SLIPT** gene candidates were consistently upstream or downstream of **siRNA** gene candidates within pathways.

A model of synthetic lethality was used to simulate gene expression data with synthetic lethal partners of a gene. The **SLIPT** methodology had high statistical performance, detecting few synthetic lethal partners, which diminished with more synthetic lethal partners or lower sample size. The **SLIPT** methodology performed better than Pearson correlation or the  $\chi^2$ -test. In particular, it performed well with high specificity for datasets containing thousands of genes or genes positively correlated with the query gene (as expected to occur in expression data). **SLIPT** was robust across correlation structures, including those derived from complex pathway structures and often distinguished synthetic lethal genes from those positively or negatively correlated with them. Therefore **SLIPT** is appropriate to identify

synthetic lethal genes within pathways and use candidate synthetic lethal genes (and their correlates) to identify synthetic lethal pathways.

## **Summary**

Thus this thesis has developed, evaluated, and refined a bioinformatics approach to discovery of synthetic lethal genes solely from gene expression data. This approach has been demonstrated to detect biologically informative and clinically relevant candidate partners for *CDH1* in breast and stomach cancers. These investigations have also involved the development of network analysis and simulation procedures which may be more widely applicable.

## Acknowledgements

I thank my supervisors A/Prof. Mik Black and Prof. Parry Guilford for their support and guidance throughout this my postgraduate studies. It has been a great experience, I look forward to seeing what your research groups produce in the future, may this not be the end for us.

I am also thankful for the guidance and mentorship of Prof. Hamish Spencer for career advice throughout my studies and time in his research group.

I am also grateful to the past and current members of these research groups, and my peers at the laboratory benches and computers across campus. The peer support, camaraderie, and guidance of newer students has been an incredible part of my time at Otago and has made my thesis studies not just easier but possible at all. The postgraduate community is very special here and I have truly made some lifelong friends from all over the world. You are talented researchers and amazing people. May we meet again some day. Where-ever you may end up, its small world and there's always time to catch up. I'd be delighted to host some visits while working abroad.

I cannot thank my friends, flatmates, family, and diligent proofreaders enough for their patience and support during such as massive, challenging, and (I'm sure you've heard too often) stressful undertaking during both my PhD and the study leading up to it. There are too many of you to name everyone here without leaving someone out, so thank you all for everything you've done, both the good times and the tough. Thank you for at least pretending to understand complex math oft brought up at the wrong moment. Thank you for checking my writing or slides, even when sprung on you last minute. Thank for your time when what I really needed was a chat, a walk, a drink with "the guys", or a moment to think clearly.

I thank the various organisations that supported this research project:

- This thesis was supported by the Postgraduate Tassell Scholarship in Cancer Research, a University of Otago Doctoral Scholarship.
- The New Zealand eScience Infrastructure (NeSI) provided access to the Intel Pan high-performance computing cluster, support, and training to use it effectively. Various aspects of this thesis would not have been possible without access to such an incredible national resource.
- The Health Research Council (HRC) of New Zealand provided funding for experimental research in the Cancer Genetics Laboratory. Some aspects of this project would not have been possible without access to the data and findings funded by this grant.
- The Allan Wilson Centre and Otago School of Biomedical Sciences provided funding for summer research placements which was a valuable opportunity to gain experience and training used in this thesis project.

I thank the following organisations for support towards presenting findings in this thesis at conference and seminars:

- Google (eResearch 2014, Hamilton)
- NeSI (Software Carpentry training and Research Bazaar 2015, Melbourne)
- REANNZ, NZGL, and NeSI (eResearch 2016, Queenstown)
- Otago Division of Health Sciences, Oxford Global, and Maurice and Phyllis Paykel Trust (NGS Asia 2016, Singapore)
- RIKEN Division of Genomic Technologies and the Okinawa Institute of Science and Technology (seminar visits in Japan)

Thanks most of all to my fianceé, Dr Yui Kawagishi, you've been an inspiration. Thank you for your support and encouragement, every day, even from afar: it has always made a difference. It's been incredible to see you flourish in your career and I look forward to joining you again soon. May the next chapter of our adventures involve a bit less Skype across timezones.

どうもありがとうございます。頑張った!もうすぐ行きます。!また来月 !

# Contents

<b>Glossary</b>	<b>xx</b>
<b>Acronyms</b>	<b>xxiv</b>
<b>1 Introduction and Literature Review</b>	<b>1</b>
1.1 Cancer Research in the Post-Genomic Era . . . . .	1
1.1.1 Cancer is a Global Health Issue . . . . .	2
1.1.1.1 The Genetics and Molecular Biology of Cancers . . . . .	3
1.1.2 The Genomics Revolution in Cancer Research . . . . .	3
1.1.2.1 High-Throughput Technologies . . . . .	4
1.1.2.2 Bioinformatics and Genomic Data . . . . .	5
1.1.3 Genomics Projects . . . . .	5
1.1.3.1 The Cancer Genome Project . . . . .	6
1.1.3.2 The Cancer Genome Atlas Project . . . . .	6
1.1.4 Genomic Cancer Medicine . . . . .	8
1.1.4.1 Cancer Genes and Driver Mutations . . . . .	8
1.1.4.2 Precision Cancer Medicine . . . . .	9
1.1.4.3 Molecular Diagnostics and Pan-Cancer Medicine . . . . .	9
1.1.4.4 Targeted Therapeutics and Pharmacogenomics . . . . .	10
1.1.5 Systems and Network Biology . . . . .	11
1.2 Synthetic Lethal Cancer Medicine . . . . .	12
1.2.1 Synthetic Lethal Genetic Interactions . . . . .	12
1.2.2 Synthetic Lethal Concepts in Genetics . . . . .	14
1.2.3 Synthetic Lethality in Model Systems . . . . .	14
1.2.3.1 Synthetic Lethal Pathways and Networks . . . . .	15
1.2.3.2 Evolution of Synthetic Lethality . . . . .	15
1.2.4 Synthetic Lethality in Cancer . . . . .	16
1.2.5 Clinical Impact of Synthetic Lethality in Cancer . . . . .	18
1.2.6 High-throughput Screening for Synthetic Lethality . . . . .	19
1.2.6.1 Synthetic Lethal Screens . . . . .	21
1.2.7 Computational Prediction of Synthetic Lethality . . . . .	22
1.2.7.1 Bioinformatics Approaches to Genetic Interactions . . . . .	22
1.2.7.2 Comparative Genomics . . . . .	23
1.2.7.3 Analysis and Modelling of Protein Data . . . . .	26
1.2.7.4 Differential Gene Expression . . . . .	27
1.2.7.5 Data Mining and Machine Learning . . . . .	28

1.2.7.6	Mutually Exclusive Bimodality . . . . .	31
1.2.7.7	Rationale for Further Development . . . . .	32
1.3	E-cadherin as a Synthetic Lethal Target . . . . .	32
1.3.1	The <i>CDH1</i> gene and its Biological Functions . . . . .	33
1.3.1.1	Cytoskeleton . . . . .	33
1.3.1.2	Extracellular and Tumour Micro-environment . . . . .	33
1.3.1.3	Cell-Cell Adhesion and Signalling . . . . .	34
1.3.2	<i>CDH1</i> as a Tumour (and Invasion) Suppressor . . . . .	34
1.3.2.1	Breast Cancers and Invasion . . . . .	34
1.3.3	Hereditary Diffuse Gastric (and Lobular Breast) Cancer . . . . .	35
1.3.4	Cell Line Models of <i>CDH1</i> Null Mutations . . . . .	36
1.4	Summary and Research Direction of Thesis . . . . .	37
1.4.1	Thesis Aims . . . . .	38
<b>2</b>	<b>Methods and Resources</b>	<b>40</b>
2.1	Bioinformatics Resources for Genomics Research . . . . .	40
2.1.1	Public Data and Software Packages . . . . .	40
2.1.1.1	Cancer Genome Atlas Data . . . . .	41
2.1.1.2	Reactome and Annotation Data . . . . .	42
2.2	Data Handling . . . . .	42
2.2.1	Normalisation . . . . .	42
2.2.2	Sample Triage . . . . .	43
2.2.3	Metagenes and the Singular Value Decomposition . . . . .	43
2.2.4	Candidate Triage and Integration with Screen Data . . . . .	45
2.3	Techniques . . . . .	46
2.3.1	Statistical Procedures and Tests . . . . .	46
2.3.2	Gene Set Over-representation Analysis . . . . .	47
2.3.3	Clustering . . . . .	47
2.3.4	Heatmap . . . . .	47
2.3.5	Modelling and Simulations . . . . .	48
2.3.5.1	Receiver Operating Characteristic Curves . . . . .	49
2.3.6	Resampling Analysis . . . . .	49
2.4	Pathway Structure Methods . . . . .	50
2.4.1	Network and Graph Analysis . . . . .	50
2.4.2	Sourcing Graph Structure Data . . . . .	51
2.4.3	Constructing Pathway Subgraphs . . . . .	51
2.4.4	Network Analysis Metrics . . . . .	52
2.5	Implementation . . . . .	53
2.5.1	Computational Resources and Linux Utilities . . . . .	53
2.5.2	R Language and Packages . . . . .	54
2.5.3	High Performance and Parallel Computing . . . . .	57
<b>3</b>	<b>Methods Developed During Thesis</b>	<b>59</b>
3.1	A Synthetic Lethal Detection Methodology . . . . .	59
3.2	Synthetic Lethal Simulation and Modelling . . . . .	61
3.2.1	A Model of Synthetic Lethality in Expression Data . . . . .	62

3.2.2	Simulation Procedure . . . . .	66
3.3	Detecting Simulated Synthetic Lethal Partners . . . . .	69
3.3.1	Binomial Simulation of Synthetic Lethality . . . . .	69
3.3.2	Multivariate Normal Simulation of Synthetic Lethality . . . . .	71
3.3.2.1	Multivariate Normal Simulation with Correlated Genes	73
3.3.2.2	Specificity with Query-Correlated Pathways . . . . .	81
3.4	Graph Structure Methods . . . . .	83
3.4.1	Upstream and Downstream Gene Detection . . . . .	83
3.4.1.1	Permutation Analysis for Statistical Significance . . . . .	84
3.4.1.2	Hierarchy Based on Biological Context . . . . .	84
3.4.2	Simulating Gene Expression from Graph Structures . . . . .	85
3.5	Customised Functions and Packages Developed . . . . .	90
3.5.1	Synthetic Lethal Interaction Prediction Tool . . . . .	90
3.5.2	Data Visualisation . . . . .	91
3.5.3	Extensions to the iGraph Package . . . . .	93
3.5.3.1	Sampling Simulated Data from Graph Structures . . . . .	93
3.5.3.2	Plotting Directed Graph Structures . . . . .	93
3.5.3.3	Computing Information Centrality . . . . .	94
3.5.3.4	Testing Pathway Structure with Permutation Testing .	94
3.5.3.5	Metapackage to Install iGraph Functions . . . . .	95
<b>4</b>	<b>Synthetic Lethal Analysis of Gene Expression Data</b>	<b>96</b>
4.1	Synthetic Lethal Genes in Breast Cancer . . . . .	97
4.1.1	Synthetic Lethal Pathways in Breast Cancer . . . . .	98
4.1.2	Expression Profiles of Synthetic Lethal Partners . . . . .	100
4.1.2.1	Subgroup Pathway Analysis . . . . .	103
4.2	Comparing Synthetic Lethal Gene Candidates . . . . .	105
4.2.1	Primary siRNA Screen Candidates . . . . .	105
4.2.2	Comparison with Correlation . . . . .	105
4.2.3	Comparison with Primary Screen Viability . . . . .	108
4.2.4	Comparison with Secondary siRNA Screen Validation . . . . .	110
4.2.5	Comparison to Primary Screen at Pathway Level . . . . .	111
4.2.5.1	Resampling Genes for Pathway Enrichment . . . . .	113
4.2.6	Integrating Synthetic Lethal Pathways and Screens . . . . .	118
4.3	Metagene Analysis . . . . .	119
4.3.1	Pathway Expression . . . . .	119
4.3.2	Somatic Mutation . . . . .	122
4.3.3	Synthetic Lethal Pathway Metagenes . . . . .	125
4.3.4	Synthetic Lethality in Breast Cancer . . . . .	127
4.4	Replication in Stomach Cancer . . . . .	127
4.5	Discussion . . . . .	128
4.5.1	Strengths of the SLIPT Methodology . . . . .	128
4.5.2	Synthetic Lethal Pathways for E-cadherin . . . . .	129
4.5.3	Replication and Validation . . . . .	131
4.5.3.1	Integration with short interfering RNA (siRNA) Screening . . . . .	131

4.5.3.2	Replication across Tissues . . . . .	132
4.6	Summary . . . . .	133
<b>5</b>	<b>Synthetic Lethal Pathway Structure</b>	<b>135</b>
5.1	Synthetic Lethal Genes in Reactome Pathways . . . . .	135
5.1.1	The PI3K/AKT Pathway . . . . .	136
5.1.2	The Extracellular Matrix . . . . .	138
5.1.3	G Protein Coupled Receptors . . . . .	141
5.1.4	Gene Regulation and Translation . . . . .	141
5.2	Network Analysis of Synthetic Lethal Genes . . . . .	142
5.2.1	Gene Connectivity and Vertex Degree . . . . .	143
5.2.2	Gene Importance and Centrality . . . . .	144
5.2.2.1	Information Centrality . . . . .	144
5.2.2.2	PageRank Centrality . . . . .	146
5.3	Relationships between Synthetic Lethal Genes . . . . .	148
5.3.1	Hierarchical Pathway Structure . . . . .	148
5.3.1.1	Contextual Hierarchy of PI3K . . . . .	148
5.3.1.2	Testing Contextual Hierarchy of Synthetic Lethal Genes	148
5.3.2	Upstream or Downstream Synthetic Lethality . . . . .	152
5.3.2.1	Measuring Structure of Candidates within PI3K . . .	152
5.3.2.2	Resampling for Synthetic Lethal Pathway Structure .	154
5.4	Discussion . . . . .	156
5.5	Summary . . . . .	158
<b>6</b>	<b>Simulation and Modelling of Synthetic Lethal Pathways</b>	<b>159</b>
6.1	Synthetic Lethal Detection Methods . . . . .	160
6.1.1	Performance of SLIPT and $\chi^2$ across Quantiles . . . . .	161
6.1.1.1	Correlated Query Genes affects Specificity . . . . .	164
6.1.2	Alternative Synthetic Lethal Detection Strategies . . . . .	166
6.1.2.1	Correlation for Synthetic Lethal Detection . . . . .	167
6.1.2.2	Testing for Bimodality with BiSEp . . . . .	168
6.2	Simulations with Graph Structures . . . . .	169
6.2.1	Performance over Graph Structures . . . . .	170
6.2.1.1	Simple Graph Structures . . . . .	170
6.2.1.2	Constructed Graph Structures . . . . .	173
6.2.2	Performance with Inhibitions . . . . .	175
6.2.3	Synthetic Lethality across Graph Structures . . . . .	181
6.2.4	Performance within a Simulated Human Genome . . . . .	184
6.3	Simulations in More Complex Graph Structures . . . . .	189
6.3.1	Simulations over Pathway-based Graphs . . . . .	190
6.3.2	Pathway Structures in a Simulated Human Genome . . . . .	192
6.4	Discussion . . . . .	195
6.4.1	Simulation Procedure . . . . .	195
6.4.2	Comparing Methods with Simulated Data . . . . .	196
6.4.3	Design and Performance of SLIPT . . . . .	197
6.4.4	Simulations from Graph Structures . . . . .	199

6.5	Summary . . . . .	200
<b>7</b>	<b>Discussion</b>	<b>202</b>
7.1	Synthetic Lethality and <i>CDH1</i> Biology . . . . .	202
7.1.1	Established Functions of <i>CDH1</i> . . . . .	203
7.1.2	The Molecular Role of <i>CDH1</i> in Cancer . . . . .	203
7.2	Significance . . . . .	204
7.2.1	Synthetic Lethality in the Genomic Era . . . . .	204
7.2.2	Clinical Interventions based on Synthetic Lethality . . . . .	206
7.3	Future Directions . . . . .	207
7.4	Conclusions . . . . .	209
	<b>Bibliography</b>	<b>211</b>
<b>A</b>	<b>Sample Quality</b>	<b>235</b>
A.1	Sample Correlation . . . . .	235
A.2	Replicate Samples in The Cancer Genome Atlas (TCGA) Breast . . . . .	237
<b>B</b>	<b>Software Used for Thesis</b>	<b>241</b>
<b>C</b>	<b>Mutation Analysis in Breast Cancer</b>	<b>250</b>
C.1	Synthetic Lethal Genes and Pathways . . . . .	250
C.2	Synthetic Lethal Expression Profiles . . . . .	253
C.3	Comparison to Primary Screen . . . . .	256
C.3.1	Resampling Analysis . . . . .	258
C.4	Compare Synthetic Lethal Interaction Prediction Tool (SLIPT) genes .	260
C.5	Metagene Analysis . . . . .	262
C.6	Expression of Somatic Mutations . . . . .	263
C.7	Metagene Expression Profiles . . . . .	266
<b>D</b>	<b>Intrinsic Subtyping</b>	<b>269</b>
<b>E</b>	<b>Stomach Expression Analysis</b>	<b>271</b>
E.1	Synthetic Lethal Genes and Pathways . . . . .	271
E.2	Comparison to Primary Screen . . . . .	275
E.2.1	Resampling Analysis . . . . .	277
E.3	Metagene Analysis . . . . .	279
<b>F</b>	<b>Synthetic Lethal Genes in Pathways</b>	<b>280</b>
<b>G</b>	<b>Pathway Connectivity for Mutation SLIPT</b>	<b>288</b>
<b>H</b>	<b>Information Centrality for Gene Essentiality</b>	<b>292</b>
<b>I</b>	<b>Pathway Structure for Mutation SLIPT</b>	<b>295</b>
<b>J</b>	<b>Performance of SLIPT and <math>\chi^2</math></b>	<b>298</b>
J.1	Correlated Query Genes affects Specificity . . . . .	304

<b>K Simulations on Graph Structures</b>	<b>310</b>
K.0.1 Simulations from Inhibiting Graph Structures . . . . .	311
K.1 Simulation across Graph Structures . . . . .	314
K.2 Simulations from Complex Graph Structures . . . . .	318
K.2.1 Simulations from Complex Inhibiting Graphs . . . . .	321
K.3 Simulations from Pathway Graph Structures . . . . .	327

# List of Tables

1.1	Methods for predicting genetic interactions . . . . .	22
1.2	Methods for predicting synthetic lethality in cancer . . . . .	23
1.3	Methods used by Wu <i>et al.</i> (2014) . . . . .	25
2.1	Excluded samples by batch and clinical characteristics. . . . .	43
2.2	Computers used during thesis . . . . .	53
2.3	Linux utilities and applications used during thesis . . . . .	54
2.4	R installations used during thesis . . . . .	55
2.5	R Packages used during thesis . . . . .	55
2.6	R packages developed during thesis . . . . .	57
4.1	Candidate synthetic lethal gene partners of <i>CDH1</i> from SLIPT . . . . .	98
4.2	Pathways for <i>CDH1</i> partners from SLIPT . . . . .	99
4.3	Pathways for clusters of <i>CDH1</i> partners from SLIPT . . . . .	104
4.4	ANOVA for synthetic lethality and correlation with <i>CDH1</i> . . . . .	107
4.5	Comparison of SLIPT genes against secondary siRNA screen . . . . .	111
4.6	Pathways for <i>CDH1</i> partners from SLIPT and siRNA . . . . .	112
4.7	Pathways for <i>CDH1</i> partners from SLIPT . . . . .	116
4.8	Pathways for <i>CDH1</i> partners from SLIPT and siRNA primary screen . . . . .	117
4.9	Candidate synthetic lethal metagenes against <i>CDH1</i> from SLIPT . . . . .	126
5.1	ANOVA for synthetic lethality and vertex degree . . . . .	144
5.2	ANOVA for synthetic lethality and information centrality . . . . .	146
5.3	ANOVA for synthetic lethality and PageRank centrality . . . . .	148
5.4	ANOVA for synthetic lethality and PI3K hierarchy . . . . .	151
5.5	Resampling for pathway structure of synthetic lethal detection methods	155
B.1	Complete list of R packages used during this thesis . . . . .	241
C.1	Candidate synthetic lethal gene partners of <i>CDH1</i> from mtSLIPT . . . . .	251
C.2	Pathways for <i>CDH1</i> partners from mtSLIPT . . . . .	252
C.3	Pathways for clusters of <i>CDH1</i> partners from mtSLIPT . . . . .	255
C.4	Pathways for <i>CDH1</i> partners from mtSLIPT and siRNA . . . . .	257
C.5	Pathways for <i>CDH1</i> partners from mtSLIPT . . . . .	258
C.6	Pathways for <i>CDH1</i> partners from mtSLIPT and siRNA primary screen . . . . .	259
C.7	Candidate synthetic lethal metagenes against <i>CDH1</i> from mtSLIPT . . . . .	262
D.1	Comparison of intrinsic subtypes . . . . .	269

E.1	Synthetic lethal gene partners of <i>CDH1</i> from SLIPT in stomach cancer	271
E.2	Pathways for <i>CDH1</i> partners from SLIPT in stomach cancer . . . . .	272
E.3	Pathways for clusters of <i>CDH1</i> partners in stomach SLIPT . . . . .	274
E.4	Pathways for <i>CDH1</i> partners from SLIPT and siRNA . . . . .	276
E.5	Pathways for <i>CDH1</i> partners from SLIPT in stomach cancer . . . . .	277
E.6	Pathways for <i>CDH1</i> partners from SLIPT in stomach and siRNA . . . .	278
E.7	Synthetic lethal metagenes against <i>CDH1</i> in stomach cancer . . . . .	279
G.1	ANOVA for synthetic lethality and vertex degree . . . . .	291
G.2	ANOVA for synthetic lethality and information centrality . . . . .	291
G.3	ANOVA for synthetic lethality and PageRank centrality . . . . .	291
H.1	Information centrality for genes and molecules in the Reactome network	293
I.1	ANOVA for synthetic lethality and PI3K hierarchy . . . . .	295
I.2	Resampling for pathway structure of synthetic lethal detection methods	297

# List of Figures

1.1	Synthetic genetic interactions . . . . .	13
1.2	Synthetic lethality in cancer . . . . .	17
2.1	Read count density . . . . .	44
2.2	Read count sample mean . . . . .	44
3.1	Framework for synthetic lethal prediction . . . . .	60
3.2	Synthetic lethal prediction adapted for mutation . . . . .	61
3.3	A model of synthetic lethal gene expression . . . . .	63
3.4	Modelling synthetic lethal gene expression . . . . .	64
3.5	Synthetic lethality with multiple genes . . . . .	65
3.6	Simulating gene function . . . . .	67
3.7	Simulating synthetic lethal gene function . . . . .	67
3.8	Simulating synthetic lethal gene expression . . . . .	68
3.9	Performance of binomial simulations . . . . .	70
3.10	Comparison of statistical performance . . . . .	70
3.11	Performance of multivariate normal simulations . . . . .	72
3.12	Simulating expression with correlated gene blocks . . . . .	74
3.13	Simulating expression with correlated gene blocks . . . . .	75
3.14	Synthetic lethal prediction across simulations . . . . .	77
3.15	Performance with correlations . . . . .	78
3.16	Comparison of statistical performance with correlation structure . . . . .	79
3.17	Performance with query correlations . . . . .	80
3.18	Statistical evaluation of directional criteria . . . . .	81
3.19	Performance of directional criteria . . . . .	82
3.20	Simulated graph structures . . . . .	86
3.21	Simulating expression from a graph structure . . . . .	87
3.22	Simulating expression from graph structure with inhibitions . . . . .	88
3.23	Demonstration of violin plots with custom features . . . . .	92
3.24	Demonstration of annotated heatmap . . . . .	92
3.25	Simulating graph structures . . . . .	94
4.1	Synthetic lethal expression profiles of analysed samples . . . . .	101
4.2	Comparison of SLIPT with siRNA . . . . .	106
4.3	Comparison of SLIPT and siRNA genes with correlation . . . . .	106
4.4	Comparison of SLIPT and siRNA genes with correlation . . . . .	108
4.5	Comparison of SLIPT and siRNA genes with screen viability . . . . .	109

4.6	Comparison of SLIPT genes with siRNA screen viability . . . . .	109
4.7	Resampled intersection of SLIPT and siRNA candidates . . . . .	114
4.8	Pathway metagene expression profiles . . . . .	121
4.9	Expression profiles for constituent genes of PI3K . . . . .	123
4.10	Expression profiles for estrogen receptor related genes . . . . .	124
4.11	Somatic mutation against the PI3K metagene . . . . .	125
5.1	synthetic lethality in the PI3K cascade . . . . .	137
5.2	synthetic lethality in Elastic Fibre Formation . . . . .	139
5.3	Synthetic lethality in Fibrin Clot Formation . . . . .	140
5.4	Synthetic lethality and vertex degree . . . . .	143
5.5	Synthetic lethality and centrality . . . . .	146
5.6	Synthetic lethality and PageRank . . . . .	147
5.7	Hierarchical structure of PI3K . . . . .	149
5.8	Hierarchy score in PI3K against synthetic lethality in PI3K . . . . .	150
5.9	Structure of synthetic lethality in PI3K . . . . .	151
5.10	Structure of synthetic lethality resampling in PI3K . . . . .	153
6.1	Performance of $\chi^2$ and SLIPT across quantiles . . . . .	162
6.2	Performance of $\chi^2$ and SLIPT across quantiles with more genes . . . . .	163
6.3	Performance of $\chi^2$ and SLIPT across quantiles with query correlation .	164
6.4	Performance of $\chi^2$ and SLIPT across quantiles with query correlation and more genes . . . . .	165
6.5	Performance of negative correlation and SLIPT . . . . .	168
6.6	Simple graph structures . . . . .	171
6.7	Performance of simulations on a simple graph . . . . .	172
6.8	Performance of simulations is similar in simple graphs . . . . .	173
6.9	Performance of simulations on a pathway . . . . .	174
6.10	Performance of simulations on a simple graph with inhibition . . . . .	176
6.11	Performance is higher on a simple inhibiting graph . . . . .	178
6.12	Performance of simulations on a constructed graph with inhibition . . .	179
6.13	Performance is affected by inhibition in graphs . . . . .	180
6.14	Detection of synthetic lethality within a graph structure . . . . .	182
6.15	Performance of simulations including a simple graph . . . . .	186
6.16	Performance on a simple graph improves with more genes . . . . .	187
6.17	Performance on an inhibiting graph improves with more genes . . .	188
6.18	Performance of simulations on the PI3K cascade . . . . .	191
6.19	Performance of simulations including the PI3K cascade . . . . .	193
6.20	Performance on pathways improves with more genes . . . . .	194
A.1	Correlation profiles of removed samples . . . . .	235
A.2	Correlation analysis and sample removal . . . . .	236
A.3	Replicate excluded samples . . . . .	237
A.4	Replicate samples with all remaining . . . . .	238
A.5	Replicate samples with some excluded . . . . .	239
C.1	Synthetic lethal expression profiles of analysed samples . . . . .	254

C.2	Comparison of mtSLIPT to siRNA . . . . .	256
C.3	Compare mtSLIPT and siRNA genes with correlation . . . . .	260
C.4	Compare mtSLIPT and siRNA genes with correlation . . . . .	260
C.5	Compare mtSLIPT and siRNA genes with siRNA viability . . . . .	261
C.6	Somatic mutation against PIK3CA metagene . . . . .	263
C.7	Somatic mutation against PI3K protein . . . . .	264
C.8	Somatic mutation against AKT protein . . . . .	265
C.9	Pathway metagene expression profiles . . . . .	266
C.10	Expression profiles for p53 related genes . . . . .	267
C.11	Expression profiles for BRCA related genes . . . . .	268
E.1	Synthetic lethal expression profiles of stomach samples . . . . .	273
E.2	Comparison of SLIPT in stomach to siRNA . . . . .	275
F.1	Synthetic lethality in the PI3K/AKT pathway . . . . .	280
F.2	Synthetic lethality in the PI3K/AKT pathway in cancer . . . . .	281
F.3	Synthetic lethality in the Extracellular Matrix . . . . .	282
F.4	Synthetic lethality in the GPCRs . . . . .	283
F.5	Synthetic lethality in the GPCR Downstream . . . . .	284
F.6	Synthetic lethality in the Translation Elongation . . . . .	285
F.7	Synthetic lethality in the Nonsense-mediated Decay . . . . .	286
F.8	Synthetic lethality in the 3' UTR . . . . .	287
G.1	Synthetic lethality and vertex degree . . . . .	288
G.2	Synthetic lethality and centrality . . . . .	289
G.3	Synthetic lethality and PageRank . . . . .	290
H.1	Information centrality distribution . . . . .	294
I.1	Synthetic lethality and heirarchy score in PI3K . . . . .	295
I.2	Heirarchy score in PI3K against synthetic lethality in PI3K . . . . .	296
I.3	Structure of synthetic lethality in PI3K . . . . .	296
I.4	Structure of synthetic lethality resampling . . . . .	297
J.1	Performance of $\chi^2$ and SLIPT across quantiles . . . . .	298
J.2	Performance of $\chi^2$ and SLIPT across quantiles . . . . .	300
J.3	Performance of $\chi^2$ and SLIPT across quantiles with more genes . . . . .	302
J.4	Performance of $\chi^2$ and SLIPT across quantiles with query correlation . . . . .	304
J.5	Performance of $\chi^2$ and SLIPT across quantiles with query correlation . . . . .	306
J.6	Performance of $\chi^2$ and SLIPT across quantiles with query correlation and more genes . . . . .	308
K.1	Performance of simulations on a simple graph . . . . .	310
K.2	Performance of simulations on an inhibiting graph . . . . .	311
K.3	Performance of simulations on a constructed graph with inhibition . . . . .	312
K.4	Performance of simulations on a constructed graph with inhibition . . . . .	313
K.5	Detection of synthetic lethality within a graph structure . . . . .	314
K.6	Detection of synthetic lethality within an inhibiting graph . . . . .	316

K.7	Detection of synthetic lethality within an inhibiting graph . . . . .	317
K.8	Performance of simulations on a branching graph . . . . .	318
K.9	Performance of simulations on a complex graph . . . . .	319
K.10	Performance of simulations on a large graph . . . . .	320
K.11	Performance of simulations on a branching graph with inhibition . . . . .	321
K.12	Performance of simulations on a branching graph with inhibition . . . . .	322
K.13	Performance of simulations on a complex graph with inhibition . . . . .	323
K.14	Performance of simulations on a complex graph with inhibition . . . . .	324
K.15	Performance of simulations on a large constructed graph with inhibition	325
K.16	Performance of simulations on a large constructed graph with inhibition	326
K.17	Performance of simulations on the $G_{\alpha i}$ signalling pathway . . . . .	327
K.18	Performance of simulations including the $G_{\alpha i}$ signalling pathway . . . . .	328

# Glossary

allele	A gene variant with a specific sequence and phenotype
bioinformatics	Statistical or computational approaches to biological data or research tools
cancer	A class of diseases, formally “malignant neoplasm”, of abnormal cellular growth and spread to other organs
cancer gene	A gene which is involved in the malignancy of some cancers, encompassing <a href="#">oncogenes</a> and <a href="#">tumour suppressors</a> , which have molecular aberrations in cancer or variants which predispose individuals to cancer
centrality	A network metric which identifies important <a href="#">vertices</a>
chemoprevention	The use of drugs to prevent early-stage cancers, generally applied to high-risk mutation carriers
chemotherapy	The use of cytotoxic drugs to treat cancers, in combinations, generally applied to advanced stage cancers
compound screen	A <a href="#">high-throughput screen</a> performed using a library of chemical compounds
computational biology	Applying computational or mathematical modelling to understanding biological systems and relationships
driver mutation	A <a href="#">mutation</a> which promotes cancer growth
E-cadherin	Epithelial cadherin (calcium-dependent adhesion), a cell-adhesion protein encoded by <i>CDH1</i>
edge or link	A relationship connecting a pair of elements of a graph structure or network, may be weighted or directional
epistasis (biological)	The effects of a gene modifying or masking the phenotype of another gene
epistasis (statistical)	A divergence of the observed double <a href="#">mutant</a> phenotype from that expected based on the respective phenotypes of single <a href="#">mutant</a> ( <a href="#">Fisher, 1919</a> )
essential	A gene which is required to be functional or expressed for a cell or organism to be viable, grow or develop
familial	A trait recurrently occurring in families, not necessarily with a genetic cause
functional redundancy	Genes which perform a common function, also known as genetic redundancy

gene expression	A measure of the relative expression of each gene from the mRNA extracted from (pooled) cells
genetic robustness	A system of biological pathways which (has evolved to) continue to function as a whole under various conditions, including the inactivation of various individual genes
genome	All of the DNA sequence in the genome
genomic	The use of data from all genes in the genome
germline mutation	A <b>mutation</b> that occurred in germline cells and is passed between generations
graph or network	A mathematical structure modelling or depicting the relationships between elements
hereditary	A trait or disease which has a genetic cause and is inherited from family members
high-throughput screen	An experimental procedure to perform a large scale series of chemical, genetic, or pharmacological tests
hub	A central or highly connected component of a network
induced essentiality	A gene becoming <b>essential</b> to viability under certain conditions, including inactivation of a synthetic lethal partner
information centrality	A network <b>centrality</b> metric which uses the impact of removing a <b>vertex or node</b> on connections in the network
intrinsic subtype	Distinguishing cancer by molecular and genetic features
metagene	A consistent signal of expression for a collection of genes such as a biological pathway, derived from singular value decomposition
methylation	A measure of the epigenetic regulation of DNA at <b>CpG dinucleotide (CpG)</b> sites
microarray	A high-throughput technique to measure presence or abundance of nucleic acid sequences from binding to probes
molecular profile	A combination of genetic and biochemical measures which identifies characteristic traits of a tumour
molecular subtype	A classification of cancers based on an identification using molecular properties
mutant	A variant or dysfunctional phenotype arising from a <b>mutation</b> in a gene
mutation	A change in DNA sequence that disrupts gene function
non-oncogene addiction	The dependence of a cancer cell on functioning non-mutant genes
'omics	A combination of approaches to generating biological data with high-throughput procedures such as genomics, proteomics or metabolomics

oncogene	A gene that potentially causes cancer, typically by over-expression or mutant gene variants
oncogene addiction	The dependence of a cancer cell on a specific oncogenic pathway
PageRank centrality	A network <a href="#">centrality</a> metric which uses eigenvectors with a scaling factor ( <a href="#">Brin and Page, 1998</a> )
pan cancer	A focus on the molecular and genetic features across cancers in different tissues
passenger mutation	A <a href="#">mutation</a> that occurs in cancers but does not affect the growth of cancers
pathway	A series of biomolecules that produces a particular product or biological function
pleiotropy	When a gene has multiple biological functions
precision medicine	The application of prevention and treatment measures to target diseases by molecular and genetic features
recurrent mutation	The repeated occurrence of mutations in a particular gene across cancers
RNAi screen	A <a href="#">high-throughput screen</a> performed using a <a href="#">RNA interference (RNAi)</a>
RNA-Seq	The generation of transcriptome data from sequencing RNA
scale-free	A property of a network which has a power law <a href="#">vertex degree</a> distribution, that is several highly connected <a href="#">hub</a> genes and many with very few connections
shortest path	A path with the fewest possible <a href="#">edges</a> which connects two particular <a href="#">vertices</a>
small world	A property of a network which is highly connected and has a low characteristic path length, derived from the mean <a href="#">shortest path</a> length across all pairs of nodes
somatic mutation	A <a href="#">mutation</a> that occurs in somatic cells, during a patient's lifespan
sporadic cancer	Cancers which do occur in patients with a family history or carry a high-risk genetic variant
synthetic dosage lethal	A <a href="#">synthetic genetic interaction (SGI)</a> analogous to <a href="#">synthetic lethality</a> where one gene is inactivated and the other over-expressed
synthetic lethal	Genetic interactions where inactivation of multiple genes is inviable (or deleterious) which are viable if inactivated separately
synthetic lethal screen	A <a href="#">high-throughput screen</a> performed on isogenic cell lines to detect genes for which inhibition specifically deleterious to the null <a href="#">mutant</a> genotype

synthetic rescue	A <b>synthetic genetic interaction</b> when the combined <b>mutations</b> restores the <b>wild-type</b> the phenotype of one of the <b>mutations</b>
synthetic sick	Genetic interactions where inactivation of multiple genes is deleterious which are viable if inactivated separately
synthetic suppression	A <b>synthetic genetic interaction</b> when the combined <b>mutations</b> (partially) suppresses the <b>mutant</b> phenotype of one of the <b>mutations</b>
targeted therapy	Cancer treatment that specifically acts against a molecular target, in contrast to standard chemotherapy
transcriptome	All of the genes expressed in the genome
treatment	Medical procedures for a disease to improve patient outcomes
tumour	An abnormal lump of tissue or growth of cells, may be cancerous
tumour suppressor	A gene potentially causes cancer, typically by disruption of functions which protect the cell from cancer
vertex degree	A network metric of connectivity of <b>vertices</b> which uses the number of edges connected to each <b>vertex or node</b>
vertex or node	An element of a graph structure or network
wild-type	A natural phenotype of a trait or the normally functional <b>allele</b> which encodes it

# Acronyms

ADP	Adenosine Diphosphate
AMP	Adenosine Monophosphate
AMPK	<a href="#">AMP</a> -activated Protein Kinase
ANOVA	Analysis of Variance
AUROC	Area Under the Receiver Operating Characteristic (curve)
Bash	Bourne Again Shell
BioPAX	Biological Pathway Exchange
BiSEp	Bimodal Subsetting Expression
BMP	Bone Morphogenic Protein
CCLE	Cancer Cell Line Encyclopaedia
cDNA	Complementary DNA (from mRNA)
CGP	Cancer Genome Project
CNV	Copy Number Variation
COSMIC	Catalogue Of Somatic Mutations In Cancer
CpG	5'-C-phosphate-G-3'
CPM	Counts Per Million mapped reads
CPU	Central Processing Unit
CRAN	comprehensive R archive network
CXCR	Chemokine Receptor
DAISY	Data Mining Synthetic Lethal Identification Pipeline
DNA	Deoxyribonucleic Acid
EMT	Epithelial-Mesenchymal Transition
ER	Estrogen Receptor
FDR	False Discovery Rate
GO	Gene Ontology
GPCR	G Crotein Coupled Receptor
HDAC	Histone Deacetylase
HDGC	Hereditary Diffuse Gastric Cancer
HPC	High Performance Computing
ICGC	International Cancer Genome Consortium
JAK	Janus Kinase
microRNA	Micro RNA
mRNA	Messenger RNA
MSI	Microsatellite Instability
mtSLIPT	Synthetic Lethal Interaction Prediction Tool (against mutation)

NeSI	New Zealand eScience Infrastructure
NGS	Next-Generation Sequencing
NMD	Nonsense-Mediated Decay
PAM50	Prediction Analysis of Microarray 50
PARP	Poly- <b>ADP</b> -Ribose Polymerase
PCR	Polymerase Chain Reaction
PDE	Phosphodiesterase
PI3K	Phosphoinositide 3-kinase
PIP <sub>2</sub>	Phosphatidylinositol-(4,5)-bisphosphate
PIP <sub>3</sub>	Phosphatidylinositol-(3,4,5)-trisphosphate
PPI	Protein-Protein Interaction
PR	Progesterone Receptor
RGS	G-protein Signalling
RHO	Ras Homolog Family
RNA	Ribonucleic Acid
RNAi	RNA Interference
ROC	Reciever Operating Characteristic (curve)
RPPA	Reverse Phase Protein Arrays
RSEM	RNA-Seq by Expectation Maximization (normalisation)
SGA	Synthetic Gene Array (technique)
SGI	Synthetic Genetic Interaction
shRNA	Short Hairpin RNA
siRNA	Short Interfering RNA
SL	Synthetic Lethal
SLIPT	Synthetic Lethal Interaction Prediction Tool
Slurm	Simple Linux Utility for Resource Management
SNP	Single Nucleotide Polymorphism
SOCKS	Socket Secure
SR	Synthetic Rescue (or viability)
SS	Synthetic Suppression
SSL	Synthetic Sick
TCGA	The Cancer Genome Atlas (genomics project)
TGF $\beta$	Transforming Growth Factor $\beta$
UCSC	University of California, Santa Cruz
UTR	Untranslated Region (of mRNA)
WNT	Wingless-Related Integration Site

# Chapter 1

## Introduction and Literature Review

This thesis presents research into genetic interactions using [genomics](#) data and [bioinformatics](#) approaches. Chapter 1 introduces recent developments in [genomics](#) and [bioinformatics](#), particularly in their application to [cancer](#) research. Studies of [synthetic lethal](#) interactions, which have fundamental importance in genetics in model organisms and renewed relevance in [cancer](#) biology specifically, will be discussed and reviewed in detail. A bioinformatic approach to [synthetic lethal](#) interactions enables a wider exploration of the function of genes and proteins in [cancer](#) cells, in contrast with candidate gene and experimental screening approaches. Synthetic lethal drug design aims to develop [treatments](#) to specificity against loss of function [mutations](#) in [tumour suppressor](#) genes, such as *CDH1* (which encodes [E-cadherin](#)) and was the focus of the analysis in this thesis. The role of *CDH1* in cellular and [cancer](#) biology is therefore also briefly reviewed.

### 1.1 Cancer Research in the Post-Genomic Era

Genomic technologies are expected to significantly impact on the clinical treatment of cancers along with wider applications of genetics ([Goodwin et al., 2016](#); [Roychowdhury and Chinnaiyan, 2016](#)). These technologies enable focused genetics investigations on candidate genes selected from [bioinformatics](#) analysis of [genomics](#) data. Facilitated by rapidly developing technologies, large-scale projects have investigated populations ([1000 Genomes, 2010](#)), cancers ([Dickson, 1999](#); [Zhang et al., 2011](#)), and functional genomics ([Kawai et al., 2001](#); [ENCODE, 2004](#)), however, genomic technologies have yet to be widely adopted in healthcare or oncology ([Roychowdhury and Chinnaiyan, 2016](#); [Waldron, 2016](#)). [bioinformatics](#) analysis for interpretation of [genomic](#) data is one of the main approaches to address this disparity ([Goodwin et al., 2016](#)). Here, I outline

the [cancer genomics](#) projects and findings which have led to availability of [genomics](#) data used in this thesis, and recent findings in [cancer](#) research which demonstrate potential applications of using this data.

### 1.1.1 Cancer is a Global Health Issue

Cancers are diseases of malignant cellular growth which typically involve [tumour](#) formation, invasion of tissues and spread to other organs. Cancers are the second leading cause of death globally ([WHO, 2017](#)), with an estimated annual incidence of 14.1 million cases and annual mortality of 8.2 million people ([Ferlay et al., 2015](#)). Breast and stomach [cancers](#) are among the most prevalent [cancers](#). Breast cancer is the most common [cancer](#) in women and has an estimated annual incidence of 1.6 million cases and mortality of 520,000 people. Stomach cancer has an estimated annual incidence of 950,000 cases and a mortality of 723,000 people. Cancer is also a major health concern here in New Zealand, with 19,100 people (including 2500 cases of breast cancer and 370 cases of stomach cancer) diagnosed annually ([Hanna, 2003](#)), near the highest incidence (age-standardised per capita) of [cancer](#) in the world ([Ferlay et al., 2015](#)).

While environmental factors often play a role, genetics is an important contributor to cancer risk. Most [cancers](#) occur more frequently with age and family history. Cancers arise from dysregulated cellular growth or differentiation. These can occur through genetic [mutations](#) or alterations in gene regulation or [expression](#) which generally accumulate as the disease develops. Therefore, early diagnosis is important to ensure patient survival and quality of life. Identification of patients with genetic variants or family histories at a high-risk of particular cancers is an important health issue. These high-risk individuals are regularly monitored for some cancers and are sometimes offered preventative surgery or treatment for pre-cancerous tissue ([Guilford et al., 2010](#); [Scheuer et al., 2002](#)).

[Chemotherapy](#) is a treatment for many advanced stage cancers, designed to inhibit rapidly growing cells. However, this approach often has severe adverse effects, a narrow therapeutic window, and is not suitable for [chemopreventative](#) application in many cases ([Kaelin, Jr, 2009](#)). Patients at high-risk of cancers are offered surveillance and preventative surgery but these approaches are not completely effective at preventing cancers and may impact on quality of life ([Guilford et al., 2010](#)). Alternative [chemoprevention](#) and treatment strategies based on molecular biology and other fields are being investigated, including targeted molecular therapeutics ([Bozovic-Spasojevic et al., 2012](#)).

### 1.1.1.1 The Genetics and Molecular Biology of Cancers

Cancers involve dysregulation of genes including **mutations** which occur during a patient's lifetime and **hereditary mutations** which predispose them to high-risk cancers (American Cancer Society, 2017; Guilford *et al.*, 1998; NCI, 2015). Due to these **familial** cancer syndromes, **hereditary** risk factors, and the molecular changes occurring in them, **cancers** are in part a genetic disease involving many **cancer genes** (Stratton *et al.*, 2009; Vogelstein *et al.*, 2013). The occurrence of **somatic mutation** mutations increases the risk of **cancer** with age. An association of cancer incidence with the stem cell divisions in which **mutations** could occur across tissue types, suggests that cancers may be inseparably coupled with aging (Tomasetti and Vogelstein, 2015).

Hanahan and Weinberg (2000) proposed the “hallmarks of cancer”, molecular and cellular traits shared across cancers. These form the basis of a rational approach to categorising the complex changes that occur in **cancer**. These traits include limitless replication potential, signals for indefinite growth, and invasive or metastatic capabilities. **Cancers** also evade apoptosis and the immune system, and sustain angiogenesis and energy metabolism (Hanahan and Weinberg, 2011). To achieve this, **cancer** cells change their **genomes** and the **tumour** microenvironment. **Genomic** instability has a role in the survival and proliferation of **cancer** cells and the progression of disease, as these malignant characteristics are acquired. Identifying the genetic mechanisms involved in the acquisition of these traits is important for understanding and effectively inhibiting **cancer**.

### 1.1.2 The Genomics Revolution in Cancer Research

**Genomic** technologies have transformed genetics research, including the study of health and disease (Goodwin *et al.*, 2016; Lander, 2011). **Genomics** enables systematic, unbiased studies across all of the genes in the **genomes**. Cancer **genomics** investigations have been widely applied to different tissues across **molecular profiles** (Bamford *et al.*, 2004; Weinstein *et al.*, 2013; Zhang *et al.*, 2011). **Genomes** sequencing technologies continue to improve and become feasible in a wider range of applications.

**Genomics** has been used in many investigations (Goodwin *et al.*, 2016) but relatively few of the potential applications in healthcare have been realised yet (Roychowdhury and Chinnaiyan, 2016; Tran *et al.*, 2012). Cancer **genomics**, in particular, could have numerous benefits across diagnostics, prognosis, management, and treatment (Roychowdhury and Chinnaiyan, 2016). While direct impact of **genomics** on the clinic has

been limited thus far, the cancer genes and therapeutic targets identified have begun to be introduced in the clinic (Stratton *et al.*, 2009).

### 1.1.2.1 High-Throughput Technologies

These investigations have been enabled by recent developments in genomics technologies, including microarrays and more recently “Next-Generation Sequencing” (NGS), which can both be used to generate high-throughput expression data. Microarray are a high-throughput molecular technique, reducing the cost, time, and labour required to study genes at the “genome” scale (Schena, 1996). Microarray can detect genotype or expression across many genes, making it feasible to perform on a statistically informative number of samples. Microarray are manufactured with probes which measure binding of nucleotides which either detect the presence of a sequence such as a single nucleotide polymorphism (SNP) or quantify sequences for DNA copy number, gene expression, or DNA CpG methylation. In addition to being more versatile, with higher-throughput than polymerase chain reaction (PCR) based techniques, microarrays are considered cost-effective, particularly when scaled up to a large number of probes.

The introduction of massively parallel sequencing technologies has further expanded high-throughput molecular studies and the availability of genomics data. NGS enables rapid *de novo* genomes and transcriptome sequencing, in addition to gene expression studies (Goodwin *et al.*, 2016). However, the cost of sequencing for gene expression studies is still considerably higher than a microarray study, limiting feasible sample sizes, and NGS studies have large compute requirements to handle the raw data. In many cases, the benefits of NGS technologies outweigh the additional cost. NGS technologies have the advantage of greater potential accuracy and sensitivity than microarrays. NGS has a wider dynamic range than microarrays and are not limited to genes with an already characterised sequence or functions (TaraZona *et al.*, 2011).

NGS is highly adaptable to different applications, including DNA sequencing (obtaining the base sequence for the exome or whole genome) or RNA-Seq (Goodwin *et al.*, 2016; Tran *et al.*, 2012; Waldron, 2016). RNA-Seq of the transcriptome is a common adaptation where RNA is reverse transcribed and sequenced from the resulting complementary DNA (cDNA). This is utilised to quantify the levels of RNA and identify which regions of DNA are expressed. Subsets of the nucleic acid may be extracted for sequencing such as the coding regions of DNA (for the “exome”), mRNA, or micro RNA (microRNA). These “omics” technologies (Roychowdhury and Chinnaiyan, 2016;

Waldron, 2016) are applicable across a wide range of biomolecules to generate “” of a cell or sample (Perou *et al.*, 2000).

NGS technologies continue to be refined (Goodwin *et al.*, 2016) with Illumina (the platform used to generate data in this project) and competitors continuing to improve products and decrease costs. As such, RNA-Seq for examining transcriptomes or expression studies is a growing field and will continue to be generated for a range of samples. The technology may yet improve (Goodwin *et al.*, 2016) with developments in speed and accuracy (such as semi-conductor platforms) or long reads, single molecule sequences (such as Pacific Biosciences, Oxford Nanopore, and Quantum Biosystems Japan). Due to the benefits of sequencing and the availability of public data, this thesis has focused on gene expression data generated by RNA-Seq. RNA-Seq data is publicly available from large-scale cancer genomics projects and the methods analysis developed for RNA-Seq data could be applied to future genomics technologies.

### 1.1.2.2 Bioinformatics and Genomic Data

Genomic technologies have generated data at a scale which requires computational, mathematical, and statistical expertise to handle this data effectively (Markowetz, 2017; Tran *et al.*, 2012), in addition to an understanding of the biological context and research questions. The interdisciplinary field of “bioinformatics”, which draws upon these skills, focuses specifically on making inferences from genomics data or developing the tools to do so. Gene expression analysis is the focus of many bioinformatics research groups, drawing upon statistical approaches to appropriately handle microarray and RNA-Seq data along with making biological inferences from a large number of statistical tests.

Bioinformatics is often confused with the broader field “computational biology” (Markowetz, 2017), which focuses on modelling and simulating aspects of biology and is not necessarily limited to genetics or data analysis. In practice, many researchers identify with both bioinformatics and computational biology or use techniques in both fields. This thesis uses many of these approaches, mainly in bioinformatics, to address biological research questions pertaining to synthetic lethal interactions.

### 1.1.3 Genomics Projects

Genomic projects have also been applied to various organisms, functional genetics (Kawai *et al.*, 2001; ENCODE, 2004), and human populations focusing on variability between individuals and health or disease risk (HapMap, 2003; 1000 Genomes, 2010). International projects and consortiums have begun to release data gathered using com-

mon agreed upon protocols across laboratories. These include many [genomics](#) projects including cancer [genomics](#) projects discussed below. The quality, consistency, and accessibility of these international projects is appealing, particularly for [gene expression](#) datasets where the more recent, larger projects have switched from [microarray](#) to [RNA-Seq](#) technologies.

#### 1.1.3.1 The Cancer Genome Project

The [Cancer Genome Project \(CGP\)](#) was among the first [genomics](#) investigations into cancer (Dickson, 1999), using the human [genomes](#) sequence (Collins and Barker, 2007; Lander *et al.*, 2001), the cancer research literature, and sequencing the genes of cancers themselves. The main aim of the Cancer [Genomes](#) Project was to discover “[cancer genes](#)”, which are frequently mutated in cancers by comparing cancer and normal tissue samples. These include both “[oncogenes](#)” (which drive cancer growth) and “[tumour suppressors](#)” (which protect against cancers) that are functionally activated and inactivated in cancers respectively. This project is ongoing and continues to maintain the [Catalogue Of Somatic Mutations In Cancer \(COSMIC\)](#), a database of cancer genes (COSMIC, 2016). It includes 1,257,487 samples with 4,175,8787 gene [mutations](#) curated from 23,870 publications, including 29,112 whole [genomes](#) (COSMIC, 2016).

#### 1.1.3.2 The Cancer Genome Atlas Project

The [Cancer Genome Atlas \(TCGA\)](#) network initially set out to demonstrate utility in a pilot project on brain (McLendon *et al.*, 2008), ovarian (Bell *et al.*, 2011), and squamous cell lung (Hammerman *et al.*, 2012) cancers. The project then expanded, aiming to analyse 500 samples each for 20-25 [tumour](#) tissue types. [TCGA](#) has since exceeded that goal, with data available for 33 cancer types including 10 “rare” cancers, a total of over 10,000 samples (TCGA, 2017). The [TCGA](#) projects set out to generate a molecular “profile” of the [tumour](#) (and some matched normal tissue) samples: genotype, [somatic mutations](#), [gene expression](#), [microRNA](#), [DNA](#) copy number, [DNA](#) methylation, and protein levels. Data which cannot be used to identify the patients are publicly available

The [Cancer Genome Atlas](#) pilot projects (Bell *et al.*, 2011; Hammerman *et al.*, 2012; McLendon *et al.*, 2008) serve to demonstrate the power of applying [genomic](#) technologies to cancer research at such a scale. [TCGA](#) demonstrated the potential discovery of the molecular basis of cancer with these tissues, including the describing recurrently mutated genes in each cancer, identifying differentially methylated regions, and proposing transcriptional subtypes for ovarian cancers. The molecular aberrations

in each cancer represent potential therapeutic targets in some cases and some were shown to have an impact on patient survival.

The TCGA breast cancer analysis (Koboldt *et al.*, 2012) consisted of 802 samples with exomes, copy number variants, RPPA protein quantification, and DNA methylation, mRNA, and microRNA arrays, with 97 whole genomes sequenced. Four main molecular classes were identified to subtype the samples, despite considerable heterogeneity between samples. Recurrent mutations across more than 10% of samples were identified in the *TP53*, *PIK3CA*, and *GATA3* genes. In a further analysis of 817 breast cancer samples including 127 invasive lobular breast and 88 mixed type samples (Ciriello *et al.*, 2015), 3 molecular subtypes of lobular breast cancer were identified. Lobular breast cancer was also characterised by recurrent mutations in the *CDH1*, *PTEN*, *TBX2*, and *FOXA1* genes.

TCGA stomach cancer analysis of 295 samples (Bass *et al.*, 2014) identified molecular subtypes of stomach cancers characterised by: the Epstein-Barr virus, microsatellite instability (MSI), genomic instability, and chromosomal instability. Aberrations in *PD-L1*, *PIK3CA*, and *JAK2* were also identified in stomach cancers which may present therapeutic targets.

TCGA has identified various genes as recurrent, driver mutations across cancer types which are likely to have a role in driving the development of these cancers and present a molecular target that could be applied across tissue types. In addition to disregarding the tissue-based distinction between colon and rectal cancers based on molecular similarity (Muzny *et al.*, 2012), TCGA has observed differences within tumour types and proposed molecular subtyping for breast, clear cell renal, papillary renal, stomach, skin, bladder, and prostate cancers (Abeshouse *et al.*, 2015; Akbani *et al.*, 2015; Bass *et al.*, 2014; Ciriello *et al.*, 2015; Creighton *et al.*, 2013; Hammerman *et al.*, 2012; Koboldt *et al.*, 2012; Linehan *et al.*, 2016; Muzny *et al.*, 2012; Weinstein *et al.*, 2014).

The “Pan Cancer” TCGA project (Hoadley *et al.*, 2014; Weinstein *et al.*, 2013) analysed 3527 samples across 12 tissue types. This project performed a comprehensive analysis of molecular data across cancer types to identify molecular similarities and differences. These included recurrent *TP53*, *BRCA1* and *BRCA2* mutations, HER2 over-expression, and MSI across cancer types. The Pan Cancer project has identified 11 molecular subtypes across these tissues, with only 5 of these corresponding to tissue cancer types due to molecular similarities shared across cancer types (Hoadley *et al.*, 2014). The project further supports the genomic stratification of cancer patients,

demonstrated in breast cancer (Parker *et al.*, 2009; Pereira *et al.*, 2016; Perou *et al.*, 2000), and there being core molecular characteristics across cancers (Hanahan and Weinberg, 2000, 2011).

While these findings contribute to further understanding cancer biology within and across tissue types, the main objective of such projects is to publicly release data to analyse in future investigations (McLendon *et al.*, 2008; TCGA, 2017; Weinstein *et al.*, 2013). These serve as a vast resource of common and rare cancer types and are publicly available for further analysis (cBioPortal, 2017; TCGA, 2017; Zhang *et al.*, 2011).

### 1.1.4 Genomic Cancer Medicine

Cancer genomics has substantial potential for impacts in cancer medicine: from diagnosis to treatment (Roychowdhury and Chinnaiyan, 2016; Tran *et al.*, 2012). Beyond direct use of genomes or RNA-Seq in clinical laboratories, genomic studies also generate biomarkers and inform development of treatments. These are likely to have a more immediate patient benefit considering the cost of routine genomes sequencing for diagnostics.

#### 1.1.4.1 Cancer Genes and Driver Mutations

There are two main classes of “cancer genes” (Futreal *et al.*, 2001). Oncogenes are activated in cancers either by gain of function mutations in proto-oncogenes, amplification of DNA, or elevated gene expression. Their normal functions are typically to regulate stem cells or to promote cellular growth, with recurrent mutations that are typically concentrated to particular gene regions (“hotspots”). Conversely, tumour suppressor genes are those inactivated in cancer either by loss of function mutations, deletion of DNA copies, or reduced of gene expression, including hypermethylation. Their normal functions are typically to regulate cell division, DNA repair, and cell signalling. Detecting these cancer genes has accelerated with genomic technologies, as demonstrated by COSMIC and TCGA (COSMIC, 2016; Weinstein *et al.*, 2013). Recurrent mutations, DNA copy number variants, differential gene expression, or differential DNA methylation are all indicative of cancer genes (Mattison *et al.*, 2009), which can be detected in genomics data (Pereira *et al.*, 2016; Weinstein *et al.*, 2013).

Distinguishing important “driver” mutations in cancer genes from “passenger mutation” mutations is challenging due to patient variation, tumour heterogeneity, and genomic instability producing many variant gene sequences (Stratton *et al.*, 2009; Tran *et al.*, 2012). Driver mutations can be identified by whether they co-occur or are mutually exclusive with mutations in other genes in cancers, are recurrently mutated

across a significant proportion of samples for a specific tissue type, or if mutations are recurrent across different cancer tissue types (cBioPortal, 2017; Pereira *et al.*, 2016; COSMIC, 2016; Weinstein *et al.*, 2013; Zhang *et al.*, 2011). Approximately 140 driver mutations have been identified, including many novel genes in particular cancers from genomic studies, with 2–8 in typically occurring in each tumour usually affecting cell fate, survival, or genomes maintenance (Vogelstein *et al.*, 2013). There remains a need to translate the identification of many cancer genes and driver mutations to patient benefit by repurposing or designing of therapeutic interventions against these molecular targets.

#### 1.1.4.2 Precision Cancer Medicine

The importance of genomics is emphasised in translational cancer research in contrast with current strategies of healthcare based on what works well for the most of the population. Cancers could eventually be treated by their genomic features (Roychowdhury and Chinnaiyan, 2016), particularly grouping patients by the mutation, expression, or DNA methylation profiles of their cancers, which is already done in part (Parker *et al.*, 2009). Identifying actionable molecular targets is a key aspect of “precision medicine”, the rationale to target molecular subtypes with separate treatment strategies (Glaire *et al.*, 2017). To this end many driver mutations and gene expression signatures for distinguishing cancers have been identified. Some oncogenic driver mutations have effective pharmacological inhibitors designed against them but there remain many cancer genes and mutations, particularly tumour suppressors, for which there is not yet a targeted therapy.

#### 1.1.4.3 Molecular Diagnostics and Pan-Cancer Medicine

Molecular features such as mutations or gene expression signatures have been proposed to diagnose tumour subtypes. In breast cancer, several distinct “intrinsic subtypes” have been identified, distinguished by molecular mechanisms, with differences in malignancy and patient outcome (Parker *et al.*, 2009; Perou *et al.*, 2000). Conversely, common molecular mechanisms may be shared between cancers across tissue types as discovered by the “Pan Cancer” TCGA project, which combined molecular profiles across tissue types (Weinstein *et al.*, 2013). Molecular subtypes could feasibly be included in clinical testing as a panel of biomarkers for diagnosis, monitoring drug response, or predicting risk of recurrence. As these molecular subtypes and genetic aberrations specific to cancers have been identified, there is an increasingly clear need for further development of treatments that target them.

Gene expression can be used to characterise breast cancers. The “intrinsic subtypes” identified were characterised by estrogen receptor, *HER2*, and basal, epithelial signalling (Perou *et al.*, 2000). The expression profiles were similar across independent samples of the same tumour or the same patient and therefore represent the molecular state of a tumour. The molecular intrinsic subtypes “luminal A”, “luminal B”, “*HER2*-enriched”, “basal-like”, and “normal-like” have been replicated across microarray studies (Hu *et al.*, 2006), with their relevance to prognosis demonstrated, and a 50-gene subtype predictor developed (Parker *et al.*, 2009; Sørlie *et al.*, 2001). Despite specific differences in subtyping, there is widespread agreement that distinguishing luminal, *HER2*-enriched, and triple negative tumours has prognostic importance for patients (Dai *et al.*, 2015). The “Pan Cancer” The Cancer Genome Atlas project (discussed in Section 1.1.3.2) demonstrates the importance of molecular similarities and differences between cancers across cancer tissue types (Weinstein *et al.*, 2013).

Gatza *et al.* (2010) used gene signatures for 18 cellular pathways in breast cancer to define subtypes with distinct molecular pathway activity. A “metagene” is a measure pathway activation (derived from eigenvectors or principal components) which gives a consistent signal of gene expression (Anjomshoaa *et al.*, 2008; Huang *et al.*, 2003; Nagalla *et al.*, 2013). Unsupervised hierarchical clustering defined subtypes with common pathway activity, despite variation in mutations. These subtypes intrinsic subtypes and provide finer molecular stratification with a functional basis (Gatza *et al.*, 2014; Parker *et al.*, 2009). The subtypes with shared pathway activity have similar molecular characteristics (such as DNA copy number) and clinical properties including prognosis.

#### 1.1.4.4 Targeted Therapeutics and Pharmacogenomics

Targeted therapies with specificity against a molecular target are examples of precision cancer medicine. Molecular targets can be tested in laboratory conditions with RNA interference (RNAi) or pharmacological agents (Fece de la Cruz *et al.*, 2015). Identification of molecular targets is important for developing novel anti-cancer treatments along with validation and drug testing. For oncogenic mutations, the recurrent mutant variant or over-expressed gene can be directly inhibited, however, oncogenes with high homology to other genes or tumour suppressor genes are not amenable to direct targeting (Kaelin, Jr, 2009). Targeted anticancer therapeutics can exploit complex interactions to distinguish normal and cancerous cells which may benefit from studies of gene regulation or interaction networks (Hopkins, 2008). Targeted therapeutics have already been successfully applied as monoclonal antibodies against oncogenes, such as *HER2* in breast cancer (Miles, 2001).

### 1.1.5 Systems and Network Biology

Driver mutations in [oncogenes](#) and [tumour suppressor](#) genes do not occur in isolation. The genetic interactions, regulatory and cellular signalling, and metabolic reactions are inter-related and may each be perturbed by aberrations in gene function occurring in [cancers](#). These relationships can be represented by biological networks of connected pairs of genes with a relationship. Due to the complexity of a cell, these molecular networks are very large, consisting of thousands of [nodes](#) comprised by genes or proteins.

The properties of large [networks](#) were first studied by constructing random [networks](#) by randomly linking a fixed number of [nodes](#) ([Erdős and Rényi, 1959, 1960](#)). Despite the random nature of these [networks](#), properties such as their connectivity were well characterised. The [vertex](#) degree (number of partners for each [node](#)) of their random [networks](#) followed a Poisson distribution, however this property does not hold in nature. Thus natural [networks](#) are non-random or not formed in this way ([Barabási and Oltvai, 2004](#)).

This work formed the foundation for studying complex [networks](#) ([van Steen, 2010](#)), which model features of observed [networks](#) not found in Erdő and Rényi's random [networks](#) ([Erdős and Rényi, 1959, 1960](#)). The [small world](#) property, made popular by findings in social [networks](#) ([Travers and Milgram, 1969](#)), is the remarkably short path lengths between any [nodes](#) in a [small world network](#). A [small world network](#) is well-connected with a characteristic path length (the average length of [shortest paths](#) between all pairs of [nodes](#)) proportional to the logarithm of the number of [nodes](#). [Watts and Strogatz \(1998\)](#) developed a model of random rewiring of a regular [network](#) to construct random [networks](#) with the [small world](#) property and a high clustering coefficient. While these properties are more representative of [networks](#) occurring in nature, their model was limited by the degree distribution which converges to a Poisson distribution as it is rewired ([Barrat and Weigt, 2000](#)). The [vertex](#) degree distribution of naturally occurring [networks](#) often follows a power law distribution with most [nodes](#) having far fewer connections than average and a small subset of highly connected network 'hubs' ([Barabási and Albert, 1999](#)).

[Barabási and Albert \(1999\)](#) constructed a [network](#) model in an entirely different way to randomly generate [scale-free networks](#) which have a power law degree distribution. They constructed random [networks](#) by preferential attachment, modelling growth of a [network](#) by sequentially adding [nodes](#) with [links](#) to existing [nodes](#). The [scale-free](#) nature of the random [networks](#) was ensured by adding new [nodes](#) with an increasing probability

of attachment to an existing **node** if it had a higher degree. These networks successfully captured the **scale-free** nature of many observed **networks** with short characteristic path length and low eccentricity resulting in super **small worlds** (Barabási and Albert, 1999).

High-throughput technologies such as **siRNA** screens, two-hybrid screens, **microarrays** and massively parallel sequencing have generated **genomes-scale** data and enabled analysis of biological **networks** (Barabási and Oltvai, 2004; Boone *et al.*, 2007; Goodwin *et al.*, 2016). Molecular networks are biological networks consisting of biological molecules including genes, transcripts (with non-coding and **microRNAs**), or proteins related by known interactions and gene regulatory or metabolic **pathways**. Many types of molecular networks can be constructed, depending on the biological application (). **Synthetic genetic interactions** are relatively unexplored within molecular networks and may lead to better understanding of the role of gene functions in cellular function and disease. **High-throughput screens** in humans, mammals, and non-model organisms are costly and labour-intensive (Fece de la Cruz *et al.*, 2015). Computational approaches with effective predictive models are therefore a more feasible alternative to study the connectivity of a biological **network** in a complex metazoan cell at the **genomes-scale**.

## 1.2 Synthetic Lethal Cancer Medicine

**Synthetic lethality** has vast potential to improve cancer medicine by expanding application of **targeted therapeutic** to include inactivation of **tumour suppressors** and genes that are difficult to target directly. **Synthetic lethal** interactions are also studied for gene function and drug mode-of-action in model organisms. This section introduces the concept of **synthetic lethality** as it was originally conceived and how it has been adopted conceptually in cancer research. Detecting these interactions at scale and interpreting them is the focus of this thesis, hence we start with an overview of the concepts involved, initial work on the interaction, and the rationale for applications to cancer. Specific investigations into **synthetic lethality** in cancer, detection by experimental screening, and prediction by computational analysis will then be reviewed.

### 1.2.1 Synthetic Lethal Genetic Interactions

Genetic interactions are a core concept of molecular biology, discovered among earliest investigations of Mendelian genetics, and have received revived interest with new technologies and potential applications. **Biological epistasis** is the effect of an **allele** at one locus “masking” the phenotype of another locus (Bateson and Mendel, 1909). **Statistical epistasis** is where there is significant disparity between the observed and ex-

pected phenotype of a double **mutant**, compared to the respective phenotypes of single **mutant** and the **wild-type** (Fisher, 1919). Fisher's definition lends itself to quantitative traits and more broadly encompasses **synthetic genetic interactions**. These have become popular for studies in yeast genetics and cancer drug design (Boone *et al.*, 2007; Kaelin, Jr, 2005).

**SGIs** are substantial deviations of growth or viability from the expected null mutant phenotype (of an organism or cell) assuming additive (deleterious) effects of the single **mutant**. The double **mutant** does not necessarily have either of the single **mutant** phenotypes (as shown for cellular growth phenotypes in Figure 1.1). Most **SGIs** are more viable than either single **mutant** or less viable than the expected double **mutant**. Mutations are “synergistic” in negative **SGI** with more deviation from the **wild-type** than expected. Formally, “**synthetic sick**” (**SSL**) and “**synthetic lethal**” (**SL**) interactions are negative **SGIs** giving growth inhibition and complete inviability respectively. In cancer research, **synthetic lethality** more broadly describes any negative **SGI** with specific inhibition of a **mutant** cell, including **SSL** interactions. Mutations are “alleviating” in positive **SGI** with less deviation from the **wild-type** than expected. For viability, “**suppression**” (**SS**) and “**rescue**” (**SR**) are positive **SGIs** giving at least partial restoration of **wild-type** growth from single **mutant** with growth impairment and lethal phenotypes respectively. Negative **SGIs** were markedly more common than positive **SGIs** in a number of studies in model systems (Boucher and Jenna, 2013; Tong *et al.*, 2004).

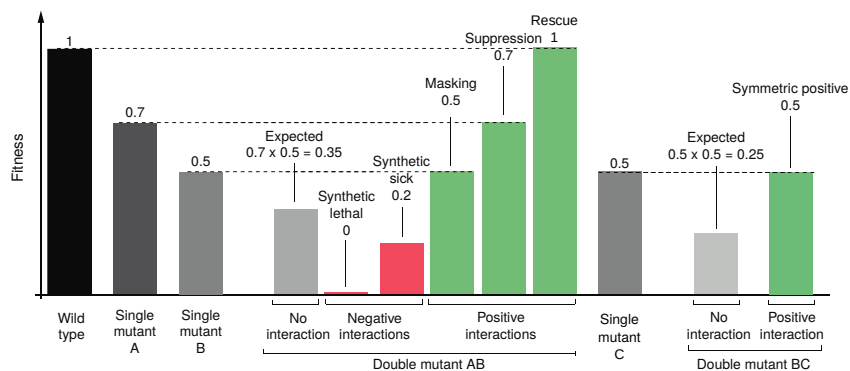


Figure 1.1: **Synthetic genetic interactions.** Impact of various negative and positive **SGIs**: negative interactions involve deleterious (sick) or inviable (lethal) phenotypes whereas positive interactions involve restoring viability by masking or suppressing the other **mutation** or complete rescue of the **wild-type** phenotype. Figure adapted from (Costanzo *et al.*, 2011) concerning growth viability fitness in yeast.

### 1.2.2 Synthetic Lethal Concepts in Genetics

Synthetic lethal genes are generally regarded to arise due to functional redundancy (Boone *et al.*, 2007). Due to the functional level of SGIs, synthetic lethal genes do not need to directly interact, nor be expressed in the same cell or at the same developmental stage: serving related functions is sufficient to affect cell (or organism) viability and be relevant to drug-mode-of-action cancer biology. Combined loss of genes performing an essential or important function in a cell are therefore deleterious. Synthetic lethal gene pairs are therefore pairwise essential with “induced essentiality”: each synthetic lethal gene becomes essential to the cell upon loss of the other (Ashworth *et al.*, 2011; Kaelin, Jr, 2005).

Since synthetic lethal gene partners can be affected by extracellular stimuli such as chemicals, essentiality of synthetic lethal genes can be induced by the environment of a cell. An environmental stress condition may inhibit one or the other synthetic lethal gene, such as exposure to chemicals, in which case the synthetic lethal partner gene is “conditionally essential” (Hillenmeyer, 2008). Thus the evolutionary rationale for the abundance of SGIs (compared to the surprisingly low number of essential genes) in a Eukaryotic genomes can be attributed to genetic functional redundancy and network robustness of a cell which are advantageous to survival.

Biological functions are typically performed by a pathway of genes (or their products). Synthetic lethal genes occur within the same biological pathway and between them (Boone *et al.*, 2007; Costanzo *et al.*, 2010; Kelley and Ideker, 2005). Many genes of the same pathway may be functionally interchangeable, synthetic lethal partners of a particular gene. Therefore biological pathways can exhibit induced essentiality with loss of the synthetic lethal partner gene and synthetic lethality may occur at pathway level or in a gene regulation network.

### 1.2.3 Synthetic Lethality in Model Systems

Genetic high-throughput screens have identified unexpected, functionally informative, and clinically relevant synthetic lethal interactions; including synthetic lethal partners of genes recurrently mutated in cancer or attributed to familial early-onset cancers (Lord *et al.*, 2015). While screening presents an appealing strategy for synthetic lethal discovery, computational approaches are becoming popular as an alternative or complement to experimental methods to overcome inherent bias and limitations of experimental screens. An array of recently developed computational methods (Jerby-Arnon *et al.*, 2014; Lu *et al.*, 2015; Tiong *et al.*, 2014; Wang and Simon, 2013; Wappett, 2014)

show the need for synthetic lethal discovery in the fundamental genetics and translational cancer research community. However, many existing computational methods are not suitable for queries of genomic data for interacting partners of a particular gene, as (1) they have been applied pairwise across the genomes, (2) they do not have software released to apply the methodology, or (3) they lack statistical measures of error for further analysis. A robust prediction of gene interactions is an effective and practical approach at a scale of the entire genomes for ideal translational applications, analysis of biological systems, and constructing functional gene networks.

#### 1.2.3.1 Synthetic Lethal Pathways and Networks

SGIs are common in genomes, four-fold more interactions were detected with synthetic gene array (SGA) mating screens than protein-protein interactions detected with yeast-2-hybrid (Tong *et al.*, 2004). The SGI network was scale-free and had a low average shortest path length, as expected for a complex biological network (Barabási and Oltvai, 2004). Highly connected “hub” genes with the highest number of links (vertex degree) are functionally important with many negative SGI hubs involved in cell cycle regulation, and many positive SGIs involved in translation (Baryshnikova *et al.*, 2010b; Costanzo *et al.*, 2010). Negative SGIs were far more common than positive SGIs, with synthetic gene loss being more likely to be deleterious to cell than advantageous, which indicates that synthetic lethality may be comparably easier to detect than other SGIs.

Essential pathways are highly buffered, with five-fold more interactions than other SGIs, consistent with strong selection for survival, as found with conditional and partial mutations in essential genes (Davierwala *et al.*, 2005). This SGI network had scale-free topology and rarely shared interactions with the protein-protein interaction network. These networks are related by an “orthogonal” relationship: shared partners in one network tend to be themselves connected directly in the other network. Essential genes were likely to have closely related functions, whereas non-essential networks were relatively more inclined to have SGIs between distinct biological pathways.

#### 1.2.3.2 Evolution of Synthetic Lethality

There is poor conservation of specific SGIs between *S. cerevisiae* and *S. pombe* with 29% of the interactions tested in both distantly related species being conserved between them (Dixon *et al.*, 2008). The remaining interactions show high species-specific differences, however, many of the species-specific interactions were still conserved between biological pathways, protein complexes, or protein-protein interaction modules.

Similarly, conservation of pathway redundancy was also found between Eukaryotes (*S. cerevisiae*) and prokaryotes (*E. coli*) (Butland *et al.*, 2008). Negative SGIs were more likely to be conserved between biological pathways, whereas positive SGIs were more likely to be conserved within a pathway or protein complex (Roguev *et al.*, 2008).

A modest 5% of interactions were conserved between unicellular (*S. cerevisiae*) and multicellular (*C. elegans*) organisms. However, the nematode SGI network had similar scale-free topology and modularity despite differences in methodology: metazoan synthetic lethal screens with RNA interference (RNAi) are incomplete knockouts, whereas screening null mutations is feasible in yeast (Bussey *et al.*, 2006). The nematode SGI screen identified network hubs with important interactions to orthologues of known human disease genes (Lehner *et al.*, 2006). Despite the lack of direct conservation of SGIs between yeasts and nematode worms, genetic redundancy was consistent with an “induced essentiality” model of SGIs where gene functions are conserved with network restructuring over evolutionary change (Tischler *et al.*, 2008).

While nematode models are more closely related to human cells which are also screened with RNAi, cancer cells can present growth and viability phenotypes more comparable to yeast models. Therefore findings from both SGA and RNAi models are relevant to understanding human and cancer cells. RNAi has also been applied to human and mouse cancer cells with short interfering RNA (siRNA) in cell culture and genetic screening experiments. These findings suggest that SGI network “rewiring” is a concern for identifying specific synthetic lethal interactions in cancer as specific synthetic lethal genes may vary between genetic backgrounds. Thus it is expected at a pathway approach will be more robust in the context of evolution, patient variation, tumour heterogeneity, or disease progression.

#### 1.2.4 Synthetic Lethality in Cancer

Loss of function occurs in many genes in cancers, including tumour suppressors, yet few interventions target such mutations compared to targeted therapies for gain of function mutation in oncogenes (Kaelin, Jr, 2005). Synthetic lethality is a powerful design strategy for therapies selective against loss of gene function with potential for application against a range of genes and diseases (Fece de la Cruz *et al.*, 2015; Kaelin, Jr, 2009). When genes are disrupted in cancers, the induced essentiality of synthetic lethal partners presents a vulnerability that may be exploited for anti-cancer therapy. Since synthetic lethality affects cellular viability by indirect functional relationships between genes, it is suitable for indirectly targeting mutations in cancers via synthetic lethal

partners with **targeted therapeutic**. These have could be highly specific against cancer cells (with the target **mutation**) over non-cancer cells (with a functional compensating gene). Analogous to “**oncogene addiction**”, where cancer cells adapt to particular oncogenic growth signals and become reliant on them to remain viable (Luo *et al.*, 2009; Weinstein, 2000), synthetic lethal partners of inactivated **tumour suppressors** are required to maintain cancer cell viability and proliferation. As such cancers are subject to “**non-oncogene addiction**” and these genes are feasible anti-cancer drug targets.

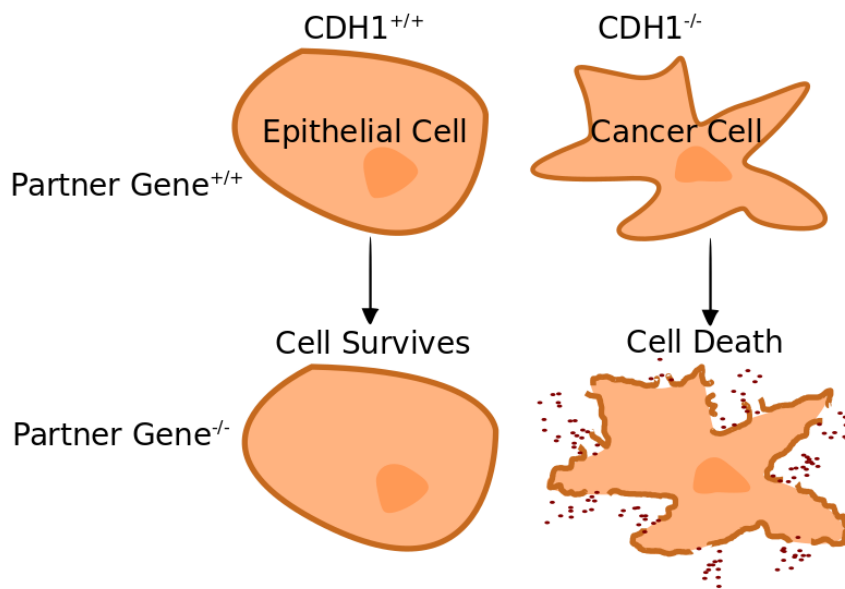


Figure 1.2: **Synthetic lethality in cancer**. Rationale of exploiting **synthetic lethality** for specificity against a **tumour suppressor** gene (e.g., *CDH1*) while other cells are spared under the inhibition of a partner gene.

The synthetic lethal approach to cancer medicine is most amenable to loss of function **mutations** in **tumour suppressor** genes, where it would feasibly be effective against any loss of function **mutation** across the **tumour suppressor** with a viable **synthetic lethal** partner gene (as shown in Figure 1.2). However, the approach may also be suitable for cases where cancer cells have **mutations** where the normal function of the gene is disrupted such as if it were over-expressed (“**synthetic dosage lethality**”) or if an oncogenic **mutation** interfered with the function of the proto-oncogene. Thus **synthetic lethality** makes it feasible to target a range of cancer-specific **mutations** with **targeted therapeutic**, including inactivated **tumour suppressor** genes. **synthetic lethality** may also enable distinguishing highly homologous **oncogenes** by functional differences by targeting their **synthetic lethal** partners.

### 1.2.5 Clinical Impact of Synthetic Lethality in Cancer

The synthetic lethal interaction of *BRCA1* or *BRCA2* with *PARP1* in breast cancer is an example of how gene interactions are important in cancer and these discovery of these interactions has lead to translation to the clinic. These genetic interactions enable specific targeting of mutations in *BRCA1* or *BRCA2* tumour suppressor genes with Poly-ADP-ribose polymerase (PARP) inhibitors by inducing synthetic lethality in breast cancer (Farmer *et al.*, 2005). PARP inhibitors were one of the first targeted therapeutic against a tumour suppressor mutation to exhibit success in clinical trials.

*BRCA1/BRCA2* and *PARP1* genes demonstrate the application of the synthetic lethal approach to cancer therapy (Ashworth, 2008; Kaelin, Jr, 2005). *BRCA1* and *BRCA2* are homologous DNA repair genes, widely known as tumour suppressors; mutation carriers have substantially increased risk of breast (risk by age 70 of 57% for *BRCA1* and 59% for *BRCA2*) and ovarian cancers (risk by age 70 of 40% for *BRCA1* and 18% for *BRCA2*) (Chen and Parmigiani, 2007). The *BRCA1* or *BRCA2* genes, which usually repair DNA or destroy the cell if it cannot be repaired, have inactivating somatic mutations in some familial and sporadic cancers. Poly-ADP-ribose polymerase (PARP) genes are tumour suppressor genes involved in base excision DNA repair. Loss of PARP activity results in single-stranded DNA breaks. However, *PARP1*<sup>-/-</sup> knockout mice are viable and healthy indicating low toxicity from PARP inhibition (Bryant *et al.*, 2005).

Bryant *et al.* (2005) showed that *BRCA2* cells were sensitive to PARP inhibition by siRNA of *PARP1* or drug inhibition (which targets *PARP1* and *PARP2*) using Chinese hamster ovary cells, MCF7 and MDA-MB-231 breast cell lines. This effect was sufficient to kill mouse tumour xenografts and showed high specificity to *BRCA2* deficient cells in culture and xenografts. Farmer *et al.* (2005) replicated these results in embryonic stem cells and showed that *BRCA1* cells were also sensitive to PARP inhibition relative to the wild-type with siRNA and drug experiments in cell culture and drug activity against *BRCA1* or *BRCA2* deficient embryonic stem cell mouse xenografts. They found evidence that PARP inhibition causes DNA lesions, usually repaired in wild-type cells, which lead to chromosomal instability, cell cycle arrest, and induction of apoptosis in *BRCA1* or *BRCA2* deficient cells. The combined loss of DNA repairs pathways gives a plausible mechanism for an effective anti-cancer treatment.

Thus PARP inhibitors could be applied with clinical use against *BRCA1* or *BRCA2* mutations in both hereditary and sporadic cancers (Ashworth, 2008; Kaelin, Jr, 2005). PARP inhibition has been found to be effective in ovarian cancer patients carrying

*BRCA1* or *BRCA2* mutations and some patient without these mutations, suggesting synthetic lethality between PARP and other DNA repair pathways (Ström and Helleday, 2012). This supports the potential for PARP inhibition as a chemo-preventative alternative to prophylactic surgery for high-risk individuals with *BRCA1* or *BRCA2* mutations (Ström and Helleday, 2012). Hormone-based therapy has also been suggested as a chemo-preventative in such high-risk individuals and aromatase inhibitors have completed phase I clinical trials for this purpose (Bozovic-Spasojevic *et al.*, 2012). Ström and Helleday (2012) also postulate increased efficacy of PARP inhibitors in the hypoxic DNA-damaging tumour micro-environment.

A PARP inhibitor, olaparib, showed fewer adverse effects than cytotoxic chemotherapy and anti-tumour activity in various clinical trials against *BRCA1* or *BRCA2* deficient familial or sporadic breast, ovarian, and prostate cancers (Audeh *et al.*, 2010; Fong *et al.*, 2009, 2010; Tutt *et al.*, 2010). This treatment has a favourable therapeutic window and similarly low toxicity between mutation carriers of *BRCA1* or *BRCA2* mutations and sporadic cases. These PARP inhibitors have been FDA approved for some cancers McLachlan *et al.* (2016), are effective against germline mutation and sporadic *BRCA1* or *BRCA2* mutations, and are a potential prevention alternative to prophylactic surgery for high-risk mutation carriers Ström and Helleday (2012).

This demonstrates the clinical impact of a well characterised system of synthetic lethality with known cancer risk genes. Synthetic lethality has the benefit of being effective against inactivation of tumour suppressor genes by any means, broader than targeting a specific oncogenic mutation (Kaelin, Jr, 2005). The targeted therapy is effective in both sporadic and hereditary *BRCA1* or *BRCA2* deficient tumours acting against an oncogenic molecular aberration across several tissues.

### 1.2.6 High-throughput Screening for Synthetic Lethality

RNA interference (RNAi) technologies have enabled extensive investigations of genetic redundancy in mammalian experimental models including testing experimentally for synthetic lethality (Fraser, 2004). Synthetic lethal RNAi screens are performed, using short interfering RNA (siRNA) or short hairpin RNA (shRNA) to target specific genes in isogenic cells. Identifying synthetic lethality is crucial for studying gene function, drug mechanisms, and design novel therapies (Lum *et al.*, 2004). Candidate selection of synthetic lethal gene pairs relevant to cancer has shown some success but is limited because interactions are difficult to predict; they can occur between seemingly unrelated pathways in model organisms (Costanzo *et al.*, 2011). While biologically informed

hypotheses have had some success in synthetic lethal discovery (Bitler *et al.*, 2015; Bryant *et al.*, 2005; Farmer *et al.*, 2005), interactions occurring indirectly between distinct pathways would be missed (Boone *et al.*, 2007; Costanzo *et al.*, 2011). Scanning the entire genomes for interactions against a clinically relevant gene is an emerging strategy being explored with high-throughput screens (Fece de la Cruz *et al.*, 2015) and computational approaches (Boucher and Jenna, 2013; van Steen, 2012).

Experimental screening for synthetic lethality is an appealing strategy for wider discovery of functional interactions *in vivo* despite many potential sources of error which must be considered. The synthetic lethal concept has both genetic and pharmacological screening applications to cancer research. Genetic screens, with RNAi to discover the specific genes involved, inform development of targeted therapies with a known mode of action, anticipated mechanisms of resistance, and biomarkers for treatment response. RNAi is a transient knockdown of gene expression more similar to the effect of drugs than complete gene loss and is more representative of disease than model organisms (Bussey *et al.*, 2006). The RNAi gene knockdown process has inherent toxicity to some cells, potential off-target effects, and issues with a high false positive rate. Therefore, it is important to validate any candidates in a secondary screen and replicate knockdown experiments with a number of independent shRNAs. Genetic screens have potential for quantitative gene disruption experiments to selectively target over-expressed genes in cancer via synthetic dosage lethality. While powerful for understanding fundamental cellular function, analysis of isogenic cell lines is inherently limited by assuming only a single mutation differs between them and cannot account for diverse genetic backgrounds or tumour heterogeneity (Fece de la Cruz *et al.*, 2015). Genetic screens can thus identify targets to develop, or can repurpose targeted therapies for disease, but alone will not directly identify a lead compound to develop for the market or for clinical translation.

Chemical screens are immediately applicable to the clinic, as they are directly screening for selective lead compounds with suitable pharmacological properties. However, chemical screens lack a known mode of action, may affect many targets, and screen a narrow range of genes with existing drugs. With either approach there are still many challenges to translating candidates into the clinic. Identifying specific target genes may contribute to overcoming such challenges, which can be approached with genetic screens and computational alternatives. Screening methods have proven a fruitful area of research, despite being costly, laborious, and having many different

sources of error. These limitations suggest a need for complementary computational approaches to synthetic lethal discovery.

#### 1.2.6.1 Synthetic Lethal Screens

Hereditary diffuse gastric cancer (HDGC) is a cancer syndrome of predisposition to early-onset malignant stomach and breast cancers attributed to mutations in E-cadherin, encoded by *CDH1* (as discussed in Section 1.3). Telford *et al.* (2015) performed an RNAi screen on MCF10A breast cells for synthetic lethality with *CDH1*. They found enrichment of G protein coupled receptors and cytoskeletal gene functions. The results were consistent with a concurrent drug compound screen with several candidates validated by lentiviral shRNA gene knockdown and drug testing including inhibitors of Janus kinase (JAK), histone deacetylase (HDAC), phosphoinositide 3-kinase (PI3K), aurora kinase, and tyrosine kinases. Therefore the synthetic lethal strategy has potential for clinical impact against HDGC, with an interest in interventions with low adverse effects for chemo-prevention, including repurposing existing approved drugs for activity against *CDH1* deficient cancers.

The examples above show that high-throughput screens are an effective approach to discover synthetic lethality in cancer with a wide range of applications. Screens are more comprehensive than hypothesis-driven candidate gene approaches and successfully find known and novel synthetic lethal interactions with potential for rapid clinical application. They have the power to test mode of action of drugs, find unexpected synthetic lethal interactions between pathways, or identify effective treatment strategies without needing a clear mechanism. However, synthetic lethal screens are costly, labour-intensive, error-prone, and biased towards genes with effective RNAi knockdown libraries. Limited genetic background, lethality to wild-type cell during gene knockdown, off-target effects, and difficulty replicating synthetic lethality across different cell lines, tissues, laboratories, or conditions stems from a high false positive rate and a lack of standardised thresholds to identify synthetic lethality in a high-throughput screen. Therefore there is a need for replication, validation, and alternative approaches to identify synthetic lethal candidates. In addition, varied conditions across experimental screens and differences between RNAi and drug screens makes meta-analysis extremely challenging.

Genome-scale synthetic lethal experiments (across gene pairs) are not feasible, even in model organisms, and they typically focus on specific gene candidates or the partners of a gene of interest (such as importance in health). Therefore a computational ap-

proach is more suitable for this task and may further augment experimental screening to replicate screen candidates beyond experimental models.

## 1.2.7 Computational Prediction of Synthetic Lethality

### 1.2.7.1 Bioinformatics Approaches to Genetic Interactions

Prediction of gene interaction networks is a feasible alternative to high-throughput screening, and has both biological importance and clinical relevance. There are many existing methods to predict gene networks, as reviewed by [van Steen \(2012\)](#) and [Boucher and Jenna \(2013\)](#) and summarised in Table 1.1. However, many of these methods have limitations, including the requirement for existing [SGI](#) data, several data inputs, and reliability of gene function annotation. Many of the existing methods also assume conservation of individual interactions between species, which has been found not to hold in yeast studies ([Dixon \*et al.\*, 2008](#)). Tissue specificity is important in gene regulation and [gene expression](#), which are used as predictors of genetic interaction. However, tissue specificity of genetic interactions cannot be explored in yeast studies and has not been considered in many studies of multicellular model organisms, human networks, or cancers. Similarly, investigation into tissue specificity of [PPIs](#), an important predictor of genetic interactions, is difficult given that high-throughput two-hybrid screens occur out of cellular context for multicellular organisms ([Brückner \*et al.\*, 2009](#)).

Table 1.1: Methods for predicting genetic interactions

Method	Input Data	Species	Source	Tool Offered
Between Pathways Model	PPI, SGI	<i>S. cerevisiae</i>	Kelley and Ideker (2005)	
Within Pathways Model	PPI, SGI	<i>S. cerevisiae</i>	Kelley and Ideker (2005)	
Decision Tree	PPI, expression, phenotype	<i>S. cerevisiae</i>	Wong <i>et al.</i> (2004)	2 Hop
Logistic Regression	SGI, PPI, co-expression, phenotype	<i>C. elegans</i>	Zhong and Sternberg (2006)	Gene Orienteer
Network Sampling	SGI, PPI, GO	<i>S. cerevisiae</i>	Le Meur and Gentleman (2008) Le Meur <i>et al.</i> (2014)	SLGI(R)
Random Walk	GO, PPI, expression	<i>S. cerevisiae</i> <i>C. elegans</i>	Chipman and Singh (2009)	
Shared Function	Co-expression, PPI, text mining, phylogeny	<i>C. elegans</i>	Lee <i>et al.</i> (2010b)	WormNet
Logistic Regression	Co-expression, PPI, phenotype	<i>C. elegans</i>	Lee <i>et al.</i> (2010a)	GI Finder
Jaccard Index	GO, SGI, PPI, phenotype	Eukarya	Hoehndorf <i>et al.</i> (2013)	
Machine Learning			Pandey <i>et al.</i> (2010)	MNMC
Machine Learning Meta-Analysis			Wu <i>et al.</i> (2014)	MetaSL
Flux Variability Analysis		<i>E. coli</i>		
Flux Balance Analysis	Metabolism	<i>M. pneumoniae</i>	Güell <i>et al.</i> (2014)	
Network Simulation				

There are existing computational methods for predicting [synthetic lethal](#) gene pairs

Table 1.2: Methods for predicting synthetic lethality in cancer

Method	Input Data	Source	Tool Offered
Network Centrality	protein-protein interactions	Kranthi <i>et al.</i> (2013)	
Differential Expression	Expression Mutation	Wang and Simon (2013)	
Comparative Genomic Chemical-Genomic	Yeast synthetic gene interactions Homology	Heiskanen and Aittokallio (2012)	
Comparative Genomic	Yeast synthetic gene interactions Homology	Deshpande <i>et al.</i> (2013)	
Machine Learning		Discussed by Babyak (2004) and Lee and Marcotte (2009)	
Differential Expression	Expression	Tiong <i>et al.</i> (2014)	
Literature Database		Li <i>et al.</i> (2014)	Syn-Lethality
Meta-Analysis	Meta-Analysis Machine Learning	Wu <i>et al.</i> (2014)	MetaSL
Pathway Analysis		Zhang <i>et al.</i> (2015)	
Protein Domains	Homology	Kozlov <i>et al.</i> (2015)	
Data-Mining Machine Learning	Expression Somatic mutation and DNA CNV siRNA in cell lines	Jerby-Arnon <i>et al.</i> (2014) Ryan <i>et al.</i> (2014) Crunkhorn (2014) Lokody (2014)	DAISY (method)
Genome Evolution	Expression	Lu <i>et al.</i> (2013)	
Hypothesis Test	DNA CNV	Lu <i>et al.</i> (2015)	
Machine Learning	Known SL		
Bimodality	Expression DNA CNV Somatic Mutation	Wappett (2014) Wappett <i>et al.</i> (2016)	BiModal Subsetting ExPression (BiSEp)
Directional Chi-Square	Expression (microarray) Somatic mutation	Kelly, S. T., Guilford, P. J., and Black, M. A. Dissertation (Kelly, 2013) and developed here	SLIPT

in humans, with a specific emphasis on cancer (as summarised in 1.2). While these demonstrate the power and need for predictions of **synthetic lethality** in human and cancer contexts, limitations of previous methods could be met with a different approach. Existing computational approaches to **synthetic lethal** prediction are often difficult to interpret or replicate for new genes, or are reliant on data types not available for a wider range of genes to test.

### 1.2.7.2 Comparative Genomics

A comparative genomic approach by Deshpande *et al.* (2013) used the results of well characterised high-throughput **mutation** screens in *S. cerevisiae* as candidates for **synthetic lethality** in humans (Baryshnikova *et al.*, 2010a; Costanzo *et al.*, 2010, 2011; Tong *et al.*, 2001, 2004). Yeast **synthetic lethal** partners were compared to human orthologues to find cancer relevant **synthetic lethal** candidate pairs with direct therapeutic potential. Proposed as a complementary approach to **siRNA** screens, approximately 24,000 of the 116,000 negative **SGI** in yeast (Costanzo *et al.*, 2011) were matched to human orthologues, with over 500 involving a **cancer gene** (Futreal *et al.*, 2004). Under strict criteria of one-to-one orthologues, large effect size and significant interaction in yeast data, 1522 interactions were identified with 70 involving **cancer genes**. Of the

21 gene interactions tested with pairs of **siRNA** in IMR1 fibroblast cells, 6 exhibited **synthetic lethal** effects. The two strongest interactions (*SMARCB1* with *PSMA4* and *ASPSCR1* with *PSMC2*) were successfully validated by protein analysis of human cells and replication with tetrad analysis for yeast orthologues.

Another approach to systematic **synthetic lethality** discovery specific to human cancer (in contrast to the plethora of yeast **synthetic lethality** data) was to build a database as done by [Li et al. \(2014\)](#). In their relational database, called “Syn-lethality”, they have curated both known experimentally discovered **synthetic lethal** pairs in humans (113 pairs) from the literature and those predicted from **synthetic lethality** between orthologous genes in *S. cerevisiae* yeast (1114 pairs). This knowledge-based database is the first dedicated to human cancer **synthetic lethal** interactions and integrates gene function annotation, **pathway** and molecular mechanism data with experimental and predicted **synthetic lethal** gene pairs. This combination of data sources is intended to tackle the trade-off between more conclusive **synthetic lethal** experiments in yeast and more clinically relevant **synthetic lethal** experiments in human cancer models, such as **RNAi**, especially when high-throughput screens are costly and prone to false positives in either system and are difficult to replicate across gene backgrounds. This database centralises a wealth of knowledge scattered in the literature including cancer relevant genes, including the previously mentioned interactions of *BRCA1* and *BRCA2* with *PARP1*, and *TP53* with *WEE1* and *PLK1*, although the computational methodology was not released and was limited to 647 human genes. Their future directions were promising, such as constructing networks of known **synthetic lethality**, applying known **synthetic lethality** to cancer treatment, data mining, replicating the approach for **synthetic lethality** in model organisms, signalling pathways, and developing a complete global network in human cancer or yeast (both of which are still incomplete with experimental data), some of which has been implemented in “SynLethDB” ([Guo et al., 2016](#)).

Machine learning approaches have also been explored for **synthetic lethal** discovery ([Babyak, 2004](#); [Lee and Marcotte, 2009](#)). Due to concerns that these may be subject to overfitting or noise, [Wu et al. \(2014\)](#) developed a meta-analysis method (based on the machine learning methods in Table 1.3). They focused on **synthetic lethal** gene pairs relevant to developing selective drugs against human cancer, building upon their previous database ([Li et al., 2014](#)). Their “metaSL” approach utilises **genomic**, **proteomic** and annotation data and had a high statistical performance in yeast data with an area under receiver operating characteristic (**AUROC**) of 0.871 (as described in

Table 1.3: Machine Learning Methods used by Wu *et al.* (2014)

Method	Source	Tool Offered
Random Forest	Breiman (2001)	
Random Forest		
J48 (decision tree)		
Bayes (Log Regression)		
Bayes (Network)	Hall <i>et al.</i> (2009)	WEKA
PART (Rule-based)		
RBF Network		
Bagging / Bootstrap		
Classification via Regression		
Support Vector Machine (Linear)	Vapnik (1995)	
Support Vector Machine (RBF – Gaussian)	Joachims (1999)	
Multi-Network Multi-Class (MNMC)	Pandey <i>et al.</i> (2010)	
MetaSL (Meta-Analysis)	Wu <i>et al.</i> (2014)	MetaSL

Section 2.3.5.1). They predicted orthologous synthetic lethal partners in human data were not experimentally validated but some were relevant to cancer such as *EGFR* with *PRKCZ*.

Computational approaches scale-up across the genomes at lower cost than experimental screen (Wu *et al.*, 2014). Wu *et al.* (2014) provided their most supported interactions online but the method is not available for analysis of other genes. Syn-Lethality (Li *et al.*, 2014) and MetaSL (Wu *et al.*, 2014) demonstrate the value of computational approaches to synthetic lethality but omit many genes of importance in cancer, such as *CDH1*. Accordingly, there remains a need to enable biological researchers to query further genes and do so in a particular tissue or genetic background.

There is also concern for analyses based on yeast data that many synthetic lethal interactions may not be conserved between species (Dixon *et al.*, 2009), although interactions between pathways may be more comparable. It is unsurprising that many of the interactions identified were not experimentally validated. There have been many gene duplications in the separate evolutionary histories of humans and yeast which may lead to differences in genetic redundancy. Yeast cells are not an ideal human cancer model because they do not have tissue specificity, multicellular gene regulation, or orthologues to several known cancer genes such as p53 (Guaragnella *et al.*, 2014). Although these studies have tried to anticipate these issues with stringent criteria such

as requiring one-to-one orthologues (Deshpande *et al.*, 2013; Heiskanen and Aittokallio, 2012; Kranthi *et al.*, 2013), there remains the possibility that changes in gene function may affect whether these are solely redundant such as if functions had co-evolved without sequence homology. Many genes will also be excluded since they lack homologues in yeast, the corresponding experimental data, or having paralogues in either species. Thus conservation of yeast interactions is not an ideal strategy and analysis of human data directly for comparison with human experimental data will be the focus of this thesis.

### 1.2.7.3 Analysis and Modelling of Protein Data

Kranthi *et al.* (2013) took a network approach to discovery of synthetic lethal candidate selection applying the concept to “centrality” to a human PPI network involving interacting partners of known cancer genes. The effect of removing pairs of genes on connectivity of the network was used as a surrogate for viability which is supported by observations that the PPI and synthetic lethal networks are orthogonal in *S. cerevisiae* studies (Tong *et al.*, 2004). They showed that the human cancer protein interaction network derived protein interactions and cancer gene databases (Futreal *et al.*, 2004; Higgins *et al.*, 2007; Keshava Prasad *et al.*, 2009), consisting of 1539 proteins and 6471 interactions, exhibits the power law distribution expected of a scale-free synthetic lethal network with high connectivity (average vertex degree of 23.67 and network efficiency of 0.2952). Their top 100 candidate interactions included interactions of the tumour suppressor *TP53* with *BRCA1*, *CDKNA1*, *CDKNA2*, *MET*, and *RB1* which have been detected by prior studies. The gene pairs were often observed to be in the same or a plausible compensatory pathway. This demonstrated that network structure is important in the biological functions of cancers and could be exploited for targeting *TP53* loss of function mutations.

However, the approach of Kranthi *et al.* (2013) was limited to known cancer genes and is not applicable to genes that do not have PPI data. Other nucleotide sequencing data types are more commonly available for cancer studies at a genomic scale. Of further concern is that the results were enriched for p53 synthetic lethal partners, which is relevant to many cancers but this genomes-wide approach did not detect many other cancer genes due to the extent of multiple testing. This enrichment may be due to the known drastic effect of removing p53 itself from the network as a highly connected, master regulator, and cancer driving tumour suppressor gene. The focus on cancer genes is useful for translation into therapeutics but does not account for variable genetic backgrounds or effect of protein removal on the cellular network.

Focusing on the potential for synthetic lethality to be an effective anti-cancer drug target, Zhang *et al.* (2015) used modelling of signalling pathways to identify synthetic lethal interactions between known drug targets and cancer genes by simulating gene knockdowns. A computational approach was applied to avoid the limitations of experimental RNAi screens such as scale, instability of knockdown, and off-target effects. This ‘hybrid’ method of a data-driven model and known signalling pathways showed potential to predict cell death in single and combination gene knockouts. They used time series protein phosphorylation data (Lee *et al.*, 2012) for 28 signalling proteins and Gene Ontology (GO) pathways (Ashburner *et al.*, 2000; Blake *et al.*, 2015). This approach successfully detected many known essential genes in the human gene essentiality database, known synthetic lethal partners in the Syn-Lethality database (Li *et al.*, 2014), and predicted novel synthetic lethal gene pairs.

These novel results contained many TP53 and AKT synthetic lethal partners (Zhang *et al.*, 2015), genes known to be important in many cancers. However, these genes also have a severe impact on the signalling pathways in an essentiality analysis of single gene disruptions and large phenotypic changes in cancer (Zhang *et al.*, 2015). This approach is amenable to detect functionally related pathways and protein complexes across the molecular function, cellular component, and biological process annotations provided by Gene Ontology. The results were consistent with the experimental results in the literature but the novel synthetic lethal interactions have yet to be validated. While the mathematical reasoning and algorithms are given, the code was not released to replicate the findings or apply the methodology beyond the signalling pathways analysed by (Zhang *et al.*, 2015). While this is an interesting approach, the analysis of this thesis will focus on gene expression and RNAi data, the widespread availability which allows testing of a broader range of candidate gene pairs.

#### 1.2.7.4 Differential Gene Expression

Differential gene expression has been explored to predict synthetic lethal pairs in cancer which would be widely applicable due to the availability of public gene expression data for many samples and cancer types. Wang and Simon (2013) found differentially expressed genes (by the t-test, adjusted by False discovery rate (FDR)) between tumours with or without functional p53 mutations in TCGA (McLendon *et al.*, 2008) and Cancer Cell Line Encyclopaedia (CCLE) (Barretina *et al.*, 2012) RNA-Seq gene expression data as candidate synthetic lethal partner pathways of p53. They identified 2, 8, and 21 candidate synthetic lethal partner genes in 3 microarray datasets from the NCI60 cell lines, 31 partner genes from the CCLE RNA-Seq data (Barretina *et al.*, 2012), and

50 in TCGA RNA-Seq data (Muzny *et al.*, 2012). *PLK1* was replicated across 4 of these analyses and 17 other genes were replicated across 2 analyses (including *MTOR*, *PLK4*, *MAST2*, *MAP3K4*, *AURKA*, *BUB1* and 6 CDK genes) with many playing a role in cell cycle regulation. This was supported by a drug sensitivity experiment on the NCI60 cell lines which found that cells lacking functional p53 were more sensitive to paclitaxel (which targets *PLK1*, *AURKA*, and *BUB1*). This demonstrated the potential of gene expression as a surrogate for gene function, and the use of public genomic data to predict synthetic lethal gene pairs in cancer. Wang and Simon (2013) advocated for pre-screening of expression profiles to augment future RNAi screens, however, their analyses were limited to kinase genes and focused on currently druggable targets, lacking wider application of synthetic lethal prediction methodology. This approach may not be feasible or applicable in cancer genes with a lower mutation rate than p53.

Tiong *et al.* (2014) also investigated gene expression as a predictor of synthetic lethal pairs with colorectal cancer microarrays from a Han Chinese population with a sample size of 70 tumours and 12 normal tissue samples. Simultaneously differential expressed “tumour dependent” gene pairs (which includes co-expression) between cancer and normal tissue were used to rank 663 candidate synthetic lethal interactions identified in cell line siRNA experiments. Of the top 20 gene pairs, 17 were tested for differential expression at the protein level with immunohistochemistry staining and correlation with clinical characteristics, with 11 pairs exhibiting synergistic effects. Some of the predicted synthetic lethal pairs were consistent with the literature (including *TP53* with *S6K1* and partners of *KRAS*, *PTEN*, *BRCA1*, and *BRCA2*) and two novel synthetic lethal interactions (*TP53* with *CSNK1E* and *CTNNB1*) were validated in pre-clinical models. This serves as a valuable proof-of-concept for integration of *in silico* approaches to synthetic lethal discovery in cancer, demonstrating its utility to triage and identify synthetic lethal partners of p53 applicable to colorectal tissues. Although the experimental work was the focus of the paper, these findings show that bioinformatics synthetic lethal candidates can be validated in patient tissue samples to find those applicable to colorectal cancers (including in a non-Caucasian population).

#### 1.2.7.5 Data Mining and Machine Learning

Recognising the utility of synthetic lethality to drug inhibition and specificity of anti-cancer treatments, Jerby-Arnon *et al.* (2014) also saw the need for effective prediction of gene essentiality and synthetic lethality to augment experimental studies of SL. They developed the “DAta mIning SYnthetic lethal identification pipeline” (DAISY), a data-driven approach for genomes-wide analysis of synthetic lethality in public cancer

genomics data from TCGA and CCLE (Barretina *et al.*, 2012). DAISY is intended to predict the candidate synthetic lethal partners of a query gene such as genes recurrently mutated in cancer.

Jerby-Arnon *et al.* (2014) combined a computational approach to triage candidates with a conventional RNAi screen to validate synthetic lethal partners. They screened a selection of computationally predicted candidates and randomly selected genes with RNAi against *VHL* loss of function mutation in RCC4 renal cell lines. The computational method had a high AUROC of 0.779 and predictions were enriched 4-fold for validated RNAi hits over randomly selected genes. This approach detected known synthetic lethal pairs such as *BRCA1* or *BRCA2* genes with *PARP1*, and *MSH2* with *DHFR*. The synthetic lethal candidates identified with both RNAi screening and computational prediction formed an extensive network of 2077 genes with 2816 synthetic lethal interactions, and a similar network of 3158 genes with 3635 synthetic dosage lethal interactions (for synthetic lethality with over-expression). Each network was scale-free, as expected of a biological network, and was enriched for known cancer genes and for essential genes in mice which could be harnessed for predicting prognosis and drug response.

The DAISY methodology (Jerby-Arnon *et al.*, 2014) compares the results of analysis of several data types to predict synthetic lethality, namely: DNA copy number and somatic mutation for TCGA patient samples and CCLE cell lines. The cell lines were also analysed with gene expression and gene essentiality (shRNA screening) profiles. Genes were classed as inactivated by copy number deletion, somatic loss of function mutation, or low expression and tested for synthetic lethal gene partners which are either essential in screens or not deleted with copy number variants. Co-expression is also used for synthetic lethality prediction based on studies in yeast (Costanzo *et al.*, 2010; Kelley and Ideker, 2005). Copy number, gene expression, and essentiality analyses were stringently compared by adjusting each for multiple tests with Bonferroni correction and only taking candidates identified in all analyses. The predictions performed well and an RNAi screen, for the example of *VHL* in renal cancer, validated predicted synthetic lethal partners of *VHL* demonstrating the feasibility of combining approaches to synthetic lethal discovery in cancer and using computational predictions to enable more efficient high-throughput screening. While DAISY performed well statistically, co-expression and shRNA functional examination contributed less to this than the mutation and copy number analysis (AUROC 0.683 alone). However, this methodology was very stringent, missing potentially valuable synthetic lethal candi-

dates. Additionally, the software for the procedure has not been publicly released for replication.

Although the DAISY procedure performed well and has been well received by the scientific community (Crunkhorn, 2014; Lokody, 2014; Ryan *et al.*, 2014), showing a need for such methodology, there has not yet been widespread adoption of this approach. Co-expression analysis may exclude some synthetic lethal interactions, where inverse correlation could occur (Lu *et al.*, 2015). In the interests of a large sample size, tissue types were not tested separately despite tissue-specific synthetic lethality being likely since gene function (and by extension expression, isoforms, and clinical characteristics) in cancers may often be tissue-dependent. Some data forms and analyses used, such as gene essentiality, may not be available for all cancers, genes, or tissues, and may not be reproduced.

Lu *et al.* (2015) propose an alternative computational prediction of synthetic lethality based on machine learning methods and a “cancer genome evolution” hypothesis. Using DNA copy number and gene expression data from TCGA patient samples, a cancer genomes evolution model assumes that synthetic lethal gene pairs behave in two distinct ways in response to an inactive synthetic lethal partner gene, either a “compensation” pattern where the other synthetic lethal partner is overactive or a “co-loss underrepresentation” pattern where the other synthetic lethal partner is less likely to be lost, since loss of both genes would cause death of the cancer cell. During the genomes evolution of cancers, the cell becomes addicted to the remaining synthetic lethal partner due to induced gene essentiality. These patterns would explain why DAISY detects only a small number of synthetic lethal pairs, compared to the large number expected based on model organism studies (Boone *et al.*, 2007), and the disparity between screening and computationally predicted synthetic lethal candidates due to testing different classes of synthetic lethal gene pairs.

Lu *et al.* (2015) compared a genomes-wide computational model of genomes evolution and gene expression patterns to the experimental data (Laufer *et al.*, 2013; Vizeacoumar *et al.*, 2013). This more simple model performed well, with an AUROC of 0.751 (lower than DAISY), and did not rely on data from cell lines which may not represent patient disease. Lu *et al.* (2015) predicted 591,000 human synthetic lethal partners with a probability score threshold of 0.81, giving a precision of 67% and 14-fold enrichment of synthetic lethal true positives compared to randomly selected gene pairs. Discovery of such a vast number of cancer-relevant synthetic lethal interactions in humans would not be feasible experimentally and is a valuable resource for research

and clinical applications. These predictions are not limited by assuming co-expression of synthetic lethal partners or evolutionary conservation with model organisms enabling wider synthetic lethal discovery. However, there remains a lack of basis for an expectation of how many synthetic lethal partners a particular gene will have, how many pairs there are in the human genomes, and whether pathways or correlation structure would influence predicted synthetic lethal partners.

Large scale, computational approaches have yet to determine whether synthetic lethal interactions are tissue-specific, since Lu *et al.* (2015) used pan cancer data for 14136 patients with 31 cancer types. Experimental data used for comparison was a small training dataset specific to colorectal cancer, and based on screens for other phenotypes, which may limit performance of the model or application to other cancers. Proposed expansion of the computational approach to mutation, microRNA, or epigenetic modulation of gene function and tumour micro-environment or heterogeneity suggests that synthetic lethal discovery could be widely applied to the current challenges in cancer genomics. This approach was also based on machine learning methodology and was not supported by a software release for the community to develop, contribute to, or reproduce beyond the gene pairs given in the supplementary results.

#### 1.2.7.6 Mutually Exclusive Bimodality

Wappett *et al.* (2016) demonstrated a multi-omic approach to identification of synthetic lethality in cancer with a strategy to detect bimodal patterns in molecular profiles. They released this solution as the BiSEp R package (Wappett, 2014) which aims to detect subtle bimodal and non-normal patterns in expression data. Since loss of gene function is not consistently genetic. Wappett *et al.* (2016) advocate the use of gene expression (loss of mRNA) and deletion (loss of copy number) data in addition to mutation. The BiSEp procedure was demonstrated on an analysis of 881 cell lines from CCLE (Barretina *et al.*, 2012), 442 cell lines from COSMIC (Forbes *et al.*, 2015), and RNA-Seq by Expectation Maximization (RSEM) normalised RNA-Seq data for 178 TCGA lung patient samples (Collisson *et al.*, 2014). BiSEp was demonstrated to have significant enrichment of validated tumour suppressor, synthetic lethal gene pairs (detecting 76 experimentally supported gene pairs) and was improved (detecting 420) with expression data rather than relying on detecting loss of gene function by mutation or deletion. Wappett *et al.* (2016) identified interactions with genes relevant to cancer with support in experimental screens including ERCC4 with XRCC1, BRCA1 with PARP3, and SMARCA1 with SMARCA4.

Wappett *et al.* (2016) demonstrated that analysis of genomics data, particularly ex-

pression data, is relevant to augment the identification of synthetic lethal interactions with screening experiments. They further showed that this is applicable in both genetically homogeneous cell lines and heterogeneous cell population from patient samples. This approach is limited however, to genes that exhibit bimodal expression patterns which do not commonly occur, particularly in normalised gene expression data, and other approaches may need to be considered for gene such as *CDH1* which were not identified by BiSEp.

#### 1.2.7.7 Rationale for Further Development

Many of the approaches discussed here aimed to identify the strongest synthetic lethal pairs across the yeast or human genomes (Deshpande *et al.*, 2013; Lu *et al.*, 2015; Wappett *et al.*, 2016; Wu *et al.*, 2014), which may not be an ideal strategy to identify interactions in particular functions or relevance to particular cancers. These demonstrate a need for computational approaches to prioritise candidate gene pairs for validation but this thesis will focus on the interactions with *CDH1* with importance in breast and stomach cancers, although these partners may be applicable in other cancers. As such, this thesis presents a query-based method, amenable to identification of candidate partners for a selected gene of functional or translational importance such as *CDH1*.

### 1.3 E-cadherin as a Synthetic Lethal Target

E-cadherin is a transmembrane protein (encoded by *CDH1*) with several characterised functions in the cytoskeleton and cell-to-cell signalling. Here we outline the characterised functions of E-cadherin and its importance in cancer biology. *CDH1* is a tumour suppressor gene, with loss of function occurring in both familial (germline mutation mutations) and sporadic (somatic mutations) cancers. As such, *CDH1* inactivation is a prime example of a genetic event that could be targeted by synthetic lethality for anti-cancer treatments. Most notably this includes patients at risk of developing hereditary breast and stomach cancers for which conventional surgical or cytotoxic chemotherapy is not ideal and who have a known genetic aberration in their familial syndromic cancers. Effective treatments against *CDH1* inactivation would also benefit patients with sporadic diffuse gastric cancers since they often present with symptoms at a late stage.

### **1.3.1 The *CDH1* gene and its Biological Functions**

The [tumour suppressor](#) gene *CDH1* is implicated in [hereditary](#) and [sporadic](#) lobular breast cancers (Berx *et al.*, 1996; Berx and van Roy, 2009; De Leeuw *et al.*, 1997; Masciari *et al.*, 2007; Semb and Christofori, 1998; Vos *et al.*, 1997). The *CDH1* gene encodes the [E-cadherin](#) protein and is normally expressed in epithelial tissues, where it has also been identified as an invasion suppressor and loss of *CDH1* function has been implicated in breast cancer progression and metastasis (Becker *et al.*, 1994; Berx *et al.*, 1995; Christofori and Semb, 1999).

#### **1.3.1.1 Cytoskeleton**

The primary function of *CDH1* is cell-cell adhesion forming the adherens junction, maintaining the cytoskeleton and mediating molecular signals between cells. The function of the adherens complex is particularly important for cell structure and regulation because it interacts with cytoskeletal actins and microtubules. The cytoskeletal role of [E-cadherin](#) maintains healthy cellular viability and growth in epithelial tissues including cellular polarity (Jeanes *et al.*, 2008). [E-cadherin](#) is not [essential](#) to cellular viability but loss in epithelial cells does lead to defects in cytoskeletal structure and proliferation. In addition to a central role in the adherens complex, [E-cadherin](#) is involved in many other cellular functions and thus *CDH1* is regarded as a highly [pleiotropic](#) gene (Kroepil *et al.*, 2012).

#### **1.3.1.2 Extracellular and Tumour Micro-environment**

As a transmembrane signalling protein [E-cadherin](#) also interacts with the extracellular environment and other cells, most notably forming tight junctions between cells (Chen *et al.*, 2014; Tunggal *et al.*, 2005). These junctions serve to both regulate movement of ion signals between cells and separate membrane proteins on the apical and basal surfaces of a cell, maintaining cell polarity. Thus [E-cadherin](#) is an important regulator of epithelial tissues by intercellular communication (Jeanes *et al.*, 2008). It also has important roles in the extracellular matrix, including fibrin clot formation. The role of intercellular interactions and the tissue micro-environment are important themes in cancer research, being a potential mechanism for cancer progression and malignancy in addition to its potential for specifically targeting tumour cells.

### 1.3.1.3 Cell-Cell Adhesion and Signalling

The signals mediated by tight junctions are also passed on to intracellular signalling pathways and thus E-cadherin also has a role in maintaining cellular function and growth. One such example is the regulation of  $\beta$ -catenin which interacts with both the actin cytoskeleton and acts as a transcription factor via the Wingless-related integration site (WNT) pathway (Jeanes *et al.*, 2008). Similarly, the Hippo and phosphoinositide 3-kinase (PI3K)/AKT pathways are implicated in being mediated by E-cadherin (De Santis *et al.*, 2009; Kim *et al.*, 2011), having roles in promoting cell survival, proliferation, and repressing apoptosis. E-cadherin shares several downstream pathways with signalling pathways such as integrins and thus indirectly interacts with them, particularly since feedback loops may occur in such pathways. Conversely, the multifaceted roles of E-cadherin have been shown with over-expression in ovarian cells promoting tumour growth, while it maintains healthy cellular functions in other cells (Brouxhon *et al.*, 2014; Dong *et al.*, 2012).

### 1.3.2 *CDH1* as a Tumour (and Invasion) Suppressor

E-cadherin has key roles in maintaining cellular structure and regulating growth, consistent with *CDH1* being a tumour suppressor gene. Loss of *CDH1* in epithelial tissues leads to disrupted cell polarity, differentiation, and migration (Chen *et al.*, 2014). E-cadherin loss has been identified as a recurrent driver tumour suppressor mutation in sporadic cancers of many tissues including breast, stomach, lung, colon, and pancreas tissue (TCGA, 2017).

#### 1.3.2.1 Breast Cancers and Invasion

E-cadherin loss in breast cancers has been shown to cause increased proliferation, lymph node invasion, and metastasis with poor cell-cell contact Berx and van Roy (2009). Thus the *CDH1* gene has also been implicated as an invasion suppressor, with a key role in the epithelial-mesenchymal transition (EMT), an established mechanism of cancer progression (Hanahan and Weinberg, 2011). The epithelial-mesenchymal transition is important during development and wound healing but such changes in cellular differentiation also occur in cancers. If *CDH1* is inactivated by mutation or DNA methylation (Berx *et al.*, 1996; Guilford, 1999; Machado *et al.*, 2001), it is likely that EMT will drive growth of E-cadherin deficient cancers (Berx and van Roy, 2009; Graziano *et al.*, 2003; Polyak and Weinberg, 2009). While loss of E-cadherin is not sufficient to cause EMT or tumourigenesis, it is an important step in this mechanism of

tumour progression and a potential therapeutic intervention may therefore also impede cancer progression and have activity against advanced stage cancers.

### 1.3.3 Hereditary Diffuse Gastric (and Lobular Breast) Cancer

*CDH1* loss of function mutations also causes familial cancers, including diffuse gastric cancer and lobular breast cancer (Graziano *et al.*, 2003; Guilford *et al.*, 2010, 1999; Oliveira *et al.*, 2009). Individuals carrying a null mutation in *CDH1* have a syndromic predisposition to early-onset of these cancers, including hereditary diffuse gastric cancer (HDGC) (Guilford *et al.*, 1998). Due to carrying a dysfunctional allele, these individuals are prone to carcinogenic lesions in the breast or stomach if the remaining functional allele is inactivated, occurring more frequently and at an earlier age than in individuals with two functional *CDH1* allele. The loss of the second allele is most often through hypermethylation suppressing expression rather than mutation (Grady *et al.*, 2000; Graziano *et al.*, 2003; Machado *et al.*, 2001; Oliveira *et al.*, 2009), although loss of heterozygosity may also occur (Guilford *et al.*, 2010). Therefore HDGC is an autosomal dominant cancer syndrome with incomplete penetrance. The “lifetime” (until age 80 years) risk for mutation carriers of diffuse gastric cancer is 70% in males and 56% in females (Hansford *et al.*, 2015; van der Post *et al.*, 2015). In addition, the lifetime risk of lobular breast cancer is 42% in female mutation carriers (Hansford *et al.*, 2015).

HDGC affects less than one in a million people globally (Ferlay *et al.*, 2015) and represents less than 1% of gastric cancers. However, HDGC is a serious health issue for several hundred families globally. E-cadherin mutations in the germline mutation are implicated in 1-3% of gastric cancers presenting with a family history, varying between high and low incidence populations. E-cadherin is also mutated in 13% of sporadic gastric cancers.

While diagnostic testing for *CDH1* genotype has enabled more effective management of HDGC and improved patient outcomes, there are still limited options for clinical interventions (Guilford *et al.*, 2010). Individuals with a family history of HDGC are recommended to be tested for *CDH1* mutations in late adolescence and are offered prophylactic stomach surgery before the risk of developing cancers increases with age. Another option is annual endoscopic screening to diagnose early stage stomach cancers with surgical intervention once they are detected (Oliveira *et al.*, 2013). However, these early stage cancers are difficult to detect and may be missed in regular screening. Thus patients carrying *CDH1* mutations either have surgical interventions with a significant

impact on quality of life and risk of complications or remain at risk of developing advanced stage stomach cancers. Due to the lower mortality rate from stomach cancers, there are increasing concerns among these **HDGC** families about the elevated risk of lobular breast cancers for women later in life.

The current clinical management of **HDGC** still has significant risks for patients and therefore a greater understanding of the molecular and cellular function of *CDH1* is important for its role in these cancers. Such studies may lead to alternative treatment strategies such as pharmacological **treatments** with specificity against *CDH1* null cells, once they lose the second **allele**. While a loss of gene function is difficult to target directly, designing a treatment with specificity against *CDH1* may also have activity in **sporadic** cancers in a range of epithelial cancers. Thus an effective treatment against *CDH1* **mutant** cancers would potentially have significant therapeutic and preventative applications in a large number of patients.

### 1.3.4 Cell Line Models of *CDH1* Null Mutations

Previous work published by members of our research group used a model of homozygous *CDH1*<sup>-/-</sup> null **mutation** in non-malignant MCF10A breast cells to show that loss of *CDH1* alone was not sufficient to induce **EMT** with compensatory changes in the **expression** of other cell adhesion genes (Chen *et al.*, 2014). However, *CDH1* deficient cells did manifest changes in morphology, migration, and weaker cell adhesion (Chen *et al.*, 2014).

This *CDH1*<sup>-/-</sup> MCF10A model has been used in a **genomes-wide** screen of 18,120 genes using **siRNA** and a complementary drug screen using 4057 compounds to identify **synthetic lethal** partners to **E-cadherin** (Telford *et al.*, 2015). One of the strongest candidate pathways identified by Telford *et al.* (2015) were the **G protein coupled receptor (GPCR)** signalling cascades, which were highly enriched by **Gene Ontology (GO)** analysis of the candidate **synthetic lethal** partners the primary **siRNA** screen. This was supported by validation with Pertussis toxin, known to target G<sub>αi</sub> signalling (Clark, 2004), as were various candidate cytoskeletal pathways by inhibition of **Janus kinase (JAK)** and aurora kinase. The drug screen also produced candidates in **histone deacetylase (HDAC)** and **PI3K** which were supported by validation and time course experiments.

## 1.4 Summary and Research Direction of Thesis

Genomic technologies and the data available from them have immense potential for understanding of genetics and improving healthcare, including identification of genes altered in cancer for molecular diagnosis, prognostic biomarkers, and therapeutic targets. This has been demonstrated with the identification of driver genes in many cancers, distinguishing tumour subtypes by expression profiles, and the development of targeted therapies against oncogenes (such as *BRAF*) and tumour suppressors (such as *BRCA1*). Synthetic lethality is an important genetic interaction to study fundamental cellular functions and exploit them for biomarker identification and cancer treatment. They present a means to target loss of function mutations and genetic dysregulation in tumour suppressor genes by identifying interacting partners with redundant or compensating molecular functions.

*CDH1* (encoding E-cadherin) is an example of a tumour suppressor gene implicated in sporadic breast and stomach cancers. Germline mutations in *CDH1* are also found in many patients with familial early onset cancers (HDGC). Discovery of synthetic lethal partners would contribute to an understanding of the molecular mechanisms driving the growth of *CDH1* deficient tumours and identification of potential therapeutic targets or chemopreventative agents for management of HDGC. The clinical potential of the synthetic lethal approach has been demonstrated with the application of olaparib against *BRCA1* and *BRCA2* mutations (Lord *et al.*, 2015) but there remains the need to systematically identify synthetic lethal partner genes for other tumour suppressors such as *CDH1*. A synthetic lethal screen has been conducted on breast cell lines (Telford *et al.*, 2015) but these candidate synthetic lethal partners of *CDH1* may be supported by the application of computational approaches.

While there are a wide range of experimental and computational approaches to synthetic lethal discovery, many are limited to particular applications, prone to false positives, inconsistent across independent approaches, or enriched for particular genes of interest. Therefore synthetic lethal interactions are difficult to replicate or apply in the clinic. Computational approaches to synthetic lethality are not widely adopted by the cancer research community and experimental approaches cannot be combined to study synthetic lethality at a genomes-wide scale. However, these show interest in synthetic lethal discovery in the community and the need for robust predictions of synthetic lethal interactions in cancer and human tissues.

Effective screening, prediction, and analysis of synthetic lethal interactions are a

crucial part of developing next generation anti-cancer strategies. Therefore, we propose developing a computational statistical procedure to identify *synthetic lethal* interactions and construct gene networks. This will enable the development of personalised medicine targeted to particular molecular aberrations. Genetic tests and *genomic* have the potential to revolutionise cancer screening, diagnosis, and prognostics; *targeted therapeutic*, similarly, have applications in prevention and therapy of *sporadic* or *hereditary* cancers with known molecular properties.

To address the concerns raised by recent computational approaches to *synthetic lethal* discovery in cancer (*Jerby-Arnon et al.*, 2014; *Lu et al.*, 2015; *Wappett et al.*, 2016), I present similar analysis using solely *gene expression* data which is widely available for a large number of samples in many different cancers. This uses a statistical methodology the *SLIPT* developed for this purpose. To further determine the limitations and implications of *synthetic lethal* predictions, modelling and simulation was performed upon the statistical behaviour of *synthetic lethal* gene pairs in *genomics* data. Comparison of *synthetic lethal* gene candidates from public data analysis and experimental candidates, pathway analysis, and networks structure will also be presented to investigate the relationships between *synthetic lethal* candidates. Release of the R code used for simulation, prediction, and analysis will enable adoption of the methodology in the cancer research community and comparison to existing methods. Therefore this thesis aims to develop predictions for *synthetic lethal* partner genes with a focus on the example of *E-cadherin* to compare to the findings of *Telford et al.* (2015), develop of network approaches for *pathway* structure, and simulate *gene expression* on *pathway* structure with the *bioinformatics* and *computational biology* investigations.

#### 1.4.1 Thesis Aims

Understanding *synthetic lethality* is important in cancers, having shown an impact clinical practice and patient outcomes for certain genes already. Thus this thesis aims to identify *synthetic lethal* gene pairs using public *gene expression* data. Accordingly, Chapter 3 describes the methods developed to do so, including a *synthetic lethal* detection methodology (*SLIPT*) and the release of R software packages. This chapter also serves to document the original simulation and network analysis procedures developed to support the use of *SLIPT* and perform analyses throughout this thesis.

This thesis also aims to demonstrate *SLIPT* methodology for analysis of *RNA-Seq* *gene expression* data. Chapter 4 does so by performing an analysis to identify candidate synthetic lethal gene partners of *CDH1* in public breast and stomach cancer data (Bass

(*et al.*, 2014; Koboldt *et al.*, 2012). Chapter 4 demonstrates the biological relevance of these candidate synthetic lethal partners by identifying synthetic lethal pathways and comparing them with the results of an experimental siRNA screen (Telford *et al.*, 2015).

Pathway analysis was extended to include graph structures in Chapter 5, which aimed to assess the importance of synthetic lethal genes within pathway structures. Chapter 5 also uses pathway structure to identify directional relationships between SLIPT and siRNA synthetic lethal candidates and explore the disparity between them. The SLIPT methodology is supported by simulation-based investigations in Chapters 3 and 6, which evaluate the ability of SLIPT to detect known synthetic lethal genes in simulated data. Graph structures were also used in Chapter 6 to determine the effect of pathway structures of synthetic lethal detection with SLIPT in simulated data and ascertain that the simulation results were comparable to expression data containing complex correlation structures within biological pathways.

# Chapter 2

## Methods and Resources

In this Chapter, I will outline the various existing resources and methods that were used throughout this project. This includes public data repositories, stable and development releases of software packages (primarily using the R programming environment), and custom implementation of [bioinformatic](#) methods and statistical concepts with Shell or R scripts developed for this purpose. The methods and packages that have been developed specifically for this project will be covered in Chapter 3 with supporting data and demonstration of their use .

### 2.1 Bioinformatics Resources for Genomics Research

#### 2.1.1 Public Data and Software Packages

Various [bioinformatics](#) resources, such as databases and methods, have become integral parts of genetics and [genomics](#) research. Reference [genomes](#), genotyped variants, [gene expression](#), and epigenetics profiles are among the most commonly used resources. [Gene expression](#) data, in particular, is widely available from [microarray](#) and [RNA-Seq](#) projects, driven by data sharing, data mining, and the wider initiatives for publicly available data for enabling the scientific community to further utilise the data generated beyond a single research group or consortium ([Rung and Brazma, 2013](#)) These datasets are a valuable resource to examine the changes in [gene expression](#) occurring in cancers and the variation between samples. The potential for integrating findings from publicly available [genomic](#) data with experimental investigations has expanded with [RNA-Seq](#) datasets, including large-scale cancer [genomics](#) projects ([Zhang \*et al.\*, 2011](#)). This thesis presents such an investigation, enabled by the release of these datasets and tools developed to handle them.

It is now common practice for **bioinformatics** researchers to release open-source code or provide software packages to enable replication of the findings or further applications of the methods (Stajich and Lapp, 2006). This is part of a wider movement in software and data analysis, including the development of Linux and the R programming environment (R Core Team, 2016). In addition to the R packages hosted on **comprehensive R archive network** (CRAN) (CRAN, 2017), many packages specifically developed for applications in **bioinformatics** are hosted on the Bioconductor repositories (Gentleman *et al.*, 2004), and numerous packages in various stages of development are hosted on GitHub (<https://github.com/>). Packages from each of these resources have been used throughout this project and are cited wherever possible. Several R packages have been developed during this thesis project and publicly released on GitHub or will be released in conjunction with a publication.

### 2.1.1.1 Cancer Genome Atlas Data

Molecular profile data for normal and tumour samples were downloaded from publicly available sources, using the **TCGA** (TCGA, 2017) and the **International Cancer Genome Consortium** (ICGC) web portals (Zhang *et al.*, 2011). These include **gene expression** (RNA-Seq), **somatic mutations**, and clinical data. The versions were downloaded on the 6<sup>th</sup> of August 2015 (Release 19) and the 2<sup>nd</sup> of May 2016 (Release 20) for breast and stomach cancer respectively via the ICGC data portal (<https://dcc.icgc.org/>).

The **TCGA** project (Koboldt *et al.*, 2012) used widely adopted tools: “Bowtie” for alignment (Langmead *et al.*, 2009), “mapsplice” to detect splice sites (Wang *et al.*, 2010), and the **RSEM** approach to quantify reads as a measure of **gene expression** (Li *et al.*, 2010). These are widely acceptable tools for processing RNA-Seq data which were used to produce the raw counts of mapped reads (tier 1) and normalised **expression** data (tier 3) publicly downloaded from **ICGC** and **TCGA** respectively. Protein **expression** data generated from **reverse phase protein arrays** (RPPA) was normalised by **TCGA** to dilution curves using the **SuperCurve** R package (Ju *et al.*, 2015; Neeley *et al.*, 2009).

Raw count and **RSEM** normalised **TCGA** expression data from Illumina **RNA-Seq** protocols were downloaded for 1177 breast samples (113 normal, 1057 primary tumour, and 7 metastases) for 20,501 genes. **TCGA** breast **somatic mutation** data for 981 samples (976 primary tumours and 5 metastases) across 25,836 genes were downloaded. These included 969 samples (964 primary tumours and 5 metastases) with corresponding **RNA-Seq** expression data and 19,166 genes mapped from Ensembl identifiers to gene symbols. Of these genes, 16,156 had corresponding **gene expression**

information. Unless otherwise stated, the raw counts were used for further processing rather than the RSEM normalised data (provided by TCGA tier 3). Somatic mutations was reported if there were non-synonymous substitutions, frameshifts, or truncations (by premature stop codons) detected which would likely disrupt the wild-type gene function. Normalised protein expression data were downloaded (as provided by TCGA tier 3), generated from RPPA for 142 antibodies targeting 115 genes for 298 TCGA breast samples.

Raw count TCGA expression data (TCGA tier 1) from Illumina RNA-Seq was downloaded for 450 stomach samples (35 normal, 415 primary tumour) for 20,501 genes. TCGA stomach mutation data was also used for 289 samples across 25807 genes, corresponding to 19436 genes with expression data.

### 2.1.1.2 Reactome and Annotation Data

Pathway analysis was performed for human pathway annotation from the Reactome database (version 52) with pathway gene sets derived from the reactome.db R package. Entrez identifiers were mapped to gene symbols or aliases to match to TCGA expression and mutation data using the org.Hs.eg.db R package. Gene expression for breast cancer from Gatza and colleagues were also used (Gatza *et al.*, 2011; Gatza *et al.*, 2014). The gene symbols for each pathway were matched to the expression data and to construct a matrix of category membership using the safe R package (Barry, 2016).

## 2.2 Data Handling

### 2.2.1 Normalisation

Apart from the Prediction Analysis of Microarray 50 (PAM50) subtyping procedure (Parker *et al.*, 2009), which required RSEM normalised data (J.S. Parker personal communication), the analysis of the RNA-Seq data presented here was based on raw read count data. After some samples were removed for consistency (based on a Euclidean distance correlation matrix as described in Section 2.2.2), raw read counts were log-scaled and the final dataset was normalised as Counts per Million mapped reads (CPM), weighted by variance modelling, using the voom function (Law *et al.*, 2014) in the limma R package (Ritchie *et al.*, 2015). This procedure adjusts the data to account for differences in read count by sequencing depth between samples and length between genes.

## 2.2.2 Sample Triage

The [TCGA](#) breast [RNA-Seq](#) data were assessed for batch effects using a correlation matrix of the log-transformed raw counts for which a heatmap (Euclidean distance, complete linkage) is shown in Figure [A.2](#). While no major batch effects were detectable between the samples, 9 samples were excluded due to poor correlation with the remaining samples, as detailed in Table [2.1](#). These samples showed unusual density plots compared to the rest of the dataset, and exhibited low mean read count in Figures [2.1](#) and [2.2](#). A heatmap showing key clinical properties of these excluded samples and their correlation with the remainder of the samples is shown in Figure [A.1](#), and a full correlation heatmap (Figure [A.2](#)) shows these samples as relatively poorly correlated outliers in the bottom rows and left columns. In addition to the clustering analysis (in Appendix [A.1](#)), replicate tumour samples were also examined for sample quality in Appendix [A.2](#). After removal of these samples, the [TCGA](#) dataset used for analysis consisted of the remaining 1168 samples (from 1040 patients): 1049 tumour samples, 112 normal tissue for matched samples, and 7 metastases.

Table 2.1: Excluded samples by batch and clinical characteristics.

Tissue Source	Type	Batch	Plate	Patient	Samples	p53	Subtype	Treatment (History)	Clinical Subtypes (Stage)		
A7 Christiana	Tumour	47	A227	A0DB	1 of 3	NA	Luminal A	Mastectomy	(no)	Estrogen receptor (ER) <sup>+</sup>	Ductal (2)
A7 Christiana	Tumour	96	A220	A13D	1 of 3	Wildtype	Luminal A	Mastectomy	(no)	ER <sup>+</sup>	Ductal (2)
A7 Christiana	Tumour	96	A227	A13E	1 of 3	NA	Basal	Lumpectomy	(no)	ER <sup>-</sup>	Ductal (2)
A7 Christiana	Tumour	142	A277	A26E	1 of 3	NA	Basal	Lumpectomy	(no)	ER <sup>+</sup>	Ductal (2)
A7 Christiana	Tumour	47	A277	A0DC	1 of 2	NA	Luminal A	Mastectomy	(yes)	ER <sup>+</sup>	Lobular (3)
A7 Christiana	Tumour	142	A220	A26I	1 of 2	Mutant	Basal	Lumpectomy	(yes)	ER <sup>-</sup>	Ductal (2)
AC Intl Genomics	Tumour	177	A18M	A2QH	2 of 2	Mutant	Basal	Radical Mastectomy	(no)	ER <sup>-</sup>	Metaplastic (2)
AC Intl Genomics	Tumour	177	A220	A2QH	2 of 2	Mutant	Basal	Radical Mastectomy	(no)	ER <sup>-</sup>	Metaplastic (2)
GI ABS IUPUI	Normal	177	A16F	A2C8	1 of 1	NA	Luminal A	Radical Mastectomy and Neoadjuvant	(no)	ER <sup>+</sup>	Ductal (2)

Similarly, a correlation matrix of log-transformed raw counts was used to evaluate sample quality for [TCGA](#) stomach [RNA-Seq](#). A tumour sample (patient 4294) was removed due to similar quality concerns leaving a final dataset for 449 samples (from 417 patients): 414 tumour samples and 35 normal tissue samples.

## 2.2.3 Metagenes and the Singular Value Decomposition

A “metagene” offers a one-dimensional summary of [pathway](#) (expression) activation or inactivation by dimension reduction of a matrix, avoiding negatively correlated genes averaging out the signal of a mean-based centroid ([Huang et al., 2003](#)). Constructing [pathway metagenes](#) used gene sets for Reactome and the Gatza signatures ([Gatza et al., 2011, 2014](#)) as specified above (see Section [2.1.1.2](#)). The singular-value decomposition was performed ( $X = U^T DV$ , where  $X$  is the data matrix of the gene set, with genes  $\times$  samples) and the leading eigenvector (first column of  $V$ ) corresponding to the largest

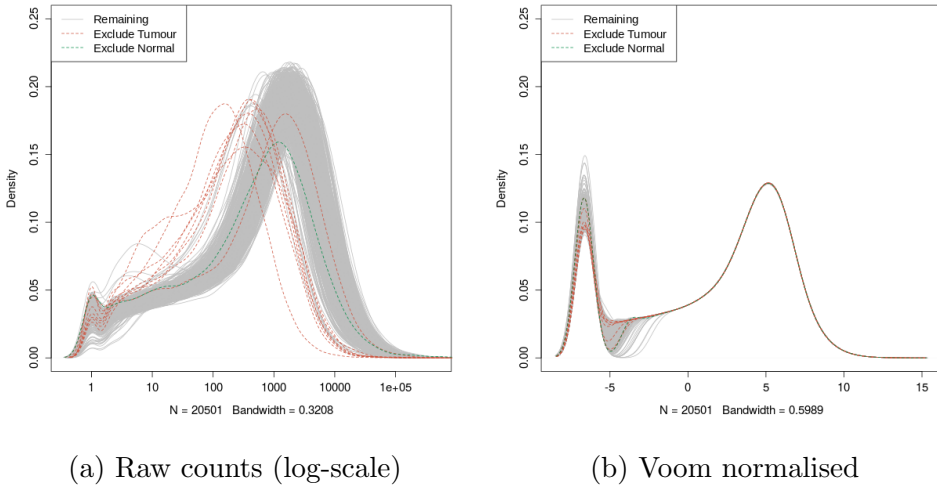


Figure 2.1: **Read count density.** Sample density plots of raw counts on log-scale and voom normalised showing samples removed due to quality concerns.

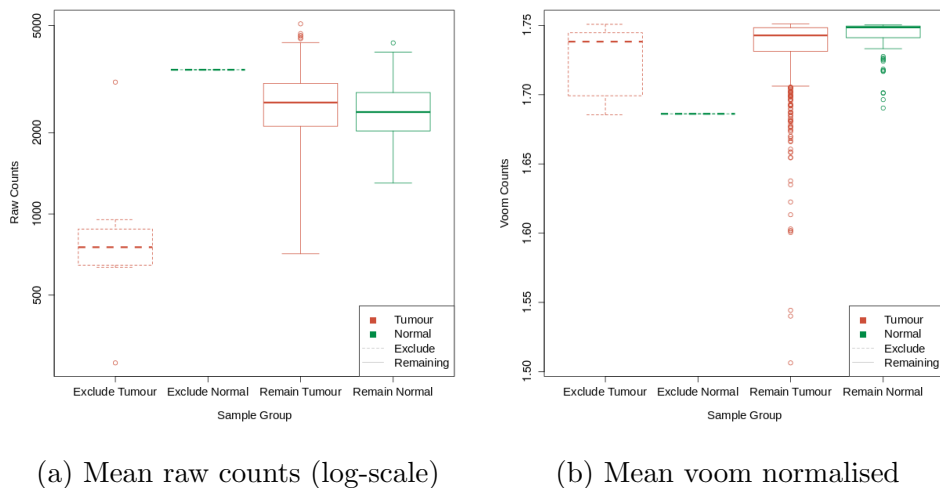


Figure 2.2: **Read count sample mean.** Boxplots of sample means for raw counts on log-scale and voom normalised show removed tumour samples with low mean read count.

singular value was used as a **metagene** for the **pathway** gene set. To ensure consistent directionality of **metagene** signals, the median of the gene set in each sample was calculated and correlated against the **metagene** with the (arbitrary) **metagene** sign adjusted as needed to conform with the majority of the gene set (i.e., positive correlation between **metagene** and the median-based centroid). To ensure that genes and **pathways** were weighted equally, **metagenes** were derived from a z-transformed (mean 0, standard deviation 1) dataset of **gene expression** and samples were scaled (by fractional ranking) for each **metagene** so that they were comparable on a [0, 1] scale.

## 2.2.4 Candidate Triage and Integration with Screen Data

Candidate triage in combination with the experimental data was intended to integrate findings of the **SLIPT** analysis with an ongoing experiment project (Chen *et al.*, 2014; Telford *et al.*, 2015). The first procedure to compare the **SLIPT** gene candidates for *CDH1* with an **siRNA** experimental screen (Telford *et al.*, 2015) was a direct comparison of the overlapping candidates, presented in a Venn diagram and tested with the  $\chi^2$  test. Since these candidates modestly overlapped at the gene level (even when excluding genes not contained in both datasets), further gene set over-representation analysis was performed for pathways specific to each detection approach and the intersection of the two.

The **pathway** composition of the intersection was further verified by a permutation resampling analysis (as described in Section 2.3.6): the same number of genes detected by **SLIPT** were sampled randomly from the universe of genes tested by both approaches. These samplings were performed over 1 million iterations and the **pathway** over-representation was compared for each of the 1652 reactome **pathways**. These over-representation scores ( $\chi^2$ ) were compared the observed over-representation in the intersection of the **SLIPT** candidates, with the proportion of resamplings with higher  $\chi^2$  values used for empirical p-values of **pathway** composition. The  $\chi^2$  test was used as an appropriation of Fisher's exact test on a hypergeometric distribution for resampling to computationally scale **pathway** over-representation tests across iterations. Pathways for which no resamplings were occurred as high as the observed were reported as  $p < 10^{-6}$ . These empirical p-values were adjusted for multiple comparisons (**FDR**). Intersection size was not assumed to be constant across resamplings, so similarly with the proportion of resamplings with higher or lower intersection size were used to evaluate significance of enrichment or depletion respectively (of **siRNA** candidate among **SLIPT** candidate genes).

## 2.3 Techniques

Various statistical, computational, and [bioinformatics](#) techniques were performed throughout this thesis. This section describes these techniques and gives the parameters used unless otherwise specified. Where relevant, the R package implementation which provided the technique will be acknowledged.

### 2.3.1 Statistical Procedures and Tests

As described in sections [2.3.4](#) and [2.2.3](#), the z-transform has been used to generate z-scores in various analyses in this thesis. Each row of the dataset ( $x_i$ ) is transformed into a scores ( $z_i$ ) using the mean ( $\bar{x}_i$ ) and standard deviation ( $s_i$ ) of the data such that:

$$z_i = \frac{x_{ij} - \bar{x}_i}{s_i}$$

This generates data where each row (gene) has a mean of 0 and standard deviation of 1. Where plotted as aa heatmap, any data more than 3 standard deviations above or below the mean was plotted as 3 or  $-3$  respectively.

Where specified, the Fisher's exact test,  $\chi^2$  test, and correlation were used to measure associations between variables, as implemented in the `stats` R package ([R Core Team, 2016](#)). Unless otherwise specified, Pearson correlation was used for correlation analyses ( $r$ ) and coefficient of determination ( $R^2$ ). Where these comparisons are discussed in more detail, Fisher's exact test and  $\chi^2$  tests are supported by a table or Venn diagram, rendered with the `limma` R package ([Ritchie \*et al.\*, 2015](#)). In some analyses, correlation is further supported by a scatter plot and a line of best fit derived by least squares linear regression.

The `t.test` function ([R Core Team, 2016](#)) has also been used to implement the t-test to compare pairs of data. Where relevant, an [analysis of variance \(ANOVA\)](#) has been performed to report significance of multivariate predictors of outcomes, or least squares linear regression performed for the adjusted coefficient of determination ( $R^2$ ) and F-statistic p-value to evaluate the fit of the predictor variables. For some analyses these are supported by boxplot or violin plot visualisation ([Adler, 2005](#)), rendered in R ([R Core Team, 2016](#)).

Multiple comparisons were accounted for with the Benjamini-Hochberg procedure to control the [FDR](#) unless otherwise specified ([Benjamini and Hochberg, 1995](#)). This procedure adjusts p-values to achieve an average of the proportion of false-positives among significant tests below a threshold,  $\alpha$ . The more stringent Holm-Bonferroni (Holm) procedure ([Holm, 1979](#)) was also applied in some cases to adjust for multiple

comparisons and control the family-wise error rate which adjusts p-values so that the probability that any one of the tests is a false-positive (type-1 error) below a threshold,  $\alpha$ .

### 2.3.2 Gene Set Over-representation Analysis

Gene set enrichment over-representation analysis was performed to test whether there was an enrichment of a gene set (e.g., a biological pathway) among a group of input genes. Such input genes may be predicted synthetic lethal candidates or a subset defined by clustering (in Section 2.3.3) or comparison with experimental candidates (see Section 2.2.4). Initially, these tests were performed using the GeneSetDB web tool (Araki *et al.*, 2012) hosted by the University of Auckland on the Reactome pathways (Croft *et al.*, 2014). Since the GeneSetDB tool used an older version of Reactome (version 40), it was difficult to directly compare with the results of other analysis (see sections 2.2.4 and 2.3.6) performed on version 52 (as described in Section 2.1.1.2). Thus an implementation of the hypergeometric test in R (R Core Team, 2016) was used to test for over-representation against Reactome (version 52) pathways. Pathways containing less than 10 genes or more than 500 (as performed in GeneSetDB by Araki *et al.*, 2012) were excluded before adjusting for multiple comparisons.

### 2.3.3 Clustering

The clustering analysis used unsupervised hierarchical clustering with complete linkage (distance calculated from the furthest possible pairing). For correlation matrices or multivariate normal parameters (e.g.,  $\Sigma$ ), the distance metric used was Euclidean distance. For empirical or simulated gene and pathway expression data correlation distance was used, calculated by  $distance = 1 - cor(t(x))$  where  $cor$  is Pearson correlation and  $t(x)$  is the transpose of the expression matrix.

### 2.3.4 Heatmap

Standardised z-scores of the data were used to plot heatmaps on an appropriate scale. Raw (log-scale) read counts or voom normalised counts per gene (as specified) were plotted as normalised z-scores on a  $[-3, +3]$  blue-red scale. Similarly, correlations were plotted on a  $[-1, +1]$  blue-red scale. Heatmap dendograms were generated using the linkage method and distance specified for the clustering performed in Section 2.3.3. The gplots R package (Warnes *et al.*, 2015) was used to generate many of the heatmaps throughout this thesis, along with a customised heatmap function (released as `heatmap.2x`, detailed in Table 2.6 and Section 3.5.2). Where clearly specified,

data have been split into subsets with clustering performed separately on each subset with these plotted alongside each other.

### 2.3.5 Modelling and Simulations

Statistical modelling and simulations were used to test various **synthetic lethal** detection procedures on simulated data. This involved constructing a statistical model of how **synthetic lethality** would appear in (continuous normally distributed) **gene expression** data. Where presented (in Section 3.2.1), the assumptions of the model are stated clearly. The model allows sampling from a multivariate normal distribution (using the `mvtnorm` R package (Genz and Bretz, 2009; Genz *et al.*, 2016)) to generate simulated data with known underlying **synthetic lethal** partners (detailed in Section 3.2.2). We can test whether statistical procedures, including those developed in this thesis (presented in Section 3.1), are capable of detecting **synthetic lethal** partners within the simulated data. This multivariate normal simulation procedure also enables the inclusion of correlation structure which is either given as correlated blocks of genes or derived from **pathway** structures (as detailed in Section 3.4.2).

When this multivariate normal distribution is sampled once and the procedure to add known **synthetic lethal** partners is performed, it generates a simulated dataset. Performing this simulation procedure and testing with a **synthetic lethal** detection procedure iteratively, these simulations can be used to assess the statistical performance of the detection procedure. The number of iterations (`Reps`) will be given for each simulation result. Typically, these are performed 1000 or 10,000 times depending on computational feasibility of doing so on larger datasets.

Several measures of statistical performance were used to assess the simulations. The following measures used the final classification of the detection procedure, statistical significance for  $\chi^2$ , significance and directional criteria met for **SLIPT** (see Section 3.1), and an arbitrary threshold:  $< -0.2$  and  $> +0.2$  for negative correlation and correlation respectively. Sensitivity (or “true positive rate”) was measured as the proportion of known **synthetic lethal** partners predicted to be **synthetic lethal**. Specificity (or “true negative rate”) was measured as the proportion of known non-synthetic lethal partners predicted not to be **synthetic lethal**. The “false positive rate” was measured here as the proportion of known non-synthetic lethal partners out of all putative partners predicted by the detection procedure. Statistical “accuracy” is the proportion of true predictions for a detection procedure, which is both the correctly predicted known **synthetic lethal** partners and correctly negative known non-synthetic lethal partners.

### 2.3.5.1 Receiver Operating Characteristic Curves

A more general procedure to measure the statistical performance of a simulation is the receiver operating characteristic (ROC) curve which does not assume a threshold for classification of synthetic lethality but demonstrates the achievable range of sensitivity and specificity for a model (Akobeng, 2007; Fawcett, 2006; Zweig and Campbell, 1993). These curves (implemented with the `ROCR` R package (Sing *et al.*, 2005)) plot the true positive rate (sensitivity) against the false positive rate (1-specificity) as the prediction threshold is varied. An ideal detection method will have a true positive rate of 1 and a false positive rate of 0, hence the Area Under the ROC curve (AUC or area under receiver operating characteristic (AUROC)) is a measure of statistical performance for a detection procedure accounting for this trade-off. AUROC values typically range from 0.5 (the value expected by random chance) to 1 for an optimal detection method, however it is possible for an AUROC below 0.5 for a poor detection method that performs worse than random chance. In cancer biology, it has been suggested that an AUROC of approximately 0.8 is a predictive biomarker suitable for publication (Hajian-Tilaki, 2013) but predictors with lower AUROC values may still be informative depending on the context. In this thesis, the AUROC values varied widely across simulation parameters and were primarily used for comparisons across these parameters, although they can also be used to refine thresholds for optimal classification.

### 2.3.6 Resampling Analysis

Resampling analyses (e.g., “permutation” analysis) are used to statistically test the significance of an observation without assuming the underlying distribution of expected test statistics (Collingridge, 2013). Instead these are derived from randomly shuffling test statistics or randomly sampling predicted candidates. For the purposes of this thesis, this involved randomly sampling genes from those tested to be analysed as putative synthetic lethal candidates. This was performed both for testing the significance of pathway composition in the intersection with experimental gene candidates (Section 2.2.4) and for assessing the significance of pathway structure among synthetic lethal candidates (Section 3.4.1.1).

These were analysed to compare the observed synthetic lethal genes against values derived from randomly sampling the same number of genes as were observed to be synthetic lethal from among the genes tested. Sampling iteratively across many resampling procedures, these resampling-based values form a null distribution that could be

expected if the null hypothesis were true. Thus the proportion of resampling-based values across these iterations that are greater than or equal to that observed, forms an empirically derived p-value to test significance.

Resampling was performed for comparison (in Section 2.2.4) with fixed experimental screen candidates (Telford *et al.*, 2015) both resampling the number of genes overlapping with the screen candidates and test statistics for *pathway* enrichment. Resampling analysis was also applied to *shortest paths* and network metrics (in Section 3.4.1.1) to test significance of directional relationships between *synthetic lethal* candidate genes within *pathway* structures.

The number of iterations determines the accuracy of these p-values. For *pathway* composition (in Section 2.2.4), a million iterations were performed using high performance computing (as detailed in Section 2.5.3) to provide sufficient accuracy after adjusting for multiple comparisons across *pathways*. For the purposes of network analysis (in Section 3.4.1.1), a thousand iterations were sufficient to reject the null hypothesis for the majority of *pathways* tested before adjusting for multiple comparisons, and thus further iterations were not performed.

## 2.4 Pathway Structure Methods

### 2.4.1 Network and Graph Analysis

Networks are important in considering the structure of relationships in molecular biology, including gene regulation, kinase cellular signalling, and metabolic *pathways* (Barabási and Oltvai, 2004). Network theory is an interdisciplinary field which combines the approaches of computer science with the metrics and fundamental principles of graph theory, an area of pure mathematics dealing with relationships between sets of discrete elements. The vast amounts of molecular and cellular data from high-throughput technologies have enabled the application of network-based and *genomes-wide bioinformatics* analysis to examine the complexity of a cell at the molecular level and understand aberrations in cancer. This thesis uses various metrics and analysis procedures developed in Graph and Network theory to analyse *graph* structure of biological *pathways*. Where feasible, these have been implemented using the *igraph* R package with such procedures described below (Csardi and Nepusz, 2006). Custom R functions were used to perform more complex analysis and visualisation of iGraph data (as described in Section 3.5.3).

Graph theory is a branch of pure mathematics which deals with the properties of sets

of discrete objects (referred to as a ‘node’ or ‘vertex’) with some pairs are joined (by a ‘link’ or an ‘edge’). While a seemingly reductionist abstraction to mathematically study relationships, graph theory has applications in a wide range of fields, including the life sciences. Network theory is the sub-discipline of graph theory that deals with networks, which has become popular due to the vast potential for applications of networks (van Steen, 2010).

Applications vary depending on the situation modelled, particularly in how the edges between vertices are defined, whether they are directed or weighted, and whether multiple redundant edges between a pair of vertices (referred to as ‘parallel edges’) or edges connecting a vertex to itself (referred to as ‘loops’) are permitted in the model. Networks are defined such that the edges represent a relationship between the vertices and may be directed, weighted, or contain parallel edges or loops depending on the application (van Steen, 2010). Unless otherwise stated, graph structures and networks in this thesis will be unweighted and have no parallel edges or loops. Where a directional relationship is known or modelled, it will be represented with a directed edge in a directed graph.

## 2.4.2 Sourcing Graph Structure Data

Pathway Commons interaction data was sourced using the Biological PAthway eX-change (BioPAX) with the paxtools-4.3.0 Java application on October 6<sup>th</sup> 2015 (Cerami *et al.*, 2011; Demir *et al.*, 2013). This utility was used to import ‘sif’ format interaction data into R (R Core Team, 2016) and extract the human Reactome (version 52) dataset of interactions was imported (Croft *et al.*, 2014), matching those used for pathway enrichment analysis. These interactions were used to construct an adjacency matrix for the Reactome network and subnetworks corresponding to each relevant biological pathway.

## 2.4.3 Constructing Pathway Subgraphs

Subgraphs for each relevant pathway were constructed by matching the nodes in the complete Reactome network to the pathway gene sets (as derived in Section 2.1.1.2). A subgraph with adjacent nodes was constructed by adding nodes which have an edge with a gene in the pathway gene set. The pathways these adjacent nodes belong to were added to form a “meta-pathway” to account for the possibility for nodes within the pathway being linked by the surrounding graph structure.

## 2.4.4 Network Analysis Metrics

The existing network analysis measures applied in this thesis (as described below) used an implementation in the `igraph` R package to compute vertex degree, shortest paths, and centrality (Csardi and Nepusz, 2006). Additionally, custom features were developed for analysis of iGraph objects in R and released as `igraph.extensions` (as described in Section 3.5.3).

Vertex degree is the number of `edges` a `node` has and is a fundamental measure of the importance and connectivity of a network (van Steen, 2010). More connected `nodes`, such as network hubs, will have a higher `vertex` degree relative to other `nodes`. For the purposes of this thesis, `vertex` degree ignored `edge` direction with loops (edges with itself) and double `edges` to the same `node` excluded.

A fundamental concept in network analysis is a “`shortest path`”, that is the shortest route via `edges` between any two particular `nodes` in a network. These are computed by Dijkstra’s algorithm (Dijkstra, 1959) in the `igraph` R package (Csardi and Nepusz, 2006). Where applicable paths will only use directed `edges` in a particular direction. Shortests paths are a useful measure of how close `nodes` are in a network. This is used to compute `information centrality`, and for further analysis of `pathway` structure (as described in Section 3.4.1).

Network `centrality` is an alternative measure of the importance or influence of a `node` to the `graph` structure (Borgatti, 2005). Various strategies are used to derive centrality, typically based on how connected the `node` is or the impact of `node` removal on the connectivity of the network. One of the most notable is the “`PageRank`” algorithm, a refinement of eigenvector `centrality` based on the eigenvectors of the adjacency matrix (Brin and Page, 1998). This is implemented in the `igraph` R package (Csardi and Nepusz, 2006).

Another network `centrality` measure that has been previously applied to biological protein interaction networks (Kranthi *et al.*, 2013) is the “`information centrality`”. The `information centrality` of a `node` is the relative impact on efficiency (transmission of information via `shortest paths`) of the network when the `node` is removed. Te `centrality` ( $C$ ) (Kranthi *et al.*, 2013) for `node`  $n$  in graph  $G$  is defined as:

$$C_n = \frac{E(G) - E(G')}{E(G)}$$

where  $G'$  is the subgraph with the `node` removed and  $E$  is the efficiency (Latora and

Marchiori, 2001), derived from [shortest paths](#) ( $d_{ij}$  between [nodes](#)  $i$  and  $j$ ).

$$E(G) = \frac{2}{N(N-1)} \sum_{i < j \in G} \frac{1}{d_{ij}}$$

The efficiency of the network can be derived from [shortest paths](#) implemented in the [igraph](#) R package and the iterative network [centrality](#) computation of each [node](#) has been released as an R package ([info.central](#)) and included in the [igraph.extensions](#) package.

## 2.5 Implementation

### 2.5.1 Computational Resources and Linux Utilities

Several computers were used to process and store data during this thesis (as summarised in Table 2.2), running different versions of Linux operating systems, including a personal laptop computer, laboratory desktop machine, departmental server, and the New Zealand eScience Infrastructure Intel Pan high-performance computing cluster (a supercomputer based at the University of Auckland). Each of these systems support a 64-bit architecture. Current workflows on local machines use Elementary OS (based on the Ubuntu versions given in Table 2.2) and the ZSH shell. However, Ubuntu OS and the [Bourne Again SHell \(Bash\)](#) were used at the inception of this project and [Bash](#) continues to be used for running scripts. Various Linux applications and command-line utilities were used on these machines (as summarised in Table 2.3). As such, the workflows developed in this project should be backwards-compatible with Ubuntu Linux (and other derivatives). The majority of novel methodology and implementations were performed in R which is a cross-platform language, packages developed in R will be available for users of Linux, Mac, and Windows machines.

Table 2.2: Computers used during thesis

	Viao Laptop	Lab Machine	Biochem Server	NeSI Pan Cluster
Operating System (OS)	Elementary OS Freya 0.3.2	Elementary OS Loki 0.4	Red Hat Enterprise Maipo 7.2	Cent OS Final 6.4
Upstream OS	Ubuntu LTS Trusty 14.04	Ubuntu LTS Xenial 16.04		
Linux Kernel	3.19.0-65-generic	4.4.0-36-generic	3.10.0-327.36.2.el7.x86_64	2.6.32-504.16.2.el6.x86_64
Shell: Bash	4.3.11(1)	4.3.46(1)	4.2.46(1)	4.2.1(1)
Shell: zsh	5.0.2	5.1.1	5.0.2	5.2

Table 2.3: Linux utilities and applications used during thesis

		Viao Laptop	Lab Machine	Biochem Server	NeSI Pan Cluster
	OS	Elementary OS Freya 0.3.2	Elementary OS Loki 0.4	Red Hat Enterprise Maipo 7.2	Cent OS Final 6.4
	Linux Kernel	3.19.0-65-generic	4.4.0-36-generic	3.10.0-327.36.2.el7.x86_64	2.6.32-504.16.2.el6.x86_64
Scripting	Shell Bash	4.3.11(1)	4.3.46(1)	4.2.46(1)	4.2.1(1)
	Shell zsh	5.0.2	5.1.1	5.0.2	5.2
Programming	Python	2.7.6	2.7.12	2.7.5	
	Java	1.8.0_101	9-ea	1.8.0_101	
	C++	4.8.4	5.4.0	4.8.5	4.4.7
Text Editor	nano	2.2.6	2.5.3	2.3.1	2.0.9
	kile (L <sup>A</sup> T <sub>E</sub> X)	2.1.3	2.1.3		
Version Control	git	1.9.1	2.11.0	1.7.1	1.8.3.1
Shell Utilities	sed	4.4.2	4.4.2	4.4.2	4.4.1
	grep	2.16-1	2.25-1	2.20	2.6.3
	nohup	8.21	8.25	8.22	8.4
Typesetting	T <sub>E</sub> X	3.1415926	3.14159265		
	TeXLive (L <sup>A</sup> T <sub>E</sub> X)	2013	2015		
	PDFT <sub>E</sub> X	2.5-1	2.6		
	pandoc	1.12.2.1	1.16.0.2		
Remote Computing	Slurm scheduler				16.05.6
	OpenSSH	7.2p2	7.2p2	6.6.1	5.3p1
	OpenSSL	1.0.2g	1.0.2g	1.0.01e-fips	1.0.01e-fips
	rsync	3.1.0p31	3.1.1p31	3.0.9p30	
	Globus Online Transfer			3.1	3.1
	Cisco AnyConnect VPN		3.1.05170		
Image Processing	Inkscape	0.48.4	0.91		
	GIMP	2.8.10	2.8.16		
	ImageMagick	6.7.7.10-6			

## 2.5.2 R Language and Packages

The R programming language has been used for the majority of this thesis. Current R installations across the machines used are given in Table 2.4. Local machines currently run the latest version of the R (at the time of writing) and remote machines run the versions and modules as managed by the system administrator.

Various scripts and packages in this thesis were developed or run in previous versions of RStudio and R but these run without error in the current version of R (and the older versions on remote machines). The R packages which were used throughout this thesis (as detailed in Table 2.5 with versions specified) were installed from the [comprehensive R archive network \(CRAN\)](#) ([CRAN, 2017](#)), Bioconductor ([Gentleman \*et al.\*, 2004](#), version 3.4; BiocInstaller 1.24.0), or GitHub (<https://github.com/>). These packages were not updated when they would change the functionality of scripts or functions in packages, in particular imported data from annotation packages (used to define gene sets) have been saved as local files to continue using stable versions of these [pathway](#) data (across machines).

This is a summary of the key packages which (in addition to their dependencies) have been used throughout this project. Where a package implementation has been central to the methods applied, they are described in more detail in the relevant section. A full table of packages used in this thesis can be found in Appendix B (Table B.1). The R packages developed during this thesis are given in Table 2.6 with the relevant sections describing their implementation and use where appropriate, in addition to further details on these functions in Section 3.5.

Table 2.4: R installations used during thesis

		Viao Laptop	Lab Machine	Biochem Server	NeSI Pan Cluster
	OS	Elementary OS Freya 0.3.2	Elementary OS Loki 0.4	Red Hat Enterprise Maipo 7.2	Cent OS Final 6.4
Programming	R	3.3.2	3.3.2	3.3.1	3.3.0-intel (module)
Development	RStudio	1.0.136	1.0.136	1.0.136 (server)	

Table 2.5: R Packages used during thesis

Package	Version Used	Built	Repository
colorspace	1.3-2	3.3.1	CRAN
curl	2.3	3.3.1	CRAN
data.table	1.9.6	3.3.1	CRAN
dendextend	1.4.0	3.3.2	CRAN
DBI	0.5-1	3.3.1	CRAN
devtools	1.12.0	3.3.1	CRAN
dplyr	0.5.0	3.3.1	CRAN
ggplot2	2.2.1	3.3.1	CRAN
git2r	0.18.0	3.3.1	CRAN
gplots	3.0.1	3.3.1	CRAN
gtools	3.5.0	3.3.1	CRAN
igraph	1.0.1	3.3.1	CRAN
matrixcalc	1.0-3	3.3.1	CRAN
mclust	5.2.2	3.3.1	CRAN
mvtnorm	1.0-6	3.3.1	CRAN
org.Hs.eg.db	3.1.2	3.1.2	Bioconductor
openssl	0.9.6	3.3.1	CRAN
plyr	1.8.4	3.3.1	CRAN
purrr	0.2.2	3.3.1	CRAN

reactome.db	1.52.1	3.2.1	Bioconductor
RColorBrewer	1.1-2	3.3.1	<a href="#">CRAN</a>
Rcpp	0.12.9	3.3.1	<a href="#">CRAN</a>
ROCR	1.0-7	3.3.1	<a href="#">CRAN</a>
roxygen2	6.0.1	3.3.2	<a href="#">CRAN</a>
shiny	1.0.0	3.3.1	<a href="#">CRAN</a>
snow	0.4-2	3.3.1	<a href="#">CRAN</a>
testthat	1.0.2	3.3.2	<a href="#">CRAN</a>
tidyverse	1.1.1	3.3.2	GitHub (hadley)
sm	2.2-5.4	3.3.1	<a href="#">CRAN</a>
Unicode	9.0.0-1	3.3.2	<a href="#">CRAN</a>
vioplot	0.2	3.3.1	<a href="#">CRAN</a>
viridis	0.3.4	3.3.2	<a href="#">CRAN</a>
xml2	1.1.1	3.3.2	<a href="#">CRAN</a>
xtable	1.8-2	3.3.1	<a href="#">CRAN</a>
zoo	1.7-14	3.3.1	<a href="#">CRAN</a>
graphics	3.3.2	3.3.2	base
grDevices	3.3.2	3.3.2	base
cluster	2.0.5	3.3.1	base
graphics	3.3.2	3.3.2	base
grDevices	3.3.2	3.3.2	base
Matrix	1.2-8	3.3.1	base
stats	3.3.2	3.3.2	base

Table 2.6: R packages developed during thesis

Package Name	Description and GitHub Repository	Section
<code>slipt</code>	Synthetic lethal detection by <a href="#">SLIPT</a> (to accompany publication) <a href="https://github.com/TomKellyGenetics/slipt">https://github.com/TomKellyGenetics/slipt</a>	3.1
visualisation	<code>vioplotx</code> Customised violin plots (based on <code>vioplot</code> ) <a href="https://github.com/TomKellyGenetics/vioplotx">https://github.com/TomKellyGenetics/vioplotx</a>	3.4
	<code>heatmap.2x</code> Customised heatmaps (based on <code>gplots</code> ) <a href="https://github.com/TomKellyGenetics/heatmap.2x">https://github.com/TomKellyGenetics/heatmap.2x</a>	
igraph.extensions	<code>igraph.extensions</code> Meta-package to install the follow iGraph functions <a href="https://github.com/TomKellyGenetics/igraph.extensions">https://github.com/TomKellyGenetics/igraph.extensions</a>	3.5.3
	<code>plot.igraph</code> Custom plotting of directed graphs <a href="https://github.com/TomKellyGenetics/plot.igraph">https://github.com/TomKellyGenetics/plot.igraph</a>	2.4.4
	<code>info.centrality</code> Computing information centrality from network efficiency <a href="https://github.com/TomKellyGenetics/info.centrality">https://github.com/TomKellyGenetics/info.centrality</a>	3.4.2
	<code>pathway.structure.permutation</code> Testing pathway structure with resampling analysis <a href="https://github.com/TomKellyGenetics/pathway.structure.permutation">https://github.com/TomKellyGenetics/pathway.structure.permutation</a>	3.4.1.1
	<code>graphsim</code> Generating simulated expression from graph structures <a href="https://github.com/TomKellyGenetics/graphsim">https://github.com/TomKellyGenetics/graphsim</a>	3.4.2

### 2.5.3 High Performance and Parallel Computing

Another enabling technology for [bioinformatics](#) is parallel computing, performing independent operations using separate [central processing unit \(CPU\)](#) cores: this “multithreading” is widely used to increase the time to compute results. [Bioinformatics](#) is particularly amenable to this since performing multiple iterations of a simulation or testing separate genes is often “embarrassingly parallel”, as [CPUs](#) completely independent of each other.

The New Zealand eScience Infrastructure ([NeSI](#)) is a [High Performance Computing \(HPC\)](#) organisation providing the Intel Pan cluster or “supercomputer”, hosted by the University of Auckland ([NeSI, 2017](#)). The Pan cluster used throughout this thesis project to optimise and perform computations which would have otherwise been infeasible in the timeframe of thesis. Such technological developments and infrastructure initiatives have enabled [bioinformatics](#) research including this project. High performance computing on the Pan cluster was used extensively in this project including for resampling analysis (in sections 2.3.6 and 3.4.1.1), calculating [information centrality](#) (in Section 2.4.4), and in simulations (in sections 2.3.5, 3.2, and 3.4.2)

Scripts and data were transferred between the Pan cluster and University of Otago computing resources by `rsync` or the Globus file transfer service ([Globus, 2017](#)). R scripts ([R Core Team, 2016](#)) were run in parallel with the “simple network of workstations” `snow` R package [Tierney et al. \(2015\)](#). This utilised the “message passing interface” ([Yu, 2002](#)) when it was feasible with memory requirements to run in parallel across multiple compute nodes, otherwise [Socket Secure \(SOCKS\)](#) was used to access

multiple cores within an instance of R and pass input data to them. R jobs were submitted to queue for available resources and run on the Pan cluster via the [Simple Linux Utility for Resource Management \(Slurm\)](#) workload manager ([Slurm, 2017](#)). Slurm array job submission and independent running of different parameters (with arguments passed to R from the shell) were used to run memory-intensive job or scripts across many parameters simultaneously. In some cases, this submission was automated across a range of parameters with [Bash](#) scripts.

# Chapter 3

## Methods Developed During Thesis

In this Chapter, I outline the rationale and development of various methods used throughout this thesis to examine [synthetic lethality](#) in gene expression data, graph structures, models and simulations. Firstly, the [Synthetic Lethal Interaction Prediction Tool \(SLIPT\)](#), a [bioinformatics](#) approach to triage [synthetic lethal](#) candidate genes, will be described. This is one of the main research outputs of this thesis project and is supported by comparisons to an experimental screen from a related project and evaluation of performance on simulated data. These supporting findings will be covered in further chapters but simulation data is included to support the use and design of [SLIPT](#). This includes the construction of a statistical model of [synthetic lethality](#) in (continuous multivariate Gaussian) [gene expression](#) data, which enables testing [SLIPT](#) upon simulated data with known [synthetic lethal](#) partners. Another key component of this simulation pipeline is the generation of simulated data from a known [graph](#) structure or simulated biological pathway (as applied in Chapter 6). The development of this simulation procedure and other statistical treatment of graph and [network](#) structures will also be covered. Various R packages have been developed to support this project, including the `slipt` package to implement the [SLIPT](#) methodology. Additional R packages for handling [graph](#) structures, simulations, and custom plotting features will be described as research outputs of this thesis, methods applied throughout, and contributions of open-source software.

### 3.1 A Synthetic Lethal Detection Methodology

The [SLIPT](#) methodology identifies [gene expression](#) patterns consistent with [synthetic lethal](#) interactions, between a query gene and a panel of candidate interacting partners. Gene expression is scored “low”, “medium”, or “high”, sorting samples by tertiles (1/3-

quantiles) for each gene. Genes with insufficient expression across all samples are excluded by requiring that the first tertile of raw counts is above zero. A  $\chi^2$  test is then performed between the query gene and each candidate partner. The p-values for the  $\chi^2$  test are corrected for multiple testing using False discovery rate (FDR) error control to reduce false positives (Benjamini and Hochberg, 1995). Significance is called for FDR adjusted  $p < 0.05$ . A synthetic lethal interaction is predicted (as shown in Figure 3.1) when (i) the  $\chi^2$  test is significant; (ii) observed low-query, low-candidate samples are less frequent than expected; and (iii) observed low-query, high-candidate and high-query, low-candidate samples are more frequent than expected.

The synthetic lethal prediction procedure has also been performed with somatic mutation data for the query gene. This is intended for a query gene known which is recurrently mutated, with the majority of mutations disrupting gene function (e.g., null or frameshift mutations). A synthetic lethal interaction is predicted (as shown in Figure 3.2) when (i) the  $\chi^2$  test is significant; (ii) observed mutant-query, low-candidate samples are less frequent than expected; and (iii) observed mutant-query,

		Candidate Gene		
		Low	Medium	High
Query Gene (e.g. CDH1)	Low	Observed less than expected		Observed more than expected
	Medium			
	High	Observed more than expected		

Figure 3.1: **Framework for synthetic lethal prediction.** SLIPT was designed to identify candidate interacting genes from gene expression data using the  $\chi^2$  test against a query gene. Samples are sorted into low, medium, and high expression quantiles for each gene to test for a directional shift. A sample being low in both genes of a synthetic lethal pair is unlikely, since loss of both genes will be deleterious, and is expected to be statistically under-represented in a gene expression dataset. We expect a corresponding (symmetric) increase in frequency of sample with low-high gene pairs. Synthetic lethal candidate partners of a gene were identified by running this procedure on all possible partner genes, selecting those with an FDR-adjusted  $\chi^2$ -derived  $p < 0.05$ , and meeting the directional criteria. Since synthetic lethal genes are partners of each other, commutatively, the symmetric direction criteria were defined such that detected synthetic lethal genes are partners of each other.

		Candidate Gene		
		Low	Medium	High
Query Gene (e.g. <i>CDH1</i> )	Mutation	Observed less than expected		→ Observed more than expected
	Wild-type	↓ Observed more than expected		

Figure 3.2: **Synthetic lethal prediction adapted for mutation.** SLIPT was also adapted to identify candidate interacting genes using (somatic) **mutation** data of the query gene in the  $\chi^2$  test. Samples are sorted into low, medium, and high **expression** quantiles for each candidate gene and tested for a directional shift against **mutation** status of the query gene. A sample having low **expression** or **mutation** for the **synthetic lethal** pair is expected to be unlikely with a corresponding increase in frequency of sample with **mutant-high** or **wild-type-low** gene pairs. **Synthetic lethal** (mtSL) candidate partners of a gene were identified from running this procedure on all possible partner genes, selecting those with an **FDR**-adjusted  $\chi^2$ -derived  $p < 0.05$ , and meeting the directional criteria.

high-candidate and **wild-type-query**, low-candidate samples are more frequent than expected.

The **SLIPT** methodology can be performed on **expression** data, including pathway **metagenes** (as generated in Section 2.2.3). The application of the **SLIPT** methodology on public **gene expression** data will be supported with simulation results (in Section 3.3 and Chapter 6), including comparison to other statistical methods. **SLIPT** results for *CDH1* were compared experimental screen results in a breast cell line (Telford *et al.*, 2015). Primary screen results are discussed in Section 4.2 and secondary screen results are presented in Section 4.2.4.

## 3.2 Synthetic Lethal Simulation and Modelling

A statistical model of **synthetic lethality** was developed to generate simulated data and to evaluate the **SLIPT** procedure. This section describes the **synthetic lethal** model and the simulation procedure for generating **gene expression** data with known **synthetic lethal** partners. Simulation results, to support usage of the **SLIPT** methodology throughout this thesis, will be presented in Section 3.3. The simulation procedure will

also be applied in Chapter 6, including in combination with simulations from graph structures (as described in Section 3.4.2).

### 3.2.1 A Model of Synthetic Lethality in Expression Data

A conceptual model of synthetic lethality was devised (see Figure 3.3), which will be used to build a statistical model of synthetic lethal gene expression and to simulate expression data for assessing various potential synthetic lethal prediction methods, including SLIPT. In the model, synthetic lethality occurs between genes with related functions, as a cell death phenotype, when these functions are inactive.

This model suggests that synthetic lethality is detectable in measures of gene inactivation across a sample population, namely mutation, DNA copy number, DNA methylation, and expression levels. While any of these mechanisms of gene inactivation could lead to synthetic lethality, expression data is readily available and changes in other mechanisms are likely to impact on the amount of expressed RNA that is detectable. Functional relationships between genes could manifest in expression data in several ways, including coexpression, mutual exclusivity and directional shifts. Co-expression is overly simplistic (Lu *et al.*, 2015) and has previously performed poorly as a predictor of synthetic lethality (Jerby-Arnon *et al.*, 2014), although this will still be tested with correlation measures in later simulations. The alternative hypothesis is that synthetic lethality will result in a detectable shift in the number of samples which exhibit low or high expression of either gene. This model does not preclude mutual exclusivity, compensating expression, or co-loss under-representation which may occur between synthetic lethal genes (Lu *et al.*, 2015; Wappett *et al.*, 2016).

The first condition of the synthetic lethal model is that if there are only two synthetic lethal genes (e.g., *CDH1* and one SL partner), then they will not both be non-functional in the same sample (in an ideal model). Gene function is thus determined for each sample in a model of synthetic lethality with the proportion of samples which are functional or non-functional for a gene being arbitrary. Whether a gene is functional can similarly be modelled by an arbitrary threshold of continuous and normally distributed gene expression data to define gene function (as shown in Figure 3.4). For the purposes of modelling synthetic lethality in cancer expression data, a threshold of the 30<sup>th</sup> percentile of the expression levels was used because approximately 30% of samples analysed had *CDH1* inactivation (mutations) in breast cancer (Koboldt *et al.*, 2012). This was generalised for a model of the proportion of samples inactivated for each gene. The threshold of the 0.3 quantile was used in simulations derived from this

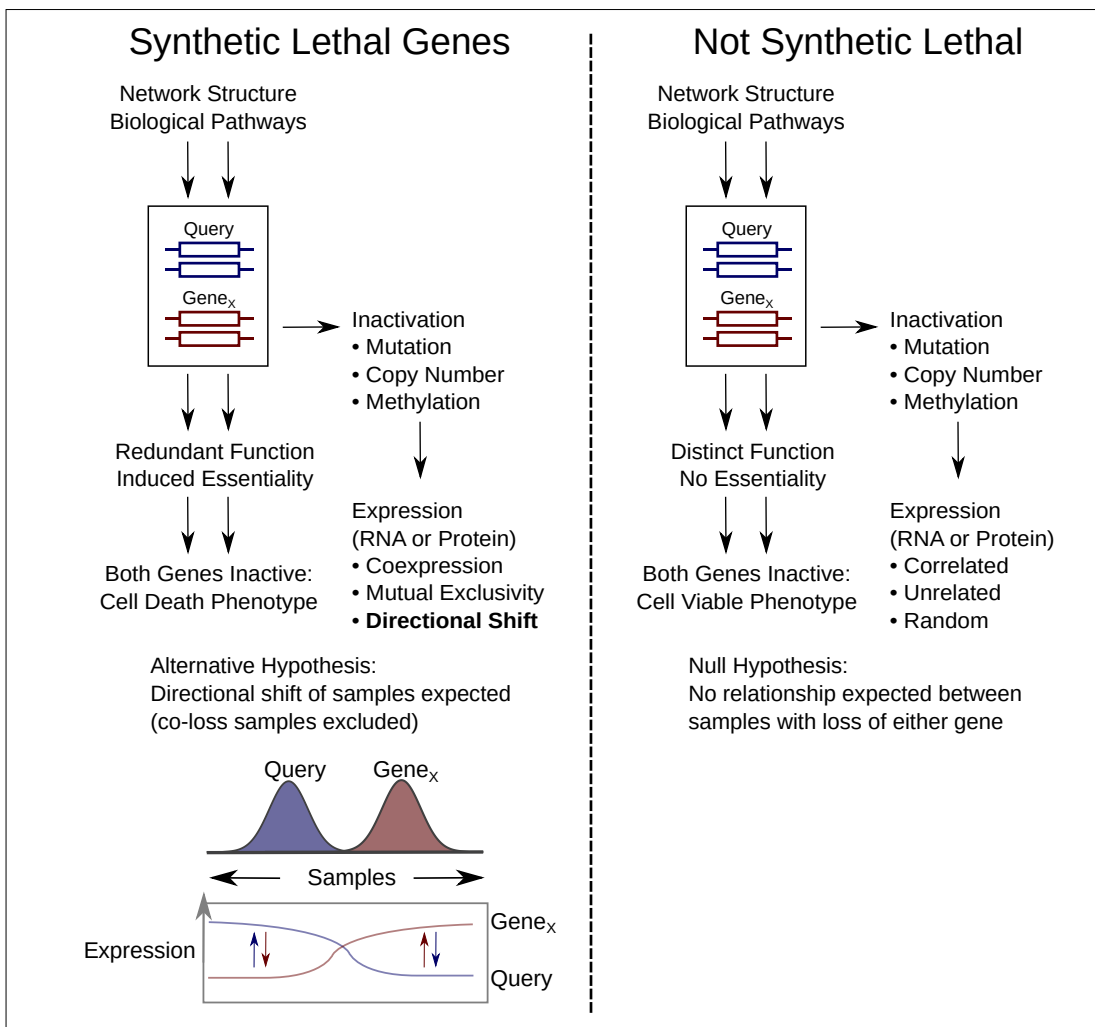


Figure 3.3: A model of **synthetic lethal** gene expression. A conceptual model of synthetic lethal interactions between a Query gene and partner gene ( $G_X$ ). Genes that are synthetic lethal may not both be non-functional in the same sample without another gene compensating for the loss of function. This is most likely to be detectable as low gene expression, whether they are lost by mutation, deletion, DNA methylation, or suppressing regulatory signals. This could manifest as coexpression, mutual exclusivity, or directional shifts in sample frequency. Thus the alternative hypothesis ( $H_A$ ) is that synthetic lethal genes will have a reduced frequency of co-loss samples while the null hypothesis ( $H_0$ ) is that non synthetic lethal gene pairs would show no such relationship, even if they may be correlated for other means such as pathway relationships. In this model synthetic lethal genes may compensate for the loss of each other but this is not assumed, only that loss of both is unfavourable to cell viability and probability of detecting samples with combined gene loss.

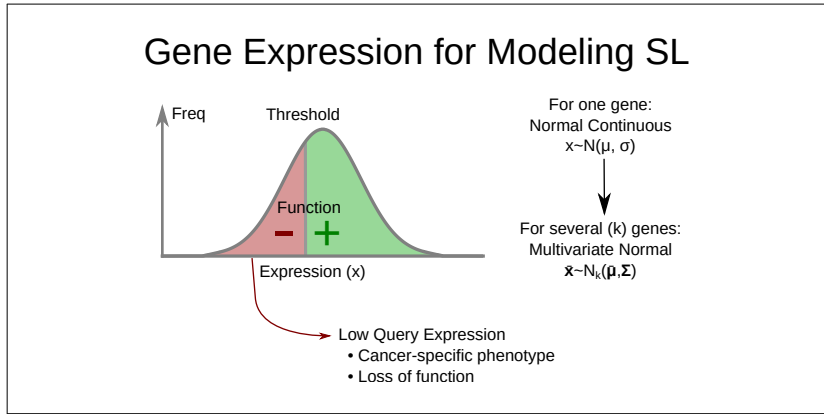


Figure 3.4: **Modelling synthetic lethal gene expression.** When modelling [synthetic lethal](#) interactions between a Query gene and partner genes ( $G_X$  and  $G_Y$ ) above, cellular viability requires that at least one of genes is not inactivated. As a model of loss of function, genes are regarded as non-functional with expression below a threshold for the purposes of modelling [synthetic lethality](#). Tumour suppressor genes with loss of function also have cancer specific phenotypes (although these thresholds are not assumed to be the same). Expression is modelled by normally (Gaussian) distributed continuous data, such as (log-scale) data from RNA (microarray or [RNA-Seq](#)), protein, or pathway [metagenes](#). This rationale generalises to several genes on a multivariate normal distribution.

model throughout this thesis. In this ideal case, no samples lowly expressing both of these genes are expected to be observed. While this was not the case, that is to be expected as it is unlikely that only two genes will have an exclusive [synthetic lethal](#) partnership.

A [synthetic lethal](#) pair of genes is unlikely to act in isolation, therefore higher-order [synthetic lethal](#) interactions (i.e., 3 or more genes) must be considered in the model as shown in Figure 3.5. Even when testing pairwise interactions, it is important to model higher level interactions that may interfere. If there are additional [synthetic lethal](#) partners, there are two possibilities for adding these: 1) that they are independent partners of the query genes interacting pairwise (and not with each other) or 2) that an additional partner gene interacts with both of the [synthetic lethal](#) genes already in the system and any of the three (or more) are required to be functional for the cell to survive.

The signal (in terms of [gene expression](#) data) will be weaker for this latter case and this model has the more stringent assumption that all [synthetic lethal](#) partner genes interact with each other: that only one of these must be expressed to satisfy

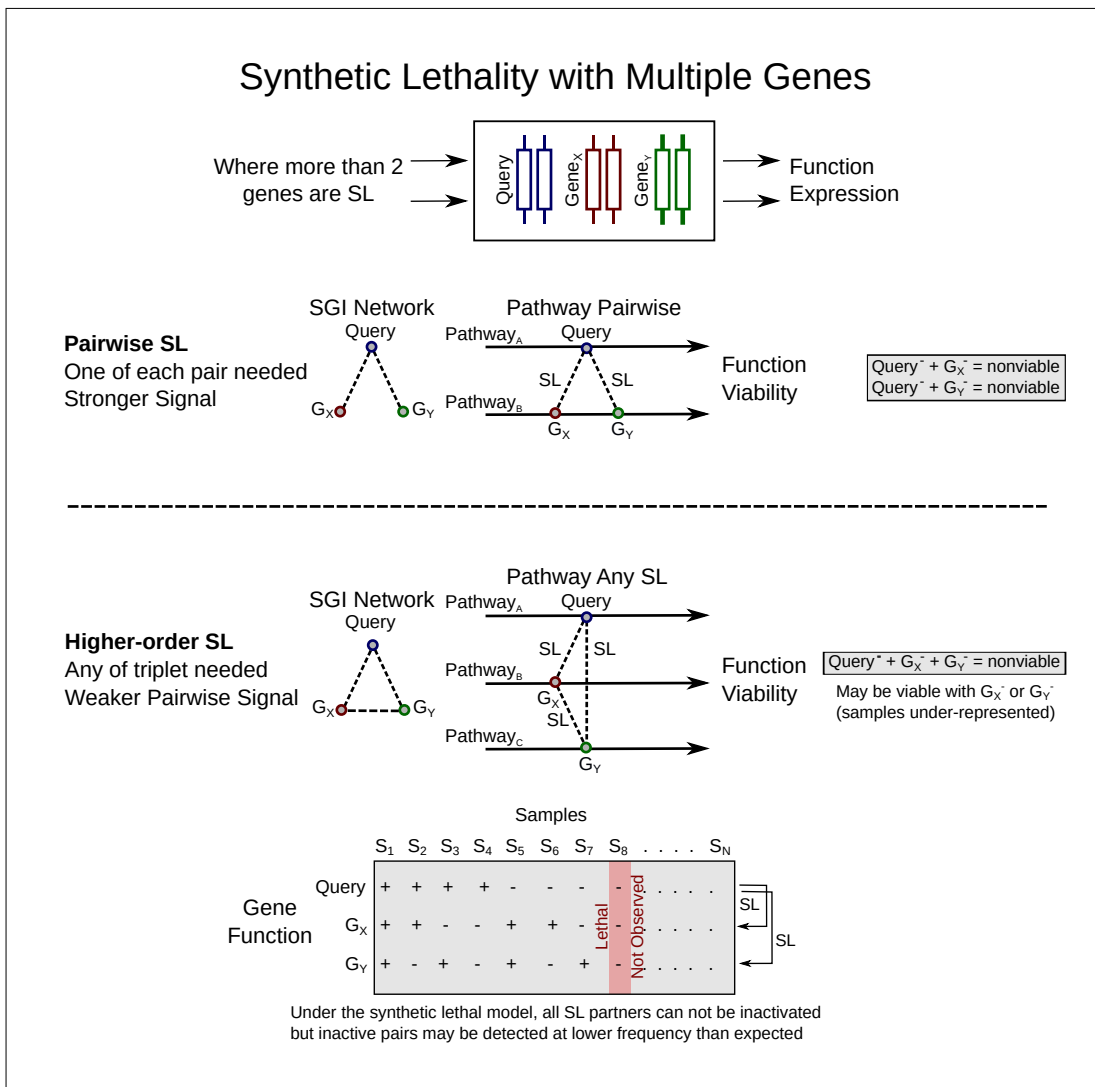


Figure 3.5: **Synthetic lethality with multiple genes.** Higher order synthetic lethal interactions may occur between 3 or more genes, affecting the simulated expression (or synthetic lethal predictions) even if undetected when observed pairwise. Consider interactions between a Query gene and two partner genes ( $G_X$  and  $G_Y$ ). They may interact with the Query pairwise (inviolate when either gene pair is lost) or form a higher-order interaction such as the “synthetic lethal triplet” if any of the genes provide an essential function (inviolate only when all are lost). Either is plausible with the potential pathway structures. A synthetic lethal triple has 8 potential combinations of gene function but one is not expected to be observed (due to inviability), however pairwise inactivation may be observed if additional partner genes are functional. The proportion of these combinations varies depending on the functional threshold.

the model of synthetic lethality. In this model, any of the synthetic lethal genes in a higher-order interaction are able to perform the essential function of the others, allowing for higher-level synthetic lethal partners to compensate for loss a synthetic lethal gene pair. While samples that express low levels of the synthetic lethal gene pairs will be under-represented, they may not be completely absent from the dataset, due to these higher-level interactions. In the example of three synthetic lethal genes (shown in Figure 3.5), only one of the genes involved in the higher-order synthetic lethal interaction is required for cell viability. For synthetic lethal pairs, only a subset of these samples will be inviable (i.e., removed from simulated data), leading to an under-representation.

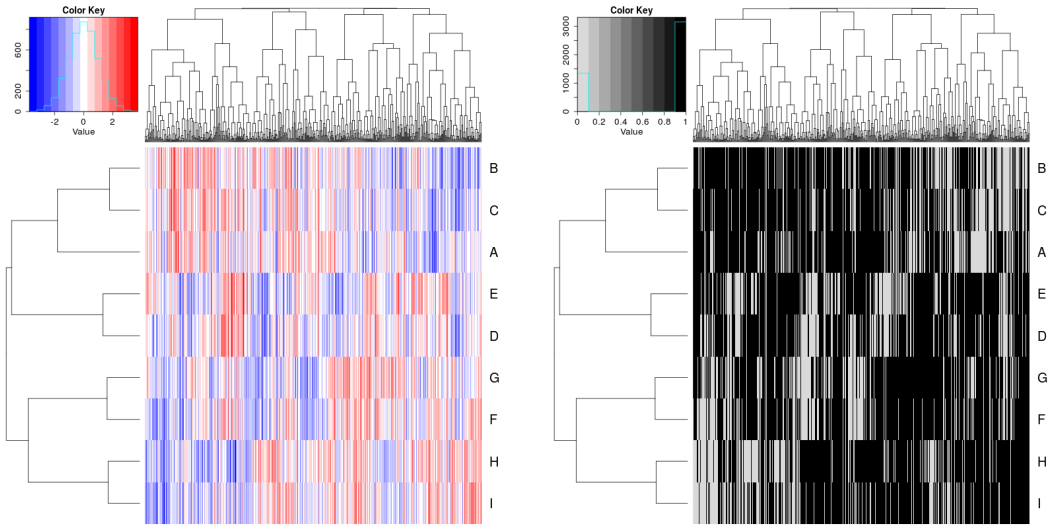
Samples were not actually removed from a simulated dataset, rather the expression and function of the query gene is generated across samples separately from the pool of potential partner genes. The query gene data was matched to simulated samples (as shown in Figure 3.7) satisfying the synthetic lethal condition with the procedure described in Section 3.2.2. This was performed to maintain a comparable samples size across simulations and the preserve the (multivariate) normal distribution of the data.

### 3.2.2 Simulation Procedure

Simulations were developed to generate normal distributions of expression data and define gene function with a threshold cut-off. While gene function was used as an intermediary step in modelling synthetic lethal genes in expression data, the normal distribution was sampled for simulated data to represent normalised empirical gene expression data for which SLIPT (and other methods) will be applicable.

Sampling a distribution for expression profiles has the advantage of enabling simulating correlation structures with the multivariate normal distribution, using the `mvtnorm` R package (Genz and Bretz, 2009; Genz *et al.*, 2016). The parameter  $\Sigma$ , the covariance matrix, defines the correlation structure between the simulated genes being sampled. With a diagonal of one, this  $\Sigma$  matrix simulates genes with a standard deviation of one and the covariance parameters between them are the correlations between each gene. In Figure 3.6, an example of such a simulated multivariate normal dataset is shown with the functional threshold applied.

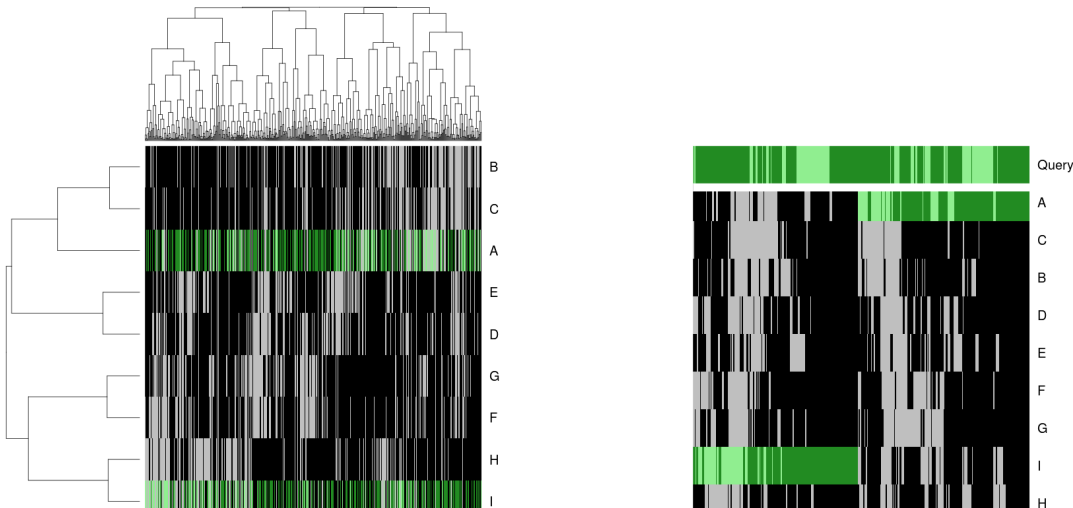
Once a simulated dataset has been generated, the samples were compared by gene function (as derived from a functional threshold). The known underlying synthetic lethal partners were selected within the dataset and a query gene was generated by sampling from the normal distribution. These were matched (as shown for two synthetic



(a) Simulated expression matrix

(b) Corresponding gene function calls

Figure 3.6: **Simulating gene function.** A simulated dataset with samples (columns) and genes A–I (rows) was transformed from a continuous (coloured blue–red) scale to a discrete matrix of gene function (black for functional levels and grey for non-functional).



(a) Simulated gene function with SL genes (b) Query gene added with SL condition

Figure 3.7: **Simulating synthetic lethal gene function.** In a discrete simulated gene function dataset (shaded for functional levels and pale otherwise) with samples (columns) and genes (rows), genes A and I are SL partners of a “Query” gene. A partner was selected (highlighted in green) randomly in each sample for simulating synthetic lethality, then ordered such that the query gene or an SL partner were functional in each sample.

lethal partners in Figure 3.7) such that the synthetic lethal condition was met: at least one of the synthetic lethal partner genes and the query gene are functional in any particular cell. The samples are ordered by functional data (without assuming correlation of underlying expression values) with the query gene in one direction and the remaining dataset ordered by the selected synthetic lethal partner.

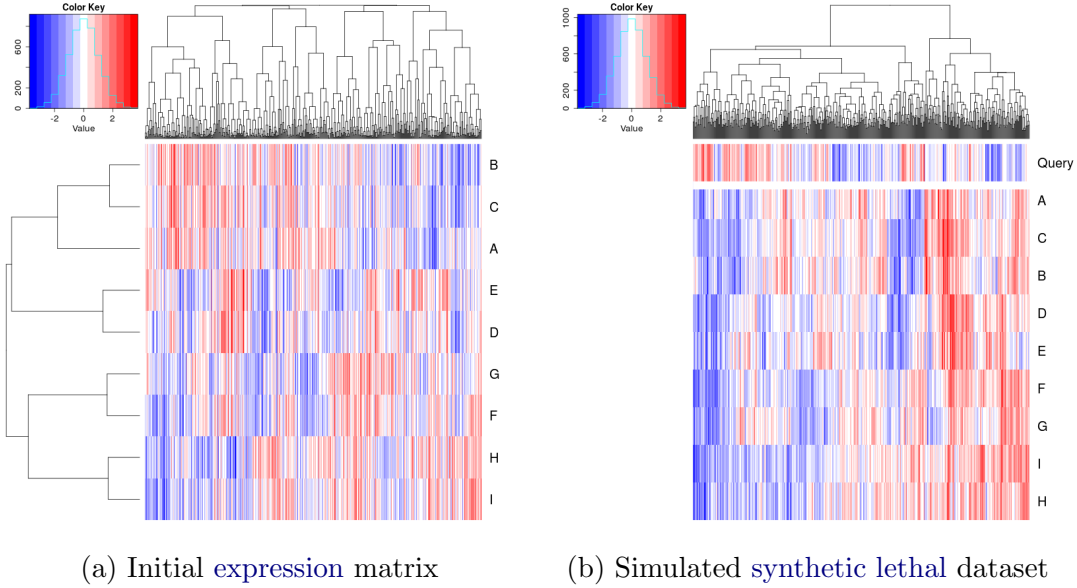


Figure 3.8: **Simulating synthetic lethal gene expression.** A simulated continuous expression dataset (blue–red scale) with samples (columns) and genes A–I (rows) was matched to a query gene such that at least one synthetic lethal partner was above a functional threshold when the query gene was below it which satisfied the synthetic lethal model.

This procedure produces a simulated dataset where samples with a non-functional query gene have at least one functional partner gene. Similarly, the query gene is functional in all samples where all of the synthetic lethal partner genes are non-functional. In this procedure, a dataset has been generated with known synthetic lethal partners (see Figure 3.8) with few assumptions about the relationships between the each synthetic lethal pair (allowing compensating functions from higher-order interactions). This procedure has been designed to have the most stringent (least detectable) synthetic lethal relationships, where higher-order interactions are possible for the purposes of testing pairwise detection procedures such as SLIPT.

### 3.3 Detecting Simulated Synthetic Lethal Partners

The [synthetic lethal](#) detection methodology ([SLIPT](#)), as described in Section 3.1, was evaluated with simulated data containing known [synthetic lethal](#) partners, generated using the procedure described in Section 3.2.2. Simulations were performed to demonstrate the methodology and support its use throughout this thesis. These simulations were performed by sampling from statistical distributions, including the multivariate normal distribution with correlated blocks of genes, generated by  $\Sigma$  matrices such as those shown. A more complex multivariate normal sampling procedure based on pathway [graph](#) structures, as described in section 3.4.2, was used for further investigations in Chapter 6.

#### 3.3.1 Binomial Simulation of Synthetic Lethality

The [synthetic lethal](#) simulation procedure (described in Section 3.2.2) initially used gene function, sampled directly from a binomial distribution using the binomial probability of observing functional gene levels ( $p = 0.3$ ) in one observation ( $n = 1$ ) for each samples:

$$X \sim \text{Bin}(n, p)$$

Once a query gene with [synthetic lethal](#) partners has been added, these functional levels were passed directly into [SLIPT](#) as “low” and “high” samples.

The simulation procedure was performed with 20,000 total genes (as occurs in [expression](#) datasets) with a variable number of true [synthetic lethal](#) partners and 500, 1000, 2000, or 5000 samples. Each [ROC](#) curve was derived from the results of 10,000 replicate simulations. The statistical performance (as shown in Figure 3.9) of the  $\chi^2$ -derived p-value declined towards random predictions (an [AUROC](#) of 0.5) with an more underlying [synthetic lethal](#) partners to detect. However, increased sample size somewhat mitigated this decline, as expected with a statistical predictor, particularly for moderate numbers of [synthetic lethal](#) partners.

Simulations using this binomial model of [synthetic lethality](#) were simplistic but informed the development of more complex simulations including [expression](#) and correlation structures. It did not represent the data that [SLIPT](#) will be applied to but the binomial simulations demonstrated that [SLIPT](#) is able to distinguish small numbers of [synthetic lethal](#) partners in a simulated system with behaviours expected with respect to sample size. This supported further development of the [synthetic lethal](#) model

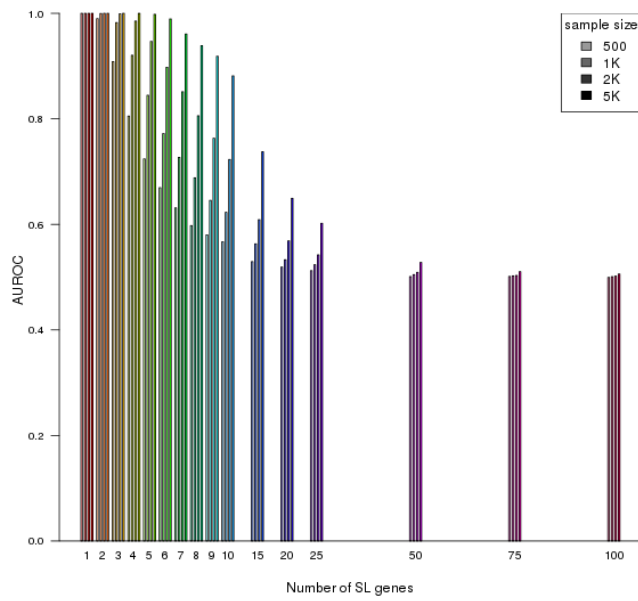


Figure 3.9: **Performance of binomial simulations.** Gene function was simulated by binomial sampling and tested for synthetic lethality by [SLIPT](#). Statistical performance declined with additional synthetic lethal partners but this was mitigated by increased sample sizes.

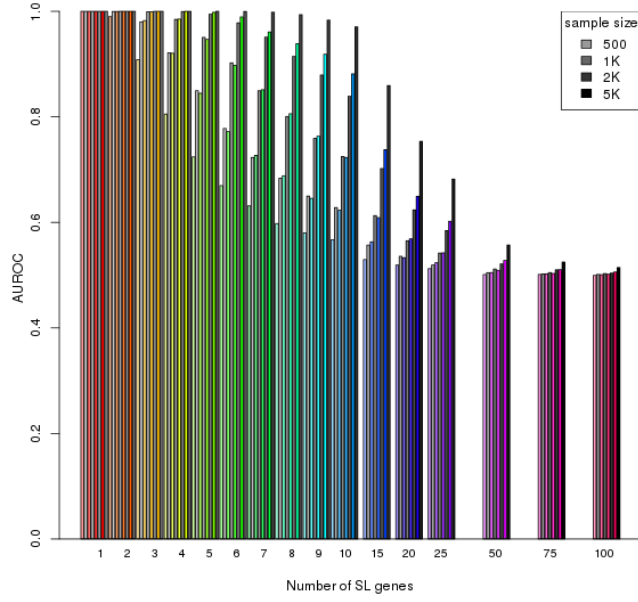


Figure 3.10: **Comparison of statistical performance.** Binomial simulation of synthetic lethality (in colour) in comparison to multivariate normal simulations (in greyscale), in which [SLIPT](#) consistently had higher performance across parameters.

and simulation pipeline (as described in Section 3.2) using the multivariate normal distribution.

The multivariate normal simulation procedure more closely recapitulates the (normalised) `expression` data that **SLIPT** was intended for and enables the methodology procedure to be tested without requiring modifications (in Section 3.3.2). Sampling continuous `expression` values from a normal distribution enabled the `expression` threshold for gene function to differ from the categorical “low” and “high” `expression` binning performed by **SLIPT** (as discussed in Section 3.2.1). The **SLIPT** procedure does not assume a known threshold for `expression` and instead uses `expression` as an estimate of gene function which does not compromise the statistical performance of the **SLIPT** in the multivariate normal simulation. The performance was an improvement over the binomial simulation procedure (shown in Figure 3.10) across simulation parameters in an equivalent simulation (without correlation structure). This multivariate normal model is also more refined since it defines the `synthetic lethal` condition, to ensure that at least one `synthetic lethal` partner was active in query-deficient samples, without disrupting the proportion of samples with each gene being functional.

### 3.3.2 Multivariate Normal Simulation of Synthetic Lethality

The multivariate normal simulation procedure was initially performed using the `mvttnorm` R package (Genz and Bretz, 2009; Genz *et al.*, 2016) (as described in Section 3.2) without correlation structure. Expression was sampled from multivariate normal distribution with a mean ( $\mu = 0$ ), standard deviation ( $\sigma = 1$ ), and no correlation between genes ( $r = 0$ ):

$$X \sim N(\bar{\mu}, \Sigma).$$

Once a query gene with synthetic lethal partners has been added, the simulated `expression` values were tested by **SLIPT**, as described in Section 3.1.

The statistical accuracy of **SLIPT** as a binary classifier was high across simulations of a full dataset of 20,000 genes (shown in Figure 3.11a). Using the  $\chi^2$ -derived p-value as a threshold for prediction, this was largely due to high specificity: the majority of non synthetic lethal genes were distinguished from the underlying `synthetic lethal` genes. Thus the **SLIPT** methodology performed better with larger datasets with more expected negatives and the results of simulations of smaller numbers of genes (e.g., the graph structures analysed in Section 6.2.1) can be applied to larger datasets, where they are expected to perform comparably or better with a lower false negative rate

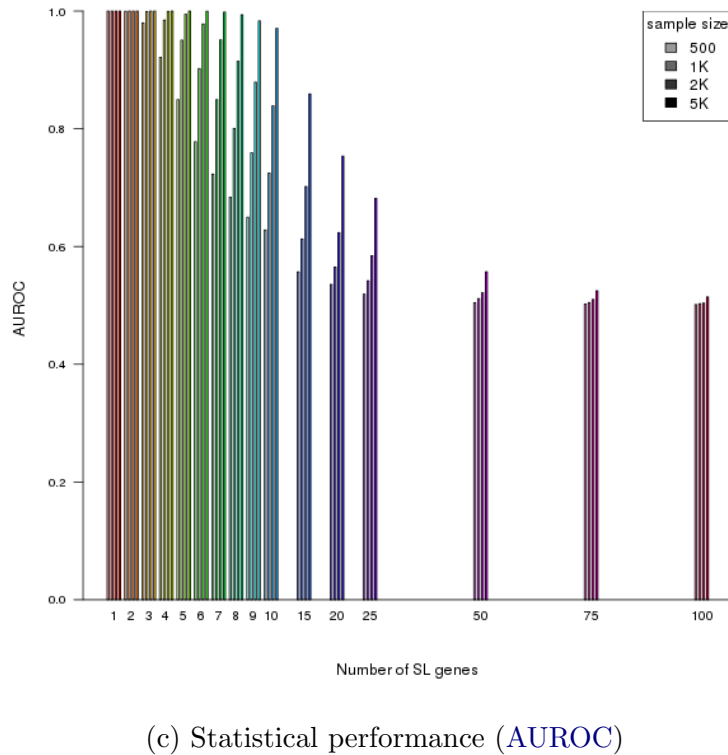
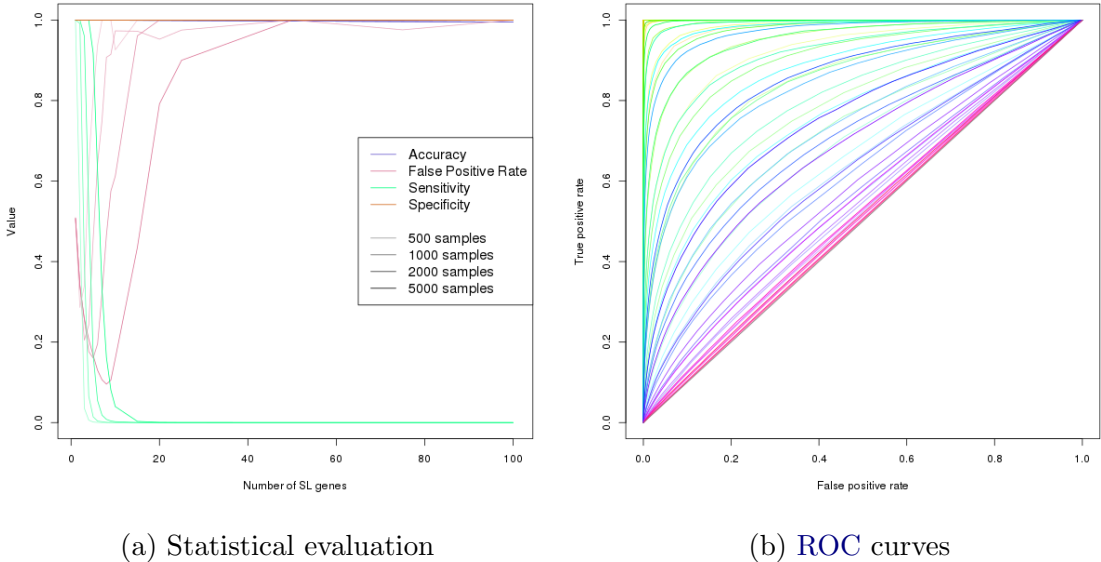


**Figure 3.11: Performance of multivariate normal simulations.** Simulation of synthetic lethality was performed by sampling from a multivariate normal distribution (without correlation structure). Performance of **SLIPT** declined with increasing numbers of synthetic lethal partners but this was mitigated by increased sample sizes (in darker colours). This occurred as the sensitivity decreased with a greater number of true positives to detect, which lead to a trade-off in accuracy as seen in a trough for false positive rate and the **ROC** curves.

(as shown in Sections 6.2.4 and 6.3.2). Accordingly, key results will be supported by replication with larger numbers of non synthetic lethal genes added to the simulations.

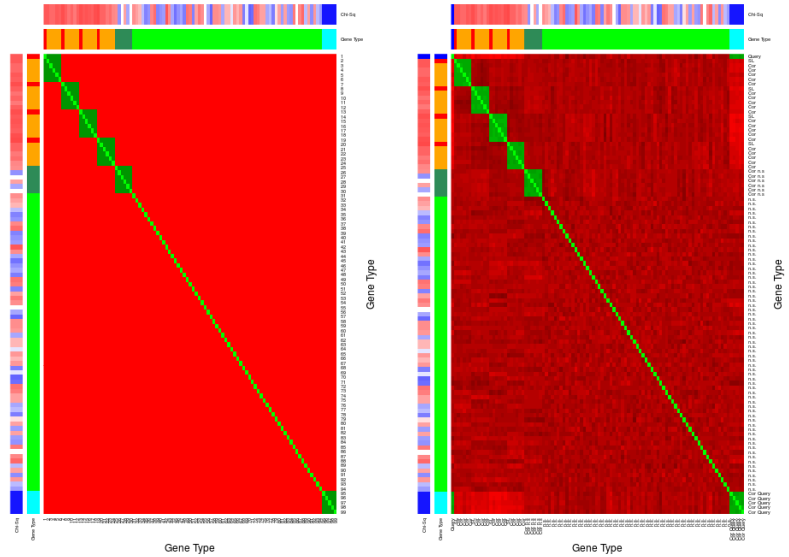
The sensitivity of **SLIPT** as a binary classifier of synthetic lethality (in Figure 3.11a) declined with higher numbers of synthetic lethal genes to detect, although this is somewhat mitigated by higher sample sizes. The minority of true synthetic lethal partners are more difficult to distinguish when there are more of them (with a weaker expression signal from each). While a reduction of the false positive rate could be achieved for moderate numbers of underlying synthetic lethal partners, the number of partners to be detected in analyses of expression data is unknown. However, this simulation procedure is amenable to assessing the performance of **SLIPT** across simulation parameters, graph structures, and comparisons to other approaches (as presented in Chapter 6).

Not all of the genes detected by **SLIPT** were true synthetic lethal genes but they were among the strongest candidates and **SLIPT** had higher performance with fewer underlying synthetic lethal genes to detect. These results support a focus on pathway analyses, in particular, the selection of pathways for further investigation. Pathway over-representation analysis was performed to detect functional groups recurrently detected by **SLIPT** since individually detected gene candidates were not necessarily synthetic lethal. The detection of functionally related genes (in Chapter 4) supports the role of a pathway in synthetic lethal relationships. The use of pathway metagenes can reduce the number of potential pathways, compared to genes, to help identify synthetic lethality. These approaches were both applied in Chapter 4 to identify the synthetic lethal pathways of *CDH1*. Pathways are also more likely to replicate across experimental models, as demonstrated by Dixon *et al.* (2008).

The ROC curves showed that **SLIPT** is subject to a near equal trade-off between sensitivity and specificity across threshold values (in Figure 3.11b). The lower sensitivity and higher specificity with a binary classification (in Figure 3.11a) results from stringent testing by **SLIPT** with FDR adjusted p-values. The area under these curves (AUROC) was used to compare statistical performance (in Figure 3.11c), which had lower performance for more underlying synthetic lethal partners, and higher performance for larger sample size in multivariate normal simulations.

### 3.3.2.1 Multivariate Normal Simulation with Correlated Genes

Correlation structures were added to the simulation procedure (with the  $\Sigma$  matrix, as discussed in Section 3.2), using correlated blocks of genes (as shown in Figure 3.12a). These correlated blocks represent genes with correlated expression, such as co-regulation or shared membership of biological pathways. The example (in Figure 3.12) shows four



(a) Input  $\Sigma$  matrix parameter (b) Simulated correlation matrix

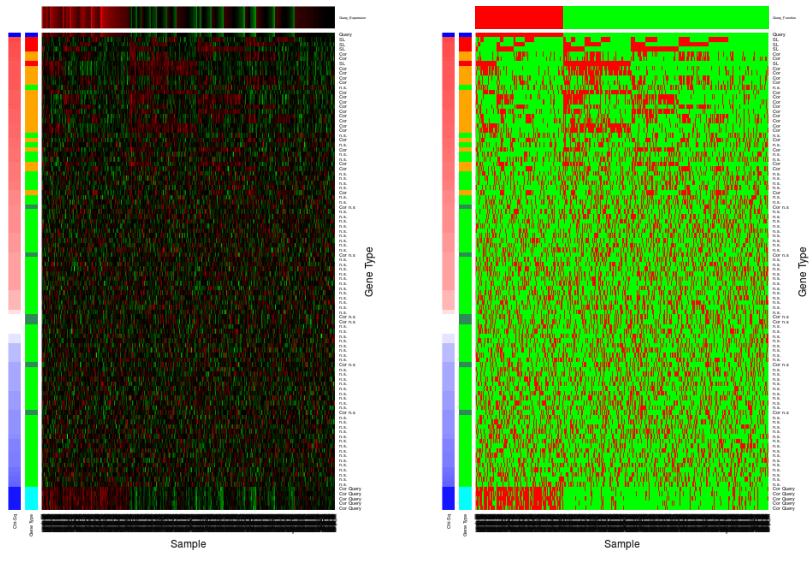


**Figure 3.12: Simulating expression with correlated gene blocks.** A  $\Sigma$  matrix (a) was used to generate 100 genes with a multivariate normal distribution, including correlated blocks of genes ( $r = 0.8$ ) with correlation (b) similar to  $\Sigma$ , on a red-to-green scale. The annotation for genes gives the  $\chi^2$  (in blue for in the direction of SLIPT or red otherwise) and the gene category (blue for query, cyan for query-correlated, red for SL, orange for SL-correlated, forest green for non synthetic lethal-correlated, and light green for non synthetic lethal). The simulated gene expression (c) and function (d) generated were ordered by  $\chi^2$  showing the functional structure of synthetic lethal genes and that they were among the strongest SLIPT results.

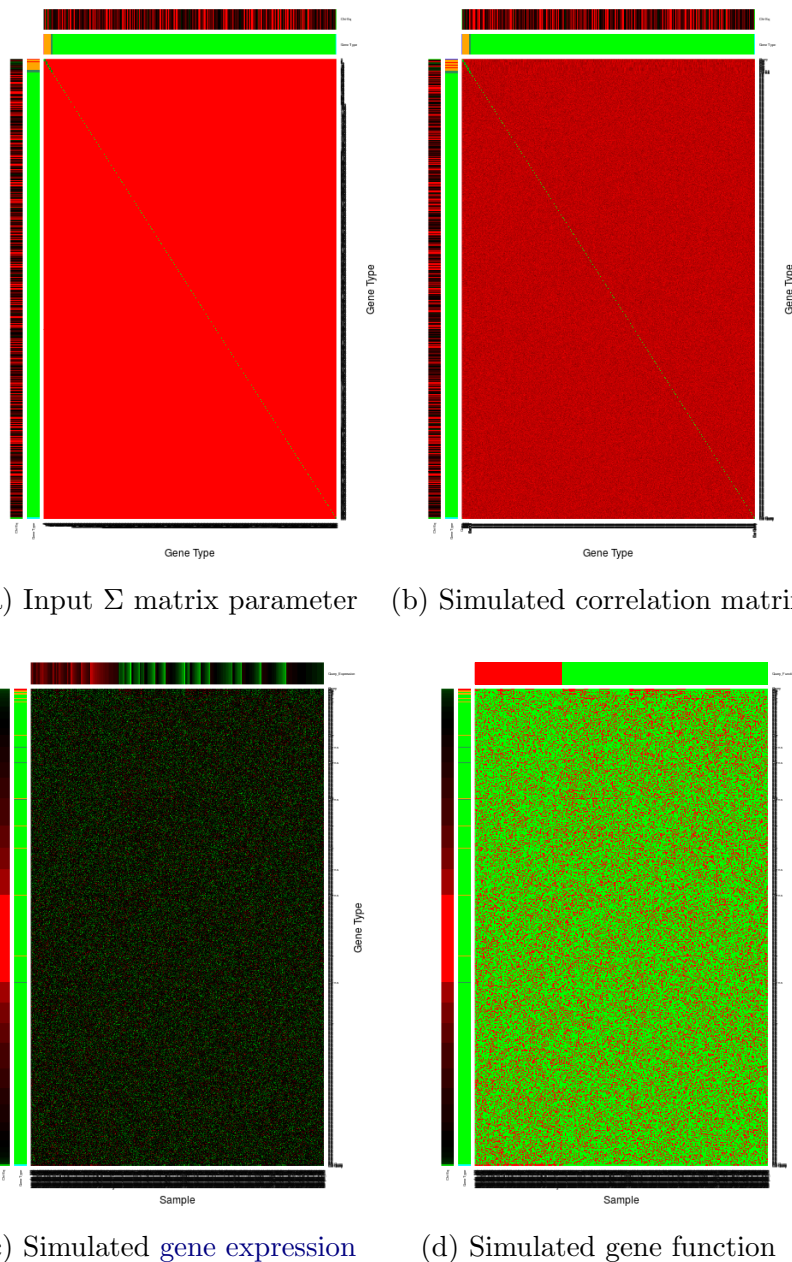


Figure 3.13: **Simulating expression with correlated gene blocks.** Using the  $\Sigma$  matrix (a), sampling 1000 genes from a multivariate normal distribution produced (b) correlated blocks of genes (correlated by 0.8) on a red-to-green scale. The simulated gene expression (c) and function (d) generated were ordered by  $\chi^2$  and SLIPT direction show that synthetic lethal genes are among the strongest SLIPT results with high specificity against many potential false positives. These are annotated for  $\log\chi^2$  (on a red-to-green scale) and category (blue for query, cyan for query-correlated, red for SL, orange for SL-correlated, forest green for non synthetic lethal-correlated, and green for non synthetic lethal) for each gene.

synthetic lethal genes (out of 100), each with five correlated genes that are not themselves synthetic lethal partners of the query gene. These simulations address whether synthetic lethal genes are distinguishable from correlated partners. The  $\Sigma$  matrix produced a similar correlation structure (Figure 3.12b) and expression profiles (Figure 3.12c). Apart from correlated blocks of genes ( $r = 0.8$ ), the remaining genes had small variations due to random sampling. The structure of the dataset, particularly between synthetic lethal genes and the query, was evident in the simulated gene expression (Figure 3.12c) and function (Figure 3.12d). When these genes were ordered by the SLIPT results, the synthetic lethal genes were highly ranked, a the majority of them were distinguishable from highly correlated genes.

The use of correlation structure was applied to larger datasets, such as the 1000 genes shown in Figure 3.13. Synthetic lethal genes were highly ranked by SLIPT and were often distinguishable from correlated genes. As previously discussed in Section 3.3.2, these synthetic lethal genes were still detectable among a larger number of non synthetic lethal genes, and the SLIPT methodology performed better on large datasets.

These plots (Figures 3.12 and 3.13) used similar correlated blocks with a non synthetic lethal gene (true negative) and the query gene (which is not synthetic lethal with itself). Neither of these were synthetic lethal but they could potentially affect performance methodology, particularly the specificity, as correlated non synthetic lethal genes may be distinguishable from synthetic lethal genes. The non synthetic lethal correlated block of genes had no impact on synthetic lethal detection but the query correlated genes were important (as shown in Sections 3.3.2.2 and and 6.1.1.1).

The simulations of gene expression data (with 100 genes) with correlations structure were used to examine the variation between detection in different samples and varying the number of underlying synthetic lethal partners. A small number of simulations (10 for each) are shown to demonstrate the variation between replicate simulations from iterative sampling from the same multivariate normal distribution (in Figure 3.14). These simulations showed that synthetic lethal genes were highly ranked by SLIPT when there are few of them and these were relatively consistent across replicate simulations. However, they were less consistent for higher numbers of synthetic lethal partners to detect and were more difficult to distinguish from other genes, particularly those correlated with them. Similarly, the  $\chi^2$  values showed clear thresholds for synthetic lethal and correlated genes in simple simulations but these were more gradual for higher numbers of synthetic lethal partners.

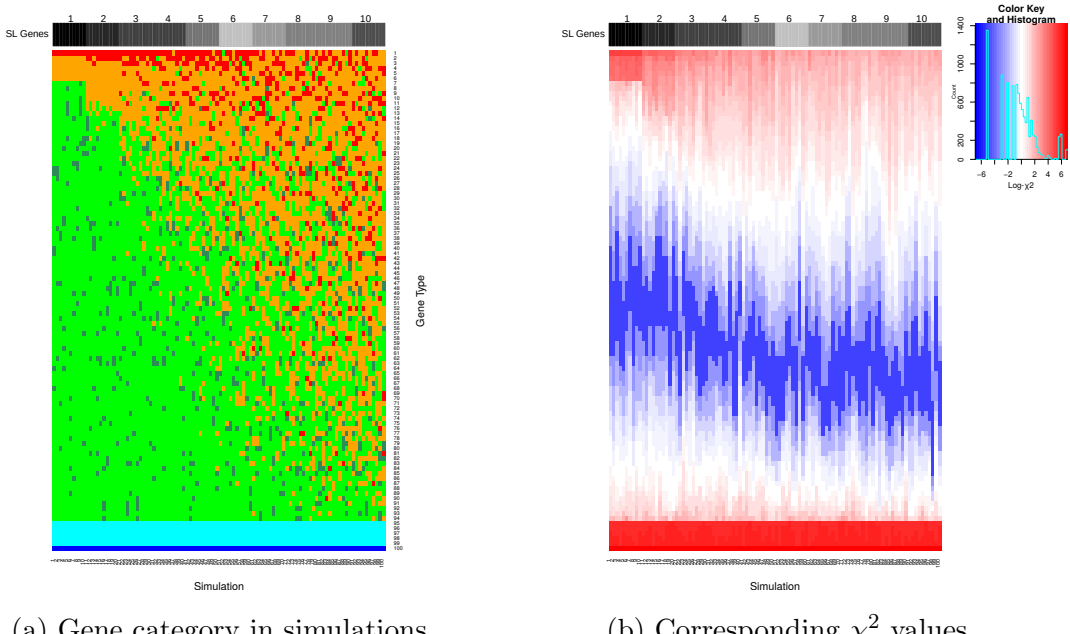
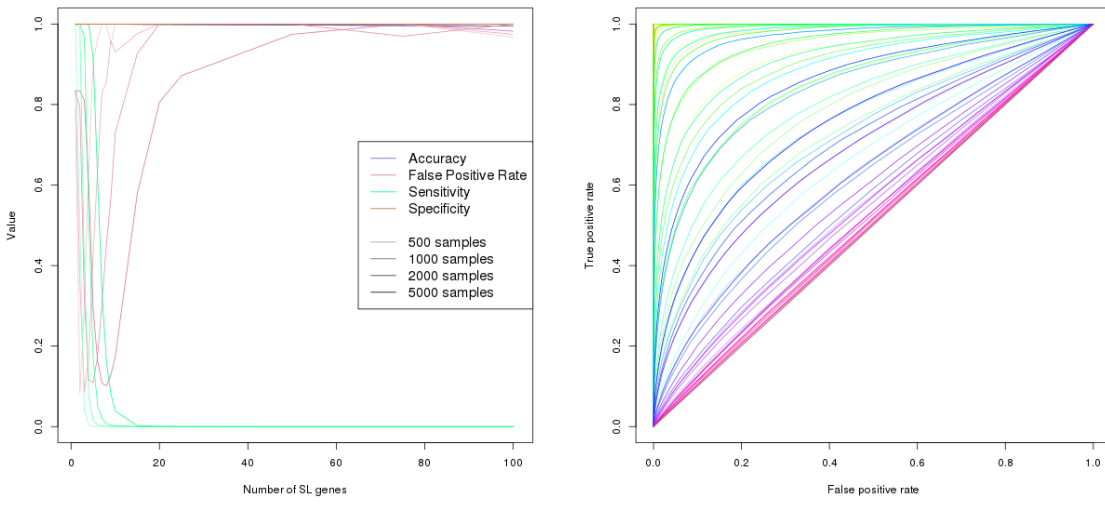


**Figure 3.14: Synthetic lethal prediction across simulations.** The gene category (a) ordered by  $\chi^2$  and the **SLIPT** directional condition is shown across simulations (blue for query, cyan for query-correlated, red for SL, orange for SL-correlated, forest green for non synthetic lethal-correlated, and green for non synthetic lethal). For each number (1–10) of synthetic lethal partners, 10 simulations show that the increasing numbers of synthetic lethal partners became harder detect (i.e., red cells become interspersed in the columns of (a)). The  $\log \chi^2$  values (b) showed a threshold for synthetic lethal and correlated genes when there are fewer of them, distinguishable from correlated genes in this case.

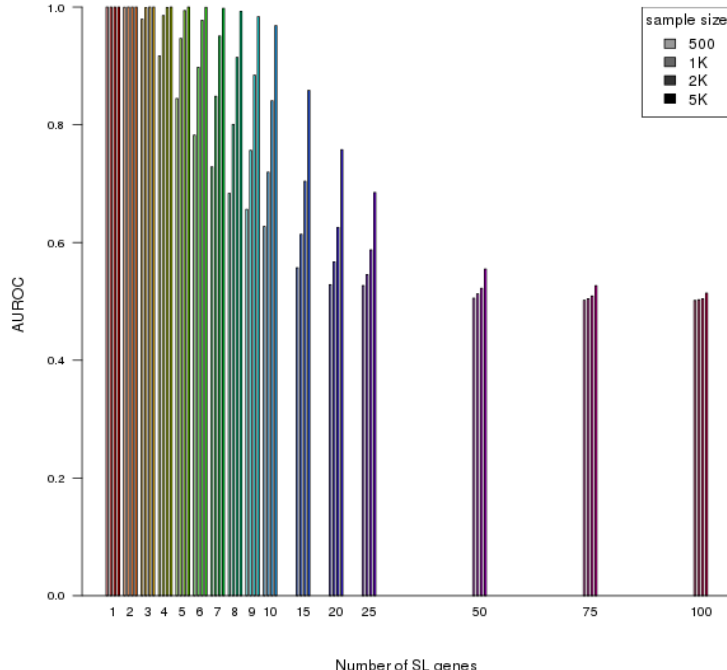
While the synthetic lethal genes were detected in simple simulations (in Figure 3.14), ROC analysis was performed to determine whether they were robustly detectable and to make further comparisons. These results (in Figure 3.15) were similar to simulations without correlation structure. As a binary classifier, **SLIPT** had low sensitivity for higher numbers of synthetic lethal partners to detect and high specificity with the vast majority of non synthetic lethal genes (for 20,000 genes). This was reflected in a similar reduction in statistical performance for higher numbers of synthetic lethal partners and a higher performance with higher sample size. Overall, the statistical performance was no different to simulations without correlation structure (as shown in Figure 3.16).

**SLIPT** was robust across correlation structures and is applicable to gene expression data, with pathway structures and correlations. These correlation structures were not intended to model specific biological pathways or represent them but showed potential



(a) Statistical evaluation

(b) ROC curves



(c) Statistical performance (AUROC)

Figure 3.15: **Performance with correlations.** Simulation of synthetic lethality was performed by sampling from a multivariate normal distribution (with correlation structure). Performance of SLIPT declines for more synthetic lethal partners but this is mitigated by increased sample sizes (darker colours). This generally occurs as the sensitivity decreases for a greater number of true positives to detect, leading to a trade-off in accuracy as seen in a trough for false positive rate and the ROC curves.

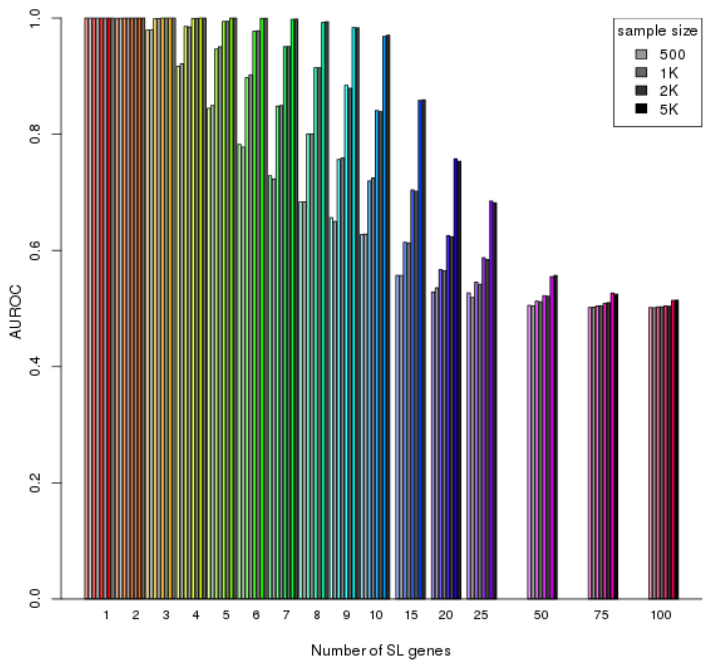


**Figure 3.16: Comparison of statistical performance with correlation structure.** Multivariate simulation of synthetic lethality with correlation structure (in colour) has comparable performance to simulation without correlations (in greyscale) with known synthetic lethal partners across parameters.

impact of correlation structure on the performance of **SLIPT** using highly correlated ( $r = 0.8$ ) gene blocks. More complex correlation structures, such as genes positively correlated with the query gene and derived from pathway graph structures (as described in 3.4.2) were examined further in Sections 3.3.2.2 and 6.2.1 respectively.

In particular, genes correlated with true synthetic lethal genes had little impact on the performance of **SLIPT** detection: synthetic lethal genes were as distinguishable from correlated genes as they are from true negative genes. Genes correlated with synthetic lethal partners did not interfere with the detection of true synthetic lethal genes, although they were often ranked next below them and may support synthetic lethal pathways by having related gene functions.

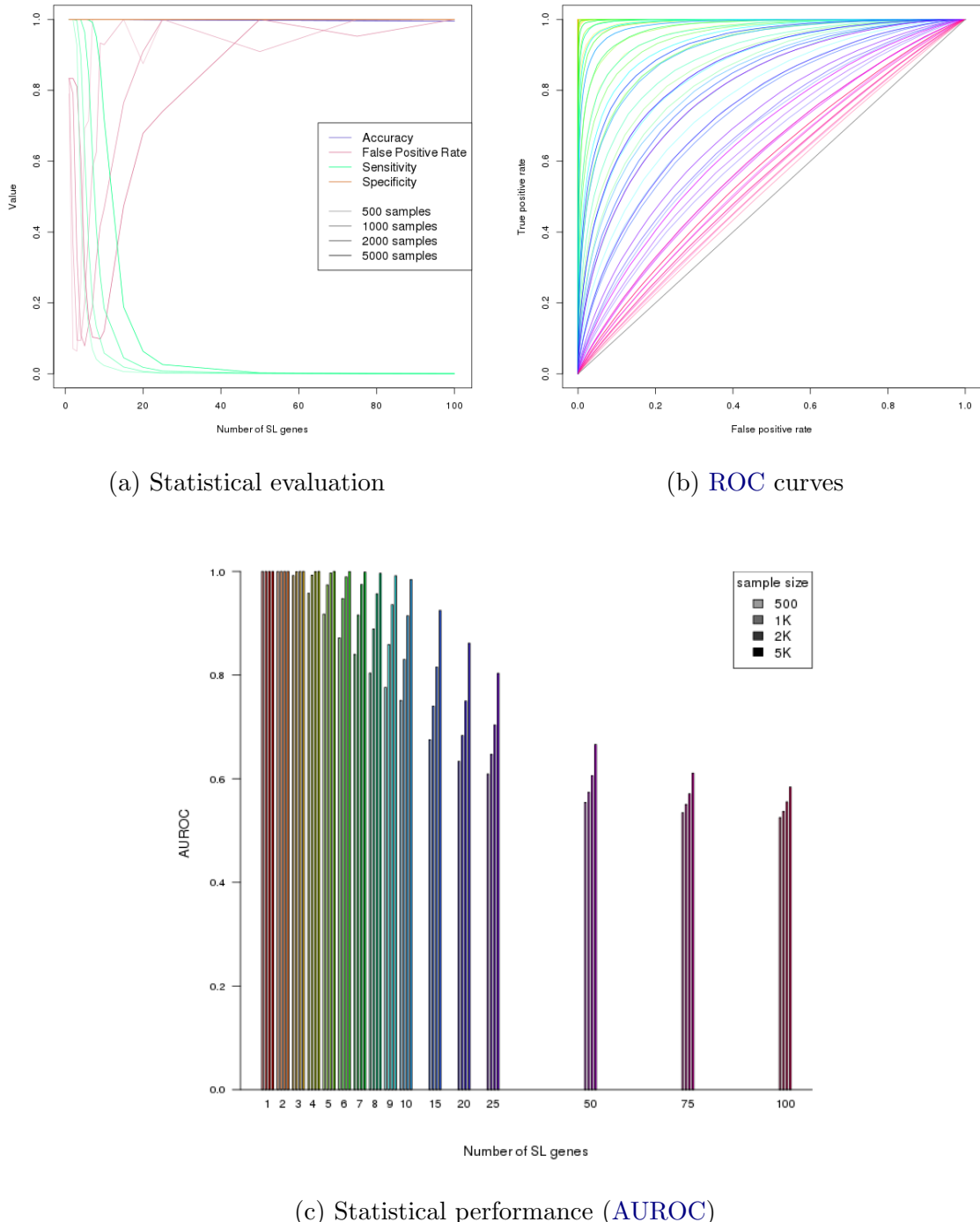


**Figure 3.17: Performance with query correlations.** Simulation of synthetic lethality was performed by sampling from a multivariate normal distribution (with correlation structure including correlated genes with non synthetic lethal and query genes). Performance of SLIPT declined for more synthetic lethal partners and is mitigated by increased sample sizes (darker colours) but the sensitivity remains higher for a greater number of true positives with corresponding improvements in ROC curves.

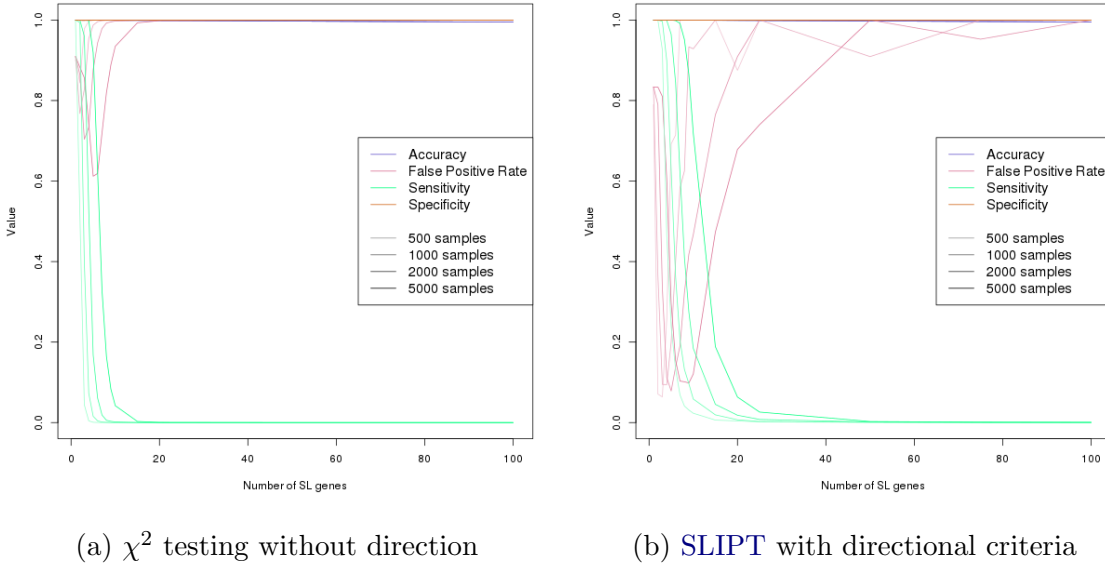


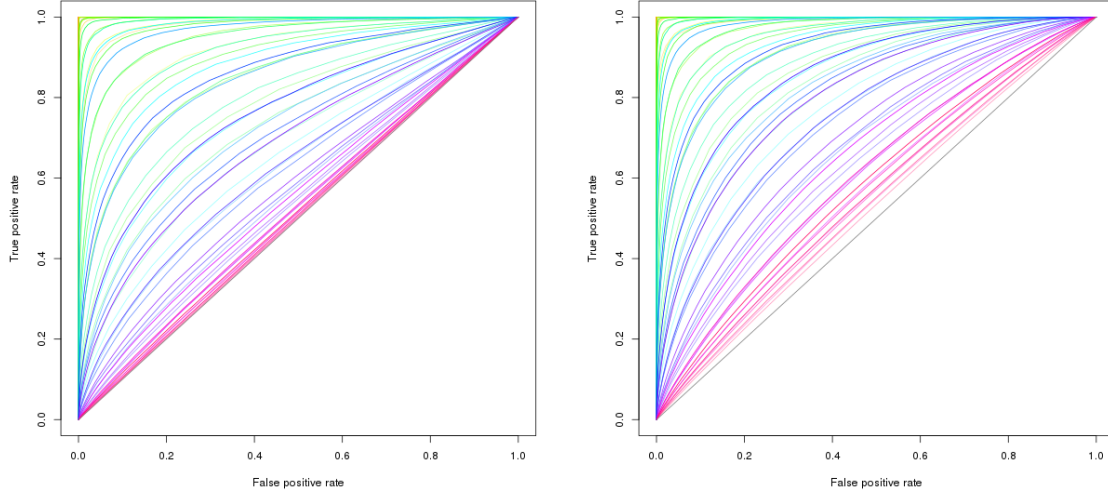
**Figure 3.18: Statistical evaluation of directional criteria.** A simulated multivariate normal dataset of 20,000 genes with correlation structures was tested by **SLIPT** with the directional condition and the  $\chi^2$  test. **SLIPT** exhibited a consistently higher sensitivity and lower false positive rate.

### 3.3.2.2 Specificity with Query-Correlated Pathways

Correlation structures were also considered for non synthetic lethal genes that were (positively) correlated genes with the query gene. Specifically, five highly correlated ( $r = 0.8$ ) with the query gene were added (as described in Section 3.3.2.1). These simulations had similar performance (in Figure 3.17) to those without these correlations with a higher specificity and a lower false positive rate (shown in Figure 3.17a).

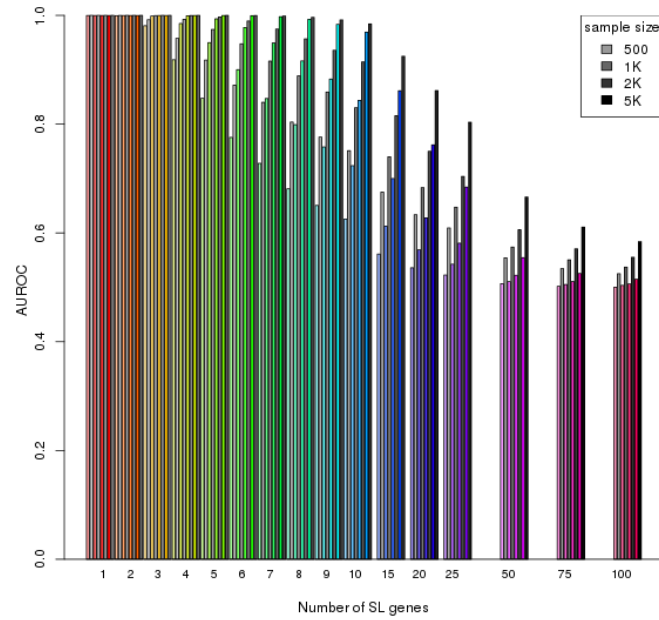
The directional criteria of the **SLIPT** procedure was important in this case, enhancing its performance, particularly in distinguishing positively correlated non synthetic lethal genes. The multivariate normal simulations were performed, with 20,000 genes, including all of the correlation structures discussed (with synthetic lethal, non synthetic lethal, and query correlated genes). These simulations were compared for the direction **SLIPT** and the  $\chi^2$  testing. There was a considerably higher statistical performance with **SLIPT**, particularly increased sensitivity and lower false positive rate (as shown in Figure 3.18).

These results show that the performance of **SLIPT** is appropriate for the analysis of **expression** datasets, where positively correlated genes commonly occur, with the



(a)  $\chi^2$  testing without direction

(b) **SLIPT** with directional criteria



(c) Statistical performance (AUROC)

Figure 3.19: **Performance with directional criteria.** A simulated multivariate normal dataset of 20,000 genes with correlation structures was tested by **SLIPT** and  $\chi^2$  test. **SLIPT** had higher performance across simulation parameters, clearly differing from random (grey diagonal) in ROC curves up to 100 SL genes (b). The performance (c) of **SLIPT** (in greyscale) was consistently higher than the  $\chi^2$  test (in color).

directional condition robustly improving the performance of **SLIPT** across simulation parameters (compared to the  $\chi^2$  test). Without assuming the underlying number of synthetic lethal genes, **SLIPT** will performed than the  $\chi^2$  test alone, irrespective of the significance threshold as shown by **ROC** analysis (in Figure 3.19). The directional **SLIPT** methodology outperformed the  $\chi^2$  test at detecting synthetic lethal partners with even up to 100 synthetic lethal genes.

Together these simulation results support the application of the **SLIPT** methodology as it has been performed throughout Chapters 4 and 5. The methodology and simulation procedure were explored further in Chapter 6, with comparison to other synthetic lethal detection approaches and the inclusion of graph structures.

## 3.4 Graph Structure Methods

Graph structures have been used in several ways in this project, including novel approaches to analysis and simulations. Procedures were developed for statistical and network analysis of gene states in pathway structures. Specifically, the relationships between siRNA and **SLIPT** genes were tested within biological pathways in Chapter 5. These graph structures were also used in Chapter 6 to derive correlation structure between simulated gene expression profiles to represent biological pathways.

### 3.4.1 Upstream and Downstream Gene Detection

Comparison of experimental and computational candidate synthetic lethal partner genes within pathway structures was performed to determine whether these sets of genes were related by pathway structure. Considering the differences in how these candidates were generated, it was unsurprising that they did not detect some identical genes within the candidate biological pathways. However, they could still be related by being upstream or downstream of each other.

Using the Reactome version 52 (Croft *et al.*, 2014), as described in Section 2.4.2, genes detected by each synthetic lethal discovery approach were mapped to the graph structure for each candidate pathway identified in Chapter 4 (with graphs defined as described in Section 2.4.3). To test whether siRNA candidate genes were upstream of **SLIPT** candidate genes, shortest paths were traced between each pair of these genes in a directed network. The paths where the siRNA candidate was upstream (“up”) and downstream (“down”) of a **SLIPT** candidate were scored. This procedure yielded the total number of shortest paths which indicated that siRNA genes were upstream or downstream of the **SLIPT** genes and measured the difference between these to de-

termine if there was an imbalance in a particular direction. While this difference was indicative of the number of paths between the gene candidate groups in either direction, it was not sufficient to statistically verify structure or relationships between **siRNA** and **SLIPT** genes. It was be combined with a permutation resampling procedure (as described in Section 3.4.1.1) to test for directional relationships in either direction.

Initially, this procedure excluded genes that were detected by both approaches since they would count in both directions. Upon further consideration, these genes were restored to accounted for since they may contribute unequally to each gene set if there are unequal numbers of genes above or below them in the **pathway** structure.

### 3.4.1.1 Permutation Analysis for Statistical Significance

A permutation procedure was developed to randomly assign members of the pathway to **siRNA** and/or **SLIPT** groups, with the same number of each candidate partner gene set as observed in the pathway. These permuted genes were measured for **pathway** structure between the permuted gene groups as performed for the observed candidates (as performed in Section 3.4.1). A distribution of **pathway** structure relationships expected by chance was generated by permuting iteratively over these pathways. The resulting null distribution was compared to the observed counts of relationships (in either direction). This procedure yielded a permutation p-value as the proportion of permutations in which had a value greater than the observed value. The null hypothesis was that there was no relationship between these gene groups compared to genes that had been selected at random. Thus both the alternate hypotheses that the **siRNA** genes were either upstream of the **SLIPT** genes or that they are downstream of them were testable.

The permutation procedure does not assume the underlying distribution of the data under the null hypothesis and accounts for the total number of **nodes**, **edges**, **siRNA**, and **SLIPT** genes in each **graph** or **network** pathway structure. The number of genes detected by both **siRNA** and **SLIPT** was not accounted for under the initial **shortest path** counts procedure that excluded them. Once they were included, it was ensured that the number of intersecting genes was equal to the number observed to test for **pathway** structure without changing the intersection size, the subject of prior analyses.

### 3.4.1.2 Hierarchy Based on Biological Context

An alternative approach to **pathway** structure was based on the biological context, given that genes at the upstream and downstream ends of a pathway perform different functions, such as a kinase signalling cascade receiving signals from external stimuli

and passing these on to ribosomes or the nucleus. Genes were assigned to a hierarchy to determine if genes of either candidate group disproportionately performed upstream or downstream functions.

A network-based approach was used to generate the pathway hierarchy of genes in a computationally rational way when applied to different biological pathways with a directed **graph** structure,  $G$  (without loops). The diameter of the network (i.e., the length of the longest possible **shortest path** between the most distant genes) was used to identify a gene ( $z$ ) at the downstream end of the pathway (at the end of a diameter spanning **shortest path**), which was assigned a hierarchy of:

$$\text{hierarchy}(z) = 1 + \text{diameter}(G).$$

Having identified the downstream end of the pathway, genes upstream (e.g., gene  $i$ ) of this were assigned a hierarchy by the length of their **shortest path** ( $d$ ) to this gene  $z$ .

$$\text{hierarchy}(i) = \text{hierarchy}(z) - d_{iz}.$$

The remaining unassigned genes (e.g., gene  $j$ ) gained the hierarchy of the length of the **shortest path** downstream from the nearest assigned gene if possible

$$\text{hierarchy}(j) = \text{hierarchy}(i) + d_{ij}.$$

This process could be performed iteratively to fill in pathway hierarchy but it was not necessary to perform further iterations for the candidate **synthetic lethal** pathways investigated which exhibited strong directional structure and the **small world** property (i.e., had a low diameter). Using this procedure, genes in a pathway **graph** structure were assigned to an integer valued hierarchy upstream to downstream by this procedure:

$$\text{hierarchy} \in \{1, 2, 3, \dots, 1 + \text{diameter}(G)\}$$

This hierarchy of pathway directionality (e.g., that shown in Figure 5.7) was used for comparison with measures of the number of **synthetic lethal** partners detected by either approach.

### 3.4.2 Simulating Gene Expression from Graph Structures

The simulation procedure was refined to generate **expression** data with correlation structure from a known **graph** structure. This enabled modelling of **synthetic lethal** partners within a biological pathway and the investigation of the impact of **pathway** structure on **synthetic lethal** prediction. Firstly, a simulated pathway was constructed

as a `graph` structure, with the `igraph` R package [Csardi and Nepusz \(2006\)](#), with the state of the `edges` (i.e, whether they activate or inhibit downstream pathway members). This simulation procedure was intended for biological pathway members with correlated gene expression (higher than the background of genes in other pathways) but it may also be applicable to modelling protein levels (e.g, in a kinase regulation cascade) or substrates and products (e.g., in a metabolic pathway).

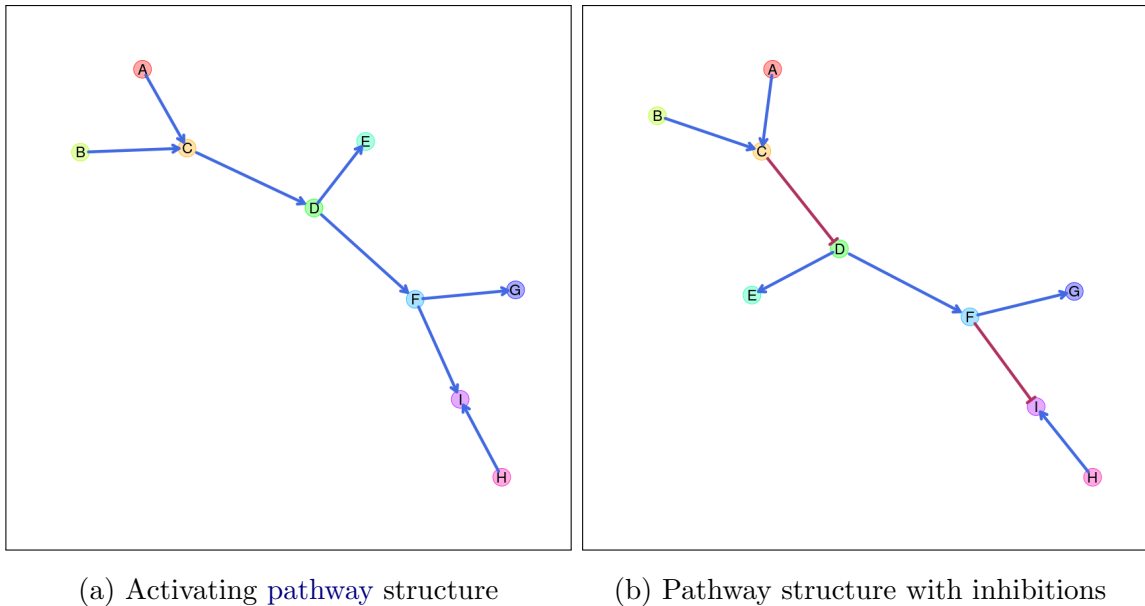
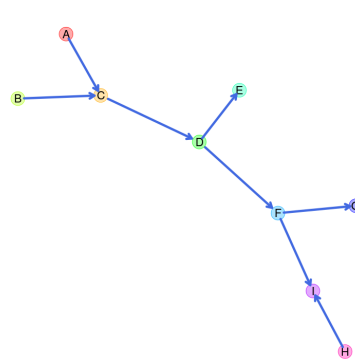


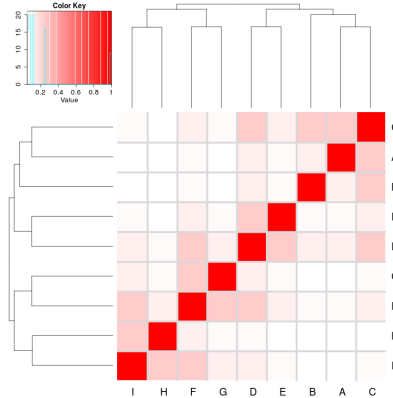
Figure 3.20: **Simulated graph structures.** A constructed `graph` structure used as an example to demonstrate the simulation procedure. Activating `links` are denoted by blue arrows and inhibiting `links` by red edges.

The `graph` structure was constructed from which simulated data will be generated from, sampling a multivariate normal distribution using the `mvtnorm` R package ([Genz and Bretz, 2009; Genz \*et al.\*, 2016](#)). Throughout this section, the simulation procedure will be demonstrated with the relatively simple constructed `graph` structure shown in Figure 3.20. This `graph` structure visualisation was specifically developed for (directed) iGraph objects in R and has been released in the `plot.igraph` package and `igraph.extensions` library (see Table 2.6 and Section 3.5.3). The `plot_directed` function enabled customisation of plot parameters for each `node` or `edge` and mixed (directed) `edge` types for indicating activation or inhibition. These inhibition links (which occur frequently in biological pathways) were demonstrated in Figure 3.20b.

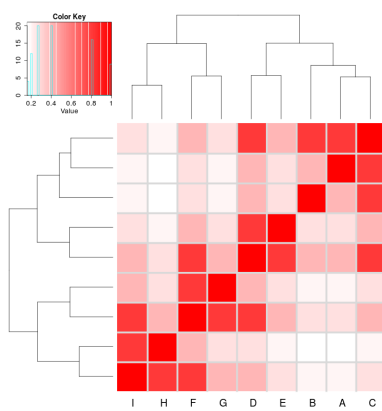
The simulation procedure was designed to use such `graph` structures to inform development of a “Sigma” variance-covariance matrix ( $\Sigma$ ) for sampling from a multi-



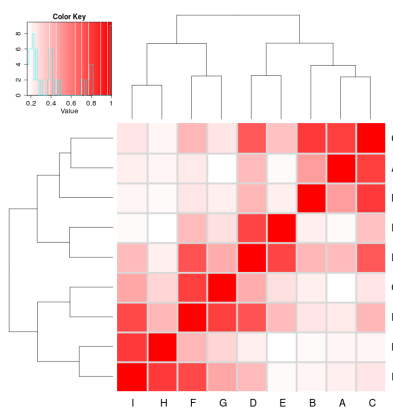
(a) Activating pathway structure



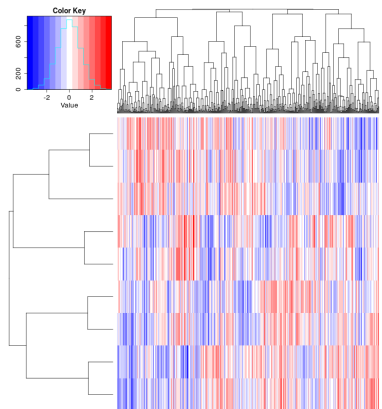
(b) Distance matrix



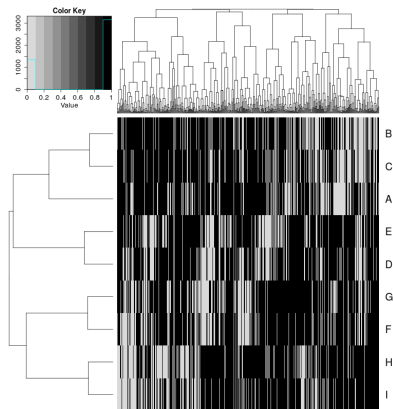
(c)  $\Sigma$  (expected correlation)



(d) Simulated correlation



(e) Simulated expression data



(f) Simulated gene function calls

Figure 3.21: **Simulating expression from a graph structure.** An example graph structure that was used to derive a correlation structure from the relative distances between nodes and simulate continuous gene expression with sampling from the multivariate normal distribution.

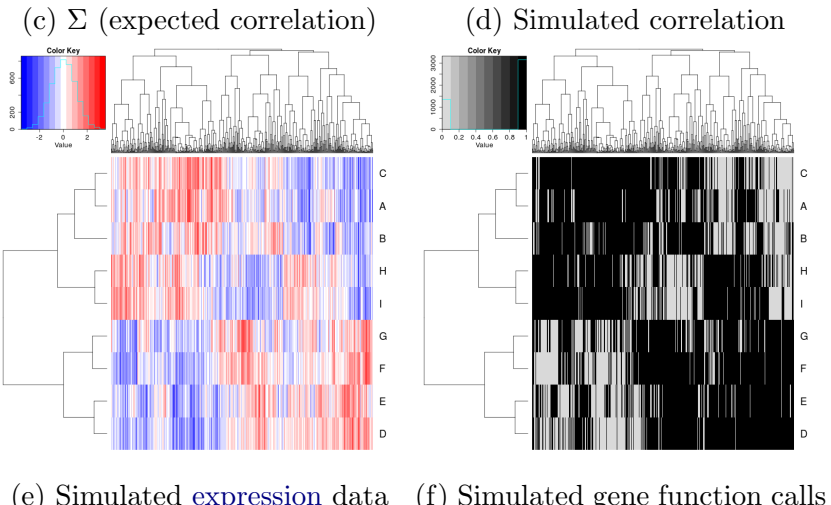
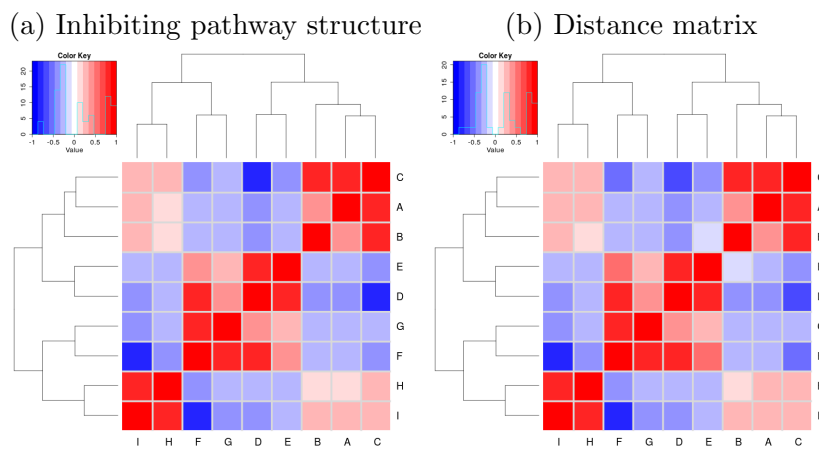
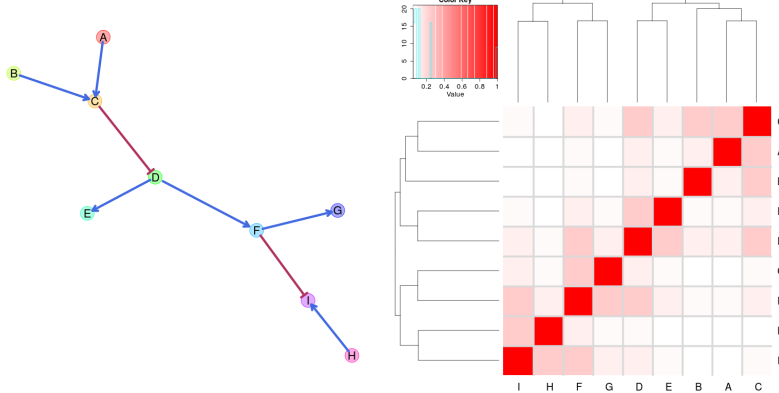


Figure 3.22: **Simulating expression from graph structure with inhibitions.** An example graph structure that was used to derive a correlation structure from the relative distances between nodes and simulate continuous gene expression with sampling from the multivariate normal distribution.

ivariate normal distribution (using the `mvtnorm` R package). Given a `graph` structure (or adjacency matrix), such as Figure 3.21a, a relation matrix was calculated based on distance such that nearer `nodes` are given higher weight than farther `nodes`. Throughout this thesis, a geometrically decreasing (relative) distance weighting was used, with each more distant `node` being related by  $1/2$  compared to the next nearest, as shown in Figure 3.21b. An arithmetically decreasing (absolute) distance weighting is also supported in the `graphsim` R package release of this procedure.

A  $\Sigma$  matrix can be derived from this distance weighting matrix, creating a matrix (with a diagonal of 1) where each `node` has a variance and standard deviation of 1. Thus covariances between adjacent `nodes` were assigned by a correlation parameter and the remaining matrix based on weighting these correlations by the geometrically weighted distance matrix (or the nearest “positive definite” matrix for  $\Sigma$  weighted for negatively correlated inhibitions). Throughout this thesis, the correlation parameter was 0.8, unless otherwise specified (as used for the example in Figure 3.21c). This  $\Sigma$  matrix was then used to sample from a multivariate normal distribution such that each gene had a mean of 0, standard deviation 1, and covariance within the range [0, 1] such that they are correlations. This procedure generated a simulated (continuous normally distributed) `expression` profile for each `node` (as shown in Figure 3.21e) with corresponding correlation structure (Figure 3.21d). The simulated correlation structure closely resembled the expected correlation structure ( $\Sigma$  in 3.21c) even for the relatively modest sample size ( $N = 100$ ) illustrated in 3.21. Once a simulated `gene expression` dataset has been generated (as in Figure 3.21e), then a discrete matrix of gene function was constructed with a functional threshold quantile to simulate functional relationships of `synthetic lethality` (as shown in Figure 3.4). Throughout this thesis, this threshold is the 0.3 quantile (as discussed in Section 3.2.1) which generates functional discrete matrices such as those used for `synthetic lethal` simulation in Section 3.2.2 (as shown Figure 3.21f).

The simulation procedure (depicted in Figure 3.21) can be used for pathways containing inhibition `links` (as shown in Figure 3.22) with several refinements. With the inhibition `links` (as shown in Figure 3.22a), distances were calculated in the same manner as before (Figure 3.22b) with inhibitions accounted for by iteratively multiplying downstream `nodes` by  $-1$  to form blocks of negative correlations (as shown in Figures 3.22c and 3.22d). A multivariate normal distribution with these negative correlations can be sampled to generate simulated data (as shown in Figures 3.22e and 3.22f).

These simulated datasets could then be used for simulating `synthetic lethal` partners

of a query gene within a graph network. The query gene was assumed to be separate from the graph network pathway and was added to the dataset using the procedure in Section 3.2.2. Thus we can simulate known synthetic lethal partner genes within a synthetic lethal partner pathway structure.

## 3.5 Customised Functions and Packages Developed

Various R packages (R Core Team, 2016) have been developed throughout this thesis using `devtools` (Wickham and Chang, 2016) and `roxygen` (Wickham *et al.*, 2017) to enable reproducibility of customised analysis and visualisation. Many of these have been documented, demonstrated in vignettes, and released on GitHub (<https://github.com/TomKellyGenetics>) to enable the research community to utilise them in their own analysis. These are summarised in Table 2.6, with the corresponding urls for their GitHub repository which contains instructions for installation with the `devtools` R package (Wickham and Chang, 2016) and links the relevant vignette(s).

### 3.5.1 Synthetic Lethal Interaction Prediction Tool

The statistical methodology for detection of synthetic lethality in gene expression data (**SLIPT**) is one of the main novel procedures developed in this thesis, as described in Section 3.1. The `slipt` R package has been prepared for release to accompany a publication demonstrating the applications of the methodology for identifying candidate interacting genes and pathways with *CDH1* in breast cancer (Koboldt *et al.*, 2012).

**SLIPT** can be used amenable to analysis of any effectively continuous measure of gene activity (e.g., microarray, RNA-Seq, protein abundance, or pathway metagenes). Executing `slipt` is straightforward: the `prep_data_for_SL` function scores samples as “low”, “medium”, or “high” for each gene, then the `detect_SL` function tests a given query gene against all potential partners by performing the chi-squared test and directional conditions. This function returns a table summarising the observed and expected sample numbers used for the directional criteria, the  $\chi^2$  values, and corresponding p-values including adjusting for multiple comparisons. The `count_of_SL` and `table_of_SL` functions serve to facilitate summary and extraction of the positive **SLIPT** hits, respectively, from the table of predictions of synthetic lethal partners.

The **SLIPT** methodology in this package release was used in later analyses rather than the corresponding source R code, including use on remote machines and upon simulated data. In particular, the functions in the package facilitate alterations to parameters, such as the proportion of samples called as exhibiting low or high gene

activity (as shown in Section 6.1.1). This release supports reproducible research and enables wider use of **SLIPT** in future investigations into other disease genes.

### 3.5.2 Data Visualisation

Customised data visualisations in R (R Core Team, 2016) were developed to present data throughout this thesis. The **vioplotx** and **heatmap.2x** packages are enhancements of the **vioplot** package (Adler, 2005) and **heatmap.2** provided by the **gplots** package (Warnes *et al.*, 2015).

The **vioplotx** package provides an alternative visualisation (of continuous variables against categories) to the more familiar boxplot, showing variability of the data by the width of the plots. As demonstrated in Figure 3.23, this version enables separate plotting parameters for each violin with vector inputs for colour, shape, and size of various elements of the median point, central boxplot, borders, and fill colour for the violin. Scaling violin width to adjust violin area and splitting data by a second categorical variable is also enabled. This function is intended to be backwards compatible with the inputs of **vioplot** (applying scalar inputs across all violins) and **boxplot** (by enabling formula inputs as an S3 method). Each of these features has been demonstrated with examples in respective vignettes on the package GitHub repository (<https://github.com/TomKellyGenetics/vioplotx>).

The **heatmap.2x** function provides extensions for annotation colour bars for both the rows and columns (as shown in Figure 3.24). Multiple bars are enabled on both axes with matrix inputs (rather than single vector for **heatmap.2**) which facilitates additional plotting of gene and sample characteristics for comparison with correlation matrices, **expression** profiles, or pathway **metagenes**. The annotation bar inputs correspond to their orientation on the plot, each colour bar is provided as a column for the row annotation on the left of the heatmap and as a row for the column annotation on top of the heatmap. Row and column annotation bars are labelled with the column or row names respectively. Additional parameters enable resizing of these annotation bar labels and control of reordering columns for when samples have been ordered in advance (e.g., ranked by a **metagene** or split into groups clustered separately). These features were used through this thesis and have been provided in a package GitHub repository (<https://github.com/TomKellyGenetics/heatmap.2x>).

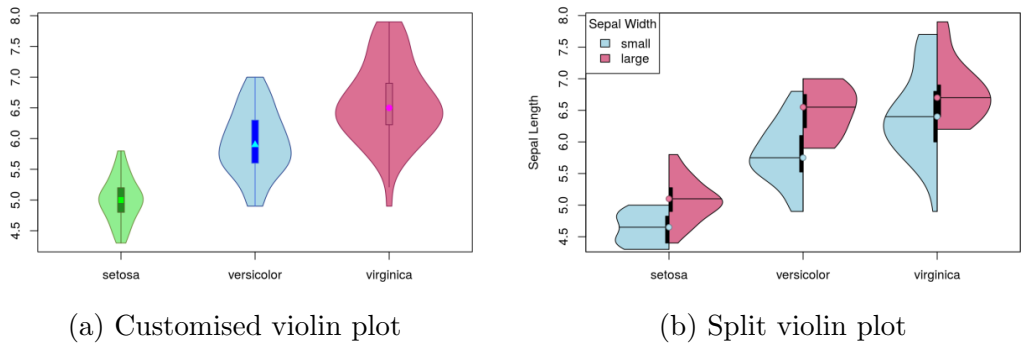


Figure 3.23: **Demonstration of violin plots with custom features.** An example of the *iris* dataset is plotted to show the custom features of the `vioplotx` package including (a) individual colour, shape and size parameters of each violin, scaling violin widths by area, and (b) splitting violins to compare subsets of data.

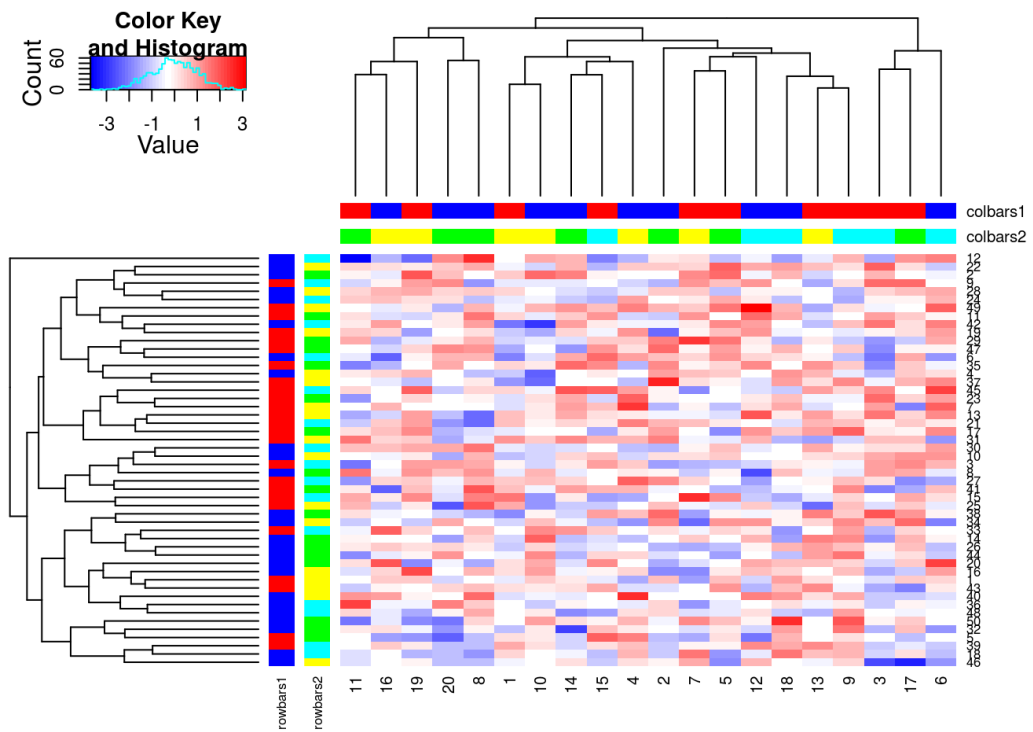


Figure 3.24: **Demonstration of annotated heatmap.** The example heatmap depicts the additional row and column annotation bars enabled by `heatmap.2x`, extending the features of `gplots` with backwards compatible inputs.

### 3.5.3 Extensions to the iGraph Package

The following features were developed during this thesis using “iGraph” data objects, building upon the `igraph` package (Csardi and Nepusz, 2006). These have been released as separate packages for each respective procedure and can be installed together as a collection of extensions to the `igraph` package (<https://github.com/TomKellyGenetics/igraph.extensions>).

#### 3.5.3.1 Sampling Simulated Data from Graph Structures

The `graphsim` package implements the procedure for simulating gene expression from `graph` structures (as described in Section 3.4.2). By default, this derives a matrix with a geometrically decreasing weighting by distance (by `shortest paths`) between each pair of `nodes` with. An absolute decreasing weighting is also available with the option of to derive correlation structures from adjacency matrices or the number of `links` common partners (i.e., size of the shared “neighbourhood” (Hell, 1976)) between each pair of `nodes`. Functions to compute these are called directly by passing parameters to them when running the `generate_expression` or `make_sigma_mat` commands. This package enables simulating `expression` data directly from a `graph` structure (with the intermediate steps automated) or generating  $\Sigma$  parameters for `mvtnorm` from `graph` structures or matrices derived from them. These functions support assignment of activating or inhibiting relationships to each `edge` (with a `state` parameter).

#### 3.5.3.2 Plotting Directed Graph Structures

The `plot.igraph` package provides the `plot_directed` function, specifically developed for directed `graph` structures, to plot activating or inhibiting for each `edge` (as described in Section 3.4.2). As shown in Figure 3.25, this function supports separate plotting parameters for each `node`, `node` label, and `edge`. This includes colours of `node` fill, border, label text, and `edges` and size of `nodes`, `edge` widths, arrowhead lengths, and font size of labels. The `state` parameter for assigning activating or inhibiting to each `edge` determines whether `edges` were depicted with 30° or 90° arrowheads. Colours are assigned separately so they may be customised. Vectorised parameters are applied across each `node` or `edge`, whereas scalar parameters apply the same plotting parameters across them. The default layout function is `layout.fruchterman.reingold` but any layout function supported by `plot` function in `igraph` (Csardi and Nepusz, 2006) was compatible, such as `layout.kamada.kawai` used to implement the Kamada–Kawai algorithm (Kamada and Kawai, 1989) for graph plots throughout this thesis.

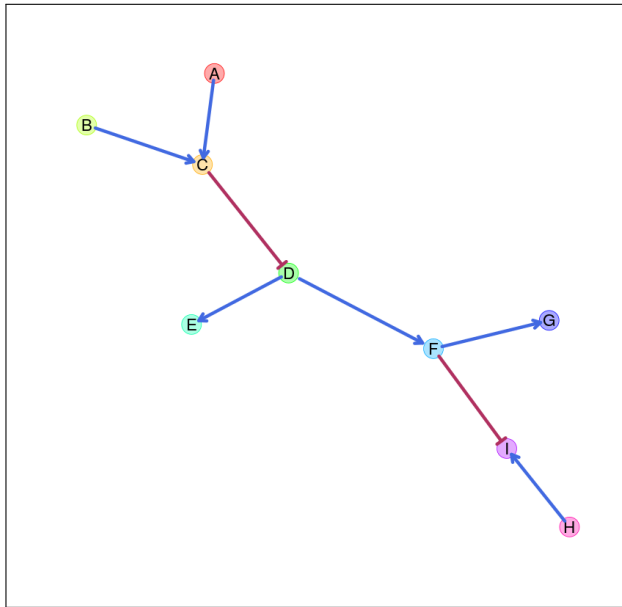


Figure 3.25: **Simulating graph structures.** An example graph structure which has been used throughout demonstrating the simulation procedure from graph structures. Activating links are denoted by blue arrows and inhibiting links by red edges.

### 3.5.3.3 Computing Information Centrality

The shortest paths of a network were computed by the `igraph` package (Csardi and Nepusz, 2006) which can be extended to calculate the network efficiency but was not provided by the package itself (as described in Section 2.4.4). The “information centrality” of a vertex is computed as the relative change in the network efficiency when the vertex is removed. Information centrality is calculated iteratively for each node and the sum of information centrality for each vertex is the information centrality for the network. These metrics were released in the `info.centrality` package (<https://github.com/TomKellyGenetics/info.centrality>).

### 3.5.3.4 Testing Pathway Structure with Permutation Testing

A network-based procedure developed was used to compare of siRNA and SLIPT candidate genes in a pathway structure. Such pathway structure relationships were tested by computing the number of shortest paths between two different groups of nodes in either direction within a graph. This pathway relationship metric was implemented in the `pathway.structure.permutation` package (<https://github.com/TomKellyGenetics/pathway.structure.permutation>) with permutation testing (as described in sections 3.4.1 and 3.4.1.1).

### 3.5.3.5 Metapackage to Install iGraph Functions

These features may be installed together with `igraph.extensions`, which can be accessed from a GitHub repository (<https://github.com/TomKellyGenetics/igraph.extensions>). This meta-package installs `igraph` (Csardi and Nepusz, 2006) and the packages described in Section 3.5.3 including their dependencies for matrix operations and statistical procedures: `Matrix`, `matrixcalc`, and `mvtnorm` (Bates and Maechler, 2016; Genz and Bretz, 2009; Genz *et al.*, 2016; Novomestky, 2012).

# Chapter 4

## Synthetic Lethal Analysis of Gene Expression Data

Having developed a statistical [synthetic lethal](#) detection methodology, [SLIPT](#), it was next applied to publicly available cancer [gene expression](#) datasets. The analysis presented in this Chapter focuses on breast cancer for which [TCGA](#) expression data ([Koboldt \*et al.\*, 2012](#)) from a patient cohort and [siRNA](#) screen data, from experiments conducted in MCF10A cells ([Telford \*et al.\*, 2015](#)), were available. Stomach cancer data ([Bass \*et al.\*, 2014](#)) was used to replicate findings in an independent dataset, with this cancer chosen because it also occurs in syndromic [HDGC](#) patients. The [TCGA](#) data also has the advantages of having other clinical and molecular profiles, including [somatic mutation](#) across many of the same samples, in addition to a considerable sample size for [RNA-Seq](#) expression data generated with common [TCGA](#) procedures to minimise batch effects.

Synthetic lethal candidate partners for *CDH1* were identified at both the gene and pathway level. [SLIPT](#) gene candidates were analysed by cluster analysis for common [expression](#) profiles across samples and relationships with clinical factors and [mutations](#) in key breast cancer genes. These genes were also compared to the gene candidates from primary and secondary (validation) screens conducted by [Telford \*et al.\* \(2015\)](#) on isogenic cell lines. For comparison, the [SLIPT](#) methodology was also applied using [mutation](#) data for *CDH1* against [expression](#) of candidate partners (as described in Section 3.1) which may better represent the null [mutations](#) in [HDGC](#) patients and the experimental cell model ([Chen \*et al.\*, 2014](#)). Pathways were analysed by overrepresentation analysis (with resampling for comparisons with [siRNA](#) data) and supported by a [metagene](#) analysis of pathway gene signatures. The pathway metagene

[expression](#) profiles were used to replicate known relationships between clinical and molecular characteristics for breast cancer and to demonstrate application of [SLIPT](#) directly on [metagenes](#) to detect [synthetic lethal](#) pathways.

## 4.1 Synthetic Lethal Genes in Breast Cancer

The [SLIPT](#) methodology (as described in Section 3.1) was applied to the normalised [TCGA](#) breast cancer [gene expression](#) dataset ( $n = 1168$ ). As shown in Table 4.1, the most significant genes had strong evidence of [expression](#)-based association with *CDH1* (high  $\chi^2$  values) with fewer samples exhibiting low [expression](#) of both genes than expected statistically. Eukaryotic translation genes were among the highest scoring gene candidates, including initiation factors, elongation factors, and ribosomal proteins. These are clearly necessary for cancer cells to grow and proliferate, with sustained [gene expression](#) needed to maintain growth signalling pathways and resist apoptosis or immune factors, translation genes may be subject to [non-oncogene addiction](#) for *CDH1*-deficient cells.

While these are among the strongest [synthetic lethal](#) candidates, translational genes are crucial to the viability of healthy cells and dosing for a selective [synthetic lethal](#) effect against these may be difficult compared to other biological functions which may also be supported among the [SLIPT](#) candidate genes. Furthermore, few known biological functions of *CDH1* were among the strongest SL candidates, so the remaining candidate genes may also be informative since they are likely to contain these expected functions in addition to novel relationships for *CDH1*. Thus further pathway level analyses were also conducted to examine biological functions over-represented among synthetic candidate genes and to identify [synthetic lethal](#) pathways.

The modified [mtSLIPT](#) methodology (as described in Section 3.1) was also applied to the normalised [TCGA](#) breast cancer [gene expression](#) dataset, against [somatic loss of function mutations](#) in *CDH1*. As shown in Appendix Table C.1, the most significant genes also had strong evidence of [expression](#) associated with *CDH1* [mutations](#) (high  $\chi^2$  values) with fewer samples with *CDH1* exhibiting low [expression](#) each candidate gene than expected statistically. These genes were not as strongly supported as the [expression](#) analysis (in Table 4.1), however, nor were as many genes detected. This is perhaps unsurprising due to the lower sample size with matching [somatic mutation](#) data and the lower frequency of *CDH1* [mutations](#) compared to low [expression](#) defined by  $1/3$  quantiles.

The [mtSLIPT](#) candidates had more genes involved in cell and gene regulation,

Table 4.1: Candidate [synthetic lethal](#) gene partners of *CDH1* from SLIPT

Gene	Observed*	Expected*	$\chi^2$ value	p-value	p-value ( <a href="#">FDR</a> )
<i>TRIP10</i>	62	130	162	$5.65 \times 10^{-34}$	$1.84 \times 10^{-31}$
<i>EEF1B2</i>	56	130	158	$3.10 \times 10^{-33}$	$9.45 \times 10^{-31}$
<i>GBGT1</i>	61	131	156	$1.08 \times 10^{-32}$	$3.14 \times 10^{-30}$
<i>ELN</i>	81	130	149	$3.46 \times 10^{-31}$	$8.82 \times 10^{-29}$
<i>TSPAN4</i>	78	130	146	$1.63 \times 10^{-30}$	$3.79 \times 10^{-28}$
<i>GLIPR2</i>	72	130	146	$1.68 \times 10^{-30}$	$3.86 \times 10^{-28}$
<i>RPS20</i>	73	131	145	$1.89 \times 10^{-30}$	$4.28 \times 10^{-28}$
<i>RPS27A</i>	80	130	143	$5.53 \times 10^{-30}$	$1.18 \times 10^{-27}$
<i>EEF1A1P9</i>	63	130	141	$1.91 \times 10^{-29}$	$3.74 \times 10^{-27}$
<i>C1R</i>	73	130	141	$2.05 \times 10^{-29}$	$3.97 \times 10^{-27}$
<i>LYL1</i>	73	130	140	$2.99 \times 10^{-29}$	$5.74 \times 10^{-27}$
<i>RPLP2</i>	71	130	139	$4.88 \times 10^{-29}$	$9.07 \times 10^{-27}$
<i>C10orf10</i>	73	130	138	$6.72 \times 10^{-29}$	$1.20 \times 10^{-26}$
<i>DULLARD</i>	74	131	138	$9.29 \times 10^{-29}$	$1.61 \times 10^{-26}$
<i>PPM1F</i>	64	130	136	$1.61 \times 10^{-28}$	$2.65 \times 10^{-26}$
<i>OBFC2A</i>	69	130	136	$2.49 \times 10^{-28}$	$3.93 \times 10^{-26}$
<i>RPL11</i>	70	130	136	$2.56 \times 10^{-28}$	$3.97 \times 10^{-26}$
<i>RPL18A</i>	70	130	135	$3.08 \times 10^{-28}$	$4.70 \times 10^{-26}$
<i>MFNG</i>	76	131	133	$7.73 \times 10^{-28}$	$1.12 \times 10^{-25}$
<i>RPS17</i>	77	131	133	$8.94 \times 10^{-28}$	$1.29 \times 10^{-25}$
<i>MGAT1</i>	73	130	132	$1.44 \times 10^{-27}$	$2.03 \times 10^{-25}$
<i>RPS12</i>	72	130	128	$8.57 \times 10^{-27}$	$1.12 \times 10^{-24}$
<i>C10orf54</i>	73	130	127	$1.37 \times 10^{-26}$	$1.75 \times 10^{-24}$
<i>LOC286367</i>	72	130	126	$2.20 \times 10^{-26}$	$2.70 \times 10^{-24}$
<i>GMFG</i>	70	130	126	$2.20 \times 10^{-26}$	$2.70 \times 10^{-24}$

Strongest candidate [synthetic lethal](#) partners for *CDH1* by [SLIPT](#) in [TCGA](#) breast cancer expression data

\* Observed and expected numbers of samples which had low [expression](#) of both genes

particularly [DNA](#) and [RNA](#) binding factors. The strongest candidates also included microtubule (*KIF12*), microfibril (*MFAP4*), and cell adhesion (*TENC1*) genes consistent with the established cytoskeletal role of *CDH1*. The elastin gene (*ELN*) was notably strongly supported by both [expression](#) and [mutation](#) [SLIPT](#) analysis of *CDH1* supporting interactions with extracellular proteins and the tumour microenvironment.

#### 4.1.1 Synthetic Lethal Pathways in Breast Cancer

Translational pathways were strongly over-represented in [SLIPT](#) partners, as shown in Table 4.2. These include ribosomal subunits, initiation, peptide elongation, and termination. Regulatory processes involving [mRNA](#) including 3' untranslated region

(UTR) binding, L13a-mediated translational silencing, and nonsense-mediated decay were also implicated. These are consistent with protein translation being subject to “non-oncogene addiction” (Luo *et al.*, 2009), as a core process that is dysregulated to sustain cancer proliferation and survival (Gao and Roux, 2015).

Immune pathways, including the adaptive immune system and responses to infectious diseases were also strongly implicated as synthetic lethal with loss of E-cadherin. This is consistent with the alterations of immune response being a hallmark of cancer Hanahan and Weinberg (2000), since evading the immune system is necessary for cancer survival. Either of these systems are potential means to target *CDH1* deficient cells, although these were not detected in an isolated cell line experimental screen (Telford *et al.*, 2015) and the differences between the findings in patient data are described in more detail in Section 4.2.5.

Table 4.2: Pathways for *CDH1* partners from SLIPT

Pathways Over-represented	Pathway Size	SL Genes	p-value (FDR)
Eukaryotic Translation Elongation	86	81	$1.3 \times 10^{-207}$
Peptide chain elongation	83	78	$5.6 \times 10^{-201}$
Eukaryotic Translation Termination	83	77	$1.2 \times 10^{-196}$
Viral mRNA Translation	81	76	$1.2 \times 10^{-196}$
Formation of a pool of free 40S subunits	93	81	$3.7 \times 10^{-194}$
Nonsense Mediated Decay independent of the Exon Junction Complex	88	77	$5.3 \times 10^{-187}$
L13a-mediated translational silencing of Ceruloplasmin expression	103	82	$9.6 \times 10^{-183}$
3' -UTR-mediated translational regulation	103	82	$9.6 \times 10^{-183}$
GTP hydrolysis and joining of the 60S ribosomal subunit	104	82	$1.9 \times 10^{-181}$
Nonsense-Mediated Decay	103	80	$6.2 \times 10^{-176}$
Nonsense Mediated Decay enhanced by the Exon Junction Complex	103	80	$6.2 \times 10^{-176}$
Adaptive Immune System	412	167	$6.5 \times 10^{-174}$
Eukaryotic Translation Initiation	111	82	$5.7 \times 10^{-173}$
Cap-dependent Translation Initiation	111	82	$5.7 \times 10^{-173}$
SRP-dependent cotranslational protein targeting to membrane	104	79	$2.0 \times 10^{-171}$
Translation	141	91	$6.1 \times 10^{-170}$
Infectious disease	347	146	$1.6 \times 10^{-166}$
Influenza Infection	117	81	$1.9 \times 10^{-163}$
Influenza Viral RNA Transcription and Replication	108	77	$1.9 \times 10^{-160}$
Influenza Life Cycle	112	77	$2.5 \times 10^{-156}$

Gene set over-representation analysis (hypergeometric test) for Reactome pathways in SLIPT partners for *CDH1*.

It is also notable that the pathways over-represented in SLIPT candidate genes have strongly significant over-representation of Reactome pathways based on the hypergeometric test (as described in Section 2.3.2). Even after adjusting stringently for multiple testing, biologically related pathways were supported together. These pathways are further supported by testing for synthetic lethality against *CDH1* mutations

(mtSLIPT) with many of these pathways also among the most strongly supported in this analysis (shown in Appendix Table C.2). This mutation-based analysis more closely represents the null *CDH1* mutations in HDGC (Guilford *et al.*, 1998) and the experimental MCF10A cell model (Chen *et al.*, 2014). There was still support for translational and immune pathways not detected in the isolated experimental system. GPCRs also among the most strongly supported pathways, supporting the experimental findings of Telford *et al.* (2015) for these intracellular signalling pathways already being targeted for other diseases.

#### 4.1.2 Expression Profiles of Synthetic Lethal Partners

Due to the sheer number of gene candidates, investigations proceeded into correlation structure and pathway over-representation. These analyses also examined expression patterns of synthetic lethal gene candidates. This serves to explore the functional similarity of the synthetic lethal partners of *CDH1*, with the eventual aim to assess their utility as drug targets. As shown in Figure 4.1 (which clusters *CDH1* lowly expressing samples separately), there were several large clusters of genes among the expression profiles of the *CDH1* synthetic lethal candidate partners. The clustering suggests co-regulation of genes or pathway correlation between partner gene candidates. A number of candidates from an experimental RNAi screen study performed by Telford *et al.* (2015) were also identified by this approach. In addition, novel gene candidates were also identified, which had not been observed affect viability in isogenic cell line experiments.

In these expression profiles, a gene with a moderate or high signal across samples exhibiting low *CDH1* expression would represent a potential drug target. However, it appears that several molecular subtypes of cancer have elevation of different clusters of synthetic lethal candidates in samples with low *CDH1*. This clustering suggests that different targets (or combinations) could be effective in different patients, suggesting potential utility for stratification. In particular, estrogen receptor negative, basal-like subtype, and “normal-like” tumours (Dai *et al.*, 2015; Eroles *et al.*, 2012; Parker *et al.*, 2009) have elevation of genes specific to particular clusters, indicative of some synthetic lethal interactions being specific to a particular molecular subtype or genetic background. Thus synthetic lethal drug therapy against these subtypes may be ineffective if it were designed against genes in another cluster.

A similar correlation structure was observed among the candidates tested against *CDH1* mutation (mtSLIPT), as shown in Appendix Figure C.1. This clustering analy-

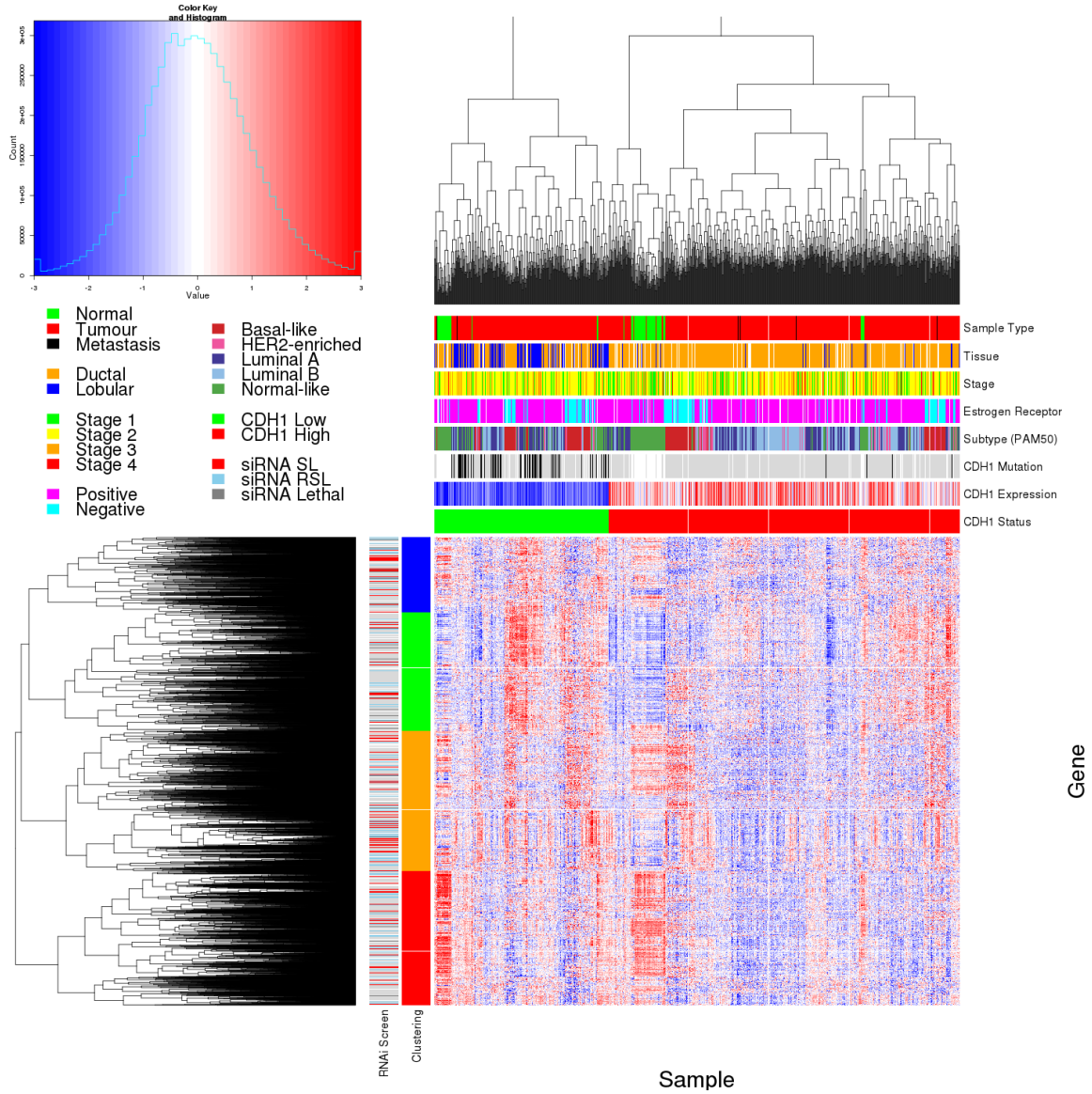


**Figure 4.1: Synthetic lethal expression profiles of analysed samples.** Gene expression profile heatmap (correlation distance, complete linkage) of all samples (separated by the 1/3 quantile of *CDH1* expression) analysed in TCGA breast cancer dataset for gene expression of 5165 candidate partners of E-cadherin (*CDH1*) from SLIPT prediction (with FDR adjusted  $p < 0.05$ ). Deeply clustered, inter-correlated genes form several main groups, each containing genes that were SL candidates or lethal in an siRNA screen (Telford *et al.*, 2015). Screen results for synthetic lethal (SL), the reverse effect (RSL), or lethal cell viability are shown as reported by Telford *et al.* (2015). Clusters had different sample groups highly expressing the synthetic lethal candidates in *CDH1* low samples, notably ‘normal-like’, ‘basal-like’, and estrogen receptor negative samples have elevated expression in one or more distinct clusters showing complexity and variation among candidate synthetic lethal partners. *CDH1* low samples also contained most of samples with *CDH1* mutations (shown in black). Negative values for mutation and screen data are shown in light grey, with missing data in white.

sis similarly identified several major clusters of putative *synthetic lethal* partner genes. In this case, many partner genes had consistently high *expression* across most of the (predominantly lobular subtype) *CDH1* breast cancer samples. However, a major exception to this in the *CDH1 expression* analysis were the normal tissue samples which were excluded from the *mutation* data (as they were not tested for tumour-specific genotypes). This supports *synthetic lethal* interventions being more applicable to *CDH1 mutant* tumours. There was still considerable correlation structure, particularly among *CDH1 wild-type* samples, sufficient to distinguish gene clusters. In contrast to the *expression* analysis the (predominantly ductal *CDH1 wild-type*) basal-like subtype and estrogen receptor negative samples had depleted *expression* among most candidate *synthetic lethal* partners. This is consistent with *synthetic lethal* interventions only being effective in lobular estrogen receptor positive breast cancers in which they are a more common, as recurrent (*driver*) *mutation*. However, the remaining samples are still informative for *synthetic lethal* analysis (by *SLIPT*) as it requires highly expressing *CDH1* samples for comparison.

The *CDH1 mutant* samples (in Figure 4.1) were predominantly among the low *CDH1* expressing samples, clustering throughout them with similar expression profiles to other samples exhibiting low *CDH1* expression. Thus the molecular profiles of *CDH1* low samples were indistinguishable from *CDH1 mutant* samples, with the exception of normal samples (that do not have *somatic mutation* data available). Conversely, many of the *CDH1 mutant* samples (in Appendix Figure C.1) had among the lowest *CDH1 expression*, and some of the *synthetic lethal* partners were also highly expressed in low expressing *CDH1 wild-type* samples, despite these not being considered as “inactivated” by *mtSLIPT* analysis.

Together these results support the use of low *CDH1* expression as a strategy for detecting *CDH1* inactivation. This has the benefit of increasing sample size (including samples such as normal tissue which do not have *somatic mutation* data available) and increasing the expected number of mutually inactive (low-low) samples for the directional criteria of (mt)*SLIPT* which enables it to better distinguish significant deviations below this (as discussed in Section 6.1). This also circumvents the assumption that all (detected) *mutations* are inactivating (although synonymous *mutations* were excluded from the analysis), which may not be the case for several highly expressing *CDH1 mutant* samples that do not cluster together in Figure 4.1 or Appendix Figure C.1. One of these exhibits among the lowest *expression* for many predicted *synthetic lethal* partners and would not be vulnerable to inactivation of these genes.

As such, correctly genotyping inactivating mutations will be essential in clinical practice for synthetic lethal targeting of tumour suppressor genes, particularly for other genes such as *TP53* where oncogenic and tumour suppressor mutations (with different molecular consequences) are both common. Using expression as a measure of gene function also avoids the assumptions that mutations are somatic, rather than germline mutation, and that gene inactivation occurs by detectable mutations, rather than other mechanisms such as epigenetic changes. These may also account for some of the lowly expressing *CDH1* wild-type samples clustering with similar profiles to mutant samples.

#### 4.1.2.1 Subgroup Pathway Analysis

Synthetic lethal gene candidates for *CDH1* from SLIPT analysis of RNA-Seq gene expression data were also used for pathway over-representation analyses (as described in Section 2.3.2). The correlation structure in the expression of candidates synthetic lethal genes in *CDH1* low tumours (lowest 1/3<sup>rd</sup> quantile of expression) was examined for distinct biological pathways in subgroups of genes elevated in different clusters of samples. These genes were highly expressed in different samples with their clinical factors including estrogen receptor status and intrinsic subtypes, from the PAM50 procedure (Parker *et al.*, 2009) shown in Figure 4.1.

As shown by the most over-represented pathways in Table 4.3, each correlated cluster of candidate synthetic lethal partners of *CDH1* contains functionally different genes. Cluster 1 contains genes with less evidence of over-represented pathways than other clusters, corresponding to less correlation between genes within the cluster, and to it being a relatively small group. While there is some indication that collagen biosynthesis, microfibril elastic fibres, extracellular matrix, and metabolic pathways may be over-represented in Cluster 1, these results are mainly based on small pathways containing few synthetic lethal genes. Genes in Cluster 2 exhibited low expression in normal tissue samples compared to tumour samples (see Figure 4.1) and show compelling evidence of over-representation of post-transcriptional gene regulation and protein translation processes. Similarly, Cluster 3 has over-representation of immune signalling pathways (including chemokines, secondary messenger, and TCR signalling) and downstream intracellular signalling cascades such as GPCR and G<sub>αi</sub> signalling events. While pathway over-representation was weaker among genes in Cluster 4, they contained intracellular signalling pathways and were highly expressed in normal samples (in contrast to Cluster 2). Cluster 4 also involved extracellular factors and stimuli such as extracellular matrix, platelet activation, ligand receptors, and retinoic acid signalling.

Based on these results, potential synthetic lethal partners of *CDH1* include pro-

Table 4.3: Pathways for clusters of *CDH1* partners from SLIPT

Pathways Over-represented in Cluster 1	Pathway Size	Cluster Genes	p-value (FDR)
Collagen formation	67	10	$4.0 \times 10^{-11}$
Extracellular matrix organisation	238	21	$1.8 \times 10^{-9}$
Collagen biosynthesis and modifying enzymes	56	8	$1.8 \times 10^{-9}$
Uptake and actions of bacterial toxins	22	5	$9.5 \times 10^{-9}$
Elastic fibre formation	37	6	$1.9 \times 10^{-8}$
Muscle contraction	62	7	$2.4 \times 10^{-7}$
Fatty acid, triacylglycerol, and ketone body metabolism	117	10	$4.9 \times 10^{-7}$
XBP1(S) activates chaperone genes	51	6	$6.6 \times 10^{-7}$
IRE1alpha activates chaperones	54	6	$1.2 \times 10^{-6}$
Neurotoxicity of clostridium toxins	10	3	$1.3 \times 10^{-6}$
Retrograde neurotrophin signalling	10	3	$1.3 \times 10^{-6}$
Assembly of collagen fibrils and other multimeric structures	40	5	$1.9 \times 10^{-6}$
Collagen degradation	58	6	$2.0 \times 10^{-6}$
Arachidonic acid metabolism	41	5	$2.1 \times 10^{-6}$
Synthesis of PA	26	4	$3.0 \times 10^{-6}$
Signalling by NOTCH	80	7	$3.3 \times 10^{-6}$
Signalling to RAS	27	4	$3.7 \times 10^{-6}$
Integrin cell surface interactions	82	7	$4.2 \times 10^{-6}$
Pathways Over-represented in Cluster 2	Pathway Size	Cluster Genes	p-value (FDR)
Eukaryotic Translation Elongation	86	75	$1.1 \times 10^{-181}$
Viral mRNA Translation	81	72	$9.8 \times 10^{-179}$
Peptide chain elongation	83	72	$1.9 \times 10^{-175}$
Eukaryotic Translation Termination	83	72	$1.9 \times 10^{-175}$
Formation of a pool of free 40S subunits	93	75	$1.9 \times 10^{-171}$
Nonsense Mediated Decay independent of the Exon Junction Complex	88	72	$9.9 \times 10^{-168}$
L13a-mediated translational silencing of Ceruloplasmin expression	103	75	$3.0 \times 10^{-159}$
3' -UTR-mediated translational regulation	103	75	$3.0 \times 10^{-159}$
Nonsense-Mediated Decay	103	75	$3.0 \times 10^{-159}$
Nonsense Mediated Decay enhanced by the Exon Junction Complex	103	75	$3.0 \times 10^{-159}$
SRP-dependent cotranslational protein targeting to membrane	104	75	$3.2 \times 10^{-158}$
GTP hydrolysis and joining of the 60S ribosomal subunit	104	75	$3.2 \times 10^{-158}$
Eukaryotic Translation Initiation	111	75	$4.5 \times 10^{-151}$
Cap-dependent Translation Initiation	111	75	$4.5 \times 10^{-151}$
Influenza Infection	117	75	$1.4 \times 10^{-145}$
Influenza Viral RNA Transcription and Replication	108	72	$5.7 \times 10^{-145}$
Translation	141	81	$8.0 \times 10^{-143}$
Influenza Life Cycle	112	72	$2.3 \times 10^{-141}$
Pathways Over-represented in Cluster 3	Pathway Size	Cluster Genes	p-value (FDR)
Adaptive Immune System	412	90	$6.1 \times 10^{-61}$
Chemokine receptors bind chemokines	52	27	$6.7 \times 10^{-56}$
Generation of second messenger molecules	29	21	$6.5 \times 10^{-55}$
Immunoregulatory interactions between a Lymphoid and a non-Lymphoid cell	64	29	$6.5 \times 10^{-55}$
TCR signalling	62	27	$8.9 \times 10^{-51}$
Peptide ligand-binding receptors	161	40	$1.5 \times 10^{-45}$
Translocation of ZAP-70 to Immunological synapse	16	14	$3.1 \times 10^{-43}$
Costimulation by the CD28 family	51	22	$4.0 \times 10^{-43}$
PD-1 signalling	21	15	$4.0 \times 10^{-41}$
Class A/1 (Rhodopsin-like receptors)	258	50	$6.7 \times 10^{-41}$
Phosphorylation of CD3 and TCR zeta chains	18	14	$1.3 \times 10^{-40}$
Interferon gamma signalling	74	24	$5.0 \times 10^{-39}$
GPCR ligand binding	326	57	$1.8 \times 10^{-38}$
Cytokine Signalling in Immune system	268	48	$8.9 \times 10^{-37}$
Downstream TCR signalling	45	18	$1.8 \times 10^{-35}$
G <sub>αi</sub> signalling events	167	33	$2.2 \times 10^{-33}$
Cell surface interactions at the vascular wall	99	21	$1.3 \times 10^{-26}$
Interferon Signalling	164	28	$1.7 \times 10^{-26}$
Pathways Over-represented in Cluster 4	Pathway Size	Cluster Genes	p-value (FDR)
Extracellular matrix organisation	238	48	$8.0 \times 10^{-41}$
Class A/1 (Rhodopsin-like receptors)	258	47	$2.8 \times 10^{-36}$
GPCR ligand binding	326	54	$2.1 \times 10^{-34}$
G <sub>αs</sub> signalling events	83	22	$1.4 \times 10^{-31}$
GPCR downstream signalling	472	68	$1.1 \times 10^{-29}$
Haemostasis	423	61	$3.3 \times 10^{-29}$
Platelet activation, signalling and aggregation	180	31	$7.1 \times 10^{-28}$
Binding and Uptake of Ligands by Scavenger Receptors	40	14	$9.9 \times 10^{-27}$
RA biosynthesis pathway	22	11	$2.5 \times 10^{-26}$
Response to elevated platelet cytosolic Ca <sup>2+</sup>	82	19	$3.0 \times 10^{-26}$
Developmental Biology	420	57	$3.5 \times 10^{-26}$
G <sub>αi</sub> signalling events	167	28	$7.3 \times 10^{-26}$
Platelet degranulation	77	18	$1.6 \times 10^{-25}$
Gastrin-CREB signalling pathway via PKC and MAPK	171	28	$2.5 \times 10^{-25}$
Muscle contraction	62	16	$4.7 \times 10^{-25}$
G <sub>αo</sub> signalling events	150	25	$3.2 \times 10^{-24}$
Retinoid metabolism and transport	34	12	$5.0 \times 10^{-24}$
Phase 1 - Functionalisation of compounds	67	16	$6.5 \times 10^{-24}$

Pathway over-representation analysis for Reactome pathways with the number of genes in each pathway (Pathway Size), number of genes within the pathway identified (Cluster Genes), and the pathway over-representation p-value (adjusted by FDR) from the hypergeometric test.

cesses known to be dysregulated in cancer, such as translational, cytoskeletal, and immune processes. Intracellular signalling cascades such as the GPCRs and extracellular stimuli for these pathways were also implicated in potential synthetic lethality with *CDH1*.

Similar translational, cytoskeletal, and immune processes were identified among SLIPT partners with respect to *CDH1* mutation, shown in Appendix Table C.3. While GPCR signalling was replicated in mtSLIPT analysis, there was also stronger over-representation for NOTCH, ERBB2, and PI3K/AKT signalling in mutation analysis consistent with these signals being important for proliferation of *CDH1* deficient tumours. The GPCR and PI3K/AKT pathways are of particular interest as pathways with oncogenic mutations that can be targeted and downstream effects on translation (a strongly supported process across analyses). Extracellular matrix pathways (e.g., elastic fibre formation) were also supported across analyses (in Table 4.3 and Appendix Table C.3) consistent with the established cell-cell signalling role of *CDH1* and the importance of the tumour microenvironment for cancer proliferation.

## 4.2 Comparing Synthetic Lethal Gene Candidates

### 4.2.1 Primary siRNA Screen Candidates

Gene candidates were compared between computational (SLIPT in TCGA breast cancer data) and experimental (the primary siRNA screen performed by Telford *et al.* (2015)) approaches in Figure 4.2. The number of genes detected by both methods did not produce a significant overlap but these may be difficult to compare due to vast differences between the detection methods. There were similar issues in the comparison of mtSLIPT genes tested against *CDH1* mutations (in Appendix Figure C.2), despite excluding genes not tested by both methods in either test. However, these intersecting genes may still be functionally informative or amenable to drug triage as they were replicated across both methods and pathway over-representation differed between the sections of the Venn diagram (see Figure 4.2).

### 4.2.2 Comparison with Correlation

Another potential means to triage drug target candidates is by correlation of expression profiles with *CDH1*. Correlation with *CDH1* was compared to SLIPT and siRNA results in Figure 4.3. The genes not detected by SLIPT (including siRNA candidates) included genes with non-significant SLIPT p-values. As expected, these genes were distributed around a correlation of zero. Genes with higher correlation with *CDH1*

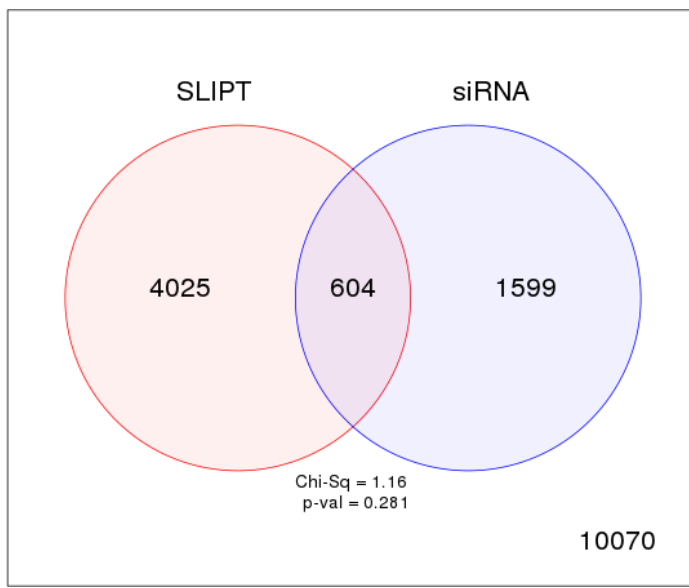


Figure 4.2: **Comparison of SLIPT with siRNA.** Testing the overlap of gene candidates for E-cadherin synthetic lethal partners between computational (**SLIPT**) and experimental screening (**siRNA**) approaches. The  $\chi^2$  test suggests that the overlap is no more than would be expected by chance ( $p = 0.281$ ). Only genes tested by both methods were included.

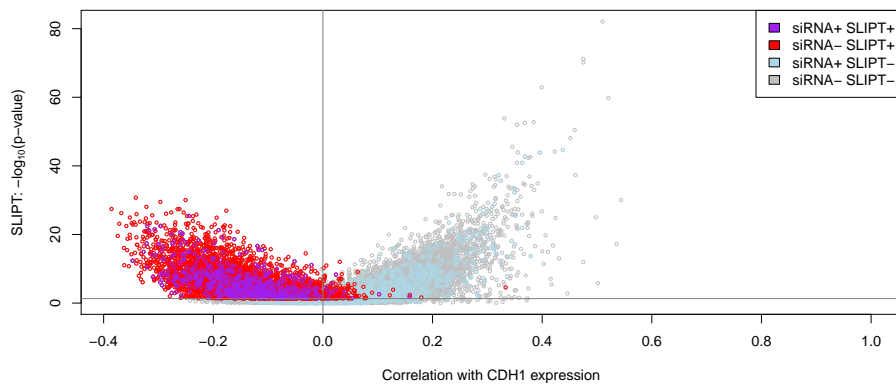


Figure 4.3: **Comparison of SLIPT and siRNA genes with correlation.** The  $\chi^2$  p-values for genes tested by **SLIPT** (in TCGA breast cancer) expression analysis were compared against Pearson correlation of gene expression with *CDH1*. Genes detected by **SLIPT** or **siRNA** are coloured according to the legend.

(either direction) were more significant, although there were exceptions to this trend and larger positive correlations than negative correlations. The majority of **SLIPT** candidates had negative correlations, particularly genes detected by both approaches, although these were typically weak correlations and are unlikely to be sufficient to detect such genes on their own. This is supported by simulation results in Section 6.1.

There were not strong positive correlations with *CDH1* among **siRNA** candidates, consistent with previous findings that co-expression was not predictive of **synthetic lethality** (Jerby-Arnon *et al.*, 2014; Lu *et al.*, 2015). Negative correlation may not be indicative of **synthetic lethality** either as many **siRNA** candidates also had positive correlations. The **SLIPT** methodology has shown to detect genes with both positive and negative correlations, although it does appear to preferentially detect negatively correlated genes to some extent. These findings were replicated with the **mtSLIPT** approach against *CDH1* **mutation** (in Appendix Figure C.3), although the range of the  $\chi^2$  p-values differs due to lower sample size for **mutation** analysis.

The apparent tendency for genes detected by **SLIPT** or **siRNA** to have negative correlations with *CDH1* **expression** was not due to the smaller number of genes in these groups. The distribution of *CDH1* correlations differed across these gene groups (as shown by Figure 4.4 and Appendix Figure C.4) and tended to be lower in **SLIPT** candidates (as supported by **analysis of variance (ANOVA)** in Table 4.4). However, these are relatively weak correlations and further triage of gene candidates by correlation is not suitable. The genes detected both **SLIPT** and **siRNA** did not differ from **SLIPT** genes and the number of positively correlated **SLIPT** genes was very small. The use of correlation itself is also less effective than **SLIPT** to predict **synthetic lethal** partners in the first place (as shown in Section 6.1.2.1).

Table 4.4: **ANOVA** for synthetic lethality and correlation with *CDH1*

	DF	Sum Squares	Mean Squares	F-value	p-value
siRNA	1	0.027	0.027	2.8209	0.09306
SLIPT	1	134.603	134.603	14115.9824	<0.0001
siRNA×SLIPT	1	0.000	0.000	0.0073	0.93212

Analysis of variance for correlation with *CDH1* against **synthetic lethal** detection approaches (with an interaction term). Only genes tested by both methods were included in this analysis.

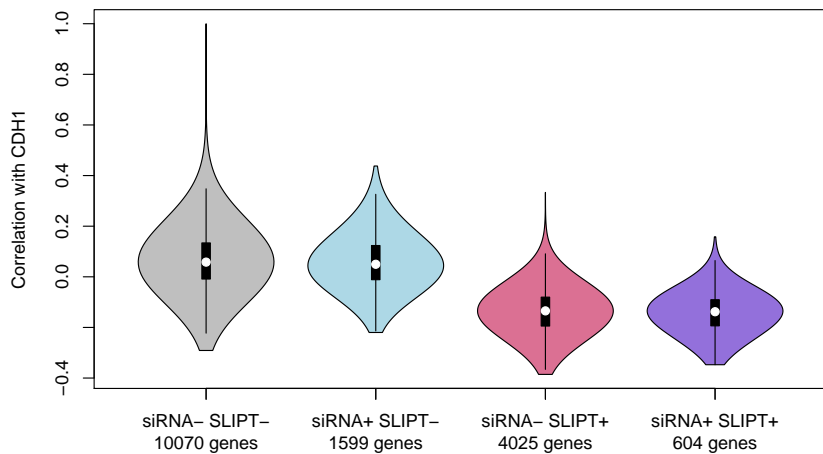
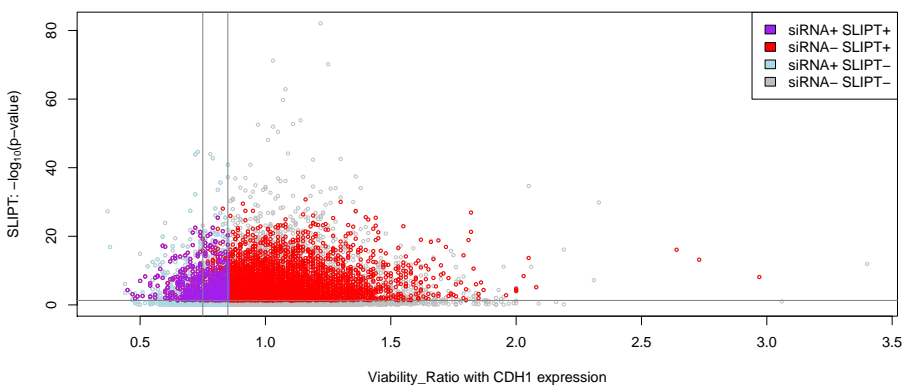


Figure 4.4: **Comparison of SLIPT and siRNA genes with correlation.** Genes detected as candidate synthetic lethal partners by SLIPT (in TCGA breast cancer) expression analysis and experimental screening (with siRNA) were compared against Pearson correlation of gene expression with *CDH1*. There were significant differences in correlation between gene groups (as shown in Table 4.4).

#### 4.2.3 Comparison with Primary Screen Viability

A similar comparison of SLIPT results was made with the viability ratio ( $CDH1^{-/-}$  mutant to wild-type) of MCF10A cells in the primary siRNA screen performed by Telford *et al.* (2015). The significance and viability thresholds used for SLIPT and siRNA detection of synthetic lethal candidate partners of *CDH1* are shown in Figure 4.5. Not all of the genes below the viability thresholds were necessarily selected to be candidate partners, however, as additional criteria were used in each case: directional criteria as for SLIPT (see Section 3.1) and minimum wild-type viability for siRNA (Telford *et al.*, 2015).

There does not appear to be a clear relationship between SLIPT and siRNA candidates. The genes detected by one approach but not the other were numerous in Figure 4.2 and Appendix Figure C.2. These genes detected by one approach are not necessarily near the thresholds for the other. In this respect, the SLIPT approach with patient data and the siRNA cell line experiments are independent means to identify synthetic lethal candidates. While genes detected by both approaches were not necessarily more strongly supported by either, the genes with a viability closer to 1



**Figure 4.5: Comparison of **SLIPT** and **siRNA** genes with screen viability.** The  $\chi^2$  p-values (log-scale) for genes tested by **SLIPT** (in TCGA breast cancer) were compared against the viability ratio of *CDH1* mutant and wild-type cells in the primary **siRNA** screen. Genes detected by **SLIPT** or **siRNA** are coloured according to the legend. Lines show the thresholds of significance with **SLIPT** and of viability used by [Telford et al. \(2015\)](#).

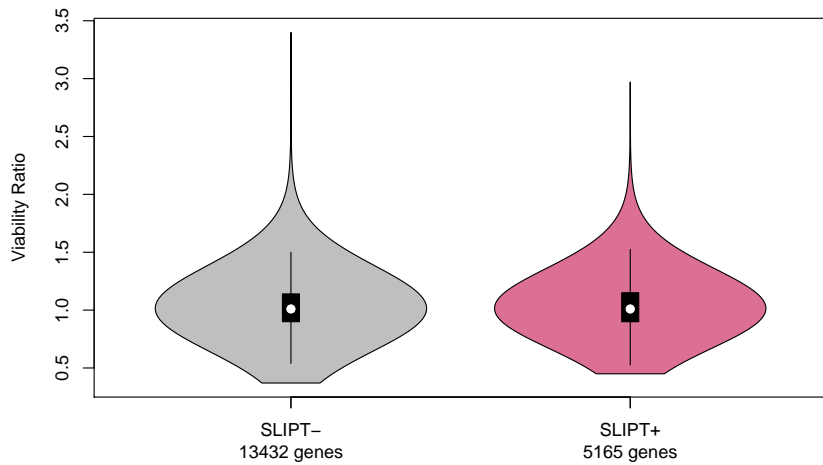


**Figure 4.6: Comparison of **SLIPT** genes with **siRNA** screen viability.** Genes detected as candidate synthetic lethal partners by **SLIPT** (in TCGA breast cancer) expression analysis were compared against the viability ratio of *CDH1* mutant and wild-type cells in the primary **siRNA** screen. There were clear no differences in viability between genes detected by **SLIPT** and those not detected. The genes identified by **SLIPT** had a higher viability ratio (by t-test:  $t = 2.1553$ ,  $p = 0.03117$ ), although the effect size was relatively small (mean SLIPT- 1.029, mean SLIPT+ 1.037).

(no synthetic lethal effect) in siRNA included those with more significant SLIPT p-values, whereas more extreme viability ratios tended to be less significant (as shown by Figure 4.5). However, it should be noted that genes with more moderate viability ratios were more common and SLIPT was capable (despite adjusting for multiple testing) of detecting significant genes with extreme viability ratios, particularly those considerably lower than 1. Lower viability ratios were used by Telford *et al.* (2015) to detect synthetic lethal candidates in the primary screen. However, there was little support for SLIPT candidates differing with respect to viability ratio (as shown in Figures 4.6 and C.5) and the vast majority of SLIPT candidate genes did not have different viability in the primary screen to genes not identified by SLIPT.

#### 4.2.4 Comparison with Secondary siRNA Screen Validation

However, it should be noted that genes with a lower viability ratio were not necessarily the most strongly supported by experimental screening. The primary screen (with 4 pooled siRNAs) has been used for the majority of comparisons in this thesis because the genomes-wide panel of target genes screened enables a large number of genes to be compared with SLIPT results from gene expression and somatic mutation analysis. A secondary screen was also performed by Telford *et al.* (2015) on the isogenic MCF10A breast cell lines to validate the individual (i.e., non-pooled) siRNAs separately, with the strongest candidates being those exhibiting synthetic lethal viability ratios replicated across independently targeting siRNAs. The strongest candidates from a primary screen were subject to a further secondary screen for validation by independent replication with 4 gene knockdowns with different targeting siRNAs. This was performed for the top 500 candidates (with the lowest viability ratio) from the primary screen and the 482 of these genes also tested by SLIPT in breast cancer.

The secondary screen results show that SLIPT candidate genes were more significantly ( $p = 7.49 \times 10^{-3}$  by Fisher's exact test) more likely to be validated in the secondary screen and are thus informative of more robust partner genes, in addition to providing support that these interactions are consistent with expression profiles from heterogeneous patient samples across genetic backgrounds. As shown in Table 4.5, there is significant association between SLIPT candidates and stronger validations of siRNA candidates. Since there were more SLIPT- genes among those not validated and more SLIPT+ genes among those validated with several siRNAs, this supports the use of SLIPT as a synthetic lethal discovery procedure which may augment such screening experiments.

Table 4.5: Comparison of **SLIPT** genes against secondary siRNA screen

		Secondary Screen					<b>Total</b>
		0/4	1/4	2/4	3/4	4/4	
<b>SLIPT+</b>	Observed	70	46	31	8	2	157
	Expected	85	44	10	4	2	
<b>SLIPT-</b>	Observed	190	90	31	10	4	325
	Expected	175	91	42	12	4	
<b>Total</b>		280	136	52	18	6	482

While the individual genes detected by either approach do not necessarily match (and are potentially false-positives), the biological functions important in *CDH1* deficient cancers and potential mechanisms for specific targeting of them can be further supported by pathway analysis of the gene detected by either method. The genes detected by both approaches may therefore be more informative at the pathway level, where it is unlikely for a pathway to be consistently detected by chance. As the **SLIPT** candidates differ from the **siRNA** candidates (and are more likely to be validated), they can provide additional mechanisms by which *CDH1* deficient cancers proliferate and vulnerabilities that may be exploited against them by using the **synthetic lethal** pathways.

#### 4.2.5 Comparison to Primary Screen at Pathway Level

These pathway over-representation analyses (performed as described in Section 2.3.2) correspond to genes separated into **SLIPT** or **siRNA** screen candidates unique to either method or detected by both (Table 4.6). The **SLIPT**-specific gene candidates were involved most strongly with translational and immune regulatory pathways, although extracellular matrix pathways were also supported. These pathways were largely consistent with those identified in Table 4.2 and in the clustering analysis (Table 4.3). The genes detected only by the **siRNA** screen had over-representation of cell signalling pathways, including many containing genes known to be involved in cancer (e.g., MAPK, PDGF, ERBB2, and FGFR), with the detection of Class A GPCRs supporting the independent analyses by Telford *et al.* (2015). The intersection of computational and experimental **synthetic lethal** partners of *CDH1* had stronger evidence for over-representation of **GPCR** pathways and more specific subclasses, such as visual

Table 4.6: Pathways for *CDH1* partners from SLIPT and siRNA

Predicted only by <b>SLIPT</b> (4025 genes)	Pathway	Size	Genes Identified	p-value (FDR)
Eukaryotic Translation Elongation		80	75	$1.5 \times 10^{-182}$
Peptide chain elongation		77	72	$2.9 \times 10^{-176}$
Viral mRNA Translation		75	70	$4.9 \times 10^{-172}$
Eukaryotic Translation Termination		76	70	$5.9 \times 10^{-170}$
Formation of a pool of free 40S subunits		87	74	$9.5 \times 10^{-166}$
Nonsense Mediated Decay independent of the Exon Junction Complex		81	70	$1.2 \times 10^{-160}$
L13a-mediated translational silencing of Ceruloplasmin expression		97	75	$3.8 \times 10^{-155}$
3' -UTR-mediated translational regulation		97	75	$3.8 \times 10^{-155}$
GTP hydrolysis and joining of the 60S ribosomal subunit		98	75	$6.0 \times 10^{-154}$
Nonsense-Mediated Decay		96	73	$5.2 \times 10^{-150}$
Nonsense Mediated Decay enhanced by the Exon Junction Complex		96	73	$5.2 \times 10^{-150}$
SRP-dependent cotranslational protein targeting to membrane		97	73	$7.8 \times 10^{-149}$
Eukaryotic Translation Initiation		105	75	$4.7 \times 10^{-146}$
Cap-dependent Translation Initiation		105	75	$4.7 \times 10^{-146}$
Translation		133	83	$4.0 \times 10^{-142}$
Influenza Viral RNA Transcription and Replication		102	71	$2.9 \times 10^{-137}$
Influenza Infection		111	74	$3.7 \times 10^{-137}$
Influenza Life Cycle		106	71	$2.3 \times 10^{-133}$
Infectious disease		326	125	$4.2 \times 10^{-120}$
Extracellular matrix organisation		189	77	$5.4 \times 10^{-95}$

Detected only by <b>siRNA</b> screen (1599 genes)	Pathway	Size	Genes Identified	p-value (FDR)
Class A/1 (Rhodopsin-like receptors)		282	44	$1.3 \times 10^{-27}$
GPCR ligand binding		363	52	$5.8 \times 10^{-26}$
G <sub>aq</sub> signalling events		159	26	$6.7 \times 10^{-23}$
Gastrin-CREB signalling pathway via PKC and MAPK		180	27	$2.0 \times 10^{-21}$
G <sub>ai</sub> signalling events		184	27	$5.3 \times 10^{-21}$
Downstream signal transduction		146	23	$7.6 \times 10^{-21}$
Signalling by PDGF		172	25	$4.0 \times 10^{-20}$
Peptide ligand-binding receptors		175	25	$8.5 \times 10^{-20}$
Signalling by ERBB2		146	22	$1.3 \times 10^{-19}$
DAP12 interactions		159	23	$2.6 \times 10^{-19}$
DAP12 signalling		149	22	$2.7 \times 10^{-19}$
Organelle biogenesis and maintenance		264	33	$5.5 \times 10^{-19}$
Signalling by NGF		266	33	$8.2 \times 10^{-19}$
Downstream signalling of activated FGFR1		134	20	$1.1 \times 10^{-18}$
Downstream signalling of activated FGFR2		134	20	$1.1 \times 10^{-18}$
Downstream signalling of activated FGFR3		134	20	$1.1 \times 10^{-18}$
Downstream signalling of activated FGFR4		134	20	$1.1 \times 10^{-18}$
Signalling by FGFR		146	21	$1.3 \times 10^{-18}$
Signalling by FGFR1		146	21	$1.3 \times 10^{-18}$
Signalling by FGFR2		146	21	$1.3 \times 10^{-18}$

Intersection of <b>SLIPT</b> and <b>siRNA</b> screen (604 genes)	Pathway	Size	Genes Identified	p-value (FDR)
Visual phototransduction		54	9	$6.9 \times 10^{-10}$
G <sub>as</sub> signalling events		48	7	$1.6 \times 10^{-7}$
Retinoid metabolism and transport		24	5	$1.7 \times 10^{-7}$
Acyl chain remodelling of PS		10	3	$6.5 \times 10^{-6}$
Transcriptional regulation of white adipocyte differentiation		51	6	$6.5 \times 10^{-6}$
Chemokine receptors bind chemokines		22	4	$6.5 \times 10^{-6}$
Signalling by NOTCH4		11	3	$6.9 \times 10^{-6}$
Defective EXT2 causes exostoses 2		11	3	$6.9 \times 10^{-6}$
Defective EXT1 causes exostoses 1, TRPS2 and CHDS		11	3	$6.9 \times 10^{-6}$
Platelet activation, signalling and aggregation		146	12	$6.9 \times 10^{-6}$
Phase 1 - Functionalisation of compounds		41	5	$1.3 \times 10^{-5}$
Amine ligand-binding receptors		13	3	$1.7 \times 10^{-5}$
Acyl chain remodelling of PE		14	3	$2.4 \times 10^{-5}$
Signalling by GPCR		300	23	$2.4 \times 10^{-5}$
Molecules associated with elastic fibres		29	4	$2.6 \times 10^{-5}$
DAP12 interactions		128	10	$2.6 \times 10^{-5}$
Cytochrome P <sub>450</sub> - arranged by substrate type		30	4	$3.2 \times 10^{-5}$
GPCR ligand binding		147	11	$3.8 \times 10^{-5}$
Acyl chain remodelling of PC		16	3	$4.0 \times 10^{-5}$
Response to elevated platelet cytosolic Ca <sup>2+</sup>		66	6	$4.2 \times 10^{-5}$

phototransduction ( $p = 6.9 \times 10^{-10}$ ) and G <sub>$\alpha$ s</sub> signalling events ( $p = 1.7 \times 10^{-7}$ ), than other signalling pathways.

The pathway analysis for **mtSLIPT** against *CDH1* mutations (in Table C.4) had concordant results for both **mtSLIPT**-specific and **siRNA**-specific pathways. While the specific pathway composition of the intersection of these analyses differed from **SLIPT** against low *CDH1* expression, signalling pathways including **GPCRs**, NOTCH, EERB2, PDGF, and SCF-KIT. These findings indicate the signalling pathways are among the most suitable vulnerability to exploit in targeting *CDH1* deficient tumours as they can be detected in both a patient cohort (with **TCGA expression** data) and tested in a laboratory system. However, it is possible that the isolated experimental system is set up to preferentially detect kinase singalling pathways (which are amenable to pharmacological inhibition and translation to the clinic) and the other pathways identified by **SLIPT** may still be informative of the role of *CDH1* loss of function in cancers or mechanisms by which further gene loss leads to specific inviability.

#### 4.2.5.1 Resampling Genes for Pathway Enrichment

Comparisons of genes between experimental screen candidates and prediction from **TCGA expression** data were less consistent than comparisons of pathways. However, this is not unexpected, since **synthetic lethal** pathways are more robustly conserved (Dixon *et al.*, 2008) and the computational approach using patient samples from complex tumour microenvironment has considerably different strengths to an experimental screen (Telford *et al.*, 2015) based on genetically homogenous cell line models in an isolated laboratory environment. For instance, it is unlikely for immune signalling to be detected in an isolated cell culture system.

The overlap between **synthetic lethal** candidates from bioinformatics **SLIPT** predictions and **siRNA** screening has raised other questions, including whether the pathways over-represented would be expected by chance. This of particular concern since the **siRNA** candidate genes themselves are highly over-represented for particular pathways (e.g., **GPCRs**) so selecting any intersect with them could be enriched for these pathways. Another pathway-based approach is to test whether pathways are over-represented in randomly sampled genes, comparing many “resamplings” or “permutations” of these genes to the enrichment statistics observed for these pathways in the **SLIPT** candidates and their intersection with the **siRNA** hits shows whether we detect these pathways more than we expect by chance (as described in Section 2.3.6).

Of particular concern are the over-represented pathways in genes detected by both methods. Pathway over-representation alone does not detect whether **SLIPT** predicted

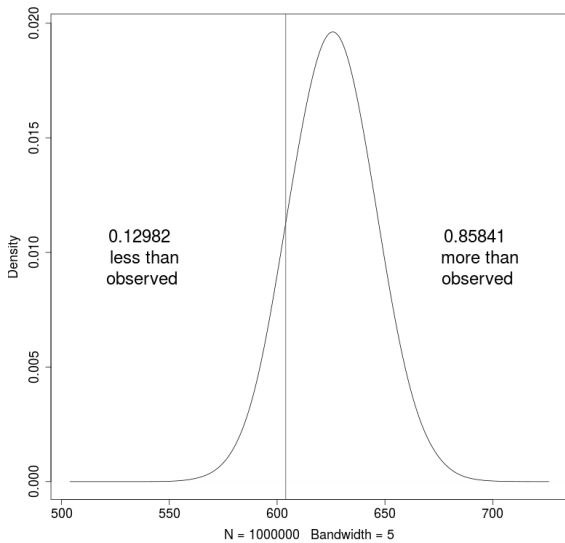


**Figure 4.7: Resampled intersection of **SLIPT** and **siRNA** candidates.** Resampling analysis of intersect size from genes detected by **SLIPT** and **siRNA** screening approaches over 1 million replicates. The proportion of expected intersection sizes for random samples below or above the observed intersection size respectively, lacking significant over-representation or depletion of **siRNA** screen candidates within the **SLIPT** predictions for *CDH1*.

genes or **siRNA** candidates are enriched within each other. This resampling analysis therefore detects whether over-represented pathways were detected by **SLIPT** independently of their over-representation among **siRNA** candidates (without assuming an underlying test statistic distribution).

A resampling approach is also applicable to testing whether the number of genes detected by each approach significantly intersected. As shown in Figure 4.7, resampling did not find evidence of significant depletion or over-representation for experimental synthetic lethal candidate genes in the computationally predicted synthetic lethal partners of *CDH1*, and thus the observed overlap may be due to chance. This is consistent with previous findings (see Figure 4.2) and does not preclude pathway relationships being supported by resampling.

A permutation analysis was performed to resample the genes tested by both approaches to investigate whether the observed pathway over-representation could have occurred in a randomly selected sample of genes from the experimental candidates, that is, whether the pathway predictions from **SLIPT** could be expected by chance (as described in Sections 2.2.4 and 2.3.6). While the number of **siRNA** candidate genes also detected by **SLIPT** was not statistically significant ( $p = 0.281$ ), this may be due

to the vastly different limitations of the approaches and the correlation structure of gene expression not being independent (as assumed for multiple testing procedures). The intersection may still be functionally relevant to *CDH1*-deficient cancers, such as the pathway data in Table 4.6. The resampling analysis for pathways was compared to the pathway over-representation for **SLIPT** predicted synthetic lethal partners in Table 4.7. Similarly, the pathway resampling for intersection between **SLIPT** predictions and experimental screen candidates was compared to pathway over-representation in Table 4.8 for intersection with **siRNA** data.

The pathway resampling approach for **SLIPT**-specific gene candidates (Table 4.7) replicates the gene set over-representation analysis for all **SLIPT** genes, detecting evidence of synthetic lethal pathways for *CDH1* in translational, immune, and cell signalling pathways including G<sub>αi</sub> signalling, GPCR downstream signalling, and chemokine receptor binding. While the immune and signal transduction pathways were not significantly over-represented in the resampling analysis, the results for the two approaches were largely consistent for translation and post-transcriptional gene regulation, supporting gene set over-representation of the **SLIPT**-specific pathways in Table 4.7. In particular, some of the most significantly over-represented pathways had higher observed  $\chi^2$  values than any of the 1 million random permutations. Similar pathways were also replicated by permutation analysis for mt**SLIPT** candidate partners against *CDH1* mutation (shown in Table C.5). This shows that many of the pathways detected specifically by **SLIPT** are replicated by permutation procedures and that the permutation approach is capable of detecting many of the most strongly over-represented pathways.

The permutation approach was then also applied to the intersection between computational and experimental candidates. The permutation analysis is testing for consistent detection of pathways was independent of their pre-existing status as experimental candidates. The pathway results for these candidate partners (in Table 4.8) differed between over-representation and resampling analyses.

Namely, many of the over-represented pathways were not significant in the resampling analysis, including visual phototransduction and retinoic acid signalling, and were likely over-represented in the intersection due to over-representation in the **siRNA** candidates rather than additional support from **SLIPT**. In contrast, pathways involving defective *EXT1* or *EXT2* genes approach significance after **FDR** adjustment for multiple tests in resampling. Of the highest over-represented pathways in the intersection, only G<sub>αs</sub> signalling events were supported by both over-representation and resampling

Table 4.7: Pathways for *CDH1* partners from SLIPT

Reactome Pathway	Over-representation	Permutation
<b>Eukaryotic Translation Elongation</b>	$1.3 \times 10^{-207}$	$< 1.241 \times 10^{-5}$
Peptide chain elongation	$5.6 \times 10^{-201}$	$< 1.241 \times 10^{-5}$
<b>Viral mRNA Translation</b>	$1.2 \times 10^{-196}$	$< 1.241 \times 10^{-5}$
<b>Eukaryotic Translation Termination</b>	$1.2 \times 10^{-196}$	$< 1.241 \times 10^{-5}$
Formation of a pool of free 40S subunits	$3.7 \times 10^{-194}$	$< 1.241 \times 10^{-5}$
Nonsense Mediated Decay independent of the Exon Junction Complex	$5.3 \times 10^{-187}$	$< 1.241 \times 10^{-5}$
<b>L13a-mediated translational silencing of Ceruloplasmin expression</b>	$9.6 \times 10^{-183}$	$< 1.241 \times 10^{-5}$
3' -UTR-mediated translational regulation	$9.6 \times 10^{-183}$	$< 1.241 \times 10^{-5}$
GTP hydrolysis and joining of the 60S ribosomal subunit	$1.9 \times 10^{-181}$	$< 1.241 \times 10^{-5}$
Nonsense-Mediated Decay	$6.2 \times 10^{-176}$	$< 1.241 \times 10^{-5}$
<b>Nonsense Mediated Decay enhanced by the Exon Junction Complex</b>	$6.2 \times 10^{-176}$	$< 1.241 \times 10^{-5}$
Adaptive Immune System	$6.5 \times 10^{-174}$	0.15753
<b>Eukaryotic Translation Initiation</b>	$5.7 \times 10^{-173}$	$< 1.241 \times 10^{-5}$
<b>Cap-dependent Translation Initiation</b>	$5.7 \times 10^{-173}$	$< 1.241 \times 10^{-5}$
<b>SRP-dependent cotranslational protein targeting to membrane</b>	$2.0 \times 10^{-171}$	$< 1.241 \times 10^{-5}$
Translation	$6.1 \times 10^{-170}$	$< 1.241 \times 10^{-5}$
Infectious disease	$1.6 \times 10^{-166}$	0.23231
<b>Influenza Infection</b>	$1.9 \times 10^{-163}$	$< 1.241 \times 10^{-5}$
<b>Influenza Viral RNA Transcription and Replication</b>	$1.9 \times 10^{-160}$	$< 1.241 \times 10^{-5}$
<b>Influenza Life Cycle</b>	$2.5 \times 10^{-156}$	$< 1.241 \times 10^{-5}$
<i>Extracellular matrix organisation</i>	$1.1 \times 10^{-152}$	0.071761
GPCR ligand binding	$1.1 \times 10^{-143}$	0.55801
Class A/1 (Rhodopsin-like receptors)	$1.5 \times 10^{-142}$	0.58901
<i>GPCR downstream signalling</i>	$7.6 \times 10^{-140}$	0.098357
Haemostasis	$1.9 \times 10^{-134}$	0.27059
Developmental Biology	$2.0 \times 10^{-123}$	0.52737
Metabolism of lipids and lipoproteins	$3.3 \times 10^{-120}$	0.724
Cytokine Signalling in Immune system	$2.6 \times 10^{-119}$	0.39661
Peptide ligand-binding receptors	$3.7 \times 10^{-109}$	0.61102
<b>G<sub>αs</sub> signalling events</b>	$8.9 \times 10^{-100}$	$< 1.241 \times 10^{-5}$

Over-representation (hypergeometric test) and Permutation p-values adjusted for multiple tests across pathways (**FDR**). Significant pathways are marked in bold (**FDR** < 0.05) and italics (**FDR** < 0.1).

analyses. Other pathways supported by both analyses were cytoplasmic elastic fibre formation, associated HS-GAG protein modification pathways, energy metabolism, and the fibrin clotting cascade.

Many of the pathways supported in the intersection by permutation analysis were also replicated in the **mtSLIPT** analysis of partners tested with *CDH1 mutation* (in Table C.6), including G<sub>αs</sub>, elastic fibres, HS-GAG, and energy metabolism. While there were differences between the pathways identified by over-representation analysis, those replicated by permutation were highly concordant, supporting the combined use of these pathway approaches to identify synthetic lethal gene functions and targets.

While this indicates that G<sub>αs</sub> and **GPCR** class A/1 signalling events were significantly detected by both approaches, **GPCR** signalling pathways overall were not. It is likely that **GPCRs** were primarily over-represented in the intersection with the experimental candidates due to strong over-representation of these pathways in experimental candidates, rather than detection by **SLIPT**, which may be driven by these more specific constituent pathways.

Table 4.8: Pathways for *CDH1* partners from SLIPT and siRNA primary screen

Reactome Pathway	Over-representation	Permutation
Visual phototransduction	$6.9 \times 10^{-10}$	0.91116
<b>G<sub>as</sub> signalling events</b>	$1.6 \times 10^{-7}$	0.012988
Retinoid metabolism and transport	$1.7 \times 10^{-7}$	0.20487
Transcriptional regulation of white adipocyte differentiation	$6.5 \times 10^{-6}$	0.38197
Acylic chain remodelling of PS	$6.5 \times 10^{-6}$	0.58485
Chemokine receptors bind chemokines	$6.5 \times 10^{-6}$	0.97255
<i>Defective EXT2 causes exostoses 2</i>	$6.9 \times 10^{-6}$	0.056437
<i>Defective EXT1 causes exostoses 1, TRPS2 and CHDS</i>	$6.9 \times 10^{-6}$	0.056437
Signalling by NOTCH4	$6.9 \times 10^{-6}$	0.15497
Platelet activation, signalling and aggregation	$6.9 \times 10^{-6}$	0.53358
Phase 1 - Functionalisation of compounds	$1.3 \times 10^{-5}$	0.24836
Amine ligand-binding receptors	$1.7 \times 10^{-5}$	0.3195
Acylic chain remodelling of PE	$2.4 \times 10^{-5}$	0.7307
Signalling by GPCR	$2.4 \times 10^{-5}$	0.9939
<b>Molecules associated with elastic fibres</b>	$2.6 \times 10^{-5}$	0.0072929
DAP12 interactions	$2.6 \times 10^{-5}$	0.78273
Cytochrome P <sub>450</sub> - arranged by substrate type	$3.2 \times 10^{-5}$	0.87019
GPCR ligand binding	$3.8 \times 10^{-5}$	0.99417
Acylic chain remodelling of PC	$4.0 \times 10^{-5}$	0.65415
Response to elevated platelet cytosolic Ca <sup>2+</sup>	$4.2 \times 10^{-5}$	0.55461
<i>Arachidonic acid metabolism</i>	$4.4 \times 10^{-5}$	0.060298
Defective B4GALT7 causes EDS, progeroid type	$4.9 \times 10^{-5}$	0.15497
Defective B3GAT3 causes JDSSDHD	$4.9 \times 10^{-5}$	0.15497
<b>Elastic fibre formation</b>	$4.9 \times 10^{-5}$	0.0019227
<b>HS-GAG degradation</b>	$6.2 \times 10^{-5}$	0.017747
Bile acid and bile salt metabolism	$6.2 \times 10^{-5}$	0.15497
Netrin-1 signalling	$7.1 \times 10^{-5}$	0.95056
<b>Integration of energy metabolism</b>	$7.1 \times 10^{-5}$	0.0019287
DAP12 signalling	$7.9 \times 10^{-5}$	0.67835
GPCR downstream signalling	$8.1 \times 10^{-5}$	0.88678
<b>Diseases associated with glycosaminoglycan metabolism</b>	$8.7 \times 10^{-5}$	0.017747
<b>Diseases of glycosylation</b>	$8.7 \times 10^{-5}$	0.017747
Signalling by Retinoic Acid	$8.7 \times 10^{-5}$	0.13592
Signalling by Leptin	$8.7 \times 10^{-5}$	0.15497
Signalling by SCF-KIT	$8.7 \times 10^{-5}$	0.73399
Opioid Signalling	$8.7 \times 10^{-5}$	0.99417
Signalling by NOTCH	0.0001	0.26453
Platelet homeostasis	0.0001	0.55912
Signalling by NOTCH1	0.00011	0.13797
Class B/2 (Secretin family receptors)	0.00011	0.4659
Diseases of Immune System	0.00013	0.15497
Diseases associated with the TLR signalling cascade	0.00013	0.15497
A tetrasaccharide linker sequence is required for GAG synthesis	0.00013	0.33566
Nuclear Receptor transcription pathway	0.00016	0.22735
<b>Formation of Fibrin Clot (Clotting Cascade)</b>	0.00016	0.0054639
Syndecan interactions	0.00016	0.3974
Class A/1 (Rhodopsin-like receptors)	0.00016	0.99454
HS-GAG biosynthesis	0.0002	0.37199
Platelet degranulation	0.0002	0.39003
EPH-ephrin mediated repulsion of cells	0.00021	0.6193

Over-representation (hypergeometric test) and Permutation p-values adjusted for multiple tests across pathways (**FDR**). Significant pathways are marked in bold (**FDR** < 0.05) and italics (**FDR** < 0.1).

However, several pathways, including some immune functions and neurotransmitters, were supported by the resampling analysis (in Tables 4.8 and C.6) when the initial pathway over-representation test was not significant. These functions appear to have been detected by both approaches more than expected by chance but must be interpreted with caution since they were still not common enough to be detected in pathway over-representation analysis.

#### 4.2.6 Integrating Synthetic Lethal Pathways and Screens

Based on these results, it appears that computational and experimental approaches to synthetic lethal screening for *CDH1* lead to a broader functional characterisation, and many candidate partners, when combined, despite different strengths and limitations. Compared to candidate gene approaches, experimental genomes-wide screens are an appealing unbiased strategy for identifying synthetic lethal interactions. Since these screens are costly, laborious, and specific to genetic background, computational analysis can augment candidate triage to either reduce the initial panel of screened genes or prioritise validation.

GPCR pathways were detected among both computational and experimental synthetic lethal candidates, with more support in the experimental screen (Table 4.8). The homogeneous cell line model may be more likely to detect particular pathways. For instance, SLIPT identified immune pathways, not expected to be detected in isolated cell culture. GPCR signalling was supported in experimental models Telford *et al.* (2015) with some of these pathways replicated in varied genetic backgrounds of patient samples. These pathways require further investigation such as identification of more specific pathways, higher order interactions, and modes of resistance.

The pathway composition across computational and experimental synthetic lethal candidates was informative with over-representation (Table 4.6) and supported by resampling analysis (Table 4.8), despite a modest intersection of genes between them (Figure 4.2). Either approach may be significant for a pathway in this intersection without being supported by the other: resampling analysis may support pathways that were not over-represented due to small effect sizes, thus both tests are required for a candidate pathway. The pathways detected by both over-representation and resampling are the strongest candidates for further investigation, such as  $G_{\alpha s}$  signalling, a strong candidate in prior analyses with a role in the regulation of translation in cancer Gao and Roux (2015), another function supported by SLIPT analysis.

The predicted synthetic lethal partners occurred across functionally distinct path-

ways, including characterised functions of *CDH1*. This diversity is consistent with the wide ranging role of *CDH1* in cell-cell adhesion, cell signalling, and the cytoskeletal structure of epithelial tissues. Pathway structure may be relevant to identifying potential drug targets from gene expression signatures, indicating downstream effector genes and mechanisms leading to cell inviability. These distinct synthetic lethal gene clusters and pathways may further lead to the elucidation of drug resistance mechanisms.

## 4.3 Metagene Analysis

The gene signatures (Gatza *et al.*, 2011, 2014) were used to demonstrate to utility of the metagene approach for use on a wider range of pathways as was performed with the Reactome (Croft *et al.*, 2014) pathways as an alternative approach to identification of synthetic lethal pathways. Metagenes serve as a summary of activity for each pathway. The direction of metagenes (derived by the singular value matrix decomposition) is generally arbitrary but care has been taken to ensure that these occur in a direction which reflect overall activation of the pathway (as described in Section 2.2.3). Metagenes were derived for well characterised gene signatures in breast cancer (Gatza *et al.*, 2011, 2014) to verify that that these pathway signatures are consistent with expected molecular properties of each molecular subtype (Parker *et al.*, 2009; Perou *et al.*, 2000). This was performed by examining the pathway expression of these breast cancer gene signatures in TCGA expression data. These metagenes were also compared to somatic mutation to evaluate mutation as a measure of gene activity in comparison to gene and protein expression.

The gene signatures (Gatza *et al.*, 2011, 2014) were used to demonstrate to utility of the metagene approach for use on a wider range of pathways. Having established that metagenes generated with this procedure reflect gene activity, the metagene procedure (in Section 2.2.3) was then applied to the Reactome pathways (Croft *et al.*, 2014). These Reactome metagenes were used for synthetic lethal analysis of pathways with SLIPT, directly using pathway activity for identifying synthetic lethal pathways with *CDH1*.

### 4.3.1 Pathway Expression

Pathway metagenes (generated as described in Section 2.2.3) for gene signatures of key processes in breast cancer (Gatza *et al.*, 2011) were used to check that metagenes were generated in the correct direction to indicate pathway activation. Some of these gene signatures are plotted in Figure 4.8 for comparison with clinical factors and somatic

mutations. The “intrinsic subtypes” was computed by performing the PAM50 procedure Parker *et al.* (2009) for RNA-Seq data which was highly concordant ( $\chi^2 = 1305.9$ ,  $p = 2.73 \times 10^{-268}$ ) with the subtypes provided by University of California, Santa Cruz (UCSC) (UCSC, 2012) for TCGA samples (Koboldt *et al.*, 2012) previously analysed by microarrays (as shown in Appendix D). Somatic mutations were reported for gislinkrecurrent mutationrecurrently mutated genes in breast cancer, as reported by TCGA (Koboldt *et al.*, 2012), related genes, and those previously discussed to be important in hereditary breast cancers (*BRCA1*, *BRCA2*, and *CDH1*).

These gene signatures reflect intrinsic subtypes as expected. In particular, the estrogen and progesterone receptor signatures are low in the predominantly ER<sup>-</sup> and Progesterone receptor (PR)<sup>-</sup> basal-like subtype tumours. These tumours also had the highest frequency of *TP53* mutations and a corresponding reduction of p53 metagene activity, as expected for loss of a tumour suppressor. The luminal A and luminal B tumour subtypes are the most similar, which is reflected in these metagenes signatures, although they are distinguishable molecular subtypes as shown by elevated PI3K, AKT, RAS, and  $\beta$ -catenin signalling in luminal B tumours. However, these pathways were also elevated in basal-like and HER2-enriched subtypes and lowly expressed in the “normal-like” subtype (which contained the normal samples). These intrinsic subtypes specific gene signature profiles were further supported with metagenes for an extended set of signatures (Gatza *et al.*, 2014), as shown in Figure C.9.

*TP53* mutations were the most frequent and more common in the basal-like subtype. Similarly, *GATA3* mutations were more common in luminal subtype tumours. PI3K mutations were more frequent across breast tumours, although these were less common in the basal-like subtype despite an elevated metagene (this discrepancy will be discussed further in Section 4.3.2). *CDH1* mutations similarly occurred across molecular subtypes with the exception of the basal-like subtype (as observed in gene expression with Figure 4.1). *CDH1* low samples occurred in all subtypes but were predominantly of the lobular histological subtype. Apart from these genes, mutations did not show clear specificity to a particular subtype and the variation between samples reflects the range of molecular cascades that can result in tumours with similar molecular profiles, supporting the use of gene expression data for cancer diagnostics and identification of molecular targets.

The direction of each metagene was consistent with the clinical characteristics, which formed a consensus of gene activity as shown for the PI3K and ER signatures (Gatza *et al.*, 2011) in Figures 4.9 and 4.10, respectively. Supporting data for p53 and

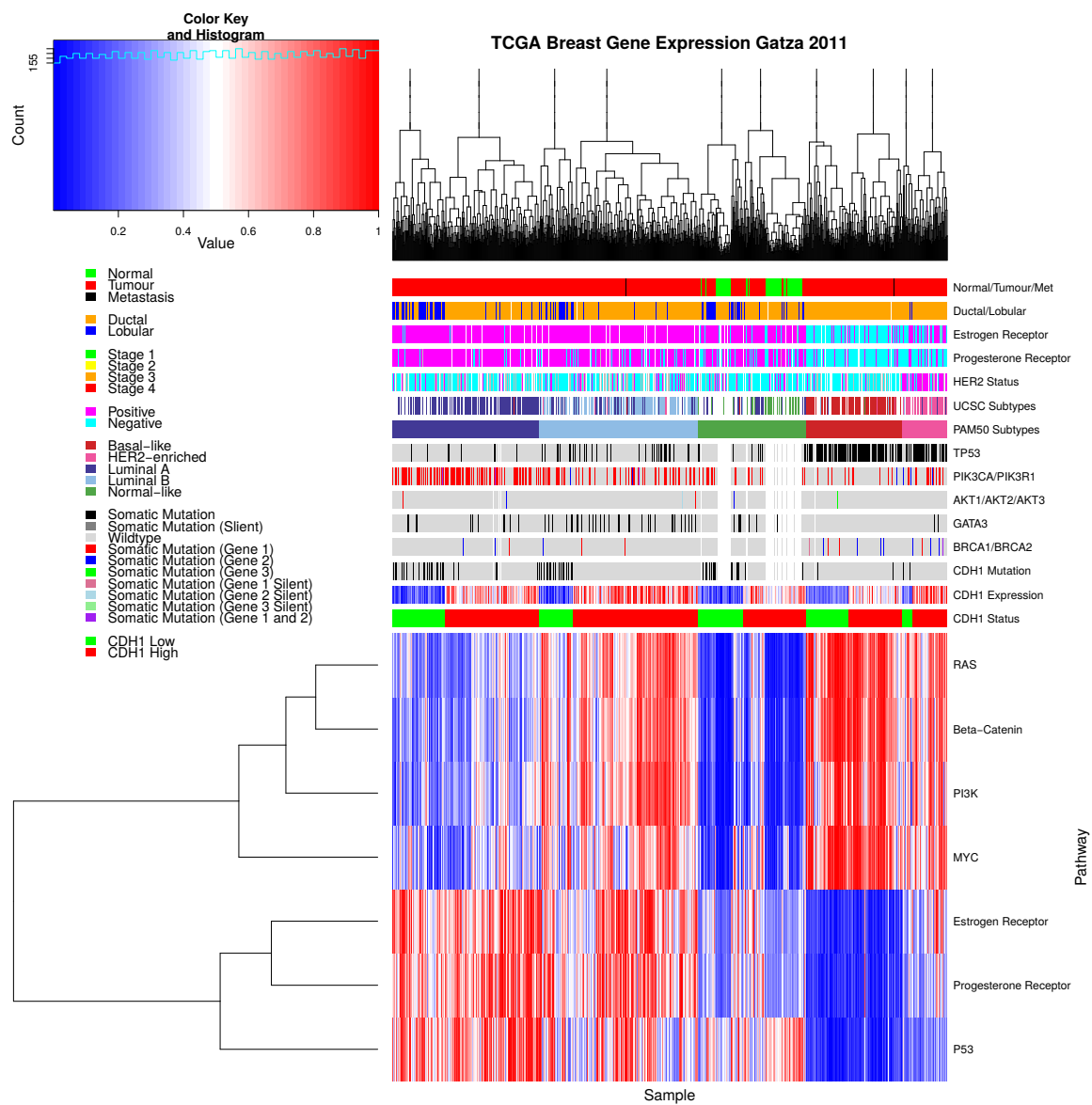


Figure 4.8: **Pathway metagene expression profiles.** Expression profiles for **metagene** signatures from [Gatza \*et al.\* \(2011\)](#) in **TCGA** breast data, annotated for clinical factors (with sample types and histological results coloured according to the legend) and cancer gene **mutations** (Negative values for **mutation** are light grey with missing data in white). Intrinsic subtypes are shown as derived from **microarray** (UCSC) and **RNA-Seq** (PAM50) data ([Koboldt \*et al.\*, 2012](#); [Parker \*et al.\*, 2009](#)). Samples were clustered independently for each **intrinsic subtypes** and by **CDH1** **expression** status. Pathway **expression** signatures are consistent with **mutations** and clinical subgroups.

BRCA metagenes (Gatza *et al.*, 2011, 2014) are given in the Appendix (Figures C.10 and C.11). In each of the examples for gene signatures, the expression of the majority of the genes were highly concordant with the metagene, being either positively or negatively correlated. These were generally consistent with established clinical and molecular subtypes of breast cancer and the recurrent mutations shown. However, the *PIK3CA* and *PIK3R1* mutant samples did not necessarily have elevated PI3K pathway metagene activity (as shown in Figure 4.9).

### 4.3.2 Somatic Mutation

It should be noted that metagenes, while consistent with the consensus of constituent expressed genes, were not necessarily reflecting the somatic mutation status. The PI3K (Gatza *et al.*, 2011) metagene levels in particular, were not statistically significantly varying between mutant and wild-type *PIK3CA* samples (shown in Figure 4.11). However, the PI3K metagene differed across *CDH1* and *TP53* mutations, remarkably in opposite directions considering that PI3K is an oncogenic growth pathway and these are both most frequently tumour suppressors inactivated in cancers. This shows that *CDH1* and *TP53* deficient tumours have distinct molecular growth pathways and that synthetic lethal interventions against loss of *CDH1* function may not be applicable to other cancers with driver mutations such as *TP53*, although these were kept in the analysis for comparison. These differences may be related to these mutations being more frequent in tumours with difference clinical characteristics (as observed in Section 4.3.1). Thus mutations do not necessarily have corresponding changes in pathway expression, particularly for oncogenes which may change in function rather than being upregulated.

While the more specific *PIK3CA* (Gatza *et al.*, 2014) metagene showed significant differences with *PIK3CA* and *PIK3R1* mutations (as shown in Figure C.6), this metagene replicated stronger differences for *CDH1* and *TP53*. These differences were less pronounced in the protein levels of p110 $\alpha$  (enocded by *PIK3CA*) and the downstream AKT gene (shown in Figures C.7 and C.8 respectively). However, this may be due to this regulatory cascade (kinases) being transmitted as a change in protein state (phosphorylation) rather than changes in expression levels. Another consideration is that mutations at different loci have different effects on protein function, particularly for oncogenes.

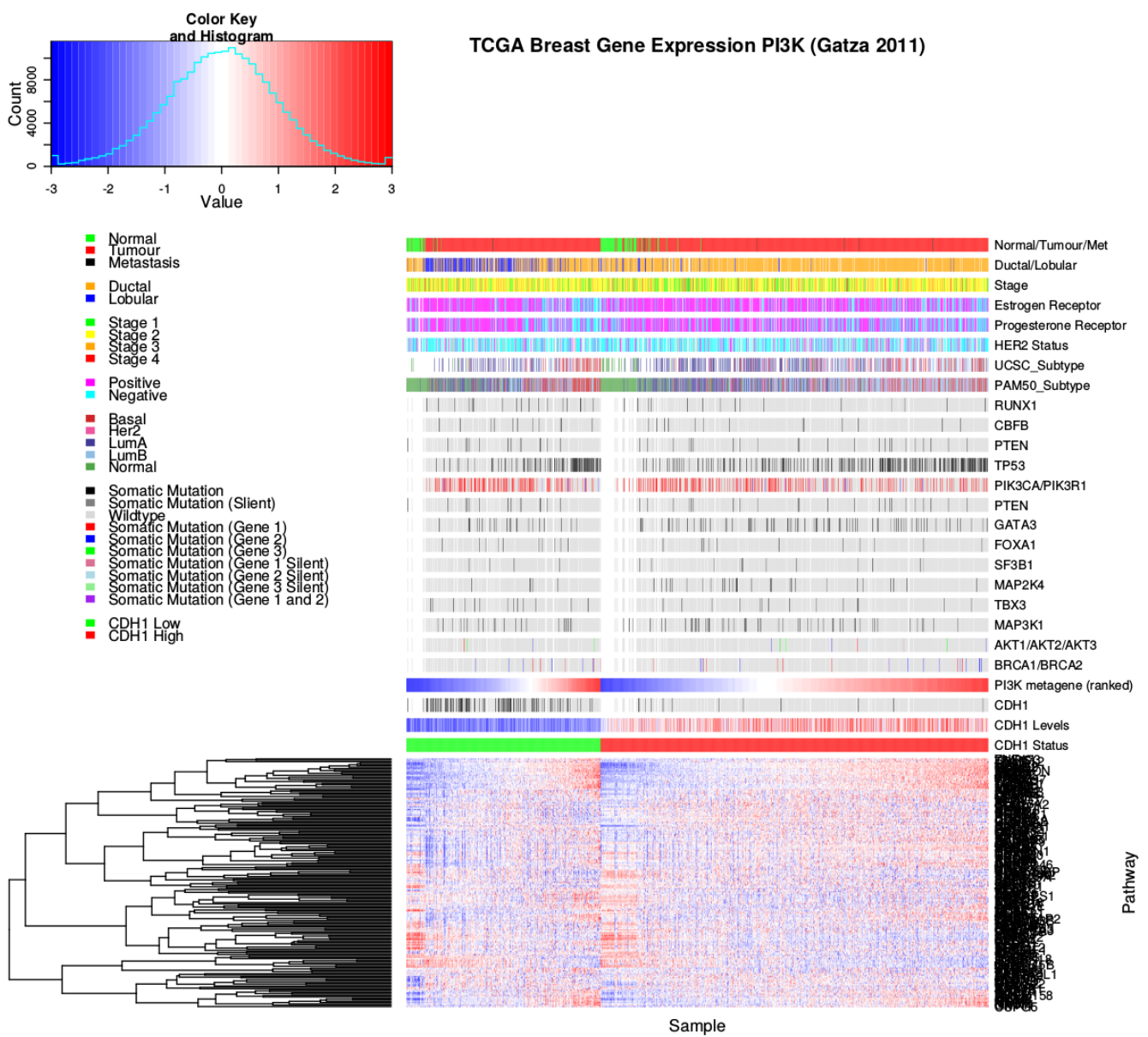


Figure 4.9: **Expression profiles for constituent genes of PI3K.** Expression profiles the genes contained in the PI3K gene signature from [Gatza et al. \(2011\)](#) in TCGA breast data, annotated for clinical factors and cancer gene mutations. Samples are separated by *CDH1* expression status and sorted by the metagene. In both cases, the majority of genes were consistent with the direction of the PI3K metagene, although considerable proportion were inversely correlated with the metagene. Normal samples had low PI3K metagene expression and *TP53* mutant samples had high PI3K expression. Although, oncogenic *PIK3CA* and tumour suppressor *PIK3R1* mutations across samples including those with low metagene response.

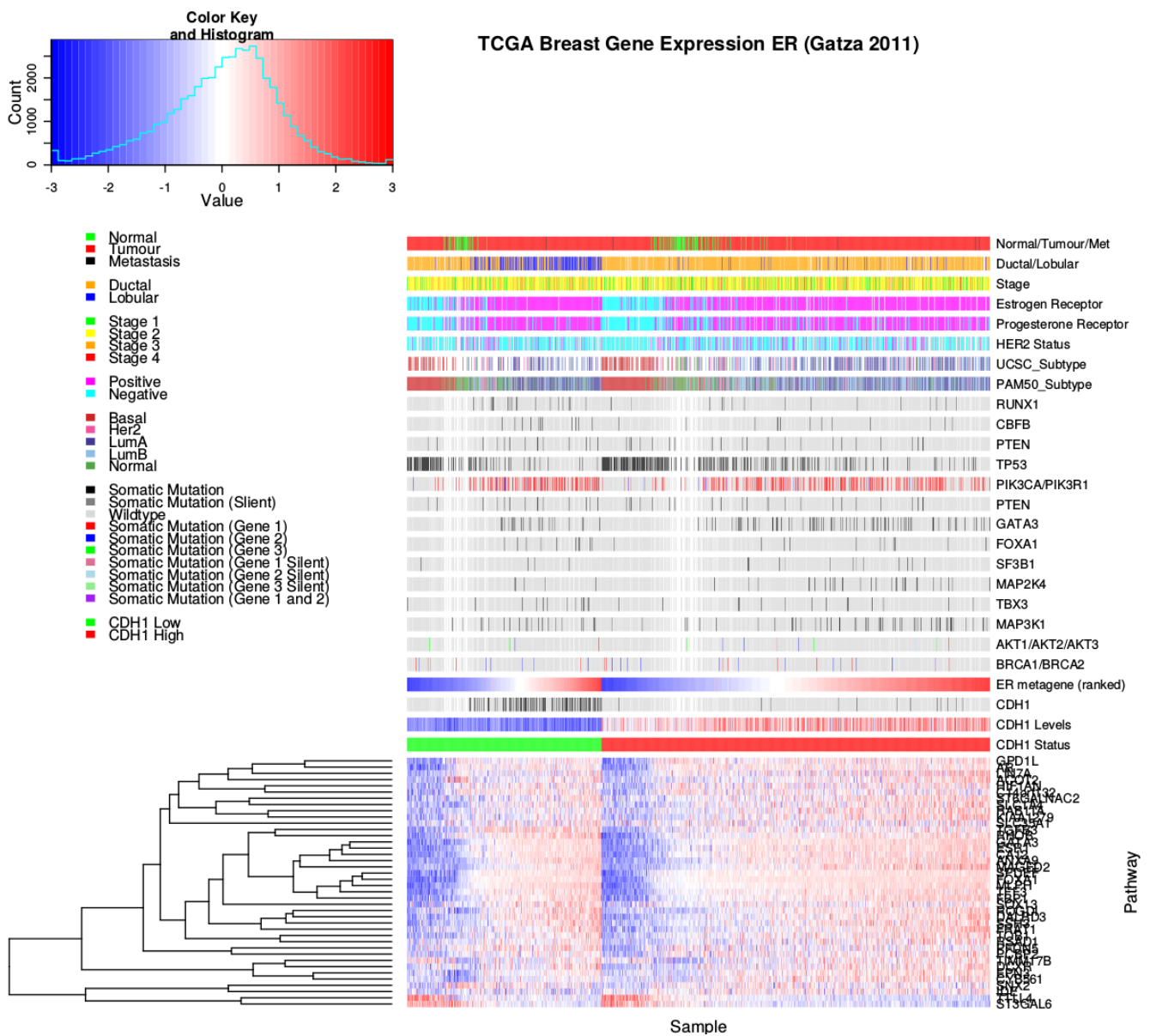


Figure 4.10: **Expression profiles for estrogen receptor related genes.** Expression profiles the genes contained in the estrogen receptor (ER) gene signature from [Gatza et al. \(2011\)](#) in TCGA breast data, annotated for clinical factors and cancer gene [mutations](#). Samples are separated by **CDH1 expression status** and sorted by the [metagene](#). In both cases, the majority of genes were consistent with the direction of the [metagene](#), with very few exceptions being inversely correlated. Estrogen receptor (by antibody staining) negative samples had low [metagene expression](#), as expected. These were more likely to be ductal and basal subtypes, lacking **CDH1** or **PIK3CA** mutations.

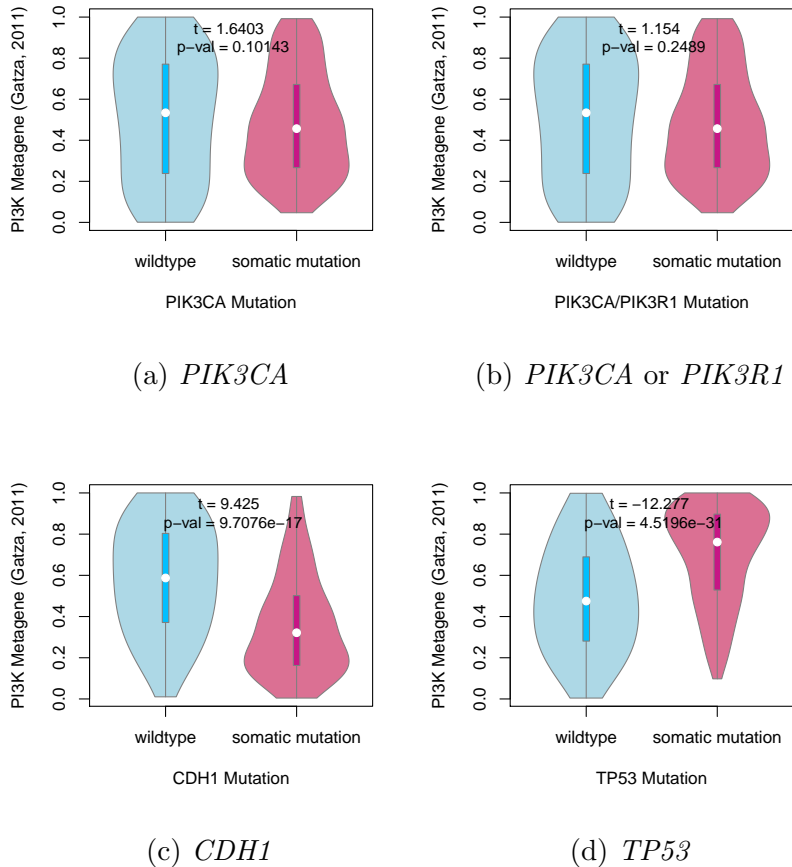


Figure 4.11: **Somatic mutation against the PI3K metagene.** Mutations in *PIK3CA*, *PIK3R1*, *CDH1*, and *TP53* were examined in TCGA breast cancer for their association with the PI3K (Gatza *et al.*, 2011) pathway metagene. The tumour suppressors *CDH1* and *TP53* showed an increase and decrease in the metagene respectively, whereas *PIK3CA* and *PIK3R1* mutations had little effect on the metagene levels.

### 4.3.3 Synthetic Lethal Pathway Metagenes

Pathway metagenes for Reactome pathways (generated as described in Section 2.2.3) were also used for testing synthetic lethal partner pathways with *CDH1* by SLIPT. Since the metagenes have are higher when the pathway as a whole is activated, they are amenable to SLIPT analysis using low metagene levels for inactivated pathways. These synthetic lethal metagenes differed to the over-represented pathways among synthetic lethal gene candidates. However, there were some similarities to previous findings, as shown in Tables 4.9. In particular, translational pathways were replicated

as observed in Table 4.2. While the specific pathways differ, immune pathways (e.g., NF- $\kappa$ B) were also supported by **metagene synthetic lethal** analysis.

Table 4.9: Candidate **synthetic lethal metagenes** against *CDH1* from SLIPT

Pathway	ID	Observed	Expected	$\chi^2$ value	p-value	p-value (FDR)
Glycogen storage diseases	3229121	68	130	176	$6.62 \times 10^{-37}$	$1.82 \times 10^{-34}$
Myoclonic epilepsy of Lafora	3785653	68	130	176	$6.62 \times 10^{-37}$	$1.82 \times 10^{-34}$
Diseases of carbohydrate metabolism	5663084	68	130	176	$6.62 \times 10^{-37}$	$1.82 \times 10^{-34}$
Arachidonic acid metabolism	2142753	81	130	157	$8.13 \times 10^{-33}$	$1.49 \times 10^{-30}$
Translation initiation complex formation	72649	70	130	152	$7.08 \times 10^{-32}$	$1.17 \times 10^{-29}$
Synthesis of 5-eicosatetraenoic acids	2142688	68	130	151	$1.25 \times 10^{-31}$	$1.88 \times 10^{-29}$
SRP-dependent cotranslational protein targeting to membrane	1799339	69	130	150	$2.01 \times 10^{-31}$	$2.76 \times 10^{-29}$
L13a-mediated translational silencing of Ceruloplasmin <b>expression</b>	156827	72	130	148	$5.91 \times 10^{-31}$	$6.44 \times 10^{-29}$
3' -UTR-mediated translational regulation	157279	72	130	148	$5.91 \times 10^{-31}$	$6.44 \times 10^{-29}$
Activation of the mRNA upon binding of the cap-binding complex and eIFs, and subsequent binding to 43S	72662	70	130	147	$1.14 \times 10^{-30}$	$9.28 \times 10^{-29}$
Formation of the ternary complex, and subsequently, the 43S complex	72695	70	130	147	$1.14 \times 10^{-30}$	$9.28 \times 10^{-29}$
Ribosomal scanning and start codon recognition	72702	70	130	147	$1.14 \times 10^{-30}$	$9.28 \times 10^{-29}$
Eukaryotic Translation Elongation	156842	72	130	146	$1.19 \times 10^{-30}$	$9.28 \times 10^{-29}$
Nonsense Mediated Decay independent of the Exon Junction Complex	975956	71	130	146	$1.24 \times 10^{-30}$	$9.28 \times 10^{-29}$
Viral mRNA Translation	192823	70	130	146	$1.51 \times 10^{-30}$	$1.04 \times 10^{-28}$
Eukaryotic Translation Termination	72764	70	130	146	$1.51 \times 10^{-30}$	$1.04 \times 10^{-28}$
NF- $\kappa$ B is activated and signals survival	209560	71	130	145	$1.90 \times 10^{-30}$	$1.19 \times 10^{-28}$
Peptide chain elongation	156902	72	130	145	$1.91 \times 10^{-30}$	$1.19 \times 10^{-28}$
Influenza Life Cycle	168255	70	130	145	$1.95 \times 10^{-30}$	$1.19 \times 10^{-28}$
Formation of a pool of free 40S subunits	72689	73	130	145	$2.01 \times 10^{-30}$	$1.19 \times 10^{-28}$
Nonsense-Mediated Decay	927802	71	130	145	$2.44 \times 10^{-30}$	$1.34 \times 10^{-28}$
Nonsense Mediated Decay enhanced by the Exon Junction Complex	975957	71	130	145	$2.44 \times 10^{-30}$	$1.34 \times 10^{-28}$
GTP hydrolysis and joining of the 60S ribosomal subunit	72706	72	130	145	$2.58 \times 10^{-30}$	$1.37 \times 10^{-28}$
Influenza Viral RNA Transcription and Replication	168273	72	130	144	$4.01 \times 10^{-30}$	$2.07 \times 10^{-28}$
Signalling by NOTCH1 HD Domain Mutants in Cancer	2691230	79	130	143	$5.99 \times 10^{-30}$	$2.82 \times 10^{-28}$

Strongest candidate **synthetic lethal** partners for *CDH1* by **SLIPT** with observed and expected numbers of TCGA breast cancer samples with low **expression** of both *CDH1* and the **metagene**.

Signalling pathways were more strongly supported by **mtSLIPT** analysis of **metagene** pathway **expression** against *CDH1* **mutation**, as shown in Table C.7, although these results were generally less statistically significant than **expression** analyses. Signalling pathways detected as **synthetic lethal metagenes** include G $_{\alpha z}$ , insulin-related growth factor (IGF), GABA receptor, G $_{\alpha s}$ , S6K1 and various toxin responses mediated by **GPCRs**. Metabolic processes including processing of carbohydrates and fatty acids were also implicated across these analyses.

The **metagene** analyses differ more between expression and *CDH1* **mutation** than previous analyses, with more specific signalling pathways identified in the **mutation** analysis. This supports the usage of a complete null **mutant** model in experimental testing for **synthetic lethality** of signalling pathways against CDH1 inactivation rather than a knockdown in **expression**. However, low **expression** of partners has been used in either case to be applicable to dose-dependent pharmacological inhibition and across genes where **mutations** have different functional consequences, including variants of unknown significance.

These results show an independent pathway-based approach to detecting synthetic lethal gene functions interacting with *CDH1*. The use of synthetic lethal metagenes replicates support for these pathways independent of pathway size (as genes are weighted equally). Along with the verifying that the direction of metagenes recapitulates the activity of a pathway, these demonstrate that many of the pathways previously identified from over-represented synthetic lethal genes (detected by SLIPT) are synthetic lethal pathways with their activity dependent on synthetic lethal genes rather than containing synthetic lethal genes as inhibitors or peripheral regulators of the pathways.

#### 4.3.4 Synthetic Lethality in Breast Cancer

The synthetic lethal analysis against low *CDH1* expression supports prior findings in translational and immune pathways even if they were not able to be detected in an experimental screen (Telford *et al.*, 2015). Together these findings support the role of *CDH1* loss in cancer disrupting cell signalling with wider effects on protein translation and metabolism necessary for the proliferation of cancer cells. This is consistent with the GPCR pathways such as G<sub>αs</sub> signalling being supported by SLIPT gene candidates and the experimental primary siRNA screen, as shown by resampling in Section 4.2.5.1.

### 4.4 Replication in Stomach Cancer

*CDH1* is also important in stomach cancer biology as a driver tumour suppressor gene, including as a germline mutation mutation in many cases of hereditary diffuse gastric cancer. The synthetic lethal analysis of genes and pathways (previously identified for TCGA breast cancer data) was replicated in TCGA stomach cancer. The accompanying data for SLIPT analysis against *CDH1* expression is provided in Appendix E.

While the sample size was lower for TCGA stomach cancer (particularly for mutations), these results serve to support the findings in breast cancer in an independent patient cohort and tissue samples. The molecular profiling, including RNA-Seq expression, were performed by TCGA using the sample procedures as for breast cancer and the findings reported here were performed used data analysis techniques identical to those presented previously. These procedures should ensure as close comparison as feasible across cancer types for those relevant to HDGC and recurrent *CDH1* mutations.

The strongest SLIPT genes for stomach cancer (shown in Table E.1) did not necessarily directly correspond to those observed in breast cancer (shown in Table 4.1). However, several gene functions were replicated in stomach cancer. Together, these gene candidates indicate widespread functions of *CDH1* and strongly detectable syn-

thetic lethality with many genes from a strategy that can be applied across cancer types. More specifically, the signalling genes included GPCR signalling genes, which was one of the most supported synthetic lethal pathways in breast cancer analysis, the experimental screen (Telford *et al.*, 2015). These findings were further supported by the pathways over-represented in SLIPT candidates from TCGA stomach cancer (shown in Table E.2) which replicated the translational and immune pathways observed in TCGA breast cancer (shown in Table 4.2) and further supported GPCR signalling pathways, including the class A/1 receptors. The extracellular matrix was also detected at the pathway level in stomach cancer, including elastic fibres, glycosylation, collagen, and integrin cell-surface interactions. While fewer pathways were supported by resampling for the intersection of SLIPT and experimental screen (Telford *et al.*, 2015) candidate partners in stomach cancer than breast cancer, many of those detected (shown in Table E.6) replicate those detected in breast cancer (shown in Table 4.8). The pathways detected by both permutation and over-representation were more likely to be replicated across stomach and breast cancer than those detected by over-representation alone, supporting the use of this procedure to detect synthetic lethal pathways applicable across cancer types. The include  $G_{\alpha s}$  signalling and elastic fibre formation as discussed for breast cancer (in Section 4.2.5.1).

## 4.5 Discussion

### 4.5.1 Strengths of the SLIPT Methodology

Synthetic lethal discovery with SLIPT used established statistical procedures to identify putative partner genes from gene expression data. Such use of the  $\chi^2$ -value is amenable to pathway or permutation analyses and could feasibly be applied to other disease gene or pair-wise across the genomes, although genomes-wide approaches were unable to find informative candidate genes for E-cadherin (Lu *et al.*, 2015). Synthetic lethal discovery in cancer has focused on genes with severe cellular mutant phenotypes, such as essential genes or the oncogenes TP53 and AKT (Lu *et al.*, 2015; Tiong *et al.*, 2014; Wang and Simon, 2013), with other cancer genes, such as CDH1, requiring more focused investigations. Prior computational approaches for synthetic lethal discovery, in cancer, vary widely (Jerby-Arnon *et al.*, 2014; Lu *et al.*, 2015; Tiong *et al.*, 2014; Wappett *et al.*, 2016). There is no consensus as to which approach is more appropriate, and the methods are difficult to compare, as they either do not have a released code implementation or do not make predictions solely from normalised expression data.

However, the query-based approach demonstrated by **SLIPT** analysis is suitable for wider application on **expression** data and for augmenting experimental studies such as high-throughput screens. This approach has identified biologically plausible **synthetic lethal** pathways for *CDH1*, triaged candidates from experimental screening (Telford *et al.*, 2015), and replicates genes and pathways across breast and stomach cancer datasets. In addition, **SLIPT** avoids critical assumptions underlying the design of some approaches such as co-expression of synthetic candidates or that interacting gene pairs will have known (annotated) similarities in function.

The DAISY methodology Jerby-Arnon *et al.* (2014), which took a similar query-based approach with the **tumour suppressor** *VHL*, has been critiqued for being too stringent (Lu *et al.*, 2015) which impedes pathway analysis. Since **functional redundancy** does not require genes to be expressed at the same time, the **SLIPT** approach does not assume co-expression of **synthetic lethal** genes which may enrich for **synthetic lethal** genes in established coregulated pathways. Rather, the interpretation of **synthetic lethality** for **SLIPT** was similar to other computational methods based on ‘co-loss under-representation’, ‘compensation’, or ‘simultaneous differential **expression**’ (Lu *et al.*, 2015; Tiong *et al.*, 2014; Wang and Simon, 2013).

Genomics analyses are prone to false-positives and require statistical caution, particularly where working with gene-pairs scale up the number of multiple tests drastically, at the expense of statistical power. Experimental screens for **synthetic lethality** are also error-prone (Fece de la Cruz *et al.*, 2015; Lord *et al.*, 2015; Lu *et al.*, 2015), especially with false-positives, raising the need for understanding the expected behaviour and number of functional relationships and genetic interactions in the **genomes**, or in discovery of **synthetic lethal** partners of a particular query gene. Thus analyses throughout this thesis have focused on querying for partners of a particular gene of interest. Statistical modelling and simulations (in Section 3.3 and Chapter 6) will further support the design decisions underlying **SLIPT** analysis and its strengths over other approaches.

#### 4.5.2 Synthetic Lethal Pathways for **E-cadherin**

Specific genes were difficult to replicate across experiments. This is consistent with **gene expression** profiles for **synthetic lethal** partners reflecting the complexity of biological pathways which are subject to higher-order interactions and do not consistently compensate for loss of gene function across all samples (Jerby-Arnon *et al.*, 2014; Kelly, 2013; Lu *et al.*, 2015). The predicted **synthetic lethal** partners of *CDH1* (with FDR correction) were investigated with **gene expression** profiles and clinical variables to

find relationships in gene expression, gene function, and clinical characteristics. The large number of genes detected indicates that synthetic lethal detection is potentially error-prone, and that identifying genes relevant for clinical application will be difficult without a supporting biological pathway rationale. As such, investigations into the genes identified by SLIPT, the correlation structure between them, and those which were validated by experimental screening (Telford *et al.*, 2015) focused at the pathway level throughout this Chapter. Similarly, comparisons across analyses were largely made at the pathway level, including comparisons between expression and mutation, breast and stomach TCGA datasets.

Potential synthetic lethal partners of *CDH1* identified by SLIPT had many distinct functions, with each gene cluster highly expressed in different patient subgroups (Figure 4.1). The expression profiles of the SL partners of *CDH1* predicted from TCGA breast cancer RNA-Seq data (expected to have compensating high or stable expression) and their corresponding functional enrichment found in subgroups of genes, particularly among *CDH1* low breast tumours. Ductal breast cancers showed higher expression of synthetic lethal partners suggesting treatment would be more effective in this tumour subtype. However, there was consistently low expression of SL partners in estrogen receptor negative tumours, although this is independent of tumour stage and consistent with poor prognosis in these patients and could inform other treatment strategies or prevent ineffective treatment further impacting quality of life in these patients. These results suggest that synthetic lethal partner expression varies between patients; that these different tumour classes would react differently to the same treatment; that treatment of different pathways and combinations in different patients is the most effective approach to target genes compensating for *CDH1* gene loss; and that the expression of synthetic partners could be a clinically important biomarker.

The pathways that synthetic lethal partners of *CDH1* identified by SLIPT were involved in a diverse range of biological functions and differed to those detected experimentally. This discrepancy may be accounted for by gene expression analyses detecting both synthetic lethal partners, as screened for experimentally by Telford *et al.* (2015), and their downstream targets (not detected by siRNA), capturing the wider pathways and mechanisms involved in synthetic lethality with *CDH1* inactivation. In particular, GPCR phosphorylation cascades (which regulate gene expression and translation in cancers (Gao and Roux, 2015)) were predicted to be synthetic lethal with *CDH1*. The predicted synthetic lethal partners occurred across functionally distinct pathways, including characterised functions of *CDH1*. The most consistently supported pathways

included elastic fibres in the extracellular matrix, GPCR signalling, and translation presenting vulnerabilities for *CDH1* deficient cancer cells from extracellular stimuli to the core growth mechanisms of a cell.

This diversity in synthetic lethal functions is consistent with the wide ranging role of *CDH1* in cell-cell adhesion, cell signalling, and the cytoskeletal structure of epithelial tissues. Pathway structure may be relevant to identifying potential drug targets from gene expression signatures, indicating downstream effector genes and mechanisms leading to cell inviability. Identification of distinct synthetic lethal gene clusters may further lead to the elucidation of drug resistance mechanisms. While these pathways are indicative of the main functions of E-cadherin and synthetic lethal partners, it remains to identify the genes within these pathways that are the most actionable or supported across SLIPT analysis in patient samples and detected by experiments in preclinical models (Chen *et al.*, 2014; Telford *et al.*, 2015). The specific genes within key pathways will be discussed in Chapter 5, along with further investigations into their relation to pathway structure. While these are important clinical implications, the synthetic lethal predictions lack enough confidence for direct translation into pre-clinical models or clinical applications leading to a need for statistical modelling and simulation of synthetic lethality in genomics expression data.

These synthetic lethal pathways have potential clinical implications, particularly those supported in pre-clinical models and in patient expression data. However, further validation of gene candidates will be necessary to ensure that these are able to be reproduced in further pre-clinical studies, they are applicable to tumours *in vivo*, and that effective inhibitory agents can be repurposed or designed against them.

### 4.5.3 Replication and Validation

#### 4.5.3.1 Integration with siRNA Screening

The pathway composition across computational and experimental synthetic lethal candidates was informative with over-representation (Table 4.6) and supported by resampling analysis (Table 4.8), despite a modest intersection of genes between them (Figure 4.2). Either approach may be significant for a pathway in this intersection without being supported by the other: resampling analysis may support pathways that were not over-represented due to small effect sizes, thus both tests are required for a candidate pathway.

The pathways detected by both over-representation and resampling are the strongest candidates for further investigation and the pathway structure analyses in Chapter 5

will focus on these pathways detected by both over-representation and resampling. Particularly, those replicated across datasets or with pathway [metagenes](#). In addition to GPCR pathways detected across these analyses, the [PI3K](#) cascade will also be investigated in Chapter 5, this signalling pathway is a well characterised mediator between GPCR receptors and regulation of translation (Gao and Roux, 2015) (both detected throughout this Chapter) and exhibited unexpected behaviour with pathway the [metagenes](#) (in Section 4.3). This pathway is activated by protein Phosphorylation states and thus inactivation may not be detectable with [expression](#).

However, the [SLIPT](#) approach was shown to be predictive of which [siRNA](#) primary screen candidate partners of *CDH1* were validated in a secondary screen (as shown in Section 4.2.4). These results further support [SLIPT](#) for identifying robust [synthetic lethal](#) candidates which can be validated and as a triage approach for interpreting screening experiments.

#### 4.5.3.2 Replication across Tissues

Furthermore, [synthetic lethal](#) partners identified by [SLIPT](#) were replicated across breast and stomach cancer. These were particularly concordant at the pathway level, as expected between tissues since [synthetic lethal](#) pathways have higher conservation between species (Dixon *et al.*, 2008). These findings support gene functions conserved across *CDH1* deficient cancers in breast and stomach tissues, presenting vulnerabilities that could be applied against molecular targets in both cancers. In addition, these analyses serve as a replication across independent patient cohorts from breast and stomach cancers, decreasing the likelihood of the [synthetic lethal](#) pathways detected being false positives or artifacts of either dataset.

Synthetic lethal pathways were also replicated across [expression](#) analyses of [TCGA](#) patient samples in heterogeneous tumours and homogeneous cell line isolates. This further supports that the subset of [synthetic lethal](#) functions detectable in experimental models (Chen *et al.*, 2014; Telford *et al.*, 2015) would be applicable to tumours of patients with *CDH1* deficient cancers.

There are many gene functions replicated across breast cancer [gene expression](#) analyses. Many of these were also replicated with [mutation](#) analysis and with stomach cancer or cell line [expression](#) data. These pathways were more consistent across replication analyses than previous investigations with [TCGA microarray](#) data (Kelly, 2013).

## 4.6 Summary

We have developed a simple, interpretable, computational approach to predict synthetic lethal partners from genomics data. The analyses focus on gene expression data as it is widely available for applications in other cancers and other disease genes, particularly those with malignant loss of function.

This approach has been applied to robustly detect synthetic lethal pathways for the E-cadherin (*CDH1*) in TCGA breast cancer molecular profiles with comparisons to experimental screening (Telford *et al.*, 2015) in cell lines, and replication in TCGA stomach cancer molecular profiles and across cell types in the cancer cell line encyclopaedia. The pathway replicated across several analyses included extracellular matrix pathways (e.g., elastic fibres formation), cell signalling (including GPCRs), and core gene regulation and translation processes crucial for the growth and proliferation of cancer cells. These pathways show evidence of non-oncogene addiction for *CDH1* deficient cells and present vulnerabilities which may be exploited for specific treatment against *CDH1* mutations in HCGC and sporadic cancers. There was also support for synthetic lethal pathways with *CDH1* in cell adhesion and cytoskeletal processes to which *CDH1* belongs, supporting the finding that synthetic lethality occurs within biological pathways (Boone *et al.*, 2007; Kelley and Ideker, 2005).

While translational and immune pathways detected by SLIPT were not supported by primary siRNA screening (Telford *et al.*, 2015), these were replicated across various analyses. Due to the differences between an experimental cell line model (Chen *et al.*, 2014; Fece de la Cruz *et al.*, 2015) and patient molecular profiles (Bass *et al.*, 2014; Koboldt *et al.*, 2012), these would not be expected to be completely concordant. Furthermore, many pathways are difficult to test in an isolated experimental system. Nevertheless, many of the genes and pathways detected by SLIPT are suitable to inform further investigations and triage of therapeutic targets against *CDH1* deficient tumours in combination with experimental screening.

A characteristic of gene interaction networks is a scale-free topology leading to highly interacting ‘hub’ genes, these represent important genes in a functional network. Cell surface interactions, the extracellular matrix, and cell signalling (particularly PI3K/AKT signalling) were also found to be synthetic lethal hubs with more interactions detected than other genes. This indicates that these pathways are functionally important to survival of cancer cells since they are subject to high functional redundancy, despite frequent disruptions in cancer. These pathways being involved in

a disproportionate number of [synthetic lethal](#) interactions is also consistent with their detection for *CDH1*.

Thus [synthetic lethal](#) pathways have been identified using [TCGA](#) patient molecular profiles and experimental screening results. Some of these were robustly replicated across these datasets and against *CDH1* [mutation](#) or [expression](#) analysis. However, there remains the need to identify actionable genes within these pathways, relationships with experimental candidates, and how these pathways may affect viability when lost. While the genes identified between these analyses were less concordant the results of the [TCGA](#) breast cancer analysis will be used to test [pathway](#) structure relationships and further examine the [synthetic lethal](#) genes detected in the following Chapter.

# Chapter 5

## Synthetic Lethal Pathway Structure

Having identified key pathways implicated in [synthetic lethal](#) genetic interactions with *CDH1* (in Chapter 4), these were investigated for the [synthetic lethal](#) genes within them and their relationships to [pathway](#) structure in Reactome pathways. This chapter will focus on the [pathway](#) structure of biological pathways detected across analyses in Chapter 4.

The [synthetic lethal](#) genes identified were further examined within the context of biological pathways. Specifically, investigations were performed on whether [synthetic lethal](#) candidates, detected by [SLIPT](#) or [siRNA](#), exhibited differences with respect to network metrics of [pathway](#) structure of connectivity and importance in the network (as described in Sections 2.4.4 and 3.5.3). The relationships between [synthetic lethal](#) candidates, detected by either approach, were also considered to detect whether genes detected by [SLIPT](#) were upstream or downstream of genes detected by [siRNA](#). These directional relationships were tested by resampling (as described in Sections 3.4.1 and 3.4.1.1) and comparisons to the pathway hierarchical score based on biological context (as derived in Section 3.4.1.2). Together these investigations into structural relationships demonstrate how a combination of network biology and statistical techniques can be performed with genes identified by a [bioinformatics](#) analysis.

### 5.1 Synthetic Lethal Genes in Reactome Pathways

The [graph](#) structure for Reactome pathways was obtained from Pathway Commons via [BioPAX](#) (as described in Section 2.4.2). The pathways describe the (directional) relationships between biomolecules, including genes that encode proteins in biological pathways. These relationships include cell signalling (e.g., kinase phosphorylation cascades), gene regulation (e.g., transcription factors, chromatin modifiers, [RNA](#) bind-

ing proteins), and metabolism (e.g., the product of an enzyme being the substrate of another). Together these relationships describe the known functional pathways in a human cell with a reasonable resolution, from a curated database supported by publications documenting pathway relationships.

Pathway structures from the Reactome network (as described in Section 2.4.3) were used to derive the graph structure of each biological pathway. The synthetic lethal candidate genes for notable pathways discussed in Chapter 4, including candidate synthetic lethal pathways of *CDH1*, were examined to show the SLIPT and siRNA candidates within these pathways. The synthetic lethal genes considered here are those candidates detected by SLIPT (as described in Section 3.1) in TCGA breast cancer expression and mutation data (Koboldt *et al.*, 2012) in comparison to the candidate gene partners from the siRNA screening in breast cell lines (Telford *et al.*, 2015).

### 5.1.1 The PI3K/AKT Pathway

The phosphoinositide 3-kinase (PI3K) cascade signalling pathway exhibited unexpected results with metagene analyses (as discussed in Section 4.3). This pathway is also of interest because mediating signals between the GPCRs and regulation of protein translation have both been strongly implicated to be synthetic lethal pathways with loss of *CDH1* function (in Chapter 4). These pathways have all subject to dysregulation in cancer (Courtney *et al.*, 2010; Dorsam and Gutkind, 2007; Gao and Roux, 2015). Thus the PI3K cascade will be examined along with the most supported synthetic lethal pathways (as identified in Chapter 4).

The PI3K pathway is also an ideal pathway in which to test pathway structure because it has an established direction of signal transduction from extracellular stimuli (and membrane bound receptors) to the inner mechanisms of the cell, namely, the regulation of protein translation. The production of proteins is necessary for the growth of the cell so it is reasonable to suggest that these processes may be subject to (non-oncogene) addiction in some cancer cells which rely upon them for sustained protein production and cell growth. This is also supported by the oncogenes *PIK3CA* and *AKT1* being involved with the PI3K cascade and related PI3K/AKT pathway which may be subject to oncogene addiction when these proto-oncogenes are activated.

The PI3K cascade was not supported across SLIPT in TCGA breast expression data and the siRNA primary screen by over-representation (in Section 4.2.5) or resampling (in Section 4.2.5.1) but genes were detectable by either approach (as shown in Figure 5.1). While few genes were identified by both approaches, these include genes

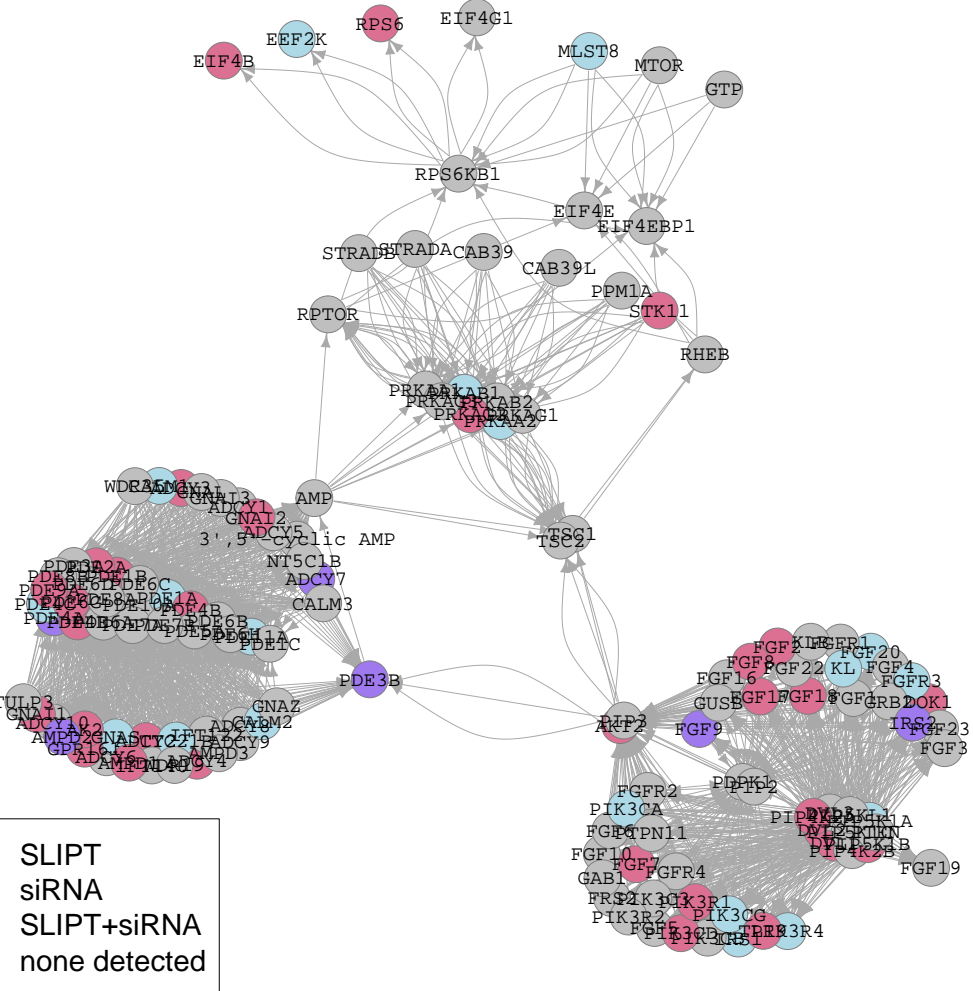


Figure 5.1: **synthetic lethality in the PI3K cascade.** The Reactome PI3K Cascade pathway with **synthetic lethal** candidates coloured as shown in the legend.

that are highly connected in the PI3K cascade and are hubs to information transmission such as *FGF9*, *PDE3B*, and *PDE4A*. The key upstream genes *PIK3CA* and *PIK3CG* were detected by siRNA whereas the downstream *PIK3R1* and *AKT2* genes were detected by SLIPT. Gene detected by either method were also prevalent in the PI3K, phosphodiesterase (PDE), and AMP-activated protein kinase (AMPK) modules, in addition to the downstream translation factors and ribosomal genes (*EIF4B*, *EEF2K*, and *RPS6*). Together these suggest that there may be further structure between the SLIPT and siRNA candidate partners of *CDH1* in pathways as illustrated by PI3K. As

such, **pathway** structure will be investigated to detect differences in the upstream and downstream gene candidates of those detected by either method. Pathway structure may account for the disparity between **SLIPT** and **siRNA** genes, even in pathways such as PI3K where they did not significantly intersect. For instance, **SLIPT** gene partners may be downstream of **siRNA** candidates rather than replicating them directly.

This disparity between **SLIPT** and **siRNA** gene candidate **synthetic lethal** partners of *CDH1*, that is a high number of genes detected by either approach with few detected by both, was replicated in the related PI3K/AKT pathway and the “PI3K/AKT in cancer” pathway (shown in Appendix Figures F.1 and F.2). Many **synthetic lethal** candidates were at the upstream core of these pathway networks and the downstream extremities. It is particularly notable that the many genes important in cell signalling and gene regulation were detected by either **synthetic lethal** detection approach. These include *AKT1*, *AKT2*, and *AKT3*, the Calmodulin signalling genes *CALM1* and *CAMK4*, and the forkhead family transcription factors *FOXO1* (a **tumour suppressor**) and *FOXO4* (an inhibitor of **EMT**).

### 5.1.2 The Extracellular Matrix

The extracellular pathways “elastic fibre formation” and “fibrin clot formation” (shown in Figures 5.2 and 5.3 respectively) were both supported across analyses (in Chapter 4). Significant over-representation and resampling the intersection between **SLIPT** (for **TCGA** breast cancer) and **siRNA** gene candidates showed that both approaches identified these pathways.

Particularly for elastic fibres (Figure 5.2), the vast majority of genes were detected by either approach in addition to a significant proportion of genes detected by both approaches (as determined in Section 4.2.5). The genes detected by both approaches also appeared to have a non-random distribution in the network with *TFGB1*, *ITGB8*, and *MFAP2* exhibiting high connectivity, and having a central role in their respective pathway modules. In addition to a structural role in the extracellular matrix and connective tissue (including the tumour microenvironment), these proteins including Furin, **transforming growth factor  $\beta$  (TGF $\beta$ )**, and the **bone morphogenic proteins (BMPs)**, are also involved in responses to endocrine signals and interact with the cellular receptors for signalling pathways. Therefore it is plausible that *CDH1* deficient tumours will be subject to **non-oncogene addiction** to the extracellular environment and growth signals arising from this pathway. The **pathway** structure also indicative for further investigation that the genes detected by **siRNA** (or both approaches) may

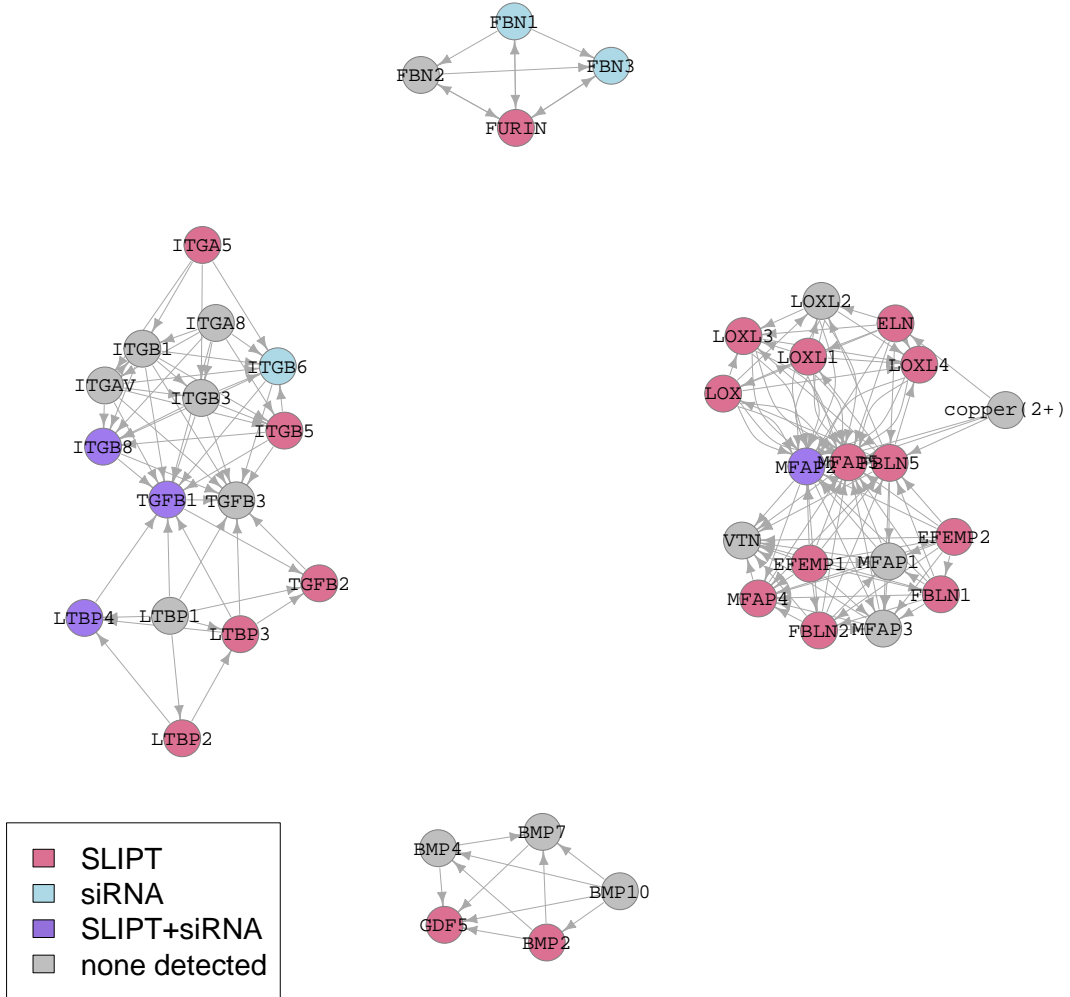


Figure 5.2: **synthetic lethality in Elastic Fibre Formation.** The Reactome Elastic Fibre Formation pathway with [synthetic lethal](#) candidates coloured as shown in the legend.

be downstream of those detected by [SLIPT](#), in addition to whether connectivity or [centrality](#) is higher for [synthetic lethal](#) candidates than other genes in the pathway.

Genes detected as [synthetic lethal](#) partners of *CDH1* by [SLIPT](#) or [siRNA](#) screening were also common in the Fibrin clot formation pathway (shown in Figure 5.3). This is consistent with the established pleiotropic role of *CDH1* in regulating fibrin clotting. It is also notable that the genes detected by either method appear to be highly connected such as *C1QBP*, *KNG1*, *F8*, *F10*, *F12*, *F13A*, and *PROC* (including many of the coagulation factors). [Synthetic lethal](#) candidates also include *SERPINE2* and *PRCP*,

which only affect downstream genes, in addition to *PROCR* and *VWF*, which are only affected by upstream genes.

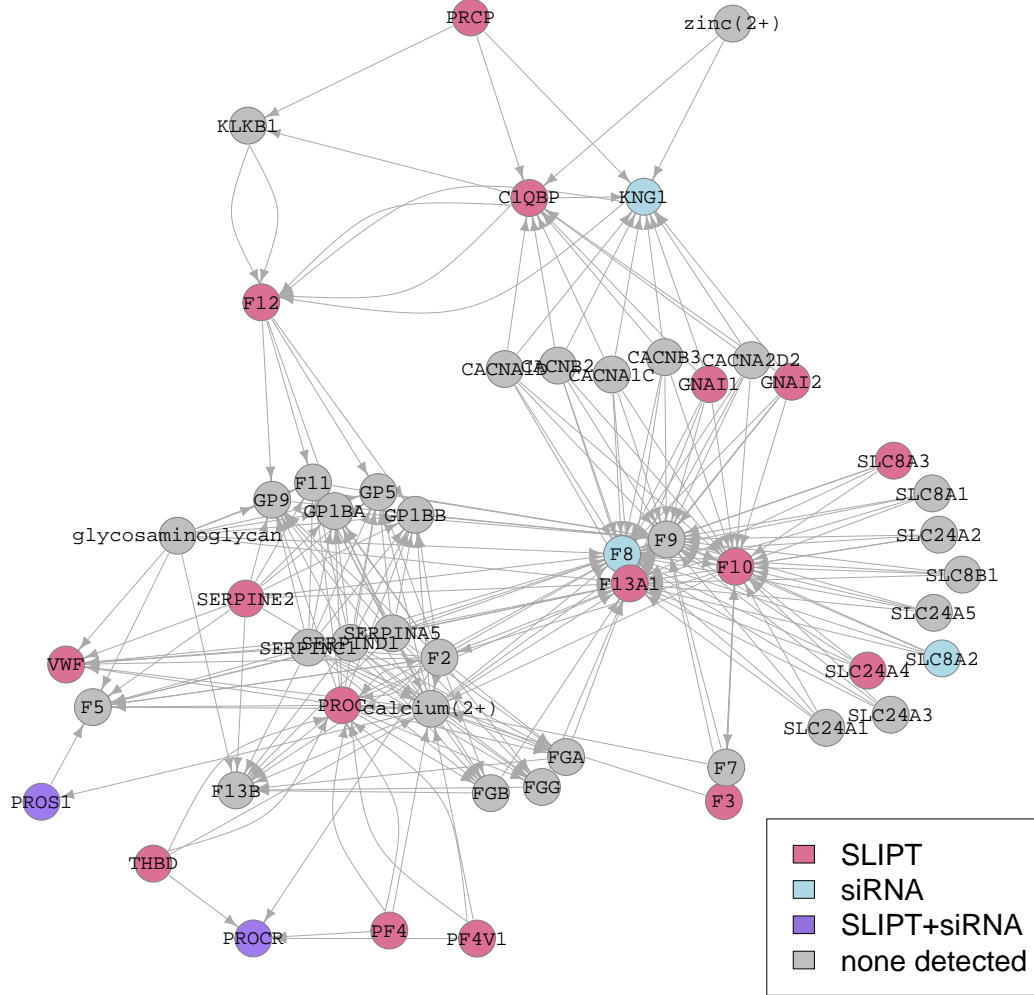


Figure 5.3: **Synthetic lethality in Fibrin Clot Formation.** The Reactome Fibrin Clot Formation pathway with synthetic lethal candidates coloured as shown in the legend.

Many of these genes are involved in the larger Extracellular Matrix pathway (shown in Appendix Figure F.3), including many of the synthetic lethal candidates discussed for elastic fibres. The number of SLIPT candidate genes outnumbers those identified by siRNA, as expected from an isolated cell model. However, the endocrine response genes (e.g., *TGFB1* and *LTPB4*) which are potentially artifacts of the cell line growth process were replicated with SLIPT analysis in patient tumours (TCGA breast cancer

data). There is also additional support for **synthetic lethal** genes (e.g., *ITGB2*, *MFAP2*, and *SPARC*) being highly connected networks hubs of the pathway. The complexity of the extracellular matrix pathway lends credence to the need for formal network analysis approaches to interpret the **pathway** structure of **synthetic lethal** candidates. Furthermore statistical approaches are needed to determine whether structural relationships are unlikely to be observed between **synthetic lethal** candidates by sampling error.

### 5.1.3 G Protein Coupled Receptors

**G protein coupled receptor (GPCR)** pathways are highly complex (as shown in Appendix Figures F.4 and F.5). Many of genes in these pathways were **synthetic lethal** candidates, detected by either **SLIPT** or **siRNA** screening, including genes frequently detected with both approaches, consistent with these pathways being supported by prior analyses (in Sections 4.2.5 and 4.2.5.1). **Synthetic lethal** candidates include the **PDE** and Calmodulin genes (as discussed in Section 5.1.3) in addition to others such as the regulators of **G-protein signalling (RGS)**, **chemokine receptors (CXCR)**, **Janus kinase (JAK)**, and the **Ras homolog family (RHO)** genes. These are important regulatory signalling pathways necessary for cellular growth and cancer proliferation. Thus the **GPCR** pathways (and downstream PI3K/AKT signals) are a potentially actionable vulnerability against *CDH1* deficient cancers, particularly since many existing drug targets exist among these signalling pathways, some of which have been experimentally validated (Kelly *et al.*, unpublished; Telford *et al.*, 2015). However, the complexity of **GPCR** networks containing hundreds of genes requires the relationships between **SLIPT** and experimental candidates to be tested with a network based statistical approach, although statistically significant number of genes in GCPR pathways was detected by both approaches (in Sections 4.2.5 and 4.2.5.1).

### 5.1.4 Gene Regulation and Translation

While very few **synthetic lethal** genes were detected in translational pathways in an experimental screen against *CDH1* (Telford *et al.*, 2015), these were highly overrepresented in translational elongation (as shown in Appendix Figure F.6). These **SLIPT** genes include many ribosomal proteins and the regulatory “elongation factors” which may be subject to responses in the upstream signalling pathways. This observation lends support to the notion of **pathway** structure among **synthetic lethal** candidates detected by **SLIPT** in comparison with **siRNA**. The computational approach with **SLIPT** displays the ability to detect downstream genes in the core translational processes which experimental screening did not identify. The experimental screening

may similarly detect upstream regulatory genes less sensitive to inactivation, that is, genes that are less likely to be indiscriminately lethal to both genotypes at high doses of inactivation.

Many of these **SLIPT** candidate genes are also among the **nonsense-mediated decay (NMD)** pathway (shown in Appendix Figure F.7) or **3' untranslated region (UTR)** mediated translational regulation (shown in Appendix Figure F.8). While genes in these pathways were also supported by experimental screening with **siRNA**, there was differences in which genes were detected within the **pathway** structures. In particular, *UPF1* was detected in the **siRNA** screen and is the focal downstream gene for the entire **NMD** pathway showing that (in this case) **siRNA** genes are downstream effectors of those detected by **SLIPT**. **3' UTR** mediated translational regulation has a similar structure with two modules connected solely by *RPL13A*, giving an example of **SLIPT** candidate genes with high connectivity, although there were many ribosomal proteins detected by **SLIPT**. However, the detection of *EIF3K*, a regulatory elongation factor (not **essential** to ribosomal function) was replicated across **SLIPT** and **siRNA** screening, while the majority of the elongation factors were not detected by either approach. Regulatory genes, being more amenable to experimental validation, also support further investigation into **pathway** structure. The **SLIPT** candidates may support experimental candidates in biological pathways by detecting downstream genes, which may not be detectable by experimental screening with high dose inhibitors. This difference between the approaches may explain the greater number of **SLIPT** candidate partners of *CDH1* than those experimentally identified.

## 5.2 Network Analysis of Synthetic Lethal Genes

Genes detected as **synthetic lethal** partners of *CDH1* with the **SLIPT** computational approach and the **siRNA** screen (Telford *et al.*, 2015) were compared across network metrics in the example of the PI3K cascade pathway (where the genes differed considerably between **synthetic lethal** detection methods). These were used to test whether network metrics differed between groups of genes detected by either or both approaches. These analyses serve to test both whether **synthetic lethal** gene candidates had higher connectivity or importance in a network and whether either detection approach is biased towards genes with different network properties.

### 5.2.1 Gene Connectivity and Vertex Degree

Vertex degree (the number of connections) for each gene is a fundamental property of a network. The vast majority of genes had a relatively modest number of connections, each with only a few genes in the PI3K pathway (shown in Figure 5.4) having pathway relationships with a high number of genes, consistent with the [scale-free](#) property of biological networks ([Barabási and Oltvai, 2004](#)). There were few differences in the number of connections between gene groups (by [synthetic lethal](#) detection), although genes detected by [siRNA](#) included those with the fewest connections. The median connectivity of genes detected by both approaches was marginally higher.

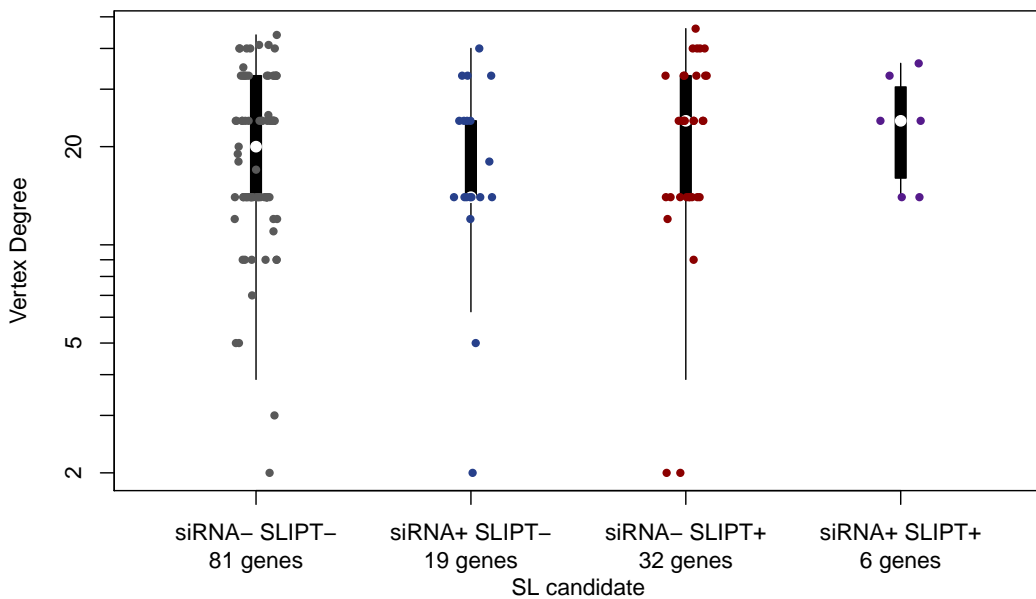


Figure 5.4: **Synthetic lethality and vertex degree.** The number of connected genes ([vertex degree](#)) was compared (on a log-scale) across genes detected by [SLIPT](#) and [siRNA](#) screening in the Reactome PI3K cascade pathway. There were very few differences in [vertex](#) degree between the groups, although genes detected by [siRNA](#) included those with the fewest connections.

Table 5.1: ANOVA for synthetic lethality and vertex degree

	DF	Sum Squares	Mean Squares	F-value	p-value
siRNA	1	15	15.50	0.0134	0.9082
SLIPT	1	506	506.01	0.4378	0.5105
siRNA × SLIPT	1	0	0.05	0.0000	0.9947

Analysis of variance for `vertex` degree against `synthetic lethal` detection approaches (with an interaction term)

The results for the PI3K pathway were very similar when testing `synthetic lethality` against `CDH1 mutation` (`mtSLIPT`). In this case, there is also indication that `mtSLIPT`-specific genes may have higher connectivity than those detected by `siRNA` screening (shown in Appendix Figure G.1).

However, these apparent differences in `vertex` degree may be due to fewer genes being detected by either approach. There was no statistically significant effect of either computational or experimental synthetic lethal detection method on `vertex` degree, as determined by analysis of variance (ANOVA) (shown by Table 5.1 and Appendix Table G.1). Thus `synthetic lethal` detection does not discriminate among genes by their connectivity in a pathway network, nor is either approach constrained to detecting highly connected genes. Both approaches have been demonstrated to detect genes with many and very few connections.

## 5.2.2 Gene Importance and Centrality

### 5.2.2.1 Information Centrality

`Information centrality` is a measure of the importance of `nodes` in a network by how vital they are to the transmission of information throughout the network. This applies well to biological pathways, particularly gene regulation and cell signalling. The `nodes` with the highest `information centrality` are not necessarily the most connected, as they may also include `nodes` that pass signals between highly connected network hubs. `Information centrality` therefore provides a distinct metric for the connectivity of a gene in a pathway, which has the added benefit of being directly related to the disruption of pathway function were it to be inactivated or removed.

`Information centrality` has also been suggested to indicate essentiality of genes or proteins (Kranthi *et al.*, 2013). The `information centrality` for each gene was computed across the entire Reactome network (as discussed in Appendix H). Reactome contains substrates and cofactors in addition to genes and proteins. In support of `centrality`

as a measure of essentiality or importance to the network, a number of **nodes** with the highest **centrality** (shown in Appendix Table H.1) were **essential** nutrients, including Mg<sup>2+</sup>, Ca<sup>2+</sup>, Zn<sup>2+</sup>, and Fe.

Genes important in development of epithelial tissues and breast cancer were also detected with relatively high **information centrality** (as shown by the distribution across the Reactome network in Appendix Figure H.1). Interleukin 8 (encoded by *IL8*) is a chemokine important in epithelial cells, the innate immune system, and binding GPCRs. *GATA4* is an embryonic transcription factor involved in heart development, EMT, and has been shown to be recurrently mutated in breast cancer (Koboldt *et al.*, 2012).  $\beta$ -catenin (encoded by the proto-oncogene *CTNNB1*) is a regulatory protein which binds to E-cadherin, being involved in cell-cell adhesion and Wingless-related integration site (WNT) signalling. Together these show that **information centrality** identifies **nodes** of importance to biological functions in pathway networks, including those relevant to *CDH1* deficient breast cancers.

Within the PI3K pathway, genes detected by **siRNA** did not include those with lower **centrality** (shown in Figure 5.5), although the median **information centrality** across gene groups detected by either **synthetic lethal** approach did not differ. The genes with the highest **information centrality** included the synthetic candidates *PDE3B* (detected by SLIPT and **siRNA**) and *AKT2* (detected by SLIPT) which were markedly higher than most other genes in the pathway. The higher **centrality** of these genes is consistent with their known biological role in PI3K/AKT signalling and the **pathway** structure (shown in Figure 5.1). Other biomolecules with high **centrality** included the *RPS6KB1* and *RP-TOR* genes, adenosine monophosphate (AMP), phosphatidylinositol-(4,5)-bisphosphate (PIP<sub>2</sub>), and phosphatidylinositol-(3,4,5)-trisphosphate (PIP<sub>3</sub>).

These findings were replicated (shown in Appendix Figure G.2) when testing synthetic lethality against *CDH1* mutation (mtSLIPT). The differences in network **centrality** between gene groups detected by either method were not statistically significant as determined by **ANOVA** (shown by Table 5.2 and Appendix Table G.2). Thus neither method was unable to detect **synthetic lethal** genes with particular **centrality** constraints, although they were also not detecting genes with higher **centrality** than expected by chance.

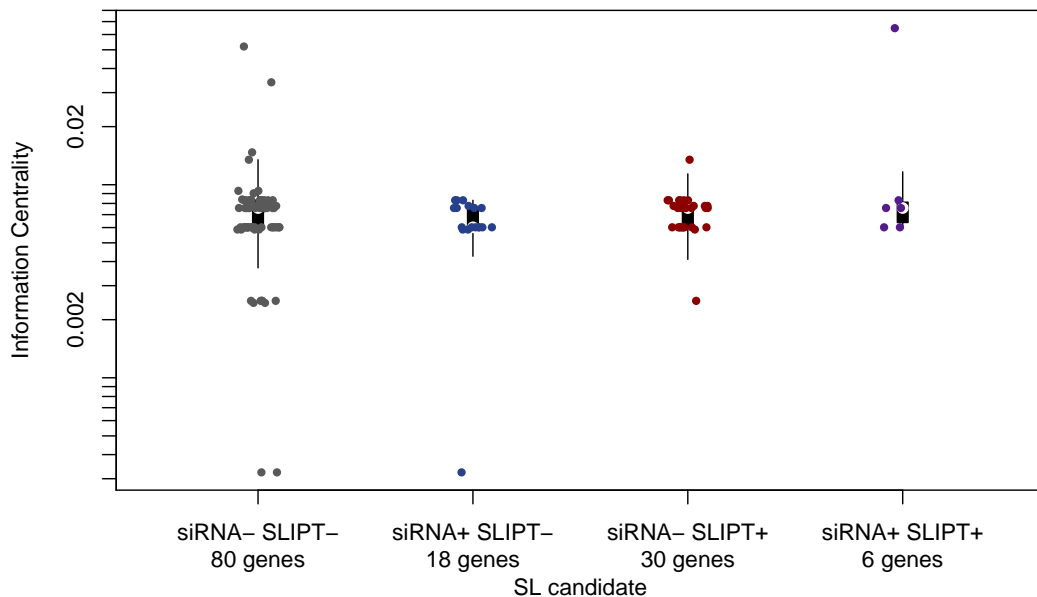


**Figure 5.5: Synthetic lethality and centrality.** The [information centrality](#) was compared (on a log-scale across genes detected by [SLIPT](#) and [siRNA](#) screening in the Reactome PI3K cascade pathway. Genes detected by [SLIPT](#) or [siRNA](#) did not have higher connectivity than other genes. The gene with the highest [centrality](#) was detected by both approaches.

Table 5.2: [ANOVA](#) for synthetic lethality and information centrality

	DF	Sum Squares	Mean Squares	F-value	p-value
siRNA	1	0.000256	0.0002561	0.1854	0.6682
SLIPT	1	0.003827	0.0038275	2.7717	0.1008
siRNA×SLIPT	1	0.000804	0.0008036	0.5820	0.4483

Analysis of variance for [information centrality](#) against [synthetic lethal](#) detection approaches (with an interaction term)

### 5.2.2.2 PageRank Centrality

[PageRank centrality](#) is another network analysis procedure to infer a hierarchy of gene importance from a network using connections and structure ([Brin and Page, 1998](#)). In contrast to the [information centrality](#) approach of removing [nodes](#), PageRank uses the eigenvalue properties of the adjacency matrix to rank genes according to the number of connections and paths they are involved in.

This distinction is immediately clear within the PI3K pathway (shown in Figure 5.6), which differs considerably from the information centrality scores. Genes detected by SLIPT span the complete range of PageRank centrality values for this pathway, which was replicated when testing synthetic lethality against *CDH1* mutation (shown in Appendix Figure G.3). However, the genes detected by both SLIPT and siRNA screening have a higher median PageRank centrality, although the differences in PageRank centrality between these methods were not statistically significant as determined by ANOVA (shown by Table 5.3 and Appendix Table G.3).

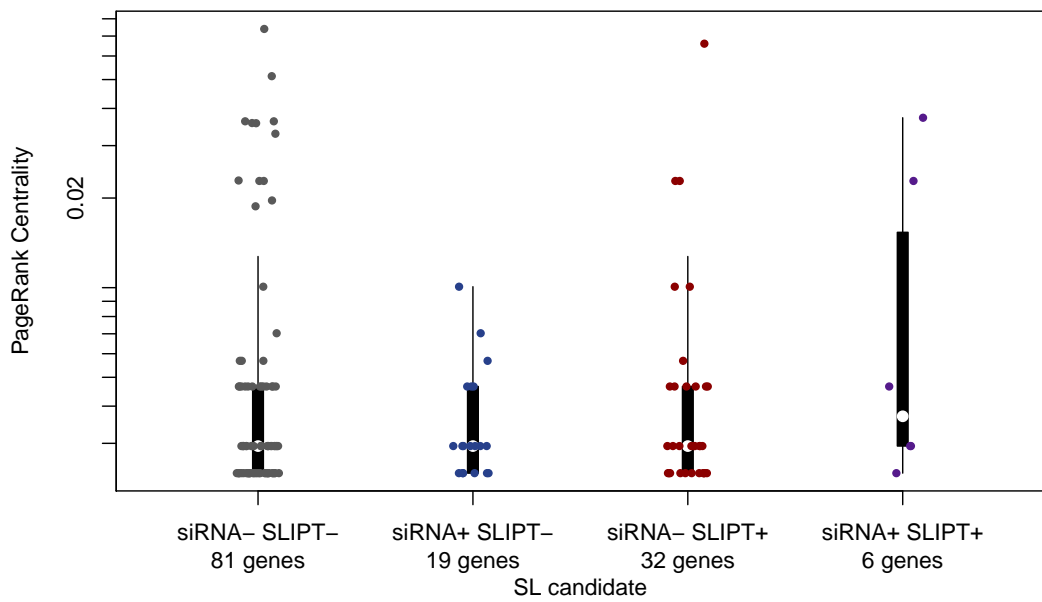


**Figure 5.6: Synthetic lethality and PageRank.** The PageRank centrality was compared (on a log-scale across genes detected by mtSLIPT and siRNA screening in the Reactome PI3K cascade pathway. Genes detected by siRNA had a more restricted range of centrality values (which may be constrained experimental detection in a cell line model) than other genes not detected by either approach, although these groups also had fewer genes and a higher median.

Table 5.3: ANOVA for synthetic lethality and PageRank centrality

	DF	Sum Squares	Mean Squares	F-value	p-value
siRNA	1	0.0002038	$2.0385 \times 10^{-4}$	1.1423	0.2892
SLIPT	1	0.0000208	$2.0752 \times 10^{-5}$	0.1163	0.7342
siRNA × SLIPT	1	0.0000137	$1.3743 \times 10^{-5}$	0.0770	0.7823

Analysis of variance for [PageRank centrality](#) against [synthetic lethal](#) detection approaches (with an interaction term)

## 5.3 Relationships between Synthetic Lethal Genes

### 5.3.1 Hierarchical Pathway Structure

#### 5.3.1.1 Contextual Hierarchy of PI3K

A contextual hierarchy of genes in the [PI3K](#) pathway was performed (as described in in Section 3.4.1.2) to assign scores for their relative order in the pathway. In the case of [PI3K](#) (shown in Figure 5.7), this orders genes from the upstream genes, which respond to signals from extracellular stimuli, to the downstream genes which transmit these to the [gene expression](#) (translation) responses of the cell. The directionality of this pathway is evident in transmitting signals from the [PI3K](#) complex, via AKT, [PDE](#), and mTOR to the ribosomal regulatory proteins. This hierarchical procedure enables testing whether the biological context of a gene in a pathway is relevant to detection as a [synthetic lethal](#) candidate by either computational [SLIPT](#) analysis or experimental [siRNA](#) screening.

#### 5.3.1.2 Testing Contextual Hierarchy of Synthetic Lethal Genes

This pathway hierarchy in the [PI3K](#) cascade was tested for differences between genes detected across [SLIPT](#) and [siRNA](#) screening. The [synthetic lethal](#) candidates for *CDH1* detected by either method (as shown by Figure 5.8a) did not differ, each being distributed throughout the pathway. When adjusted for being more numerous, there was little indication that [SLIPT](#) candidate genes are more frequently upstream or downstream of [siRNA](#) candidate genes (as shown by Figure 5.8b) and were more frequent at moderate hierarchies which contained more genes. [Synthetic lethal](#) candidates from both methods were less frequently detected in the downstream effectors of the pathway (e.g., the mTOR complex), although core pathway genes (e.g., *AKT2* and *PDE3B*) were detectable as [synthetic lethal](#) candidates (as discussed for Figures 5.1 and 5.6).

Similarly, when testing [synthetic lethality](#) against [CDH1 mutation](#) (mtSLIPT), the

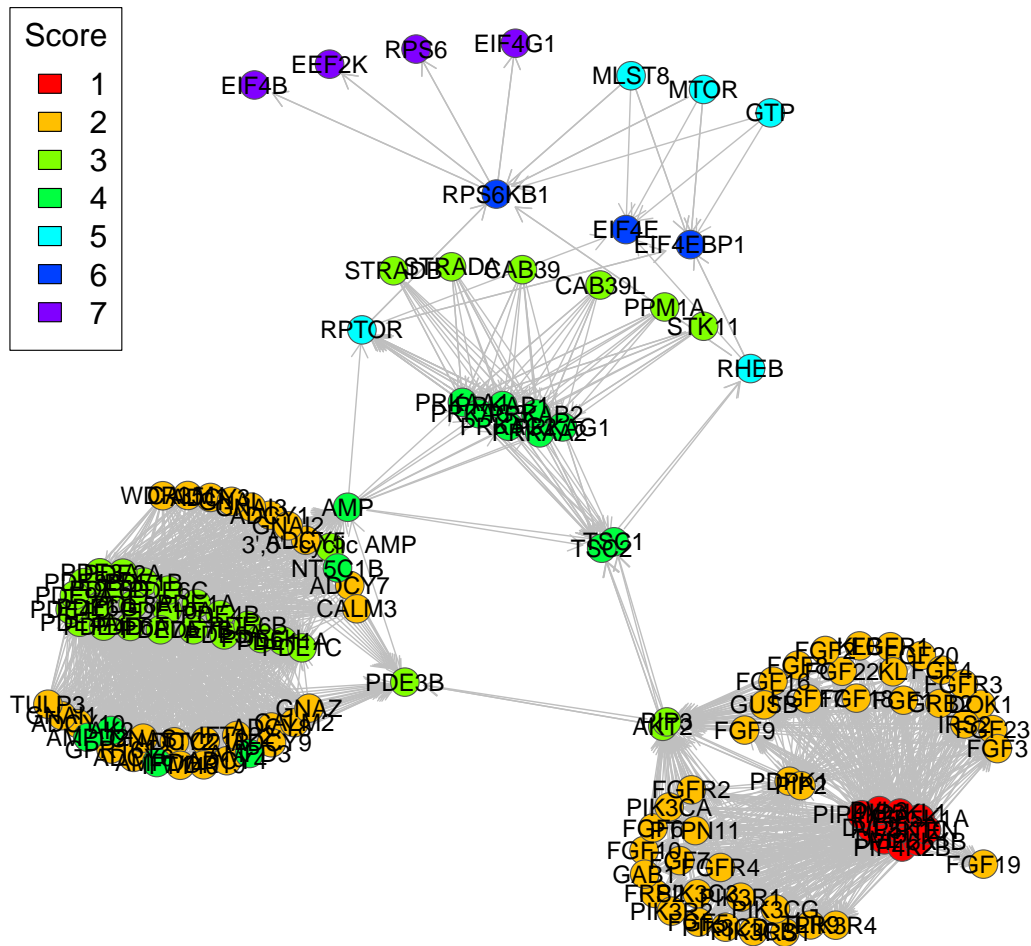
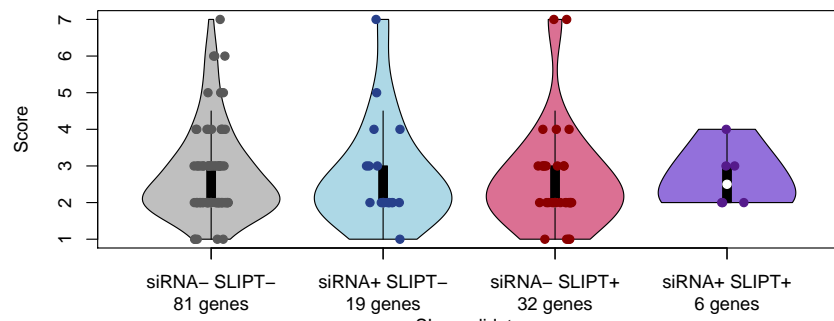


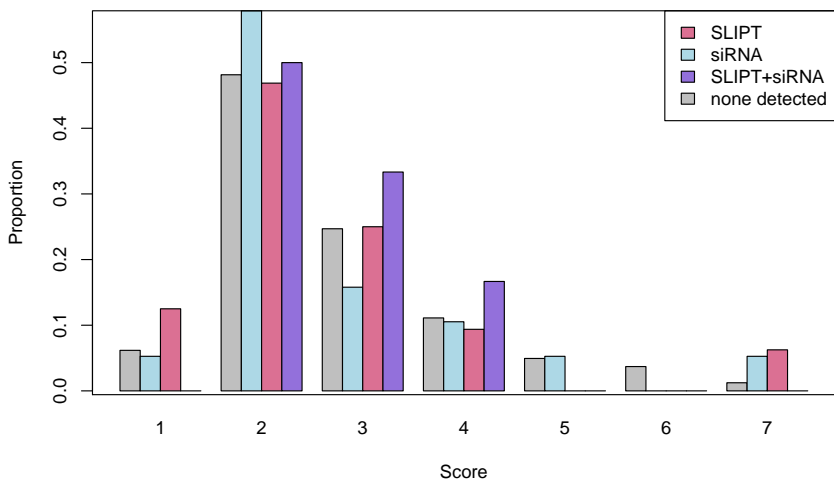
**Figure 5.7: Hierarchical structure of PI3K.** A contextual score was used for ranking genes within the PI3K Cascade to demonstrate a pathway structure analysis to examine whether genes detected by either SLIPT or siRNA were more frequently upstream or downstream in the PI3K pathway.

hierarchical score for the PI3K pathway did not differ between mtSLIPT-specific and siRNA-specific gene candidates (as shown by Appendix Figure I.1). The median among genes detected by both approaches was marginally elevated such that these genes may be further downstream in the pathway than other synthetic lethal candidate partners of *CDH1*. There were fewer genes overall with higher scores (shown in Appendix Figure I.2). While these were more frequently detected by both SLIPT and siRNA,

there was no significant effect variation in pathway hierarchy (shown by ANOVA in Table 5.4 and Appendix Table I.1) accounted for by **SLIPT** or **siRNA** detection in the PI3K pathway (as shown in Figure 5.1). Thus these hierarchical scores may be observed by sampling variation and there is no indication that **SLIPT** or **siRNA** detection differs along the direction of the pathway. Genes detected by either method are no more or less common among upstream or downstream of the pathway.



(a) Hierarchical Distance Score



(b) Proportion of Genes

Figure 5.8: **Hierarchy score in PI3K against synthetic lethality in PI3K**. The hierarchical distance scores were similarly distributed across **SLIPT** and **siRNA** genes. The number of **SLIPT** and **siRNA** genes against the hierarchical distance scores showing no significant tendency for either method to either of the pathway upstream or downstream extremities.

Table 5.4: ANOVA for synthetic lethality and PI3K hierarchy

	DF	Sum Squares	Mean Squares	F-value	p-value
siRNA	1	0.001	0.00066	0.0004	0.9842
SLIPT	1	0.456	0.45605	0.2740	0.6016
siRNA×SLIPT	1	0.019	0.01878	0.0113	0.9156

Analysis of variance for PI3K hierarchy score against synthetic lethal detection approaches (with an interaction term)

[remove this paragraph and Figures 5.9 and I.3?]

Furthermore the pathway hierarchical scores did not exhibit different more or less SLIPT than siRNA genes above or below the given threshold. Since the ideal threshold to detect pathway structure is unclear, an exploratory analysis was performed, with  $\chi^2$ -test for the SLIPT or siRNA candidate genes upstream or downstream of each gene. It is unsurprising that these  $\chi^2$  tests were highest when the gene used as a threshold was in the middle of the pathway (as shown in Figure 5.9). However, there was no statistically significant support for pathway structure by this approach, as none of the  $\chi^2$  values were high enough to detect pathway structure between SLIPT and siRNA gene candidates. Nor was structure detectable for mtSLIPT testing synthetic lethality against CDH1 mutation (as shown in Appendix Figure I.3).

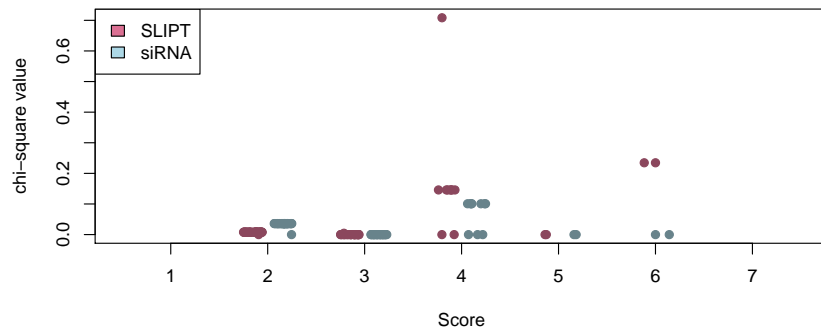


Figure 5.9: Structure of synthetic lethality in PI3K. The number of SLIPT and siRNA genes upstream or downstream of each gene in the Reactome PI3K pathway were tested (by the  $\chi^2$ -test). These are plotted as a split jitter stripchart against the hierarchical distance scores showing no significant tendency for either method to either of the pathway upstream or downstream extremities.

### 5.3.2 Upstream or Downstream Synthetic Lethality

This approach does not ascertain whether **SLIPT** and **siRNA** candidate partners of **CDH1** are upstream or downstream of one and other within a pathway such as the **PI3K** cascade. The hierarchical approach is designed to detect differences in pathway location between gene groups. An alternative **pathway** structure method has been devised to use **network** structures to identify directional relationships between individual **SLIPT** and **siRNA** genes. This **pathway** structure methodology will be applied (as described in Section 3.4.1) to detect the direction of **shortest paths** between **SLIPT** and **siRNA** gene candidates. This will be used to demonstrate the methodology on the **PI3K** pathway, to develop a statistical test for **pathway** structure between between **SLIPT** and **siRNA** gene candidate using resampling (as described in Section 3.4.1.1), and to apply this test for **pathway** structure among **synthetic lethal** gene candidates to the pathways identified in Chapter 4 and discussed in Section 5.1.

#### 5.3.2.1 Measuring Structure of Candidates within PI3K

Shortest paths in a pathway network were used to devise a strategy to detect **pathway** structure between **SLIPT** and **siRNA** gene candidate partners of **CDH1** (as described in Section 3.4.1). Thus we can determine whether individual **SLIPT** genes have upstream or downstream **siRNA** candidates (scored as “up” or “down” events respectively). This procedure enables the detection of directional relationships between **SLIPT** and **siRNA** gene candidates (in contrast to the hierarchical approach).

The total number of gene candidate pairs in either direction can be compared within a pathway network to assess the overall directional relationships in a pathway. This directionality is detectable by the difference between the number of **SLIPT** candidate genes with upstream and downstream **siRNA** gene partners. However, this measure alone is not sufficient to determine whether there is evidence of **pathway** structure between **SLIPT** and **siRNA** gene candidate partners of **CDH1** in a pathway network. Nevertheless, it does serve to measure the magnitude (and direction) of the consensus of directional relationships (upstream and downstream) between **SLIPT** and **siRNA** gene candidate partners. This measure of **pathway** structure can be used for testing for statistical significance of **pathway** structure by resampling, using a permutation procedure to test whether these relationships are detectable among randomly selected gene groups rather than the detected **SLIPT** and **siRNA** gene candidate partners (as described in Sections 2.3.6 and 3.4.1.1).

This resampling procedure was performed for the **PI3K** network to generate a null

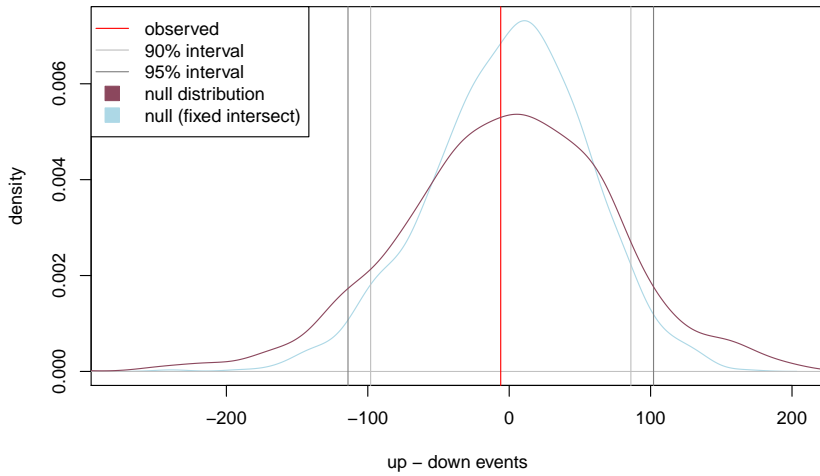


Figure 5.10: **Structure of synthetic lethality resampling in PI3K.** A null distribution with 10,000 iterations of the number of **siRNA** genes upstream or downstream of **SLIPT** genes (depicted as the difference of these) in the **PI3K** pathway. To assess significance, the observed events (with **shortest paths**) were compared to the 90% and 95% intervals for the null distribution (shown in violet). Genes detected by both methods were fixed to the same number as observed for the alternative null distribution (shown in blue), although the observed number of events (red) was not significant in either case. In both cases, these genes detected by both approaches were included in computing the number of **shortest paths** (in either direction) between **SLIPT** and **siRNA** genes.

distribution for the difference in the number of “up events” and “down events” for this pathway (as shown in Figure 5.1). Resampling yields a distribution to detect whether genes detected by **SLIPT** had significantly more upstream or downstream **siRNA** candidates. While there was modest indication that **siRNA** genes were downstream of **SLIPT** candidate genes, resampling for the **PI3K** pathway (as shown in Figure 5.10) did not detect a significant number of **siRNA** genes upstream or downstream.

In contrast, when testing **synthetic lethality** against **CDH1** mutation (**mtSLIPT**) there was modest indication that **siRNA** genes were upstream of **SLIPT** candidate genes. However, resampling (as shown in Appendix Figure I.4) was also unable to detect a significant number of **siRNA** genes upstream or downstream of **mtSLIPT** candidates. Neither fixing the number of genes detected by both approaches (as shown by the blue line in Figure 5.10 and Appendix Figure I.4) nor excluding these jointly detected genes altered the findings of this approach. These genes were included in

the analysis because they can disproportionately count towards **siRNA** genes being upstream (or downstream) of **SLIPT** genes as they may still have different proportions of gene detected by either approach upstream (or downstream) of them. Furthermore, expanding the range of **shortest paths** to consider **links** in related pathways (using the “metapathways” constructed in Section 2.4.3) also had little effect on the null distribution generated, despite increasing the computational demands of the procedure.

### 5.3.2.2 Resampling for Synthetic Lethal Pathway Structure

The permutation procedure (as described in Section 3.4.1.1) that was performed in Section 5.3.2.1 for the **PI3K** cascade was also applied to other pathways identified in Chapter 4 and discussed in Section 5.1. These include extracellular matrix (with constituent elastic fibre and fibrin pathways), cell signalling (by PI3K/AKT and GCPRs), and translational pathways (with **NMD** and 3'UTR regulation). The resampling results across these pathways (as shown in Table 5.5) had limited support for association between **pathway** structure and detection of **synthetic lethal** genes, with the majority of these being non-significant as shown for **PI3K** (in Appendix Figure I.4). However, the distribution for these pathways will differ depending on their structure, the number of genes they consist of, and the proportion of **synthetic lethal** candidates among them (including a higher frequency of genes detected by both methods for the pathways identified in Section 4.2.5.1). This resampling is an appropriate procedure to use to detect structural relationships across pathways as it does not assume an underlying test statistic distribution.

Pathway structure was supported for the **NMD** pathway (which is consistent with **siRNA** being downstream in Appendix Figure F.7). However, this observation rests upon a single gene and was not replicated when testing **synthetic lethality** (**mtSLIPT**) against **CDH1 mutation** (as shown in Appendix Table I.2) nor was it supported by the related 3'UTR regulation and translational elongation pathways.

There does not appear to be a consensus on the directionality of **SLIPT** and **siRNA** candidates across pathways as distinct pathways showed stronger tendency for **siRNA** genes to be either upstream or downstream. Even related pathways such as **PI3K** and **PI3K/AKT** signalling showed directional events in opposite directions. The strongest pathway (among those tested) with support for directional pathways structure is  $G_{\alpha i}$  signalling which showed significant downstream **siRNA** genes for both **SLIPT** and **mt-SLIPT** from a large number of **shortest paths** (in Table 5.5 and Appendix Table I.2). This would indicate that **SLIPT** detects upstream regulators of genes experimentally validated by **siRNA**. However, these results are borderline significant (with raw permu-

Table 5.5: Resampling for *pathway* structure of synthetic lethal detection methods

Pathway	Graph		States		Observed				Permutation p-value	
	Nodes	Edges	SLIPT	siRNA	Up	Down	Up–Down	Up/Down	Up–Down	Down–Up
PI3K Cascade	138	1495	38	25	122	128	-6	0.953	0.5326	0.4606
PI3K/AKT Signalling in Cancer	275	12882	98	44	779	679	100	1.147	0.3255	0.6734
<b>G<sub>αi</sub> Signalling</b>	292	22003	95	58	836	1546	-710	0.541	0.9971	0.0029
GPCR downstream	1270	142071	312	160	9755	9261	494	1.053	0.3692	0.6305
Elastic fibre formation	42	175	24	7	1	2	-1	0.500	0.5461	0.3865
Extracellular matrix	299	3677	127	29	547	455	92	1.202	0.3351	0.6636
Formation of Fibrin	52	243	18	5	12	17	-5	0.706	0.6198	0.3564
<b>Nonsense-Mediated Decay</b>	103	102	74	2	0	74	-74	0	1.0000	< 0.0001
3' -UTR-mediated translational regulation	107	2860	77	1	0	0	0		0.4902	0.5027
Eukaryotic Translation Elongation	92	3746	76	0	0	0	0		0.4943	0.4933

Pathways in the Reactome network tested for structural relationships between **SLIPT** and **siRNA** genes by resampling. The raw p-value (computed without adjusting for multiple comparisons over pathways) is given for the difference in upstream and downstream paths from **SLIPT** to **siRNA** gene candidate partners of *CDH1* with significant pathways highlighted in bold. Sampling was performed only in the target pathway and **shortest paths** were computed within it. Loops or paths in either direction that could not be resolved were excluded from the analysis. The gene detected by both **SLIPT** and **siRNA** (or resampling for them) were included in the analysis and the number of these were fixed to the number observed.

tation p-values) and are unlikely to be detected after adjusting for multiple comparisons across the 10 pathways presented here (nor in the 1652 Reactome pathways used previously in Chapter 4).

Therefore, there is insufficient evidence to determine whether there is *pathway* structure, gene detected upstream or downstream by either method, between the **SLIPT** and **siRNA** candidates in many of the *synthetic lethal* pathways (identified in Chapter 4). In particular, directional structure among *synthetic lethal* candidates for *CDH1* was not strongly supported in signalling pathways upon which the rationale for *pathway* structure hypotheses were based on. Despite the design of a robust resampling approach to test relationships between gene groups, this did not detect many structural relationships between **SLIPT** and **siRNA** gene candidates, although it may apply more broadly to gene networks. Furthermore, the pathway relationships are unlikely to be statistically supported by resampling when testing across the search space of Reactome pathways and adjusting for multiple comparisons. While there is statistically significant over-representation of many of these pathways in genes detected by both **SLIPT** and **siRNA** (as described in Chapter 4), these did not consistently show *pathway* structure. Furthermore, *pathway* structure did not account for the discrepancy between **SLIPT** and **siRNA** gene candidates which did not significantly intersect such as the **PI3K** cascade.

## 5.4 Discussion

These investigations used a functional pathway network that encapsulates protein complexes and functional modules. The Reactome network (Croft *et al.*, 2014) uses curated, experimentally identified pathways to determine relationships between genes and does not have the limitation of relying solely on protein binding or text-mining which are prone to false positives. While it is not documented whether these relationships are activating or inhibitory, the Reactome network (Croft *et al.*, 2014) is sufficient to test pathway relationships with directional information.

Synthetic lethal genes and pathways (for *CDH1* loss in cancer) were identified across gene expression and mutation datasets in Chapter 4. These pathway structure investigations extend those investigations into synthetic lethal gene candidates including exploring the discrepancy between SLIPT and siRNA candidate genes in a pathway such as PI3K in which they did not significantly intersect. Pathways with replicated synthetic lethal genes across these detection methods, breast and stomach cancer data, and patient and cell line data were also investigated including pathways from the extracellular microenvironment to core translational pathways and the signalling pathways between them.

Synthetic lethal gene candidates in the context of pathway structures can also be interpreted to provide additional mechanisms and support for belonging to a synthetic lethal pathway. Gene candidates with known mechanisms are ideal for triage of targets specific to *CDH1* deficient tumours and for further experimental validation in preclinical models. This chapter presents computational methods to use pathway structure in an attempt to detect genes with importance in a pathway and reconcile the differences between SLIPT and siRNA candidate genes with pathway relationships (e.g., one group being downstream of the other).

Many genes were detected by either method and the differences between the computational and experimental screening approaches could feasibly lead to differences in which genes within a synthetic lethal pathway are identified. Genes detected by synthetic lethal detection strategies included those of biological importance within synthetic lethal pathways, those which are actionable drug targets, and those with functional implications for the biological growth mechanisms or vulnerabilities of *CDH1* deficient tumours. It appeared that genes detected by both approaches were highly connected (or of importance) in the network structure or some pathways and that there may be some structure with SLIPT and siRNA upstream or downstream of each other.

However, the complexity of biological pathways meant that relationships between gene candidates were difficult to discern without formal mathematical and computational approaches and thus these were used to analyse large biological networks.

Network analysis techniques were therefore applied to formalise and quantify the connectivity and importance (centrality) of genes within pathways (using PI3K as an example). However, these network techniques were unable to identify distinct differences in the network properties of genes detected as synthetic lethal candidates by computational or experimental methods. These network metrics support the application of synthetic detection across pathways (and the findings using pathways as gene sets in Chapter 4) as neither synthetic lethal detection approach was biased towards genes of higher importance or connectivity and neither approach was insensitive to genes of lower importance or connectivity. SLIPT is therefore not biased towards genes with more crucial role in the pathway as inferred by pathway connectivity and centrality measures and detects genes irrespective of pathway structure.

Similarly, a network hierarchy based on biological context (ordered from receiving extracellular stimuli to affecting downstream gene expression and cell growth) was devised to test whether PI3K genes of a particular upstream or downstream level were more frequently detected as synthetic lethal candidates. However, this approach was unable to ascertain whether genes detected by either method were further upstream or downstream in the pathway and there was no statistical evidence that either method differed in which levels of this structure were detected.

A measure of pathway structure between individual SLIPT and siRNA genes within a pathway was also devised using the direction of shortest paths in a directed graph structure. This is amenable to detecting the consensus directionality of the pathway across pairs of genes detected by either method. The pathway structure methodology developed here is generally applicable to comparison of node groups (allowing overlapping) including genes in biological pathways and their detection by different methodologies. While the pathway structure measure alone is not able to detect structural relationships between gene groups (e.g., SLIPT and siRNA gene candidates), it is amenable to resampling to determine whether these relationships are statistically significant.

## 5.5 Summary

Together these analyses of biological pathways, network metrics, and statistical procedures devised specifically for this purpose were applied to Reactome pathway structures to test whether structural relationships exist between synthetic lethal candidates. Of particular interest was whether these relationships relate to the differences between the computational (SLIPT) and experimental (siRNA) synthetic lethal candidate partners of *CDH1* (in the pathways discussed in Chapter 4).

While biologically relevant relationships were observed in specific pathways, there were few detectable structural relationships between SLIPT and siRNA gene candidates. These candidates did not exhibit significant differences in network connectivity or centrality measures. Network analyses were also unable to ascertain whether the candidates detected by either method stratified into upstream and downstream genes on the pathway and they likely do not.

A statistical resampling procedure was applied to shortest path analysis to test whether pairs of SLIPT and siRNA gene candidates were more likely to be upstream or downstream of each other. This approach detected very few structural relationships in the synthetic lethal pathways identified in Chapter 4. Overall, support for pathway structure between SLIPT and siRNA gene candidates is weak and the direction is inconsistent between pathways. Therefore pathway structure does not account for the differences between the SLIPT and siRNA gene candidates, although this does support the validity of gene set analyses in Chapter 4 and the synthetic lethal pathways identified.

Furthermore, the resampling procedure demonstrated in this chapter is more widely applicable to gene states in network structures and may be of further utility in the analysis of biological pathways or networks. This approach was able to quantify structural relationships that were otherwise difficult to interpret and to conclusively exclude many potential relationships. In this respect, the network resampling methodology may also be applicable to triage of experimental validation.

# Chapter 6

## Simulation and Modelling of Synthetic Lethal Pathways

Simulation and modelling of synthetic lethality in gene expression was revisited in greater detail in this chapter, building upon the results which supported the use of **SLIPT** (in Section 3.3). In Chapter 3, a simulation procedure for generating simulated data with underlying (known) synthetic lethal partners of a query gene, such as *CDH1*, was developed (as described in Section 3.2.2) by sampling from a Multivariate normal distribution based on a statistical model of synthetic lethality in expression data (as described in Section 3.2.1). This simulation framework was applied to simulated data (in Section 3.3), including simple correlation structures to assess the statistical performance of the **SLIPT** methodology and support its use as a computational approach for detecting synthetic lethal candidates from expression data throughout this thesis (Chapters 4 and 5).

While this basic framework was provided some support for the use of **SLIPT**, further investigations with simulations were conducted to assess the strengths and limitations of the **SLIPT** methodology, compare it to alternative statistical approaches to synthetic lethal detection, and assess its performance under more complex correlation structures. Together these simulation investigations assess the performance of the **SLIPT** methodology, including on pathway graph structures (e.g., those discussed in Chapter 5) and indicate whether the **SLIPT** methodology (or similar refined bioinformatics strategies) are statistically rigorous or suitable for wider genomics applications.

These simulation investigations continue to utilise the Multivariate Normal simulation procedure (as applied in Section 3.3) with further refinements. The **SLIPT** methodology (and the  $\chi^2$  test) were applied across a range of parameters (including

altering the quantiles for detecting **synthetic lethal** direction and compared to correlation). This was also applied to query correlated genes (as performed in Section 3.3).

A refined simulation procedure was developed specifically to extend the methodology described in Section 3.2 to utilise pathway **graph** structures for the correlation structures of simulated datasets (as described in Section 3.4.2). This methodology can be applied to simulated correlation structures across simple **graph** structures to test specific network modules or use **pathway** structures based on biological pathways. Thus **graph** structure and simulation approaches were combined to test whether a gene locus in a pathway affects detection by **SLIPT** and whether **SLIPT** performance is affected by **pathway** structure. The simulation procedure based on **graph** structures was applied in a computational pipeline across many parameter combinations using high-performance computing resources (as discussed in Section 2.5.3) and the core simulation functions have been released as a software package for wider use to test **bioinformatics** and statistical methods on **graph** structures (as described in Section 3.5.3).

## 6.1 Synthetic Lethal Detection Methods

The **SLIPT** methodology (as it has been applied throughout Chapters 4 and 5) was compared for alternative computational approaches to detecting **synthetic lethality** in simulated **gene expression** data. As discussed in Section 3.3, this procedure enabled testing ability of **SLIPT** to detect known **synthetic lethal** partner genes by sampling from a statistical model of **synthetic lethality**. While comprehensive benchmarking has not been performed, several approaches to **synthetic lethal** detection are considered (e.g., Pearson correlation, the  $\chi^2$  test, and testing for bimodality) to evaluate the strengths of the **SLIPT** methodology, including modifications to the parameters of **SLIPT**.

The following comparisons of simulations of computational detection of **synthetic lethality** with different statistical rationales suffice to discuss the strengths of **SLIPT**, evaluate whether it is appropriate for further application in **genomics** research, and identify limitations which may be addressed with further developments. Some potential avenues for further development of computational **synthetic lethal** discovery will be discussed in Section 7.3.

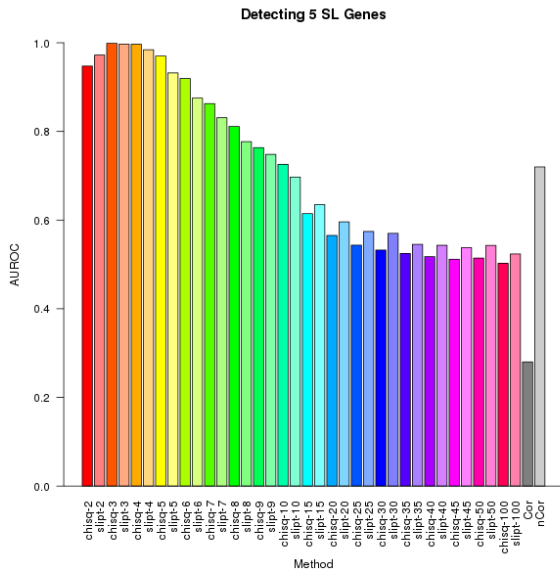
### 6.1.1 Performance of SLIPT and $\chi^2$ across Quantiles

Simulated datasets with synthetic lethal partner genes were generated using the multivariate normal simulation procedure (as described in Section 3.2.2) with performance assessed using AUROC analysis (as described in Section 2.3.5). Synthetic lethal detection was compared for modifications to the SLIPT methodology (as described in Section 3.1), namely that the quantiles used to define low and high expression was varied. Rather than  $1/3$  (as used throughout this thesis) the samples below the lowest  $1/n$  quantile and above the highest  $1/n$  quantile were used for SLIPT (and the  $\chi^2$ -test) to detect lowly and highly expressing samples respectively. The quantiles tested range from 2, splitting at the  $1/2$  quantile (the median), to 100, using the lowest (1%) and highest (99%) percentiles.

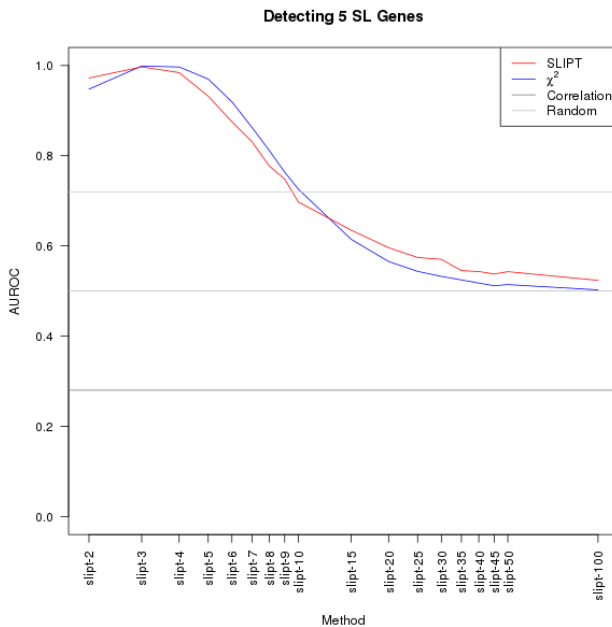
This enabled testing of the threshold for lowly expressing genes which is most able to distinguish synthetic lethal genes, even with higher-order synthetic lethal interactions (as discussed in Section 3.2.1). Both SLIPT with the directional criteria for synthetic lethality and significance of the equivalent  $\chi^2$  test were performed for each quantile. Pearson correlation was also tested on simulated continuous expression data for synthetic lethal detection in simulated data, considering both positive and negative correlations separately as predictors of synthetic lethality for comparison with  $\chi^2$  based approaches, using discrete categories of gene function deriving from quantiles.

The results presented throughout this section use the example of 5 synthetic lethal partners to illustrate the differences in performance between the standard SLIPT procedure (slipt-3) to  $n$  quantiles (slipt- $n$ ), the  $\chi^2$ -test on the same quantiles, and positive or negative correlation. However, similar results across different numbers of known synthetic lethal genes are shown in Appendix J. The synthetic lethal detection procedures were compared with 10,000 simulations of a small dataset of 100 genes and 1000 samples without correlation structure between genes, as performed in Section 3.3.2). As shown in Figure 6.1, the 3-quantiles previously used have optimal performance and SLIPT has a comparable or higher performance than the  $\chi^2$ -test alone across quantiles.

Pearson correlation was also tested as a predictor of synthetic lethality (i.e., whether highly positive or negative correlations with the query gene detected synthetic lethal partners). Positive correlation performed worse than random (with an AUROC lower than 0.5) as thus coexpression of genes is not predictive of synthetic lethality in simulated data. Conversely, negative correlation is predictive of synthetic lethality, consistent with synthetic lethal gene activity being mutually exclusive. However, neither



(a) Barplot of  $\chi^2$ , SLIPT, and correlation.



(b) Lineplot of  $\chi^2$ , SLIPT, and correlation.

Figure 6.1: **Performance of  $\chi^2$  and SLIPT across quantiles.** Synthetic lethal detection (of 5 genes) with quantiles as on the axes. The barplot uses the same hues for each quantile (grey for correlation) and darker for  $\chi^2$  (and positive correlation). The line plot (with log-scale quantiles) is coloured according to the legend. SLIPT and  $\chi^2$  perform similarly, peaking at  $1/3$ -quantiles and converging to random (0.5). Negative correlation was higher than positive but not optimal quantiles for SLIPT or  $\chi^2$ .

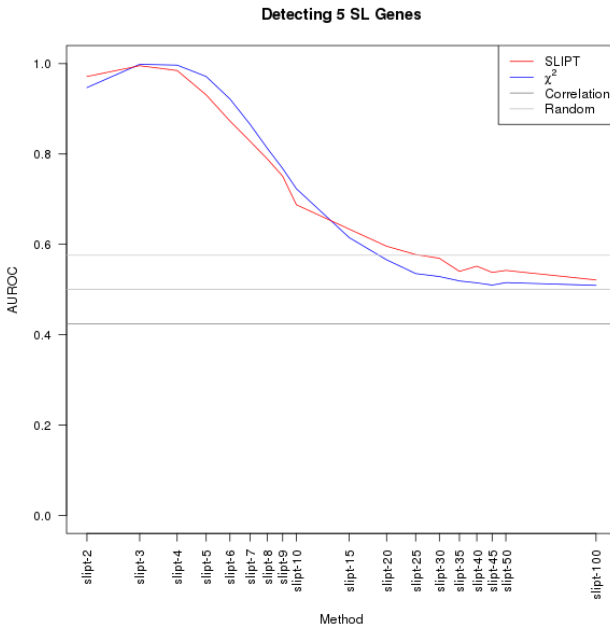


Figure 6.2: **Performance of  $\chi^2$  and SLIPT across quantiles with more genes.** Synthetic lethal detection (of 5 genes in 20,000) with quantiles as in axis labels. The line plot (with log-scale quantiles) is coloured according to the legend. As for simulations with fewer genes, SLIPT and  $\chi^2$  perform similarly, peaking at  $1/3$ -quantiles and converging to random (0.5). Negative correlation was higher than positive but not optimal quantiles for SLIPT or  $\chi^2$ .

correlation approach performed as well as the optimal quantiles for the SLIPT procedure or  $\chi^2$ -test.

These results are shown in both a bargraph and lineplot to show the individual results of each parameter, and to compare SLIPT with the  $\chi^2$ -test side-by-side across quantiles. Similarly, these plots are given for detecting a range of known synthetic lethal partners in the simulations in Figures J.1 and J.2. These demonstrate that the findings shown for 5 synthetic lethal genes are robust across different numbers of underlying synthetic lethal genes.

The synthetic lethal detection procedures were also tested with 1000 simulations of a larger dataset of 20,000 genes and 1000 samples. While fewer simulations gives a less accurate ROC result, this is sufficient to replicate the above findings with a feasible number of genes in a human gene expression dataset and assess the impact of a higher proportion of non synthetic lethal genes (potential false positives). Simulated datasets of this size were also used in Section 3.3.2 to test the specificity in a number of genes

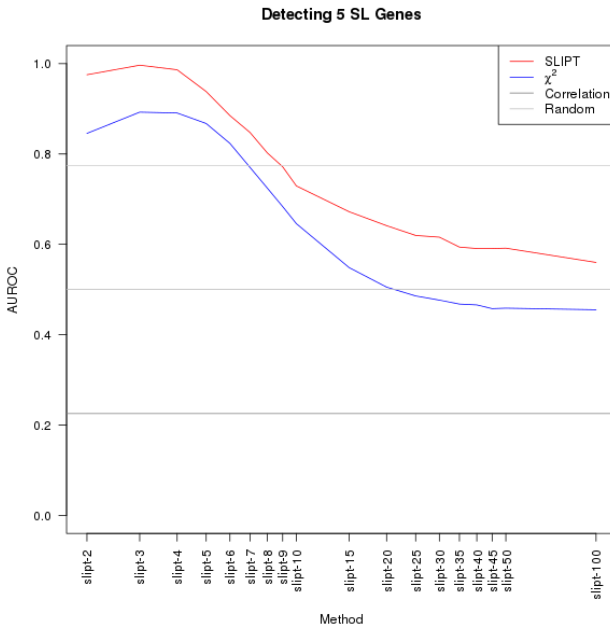
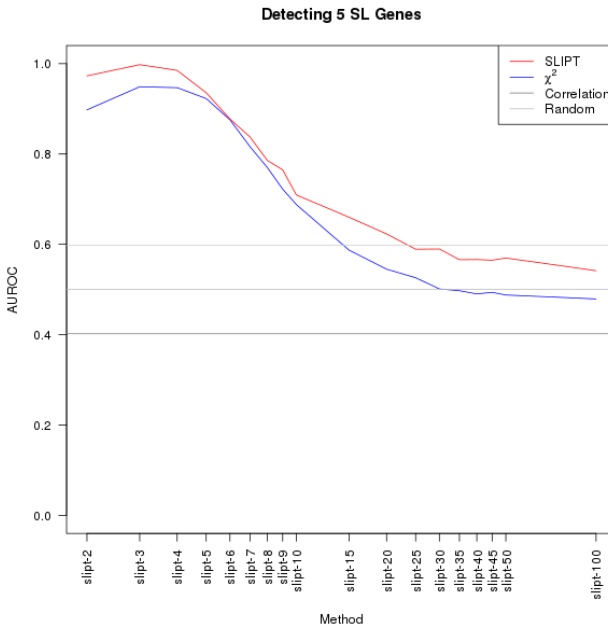


Figure 6.3: **Performance of  $\chi^2$  and SLIPT across quantiles with query correlation.** Synthetic lethal detection (of 5 genes in 100 including 5 query correlated) with quantiles as in axis labels. The line plot (with log-scale quantiles) is coloured according to the legend. SLIPT performs consistently higher than  $\chi^2$  due to higher specificity. Negative correlation performed modestly.

similar to that in experimental datasets for cancer genomes. As shown in Figure 6.2, the above findings were replicated in simulations of a larger dataset with 20,000 genes. These were also robustly replicated across varying numbers of underlying synthetic lethal genes (as shown in Figure J.3).

#### 6.1.1.1 Correlated Query Genes affects Specificity

As discussed in Section 3.3.2.2, positively correlated genes (with the query gene) have an impact of on the performance of synthetic lethal detection. SLIPT was able to distinguish these from synthetic lethal partners and hence is likely to have a higher specificity in datasets which include positively correlated genes with the query gene (as expected in gene expression data). The synthetic lethal detection procedures were compared with 10,000 simulations of a small dataset of 100 genes (with 5 correlated with the query gene) and 1000 samples otherwise without correlation structure between genes. As shown in Figure 6.3, this specificity is reflected in the increased AUROC performance values for SLIPT (in contrast to Figure 6.1). This specificity can be



**Figure 6.4: Performance of  $\chi^2$  and SLIPT across quantiles with query correlation and more genes.** Synthetic lethal detection (of 5 genes in 20,000 including 1000 query correlated) with quantiles as in axis labels. The line plot (with log-scale quantiles) is coloured according to the legend. SLIPT performs consistently higher than  $\chi^2$  due to higher specificity. Negative correlation performed modestly.

attributed to the directional criteria (as described in Section 3.1) since the  $\chi^2$ -test alone performs comparatively poorly with positively correlated genes.

The synthetic lethal detection procedures were also compared with 1000 simulations of a larger dataset of 20,000 genes (with 1000 correlated with the query gene) and 1000 samples otherwise without correlation structure between genes. This simulation increases the number of genes (and proportion of negative genes) to those comparable with a human gene expression dataset while maintaining a comparable 5% of positively correlated genes. As shown in Figure 6.4, SLIPT still outperforms  $\chi^2$  or negative correlation and is optimal at the 3-quantile. The difference between SLIPT and  $\chi^2$  was less pronounced in a larger dataset with many weakly correlated genes. The greater specificity of SLIPT than  $\chi^2$ -test to distinguish positively correlated non synthetic lethal genes is not as evident with a large number of negative genes (as potential false positives). However, specificity is an important consideration in large-scale genomics analysis where there are potentially many false positives.

Nevertheless, SLIPT with 3-quantiles (as performed throughout Chapters 4 and 5),

had higher performance than when other quantile thresholds were used, particularly when positive correlations were present (replicating the Section 3.3.2.2). These findings hold across different numbers of underlying *synthetic lethal* genes (as shown in Figures J.5 and J.6).

Together these results support the use of **SLIPT**, particularly the use of quantiles as thresholds for gene function and specific use of 3-quantiles which perform well compared to other quantiles. A particular concern in the design of **SLIPT** for *expression* data whether the samples sizes are sufficient when the data is divided into quantiles. The **SLIPT** methodology further performed better for 3-quantiles (and other moderate values) than  $\chi^2$  or correlation as a predictor of *synthetic lethality*. These results are irrespective of sample size or p-value threshold since the results replicated across sample sizes and the **AUROC** values were independent significance thresholds. Using a moderate number of quantiles for **SLIPT** ensures that there are a sufficient number of samples expected below and above them so that deviations from these are statistically detectable. These quantiles were also optimal for the  $\chi^2$  test which uses the same expected values as the **SLIPT** directional conditions.

### 6.1.2 Alternative Synthetic Lethal Detection Strategies

The **SLIPT** approach (and  $\chi^2$ ) to detect *synthetic lethality* from binning *expression* to estimate gene function also outperforms correlations which use continuous data directly. Correlation performing poorly as a *synthetic lethal* detection strategy consistent with there not necessarily being a relationship between *synthetic lethal* partners which can be in distinct biological pathways, expressed at different times or in different cell types. Nevertheless, correlation is among the alternative detection methods considered in further detail.

The BiSEp R package (Wappett, 2014) for using bimodality to detect *synthetic lethality* (Wappett *et al.*, 2016) were also considered, along with a linear regression approach. These statistical methods span a range of computational approaches to detecting *synthetic lethality* and serve to compare alternatives to **SLIPT**, supporting its design and application. However, these comparisons are able provide supporting data from statistical modelling and simulations for the viability of the **SLIPT** methodology for *synthetic lethal* discovery in cancer (as demonstrated in Chapter 4) and further applications.

### 6.1.2.1 Correlation for Synthetic Lethal Detection

As shown in Section 6.1.1, negative (Pearson) correlation performed better than positive correlation, indicating the inverse relationships were more predictive of synthetic lethality. However, neither correlation approach performed as well as SLIPT or the  $\chi^2$  test as a predictor of synthetic lethal gene partners. It is notable that negative correlation still often performed considerably better than random chance.

Negative correlation was compared directly to the SLIPT methodology (as described in Section 3.1) across numbers of known synthetic lethal partners and sample size (ranging from 500 to 5000). This comparison used 1000 simulations of a dataset with 20,000 genes and synthetic lethal genes from within a network (sampled as in Section 3.4.2)) with a 0.8 correlation between adjacent genes. In a direct comparison of SLIPT and negative correlation (shown in Figure 6.5), SLIPT consistently has higher performance in simulated data across parameter values and (inverse) correlation-based approaches perform modestly in comparison. Thus using thresholds to categorise expression data (as performed by SLIPT and  $\chi^2$ ) does not compromise the performance of these methods by losing continuous data that would be used for calculating correlations. Similarly, the slope of a linear regression did not perform as well at synthetic lethal detection than SLIPT.

Both SLIPT and correlation had poorer performance with increasing numbers of the synthetic lethal genes to detect, while they had higher performance in higher sample sizes, as expected (as previously observed for SLIPT in Section 3.3). Thus the issue with detection of greater numbers of synthetic lethal genes is not specific to SLIPT but occurs across computational methods of synthetic lethal discovery in (simulated) expression data and likely stems from cryptic higher-order synthetic lethal interactions (as conservatively assumed in Section 3.2.1).

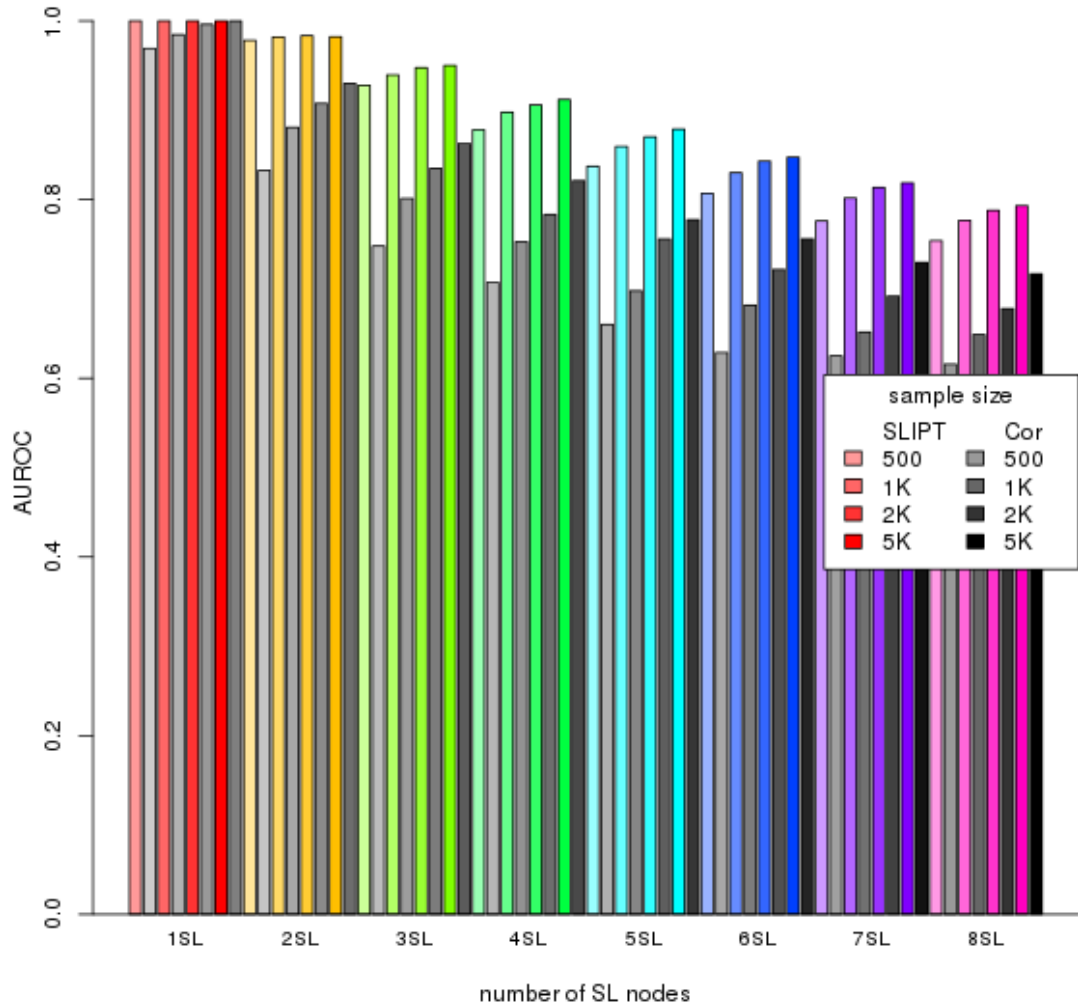


Figure 6.5: **Performance of negative correlation and SLIPT.** Synthetic lethal detection with SLIPT was compared to negative (Pearson) correlation across parameters. SLIPT consistently outperformed correlation. Both approaches had lower performance for more synthetic lethal partners and lower sample sizes. 10,000 simulations were performed with correlation structure as used in Section 6.2.1.2

#### 6.1.2.2 Testing for Bimodality with BiSEp

Extensive attempts were also made to compare SLIPT to the BiSEp methodology (Wappett *et al.*, 2016), a statistical approach to identify synthetic lethal gene pairs from mutually exclusive relationships using bimodal distributions. This synthetic lethal

detection methodology is also designed for [expression](#) analysis in cancer and is readily available as an (open-source) R package ([Wappett, 2014](#)), a practice which facilitates adoption and testing of the methodology on the same datasets and simulations procedures as previously used for [SLIPT](#).

The [BiSEp](#) package is designed for global testing of all potential gene pairs in the genomes for [synthetic lethality](#) rather than focusing on the search space of potential partners of the query gene. This approach was unable to detect [synthetic lethal](#) gene pairs in the [TCGA](#) breast cancer [expression](#) dataset ([Koboldt \*et al.\*, 2012](#)). However, this may be due to stringent thresholds under the multiple testing of millions of potential gene pairs.

For a direct comparison with the query-based [SLIPT](#) approach, the source code of the [BiSEp](#) R functions was modified to test solely for the partners of a specific gene. This approach was still unable to detect [synthetic lethal](#) partners of *CDH1* in [TCGA](#) breast cancer [expression](#) data ([Koboldt \*et al.\*, 2012](#)), even with the detection thresholds for bimodality and significance greatly relaxed from those which the package defaults to.

To circumvent multiple testing issues, [BiSEp](#) only tests gene pairs for [synthetic lethality](#) between genes with a detectable bimodal distribution. However, even with relaxed thresholds, bimodal distributions were not detectable in the normalised [TCGA](#) data ([Koboldt \*et al.\*, 2012](#)). Such normalisation [Ritchie \*et al.\* \(2015\)](#) is standard practice for [expression](#) datasets generated from [microarrays](#) or [RNA-Seq](#) and therefore [BiSEp](#) may not be appropriate to apply to this data. However, it is noted that [BiSEp](#) may also use other data types such as [DNA](#) copy number or cell line data for which it may be more applicable ([Wappett \*et al.\*, 2016](#)).

Nevertheless, attempts were made to test [BiSEp](#) on simulated datasets with underlying [synthetic lethal](#) genes (using the procedures described in Sections 3.2.2 and 3.4.2). However, [BiSEp](#) was also unable to detect genes with bimodal distributions of genes (and thus unable to detect [synthetic lethality](#)) in a limited number of computationally intensive simulations. Therefore investigations on a wider range of parameters were not performed.

## 6.2 Simulations with Graph Structures

The simulations of [synthetic lethality](#) performed in Section 3.3 included correlated blocks of genes as a rudimentary representation of [pathway](#) structure and co-regulated genes. The simulation procedure has been enhanced to account for more complex

`pathway` structures by sampling from multivariate normal distributions with correlation structure derived from `graph` structures (as described in Section 3.4.2). This approach enabled the simulation of `synthetic lethal` pathways with known correlation structure and synthetic lethal partners (of a gene not in the pathway). Using this procedure, the performance of `SLIPT` was evaluated under simple controlled correlation structures and complex correlations, such as those derived from biological networks (e.g., those described in Chapter 5). The `SLIPT` methodology was tested in artificial constructed networks to evaluate the effect of `pathway` structure on `synthetic lethal` detection. These included large biologically feasible pathways to ensure that the `SLIPT` methodology is robust under complex correlation structures and applicable to such complex `genomics` data.

These simulations combine the approach of prior simulation analyses (in Sections 3.3 and 6.1) with the `graph` structures for biological pathways (as used in Chapter 5). This enabled testing whether subtle or large differences in `pathway` structure affect `synthetic lethal` detection, whether inhibiting relationships (or inverse correlations) between genes affect `synthetic lethal` detection, and whether `synthetic lethal` detection varies by which gene is `synthetic lethal` and which genes are closely linked within the `pathway` structure. In addition, large numbers of `synthetic lethal` genes and biologically feasible numbers of genes (with many non-synthetic lethal genes) was tested to replicate the findings of Sections 3.3 and 6.1 in correlated structures derived from pathway graphs, including examples of biological pathways from Reactome (Croft *et al.*, 2014).

Simple and more complex constructed `graph` structures were used to demonstrate the impact of `pathway` structure of the performance of `SLIPT` for `synthetic lethal` detection in simulations. In addition, more complex constructed `graph` structures were compared to the PI3K and  $G_{\alpha i}$  signalling pathways derived from Reactome which were used for simulation of `pathway` structures of biological complexity (as shown in Figures 5.1 and F.4).

## 6.2.1 Performance over Graph Structures

### 6.2.1.1 Simple Graph Structures

Simple pathway modules were used to test the effect of `pathway` structure on the performance of detecting `synthetic lethal` partners within `graph` structures. For an initial comparison, the `graph` structures (shown by Figure 6.6) were used where a gene has one upstream regulator and two downstream (Figure 6.6b) or a gene has two upstream regulators and one downstream gene (Figure 6.6b). `SLIPT` has a high performance

in these simulations, detecting randomly selected [synthetic lethal](#) partners in both of these small simple networks (in Figures 6.7 and K.1).

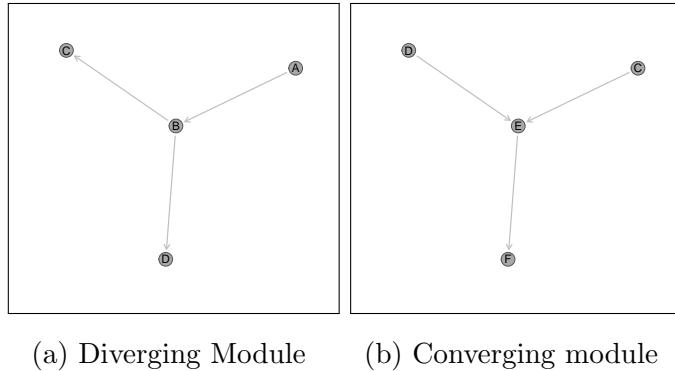
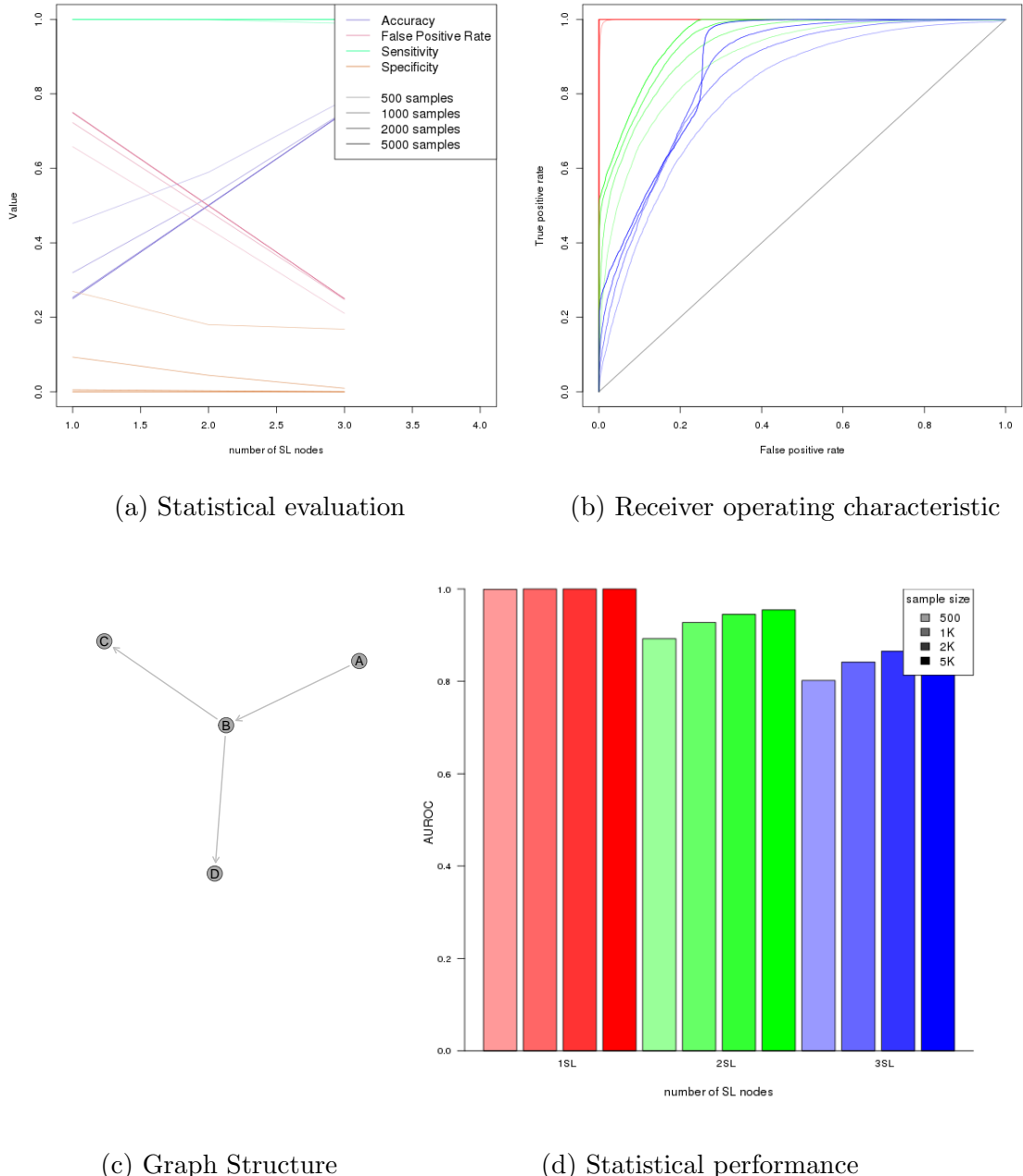


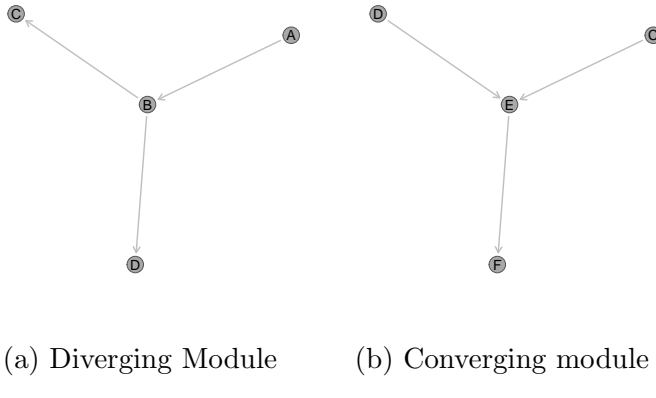
Figure 6.6: **Simple graph structures.** A simple [graph](#) structures used to demonstrate the simulation procedure. These are examples of a pathway diverging or converging respectively which enabled testing the importance of direction in [pathway](#) structures. These are used with both activating and inhibiting relationships as shown.

As previously observed (in Section 3.3), performance declined with higher numbers of [synthetic lethal](#) genes and lower sample sizes. However, the sensitivity of [SLIPT](#) is high with conventional p-value thresholds (adjusted by [FDR](#)). [Synthetic lethal](#) partners are often distinguishable for non synthetic lethal genes, even in simple highly correlated networks. The small number of genes and their high correlation has an impact on the [ROC](#) curves for higher numbers of [synthetic lethal](#) partners which are skewed compared to those observed previously. Specificity cannot be tested if all potential partner genes are [synthetic lethal](#) which limits the number of [synthetic lethal](#) genes that can be tested.

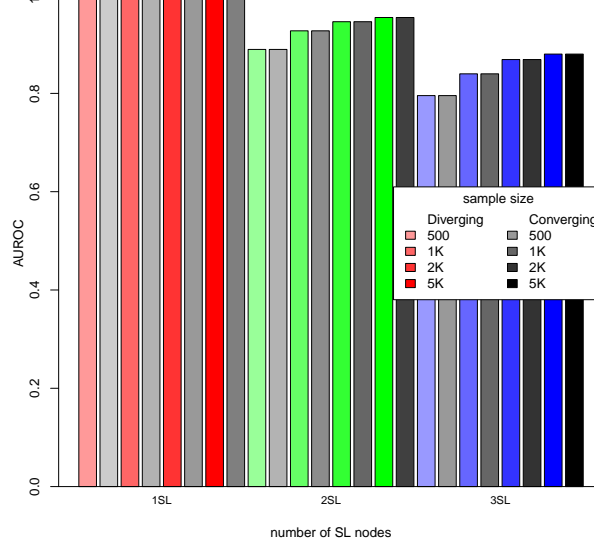
These results were consistent between the pathway modules of diverging (in Figure 6.8a) and converging signals (in Figure 6.8b). The [AUROC](#) performance and underlying curves were strikingly similar between these [graph](#) structures (as shown in Figures 6.7 and K.1). Thus the performance of [SLIPT](#) was not perturbed by [pathway](#) structure, specifically the direction of pathway relationships since these [graph](#) structures also demonstrate pathways in opposite direction. In a direct comparison (shown in Figure 6.8c), the performance of simulations did not differ across parameter values in these simple [graphs](#) and therefore [SLIPT](#) is robust to pathway direction.



**Figure 6.7: Performance of simulations on a simple graph.** Simulation of synthetic lethality was performed by sampling from a multivariate normal distribution generated from a diverging graph structure. Performance of SLIPT declines for more synthetic partners but this is mitigated by increased sample sizes (in darker colours). This manifests as a decline in specificity and the false positive rate. For each parameter value, 10,000 simulations were used. Colours of the ROC curves in Figure 6.7b correspond to the parameters in Figure 6.7d.



(a) Diverging Module      (b) Converging module

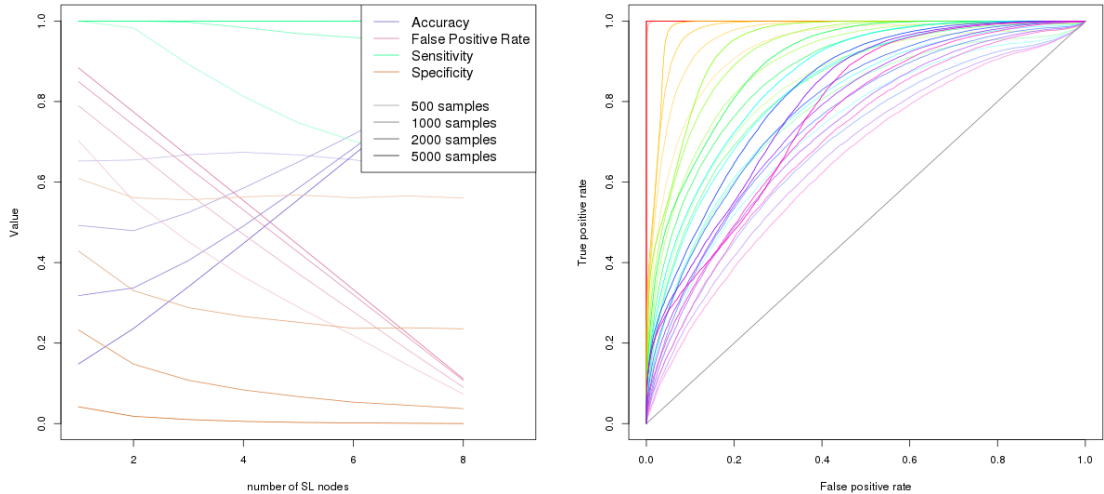


(c) Performance between Graph Structures

Figure 6.8: **Performance of simulations is similar in simple graphs.** The AUROC values for simulations of multivariate normal distributions based on each graph structure yielded indistinguishable performance across parameter values in 10,000 simulations.

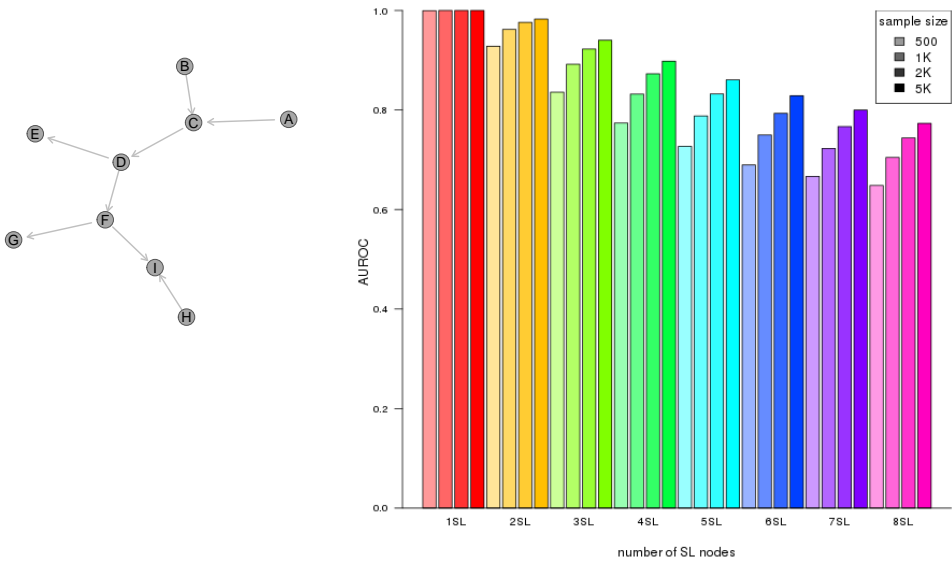
### 6.2.1.2 Constructed Graph Structures

A more complex graph structure was used to examine the performance of detecting synthetic lethal partners with **SLIPT** in simulated expression data with pathway correlation structures. For a simple chain of gene representing a pathway (shown in Figure 6.9), the above findings were generally replicated. Performance was high across parameter values in small networks, with similar decreases in higher numbers of synthetic lethal genes to detect and lower sample size.



(a) Statistical evaluation

(b) Receiver operating characteristic



(c) Graph Structure

(d) Statistical performance

Figure 6.9: **Performance of simulations on a pathway.** Simulation of synthetic lethality was performed by sampling from a multivariate normal distribution generated from a pathway structure. Performance of SLIPT declines for more synthetic partners and lower sample sizes (in darker colours). For each parameter value, 10,000 simulations were used. Colours of the ROC curves in Figure 6.9b correspond to the parameters in Figure 6.9d.

When detecting **synthetic lethal** genes with **SLIPT** using adjusted (**FDR**) p-value thresholds, the performance differences were primarily due to changes in specificity, as the small numbers of **synthetic lethal** genes still had highly significant p-values. Despite lower specificity and performance in **ROC** curves, the accuracy increases and false positive rate decreases desirably with higher numbers of **synthetic lethal** genes due to the high sensitivity and proportion of **synthetic lethal** genes detected. Therefore the thresholds imposed by adjusted p-values appear to be appropriate for detecting **synthetic lethal** partners, even in strongly correlated pathways, at least in these small-scale test cases.

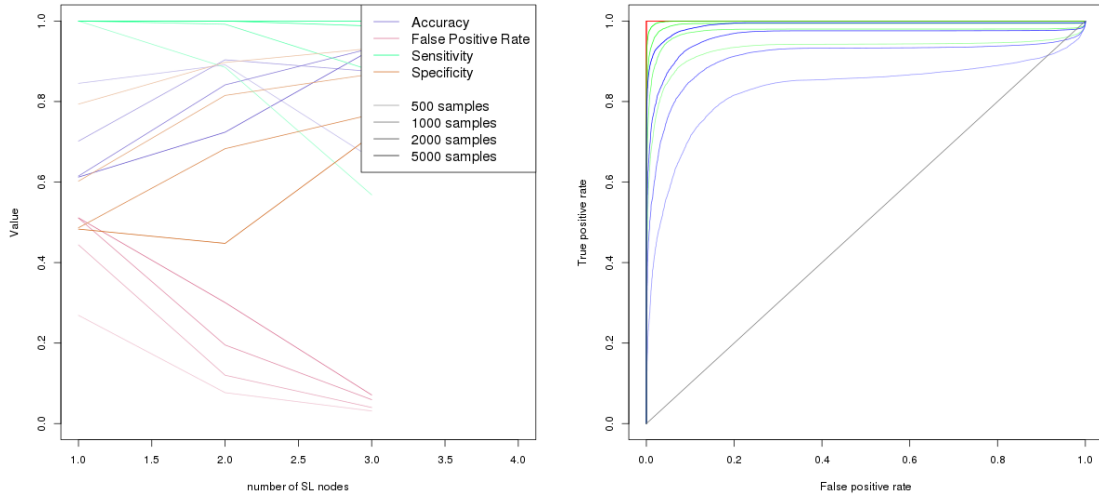
An artifact of these small test cases led to the skewed **ROC** curves (as discussed in Section 6.2.1.1), which may be the result of the low number of non-synthetic lethal genes to identify as true negatives, affecting the accuracy of specificity. This issue does not occur in larger, more complex **graph** structures, even with modest total numbers of genes and high correlations (as shown in Section 6.3). This issue is unlikely to occur in large **expression** datasets with many non synthetic lethal genes, as shown previously (in Section 3.3 and 6.2.1.1) with **graph** structures in larger datasets (in Section 6.2.4).

## 6.2.2 Performance with Inhibitions

Simulations of **synthetic lethality** in **expression** data were also performed with correlation structures derived from **graphs** containing inhibiting relationships (as are commonplace in biological pathways) which produce negative correlations. As shown in Figure 6.10, these are not an issue for detection by **SLIPT**. Rather, the **SLIPT** procedure performs well on simple graph modules with highly negative correlations. With **synthetic lethal** detection based on p-value (adjusted by **FDR**), there was higher specificity, higher accuracy, and lower false positive rate in an inhibitory graph than the same graph with activating relationships (as shown by Figure 6.7).

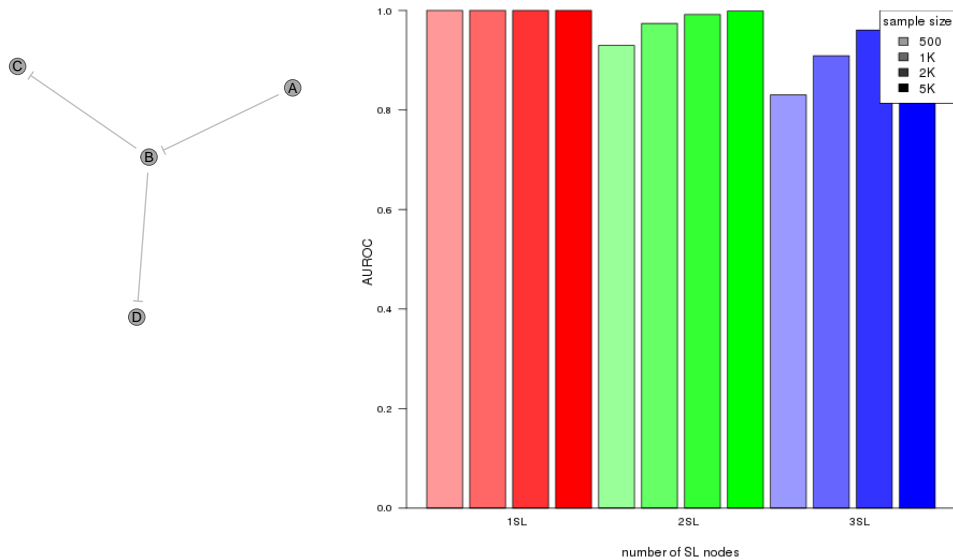
The **ROC** curves for an inhibiting graph also show consistently high specificity irrespective of detection threshold with only the upper extreme of the curve exhibiting a skew below random performance (in Figure 6.10). Nevertheless, the **AUROC** values show a high performance across parameter values, particularly avoiding issues with higher numbers of **synthetic lethal** partners (as observed in Section 6.2.1.1). However, performance was marginally lower for higher numbers of **synthetic lethal** genes to detect and lower sample sizes, consistent with previously observations.

Negatively correlated simulated datasets are also unperturbed by minor differences in **graph** structure, such as changing in the direction of the graph module. As observed



(a) Statistical evaluation

(b) Receiver operating characteristic



(c) Graph Structure

(d) Statistical performance

Figure 6.10: **Performance of simulations on a simple graph with inhibition.** Simulation of [synthetic lethality](#) was performed by sampling from a multivariate normal distribution generated from an inhibiting graph. Performance of [SLIPT](#) declines for more synthetic partners and lower sample sizes. For each parameter value, 10,000 simulations were used. Colours of the [ROC](#) curves in Figure 6.10b correspond to the parameters in Figure 6.10d.

for activating relationships in these graph modules, the performance was highly concordant between the graph modules (shown by similar results in Figures 6.10 and K.2).

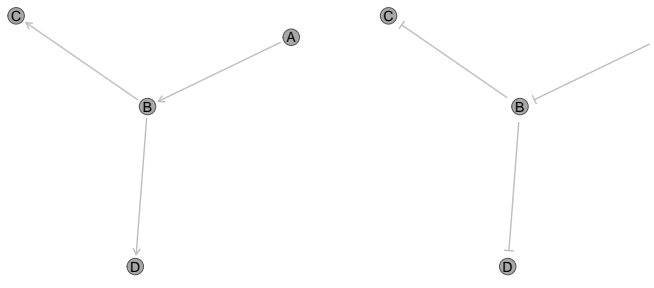
Detection of synthetic lethality by SLIPT in simulated data with inhibiting relationships outperforms simulations with activating relationships in the same graph structure (as shown in Figure 6.11). Thus SLIPT is robust in gene expression datasets with inverse correlations and performs well in them, at least in simple test cases. This is important because such relationships occur frequently in biological pathways and therefore the findings inferred from graph structures without inhibiting relationships are a conservative estimate.

The SLIPT methodology likely performs better in biological pathways (which contain negative correlations) than the graph structures discussed previously (in Section 6.2.1). This is likely since negative correlations lead to synthetic lethal partners and inversely correlated genes which are positively correlated with the query gene. As previously shown, the SLIPT methodology performs well with specificity against positively correlated query genes (in Sections 3.3.2.2 and 6.1.2.1).

Similarly, more complex graph structures with entirely inhibiting relationships (negative correlations) also perform desirably on p-value thresholds (adjusted by FDR) and have high performance across increasing numbers of synthetic lethal genes, particularly for sufficiently high sample sizes (as shown by Figure K.3). However, this is not necessarily the case for graph structures with a combination of activating and inhibiting relationships (i.e., containing positive and negative correlations) As shown by Figure K.4, such a mixed network structure does not necessarily have high performance across parameters as observed for purely inhibiting networks.

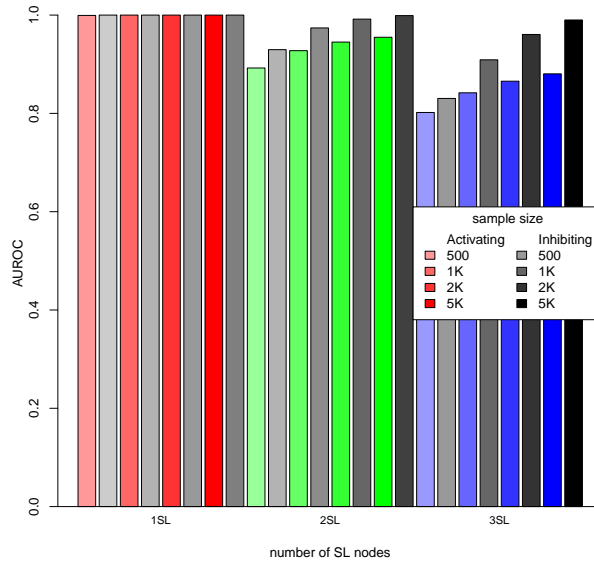
These still appear to have desirably high sensitivity, high accuracy, and low false positive rate for detecting more synthetic lethal genes, despite poor specificity. The ROC curves are particularly skewed for high proportions of the network being synthetic lethal and may stem from low numbers of true negative genes to detect (as discussed in Section 6.2.1.1). In a direct comparison of performance (shown in Figure 6.13), the purely inhibiting graph had consistently higher performance than the activating one as observed for simpler graphs (in Figure 6.11).

In contrast, the combination of activating and inhibiting relationships had slightly lower performance across parameters compared to the same graph structure with activating relationships. Therefore correlation structure can impact on the performance of SLIPT in a graph network, in either direction, specifically the addition of negative correlations. However, this may be an artifact of the simulation procedure as synthetic



(a) Activating Graph

(b) Inhibiting Graph

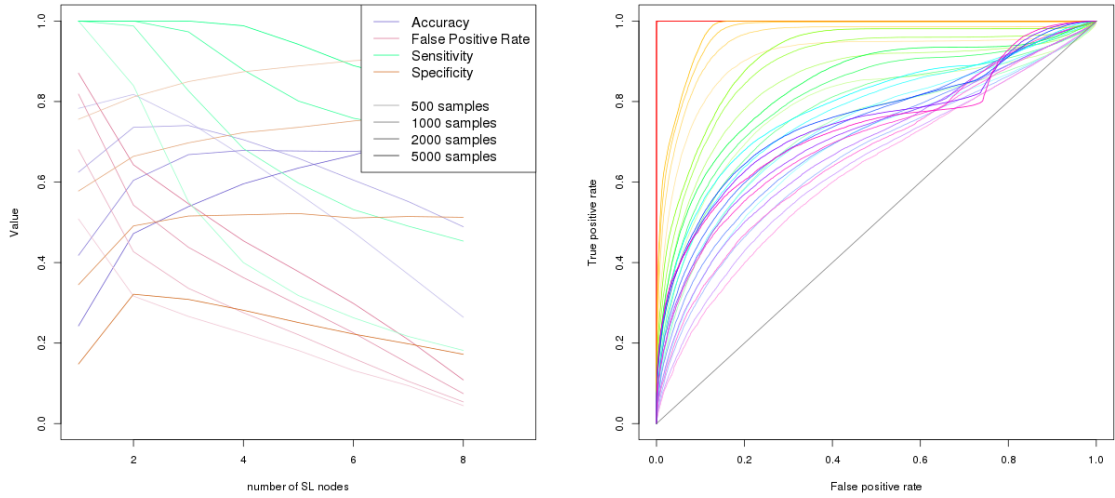


(c) Performance between Graph Structures

**Figure 6.11: Performance is higher on a simple inhibiting graph.** The AUROC values for simulations of multivariate normal distributions based on inhibitions in the Graph structure yielded consistently higher performance across parameter values in 10,000 simulations.

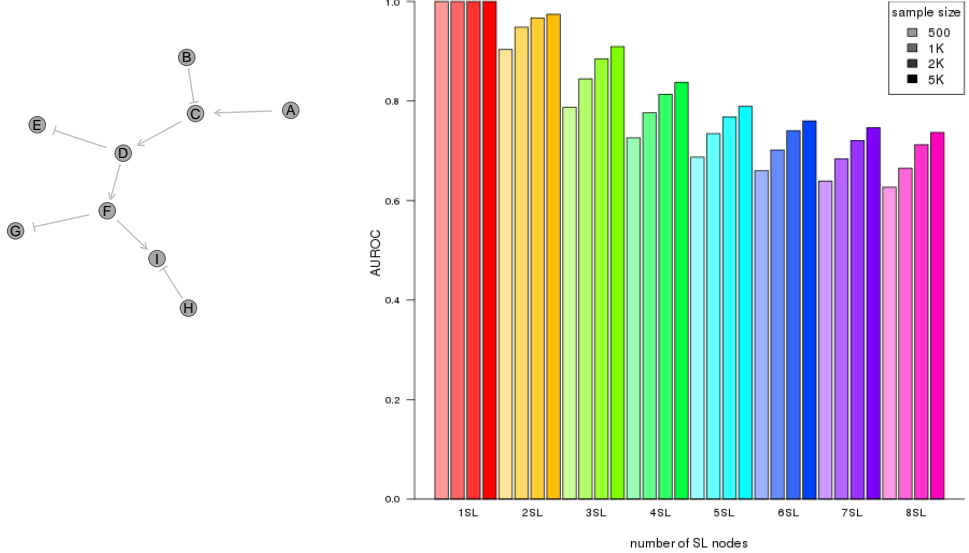
lethal genes from the correlation structure were randomly selected (without regard to their relationships), with the query gene added to ensure that conditions for synthetic lethal relationships were met.

This system for simulating inhibitory pathways is not ideal since it lead to synthetic lethal gene combinations, by randomly selecting them, which are unlikely to occur in biological pathways. These randomly selected synthetic lethal genes may account for the detection results being suboptimal (i.e., difficult to detect synthetic lethal partners) compared to previous investigations. It is expected that inversely correlated synthetic



(a) Statistical evaluation

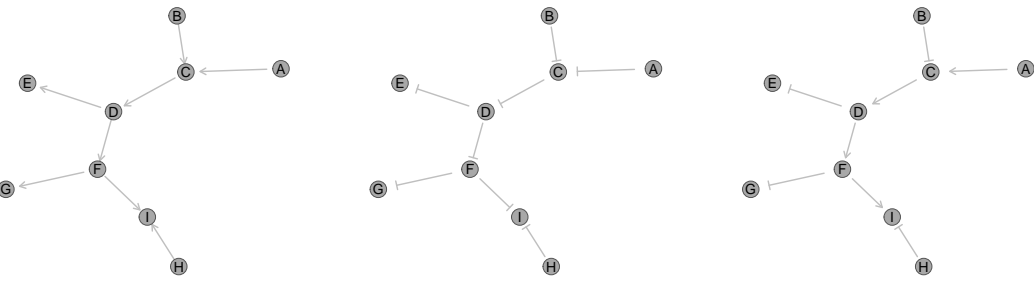
(b) Receiver operating characteristic



(c) Graph Structure

(d) Statistical performance

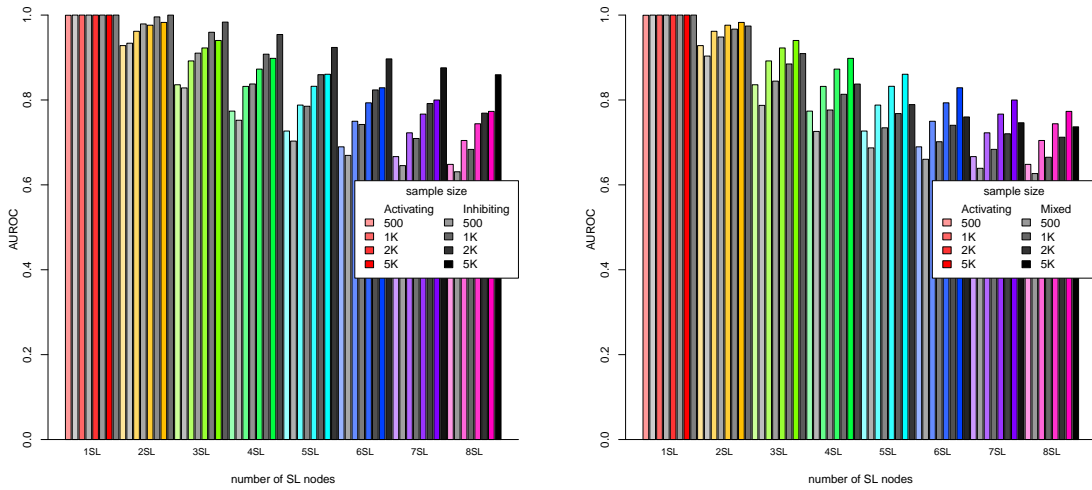
**Figure 6.12: Performance of simulations on a constructed graph with inhibition.**  
 Simulation of synthetic lethality was performed by sampling from a multivariate normal distribution generated from pathway structure with a combination of inhibitions. Performance of SLIPT declines for more synthetic partners and lower sample sizes. For each parameter value, 10,000 simulations were used.



(a) Activating Graph

(b) Inhibiting Graph

(c) Mixed Graph



(d) Performance between Graphs (a) and (b) (e) Performance between Graphs (a) and (c)

Figure 6.13: **Performance is affected by inhibition in graphs.** The AUROC values for simulations of multivariate normal distributions based on graph structure containing only inhibitions in the Graph structure yielded consistently higher performance across parameter values in 10,000 simulations. A combination of activating and inhibiting relationships had lower performance but was more similar to the activating graph.

partner genes will be highly expressed in a mutually exclusive manner such that at least one of them will be compensating for loss of the query gene in most samples, leading to a weak synthetic lethal signature in expression data in this case. Furthermore, this case may not be representative of empirical biological data with synthetic lethal partners of tumour suppressor genes which are commonly inversely correlated to the query gene (to some extent) and therefore it is unlikely that they are strongly negative correlated with each other, unless they are synthetic lethal partners of each other as well. It is plausible

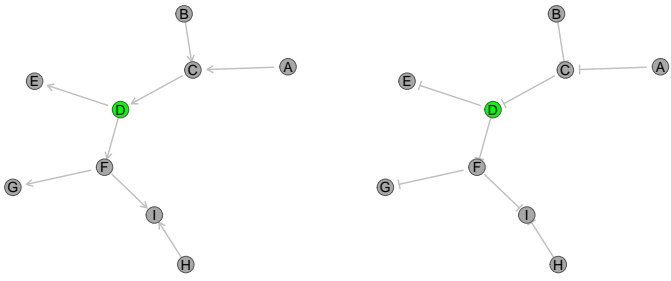
that many **synthetic lethal** partner genes will serve to separately compensate for the loss of query gene function and be positively correlated with each other. Nonetheless, these simulations are sufficient to demonstrate that correlation structure (particularly negative correlations) have an impact on the detection of **synthetic lethality**. However, **SLIPT** is still able to perform well across **graphs** with different activating and inhibiting relationships and the perturbations in performance are marginal, particularly those reducing performance compared to an activating network.

### 6.2.3 Synthetic Lethality across Graph Structures

While **synthetic lethal** genes are distinguishable in principle from those highly positively correlated with them (as shown by **ROC** analysis), they are not necessarily distinguished as reflected by low specificity and high false positive rates in poorly performing simulations throughout this section. The negative correlations are not subject to the same issue, they sometimes perturb the correlation structure between **synthetic lethal** partner genes making it difficult to detect many of them. Thus far, **synthetic lethal** genes have been selected randomly which is a limited approach. To examine the impact of pathway relationships in more detail, specific genes will be selected to be **synthetic lethal** within a network. Replicate simulations were performed for **synthetic lethal** detection with a fixed **synthetic lethal** gene, in contrast to previous investigations (randomly selecting **synthetic lethal** genes). This investigation was performed to demonstrate the impact of these genes being **synthetic lethal** in the detection of neighbouring genes in the pathway network, under **graph** structure activating and inhibiting relationships.

For instance, detection of a **synthetic lethal** gene in an activating **graph** structure (as shown in Figure 6.14a) is straightforward: the  $\chi^2$  values across simulations are clearly distinguishable from non synthetic lethal genes (shown in Figure 6.14c). A small number of simulations were performed for each gene being designated as **synthetic lethal**. In each case (of each gene being the **synthetic lethal** partner), the **synthetic lethal** gene was detectable with highest  $\chi^2$  value, being distinguishable amongst 20,000 genes including the highly correlated graph network (as shown in Figure K.5).

This is consistent with previous observations that **SLIPT** performed optimally for a single **synthetic lethal** partner in this network (in Figure 6.9). Despite optimal performance in a **ROC** curve irrespective of detection threshold, many of the highly correlated genes would be detected as false positives using a conventional p-value threshold (even if adjusted by **FDR**) from a  $\chi^2$  test with 4 degrees of freedom as performed by **SLIPT**.



(a) Activating Graph

(b) Inhibiting Graph

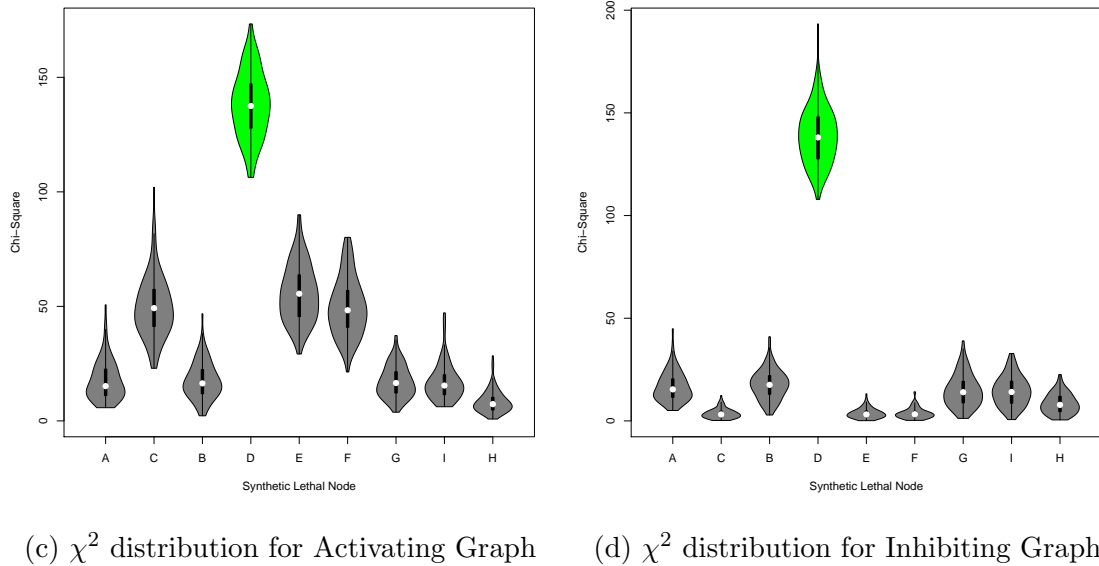


Figure 6.14: **Detection of synthetic lethality within a graph structure.** The gene “D” was designated to be synthetic lethal and the  $\chi^2$  value from [SLIPT](#) was computed for each gene across each graph structure. The  $\chi^2$  values were computed in 100 simulations of datasets of 20,000 genes including the graph structure and 1000 samples. Adjacent genes exhibited lower  $\chi^2$  values with inhibiting relationships.

(as described in Section 3.1). In particular, the genes that are adjacent to the synthetic lethal gene “D” within the graph structure exhibited high test statistics across simulations which would often be reported as false positives (as shown in Figure 6.14c). This is not specific to example of gene “D”, with the neighbouring genes exhibiting higher  $\chi^2$  test statistics for each gene in the network when it is designated as the synthetic lethal partner (as shown in Figure K.5).

Thus the synthetic lethal signal propagates from the true synthetic lethal gene

throughout the network such genes nearer to the true **synthetic lethal** gene (more highly correlated) have higher test statistics and are more likely to be detected by **SLIPT** as false positives. This tendency for adjacent genes to be detected as **synthetic lethal** false positives is consistent with the **synthetic lethal** pathways being more concordant between **SLIPT** in **TCGA** data (Koboldt *et al.*, 2012) and the **siRNA** screen (Telford *et al.*, 2015) than individual gene results (in Chapter 4). False positive genes are therefore still more likely to be involved in a **synthetic lethal** pathway by being correlated with a true **synthetic lethal** gene and **synthetic lethal** pathways are likely to have many genes detected by **SLIPT** giving a consensus of evidence, supporting the pathway over-representation approach in particular which may account for how it differs from pathway **metagenes**. Furthermore, **SLIPT** is still viable to detect true **synthetic lethal** partners or prioritise those most likely to be experimentally validated since those with the strongest support (i.e, higher  $\chi^2$  values and more significant p-values) are more likely to be the underlying **synthetic lethal** gene.

In contrast to an activating graph (Figure 6.14a), the immediately adjacent genes in an inhibiting graph (Figure 6.14b) had neither an elevated  $\chi^2$  test statistics indicating **synthetic lethality** nor a significant inverse effect (as shown in Figure 6.14d). Similar simulations were performed a **graph** structure with inhibiting relationships within a dataset of 20,000 genes. The adjacent genes to the **synthetic lethal** gene “D” did not have elevated  $\chi^2$  values and therefore true **synthetic lethal** partners were highly distinguishable from non synthetic lethal genes with inhibiting relationships. This was not specific to “D” and was shown across any gene in the **graph** structure if it were designated to be the **synthetic lethal** partner of the query gene (shown in Figure K.6). This is consistent with the detection of many genes involved in kinase signalling, gene regulation, and other known cancer pathways (in Chapter 4) which frequently have inhibitory steps. These results support **SLIPT** as an appropriate approach to distinguish **synthetic lethal** partners in biological pathways, including those relevant to cancer growth and inhibition.

However, it should be noted that the 2<sup>nd</sup> degree neighbours of the **synthetic lethal** gene still exhibited moderate  $\chi^2$  values (and are moderately correlated with the **synthetic lethal** gene). It is still possible for these to be detected as false positives as previously described for an activating **graph** structure although the presence of inhibitory relationships (and negative correlations) further increases the differences in test statistics for correlated genes and underlying **synthetic lethal** partners as shown by the extreme example (in Figure K.6).

These findings are consistent with simulations in a graph containing a combination of activating and inhibiting relationships which exhibits either of these  $\chi^2$  profiles depending on which gene is **synthetic lethal** and the relationships to adjacent genes (as shown in Figure K.7). Note that in this case, the **synthetic lethal** gene is distinguishable and inhibitory relationships within this **graph** structure make it easier to detect underlying **synthetic lethal** genes with **SLIPT** by a more highly significant  $\chi^2$  test. This contrasts with randomly selecting multiple **synthetic lethal** genes (in Figure 6.13) where the performance of **SLIPT** was impeded by the inhibitory relationships between **synthetic lethal** partners in this **graph** structure. Therefore the random **synthetic lethal** genes selected previously with negative correlations between them which had poor performance are likely to have created an artifact in the simulation results as they are biologically implausible and constrain the **synthetic lethal** simulation procedure.

The results with one **synthetic lethal** partner were sufficient to infer the impact of **synthetic lethal** partners within pathways on neighbouring (correlated) genes. However, it is plausible that the **synthetic lethal** signatures in **expression** data would propagate through a network with multiple **synthetic lethal** partners as sources, provided that the correlations between **synthetic lethal** partners is biological feasible. These simulations were performed on a correlated **graph** structure within a larger **gene expression** dataset of 20,000 genes (as performed in Sections 3.3 and 6.2.4), a feasible number for a full human **gene expression** dataset, and as such are comparable to the findings below.

#### 6.2.4 Performance within a Simulated Human Genome

The high proportion of **synthetic lethal** partners in small networks (and fewer true negatives) made it difficult to accurately assess the performance of **SLIPT** with higher numbers of true partners to detect (as noted in Section 6.2.1.1). The addition of more non synthetic lethal genes in previous simulations increased the performance of **SLIPT**, particularly the specificity to reduce the number of false positives (as shown in Sections 3.3 and 6.1). The **graph** structures (as used in Section 6.2.1) of genes with correlations from sampling a multivariate normal distribution were included in a larger simulated dataset of 20,000 genes. This simulation procedure enabled testing of the performance of **SLIPT** when detecting **synthetic lethal** partners within correlated **graph** structures (of a **synthetic lethal** pathway) in the context of biologically feasible numbers of genes.

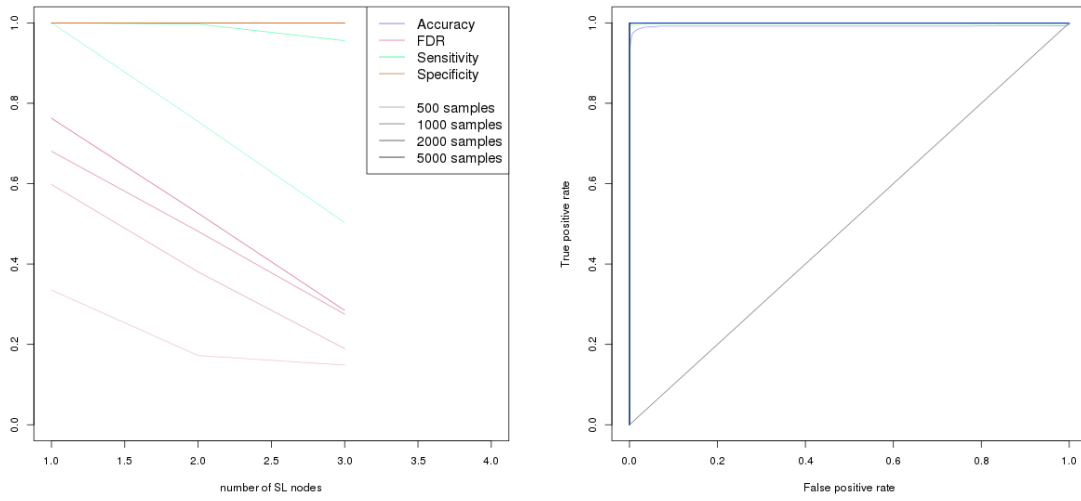
The simulations performed in Section 6.2.1.1 were replicated within a dataset of 20,000 genes with the rest being composed on non synthetic lethal genes without cor-

relation structure. The aforementioned issue with specificity in a higher number of underlying **synthetic lethal** genes did not occur in a simple **graph** structure (as shown in Figure 6.15). For such a small graph module of highly correlated genes within a **gene expression** dataset, detection of **synthetic lethal** genes within the network by **SLIPT** and distinguishing these from the larger dataset had high performance across parameter values. In this case, a reduction in sensitivity resulted in poorer performance, a higher number of non synthetic lethal genes were correctly identified, with a low false positive rate and high accuracy. Thus the the use of stringent  $\chi^2$  p-value thresholds (adjusted by **FDR**) are suitable for testing for **synthetic lethality** in **gene expression** data across the number of genes in human and cancer data.

In a direct comparison with simulations in the **graph** structure alone (as performed in Section 6.2.1.1), detection of **synthetic lethality** with **SLIPT** performs consistently better in a larger dataset with many true negative genes to detect (as shown in Figure 6.16). Thhe **SLIPT** methodology as it has a high specificity and low false positive rate, which is desirable. **SLIPT** is therefore applicable to large **gene expression** datasets where these are important considerations since the number of negative genes to correctly identify often vastly outnumbers the number of positive genes to detect.

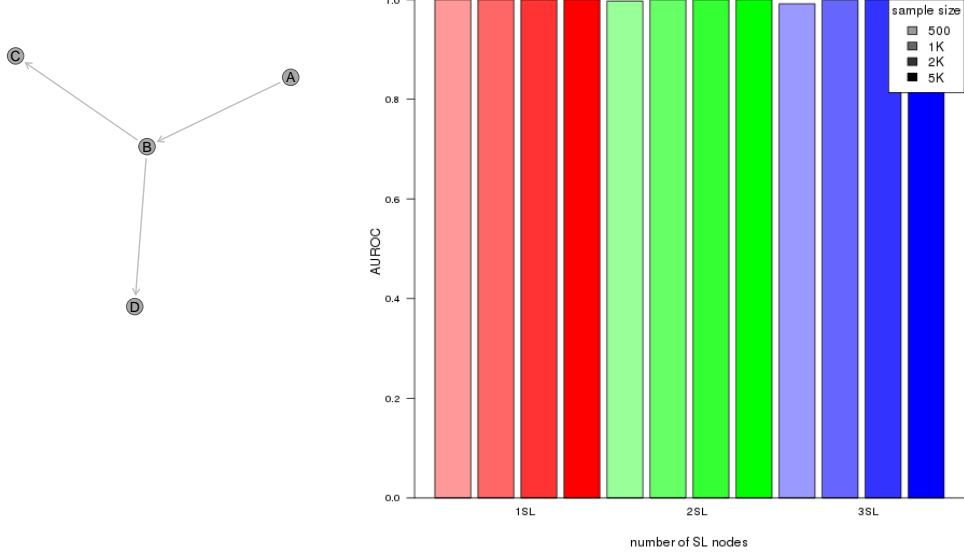
This increase in performance with more non synthetic lethal genes to detect does not necessarily apply in an inhibiting **graph** structure. This an important consideration since biological pathways commonly contain inhibiting relationships (and inverse correlations), although they are unlikely to occur across an entire pathway. While an increased performance for an activating graph was replicated, in this case, the performance of simulations of an entirely inhibiting **graph** structure did not improve within a larger dataset. Rather, the performance in the inhibiting **graph** structure was similar to simulations of the **graph** structure in isolation. It is expected that the findings based on these simulations of genes with **pathway** structures in smaller datasets (as described in Section 6.2.1) will be relevant to larger datasets. The simulation results in these inhibiting **graph** structures perform comparably or higher with more non synthetic lethal genes to distinguish from them even with inhibitory relationships within the **graph** structure

Performance of **synthetic lethal** detection of **SLIPT** in **graph** structures with inhibitions included in a larger dataset of non synthetic lethal genes did not diminish to the level of the **graph** structure simulated alone. In some cases (as shown in Figure 6.17), the performance of an inhibitory **graph** structure was consistently elevated when in-



(a) Statistical evaluation

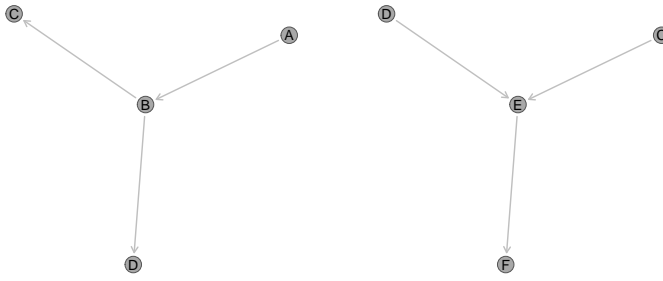
(b) Receiver operating characteristic



(c) Graph Structure

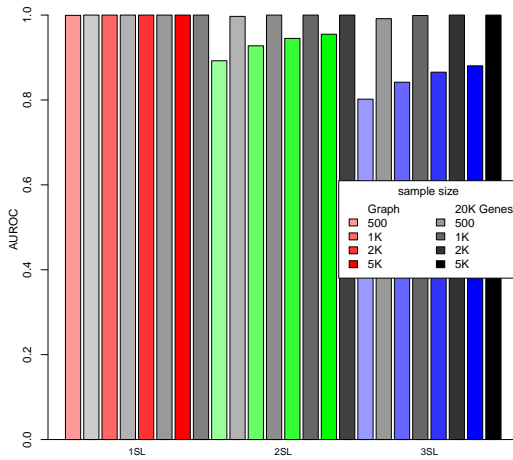
(d) Statistical performance

Figure 6.15: **Performance of simulations including a simple graph.** Simulation of synthetic lethality was performed by sampling from a multivariate normal distribution (without correlation structure apart from the graph shown). Performance of **SLIPT** was high across parameters for detecting synthetic lethality in the graph structure within a larger dataset. The sensitivity decreases for a greater number of true positives to detect but the specificity remains high with a low false positive rate.

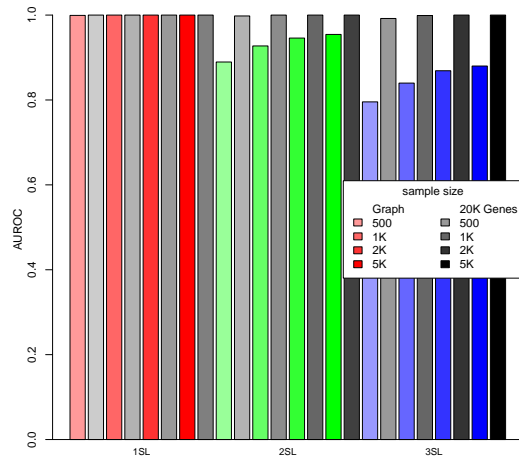


(a) Diverging Module

(b) Converging module



(c) Performance in Diverging Module

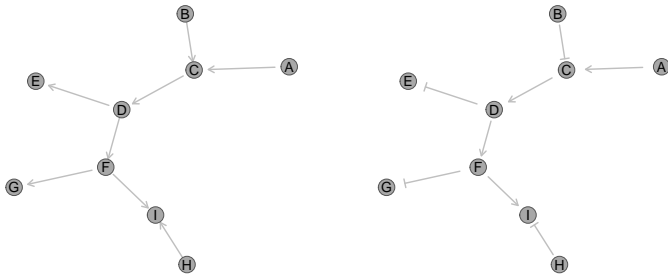


(d) Performance in Converging module

Figure 6.16: **Performance on a simple graph improves with more genes.** Simulations were performed with each of the `graph` structures to detect `synthetic lethal` partners within them. In either structure, performance of detection in a dataset containing on the `graph` structure (in colour) was lower than testing the `graph` structure within a larger dataset of non synthetic lethal genes (without correlations).

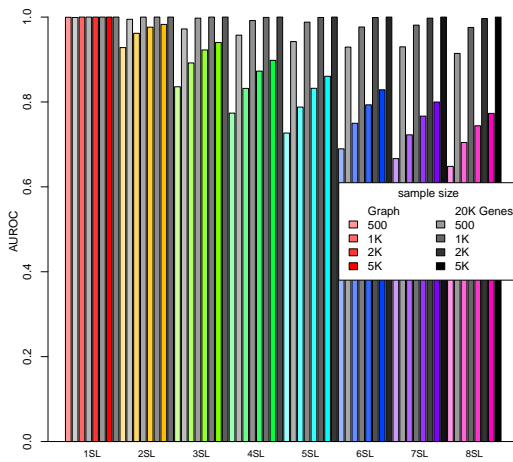
cluded within a larger data. However, these did not perform as well as the equivalent `graph` structures without inhibitory relationships within a similar dataset.

This poorer performance of inhibitory `graph` structures may be due to highly negatively correlated genes being false positives. These genes will be positively correlated with the query gene if they are negatively correlated with a `synthetic lethal` partner (i.e., within a `synthetic lethal` pathway). The `SLIPT` procedure performs well at distinguishing these positively correlated genes, as previously shown (in Sections 3.3.2.2

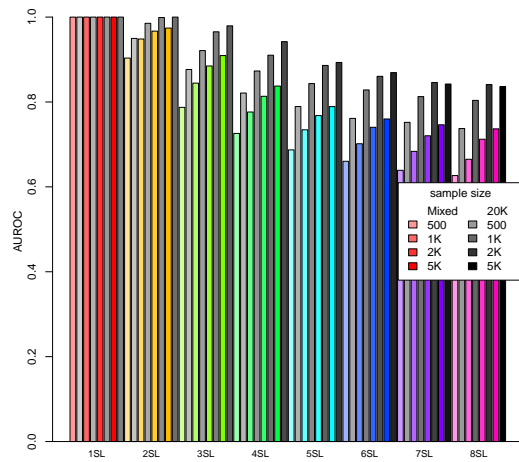


(a) Graph Structure

(b) Inhibiting Structure



(c) Performance in Graph



(d) Performance with Inhibitions

Figure 6.17: **Performance on an inhibiting graph improves with more genes.** Simulations were performed in a [graph](#) structure with activating and inhibiting relationships to detect [synthetic lethal](#) partners within them. In contrast to an activating graph, performance of detection in a dataset containing only the [graph](#) structure (in colour) was as much lower than testing the [graph](#) structure within a larger dataset of non synthetic lethal genes (without correlations) in an inhibiting [graph](#) structure with negative correlations.

and [6.1.1.1](#)). These false positives will also be a minority amongst a larger dataset of non synthetic lethal genes without correlation to the query or [synthetic lethal](#) genes.

It more likely that the poorer performance stems from negative correlations between [synthetic lethal](#) genes which makes them more difficult to individually detect (as observed in Section [6.2.2](#)). As discussed in Section [6.2.3](#), this is likely an artifact of the simulation procedure selecting random [synthetic lethal](#) genes with strong inhibitory

relationships between them. Therefore the poorer performance for inhibiting **graphs** within larger datasets is not cause for concern because the cases where **SLIPT** performs poorly are likely to be combinations of simulated **synthetic lethal** genes that are not likely to occur within biological pathways. This simulation procedure has included higher-order **synthetic lethal** to produce the weakest signal of **synthetic lethality** for individual partner genes which are still detectable by **SLIPT**.

### 6.3 Simulations in More Complex Graph Structures

Investigations with simulations based on **graph** structures were extended to larger **graphs**, enabling more synthetic lethal genes within a pathway and modelling the complexity of a biological pathway. Sensitivity declines over a greater range for the number of **synthetic lethal** partners in a larger network with a trade-off with specificity (as shown in Figures K.8–K.10). However, the accuracy declined for greater numbers of **synthetic lethal** partners and the false positive rate peaks at intermediate values. In this range, difference between simulations varied with greater sample size. The **AUROC** results were similar between these more complex **graph** structures, , although the larger **graph** (Figure K.10) differed in sensitivity and specificity at an adjusted (**FDR**) p-value threshold. This difference be due to different proportions of **synthetic lethal** and non-synthetic lethal genes to detect, since these **graphs** (in Figures K.8 and K.9) had fewer genes.

While the **graph** structures (of similar size) were highly distinct, they had similar performance profiles across parameters. **SLIPT** is therefore robust across **pathway** structures and is more affected by the number or proportion of genes to detect. Findings from previous simulations in similar correlation structures (in Section 3.3) should be applicable to **expression** data with more complex correlation structures, such as those occurring in biological pathways. Specifically, **synthetic lethal** partners are distinguishable from closely correlated genes in the context of a biological pathway networks, irrespective of thresholds (shown by **ROC**) and with the sensitivity and specificity of p-value thresholds (adjusted by **FDR**) as used for **SLIPT** (in Chapters 4 and 5).

The findings for inhibitory **graph** structures were replicated with larger more complex **graph** structures with inhibiting relationships and more **synthetic lethal** genes to detect (shown in Figures K.11–K.14). In each **graph** structure, simulations entirely with inhibiting relationships (Figures K.11, K.13, and K.15) had higher performance than the equivalent graph with entirely activating relationships (Figures K.8, K.9, and K.10) or a combination of activating and inhibiting relationships (Figures K.12, K.14, and K.16).

While the presence of negative correlations subtly affects the performance of **SLIPT**, the methodology is robust across the exact structures of genes and is therefore applicable to detecting **synthetic lethal** genes in a range of (synthetic lethal) biological pathways with different structural relationships.

### 6.3.1 Simulations over Pathway-based Graphs

Simulations of **synthetic lethality** in **gene expression** with correlation structures thus far have used simple blocks of correlated genes (as used in Section 3.3) or derived from constructed **graph** structures (as used in Section 6.2). These have been used to make inferences on the impact of correlation structure, it remains to be shown whether these findings are reproducible in the complexity of the biological **network** structure. Specifically, **SLIPT** was tested on simulated data with known underlying simulated **synthetic lethal** partners (as described in Section 3.2.2) with multivariate normal correlation structure derived from biological pathways (as described in Section 3.4.2).

The Reactome **pathway** structure for the **PI3K** cascade (as used in Chapter 5) was used to demonstrate the simulation procedure for detecting **synthetic lethality** in the **graph** structure of a biological pathway. This pathway has clear directionality and related signalling pathways were among those identified to be **synthetic lethal** candidates (in Chapter 4). The **PI3K** pathway has a relatively moderate size (138 genes) and complexity. It is therefore suitable for comparison to previous **graph** structures of a similar scale (50–100 genes) with the complexity of a biological pathway.

The performance of **synthetic lethal** detection with **SLIPT**, in simulated **expression** data based on the Reactome **PI3K** pathway (as shown in Figure 6.18), was concordant with previous findings. **SLIPT** had high performance when detecting a low number of **synthetic lethal** genes which decreased for high numbers of **synthetic lethal** genes or lower sample sizes. In particular, the performance of simulations in the **PI3K** pathway highly resembled the simulation results for constructed **graphs** of similar scale and complexity (as shown in Figures K.8 and K.9). Using thresholds based on the  $\chi^2$  p-value (adjusted by **FDR**), simulations in the biological **PI3K** pathway had a higher sensitivity and lower specificity. While the performance decreased for more **synthetic lethal** genes to detect within the simulated **PI3K** pathway, this primarily involved a reduction in sensitivity to detect **synthetic lethal** genes rather than false positives, as the false positive rate decreased, the accuracy increased, and the specificity was relatively unperturbed (being more dependent on sample size). Thus **SLIPT** was stringent in an example of a biological **graph** structure and is appropriate for detection of syn-

synthetic lethal genes in complex correlation structures in gene expression data involving biological pathways.

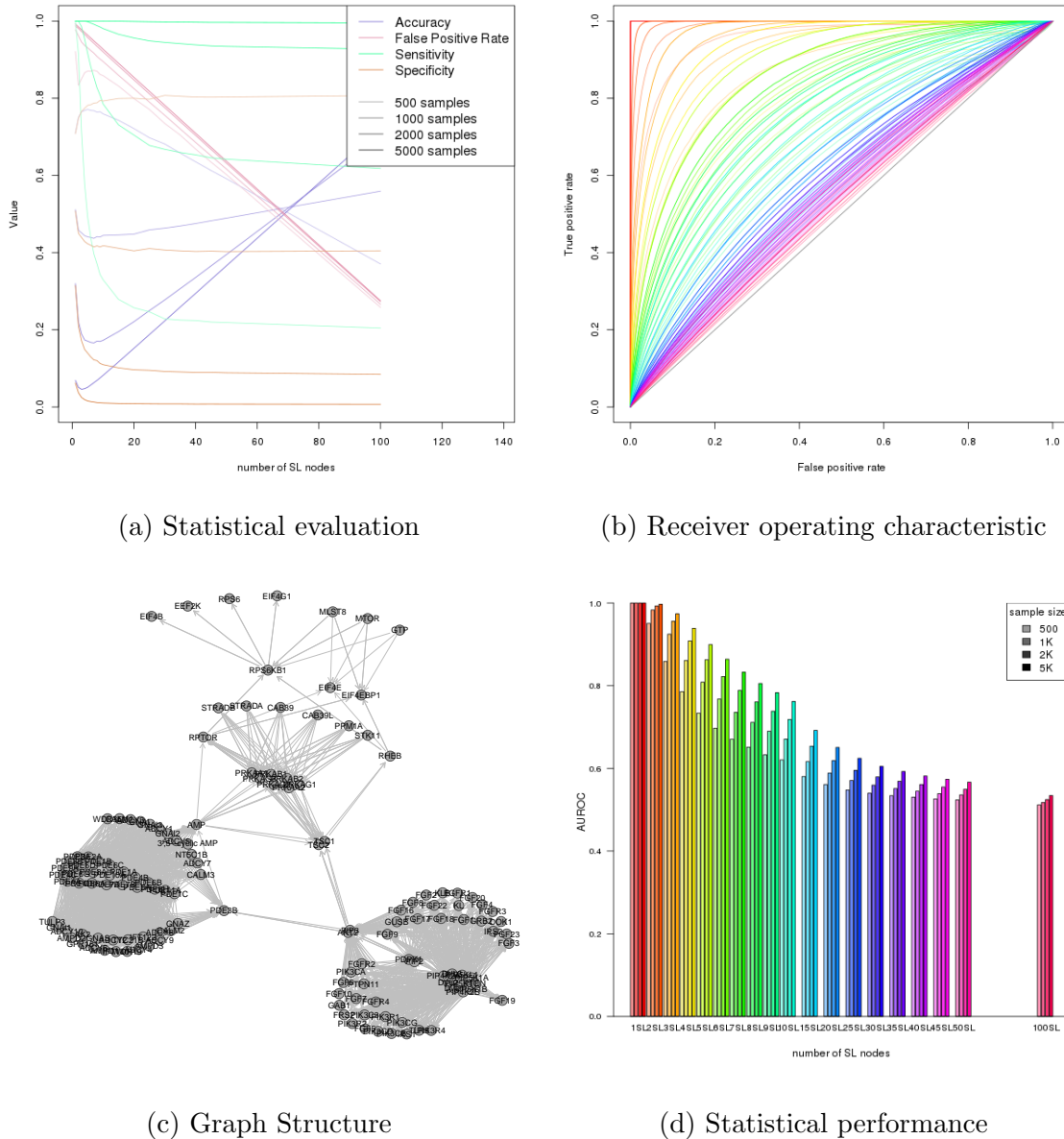


**Figure 6.18: Performance of simulations on the PI3K cascade.** Simulation of synthetic lethality was performed by sampling from a multivariate normal distribution based on the Reactome PI3K cascade. Performance of SLIPT was high across parameters for detecting synthetic lethality in the graph structure within a larger dataset. The performance decreases for a greater number of true positives to detect but the accuracy increases with a low false positive rate.

These simulations were replicated in the more complex  $G_{\alpha i}$  signalling pathway (of 292 genes), which was one of the most well supported **synthetic lethal** pathways with loss of *CDH1* in cancer (in Chapters 4 and 5). This pathway showed similar relationships between sensitivity, specificity, and false positive rate with number of **synthetic lethal** partners and sample size (as shown in Figure K.17). While the overall performance was lower than for smaller networks structures, many of the findings from previous networks were replicated in a larger more complex biological network. In the  $G_{\alpha i}$  signalling pathway, **SLIPT** had high performance for detecting low numbers of **synthetic lethal** genes and was highly stringent against false positives for higher numbers of **synthetic lethal** genes.

### 6.3.2 Pathway Structures in a Simulated Human Genome

Simulations were also performed with **graph** structures from biological pathways included in a larger dataset to simulate **gene expression** data of the scale typical for human and cancer studies. These simulations (as discussed in Section 6.2.4) showed a higher specificity and therefore **SLIPT** had higher performance. The simulated **PI3K** pathway (as shown in Figure 6.19) is no exception, with high performance across parameter values, which remained high up to many genes. While the sensitivity decreases for high numbers of **synthetic lethal** genes to detect within the **PI3K** pathway, the **SLIPT** methodology remains accurate with high specificity in a large simulated **gene expression** dataset.

Therefore the **SLIPT** methodology is a highly stringent approach suitable to be applied for detecting **synthetic lethal** genes and pathways within highly complex **expression** data with biological **pathway** structure. Even the poorly performing simulations were highly stringent with low false positive rates, which are an important consideration in a **gene expression** data with many non synthetic lethal genes. The enrichment of true **synthetic lethal** partners among detect genes makes **SLIPT** valuable for triage of candidate **synthetic lethal** partners for further validation and for pathway analysis.

The performance of simulation of **synthetic lethality** within biological pathways was markedly higher in the context of a larger dataset of thousands of genes. As shown in a direct comparison with the **graph** structures alone (in Figure 6.20c), performance was consistently higher across parameters in pathways of biological complexity from the Reactome database (Croft *et al.*, 2014) such as **PI3K** cascade and the  $G_{\alpha i}$  signalling pathway (shown in Figures K.18 and 6.20d).

These biologically complex **graph** structures, based on the Reactome pathways, as-

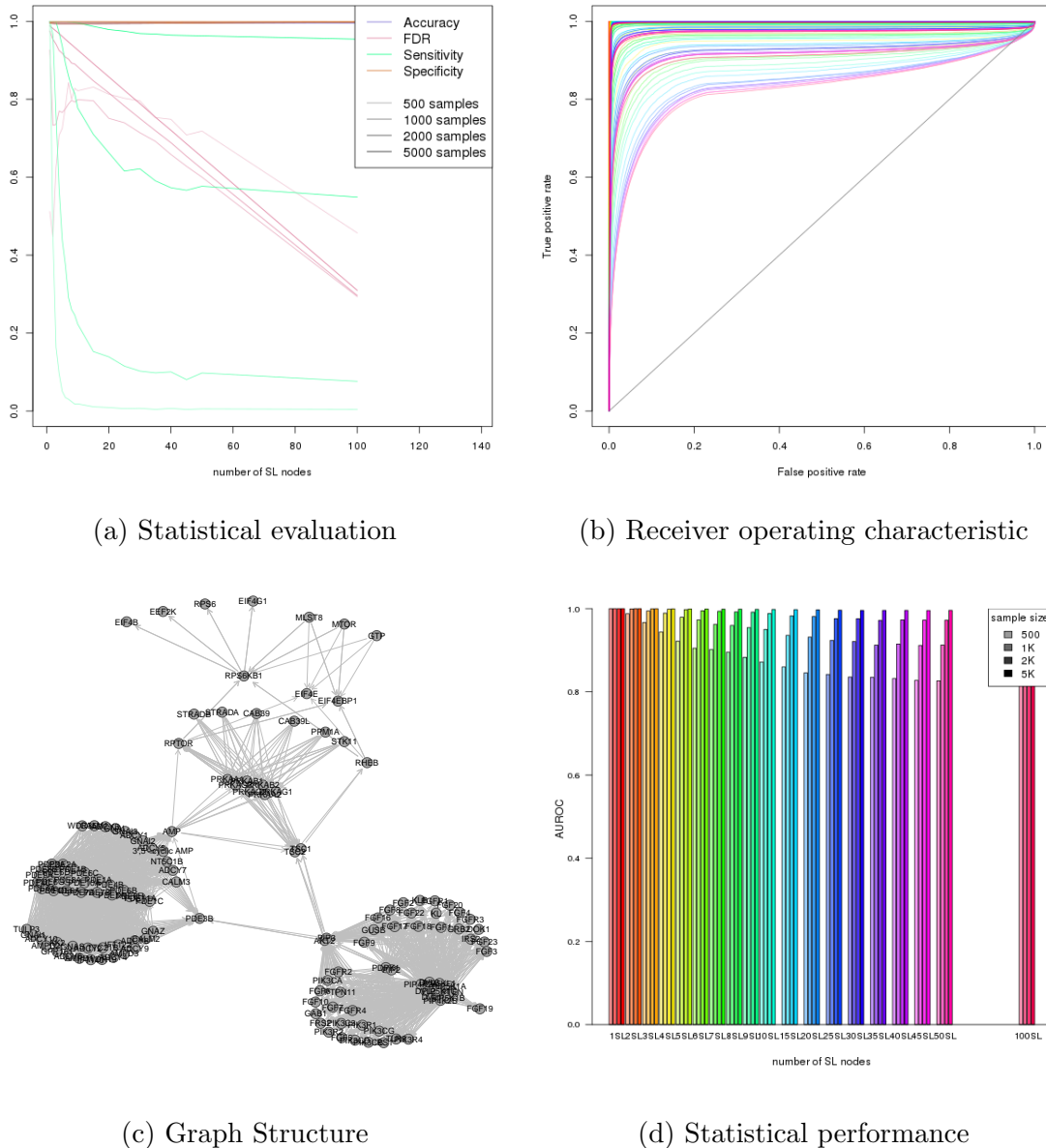
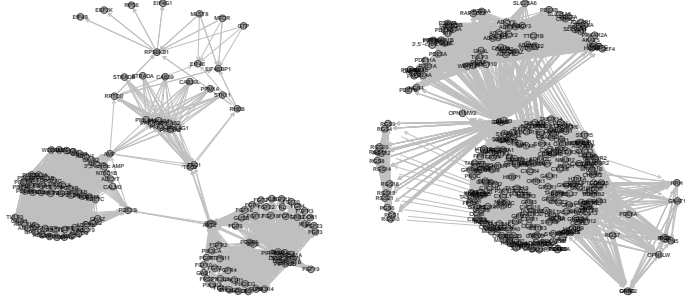
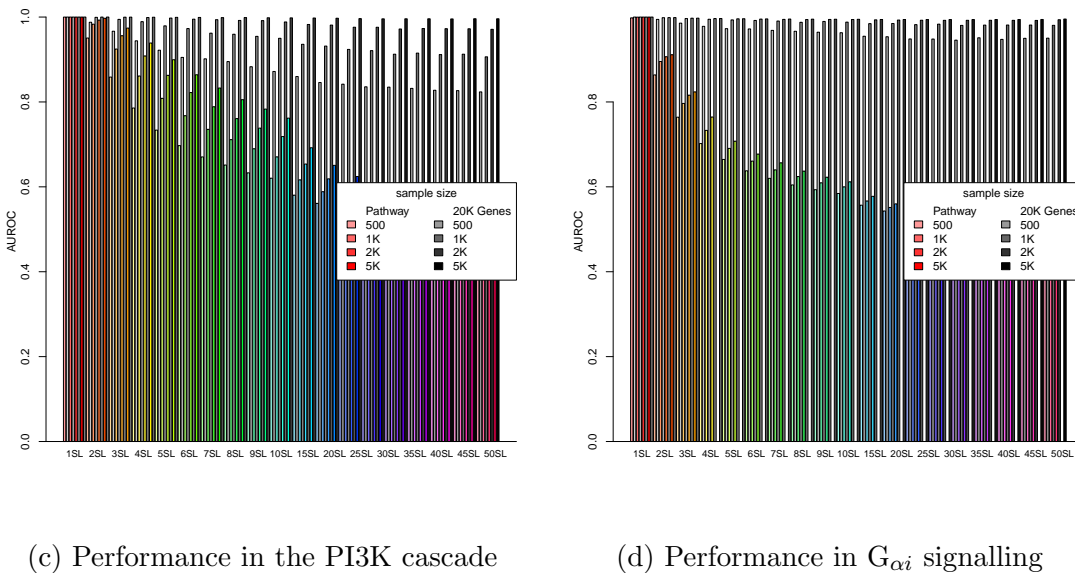


Figure 6.19: **Performance of simulations including the PI3K cascade.** Simulation of synthetic lethality was performed by sampling from a multivariate normal distribution (without correlation structure apart from the Reactome PI3K cascade). Performance of SLIPT was high across parameters for detecting synthetic lethality in the graph structure within a larger dataset. The sensitivity decreases for a greater number of true positives to detect but the specificity remains high with a low false positive rate.

sumed activating relationships to test synthetic lethal detection with SLIPT in the context of complex correlation structures. Inhibiting relationships were not distin-



(a) The PI3K cascade

(b)  $G_{\alpha i}$  signalling

(c) Performance in the PI3K cascade

(d) Performance in  $G_{\alpha i}$  signalling

Figure 6.20: **Performance on pathways improves with more genes.** Simulations were performed in a graph structures for the PI3K cascade and  $G_{\alpha i}$  signalling pathways structures to detect synthetic lethal partners within them. As for constructed graphs, performance of detection in a dataset containing only the graph structure (in colour) was as much lower than testing the graph structure within a larger dataset of non synthetic lethal genes (without correlations) for both graphs of biological complexity.

guished in the Reactome database (Croft *et al.*, 2014). However, these investigations with pathway based graph structures indicate that the findings in constructed graphs (as used in Section 6.2) are relevant to gene expression data containing real correlated pathways. Furthermore, previous comparisons between simulations with inhibiting relationships indicated that the performance of synthetic lethal detection in an equivalent graph structure with inhibitory relationships will likely be higher.

Non synthetic lethal genes, inversely correlated with the underlying synthetic lethal partners, were distinguishable by SLIPT with high specificity. Synthetic lethal genes were detectable with reasonable performance in large scale simulated gene expression data and highly (positively) correlated genes in pathway structures. These findings serve as a conservative estimate for the performance of SLIPT to detect synthetic lethal genes within a synthetic lethal biological pathway in empirical data. Synthetic lethal genes are distinguishable from correlated genes, to varying extents, in simulations. False positives are also more likely to occur within the same (synthetic lethal) pathways. Therefore SLIPT is both effective at triage of synthetic lethal candidates within a biological pathway and at identifying synthetic lethal pathways in high dimensional gene expression data.

## 6.4 Discussion

### 6.4.1 Simulation Procedure

Simulations have been performed to assess the performance of the SLIPT methodology (as described in Section 3.1 and with modifications) for detecting known underlying synthetic lethal partners of a query gene. These simulations support the the findings in empirical data (in Chapters 4 and 5) by addressing whether the methodology used to generate them is accurate or has desirable statistical performance in controlled simulated conditions. These investigations include adjusting parameters such as the numbers of synthetic lethal genes which were known in empirical data to assess the performance of the SLIPT methodology across simulation parameters and characterise the datasets for which SLIPT performs well. Simulation and statistically modelling also enabled comparison of the SLIPT methodology to other statistical approaches to synthetic lethal detection in expression data.

These simulations are based on a statistical model of synthetic lethality (as described in Section 3.2.1) which was designed stringently to ensure that if synthetic lethality is detectable in the simulated datasets it would also be detectable by the same methodology in empirical expression data. The model of synthetic lethality made conservative assumptions such as the low threshold of expression for gene function or the inclusion of cryptic higher-order synthetic lethality (when testing pairwise). These assumptions decrease the likelihood that synthetic lethal signatures would be detectable in expression data. Thus it is reassuring that synthetic lethality is still detectable in

under many simulation parameters as the performance of **SLIPT** would be expected to be higher were these assumptions to be violated in empirical data.

The simulation procedure (as described in Section 3.2.2) is designed as a computational pipeline with arguments passes to scripts. The **SLIPT** methodology and simulation of **expression** from **graph** structures were both used as R (R Core Team, 2016) software packages developed and released for this project (as described in Section 3.5). This design ensures that the simulations can be robustly applied across parameters with consistency between simulations apart from the differences discussed. The simulation procedure is also flexible to simulating other datasets, including **synthetic lethal** relationships and pathway correlation structures, should these be relevant to future investigations or **bioinformatics** tool development. The computational pipeline is also compatible with parallel computing and made use of **High Performance Computing (HPC)** infrastructure provided by the New Zealand eScience Infrastructure (NeSI) using the **Simple Linux Utility for Resource Management (Slurm)** submission system (as described in Section 2.5.3). This parallel computing pipeline enabled extensive investigations into **synthetic lethality** in simulated data, including approximately 2 million cpu-hours on NeSI.

#### 6.4.2 Comparing Methods with Simulated Data

Attempts were made to implement alternative **synthetic lethal** detection approaches such as linear regression and the **BiSEp** R package (discussed in Section 6.1). However, those tested were ineffective at detecting **synthetic lethality** in multivariate normal simulated data in comparison to **SLIPT**. While some of the published **synthetic lethal** detection methods (Jerby-Arnon *et al.*, 2014; Lu *et al.*, 2015) did not provide reproducible software releases for direct comparison, some of the central assumptions used in their design were tested by the statistical methods considered for **synthetic lethal** detection in **expression** data.

Another consideration is that **BiSEp** takes considerably more time to compute predictions than **SLIPT** or  $\chi^2$  which limited the number of simulations that were feasible and made it difficult to apply across parameters in the simulation pipeline (even when using supercomputing infrastructure as discussed in Section 2.5.3). The computationally intensive nature of the **BiSEp** procedure does not appear to be the issue for detecting **synthetic lethal** genes in **TCGA** data or simulations, although it has made more extensive simulations challenging. Rather, **BiSEp** is not suitable in either case since the **TCGA** data is normalised with **voom** (Ritchie *et al.*, 2015) and simulated

data is generated by sampling from a multivariate normal distribution. In either case, even subtle bimodal signatures in **expression** data were not consistently detectable or sufficient to detect **synthetic lethality**.

The **BiSEp** methodology may perform better on other data types but it cannot be directly compared with the results for **SLIPT** throughout this thesis which have used normalised or (multivariate) normally distributed data. Since it requires bimodal distributions, **BiSEp** is not suitable for stringently normalised **expression** data nor would it be expected to perform on (ranked) pathway **metagenes**. Thus **SLIPT** represents a distinct approach more suitable for these data types whereas **BiSEp** may be applicable to other applications in which bimodal distributions are more frequent.

This investigation also demonstrates that implementing scientific software from other research groups is not a trivial exercise, even when released as an open-source R package. Therefore, the above results were used to evaluate **SLIPT** and compare it to other statistical rationales. An comprehensive comparison to contemporary **synthetic lethal** detection approaches (and those released in the future) or further benchmarking is left to an impartial researcher to evaluate. The above findings show that the **SLIPT** approach is able to detect **synthetic lethal** genes in simulated data with comparable or better performance than a range of distinct statistical techniques and was appropriate for use throughout this thesis.

#### 6.4.3 Design and Performance of **SLIPT**

The simulation procedure using sampling from a multivariate normal distribution was used throughout the majority of the simulation investigations in this thesis. This approach has the advantages of emulating the continuous normalised **expression** data used for **gene expression** analysis and enabled the simulation of correlation structures (as discussed in Section 3.3). These simulations scaled to datasets of comparable scale to those used in **gene expression** analysis with thousands of genes. The **SLIPT** methodology was shown to perform robustly across large numbers of genes and simple correlation structures. This includes high specificity against genes positively correlated with the query gene for which the directional **SLIPT** methodology more suited to distinguishing **synthetic lethal** genes from than the  $\chi^2$  test without directional criteria on the number of samples observed.

These findings were expanded upon in this chapter. Specifically, different quantiles were compared for **SLIPT** and the  $\chi^2$  test. These approaches using threshold based discrete gene function were compared to the Pearson correlation without loss of the

continuous [expression](#) data. The 3-quantiles for [SLIPT](#) (as described in Section 3.1) were optimal for both [SLIPT](#) and the  $\chi^2$  alone. In addition to being optimal for estimating the significance of [synthetic lethal](#) interactions, these quantiles were also optimal for the directional criteria of [SLIPT](#) since this method outperformed the  $\chi^2$  test and was the most different at the 3-quantile. As previously, noted this difference was more pronounced with positively correlated genes (with the query gene) for which the specificity of [SLIPT](#) improves and was replicated in large datasets with thousands of genes as occur in human [expression](#) data. These results were not simply due to sufficient samples for significant p-values since the performance as determined by [AUROC](#) analysis is independent from significance thresholds. This indicates that the [SLIPT](#) methodology (as it has been used in Chapters 4 and 5) is optimal and the parameters used to design it were appropriate.

Both discrete functional approaches ([SLIPT](#) and  $\chi^2$ ) were able to outperform negative correlation which supports their use. In particular, this result addresses the concern that arbitrary thresholds of low and high gene function (as used by [SLIPT](#)) lose useful data by compressing the spectrum of [gene expression](#) into categorical data. However, this does not impede the performance of [SLIPT](#) and can reduce statistical if the quantiles used are optimal. The poorer performance of correlation-based detection of [synthetic lethality](#) also indicates affirms the concept of gene function for [synthetic lethality](#) being qualitative, that is [expression](#) must be sufficient for cell viability and higher [expression](#) is not necessarily higher function (as this is not the case for all genes). Furthermore, the finding that negative correlation outperforms positive correlation is also consistent with co-expression being a poor predictor of [synthetic lethality](#) compared to other approaches (Jerby-Arnon *et al.*, 2014), supporting the claims of Lu *et al.* (2015).

Compared with [SLIPT](#), neither correlation approaches nor bimodality signatures were suitable for detecting [synthetic lethality](#) in [expression](#) data. The correlation-based approaches make assumptions about the relationship between [gene expression](#) and function which do not necessarily hold for all genes. Similarly, the bimodal approach is not appropriate for normalised data since deviations from a normal distribution have already been used for ensuring data quality, as is common practice for [RNA-Seq](#) data. Other approaches were continuous data such as fitting linear models are likely to be prone to similar issues and not perform as well as [SLIPT](#). However, it is possible that these may be improved with conditioning on known [synthetic lethal](#) partners with multivariate regression or Bayesian priors. Similarly, [synthetic lethal](#)

detection could be performed by iteratively conditioning upon the strong candidate from previous analysis. These approaches may be able to better circumvent the issues of high-order **synthetic lethality** and multiple testing.

Nevertheless, the above findings are sufficient to assess the performance of **SLIPT** and present an effective straightforward approach to **synthetic lethal** detection in **gene expression** data. Further development of linear models, Bayesian inference approaches, or comparison to existing **synthetic lethal** approaches (e.g., machine learning) remain as future directions. Developing and testing more sophisticated statistical approach to **synthetic lethal** detection may benefit from the concepts discussed with regard to the relatively simple **SLIPT** methodology. Similarly, further comparisons and benchmarking of **SLIPT** against other computational approaches to **synthetic lethal** detection in **gene expression** data is more suitable for an independent researcher and the **slipt** R package has been released (as described in Section 3.5) for this purpose, in addition to further application in research.

#### 6.4.4 Simulations from Graph Structures

The simple correlation structures (as used in Section 3.3) were expanded upon to simulate correlated genes based on **graph** structures using the multivariate normal simulation procedure on correlation structures generated from graph structures (as described in Section 6.2). These simulations enable further investigations into the performance of **SLIPT** in the context of more complex correlation structures. The simulation of **expression** from **network** structures is widely applicable to simulating pathway **expression** data and as such the **graphsim** R package has been released (as described in Section 3.5).

These investigations show that **SLIPT** performs robustly across datasets with different correlation structures, including those derived from **graphs** with the complexity of biological pathways. The **SLIPT** methodology was able to detect **synthetic lethal** genes within **synthetic lethal** pathways across many **graph** structures. This methodology performed particularly well with **synthetic lethal** pathways in the context of a larger dataset with a high specificity which supports **SLIPT** as a stringent approach to **synthetic lethal** detection in highly dimensional **gene expression** data. Together these results support the use of **SLIPT** in biological gene expression data since it is able to detect **synthetic lethal** genes in highly complex correlation structures.

Similarly, the inclusion of inhibitory relationships in **graph** structures was shown to increase the performance in simple networks supporting **SLIPT** being applicable to

biological data in which these relationships are common. While these results were not replicated in more complex inhibitory **graph** structures, this is likely an artifact of the simulation procedure (which randomly selects **synthetic lethal** genes) generating biologically implausible combinations of **synthetic lethal** genes which are difficult to detect. When the test statistics in simulations with a **synthetic lethal** gene were examined in more detail, the test statistics of the **synthetic lethal** gene were consistently higher and distinguishable from nearby genes in the **graph** structure. In contrast to previous concerns with inhibiting relationships, these differences were more pronounced with genes which had inhibitory relationships with **synthetic lethal** genes. While distinguishable from nearby genes in a **pathway** structure, the genes correlated with **synthetic lethal** still had higher test statistics than more distant genes (similar to observations with correlated genes in Section 3.3).

In addition to being able to detect **synthetic lethal** genes in a pathway, the proximal genes in a pathway are most likely to be false positives and therefore **SLIPT** is also able to detect **synthetic lethal** pathways. Therefore **SLIPT** identifies genes which are likely to be constituent of a **synthetic lethal** pathway and is more likely to rank underlying **synthetic lethal** genes with greater significance. Together these findings support the use of **SLIPT** throughout this thesis, further application of **SLIPT**, and further development of such strategies for **synthetic lethal** detection. Similarly, the simulation procedures developed and demonstrated for examining **synthetic lethal** detection in **expression** data using **graph** structures is amenable to further development and investigations into **pathway** structure in **expression** data such as predicting biological pathways from **expression** data or the impact of pathways on differential **expression** analyses.

## 6.5 Summary

A statistical model and simulation procedure has been developed to test the performance of the **SLIPT** methodology in controlled conditions, using multivariate normal distributions. This simulation procedure has been developed into a computational pipeline which was able to test the statistical performance (using stringent assumptions) of **SLIPT** across many parameters and compare it to alternative **synthetic lethal** detection strategies. The **SLIPT** methodology performs well at detecting small numbers of **synthetic lethal** genes in simple systems. It does not perform as well in more complex systems but neither do alternative strategies. The **SLIPT** methodology performs well compared to Pearson correlation and similar methods based on the  $\chi^2$  test. Thus

**SLIPT** is an effective detection method for **synthetic lethal** relationships in **expression** data despite its relatively simple design.

Simulations of more complex datasets, including large numbers of genes, complex correlation structure derived from **graph** structures, and correlations with the query gene. **SLIPT** performs robustly across these, including correlation structures based on complex biological pathways. The performance of **SLIPT** improves in larger datasets, datasets with positive correlations with the query genes, and some **graph** structures which include inhibiting relationships, namely those datasets more representative of **gene expression** in biological data. **SLIPT** was both capable of recurrently detecting genes within a **synthetic lethal** pathway and distinguishing **synthetic lethal** genes from correlated with them, even in highly complex correlation structures. Therefore **SLIPT** is a stringent **synthetic lethal** detection strategy and is applicable to **gene expression** as previously demonstrated for the partners of *CDH1* in breast and stomach cancer in this thesis.

# Chapter 7

## Discussion

This thesis combines analysis of gene expression data from TCGA with experimental screening results (Telford *et al.*, 2015) to demonstrate synthetic lethal discovery for partners of *CDH1*. Together these findings further elucidate the functions of *CDH1* in the cell, functional redundancy in cancer, and represent potential targets against loss of *CDH1* function. These candidate synthetic lethal genes were further investigated for relationships within synthetic lethal pathways, developing a network-based approach to compare genes identified in genomics experiments and analyses in the process.

The synthetic lethal detection methodology, SLIPT, was applied to gene expression data throughout this thesis and was evaluated with simulated data. A simulation procedure was developed to stringently generate gene expression data from known synthetic lethal partners in simulated data. These simulations included simple and complex correlation structures and modelling synthetic lethal genes within pathways. Together, these results demonstrate SLIPT as a robust widely applicable gene expression analysis procedure (for which an R package has been released) for discovery of synthetic lethal partner genes. Performance of SLIPT on simulated data also highlights the strengths of the procedure and future directions to improve upon it.

### 7.1 Synthetic Lethality and *CDH1* Biology

The *CDH1* tumour suppressor gene was the focus of identifying synthetic lethal partners to demonstrate the novel SLIPT methodology. This gene is important in sporadic breast and stomach cancers, in addition to familial syndromes, such as HDGC. The analysis of synthetic lethal partners of *CDH1* in breast and stomach cancers was enabled by the availability of molecular data (Bass *et al.*, 2014; Koboldt *et al.*, 2012) and

a synthetic lethal screen conducted in MCF10A breast cells (Chen *et al.*, 2014; Telford *et al.*, 2015).

Synthetic lethal interactions arise due to functional redundancy (Boone *et al.*, 2007; Fece de la Cruz *et al.*, 2015; Kaelin, Jr, 2005) and as such the synthetic lethal partners of *CDH1* indicates the wide-ranging biological functions that E-cadherin is involved in. The diverse synthetic lethal pathways identified supports the known pleiotropic nature of the *CDH1* gene by detecting established functions of *CDH1*, replicating candidates from an experimental screen (Telford *et al.*, 2015), and identifying novel interactions with candidate genes and pathways for further investigation. The highly pleiotropic functions of E-cadherin was also consistent with *CDH1* being a tumour suppressor gene.

### 7.1.1 Established Functions of *CDH1*

The *CDH1* has established functions in cell-cell communication and maintaining the cytoskeleton, specifically with cell-cell adhesion by forming tight junctions and the adherens complex. More recently, additional functions of *CDH1* in the extracellular matrix and fibrin clotting have also been identified. Synthetic lethal interactions within biological pathways (i.e., partners in the same pathway as the query gene) are expected according to previous synthetic lethal experiments (Boone *et al.*, 2007; Kelley and Ideker, 2005). Synthetic lethal interactions identified in these pathways are consistent with these being functions of *CDH1*, in addition to potentially actionable targets against cancers.

### 7.1.2 The Molecular Role of *CDH1* in Cancer

The involvement of *CDH1* in the extracellular matrix is important in cancers as it indicates a mechanism by which *CDH1* loss may affect the tumour microenvironment, contributing to its role as a tumour and invasion suppressor. Furthermore, perturbations in the extracellular matrix and tumour microenvironment present a means by which to specifically inhibit (cancerous) *CDH1*-deficient cells, in addition to those currently being considered. These may be further supported in further investigations with 3D cell culture, “organoid”, or mouse xenograft cancer models.

In contrast, many of the pathways involved in cell signalling, including GPCRs, were identified by SLIPT in addition to the experimental screen (Telford *et al.*, 2015). These support the previous results in cell line models, that these pathways are essential to the growth of *CDH1*-deficient cancers and present a potential vulnerability specific to these (cancerous) cells. Furthermore, the replication of synthetic lethality

of *CDH1* with cell signalling pathways in TCGA data across cancer types and genetic backgrounds robustly supports these pathways being clinically applicable beyond the genetic background of the model system of *CDH1*<sup>-/-</sup> MCF10A cells (Chen *et al.*, 2014). While the specific synthetic lethal genes were not as consistently detected between the SLIPT analyses and siRNA screen (Telford *et al.*, 2015), they were sufficient to identify synthetic lethal pathways for further experimental investigation, which are more likely to be replicated between genetic backgrounds (Dixon *et al.*, 2008). Together these results demonstrate how SLIPT can be integrated with an experimental screen to triage potential therapeutic targets for further pre-clinical investigation.

The analysis of expression data with SLIPT is also indicative of additional biological mechanisms of synthetic lethality in pathways beyond those identified in screening experiments (Telford *et al.*, 2015). In particular, translation and regulatory pathways, involving 3' UTRs and NMD, were identified as candidate synthetic lethal pathways with *CDH1* by SLIPT. These pathways represent downstream targets regulated by the putative synthetic lethal signalling pathways which cancer cells are dependent on for sustained protein expression to proliferate and evade host defense processes such as apoptosis and immune responses (Gao and Roux, 2015) .

## 7.2 Significance

### 7.2.1 Synthetic Lethality in the Genomic Era

Development of an effective synthetic lethal discovery tool for bioinformatic analysis has a wide range of applications in genetics research including functional genomics, medical and agricultural applications. The SLIPT approach demonstrated in this thesis is widely applicable to other genes and biological questions. In addition to further query of cancer genes, including other tissues, synthetic lethal gene functions are also of wider interest for their implications for genetic redundancy. Highly redundant genes, and the genetically robust systems they give rise to, are of further relevance to evolutionary, developmental, and systems biology to understand how these change over time and play a role in fundamental development of cell types, in addition to cancers (Boone *et al.*, 2007; Nowak *et al.*, 1997; Tischler *et al.*, 2008).

Developmental genes in particular, are highly evolutionary conserved and subject to high rates of redundancy (Fromental-Ramain *et al.*, 1996; Kockel *et al.*, 1997; Nowak *et al.*, 1997). These are often difficult to study with conventional functional genetics since individual knockouts of redundant genes do not necessarily have a mutant pheno-

type. Identifying genes with a common function is therefore also important to the study of developmental genes with unknown functions. Synthetic lethal discovery methods such as **SLIPT** provide a genomic approach to further systematic characterisation of gene function including such highly redundant developmental genes.

Similarly, variants of unknown significance and modifier loci are a major concern in human genetics, including “monogenic” and “rare” diseases. Many of these could potentially be difficult to characterise individually due to synthetic lethal interactions where additional loci contribute to the disease (or only compensate for some variants). As such systematic identification of synthetic lethal interactions also has applications in the study of such “oligogenic” diseases along with similar applications in the study of heritability for traits including agricultural genomic selection.

Genetic redundancy is also a concern in pharmacology. Polypharmacology and network medicine are rationales to account for this by using drugs with multiple (known and specific) targets (Barabási *et al.*, 2011; Hopkins, 2008). Further characterisation of synthetic lethal genes will be valuable to the design of effective multi-target drugs or combination therapies in a range of therapeutic applications including molecular targeted therapies against cancer for which combination therapies are a popular solution for acquired resistance against individual targeted therapies. Characterisation of genetic interactions and combination therapies also has the potential to expand pharmacogenomic investigations. These may elucidate the impact of genotypes at multiple loci, which lead to adverse effects in a subset of the population due to variants in synthetic lethal genes.

Furthermore, redundant functions and synthetic lethal interactions also present a means to expand upon the concept of the “minimal” genome (Hutchison *et al.*, 2016). It is important to account for essential gene functions that are performed by redundant genes (or in combination with pleiotropic genes), rather than simply those that are perturbed by individual genes. An essential gene approach is likely to produce an underestimate that does not account for synthetic lethal interactions.

Synthetic lethal interactions are fundamentally important throughout genetics. Further understanding of them in a genomic context, facilitated by methods such as **SLIPT**, would contribute towards deeper understanding of gene functions and their role in traits or diseases in the post-genomic era. Genes do not function in isolation and understanding them in the context of the complexity of a cell and across genetic backgrounds is essential to further characterise their functions and ensure that findings can be validated or applied beyond experimental systems.

## 7.2.2 Clinical Interventions based on Synthetic Lethality

Synthetic lethal discovery with **SLIPT** is of particular interest in cancer research as a complementary approach to discovery of **synthetic lethal** drug targets. The cancer research community relies on cell line and mouse models for screening and validation experiments (Fece de la Cruz *et al.*, 2015) which would benefit from integration with **gene expression** analysis as demonstrated for *CDH1* and the screen conducted by Telford *et al.* (2015). **Synthetic lethal** drug design against cancer **mutations**, including gene loss or over-expression, could lead to a revolution in cancer **therapy** and **chemoprevention**. Such therapeutics would enable personalised treatment for cancer patients and high risk individuals. Examples of the **synthetic lethal** strategy (Bryant *et al.*, 2005; Farmer *et al.*, 2005) for cancer treatment have been shown to be clinically effective McLachlan *et al.* (2016). Many large-scale **RNAi** screens have been conducted recently, aiming to discover gene function and drug targets for similar application with other cancer genes, including cancers in other tissues (Fece de la Cruz *et al.*, 2015).

While **SLIPT** analysis and **RNAi** screens represent a significant step towards anti-cancer medicines, further validation is required to ensure that the **synthetic lethal** candidate genes and pathways identified for *CDH1* in breast and stomach cancer are applicable against *CDH1*-deficient cancers in the clinic. Validation with **RNAi** or pharmacological inhibitors is needed since false positives may occur in **SLIPT** analysis or **siRNA** screens. These candidates will need to be tested in pre-clinical models (cell lines and mouse xenografts) before proceeding to clinical trials. A therapeutic intervention will also require a **targeted therapeutic** to develop developed or repurposed against the **synthetic lethal** partner. Drug targets could be triaged from **synthetic lethal** genes by functions known to be amenable to drugs or structure with conserved specific sites that are not homologous to other genes, or those with existing drugs approved in trial for other applications. Both structure-aided drug design and compound screening are viable ways to target **synthetic lethal** partners.

**Targeted therapeutics** designed based on **synthetic lethal** interactions could expand the applications of “precision medicine” against molecular targets. **Synthetic lethality** expands the range of cancer genes which can be (indirectly) targeted to include **tumour suppressor** genes with loss of function, such as *CDH1*. **Oncogenes** with disrupted functions that are over-expressed or highly homologous to non-cancerous proto-oncogenes, such as *MYC*, *EGFR* or *KRAS*, may also be targeted by **synthetic lethality**. Applications against **tumour suppressor** genes is particularly important, as these cannot be approached by careful dosing. **Synthetic lethal** drug design has the benefit of being

highly specific against a particular genotype (such as *CDH1*<sup>-/-</sup>) with the potential for **targeted therapies** with a wide therapeutic index and few adverse effects, in contrast to many current anti-cancer drug regimens (Hopkins, 2008; Kaelin, Jr, 2009). These properties are highly desirable for **chemoprevention** applications, such as treatment against *CDH1*-deficient in **HDGC** patients (Guilford *et al.*, 2010), as an alternative to monitoring or surgery.

## 7.3 Future Directions

While further validation and pre-clinical testing is required to translate the findings for *CDH1* to cancer therapy or prevention, there are also further avenues for research into the detection of **synthetic lethality** in **gene expression** and other **genomics** data. The **SLIPT** methodology is amenable to wider application against a range of genes for which loss of function is deleterious, including other cancer genes in breast cancer or other tissues. **Synthetic lethal** interactions are functionally informative, particularly for mode-of-action of known drug targets, and are also relevant for identifying functions of newly characterised genes in **genomics** studies and designing specific interventions against cells with loss of function in cancer and other diseases. Thus **synthetic lethal** detection using **SLIPT** in **expression** data could be further used for many other genes, including others relevant to human health and disease.

These investigations do not need to be limited to **expression** data. While **expression** as a measure of gene function has been the focus of this thesis, other **genomics** data could be used for a similar purpose for **SLIPT** analysis. These include **DNA** copy number, **DNA** methylation, histone activation, **mutation** status, protein abundance, and protein activation state. For some applications or genes, these molecular profiles may be more informative of gene function and **synthetic lethal** relationships. However, **expression** was the focus of the investigations thus far as a widely accepted measure of gene function which has widely available **genomics** data. **SLIPT** is compatible with each of these data types (if the thresholds are selected appropriately) and may perform better for some applications with these molecular profiles or a weighted combination of these. As demonstrated, **SLIPT** is also suitable for future investigations with pathway **metagenes** and other summary data as well.

It may also be possible to improve the performance of **SLIPT** with refinements to the statistical or computational approach. This thesis has focused on rational query-based approach which computes relatively quickly, even in R (**R Core Team**, 2016), and is relatively intuitive to interpret. These computations are compatible with parallel

computing and the computational resources may be further reduced by using a different computing language. The `slipt` R package has been documented and released open-source (as described in Section 3.5) to facilitate further development, wider adoption, or comparison with other scientific software for similar purposes.

Alternative methods may be also improve on the statistical performance of `SLIPT`. In particular, the sensitivity was generally as issue with higher numbers of `synthetic lethal` partners in simulated data. While approaches using continuous data such as Pearson correlation and linear regression did not perform as well as `SLIPT`, they could be improved. A least squares regression approach in particular, enables multiple measures of relationships such as the coefficients of the fitted curve and significance of the fit (computed from the residuals). A linear modelling approach using regression is also amenable to refinement such as extending from fitting a linear relationship to a polynomial or logistic regression. Another benefit to fitting linear models is that these would enable the conditioning of known `synthetic lethal` partners to identify subtle signatures of further interacting partners.

This approach could also be applied iteratively on the strongest candidates from previous `synthetic lethal` analyses in further rounds of prediction conditioned upon them. Similarly, `synthetic lethal` prediction could also be approached with a Bayesian framework which is also amenable to Bayesian priors on known or previously predicted `synthetic lethal` partners. Either of these approaches has the potential to improve upon the `synthetic lethal` predictions which have been demonstrated as possible and biologically relevant by `SLIPT`.

## 7.4 Conclusions

Synthetic lethal interactions are important for understanding gene function and development of highly specific targeted anti-cancer treatments. Synthetic lethality could expand the repertoire of applications for precision cancer medicine to indirectly targeting loss of function in [tumour suppressor](#) genes. Synthetic lethal discovery with experimental screening is error prone and limited by the model systems in which it is performed. There is a need for [bioinformatics](#) tool to predict synthetic lethal interactions from [gene expression](#) data facilitates rapid identification of synthetic lethal candidates to augment functional genetic screens and cancer drug target triage. I present the original [Synthetic Lethal Interaction Prediction Tool \(SLIPT\)](#) methodology as a statically robust procedure which performs this analysis.

The [SLIPT](#) methodology has been demonstrated to identify biologically relevant genes and pathways. An comprehensive analysis of synthetic lethal partners of the *CDH1* was performed in [TCGA](#) breast cancer data ([Koboldt et al., 2012](#)) with many of these findings replicated in stomach cancer data ([Bass et al., 2014](#)). These genes clustered into several distinct groups, with distinct biological functions and elevated [expression](#) in different clinical subtypes. These analyses identified of synthetic lethal candidates in the *G<sub>αi</sub>* signalling, cytoplasmic microfibres, and extracellular fibrin clotting pathways which were validated in an [siRNA](#) screen performed by [Telford et al. \(2015\)](#) and consistent with the known cytoskeletal and cell signalling roles of [E-cadherin](#). These findings support interventions against these pathways being applicable to specific cancer therapeutics beyond the pre-clinical cell line models in which they were validated. [SLIPT](#) has also identified synthetic lethal partners in novel pathways for *CDH1* including the regulation of immune signalling and translational elongation which extend the range of pleiotropic functions of *CDH1* and present further biological mechanisms to investigate the malignancy and vulnerabilities of *CDH1*-deficient cancers.

While some of these pathways are not expected to be detected in an isolated experimental cell line model, [pathway](#) structure may have accounted for this disparity. Thus synthetic lethal candidates detected by [SLIPT](#) and [siRNA](#) were compared within graph structures of the candidate synthetic lethal pathways. However, this did not generally account for differences between detection by these approaches. Neither synthetic lethal detection methodology preferentially detected genes of more importance or connectivity in [pathway](#) structures using established network metrics. Nor could it

be generally established that **SLIPT** gene candidates were upstream or downstream of **siRNA** gene candidates in **pathway** structures across biological pathways.

Pathway **graph** structures were also included in investigations with simulated data to ascertain whether the **SLIPT** procedure performed desirably in data with complex correlation structures derived based on biological pathways. A simulation procedure was developed based on a statistical model of **synthetic lethality** which generates multivariate normal data with known **synthetic lethal** partners and correlation structures. The **SLIPT** methodology had high statistical performance, particularly when detecting few **synthetic lethal** genes, with large sample sizes, and a background of many non **synthetic lethal** genes to distinguish true partners from. This method had high specificity, performed better than Pearson correlation or the  $\chi^2$ -test, and had optimal performance across simulation parameter combinations for the thresholds used throughout this thesis. These findings were robust across correlation structures, including those derived from complex **pathway** structures containing strong positive and negative correlations between genes. Together, these findings support the release of the **SLIPT** software R packages and the application of the method to identify **synthetic lethal** genes within pathways and use candidate **synthetic lethal** genes to identify **synthetic lethal** pathways as demonstrated in this thesis.

Therefore, I present a widely applicable **synthetic lethal** procedure using **gene expression** data for wider use in **genomics** research, including the development of precision cancer medicine. This methodology is supported by the release of a software package in R, simulation results based on a statistical model of **synthetic lethality**, the demonstration of **bioinformatics** and network biology investigations into interactions with the *CDH1* gene in breast and stomach cancers.

# Bibliography

- Abeshouse, A., Ahn, J., Akbani, R., Ally, A., Amin, S., Andry, C.D., Annala, M., Aprikian, A., Armenia, J., Arora, A., *et al.* (2015) The Molecular Taxonomy of Primary Prostate Cancer. *Cell*, **163**(4): 1011–1025.
- Adler, D. (2005) *vioplot: Violin plot*. R package version 0.2.
- Akbani, R., Akdemir, K.C., Aksoy, B.A., Albert, M., Ally, A., Amin, S.B., Arachchi, H., Arora, A., Auman, J.T., Ayala, B., *et al.* (2015) Genomic Classification of Cutaneous Melanoma. *Cell*, **161**(7): 1681–1696.
- Akobeng, A.K. (2007) Understanding diagnostic tests 3: receiver operating characteristic curves. *Acta Paediatrica*, **96**(5): 644–647.
- American Cancer Society (2017) Genetics and cancer. <https://www.cancer.org/cancer/cancer-causes/genetics.html>. Accessed: 22/03/2017.
- Anjomshoaa, A., Lin, Y.H., Black, M.A., McCall, J.L., Humar, B., Song, S., Fukuzawa, R., Yoon, H.S., Holzmann, B., Friederichs, J., *et al.* (2008) Reduced expression of a gene proliferation signature is associated with enhanced malignancy in colon cancer. *Br J Cancer*, **99**(6): 966–973.
- Araki, H., Knapp, C., Tsai, P., and Print, C. (2012) GeneSetDB: A comprehensive meta-database, statistical and visualisation framework for gene set analysis. *FEBS Open Bio*, **2**: 76–82.
- Ashburner, M., Ball, C.A., Blake, J.A., Botstein, D., Butler, H., Cherry, J.M., Davis, A.P., Dolinski, K., Dwight, S.S., Eppig, J.T., *et al.* (2000) Gene ontology: tool for the unification of biology. The Gene Ontology Consortium. *Nat Genet*, **25**(1): 25–29.
- Ashworth, A. (2008) A synthetic lethal therapeutic approach: poly(adp) ribose polymerase inhibitors for the treatment of cancers deficient in dna double-strand break repair. *J Clin Oncol*, **26**(22): 3785–90.

- Ashworth, A., Lord, C.J., and Reis-Filho, J.S. (2011) Genetic interactions in cancer progression and treatment. *Cell*, **145**(1): 30–38.
- Audeh, M.W., Carmichael, J., Penson, R.T., Friedlander, M., Powell, B., Bell-McGuinn, K.M., Scott, C., Weitzel, J.N., Oaknin, A., Loman, N., *et al.* (2010) Oral poly(adp-ribose) polymerase inhibitor olaparib in patients with *BRCA1* or *BRCA2* mutations and recurrent ovarian cancer: a proof-of-concept trial. *Lancet*, **376**(9737): 245–51.
- Babyak, M.A. (2004) What you see may not be what you get: a brief, nontechnical introduction to overfitting in regression-type models. *Psychosom Med*, **66**(3): 411–21.
- Bamford, S., Dawson, E., Forbes, S., Clements, J., Pettett, R., Dogan, A., Flanagan, A., Teague, J., Futreal, P.A., Stratton, M.R., *et al.* (2004) The COSMIC (Catalogue of Somatic Mutations in Cancer) database and website. *Br J Cancer*, **91**(2): 355–358.
- Barabási, A.L. and Albert, R. (1999) Emergence of scaling in random networks. *Science*, **286**(5439): 509–12.
- Barabási, A.L., Gulbahce, N., and Loscalzo, J. (2011) Network medicine: a network-based approach to human disease. *Nat Rev Genet*, **12**(1): 56–68.
- Barabási, A.L. and Oltvai, Z.N. (2004) Network biology: understanding the cell's functional organization. *Nat Rev Genet*, **5**(2): 101–13.
- Barrat, A. and Weigt, M. (2000) On the properties of small-world network models. *The European Physical Journal B - Condensed Matter and Complex Systems*, **13**(3): 547–560.
- Barretina, J., Caponigro, G., Stransky, N., Venkatesan, K., Margolin, A.A., Kim, S., Wilson, C.J., Lehar, J., Kryukov, G.V., Sonkin, D., *et al.* (2012) The Cancer Cell Line Encyclopedia enables predictive modelling of anticancer drug sensitivity. *Nature*, **483**(7391): 603–607.
- Barry, W.T. (2016) *safe: Significance Analysis of Function and Expression*. R package version 3.14.0.

- Baryshnikova, A., Costanzo, M., Dixon, S., Vizeacoumar, F.J., Myers, C.L., Andrews, B., and Boone, C. (2010a) Synthetic genetic array (sga) analysis in *saccharomyces cerevisiae* and *schizosaccharomyces pombe*. *Methods Enzymol*, **470**: 145–79.
- Baryshnikova, A., Costanzo, M., Kim, Y., Ding, H., Koh, J., Toufighi, K., Youn, J.Y., Ou, J., San Luis, B.J., Bandyopadhyay, S., *et al.* (2010b) Quantitative analysis of fitness and genetic interactions in yeast on a genome scale. *Nat Meth*, **7**(12): 1017–1024.
- Bass, A.J., Thorsson, V., Shmulevich, I., Reynolds, S.M., Miller, M., Bernard, B., Hinoue, T., Laird, P.W., Curtis, C., Shen, H., *et al.* (2014) Comprehensive molecular characterization of gastric adenocarcinoma. *Nature*, **513**(7517): 202–209.
- Bates, D. and Maechler, M. (2016) *Matrix: Sparse and Dense Matrix Classes and Methods*. R package version 1.2-7.1.
- Bateson, W. and Mendel, G. (1909) *Mendel's principles of heredity, by W. Bateson*. University Press, Cambridge [Eng.].
- Becker, K.F., Atkinson, M.J., Reich, U., Becker, I., Nekarda, H., Siewert, J.R., and Höfler, H. (1994) E-cadherin gene mutations provide clues to diffuse type gastric carcinomas. *Cancer Research*, **54**(14): 3845–3852.
- Bell, D., Berchuck, A., Birrer, M., Chien, J., Cramer, D., Dao, F., Dhir, R., DiSaia, P., Gabra, H., Glenn, P., *et al.* (2011) Integrated genomic analyses of ovarian carcinoma. *Nature*, **474**(7353): 609–615.
- Benjamini, Y. and Hochberg, Y. (1995) Controlling the false discovery rate: A practical and powerful approach to multiple testing. *Journal of the Royal Statistical Society Series B (Methodological)*, **57**(1): 289–300.
- Berx, G., Cleton-Jansen, A.M., Nollet, F., de Leeuw, W.J., van de Vijver, M., Cornelisse, C., and van Roy, F. (1995) E-cadherin is a tumour/invasion suppressor gene mutated in human lobular breast cancers. *EMBO J*, **14**(24): 6107–15.
- Berx, G., Cleton-Jansen, A.M., Strumane, K., de Leeuw, W.J., Nollet, F., van Roy, F., and Cornelisse, C. (1996) E-cadherin is inactivated in a majority of invasive human lobular breast cancers by truncation mutations throughout its extracellular domain. *Oncogene*, **13**(9): 1919–25.

- Berx, G. and van Roy, F. (2009) Involvement of members of the cadherin superfamily in cancer. *Cold Spring Harb Perspect Biol*, **1**: a003129.
- Bitler, B.G., Aird, K.M., Garipov, A., Li, H., Amatangelo, M., Kossenkov, A.V., Schultz, D.C., Liu, Q., Shih Ie, M., Conejo-Garcia, J.R., *et al.* (2015) Synthetic lethality by targeting ezh2 methyltransferase activity in arid1a-mutated cancers. *Nat Med*, **21**(3): 231–8.
- Blake, J.A., Christie, K.R., Dolan, M.E., Drabkin, H.J., Hill, D.P., Ni, L., Sitnikov, D., Burgess, S., Buza, T., Gresham, C., *et al.* (2015) Gene Ontology Consortium: going forward. *Nucleic Acids Res*, **43**(Database issue): D1049–1056.
- Boone, C., Bussey, H., and Andrews, B.J. (2007) Exploring genetic interactions and networks with yeast. *Nat Rev Genet*, **8**(6): 437–49.
- Borgatti, S.P. (2005) Centrality and network flow. *Social Networks*, **27**(1): 55 – 71.
- Boucher, B. and Jenna, S. (2013) Genetic interaction networks: better understand to better predict. *Front Genet*, **4**: 290.
- Bozovic-Spasojevic, I., Azambuja, E., McCaskill-Stevens, W., Dinh, P., and Cardoso, F. (2012) Chemoprevention for breast cancer. *Cancer treatment reviews*, **38**(5): 329–339.
- Breiman, L. (2001) Random forests. *Machine Learning*, **45**(1): 5–32.
- Brin, S. and Page, L. (1998) The anatomy of a large-scale hypertextual web search engine. *Computer Networks and ISDN Systems*, **30**(1): 107 – 117.
- Brouxhon, S.M., Kyrkanides, S., Teng, X., Athar, M., Ghazizadeh, S., Simon, M., O'Banion, M.K., and Ma, L. (2014) Soluble E-cadherin: a critical oncogene modulating receptor tyrosine kinases, MAPK and PI3K/Akt/mTOR signaling. *Oncogene*, **33**(2): 225–235.
- Brückner, A., Polge, C., Lentze, N., Auerbach, D., and Schlattner, U. (2009) Yeast two-hybrid, a powerful tool for systems biology. *Int J Mol Sci*, **10**(6): 2763–2788.
- Bryant, H.E., Schultz, N., Thomas, H.D., Parker, K.M., Flower, D., Lopez, E., Kyle, S., Meuth, M., Curtin, N.J., and Helleday, T. (2005) Specific killing of *BRCA2*-deficient tumours with inhibitors of polyadprbose polymerase. *Nature*, **434**(7035): 913–7.

- Bussey, H., Andrews, B., and Boone, C. (2006) From worm genetic networks to complex human diseases. *Nat Genet*, **38**(8): 862–3.
- Butland, G., Babu, M., Diaz-Mejia, J.J., Bohdana, F., Phanse, S., Gold, B., Yang, W., Li, J., Gagarinova, A.G., Pogoutse, O., et al. (2008) esga: E. coli synthetic genetic array analysis. *Nat Methods*, **5**(9): 789–95.
- cBioPortal for Cancer Genomics (cBioPortal) (2017) cBioPortal for Cancer Genomics. <http://www.cbioportal.org/>. Accessed: 26/03/2017.
- Cerami, E.G., Gross, B.E., Demir, E., Rodchenkov, I., Babur, O., Anwar, N., Schultz, N., Bader, G.D., and Sander, C. (2011) Pathway Commons, a web resource for biological pathway data. *Nucleic Acids Res*, **39**(Database issue): D685–690.
- Chen, A., Beetham, H., Black, M.A., Priya, R., Telford, B.J., Guest, J., Wiggins, G.A.R., Godwin, T.D., Yap, A.S., and Guilford, P.J. (2014) E-cadherin loss alters cytoskeletal organization and adhesion in non-malignant breast cells but is insufficient to induce an epithelial-mesenchymal transition. *BMC Cancer*, **14**(1): 552.
- Chen, S. and Parmigiani, G. (2007) Meta-analysis of BRCA1 and BRCA2 penetrance. *J Clin Oncol*, **25**(11): 1329–1333.
- Chipman, K. and Singh, A. (2009) Predicting genetic interactions with random walks on biological networks. *BMC Bioinformatics*, **10**(1): 17.
- Christofori, G. and Semb, H. (1999) The role of the cell-adhesion molecule E-cadherin as a tumour-suppressor gene. *Trends in Biochemical Sciences*, **24**(2): 73 – 76.
- Ciriello, G., Gatza, M.L., Beck, A.H., Wilkerson, M.D., Rhie, S.K., Pastore, A., Zhang, H., McLellan, M., Yau, C., Kandoth, C., et al. (2015) Comprehensive Molecular Portraits of Invasive Lobular Breast Cancer. *Cell*, **163**(2): 506–519.
- Clark, M.J. (2004) Endogenous Regulator of G Protein Signaling Proteins Suppress G<sub>o</sub>-Dependent  $\mu$ -Opioid Agonist-Mediated Adenylyl Cyclase Supersensitization. *Journal of Pharmacology and Experimental Therapeutics*, **310**(1): 215–222.
- Collingridge, D.S. (2013) A primer on quantitized data analysis and permutation testing. *Journal of Mixed Methods Research*, **7**(1): 81–97.

- Collins, F.S. and Barker, A.D. (2007) Mapping the cancer genome. Pinpointing the genes involved in cancer will help chart a new course across the complex landscape of human malignancies. *Sci Am*, **296**(3): 50–57.
- Collisson, E., Campbell, J., Brooks, A., Berger, A., Lee, W., Chmielecki, J., Beer, D., Cope, L., Creighton, C., Danilova, L., *et al.* (2014) Comprehensive molecular profiling of lung adenocarcinoma. *Nature*, **511**(7511): 543–550.
- Costanzo, M., Baryshnikova, A., Bellay, J., Kim, Y., Spear, E.D., Sevier, C.S., Ding, H., Koh, J.L., Toufighi, K., Mostafavi, S., *et al.* (2010) The genetic landscape of a cell. *Science*, **327**(5964): 425–31.
- Costanzo, M., Baryshnikova, A., Myers, C.L., Andrews, B., and Boone, C. (2011) Charting the genetic interaction map of a cell. *Curr Opin Biotechnol*, **22**(1): 66–74.
- Courtney, K.D., Corcoran, R.B., and Engelman, J.A. (2010) The PI3K pathway as drug target in human cancer. *J Clin Oncol*, **28**(6): 1075–1083.
- Creighton, C.J., Morgan, M., Gunaratne, P.H., Wheeler, D.A., Gibbs, R.A., Robertson, A., Chu, A., Beroukhim, R., Cibulskis, K., Signoretti, S., *et al.* (2013) Comprehensive molecular characterization of clear cell renal cell carcinoma. *Nature*, **499**(7456): 43–49.
- Croft, D., Mundo, A.F., Haw, R., Milacic, M., Weiser, J., Wu, G., Caudy, M., Garapati, P., Gillespie, M., Kamdar, M.R., *et al.* (2014) The Reactome pathway knowledge-base. *Nucleic Acids Res*, **42**(database issue): D472–D477.
- Crunkhorn, S. (2014) Cancer: Predicting synthetic lethal interactions. *Nat Rev Drug Discov*, **13**(11): 812.
- Csardi, G. and Nepusz, T. (2006) The igraph software package for complex network research. *InterJournal, Complex Systems*: 1695.
- Dai, X., Li, T., Bai, Z., Yang, Y., Liu, X., Zhan, J., and Shi, B. (2015) Breast cancer intrinsic subtype classification, clinical use and future trends. *Am J Cancer Res*, **5**(10): 2929–2943.
- Davierwala, A.P., Haynes, J., Li, Z., Brost, R.L., Robinson, M.D., Yu, L., Mnaimneh, S., Ding, H., Zhu, H., Chen, Y., *et al.* (2005) The synthetic genetic interaction spectrum of essential genes. *Nat Genet*, **37**(10): 1147–1152.

- De Leeuw, W.J., Berx, G., Vos, C.B., Peterse, J.L., Van de Vijver, M.J., Litvinov, S., Van Roy, F., Cornelisse, C.J., and Cleton-Jansen, A.M. (1997) Simultaneous loss of E-cadherin and catenins in invasive lobular breast cancer and lobular carcinoma in situ. *J Pathol*, **183**(4): 404–11.
- De Santis, G., Miotti, S., Mazzi, M., Canevari, S., and Tomassetti, A. (2009) E-cadherin directly contributes to PI3K/AKT activation by engaging the PI3K-p85 regulatory subunit to adherens junctions of ovarian carcinoma cells. *Oncogene*, **28**(9): 1206–1217.
- Demir, E., Babur, O., Rodchenkov, I., Aksoy, B.A., Fukuda, K.I., Gross, B., Sumer, O.S., Bader, G.D., and Sander, C. (2013) Using biological pathway data with Paxtools. *PLoS Comput Biol*, **9**(9): e1003194.
- Deshpande, R., Asiedu, M.K., Klebig, M., Sutor, S., Kuzmin, E., Nelson, J., Piotrowski, J., Shin, S.H., Yoshida, M., Costanzo, M., *et al.* (2013) A comparative genomic approach for identifying synthetic lethal interactions in human cancer. *Cancer Res*, **73**(20): 6128–36.
- Dickson, D. (1999) Wellcome funds cancer database. *Nature*, **401**(6755): 729.
- Dijkstra, E.W. (1959) A note on two problems in connexion with graphs. *Numerische Mathematik*, **1**(1): 269–271.
- Dixon, S.J., Andrews, B.J., and Boone, C. (2009) Exploring the conservation of synthetic lethal genetic interaction networks. *Commun Integr Biol*, **2**(2): 78–81.
- Dixon, S.J., Fedyshyn, Y., Koh, J.L., Prasad, T.S., Chahwan, C., Chua, G., Toufighi, K., Baryshnikova, A., Hayles, J., Hoe, K.L., *et al.* (2008) Significant conservation of synthetic lethal genetic interaction networks between distantly related eukaryotes. *Proc Natl Acad Sci U S A*, **105**(43): 16653–8.
- Dong, L.L., Liu, L., Ma, C.H., Li, J.S., Du, C., Xu, S., Han, L.H., Li, L., and Wang, X.W. (2012) E-cadherin promotes proliferation of human ovarian cancer cells in vitro via activating MEK/ERK pathway. *Acta Pharmacol Sin*, **33**(6): 817–822.
- Dorsam, R.T. and Gutkind, J.S. (2007) G-protein-coupled receptors and cancer. *Nat Rev Cancer*, **7**(2): 79–94.
- Erdős, P. and Rényi, A. (1959) On random graphs I. *Publ Math Debrecen*, **6**: 290–297.

- Erdős, P. and Rényi, A. (1960) On the evolution of random graphs. In *Publ. Math. Inst. Hung. Acad. Sci*, volume 5, 17–61.
- Eroles, P., Bosch, A., Perez-Fidalgo, J.A., and Lluch, A. (2012) Molecular biology in breast cancer: intrinsic subtypes and signaling pathways. *Cancer Treat Rev*, **38**(6): 698–707.
- Farmer, H., McCabe, N., Lord, C.J., Tutt, A.N., Johnson, D.A., Richardson, T.B., Santarosa, M., Dillon, K.J., Hickson, I., Knights, C., *et al.* (2005) Targeting the dna repair defect in BRCA mutant cells as a therapeutic strategy. *Nature*, **434**(7035): 917–21.
- Fawcett, T. (2006) An introduction to ROC analysis. *Pattern Recognition Letters*, **27**(8): 861 – 874. {ROC} Analysis in Pattern Recognition.
- Fece de la Cruz, F., Gapp, B.V., and Nijman, S.M. (2015) Synthetic lethal vulnerabilities of cancer. *Annu Rev Pharmacol Toxicol*, **55**: 513–531.
- Ferlay, J., Soerjomataram, I., Dikshit, R., Eser, S., Mathers, C., Rebelo, M., Parkin, D.M., Forman, D., and Bray, F. (2015) Cancer incidence and mortality worldwide: sources, methods and major patterns in GLOBOCAN 2012. *Int J Cancer*, **136**(5): E359–386.
- Fisher, R.A. (1919) Xv.—the correlation between relatives on the supposition of mendelian inheritance. *Earth and Environmental Science Transactions of the Royal Society of Edinburgh*, **52**(02): 399–433.
- Fong, P.C., Boss, D.S., Yap, T.A., Tutt, A., Wu, P., Mergui-Roelvink, M., Mortimer, P., Swaisland, H., Lau, A., O'Connor, M.J., *et al.* (2009) Inhibition of poly(adp-ribose) polymerase in tumors from BRCA mutation carriers. *N Engl J Med*, **361**(2): 123–34.
- Fong, P.C., Yap, T.A., Boss, D.S., Carden, C.P., Mergui-Roelvink, M., Gourley, C., De Greve, J., Lubinski, J., Shanley, S., Messiou, C., *et al.* (2010) Poly(adp)-ribose polymerase inhibition: frequent durable responses in BRCA carrier ovarian cancer correlating with platinum-free interval. *J Clin Oncol*, **28**(15): 2512–9.
- Forbes, S.A., Beare, D., Gunasekaran, P., Leung, K., Bindal, N., Boutselakis, H., Ding, M., Bamford, S., Cole, C., Ward, S., *et al.* (2015) COSMIC: exploring the world's

knowledge of somatic mutations in human cancer. *Nucleic Acids Res*, **43**(Database issue): D805–811.

Fraser, A. (2004) Towards full employment: using RNAi to find roles for the redundant. *Oncogene*, **23**(51): 8346–52.

Fromental-Romain, C., Warot, X., Lakkaraju, S., Favier, B., Haack, H., Birling, C., Dierich, A., Doll e, P., and Chambon, P. (1996) Specific and redundant functions of the paralogous Hoxa-9 and Hoxd-9 genes in forelimb and axial skeleton patterning. *Development*, **122**(2): 461–472.

Futreal, P.A., Coin, L., Marshall, M., Down, T., Hubbard, T., Wooster, R., Rahman, N., and Stratton, M.R. (2004) A census of human cancer genes. *Nat Rev Cancer*, **4**(3): 177–183.

Futreal, P.A., Kasprzyk, A., Birney, E., Mullikin, J.C., Wooster, R., and Stratton, M.R. (2001) Cancer and genomics. *Nature*, **409**(6822): 850–852.

Gao, B. and Roux, P.P. (2015) Translational control by oncogenic signaling pathways. *Biochimica et Biophysica Acta*, **1849**(7): 753–65.

Gatza, M.L., Kung, H.N., Blackwell, K.L., Dewhirst, M.W., Marks, J.R., and Chi, J.T. (2011) Analysis of tumor environmental response and oncogenic pathway activation identifies distinct basal and luminal features in HER2-related breast tumor subtypes. *Breast Cancer Res*, **13**(3): R62.

Gatza, M.L., Lucas, J.E., Barry, W.T., Kim, J.W., Wang, Q., Crawford, M.D., Datto, M.B., Kelley, M., Mathey-Prevot, B., Potti, A., *et al.* (2010) A pathway-based classification of human breast cancer. *Proc Natl Acad Sci USA*, **107**(15): 6994–6999.

Gatza, M.L., Silva, G.O., Parker, J.S., Fan, C., and Perou, C.M. (2014) An integrated genomics approach identifies drivers of proliferation in luminal-subtype human breast cancer. *Nat Genet*, **46**(10): 1051–1059.

Gentleman, R.C., Carey, V.J., Bates, D.M., Bolstad, B., Dettling, M., Dudoit, S., Ellis, B., Gautier, L., Ge, Y., Gentry, J., *et al.* (2004) Bioconductor: open software development for computational biology and bioinformatics. *Genome Biol*, **5**(10): R80.

Genz, A. and Bretz, F. (2009) Computation of multivariate normal and t probabilities. In *Lecture Notes in Statistics*, volume 195. Springer-Verlag, Heidelberg.

- Genz, A., Bretz, F., Miwa, T., Mi, X., Leisch, F., Scheipl, F., and Hothorn, T. (2016) *mvtnorm: Multivariate Normal and t Distributions*. R package version 1.0-5. URL.
- Glaire, M.A., Brown, M., Church, D.N., and Tomlinson, I. (2017) Cancer predisposition syndromes: lessons for truly precision medicine. *J Pathol*, **241**(2): 226–235.
- Globus (Globus) (2017) Research data management simplified. <https://www.globus.org/>. Accessed: 25/03/2017.
- Goodwin, S., McPherson, J.D., and McCombie, W.R. (2016) Coming of age: ten years of next-generation sequencing technologies. *Nat Rev Genet*, **17**(6): 333–351.
- Grady, W.M., Willis, J., Guilford, P.J., Dunbier, A.K., Toro, T.T., Lynch, H., Wiesner, G., Ferguson, K., Eng, C., Park, J.G., *et al.* (2000) Methylation of the CDH1 promoter as the second genetic hit in hereditary diffuse gastric cancer. *Nat Genet*, **26**(1): 16–17.
- Graziano, F., Humar, B., and Guilford, P. (2003) The role of the E-cadherin gene (*CDH1*) in diffuse gastric cancer susceptibility: from the laboratory to clinical practice. *Annals of Oncology*, **14**(12): 1705–1713.
- Guaragnella, N., Palermo, V., Galli, A., Moro, L., Mazzoni, C., and Giannattasio, S. (2014) The expanding role of yeast in cancer research and diagnosis: insights into the function of the oncosuppressors p53 and BRCA1/2. *FEMS Yeast Res*, **14**(1): 2–16.
- Güell, O., Sagués, F., and Serrano, M. (2014) Essential plasticity and redundancy of metabolism unveiled by synthetic lethality analysis. *PLoS Comput Biol*, **10**(5): e1003637.
- Guilford, P. (1999) E-cadherin downregulation in cancer: fuel on the fire? *Molecular Medicine Today*, **5**(4): 172 – 177.
- Guilford, P., Hopkins, J., Harraway, J., McLeod, M., McLeod, N., Harawira, P., Taite, H., Scouler, R., Miller, A., and Reeve, A.E. (1998) E-cadherin germline mutations in familial gastric cancer. *Nature*, **392**(6674): 402–5.
- Guilford, P., Humar, B., and Blair, V. (2010) Hereditary diffuse gastric cancer: translation of *CDH1* germline mutations into clinical practice. *Gastric Cancer*, **13**(1): 1–10.

- Guilford, P.J., Hopkins, J.B., Grady, W.M., Markowitz, S.D., Willis, J., Lynch, H., Rajput, A., Wiesner, G.L., Lindor, N.M., Burgart, L.J., *et al.* (1999) E-cadherin germline mutations define an inherited cancer syndrome dominated by diffuse gastric cancer. *Hum Mutat*, **14**(3): 249–55.
- Guo, J., Liu, H., and Zheng, J. (2016) SynLethDB: synthetic lethality database toward discovery of selective and sensitive anticancer drug targets. *Nucleic Acids Res*, **44**(D1): D1011–1017.
- Hajian-Tilaki, K. (2013) Receiver Operating Characteristic (ROC) Curve Analysis for Medical Diagnostic Test Evaluation. *Caspian J Intern Med*, **4**(2): 627–635.
- Hall, M., Frank, E., Holmes, G., Pfahringer, B., Reutemann, P., and Witten, I.H. (2009) The weka data mining software: an update. *SIGKDD Explor Newsl*, **11**(1): 10–18.
- Hamerman, P.S., Lawrence, M.S., Voet, D., Jing, R., Cibulskis, K., Sivachenko, A., Stojanov, P., McKenna, A., Lander, E.S., Gabriel, S., *et al.* (2012) Comprehensive genomic characterization of squamous cell lung cancers. *Nature*, **489**(7417): 519–525.
- Hanahan, D. and Weinberg, R.A. (2000) The hallmarks of cancer. *Cell*, **100**(1): 57–70.
- Hanahan, D. and Weinberg, R.A. (2011) Hallmarks of cancer: the next generation. *Cell*, **144**(5): 646–674.
- Hanna, S. (2003) Cancer incidence in new zealand (2003-2007). In D. Forman, D. Bray F Brewster, C. Gombe Mbalawa, B. Kohler, M. Piñeros, E. Steliarova-Foucher, R. Swaminathan, and J. Ferlay (editors), *Cancer Incidence in Five Continents*, volume X, 902–907. International Agency for Research on Cancer, Lyon, France. Electronic version <http://ci5.iarc.fr> Accessed 22/03/2017.
- Hansford, S., Kaurah, P., Li-Chang, H., Woo, M., Senz, J., Pinheiro, H., Schrader, K.A., Schaeffer, D.F., Shumansky, K., Zogopoulos, G., *et al.* (2015) Hereditary Diffuse Gastric Cancer Syndrome: CDH1 Mutations and Beyond. *JAMA Oncol*, **1**(1): 23–32.
- Heiskanen, M.A. and Aittokallio, T. (2012) Mining high-throughput screens for cancer drug targets-lessons from yeast chemical-genomic profiling and synthetic lethality.

*Wiley Interdisciplinary Reviews: Data Mining and Knowledge Discovery*, **2**(3): 263–272.

- Hell, P. (1976) Graphs with given neighbourhoods i. problèmes combinatoires at théorie des graphes. *Proc Coll Int CNRS, Orsay*, **260**: 219–223.
- Higgins, M.E., Claremont, M., Major, J.E., Sander, C., and Lash, A.E. (2007) CancerGenes: a gene selection resource for cancer genome projects. *Nucleic Acids Res*, **35**(Database issue): D721–726.
- Hillenmeyer, M.E. (2008) The chemical genomic portrait of yeast: uncovering a phenotype for all genes. *Science*, **320**: 362–365.
- Hoadley, K.A., Yau, C., Wolf, D.M., Cherniack, A.D., Tamborero, D., Ng, S., Leiserson, M.D., Niu, B., McLellan, M.D., Uzunangelov, V., et al. (2014) Multiplatform analysis of 12 cancer types reveals molecular classification within and across tissues of origin. *Cell*, **158**(4): 929–944.
- Hoehndorf, R., Hardy, N.W., Osumi-Sutherland, D., Tweedie, S., Schofield, P.N., and Gkoutos, G.V. (2013) Systematic analysis of experimental phenotype data reveals gene functions. *PLoS ONE*, **8**(4): e60847.
- Holm, S. (1979) A simple sequentially rejective multiple test procedure. *Scandinavian Journal of Statistics*, **6**(2): 65–70.
- Hopkins, A.L. (2008) Network pharmacology: the next paradigm in drug discovery. *Nat Chem Biol*, **4**(11): 682–690.
- Hu, Z., Fan, C., Oh, D.S., Marron, J.S., He, X., Qaqish, B.F., Livasy, C., Carey, L.A., Reynolds, E., Dressler, L., et al. (2006) The molecular portraits of breast tumors are conserved across microarray platforms. *BMC Genomics*, **7**: 96.
- Huang, E., Cheng, S., Dressman, H., Pittman, J., Tsou, M., Horng, C., Bild, A., Iversen, E., Liao, M., Chen, C., et al. (2003) Gene expression predictors of breast cancer outcomes. *Lancet*, **361**: 1590–1596.
- Hutchison, C.A., Chuang, R.Y., Noskov, V.N., Assad-Garcia, N., Deerinck, T.J., Elliston, M.H., Gill, J., Kannan, K., Karas, B.J., Ma, L., et al. (2016) Design and synthesis of a minimal bacterial genome. *Science*, **351**(6280): aad6253.

- International HapMap 3 Consortium (HapMap) (2003) The International HapMap Project. *Nature*, **426**(6968): 789–796.
- Jeanes, A., Gottardi, C.J., and Yap, A.S. (2008) Cadherins and cancer: how does cadherin dysfunction promote tumor progression? *Oncogene*, **27**(55): 6920–6929.
- Jerby-Arnon, L., Pfetzer, N., Waldman, Y., McGarry, L., James, D., Shanks, E., Seashore-Ludlow, B., Weinstock, A., Geiger, T., Clemons, P., *et al.* (2014) Predicting cancer-specific vulnerability via data-driven detection of synthetic lethality. *Cell*, **158**(5): 1199–1209.
- Joachims, T. (1999) Making large-scale support vector machine learning practical. In S. Bernhard, lkopf, J.C.B. Christopher, and J.S. Alexander (editors), *Advances in kernel methods*, 169–184. MIT Press.
- Ju, Z., Liu, W., Roebuck, P.L., Siwak, D.R., Zhang, N., Lu, Y., Davies, M.A., Akbani, R., Weinstein, J.N., Mills, G.B., *et al.* (2015) Development of a robust classifier for quality control of reverse-phase protein arrays. *Bioinformatics*, **31**(6): 912.
- Kaelin, Jr, W. (2005) The concept of synthetic lethality in the context of anticancer therapy. *Nat Rev Cancer*, **5**(9): 689–98.
- Kaelin, Jr, W. (2009) Synthetic lethality: a framework for the development of wiser cancer therapeutics. *Genome Med*, **1**: 99.
- Kamada, T. and Kawai, S. (1989) An algorithm for drawing general undirected graphs. *Information Processing Letters*, **31**(1): 7–15.
- Kawai, J., Shinagawa, A., Shibata, K., Yoshino, M., Itoh, M., Ishii, Y., Arakawa, T., Hara, A., Fukunishi, Y., Konno, H., *et al.* (2001) Functional annotation of a full-length mouse cDNA collection. *Nature*, **409**(6821): 685–690.
- Kelley, R. and Ideker, T. (2005) Systematic interpretation of genetic interactions using protein networks. *Nat Biotech*, **23**(5): 561–566.
- Kelly, S.T. (2013) *Statistical Predictions of Synthetic Lethal Interactions in Cancer*. Dissertation, University of Otago.
- Kelly, S.T., Single, A.B., Telford, B.J., Beetham, H.G., Godwin, T.D., Chen, A., Black, M.A., and Guilford, P.J. (unpublished) Towards HDGC chemoprevention:

vulnerabilities in E-cadherin-negative cells identified by genome-wide interrogation of isogenic cell lines and whole tumors. Submitted to *Cancer Prev Res.*

Keshava Prasad, T.S., Goel, R., Kandasamy, K., Keerthikumar, S., Kumar, S., Mathivanan, S., Telikicherla, D., Raju, R., Shafran, B., Venugopal, A., *et al.* (2009) Human Protein Reference Database—2009 update. *Nucleic Acids Res*, **37**(Database issue): D767–772.

Kim, N.G., Koh, E., Chen, X., and Gumbiner, B.M. (2011) E-cadherin mediates contact inhibition of proliferation through Hippo signaling-pathway components. *Proc Natl Acad Sci USA*, **108**(29): 11930–11935.

Koboldt, D.C., Fulton, R.S., McLellan, M.D., Schmidt, H., Kalicki-Veizer, J., McMichael, J.F., Fulton, L.L., Dooling, D.J., Ding, L., Mardis, E.R., *et al.* (2012) Comprehensive molecular portraits of human breast tumours. *Nature*, **490**(7418): 61–70.

Kockel, L., Zeitlinger, J., Staszewski, L.M., Mlodzik, M., and Bohmann, D. (1997) Jun in drosophila development: redundant and nonredundant functions and regulation by two mapk signal transduction pathways. *Genes & Development*, **11**(13): 1748–1758.

Kozlov, K.N., Gursky, V.V., Kulakovskiy, I.V., and Samsonova, M.G. (2015) Sequence-based model of gap gene regulation network. *BMC Genomics*, **15**(Suppl 12): S6.

Kranthi, S., Rao, S., and Manimaran, P. (2013) Identification of synthetic lethal pairs in biological systems through network information centrality. *Mol BioSyst*, **9**(8): 2163–2167.

Kroepil, F., Fluegen, G., Totikov, Z., Baldus, S.E., Vay, C., Schauer, M., Topp, S.A., Esch, J.S., Knoefel, W.T., and Stoecklein, N.H. (2012) Down-regulation of CDH1 is associated with expression of SNAI1 in colorectal adenomas. *PLoS ONE*, **7**(9): e46665.

Lander, E.S. (2011) Initial impact of the sequencing of the human genome. *Nature*, **470**(7333): 187–197.

Lander, E.S., Linton, L.M., Birren, B., Nusbaum, C., Zody, M.C., Baldwin, J., Devon, K., Dewar, K., Doyle, M., FitzHugh, W., *et al.* (2001) Initial sequencing and analysis of the human genome. *Nature*, **409**(6822): 860–921.

- Langmead, B., Trapnell, C., Pop, M., and Salzberg, S.L. (2009) Ultrafast and memory-efficient alignment of short DNA sequences to the human genome. *Genome Biol*, **10**(3): R25.
- Latora, V. and Marchiori, M. (2001) Efficient behavior of small-world networks. *Phys Rev Lett*, **87**: 198701.
- Laufer, C., Fischer, B., Billmann, M., Huber, W., and Boutros, M. (2013) Mapping genetic interactions in human cancer cells with RNAi and multiparametric phenotyping. *Nat Methods*, **10**(5): 427–31.
- Law, C.W., Chen, Y., Shi, W., and Smyth, G.K. (2014) voom: precision weights unlock linear model analysis tools for RNA-seq read counts. *Genome Biol*, **15**(2): R29.
- Le Meur, N. and Gentleman, R. (2008) Modeling synthetic lethality. *Genome Biol*, **9**(9): R135.
- Le Meur, N., Jiang, Z., Liu, T., Mar, J., and Gentleman, R.C. (2014) Slgi: Synthetic lethal genetic interaction. r package version 1.26.0.
- Lee, A.Y., Perreault, R., Harel, S., Boulier, E.L., Suderman, M., Hallett, M., and Jenna, S. (2010a) Searching for signaling balance through the identification of genetic interactors of the rab guanine-nucleotide dissociation inhibitor gdi-1. *PLoS ONE*, **5**(5): e10624.
- Lee, I., Lehner, B., Vavouri, T., Shin, J., Fraser, A.G., and Marcotte, E.M. (2010b) Predicting genetic modifier loci using functional gene networks. *Genome Research*, **20**(8): 1143–1153.
- Lee, I. and Marcotte, E.M. (2009) Effects of functional bias on supervised learning of a gene network model. *Methods Mol Biol*, **541**: 463–75.
- Lee, M.J., Ye, A.S., Gardino, A.K., Heijink, A.M., Sorger, P.K., MacBeath, G., and Yaffe, M.B. (2012) Sequential application of anticancer drugs enhances cell death by rewiring apoptotic signaling networks. *Cell*, **149**(4): 780–94.
- Lehner, B., Crombie, C., Tischler, J., Fortunato, A., and Fraser, A.G. (2006) Systematic mapping of genetic interactions in *caenorhabditis elegans* identifies common modifiers of diverse signaling pathways. *Nat Genet*, **38**(8): 896–903.

- Li, B., Ruotti, V., Stewart, R.M., Thomson, J.A., and Dewey, C.N. (2010) RNA-Seq gene expression estimation with read mapping uncertainty. *Bioinformatics*, **26**(4): 493–500.
- Li, X.J., Mishra, S.K., Wu, M., Zhang, F., and Zheng, J. (2014) Syn-lethality: An integrative knowledge base of synthetic lethality towards discovery of selective anticancer therapies. *Biomed Res Int*, **2014**: 196034.
- Linehan, W.M., Spellman, P.T., Ricketts, C.J., Creighton, C.J., Fei, S.S., Davis, C., Wheeler, D.A., Murray, B.A., Schmidt, L., Vocke, C.D., *et al.* (2016) Comprehensive Molecular Characterization of Papillary Renal-Cell Carcinoma. *N Engl J Med*, **374**(2): 135–145.
- Lokody, I. (2014) Computational modelling: A computational crystal ball. *Nature Reviews Cancer*, **14**(10): 649–649.
- Lord, C.J., Tutt, A.N., and Ashworth, A. (2015) Synthetic lethality and cancer therapy: lessons learned from the development of PARP inhibitors. *Annu Rev Med*, **66**: 455–470.
- Lu, X., Kensche, P.R., Huynen, M.A., and Notebaart, R.A. (2013) Genome evolution predicts genetic interactions in protein complexes and reveals cancer drug targets. *Nat Commun*, **4**: 2124.
- Lu, X., Megchelenbrink, W., Notebaart, R.A., and Huynen, M.A. (2015) Predicting human genetic interactions from cancer genome evolution. *PLoS One*, **10**(5): e0125795.
- Lum, P.Y., Armour, C.D., Stepaniants, S.B., Cavet, G., Wolf, M.K., Butler, J.S., Hinchshaw, J.C., Garnier, P., Prestwich, G.D., Leonardson, A., *et al.* (2004) Discovering modes of action for therapeutic compounds using a genome-wide screen of yeast heterozygotes. *Cell*, **116**(1): 121–137.
- Luo, J., Solimini, N.L., and Elledge, S.J. (2009) Principles of Cancer Therapy: Oncogene and Non-oncogene Addiction. *Cell*, **136**(5): 823–837.
- Machado, J., Olivera, C., Carvalh, R., Soares, P., Berx, G., Caldas, C., Sercuca, R., Carneiro, F., and Sorbrinho-Simoes, M. (2001) E-cadherin gene (*CDH1*) promoter methylation as the second hit in sporadic diffuse gastric carcinoma. *Oncogene*, **20**: 1525–1528.

- Markowetz, F. (2017) All biology is computational biology. *PLoS Biol*, **15**(3): e2002050.
- Masciari, S., Larsson, N., Senz, J., Boyd, N., Kaurah, P., Kandel, M.J., Harris, L.N., Pinheiro, H.C., Troussard, A., Miron, P., *et al.* (2007) Germline E-cadherin mutations in familial lobular breast cancer. *J Med Genet*, **44**(11): 726–31.
- Mattison, J., van der Weyden, L., Hubbard, T., and Adams, D.J. (2009) Cancer gene discovery in mouse and man. *Biochim Biophys Acta*, **1796**(2): 140–161.
- McLachlan, J., George, A., and Banerjee, S. (2016) The current status of parp inhibitors in ovarian cancer. *Tumori*, **102**(5): 433–440.
- McLendon, R., Friedman, A., Bigner, D., Van Meir, E.G., Brat, D.J., Mastrogianakis, G.M., Olson, J.J., Mikkelsen, T., Lehman, N., Aldape, K., *et al.* (2008) Comprehensive genomic characterization defines human glioblastoma genes and core pathways. *Nature*, **455**(7216): 1061–1068.
- Miles, D.W. (2001) Update on HER-2 as a target for cancer therapy: herceptin in the clinical setting. *Breast Cancer Res*, **3**(6): 380–384.
- Muzny, D.M., Bainbridge, M.N., Chang, K., Dinh, H.H., Drummond, J.A., Fowler, G., Kovar, C.L., Lewis, L.R., Morgan, M.B., Newsham, I.F., *et al.* (2012) Comprehensive molecular characterization of human colon and rectal cancer. *Nature*, **487**(7407): 330–337.
- Nagalla, S., Chou, J.W., Willingham, M.C., Ruiz, J., Vaughn, J.P., Dubey, P., Lash, T.L., Hamilton-Dutoit, S.J., Bergh, J., Sotiriou, C., *et al.* (2013) Interactions between immunity, proliferation and molecular subtype in breast cancer prognosis. *Genome Biol*, **14**(4): R34.
- Neeley, E.S., Kornblau, S.M., Coombes, K.R., and Baggerly, K.A. (2009) Variable slope normalization of reverse phase protein arrays. *Bioinformatics*, **25**(11): 1384.
- Novomestky, F. (2012) *matrixcalc: Collection of functions for matrix calculations*. R package version 1.0-3.
- Nowak, M.A., Boerlijst, M.C., Cooke, J., and Smith, J.M. (1997) Evolution of genetic redundancy. *Nature*, **388**(6638): 167–171.

- Oliveira, C., Senz, J., Kaurah, P., Pinheiro, H., Sanges, R., Haegert, A., Corso, G., Schouten, J., Fitzgerald, R., Vogelsang, H., *et al.* (2009) Germline *CDH1* deletions in hereditary diffuse gastric cancer families. *Human Molecular Genetics*, **18**(9): 1545–1555.
- Oliveira, C., Seruca, R., Hoogerbrugge, N., Ligtenberg, M., and Carneiro, F. (2013) Clinical utility gene card for: Hereditary diffuse gastric cancer (HDGC). *Eur J Hum Genet*, **21**(8).
- Pandey, G., Zhang, B., Chang, A.N., Myers, C.L., Zhu, J., Kumar, V., and Schadt, E.E. (2010) An integrative multi-network and multi-classifier approach to predict genetic interactions. *PLoS Comput Biol*, **6**(9).
- Parker, J., Mullins, M., Cheung, M., Leung, S., Voduc, D., Vickery, T., Davies, S., Fauron, C., He, X., Hu, Z., *et al.* (2009) Supervised risk predictor of breast cancer based on intrinsic subtypes. *Journal of Clinical Oncology*, **27**(8): 1160–1167.
- Pereira, B., Chin, S.F., Rueda, O.M., Vollan, H.K., Provenzano, E., Bardwell, H.A., Pugh, M., Jones, L., Russell, R., Sammut, S.J., *et al.* (2016) Erratum: The somatic mutation profiles of 2,433 breast cancers refine their genomic and transcriptomic landscapes. *Nat Commun*, **7**: 11908.
- Perou, C.M., Sørlie, T., Eisen, M.B., van de Rijn, M., Jeffrey, S.S., Rees, C.A., Pollack, J.R., Ross, D.T., Johnsen, H., Akslen, L.A., *et al.* (2000) Molecular portraits of human breast tumours. *Nature*, **406**(6797): 747–752.
- Polyak, K. and Weinberg, R.A. (2009) Transitions between epithelial and mesenchymal states: acquisition of malignant and stem cell traits. *Nat Rev Cancer*, **9**(4): 265–73.
- R Core Team (2016) *R: A Language and Environment for Statistical Computing*. R Foundation for Statistical Computing, Vienna, Austria. R version 3.3.2.
- Ritchie, M.E., Phipson, B., Wu, D., Hu, Y., Law, C.W., Shi, W., and Smyth, G.K. (2015) limma powers differential expression analyses for RNA-sequencing and microarray studies. *Nucleic Acids Research*, **43**(7): e47.
- Roguev, A., Bandyopadhyay, S., Zofall, M., Zhang, K., Fischer, T., Collins, S.R., Qu, H., Shales, M., Park, H.O., Hayles, J., *et al.* (2008) Conservation and rewiring of functional modules revealed by an epistasis map in fission yeast. *Science*, **322**(5900): 405–10.

- Roychowdhury, S. and Chinnaiyan, A.M. (2016) Translating cancer genomes and transcriptomes for precision oncology. *CA Cancer J Clin*, **66**(1): 75–88.
- Rung, J. and Brazma, A. (2013) Reuse of public genome-wide gene expression data. *Nat Rev Genet*, **14**(2): 89–99.
- Ryan, C., Lord, C., and Ashworth, A. (2014) Daisy: Picking synthetic lethals from cancer genomes. *Cancer Cell*, **26**(3): 306–308.
- Schena, M. (1996) Genome analysis with gene expression microarrays. *Bioessays*, **18**(5): 427–431.
- Scheuer, L., Kauff, N., Robson, M., Kelly, B., Barakat, R., Satagopan, J., Ellis, N., Hensley, M., Boyd, J., Borgen, P., *et al.* (2002) Outcome of preventive surgery and screening for breast and ovarian cancer in BRCA mutation carriers. *J Clin Oncol*, **20**(5): 1260–1268.
- Semb, H. and Christofori, G. (1998) The tumor-suppressor function of E-cadherin. *Am J Hum Genet*, **63**(6): 1588–93.
- Sing, T., Sander, O., Beerenwinkel, N., and Lengauer, T. (2005) Rocr: visualizing classifier performance in r. *Bioinformatics*, **21**(20): 7881.
- Slurm development team (Slurm) (2017) Slurm workload manager. <https://slurm.schedmd.com/>. Accessed: 25/03/2017.
- Sørlie, T., Perou, C.M., Tibshirani, R., Aas, T., Geisler, S., Johnsen, H., Hastie, T., Eisen, M.B., van de Rijn, M., Jeffrey, S.S., *et al.* (2001) Gene expression patterns of breast carcinomas distinguish tumor subclasses with clinical implications. *Proc Natl Acad Sci USA*, **98**(19): 10869–10874.
- Stajich, J.E. and Lapp, H. (2006) Open source tools and toolkits for bioinformatics: significance, and where are we? *Brief Bioinformatics*, **7**(3): 287–296.
- Stratton, M.R., Campbell, P.J., and Futreal, P.A. (2009) The cancer genome. *Nature*, **458**(7239): 719–724.
- Ström, C. and Helleday, T. (2012) Strategies for the use of poly(adenosine diphosphate ribose) polymerase (parp) inhibitors in cancer therapy. *Biomolecules*, **2**(4): 635–649.
- Tarazona, S., Garcia-Alcalde, F., Dopazo, J., Ferrer, A., and Conesa, A. (2011) Differential expression in RNA-seq: a matter of depth. *Genome Res*, **21**(12): 2213–2223.

Telford, B.J., Chen, A., Beetham, H., Frick, J., Brew, T.P., Gould, C.M., Single, A., Godwin, T., Simpson, K.J., and Guilford, P. (2015) Synthetic lethal screens identify vulnerabilities in gpcr signalling and cytoskeletal organization in E-cadherin-deficient cells. *Mol Cancer Ther*, **14**(5): 1213–1223.

The 1000 Genomes Project Consortium (1000 Genomes) (2010) A map of human genome variation from population-scale sequencing. *Nature*, **467**(7319): 1061–1073.

The Cancer Genome Atlas Research Network (TCGA) (2017) The Cancer Genome Atlas Project. <https://cancergenome.nih.gov/>. Accessed: 26/03/2017.

The Catalogue Of Somatic Mutations In Cancer (COSMIC) (2016) Cosmic: The catalogue of somatic mutations in cancer. <http://cancer.sanger.ac.uk/cosmic>. Release 79 (23/08/2016), Accessed: 05/02/2017.

The Comprehensive R Archive Network (CRAN) (2017) Cran. <https://cran.r-project.org/>. Accessed: 24/03/2017.

The ENCODE Project Consortium (ENCODE) (2004) The ENCODE (ENCyclopedia Of DNA Elements) Project. *Science*, **306**(5696): 636–640.

The National Cancer Institute (NCI) (2015) The genetics of cancer. <https://www.cancer.gov/about-cancer/causes-prevention/genetics>. Published: 22/04/2015, Accessed: 22/03/2017.

The New Zealand eScience Infrastructure (NeSI) (2017) NeSI. <https://www.nesi.org.nz/>. Accessed: 25/03/2017.

Tierney, L., Rossini, A.J., Li, N., and Sevcikova, H. (2015) *snow: Simple Network of Workstations*. R package version 0.4-2.

Tiong, K.L., Chang, K.C., Yeh, K.T., Liu, T.Y., Wu, J.H., Hsieh, P.H., Lin, S.H., Lai, W.Y., Hsu, Y.C., Chen, J.Y., et al. (2014) Csnk1e/ctnnb1 are synthetic lethal to tp53 in colorectal cancer and are markers for prognosis. *Neoplasia*, **16**(5): 441–50.

Tischler, J., Lehner, B., and Fraser, A.G. (2008) Evolutionary plasticity of genetic interaction networks. *Nat Genet*, **40**(4): 390–391.

Tomasetti, C. and Vogelstein, B. (2015) Cancer etiology. Variation in cancer risk among tissues can be explained by the number of stem cell divisions. *Science*, **347**(6217): 78–81.

- Tong, A.H., Evangelista, M., Parsons, A.B., Xu, H., Bader, G.D., Page, N., Robinson, M., Raghibizadeh, S., Hogue, C.W., Bussey, H., *et al.* (2001) Systematic genetic analysis with ordered arrays of yeast deletion mutants. *Science*, **294**(5550): 2364–8.
- Tong, A.H., Lesage, G., Bader, G.D., Ding, H., Xu, H., Xin, X., Young, J., Berriz, G.F., Brost, R.L., Chang, M., *et al.* (2004) Global mapping of the yeast genetic interaction network. *Science*, **303**(5659): 808–13.
- Tran, B., Dancey, J.E., Kamel-Reid, S., McPherson, J.D., Bedard, P.L., Brown, A.M., Zhang, T., Shaw, P., Onetto, N., Stein, L., *et al.* (2012) Cancer genomics: technology, discovery, and translation. *J Clin Oncol*, **30**(6): 647–660.
- Travers, J. and Milgram, S. (1969) An experimental study of the small world problem. *Sociometry*, **32**(4): 425–443.
- Tunggal, J.A., Helfrich, I., Schmitz, A., Schwarz, H., Gunzel, D., Fromm, M., Kemler, R., Krieg, T., and Niessen, C.M. (2005) E-cadherin is essential for in vivo epidermal barrier function by regulating tight junctions. *EMBO J*, **24**(6): 1146–1156.
- Tutt, A., Robson, M., Garber, J.E., Domchek, S.M., Audeh, M.W., Weitzel, J.N., Friedlander, M., Arun, B., Loman, N., Schmutzler, R.K., *et al.* (2010) Oral poly(ADP-ribose) polymerase inhibitor olaparib in patients with *BRCA1* or *BRCA2* mutations and advanced breast cancer: a proof-of-concept trial. *Lancet*, **376**(9737): 235–44.
- University of California, Santa Cruz (UCSC) (2012) Ucsc cancer browser. Accessed 29/03/2012.
- van der Post, R.S., Vogelaar, I.P., Carneiro, F., Guilford, P., Huntsman, D., Hoogerbrugge, N., Caldas, C., Schreiber, K.E., Hardwick, R.H., Ausems, M.G., *et al.* (2015) Hereditary diffuse gastric cancer: updated clinical guidelines with an emphasis on germline CDH1 mutation carriers. *J Med Genet*, **52**(6): 361–374.
- van Steen, K. (2012) Travelling the world of gene–gene interactions. *Briefings in Bioinformatics*, **13**(1): 1–19.
- van Steen, M. (2010) *Graph Theory and Complex Networks: An Introduction*. Maarten van Steen, VU Amsterdam.
- Vapnik, V.N. (1995) *The nature of statistical learning theory*. Springer-Verlag New York, Inc.

- Vizeacoumar, F.J., Arnold, R., Vizeacoumar, F.S., Chandrashekhar, M., Buzina, A., Young, J.T., Kwan, J.H., Sayad, A., Mero, P., Lawo, S., *et al.* (2013) A negative genetic interaction map in isogenic cancer cell lines reveals cancer cell vulnerabilities. *Mol Syst Biol*, **9**: 696.
- Vogelstein, B., Papadopoulos, N., Velculescu, V.E., Zhou, S., Diaz, L.A., and Kinzler, K.W. (2013) Cancer genome landscapes. *Science*, **339**(6127): 1546–1558.
- Vos, C.B., Cleton-Jansen, A.M., Berx, G., de Leeuw, W.J., ter Haar, N.T., van Roy, F., Cornelisse, C.J., Peterse, J.L., and van de Vijver, M.J. (1997) E-cadherin inactivation in lobular carcinoma in situ of the breast: an early event in tumorigenesis. *Br J Cancer*, **76**(9): 1131–3.
- Waldron, D. (2016) Cancer genomics: A multi-layer omics approach to cancer. *Nat Rev Genet*, **17**(8): 436–437.
- Wang, K., Singh, D., Zeng, Z., Coleman, S.J., Huang, Y., Savich, G.L., He, X., Mieczkowski, P., Grimm, S.A., Perou, C.M., *et al.* (2010) MapSplice: accurate mapping of RNA-seq reads for splice junction discovery. *Nucleic Acids Res*, **38**(18): e178.
- Wang, X. and Simon, R. (2013) Identification of potential synthetic lethal genes to p53 using a computational biology approach. *BMC Medical Genomics*, **6**(1): 30.
- Wappett, M. (2014) Bisep: Toolkit to identify candidate synthetic lethality. r package version 2.0.
- Wappett, M., Dulak, A., Yang, Z.R., Al-Watban, A., Bradford, J.R., and Dry, J.R. (2016) Multi-omic measurement of mutually exclusive loss-of-function enriches for candidate synthetic lethal gene pairs. *BMC Genomics*, **17**: 65.
- Warnes, G.R., Bolker, B., Bonebakker, L., Gentleman, R., Liaw, W.H.A., Lumley, T., Maechler, M., Magnusson, A., Moeller, S., Schwartz, M., *et al.* (2015) *gplots: Various R Programming Tools for Plotting Data*. R package version 2.17.0.
- Watts, D.J. and Strogatz, S.H. (1998) Collective dynamics of 'small-world' networks. *Nature*, **393**(6684): 440–2.
- Weinstein, I.B. (2000) Disorders in cell circuitry during multistage carcinogenesis: the role of homeostasis. *Carcinogenesis*, **21**(5): 857–864.

- Weinstein, J.N., Akbani, R., Broom, B.M., Wang, W., Verhaak, R.G., McConkey, D., Lerner, S., Morgan, M., Creighton, C.J., Smith, C., *et al.* (2014) Comprehensive molecular characterization of urothelial bladder carcinoma. *Nature*, **507**(7492): 315–322.
- Weinstein, J.N., Collisson, E.A., Mills, G.B., Shaw, K.R., Ozenberger, B.A., Ellrott, K., Shmulevich, I., Sander, C., Stuart, J.M., Chang, K., *et al.* (2013) The Cancer Genome Atlas Pan-Cancer analysis project. *Nat Genet*, **45**(10): 1113–1120.
- Wickham, H. and Chang, W. (2016) *devtools: Tools to Make Developing R Packages Easier*. R package version 1.12.0.
- Wickham, H., Danenberg, P., and Eugster, M. (2017) *roxygen2: In-Line Documentation for R*. R package version 6.0.1.
- Wong, S.L., Zhang, L.V., Tong, A.H.Y., Li, Z., Goldberg, D.S., King, O.D., Lesage, G., Vidal, M., Andrews, B., Bussey, H., *et al.* (2004) Combining biological networks to predict genetic interactions. *Proceedings of the National Academy of Sciences of the United States of America*, **101**(44): 15682–15687.
- World Health Organization (WHO) (2017) Fact sheet: Cancer. <http://www.who.int/mediacentre/factsheets/fs297/en/>. Updated February 2017, Accessed: 22/03/2017.
- Wu, M., Li, X., Zhang, F., Li, X., Kwoh, C.K., and Zheng, J. (2014) In silico prediction of synthetic lethality by meta-analysis of genetic interactions, functions, and pathways in yeast and human cancer. *Cancer Inform*, **13**(Suppl 3): 71–80.
- Yu, H. (2002) Rmpi: Parallel statistical computing in r. *R News*, **2**(2): 10–14.
- Zhang, F., Wu, M., Li, X.J., Li, X.L., Kwoh, C.K., and Zheng, J. (2015) Predicting essential genes and synthetic lethality via influence propagation in signaling pathways of cancer cell fates. *J Bioinform Comput Biol*, **13**(3): 1541002.
- Zhang, J., Baran, J., Cros, A., Guberman, J.M., Haider, S., Hsu, J., Liang, Y., Rivkin, E., Wang, J., Whitty, B., *et al.* (2011) International cancer genome consortium data portal—a one-stop shop for cancer genomics data. *Database: The Journal of Biological Databases and Curation*, **2011**: bar026.
- Zhong, W. and Sternberg, P.W. (2006) Genome-wide prediction of *c. elegans* genetic interactions. *Science*, **311**(5766): 1481–1484.

Zweig, M.H. and Campbell, G. (1993) Receiver-operating characteristic (roc) plots: a fundamental evaluation tool in clinical medicine. *Clinical Chemistry*, **39**(4): 561–577.

# Appendix A

## Sample Quality

### A.1 Sample Correlation

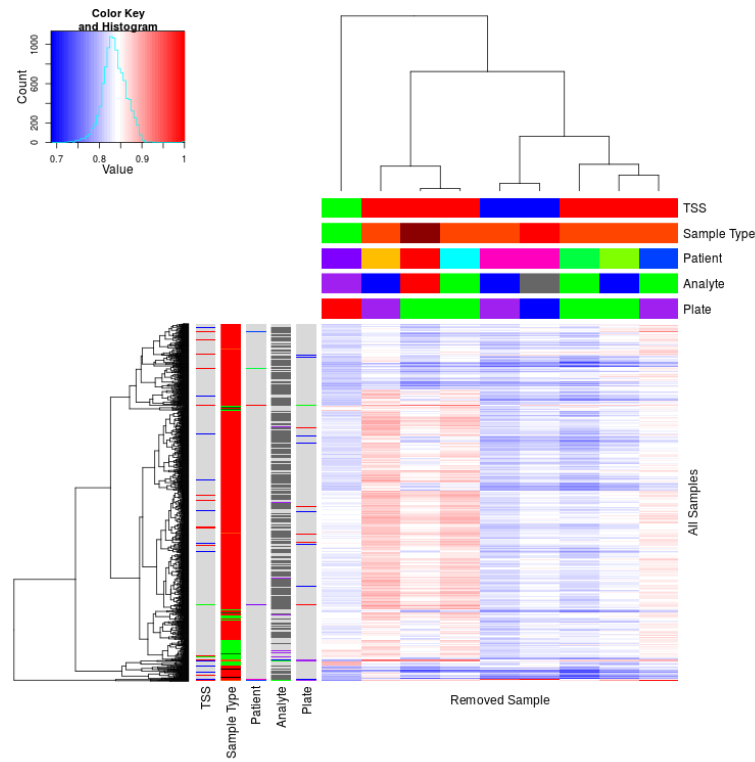
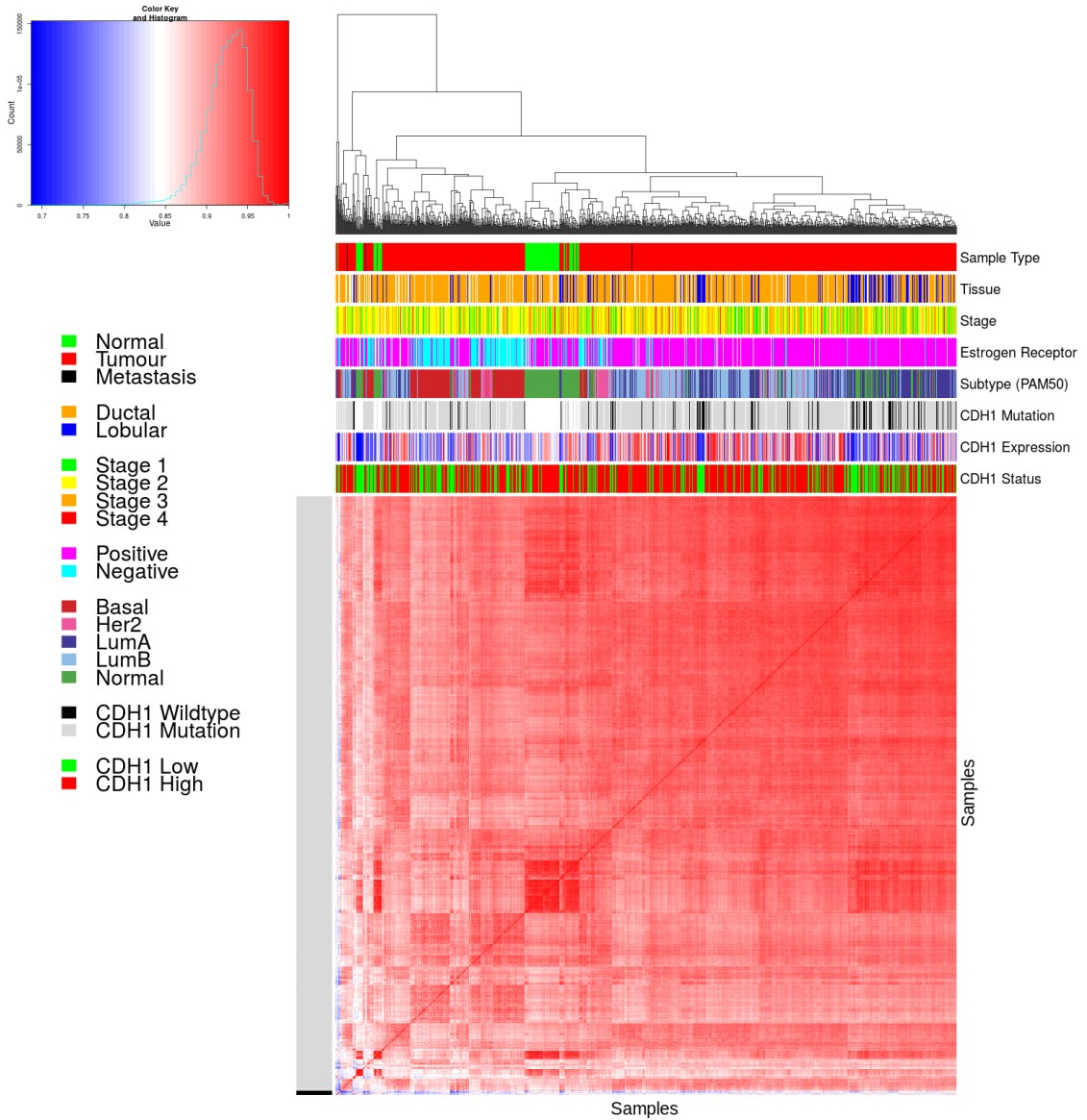


Figure A.1: **Correlation profiles of removed samples.** Heatmap (Euclidean distance) of samples in [TCGA](#) breast cancer dataset (left) clustered for all samples against removed samples (top): tissue source site (TSS), sample type with reds for tumour and greens for normal, patient (A2QH in pink), with varied analyte and plate. Excluded samples clustered at the bottom and annotation (left) show shared properties between samples in the dataset.



**Figure A.2: Correlation analysis and sample removal.** Correlation matrix heatmap (Euclidean distance) of all samples in [TCGA](#) breast cancer dataset against each other annotated for sample clinical data: sample type, tissue type, tumour stage, [ER](#) and intrinsic subtype (from the [PAM50](#) method). [CDH1](#) somatic mutation, gene expression, and status for [SLIPT](#) prediction were also annotated. Discrete variables were coloured as displayed in the legend and continuous variables on a blue–red scale as shown in the colour key. Trimmed samples cluster at the bottom of the heatmap and the colour bars of the left show which were removed for quality concerns.

## A.2 Replicate Samples in TCGA Breast

Replicate samples were picked where possible from the [TCGA](#) breast cancer gene expression data to examine for sample quality. Independent samples of the same tumour were expected to have very high Pearson correlation between their expression profiles unless there were issues with sample collection or preparation and were thus an indicator of sample quality. The log-transformed raw read counts for replicate samples were examined in Figures A.3–A.5. These were examined before normalisation which would be expected to increase sample concordance.

Another consideration was the samples which were removed for quality concerns (in Section 2.2.2). While these were selected by unbiased hierarchical clustering (See Figure A.2), many of the excluded (tumour) samples were performed in replicate despite relatively few replicate samples in the overall dataset. These samples correlate poorly with the rest of the dataset, in addition to correlation with replicate samples.

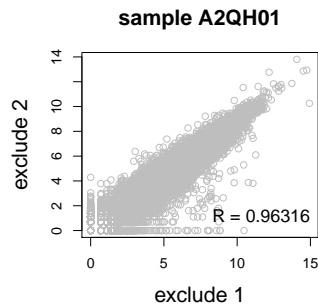


Figure A.3: **Replicate excluded samples.** Both tumour samples of patient A2QH were excluded as they were poorly correlated with other samples, although they were highly similar to each other as shown by Pearson correlation of log-raw counts.

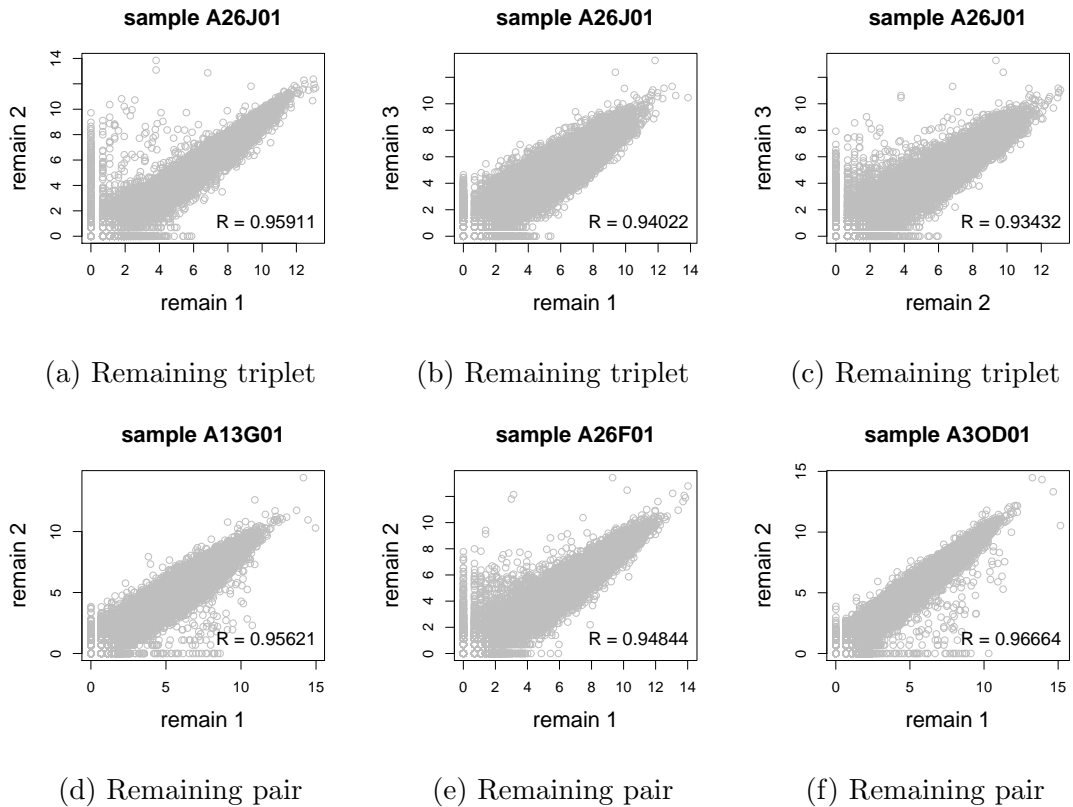


Figure A.4: **Replicate samples with all remaining.** Patient A26J was sampled 3 times and compared pairwise. Pairs of samples were also compared for other patients with replicate samples. In all cases, replicate samples remaining in the dataset were highly concordant, as shown by Pearson correlation of log-raw counts.

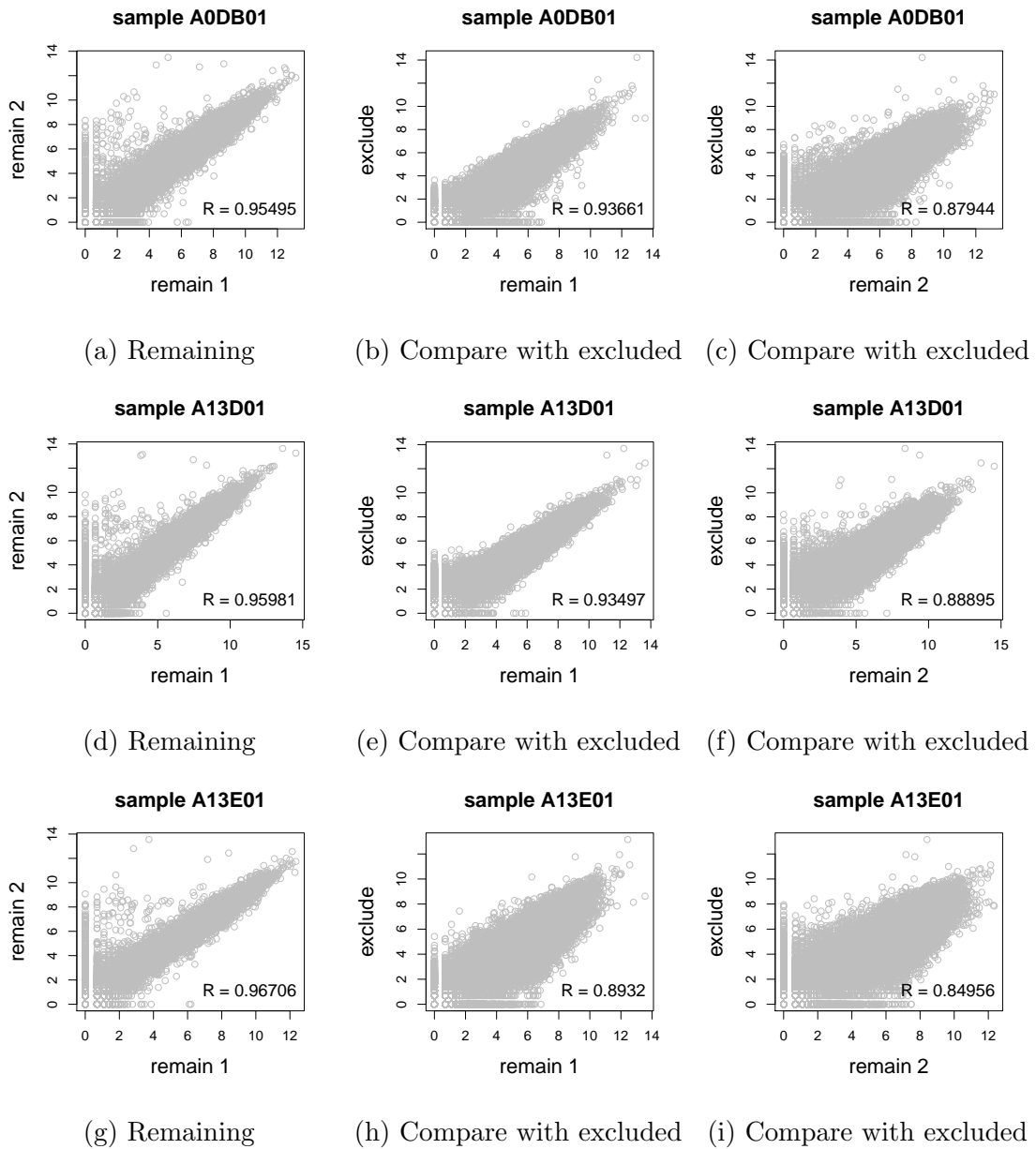


Figure A.5: **Replicate samples with some excluded.** (continued on next page)

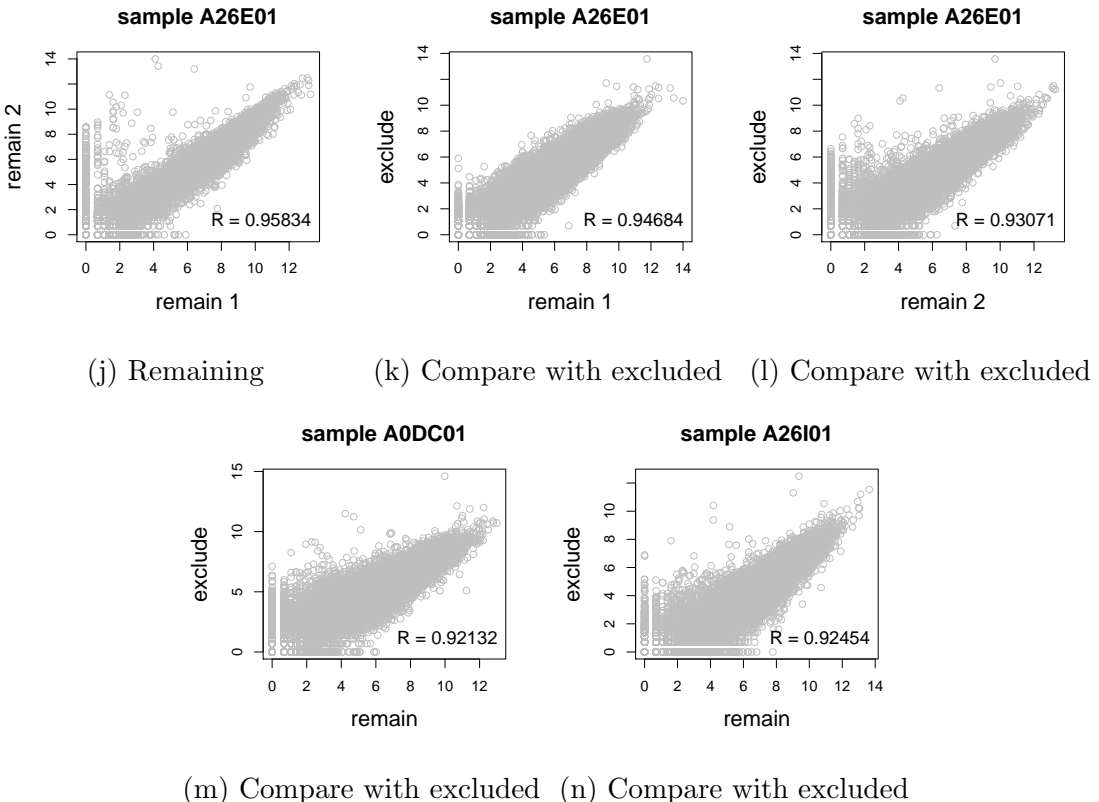


Figure A.5: **Replicate samples with some excluded.** Patients A0DB, A13D, A13E, and A26E were each sampled 3 times and compared pairwise. Pairs of samples were also compared for other patients with replicate samples. In all cases, the replicate samples remaining in the dataset more were highly concordant than those excluded from the analysis, as shown by Pearson correlation of log-log counts.

# Appendix B

## Software Used for Thesis

Table B.1: Complete list of R packages used during this thesis

Package	Repository	Laptop	Lab	Server	NeSI
base	base	3.3.2	3.3.2	3.3.1	3.3.0
abind	CRAN		1.4-5		1.4-3
acepack	CRAN		1.4.1		1.3-3.3
ade4	CRAN		1.7-5		
annaffy	Bioconductor		1.46.0		
AnnotationDbi	Bioconductor		1.36.0	1.36.0	1.34.4
apComplex	CRAN		2.40.0		
ape	CRAN		4		3.4
arm	CRAN		1.9-3		
assertthat	CRAN	0.1	0.1	0.1	0.1
backports	CRAN	1.0.5	1.0.4	1.0.5	1.0.2
base64	CRAN			2	2
base64enc	CRAN		0.1-3		0.1-3
beanplot	CRAN		1.2	1.2	1.2
BH	CRAN	1.60.0-2	1.62.0-1	1.62.0-1	1.60.0-2
Biobase	Bioconductor		2.34.0	2.34.0	2.32.0
BiocGenerics	Bioconductor		0.20.0	0.20.0	0.18.0
BiocInstaller	Bioconductor		1.24.0	1.20.3	1.22.3
BiocParallel	Bioconductor		1.8.1	1.8.1	
Biostrings	Bioconductor		2.42.1	2.42.0	
BiSEp	Bioconductor		2.0.1	2.0.1	2.0.1

bitops	CRAN	1.0-6	1.0-6	1.0-6	1.0-6
boot	base	1.3-18	1.3-18	1.3-18	1.3-18
brew	CRAN	1.0-6	1.0-6	1.0-6	1.0-6
broom	CRAN	0.4.1			
caTools	CRAN	1.17.1	1.17.1	1.17.1	1.17.1
cgdssr	CRAN		1.2.5		
checkmate	CRAN		1.8.2		1.7.4
chron	CRAN	2.3-47	2.3-48	2.3-50	2.3-47
class	base	7.3-14	7.3-14	7.3-14	7.3-14
cluster	base	2.0.5	2.0.5	2.0.5	2.0.4
coda	CRAN		0.19-1		0.18-1
codetools	base	0.2-15	0.2-15	0.2-15	0.2-14
colorRamps	CRAN		2.3		
colorspace	CRAN	1.2-6	1.3-2	1.3-2	1.2-6
commonmark	CRAN	1.1		1.2	
compiler	base	3.3.2	3.3.2	3.3.1	3.3.0
corpcor	CRAN		1.6.8	1.6.8	1.6.8
Cprob	CRAN		1.2.4		
crayon	CRAN	1.3.2	1.3.2	1.3.2	1.3.2
crop	CRAN		0.0-2	0.0-2	
curl	CRAN	1.2	2.3	2.3	0.9.7
d3Network	CRAN		0.5.2.1		
data.table	CRAN	1.9.6	1.10.0	1.10.1	1.9.6
data.tree	CRAN		0.7.0	0.7.0	
datasets	base	3.3.2	3.3.2	3.3.1	3.3.0
DBI	CRAN	0.5-1	0.5-1	0.5-1	0.5-1
dendextend	CRAN	1.4.0	1.4.0	1.4.0	
DEoptimR	CRAN	1.0-8	1.0-8	1.0-8	1.0-4
desc	CRAN	1.1.0		1.1.0	
devtools	CRAN	1.12.0	1.12.0	1.12.0	1.12.0
DiagrammeR	CRAN		0.9.0	0.9.0	
dichromat	CRAN	2.0-0	2.0-0	2.0-0	2.0-0
digest	CRAN	0.6.10	0.6.11	0.6.12	0.6.9
diptest	CRAN	0.75-7	0.75-7	0.75-7	
doParallel	CRAN	1.0.10	1.0.10	1.0.10	1.0.10

dplyr	CRAN	0.5.0	0.5.0	0.5.0	0.5.0
ellipse	CRAN		0.3-8	0.3-8	0.3-8
evaluate	CRAN		0.1	0.1	0.9
fdrtool	CRAN		1.2.15		
fields	CRAN		8.1		
flexmix	CRAN	2.3-13	2.3-13	2.3-13	
forcats	CRAN	0.2.0			
foreach	CRAN	1.4.3	1.4.3	1.4.3	1.4.3
foreign	base	0.8-67	0.8-67	0.8-67	0.8-66
formatR	CRAN		1.4	1.4	1.4
Formula	CRAN		1.2-1		1.2-1
fpc	CRAN	2.1-10	2.1-10	2.1-10	
futile.logger	CRAN		1.4.3	1.4.3	1.4.1
futile.options	CRAN		1.0.0	1.0.0	1.0.0
gdata	CRAN	2.17.0	2.17.0	2.17.0	2.17.0
geepack	CRAN		1.2-1		
GenomeInfoDb	Bioconductor		1.10.2	1.10.1	
GenomicAlignments	Bioconductor		1.10.0	1.10.0	
GenomicRanges	Bioconductor		1.26.2	1.26.1	
ggm	CRAN		2.3		
ggplot2	CRAN	2.1.0	2.2.1	2.2.1	2.1.0
git2r	CRAN	0.15.0	0.18.0	0.16.0	0.15.0
glasso	CRAN		1.8		
GO.db	Bioconductor		3.4.0	3.2.2	3.3.0
GOSemSim	Bioconductor		2.0.3	1.28.2	1.30.3
gplots	CRAN	3.0.1	3.0.1	3.0.1	3.0.1
graph	Bioconductor		1.52.0		
graphics	base	3.3.2	3.3.2	3.3.1	3.3.0
graphsim	GitHub TomKellyGenetics	0.1.0	0.1.0	0.1.0	0.1.0
grDevices	base	3.3.2	3.3.2	3.3.1	3.3.0
grid	base	3.3.2	3.3.2	3.3.1	3.3.0
gridBase	CRAN	0.4-7	0.4-7	0.4-7	0.4-7
gridExtra	CRAN	2.2.1	2.2.1	2.2.1	2.2.1
gridGraphics	CRAN		0.1-5		

gtable	<a href="#">CRAN</a>	0.2.0	0.2.0	0.2.0	0.2.0
gtools	<a href="#">CRAN</a>	3.5.0	3.5.0	3.5.0	3.5.0
haven	<a href="#">CRAN</a>	1.0.0			
heatmap.2x	GitHub TomKellyGenetics	0.0.0.9000	0.0.0.9000	0.0.0.9000	0.0.0.9000
hgu133plus2.db	Bioconductor		3.2.3		
highr	<a href="#">CRAN</a>		0.6	0.6	0.6
Hmisc	<a href="#">CRAN</a>		4.0-2	4.0-2	3.17-4
hms	<a href="#">CRAN</a>	0.2	0.3		
htmlTable	<a href="#">CRAN</a>		1.8	1.9	
htmltools	<a href="#">CRAN</a>	0.3.5	0.3.5	0.3.5	0.3.5
htmlwidgets	<a href="#">CRAN</a>		0.8	0.8	
httpuv	<a href="#">CRAN</a>	1.3.3		1.3.3	
httr	<a href="#">CRAN</a>	1.2.1	1.2.1	1.2.1	1.1.0
huge	<a href="#">CRAN</a>		1.2.7		
hunspell	<a href="#">CRAN</a>		2.3		2
hypergraph	<a href="#">CRAN</a>		1.46.0		
igraph	<a href="#">CRAN</a>	1.0.1	1.0.1	1.0.1	1.0.1
igraph.extensions	GitHub TomKellyGenetics	0.1.0.9001	0.1.0.9001	0.1.0.9001	0.1.0.9001
influenceR	<a href="#">CRAN</a>		0.1.0	0.1.0	
info.centrality	GitHub TomKellyGenetics	0.1.0	0.1.0	0.1.0	0.1.0
IRanges	Bioconductor		2.8.1	2.8.1	2.6.1
irlba	<a href="#">CRAN</a>	2.1.1	2.1.2	2.1.2	2.0.0
iterators	<a href="#">CRAN</a>	1.0.8	1.0.8	1.0.8	1.0.8
jpeg	<a href="#">CRAN</a>		0.1-8		
jsonlite	<a href="#">CRAN</a>	1.1	1.2	1.3	0.9.20
KEGG.db	Bioconductor		3.2.3		
kernlab	<a href="#">CRAN</a>	0.9-25	0.9-25	0.9-25	
KernSmooth	base	2.23-15	2.23-15	2.23-15	2.23-15
knitr	<a href="#">CRAN</a>		1.15.1	1.15.1	1.14
labeling	<a href="#">CRAN</a>	0.3	0.3	0.3	0.3
lambda.r	<a href="#">CRAN</a>		1.1.9	1.1.9	1.1.7
lattice	base	0.20-34	0.20-34	0.20-34	0.20-33

latticeExtra	CRAN		0.6-28		0.6-28
lava	CRAN		1.4.6		
lavaan	CRAN		0.5-22		
lazyeval	CRAN	0.2.0	0.2.0	0.2.0	0.2.0
les	CRAN		1.24.0		
lgtdl	CRAN		1.1.3		
limma	Bioconductor		3.30.7	3.30.3	
lme4	CRAN		1.1-12		1.1-12
lubridate	CRAN	1.6.0			
magrittr	CRAN	1.5	1.5	1.5	1.5
maps	CRAN		3.1.1		
markdown	CRAN		0.7.7	0.7.7	0.7.7
MASS	base	7.3-45	7.3-45	7.3-45	7.3-45
Matrix	base	1.2-7.1	1.2-7.1	1.2-8	1.2-6
matrixcalc	CRAN	1.0-3	1.0-3	1.0-3	1.0-3
mclust	CRAN	5.2	5.2.1	5.2.2	5.2
memoise	CRAN	1.0.0	1.0.0	1.0.0	1.0.0
methods	base	3.3.2	3.3.2	3.3.1	3.3.0
mgcv	base	1.8-16	1.8-16	1.8-17	1.8-12
mi	CRAN		1		
mime	CRAN	0.5	0.5	0.5	0.4
minqa	CRAN		1.2.4		1.2.4
mnormt	CRAN	1.5-5	1.5-5		1.5-4
modelr	CRAN	0.1.0			
modeltools	CRAN	0.2-21	0.2-21	0.2-21	
multtest	Bioconductor		2.30.0	2.30.0	
munsell	CRAN	0.4.3	0.4.3	0.4.3	0.4.3
mvtnorm	CRAN	1.0-5	1.0-5	1.0-6	1.0-5
network	CRAN		1.13.0		
nlme	base	3.1-128	3.1-128	3.1-131	3.1-128
nloptr	CRAN		1.0.4		1.0.4
NMF	CRAN	0.20.6	0.20.6	0.20.6	0.20.6
nnet	base	7.3-12	7.3-12	7.3-12	7.3-12
numDeriv	CRAN		2016.8-1		2014.2-1
openssl	CRAN	0.9.4	0.9.6	0.9.6	0.9.4

org.Hs.eg.db	Bioconductor		3.1.2		3.3.0
org.Sc.sgd.db	Bioconductor		3.4.0		
parallel	base	3.3.2	3.3.2	3.3.1	3.3.0
pathway.structure	GitHub	0.1.0	0.1.0	0.1.0	0.1.0
.permutation	TomKellyGenetics				
pbivnorm	CRAN		0.6.0		
PGSEA	Bioconductor		1.48.0		
pkgmaker	CRAN	0.22	0.22	0.22	0.22
PKI	CRAN		0.1-3		
plogr	CRAN		0.1-1	0.1-1	
plot.igraph	GitHub	0.0.0.9001	0.0.0.9001	0.0.0.9001	0.0.0.9001
	TomKellyGenetics				
plotrix	CRAN		3.6-4		
plyr	CRAN	1.8.4	1.8.4	1.8.4	1.8.3
png	CRAN		0.1-7		0.1-7
prabclus	CRAN	2.2-6	2.2-6	2.2-6	
praise	CRAN	1.0.0	1.0.0		1.0.0
pROC	CRAN		1.8	1.9.1	
prodlim	CRAN		1.5.7		
prof.tree	CRAN		0.1.0		
protools	CRAN		0.99-2		
progress	CRAN			1.1.2	
psych	CRAN	1.6.12	1.6.12		
purrr	CRAN	0.2.2	0.2.2	0.2.2	0.2.2
qgraph	CRAN		1.4.1		
quadprog	CRAN		1.5-5	1.5-5	1.5-5
R.methodsS3	CRAN		1.7.1		1.7.1
R.oo	CRAN		1.21.0		1.20.0
R.utils	CRAN		2.5.0		
R6	CRAN	2.1.3	2.2.0	2.2.0	2.1.3
RBGL	CRAN		1.50.0		
RColorBrewer	CRAN	1.1-2	1.1-2	1.1-2	1.1-2
Rcpp	CRAN	0.12.7	0.12.9	0.12.9	0.12.7
RcppArmadillo	CRAN			0.7.700.0.0	0.6.700.6.0
RcppEigen	CRAN		0.3.2.9.0		0.3.2.8.1

RCurl	<a href="#">CRAN</a>	1.95-4.8	1.95-4.8	1.95-4.8	
reactome.db	Bioconductor	1.52.1	1.52.1		
reactometree	GitHub	0.1			
	TomKellyGenetics				
readr	<a href="#">CRAN</a>	1.0.0	1.0.0		
readxl	<a href="#">CRAN</a>	0.1.1			
registry	<a href="#">CRAN</a>	0.3	0.3	0.3	0.3
reshape2	<a href="#">CRAN</a>	1.4.1	1.4.2	1.4.2	1.4.1
rgeff	<a href="#">CRAN</a>		0.15.3	0.15.3	
rgl	<a href="#">CRAN</a>			0.97.0	0.95.1441
Rgraphviz	<a href="#">CRAN</a>		2.18.0		
rjson	<a href="#">CRAN</a>		0.2.15		
RJSONIO	<a href="#">CRAN</a>		1.3-0		
rmarkdown	<a href="#">CRAN</a>		1.3	1.3	1
Rmpi	<a href="#">CRAN</a>		0.6-6		0.6-5
rngtools	<a href="#">CRAN</a>	1.2.4	1.2.4	1.2.4	1.2.4
robustbase	<a href="#">CRAN</a>	0.92-7	0.92-7	0.92-7	0.92-5
ROCR	<a href="#">CRAN</a>	1.0-7	1.0-7	1.0-7	1.0-7
Rook	<a href="#">CRAN</a>		1.1-1	1.1-1	
roxygen2	<a href="#">CRAN</a>	6.0.1	5.0.1	6.0.1	5.0.1
rpart	base	4.1-10	4.1-10	4.1-10	4.1-10
rprojroot	<a href="#">CRAN</a>	1.2	1.1	1.2	
Rsamtools	Bioconductor		1.26.1	1.26.1	
rsconnect	<a href="#">CRAN</a>		0.7		
RSQLite	<a href="#">CRAN</a>		1.1-2	1.1-2	1.0.0
rstudioapi	<a href="#">CRAN</a>	0.6	0.6	0.6	0.6
rvest	<a href="#">CRAN</a>	0.3.2			
S4Vectors	Bioconductor		0.12.1	0.12.0	0.10.3
safe	Bioconductor		3.14.0	3.10.0	
scales	<a href="#">CRAN</a>	0.4.0	0.4.1	0.4.1	0.4.0
selectr	<a href="#">CRAN</a>	0.3-1			
sem	<a href="#">CRAN</a>		3.1-8		
shiny	<a href="#">CRAN</a>	0.14		1.0.0	
slipt	GitHub	0.1.0		0.1.0	0.1.0
	TomKellyGenetics		0.1.0		

sm	CRAN	2.2-5.4	2.2-5.4		
sna	CRAN		2.4		
snow	CRAN	0.4-1	0.4-2	0.4-2	0.3-13
sourcetools	CRAN	0.1.5		0.1.5	
SparseM	CRAN		1.74		1.7
spatial	base	7.3-11	7.3-11	7.3-11	7.3-11
splines	base	3.3.2	3.3.2	3.3.1	3.3.0
statnet.common	CRAN		3.3.0		
stats	base	3.3.2	3.3.2	3.3.1	3.3.0
stats4	base	3.3.2	3.3.2	3.3.1	3.3.0
stringi	CRAN	1.1.1	1.1.2	1.1.2	1.0-1
stringr	CRAN	1.1.0	1.1.0	1.2.0	1.0.0
Summarized Experiment	Bioconductor		1.4.0	1.4.0	
survival	base	2.39-4	2.40-1	2.40-1	2.39-4
tcltk	base	3.3.2	3.3.2	3.3.1	3.3.0
testthat	CRAN	1.0.2	1.0.2		1.0.2
tibble	CRAN	1.2	1.2	1.2	1.2
tidyverse	GitHub hadley	1.1.1			
timeline	CRAN		0.9		
tools	base	3.3.2	3.3.2	3.3.1	3.3.0
tpr	CRAN		0.3-1		
trimcluster	CRAN	0.1-2	0.1-2	0.1-2	
Unicode	CRAN	9.0.0-1	9.0.0-1	9.0.0-1	
utils	base	3.3.2	3.3.2	3.3.1	3.3.0
vioplot	CRAN		0.2		
vioplotx	GitHub TomKellyGenetics	0.0.0.9000	0.0.0.9000		
viridis	CRAN	0.3.4	0.3.4	0.3.4	
visNetwork	CRAN		1.0.3	1.0.3	
whisker	CRAN	0.3-2	0.3-2	0.3-2	0.3-2
withr	CRAN	1.0.2	1.0.2	1.0.2	1.0.2
XML	base	3.98-1.3	3.98-1.1	3.98-1.5	3.98-1.4

xml2	CRAN	1.1.1	1.1.1	1.0.0
xtable	CRAN	1.8-2	1.8-2	1.8-2
XVector	Bioconductor		0.14.0	0.14.0
yaml	CRAN		2.1.14	2.1.14
zlibbioc	CRAN		1.20.0	1.20.0
zoo	CRAN	1.7-13	1.7-14	1.7-13

# Appendix C

## Mutation Analysis in Breast Cancer

### C.1 Synthetic Lethal Genes and Pathways

SLIPT expression analysis (described in Section 3.1) on TCGA breast cancer data ( $n = 969$ ) found the following genes and pathways, described in sections 4.1 and 4.1.1.

Table C.1: Candidate synthetic lethal gene partners of *CDH1* from mtSLIPT

Gene	Observed*	Expected*	$\chi^2$ value	p-value	p-value (FDR)
<i>TFAP2B</i>	8	36.7	89.5	$3.60 \times 10^{-20}$	$8.37 \times 10^{-17}$
<i>ZNF423</i>	15	36.7	78.8	$7.89 \times 10^{-18}$	$1.22 \times 10^{-14}$
<i>CALCOCO1</i>	11	36.7	76.8	$2.09 \times 10^{-17}$	$2.59 \times 10^{-14}$
<i>RBM5</i>	13	36.7	75.7	$3.65 \times 10^{-17}$	$4.00 \times 10^{-14}$
<i>BTG2</i>	7	36.7	71.7	$2.72 \times 10^{-16}$	$1.81 \times 10^{-13}$
<i>RXRA</i>	6	36.7	70.5	$5.00 \times 10^{-16}$	$2.97 \times 10^{-13}$
<i>SLC27A1</i>	11	36.7	70.3	$5.42 \times 10^{-16}$	$2.97 \times 10^{-13}$
<i>MEF2D</i>	12	36.7	69.6	$7.86 \times 10^{-16}$	$3.95 \times 10^{-13}$
<i>NISCH</i>	12	36.7	69.6	$7.86 \times 10^{-16}$	$3.95 \times 10^{-13}$
<i>AVPR2</i>	9	36.7	69.2	$9.36 \times 10^{-16}$	$4.58 \times 10^{-13}$
<i>CRY2</i>	13	36.7	68.9	$1.07 \times 10^{-15}$	$4.98 \times 10^{-13}$
<i>RAPGEF3</i>	13	36.7	68.9	$1.07 \times 10^{-15}$	$4.98 \times 10^{-13}$
<i>NRIP2</i>	10	36.7	68.2	$1.58 \times 10^{-15}$	$7.18 \times 10^{-13}$
<i>DARC</i>	12	36.7	66.4	$3.76 \times 10^{-15}$	$1.54 \times 10^{-12}$
<i>SFRS5</i>	12	36.7	66.4	$3.76 \times 10^{-15}$	$1.54 \times 10^{-12}$
<i>NOSTRIN</i>	5	36.7	65.1	$7.40 \times 10^{-15}$	$2.70 \times 10^{-12}$
<i>KIF13B</i>	12	36.7	63.4	$1.69 \times 10^{-14}$	$5.16 \times 10^{-12}$
<i>TENC1</i>	10	36.7	62.5	$2.67 \times 10^{-14}$	$7.40 \times 10^{-12}$
<i>MFAP4</i>	12	36.7	60.5	$7.17 \times 10^{-14}$	$1.67 \times 10^{-11}$
<i>ELN</i>	13	36.7	59.7	$1.07 \times 10^{-13}$	$2.32 \times 10^{-11}$
<i>SGK223</i>	14	36.7	59	$1.51 \times 10^{-13}$	$3.05 \times 10^{-11}$
<i>KIF12</i>	11	36.7	58.8	$1.74 \times 10^{-13}$	$3.34 \times 10^{-11}$
<i>SELP</i>	11	36.7	58.8	$1.74 \times 10^{-13}$	$3.34 \times 10^{-11}$
<i>CIRBP</i>	9	36.7	58.7	$1.83 \times 10^{-13}$	$3.41 \times 10^{-11}$
<i>CTDSP1</i>	9	36.7	58.7	$1.83 \times 10^{-13}$	$3.41 \times 10^{-11}$

Strongest candidate [synthetic lethal](#) partners for *CDH1* by [mtSLIPT](#) in [TCGA](#) in breast cancer expression and mutation data

\* Observed and expected numbers of *CDH1* mutant [TCGA](#) breast tumours with low expression of partner genes

Table C.2: Pathways for *CDH1* partners from mtSLIPT

Pathways Over-represented	Pathway Size	SL Genes	p-value (FDR)
Eukaryotic Translation Elongation	86	60	$2.0 \times 10^{-128}$
Peptide chain elongation	83	59	$2.0 \times 10^{-128}$
Eukaryotic Translation Termination	83	58	$2.3 \times 10^{-125}$
Viral mRNA Translation	81	57	$2.5 \times 10^{-124}$
Nonsense Mediated Decay independent of the Exon Junction Complex	88	59	$8.6 \times 10^{-124}$
Nonsense-Mediated Decay	103	61	$5.2 \times 10^{-117}$
Nonsense Mediated Decay enhanced by the Exon Junction Complex	103	61	$5.2 \times 10^{-117}$
Formation of a pool of free 40S subunits	93	58	$1.6 \times 10^{-116}$
L13a-mediated translational silencing of Ceruloplasmin expression	103	59	$1.3 \times 10^{-111}$
3' -UTR-mediated translational regulation	103	59	$1.3 \times 10^{-111}$
GTP hydrolysis and joining of the 60S ribosomal subunit	104	59	$6.2 \times 10^{-111}$
SRP-dependent cotranslational protein targeting to membrane	104	58	$2.9 \times 10^{-108}$
Eukaryotic Translation Initiation	111	59	$3.0 \times 10^{-106}$
Cap-dependent Translation Initiation	111	59	$3.0 \times 10^{-106}$
Influenza Viral RNA Transcription and Replication	108	57	$5.1 \times 10^{-103}$
Influenza Infection	117	59	$1.5 \times 10^{-102}$
Translation	141	64	$3.7 \times 10^{-101}$
Influenza Life Cycle	112	57	$1.4 \times 10^{-100}$
GPCR downstream signalling	472	116	$1.0 \times 10^{-80}$
Hemostasis	422	105	$1.4 \times 10^{-78}$

Gene set over-representation analysis (hypergeometric test) for Reactome pathways in mtSLIPT partners for *CDH1*.

The genes and pathways identified in Tables C.1 and C.2 were derived from comparing the expression profiles of potential partners to the mutation status of *CDH1* (as shown in Figure 3.2). The following analysis was limited to the samples for which both expression and somatic mutation data were available from TCGA.

## C.2 Synthetic Lethal Expression Profiles

Similar to the analysis of synthetic lethal partners against low *CDH1* expression in 4.1.2, the partners detected from *CDH1* mutation were also examined for their expression profiles and the pathway composition of gene clusters. Hierarchical clustering was performed on mtSLIPT partners for *CDH1* as showing in Figure C.1. Overrepresentation for Reactome pathways for each of the gene clusters identified is given in Table C.3.

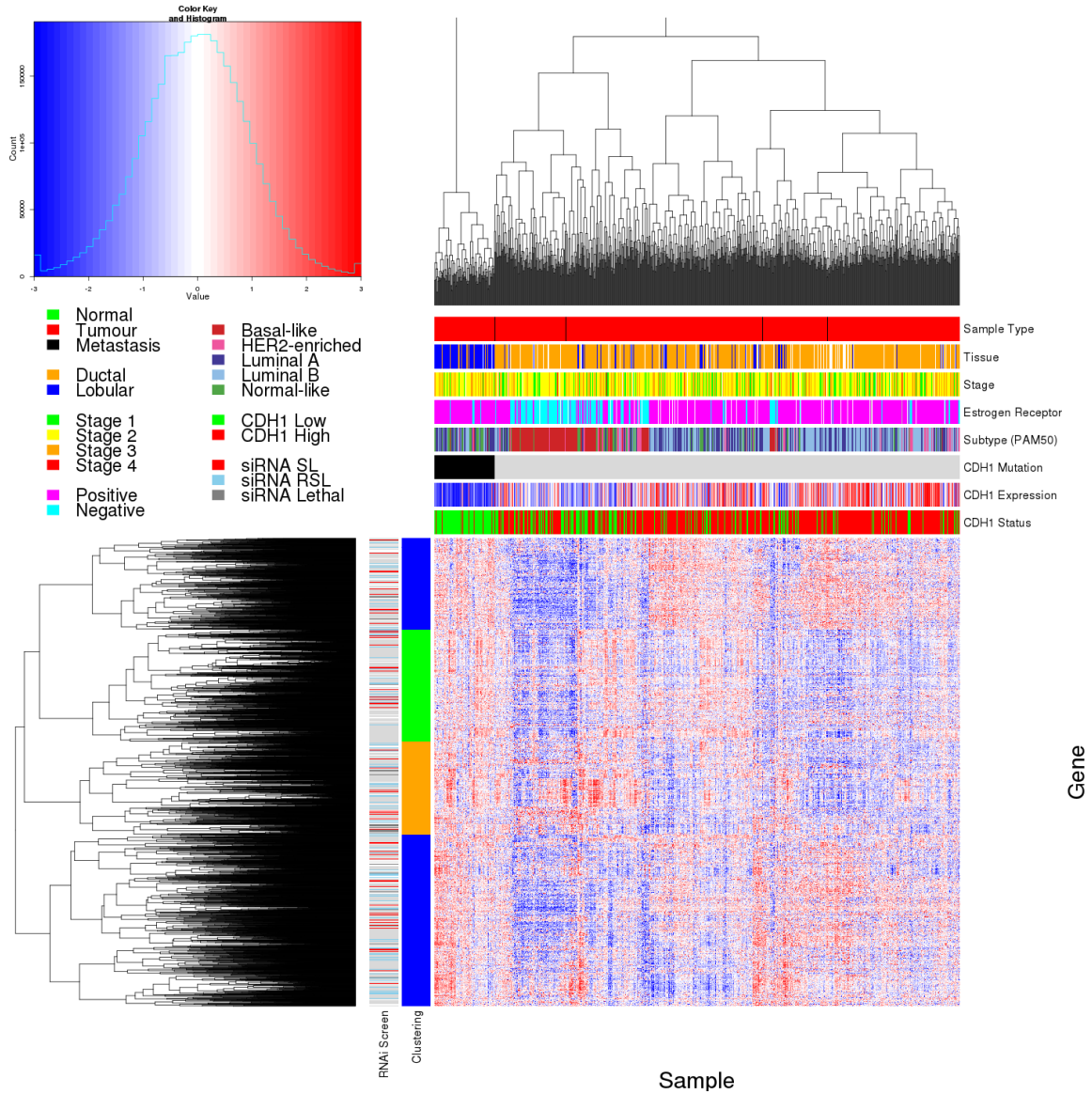


**Figure C.1: Synthetic lethal expression profiles of analysed samples.** Gene expression profile heatmap (correlation distance) of all samples (separated by *CDH1* somatic mutation status) analysed in **TCGA** breast cancer dataset for gene expression of 3743 candidate partners of **E-cadherin** (*CDH1*) from **mtSLIPT** prediction (with significant **FDR** adjusted  $p < 0.05$ ). Deeply clustered, inter-correlated genes form several main groups, each containing genes that were SL candidates or toxic in an **siRNA** screen [Telford et al. \(2015\)](#). Clusters had different sample groups highly expressing the synthetic lethal candidates in *CDH1* mutant samples and often lowly expressing *CDH1*wild-type samples (which were not tested for), although many of the *CDH1* mutant samples had among the lowest *CDH1* expression. In contrast to the expression analysis the (predominantly *CDH1*wild-type) basal subtype and **ER** negative samples have depleted expression among most candidate synthetic lethal partners.

Table C.3: Pathways for clusters of *CDH1* partners from mtSLIPT

Pathways Over-represented in Cluster 1	Pathway	Size	Cluster Genes	p-value (FDR)
Olfactory Signalling Pathway		57	8	$7.1 \times 10^{-9}$
Assembly of the primary cilium		149	14	$8.0 \times 10^{-9}$
Sphingolipid metabolism		62	8	$9.6 \times 10^{-9}$
Signalling by ERBB4		133	12	$5.1 \times 10^{-8}$
PI3K Cascade		65	7	$4.9 \times 10^{-7}$
Circadian Clock		33	5	$4.9 \times 10^{-7}$
Nuclear signalling by ERBB4		34	5	$4.9 \times 10^{-7}$
Intraflagellar transport		35	5	$4.9 \times 10^{-7}$
PI3K events in ERBB4 signalling		87	8	$4.9 \times 10^{-7}$
PIP3 activates AKT signalling		87	8	$4.9 \times 10^{-7}$
PI3K events in ERBB2 signalling		87	8	$4.9 \times 10^{-7}$
PI-3K cascade:FGFR1		87	8	$4.9 \times 10^{-7}$
PI-3K cascade:FGFR2		87	8	$4.9 \times 10^{-7}$
PI-3K cascade:FGFR3		87	8	$4.9 \times 10^{-7}$
PI-3K cascade:FGFR4		87	8	$4.9 \times 10^{-7}$
Deadenylation of mRNA		22	4	$5.6 \times 10^{-7}$
PI3K/AKT activation		90	8	$5.6 \times 10^{-7}$
Cargo trafficking to the periciliary membrane		38	5	$5.6 \times 10^{-7}$
Pathways Over-represented in Cluster 2	Pathway	Size	Cluster Genes	p-value (FDR)
G <sub>αs</sub> signalling events		83	19	$5.1 \times 10^{-25}$
Extracellular matrix organization		238	30	$1.4 \times 10^{-18}$
Hemostasis		422	46	$2.7 \times 10^{-16}$
Aquaporin-mediated transport		32	9	$2.7 \times 10^{-16}$
Transcriptional regulation of white adipocyte differentiation		56	11	$1.7 \times 10^{-15}$
Degradation of the extracellular matrix		102	15	$1.7 \times 10^{-15}$
Integration of energy metabolism		84	13	$8.8 \times 10^{-15}$
GPCR downstream signalling		472	48	$2.8 \times 10^{-14}$
G <sub>αx</sub> signalling events		15	6	$5.0 \times 10^{-14}$
Molecules associated with elastic fibres		33	8	$5.4 \times 10^{-14}$
Phase 1 - Functionalization of compounds		67	11	$5.6 \times 10^{-14}$
Platelet activation, signalling and aggregation		179	20	$5.6 \times 10^{-14}$
Vasopressin regulates renal water homeostasis via Aquaporins		24	7	$6.1 \times 10^{-14}$
Elastic fibre formation		37	8	$.03 \times 10^{-13}$
Calmodulin induced events		27	7	$3.3 \times 10^{-13}$
CaM pathway		27	7	$3.3 \times 10^{-13}$
cGMP effects		18	6	$3.6 \times 10^{-13}$
G <sub>αi</sub> signalling events		167	18	$6.3 \times 10^{-13}$
Pathways Over-represented in Cluster 3	Pathway	Size	Cluster Genes	p-value (FDR)
Eukaryotic Translation Elongation		86	55	$1.1 \times 10^{-112}$
Peptide chain elongation		83	54	$1.3 \times 10^{-112}$
Viral mRNA Translation		81	53	$1.6 \times 10^{-111}$
Eukaryotic Translation Termination		83	53	$7.1 \times 10^{-110}$
Nonsense Mediated Decay independent of the Exon Junction Complex		88	54	$1.0 \times 10^{-108}$
Formation of a pool of free 40S subunits		93	53	$4.1 \times 10^{-102}$
Nonsense-Mediated Decay		103	54	$3.9 \times 10^{-98}$
Nonsense Mediated Decay enhanced by the Exon Junction Complex		103	54	$3.9 \times 10^{-98}$
L13a-mediated translational silencing of Ceruloplasmin expression		103	53	$1.2 \times 10^{-95}$
3' -UTR-mediated translational regulation		103	53	$1.2 \times 10^{-95}$
SRP-dependent cotranslational protein targeting to membrane		104	53	$4.3 \times 10^{-95}$
GTP hydrolysis and joining of the 60S ribosomal subunit		104	53	$4.3 \times 10^{-95}$
Influenza Viral RNA Transcription and Replication		108	53	$9.6 \times 10^{-93}$
Eukaryotic Translation Initiation		111	53	$4.2 \times 10^{-91}$
Cap-dependent Translation Initiation		111	53	$4.2 \times 10^{-91}$
Influenza Life Cycle		112	53	$1.4 \times 10^{-90}$
Influenza Infection		117	53	$6.2 \times 10^{-88}$
Translation		141	55	$3 \times 10^{-81}$
Pathways Over-represented in Cluster 4	Pathway	Size	Cluster Genes	p-value (FDR)
ECM proteoglycans		66	10	$2.9 \times 10^{-11}$
deactivation of the beta-catenin transactivating complex		38	7	$5.1 \times 10^{-10}$
Arachidonic acid metabolism		41	7	$1.1 \times 10^{-9}$
G <sub>αq</sub> signalling events		149	14	$4.0 \times 10^{-9}$
HS-GAG degradation		21	5	$4.5 \times 10^{-9}$
Uptake and actions of bacterial toxins		22	5	$6.1 \times 10^{-9}$
Gastrin-CREB signalling pathway via PKC and MAPK		170	15	$6.1 \times 10^{-9}$
RNA Polymerase I, RNA Polymerase III, and Mitochondrial Transcription		64	8	$6.1 \times 10^{-9}$
Non-integrin membrane-ECM interactions		53	7	$1.5 \times 10^{-8}$
Syndecan interactions		25	5	$1.5 \times 10^{-8}$
NOTCH1 Intracellular Domain Regulates Transcription		40	6	$2.3 \times 10^{-8}$
Synthesis of Leukotrienes and Eoxins		15	4	$3.2 \times 10^{-8}$
Signalling by NOTCH1		59	7	$5.3 \times 10^{-8}$
Regulation of insulin secretion		44	6	$6.0 \times 10^{-8}$
Metabolism of lipids and lipoproteins		471	37	$8.2 \times 10^{-8}$
Signalling by NOTCH1		80	8	$1.2 \times 10^{-7}$
Platelet activation, signalling and aggregation		179	14	$1.2 \times 10^{-7}$
Recruitment of mitotic centrosome proteins and complexes		64	7	$1.2 \times 10^{-7}$

Pathway over-representation analysis for Reactome pathways with the number of genes in each pathway (Pathway Size), number of genes within the pathway identified (Cluster Genes), and the pathway over-representation p-value (adjusted by FDR) from the hypergeometric test.

### C.3 Comparison to Primary Screen

The mutation synthetic lethal partners with *CDH1* were also compared to [siRNA](#) primary screen data (Telford *et al.*, 2015), as performed in Section 4.2.1. These were expected to be more concordant with the experimental results performed on a null mutant, however this was not the case at the gene level: less genes overlapped with experimental candidates in Figure C.2. This discrepancy was may be due to lower sample size for mutations in [TCGA](#) data or lower frequency (expected value) of *CDH1* mutations compared to low expression.

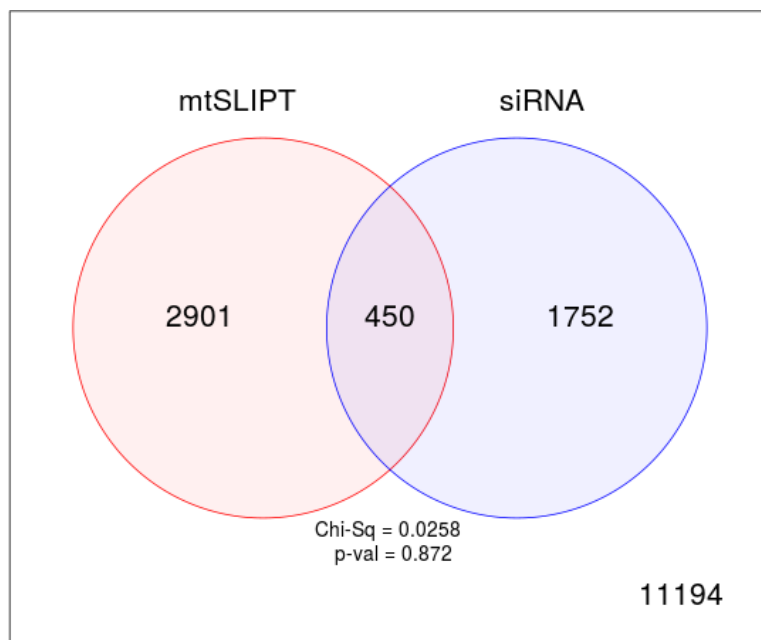


Figure C.2: **Comparison of mtSLIPT to siRNA.** Testing the overlap of gene candidates for [E-cadherin](#) synthetic lethal partners between computational (SLIPT) and experimental screening (siRNA) approaches. The  $\chi^2$  test suggests that the overlap is no more than would be expected by chance ( $p = 0.281$ ).

Despite a lower sample size (and low number of a predicted partners) for mutation analysis, the pathway composition (Tables C.2 and C.4) was similar to expression analysis, as described in Section 4.2.5. In particular, the resampling analysis (Section C.3.1) supported many of the results of expression analysis (Section 4.2.5.1). Tables C.5 and C.6 detected many of the same or functionally-related pathways.

Table C.4: Pathways for *CDH1* partners from mtSLIPT and siRNA

Predicted only by SLIPT (2901 genes)	Pathway	Size	Genes Identified	p-value (FDR)
Eukaryotic Translation Elongation		87	57	$2.8 \times 10^{-120}$
Peptide chain elongation		84	56	$3.1 \times 10^{-120}$
Eukaryotic Translation Termination		84	55	$2.8 \times 10^{-117}$
Viral mRNA Translation		82	54	$4.1 \times 10^{-116}$
Nonsense Mediated Decay independent of the Exon Junction Complex		89	55	$3.7 \times 10^{-113}$
Formation of a pool of free 40S subunits		94	55	$2.8 \times 10^{-109}$
Nonsense-Mediated Decay		104	57	$8.4 \times 10^{-108}$
Nonsense Mediated Decay enhanced by the Exon Junction Complex		104	57	$8.4 \times 10^{-108}$
L13a-mediated translational silencing of Ceruloplasmin expression		104	56	$3.4 \times 10^{-105}$
3' -UTR-mediated translational regulation		104	56	$3.4 \times 10^{-105}$
GTP hydrolysis and joining of the 60S ribosomal subunit		105	56	$1.4 \times 10^{-104}$
Eukaryotic Translation Initiation		112	56	$2.8 \times 10^{-100}$
Cap-dependent Translation Initiation		112	56	$2.8 \times 10^{-100}$
SRP-dependent cotranslational protein targeting to membrane		105	54	$2.2 \times 10^{-99}$
Influenza Viral RNA Transcription and Replication		109	54	$5.3 \times 10^{-97}$
Influenza Life Cycle		113	54	$9.6 \times 10^{-95}$
Influenza Infection		118	55	$1.7 \times 10^{-94}$
Translation		142	60	$3.5 \times 10^{-94}$
Infectious disease		349	77	$5.9 \times 10^{-62}$
Extracellular matrix organization		241	54	$3.0 \times 10^{-52}$

Detected only by siRNA screen (1752 genes)	Pathway	Size	Genes Identified	p-value (FDR)
Class A/1 (Rhodopsin-like receptors)		282	69	$1.9 \times 10^{-59}$
GPCR ligand binding		363	78	$2.7 \times 10^{-54}$
Peptide ligand-binding receptors		175	41	$1.5 \times 10^{-42}$
$G_{\alpha i}$ signalling events		184	41	$1.1 \times 10^{-40}$
Gastrin-CREB signalling pathway via PKC and MAPK		180	37	$1.5 \times 10^{-35}$
$G_{\alpha q}$ signalling events		159	34	$3.7 \times 10^{-35}$
DAP12 interactions		159	27	$1.1 \times 10^{-24}$
VEGFA-VEGFR2 Pathway		91	19	$1.0 \times 10^{-23}$
Downstream signal transduction		146	24	$1.9 \times 10^{-22}$
Signalling by VEGF		99	19	$2.6 \times 10^{-22}$
DAP12 signalling		149	24	$4.2 \times 10^{-22}$
Organelle biogenesis and maintenance		264	34	$4.3 \times 10^{-20}$
Downstream signalling of activated FGFR1		134	21	$4.3 \times 10^{-20}$
Downstream signalling of activated FGFR2		134	21	$4.3 \times 10^{-20}$
Downstream signalling of activated FGFR3		134	21	$4.3 \times 10^{-20}$
Downstream signalling of activated FGFR4		134	21	$4.3 \times 10^{-20}$
Signalling by ERBB2		146	22	$5.3 \times 10^{-20}$
Signalling by FGFR		146	22	$5.3 \times 10^{-20}$
Signalling by FGFR1		146	22	$5.3 \times 10^{-20}$
Signalling by FGFR2		146	22	$5.3 \times 10^{-20}$

Intersection of SLIPT and siRNA screen (450 genes)	Pathway	Size	Genes Identified	p-value (FDR)
HS-GAG degradation		21	4	$4.9 \times 10^{-6}$
Retinoid metabolism and transport		39	5	$4.9 \times 10^{-6}$
Platelet activation, signalling and aggregation		186	13	$4.9 \times 10^{-6}$
Signalling by NOTCH4		11	3	$4.9 \times 10^{-6}$
$G_{\alpha s}$ signalling events		100	8	$5.0 \times 10^{-6}$
Defective EXT2 causes exostoses 2		12	3	$5.0 \times 10^{-6}$
Defective EXT1 causes exostoses 1, TRPS2 and CHDS		12	3	$5.0 \times 10^{-6}$
Class A/1 (Rhodopsin-like receptors)		289	18	$2.2 \times 10^{-5}$
Signalling by PDGF		173	11	$2.9 \times 10^{-5}$
Circadian Clock		34	4	$2.9 \times 10^{-5}$
Signalling by ERBB4		139	9	$4.3 \times 10^{-5}$
Role of LAT2/NTAL/LAB on calcium mobilization		99	7	$4.4 \times 10^{-5}$
Peptide ligand-binding receptors		181	11	$4.5 \times 10^{-5}$
Defective B4GALT7 causes EDS, progeroid type		19	3	$4.5 \times 10^{-5}$
Defective B3GAT3 causes JDSSDHD		19	3	$4.5 \times 10^{-5}$
Signalling by NOTCH		80	6	$4.5 \times 10^{-5}$
$G_{\alpha q}$ signalling events		164	10	$5.1 \times 10^{-5}$
Response to elevated platelet cytosolic $\text{Ca}^{2+}$		84	6	$7.1 \times 10^{-5}$
Signalling by ERBB2		148	9	$7.1 \times 10^{-5}$
Signalling by SCF-KIT		129	8	$8.3 \times 10^{-5}$

### C.3.1 Resampling Analysis

Table C.5: Pathways for *CDH1* partners from mtSLIPT

Reactome Pathway	Over-representation	Permutation
<b>Eukaryotic Translation Elongation</b>	$3.2 \times 10^{-128}$	$< 7.035 \times 10^{-4}$
Peptide chain elongation	$3.2 \times 10^{-128}$	$< 7.035 \times 10^{-4}$
<b>Eukaryotic Translation Termination</b>	$3.7 \times 10^{-125}$	$< 7.035 \times 10^{-4}$
Viral mRNA Translation	$4.1 \times 10^{-124}$	$< 7.035 \times 10^{-4}$
Nonsense Mediated Decay independent of the Exon Junction Complex	$1.4 \times 10^{-123}$	$< 7.035 \times 10^{-4}$
Nonsense-Mediated Decay	$8.4 \times 10^{-117}$	$< 7.035 \times 10^{-4}$
Nonsense Mediated Decay enhanced by the Exon Junction Complex	$8.4 \times 10^{-117}$	$< 7.035 \times 10^{-4}$
Formation of a pool of free 40S subunits	$2.6 \times 10^{-116}$	$< 7.035 \times 10^{-4}$
L13a-mediated translational silencing of Ceruloplasmin expression	$2.0 \times 10^{-111}$	$< 7.035 \times 10^{-4}$
3' -UTR-mediated translational regulation	$2.0 \times 10^{-111}$	$< 7.035 \times 10^{-4}$
GTP hydrolysis and joining of the 60S ribosomal subunit	$9.9 \times 10^{-111}$	$< 7.035 \times 10^{-4}$
SRP-dependent cotranslational protein targeting to membrane	$4.7 \times 10^{-108}$	$< 7.035 \times 10^{-4}$
<b>Eukaryotic Translation Initiation</b>	$4.8 \times 10^{-106}$	$< 7.035 \times 10^{-4}$
Cap-dependent Translation Initiation	$4.8 \times 10^{-106}$	$< 7.035 \times 10^{-4}$
<b>Influenza Viral RNA Transcription and Replication</b>	$8.1 \times 10^{-103}$	$< 7.035 \times 10^{-4}$
<b>Influenza Infection</b>	$2.4 \times 10^{-102}$	$< 7.035 \times 10^{-4}$
<b>Translation</b>	$6.0 \times 10^{-101}$	$< 7.035 \times 10^{-4}$
<b>Influenza Life Cycle</b>	$2.2 \times 10^{-100}$	$< 7.035 \times 10^{-4}$
<b>Disease</b>	$2.1 \times 10^{-90}$	0.013347
<b>GPCR downstream signalling</b>	$1.6 \times 10^{-80}$	0.095478
Hemostasis	$2.1 \times 10^{-78}$	0.2671
Signalling by GPCR	$1.2 \times 10^{-73}$	0.44939
<i>Extracellular matrix organization</i>	$2.2 \times 10^{-67}$	0.054008
Metabolism of proteins	$1.4 \times 10^{-66}$	0.9607
Signal Transduction	$2.1 \times 10^{-66}$	0.48184
Developmental Biology	$2.5 \times 10^{-66}$	0.54075
Innate Immune System	$5.3 \times 10^{-66}$	0.9589
Infectious disease	$9.6 \times 10^{-66}$	0.21075
Signalling by NGF	$1.1 \times 10^{-62}$	0.43356
Immune System	$2.8 \times 10^{-62}$	0.23052

Over-representation (hypergeometric test) and Permutation p-values adjusted for multiple tests across pathways (**FDR**). Significant pathways were marked in bold (**FDR** < 0.05) and italics (**FDR** < 0.1).

Table C.6: Pathways for *CDH1* partners from mtSLIPT and siRNA primary screen

Reactome Pathway	Over-representation	Permutation
Visual phototransduction	$1.2 \times 10^{-9}$	0.86279
<b>G<sub>as</sub> signalling events</b>	$2.9 \times 10^{-7}$	0.023066
Retinoid metabolism and transport	$2.9 \times 10^{-7}$	0.299
Acylic chain remodelling of PS	$1.1 \times 10^{-5}$	0.42584
Transcriptional regulation of white adipocyte differentiation	$1.1 \times 10^{-5}$	0.53928
Chemokine receptors bind chemokines	$1.1 \times 10^{-5}$	0.95259
<i>Signalling by NOTCH4</i>	$1.2 \times 10^{-5}$	0.079229
Defective EXT2 causes exostoses 2	$1.2 \times 10^{-5}$	0.22292
Defective EXT1 causes exostoses 1, TRPS2 and CHDS	$1.2 \times 10^{-5}$	0.22292
Platelet activation, signalling and aggregation	$1.2 \times 10^{-5}$	0.48853
Serotonin receptors	$1.4 \times 10^{-5}$	0.34596
Nicotinamide salvaging	$1.4 \times 10^{-5}$	0.70881
Phase 1 - Functionalization of compounds	$2 \times 10^{-5}$	0.31142
Amine ligand-binding receptors	$2.5 \times 10^{-5}$	0.34934
Acylic chain remodelling of PE	$3.8 \times 10^{-5}$	0.42615
Signalling by GPCR	$3.8 \times 10^{-5}$	0.93888
<b>Molecules associated with elastic fibres</b>	$3.9 \times 10^{-5}$	0.017982
DAP12 interactions	$3.9 \times 10^{-5}$	0.71983
Beta defensins	$3.9 \times 10^{-5}$	0.91458
Cytochrome P <sub>450</sub> - arranged by substrate type	$4.7 \times 10^{-5}$	0.83493
GPCR ligand binding	$5.7 \times 10^{-5}$	0.95258
Acylic chain remodelling of PC	$6.1 \times 10^{-5}$	0.42584
Response to elevated platelet cytosolic Ca <sup>2+</sup>	$6.4 \times 10^{-5}$	0.54046
<b>Arachidonic acid metabolism</b>	$6.7 \times 10^{-5}$	0.026696
Defective B4GALT7 causes EDS, progeroid type	$7.3 \times 10^{-5}$	0.24921
Defective B3GAT3 causes JDSSDHD	$7.3 \times 10^{-5}$	0.24921
Hydrolysis of LPC	$7.3 \times 10^{-5}$	0.80663
<b>Elastic fibre formation</b>	$7.4 \times 10^{-5}$	0.0058768
<b>HS-GAG degradation</b>	$9.4 \times 10^{-5}$	0.0083179
<i>Bile acid and bile salt metabolism</i>	$9.4 \times 10^{-5}$	0.079905
Netrin-1 signalling	0.00011	0.92216
<b>Integration of energy metabolism</b>	0.00011	0.011152
Dectin-2 family	0.00012	0.10385
Platelet sensitization by LDL	0.00012	0.34596
DAP12 signalling	0.00012	0.62787
Defensins	0.00012	0.77542
GPCR downstream signalling	0.00012	0.79454
<i>Diseases associated with glycosaminoglycan metabolism</i>	0.00013	0.065927
<i>Diseases of glycosylation</i>	0.00013	0.065927
Signalling by Retinoic Acid	0.00013	0.22292
Signalling by Leptin	0.00013	0.34596
Signalling by SCF-KIT	0.00013	0.70881
Opioid Signalling	0.00013	0.96053
Signalling by NOTCH	0.00015	0.26884
Platelet homeostasis	0.00015	0.4878
Signalling by NOTCH1	0.00016	0.13043
Class B/2 (Secretin family receptors)	0.00016	0.13994
<i>Diseases of Immune System</i>	0.0002	0.0795
<i>Diseases associated with the TLR signalling cascade</i>	0.0002	0.0795
A tetrasaccharide linker sequence is required for GAG synthesis	0.0002	0.42615

Over-representation (hypergeometric test) and Permutation p-values adjusted for multiple tests across pathways (**FDR**). Significant pathways were marked in bold (**FDR** < 0.05) and italics (**FDR** < 0.1).

## C.4 Compare SLIPT genes

The mutation synthetic lethal partners with *CDH1* were also compared to siRNA primary screen data (Telford *et al.*, 2015), by correlation and siRNA viability as described in sections 4.2.2 and 4.2.3.

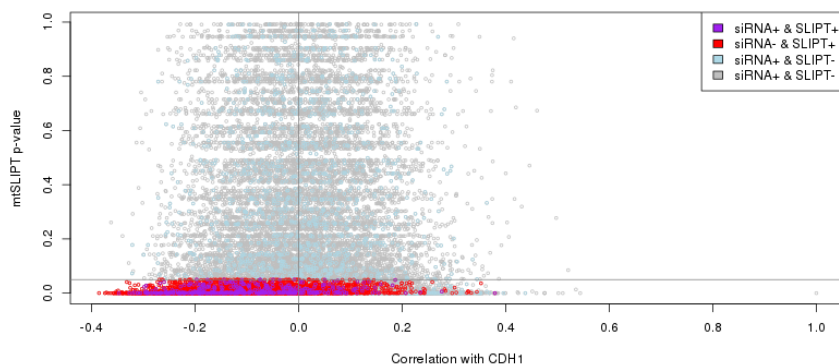


Figure C.3: **Compare mtSLIPT and siRNA genes with correlation.** The mtSLIPT p-values were compared against Pearson correlation of expression with *CDH1*. Genes detected by SLIPT or siRNA were coloured according to the legend.

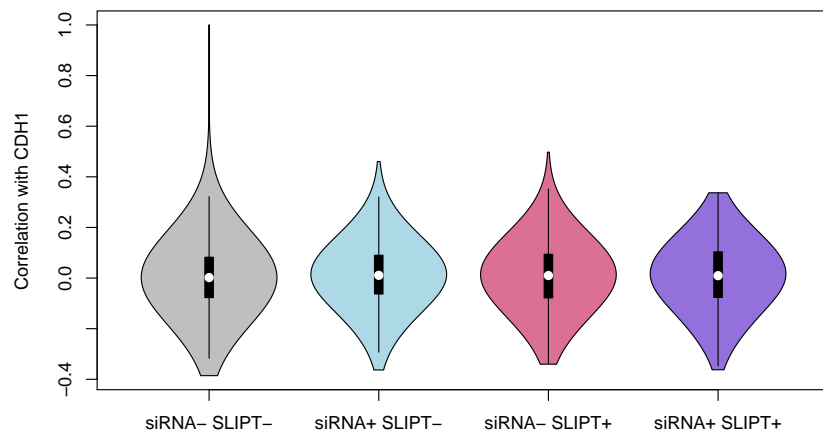
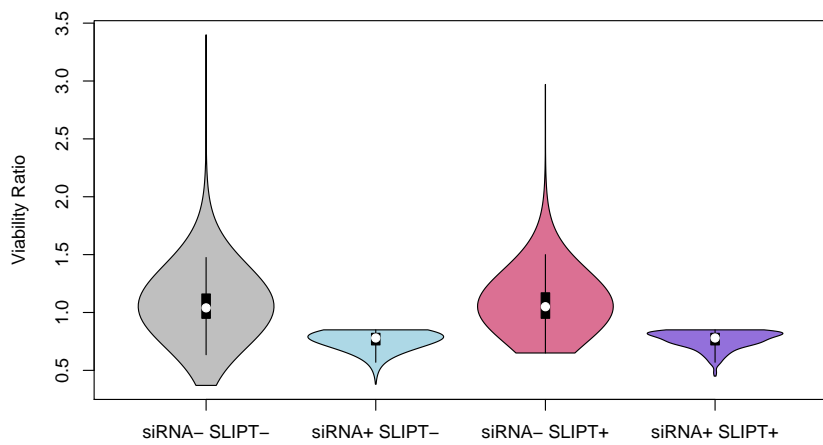


Figure C.4: **Compare mtSLIPT and siRNA genes with correlation.** Genes detected by mtSLIPT against *CDH1* mutation and siRNA screening were compared against Pearson correlation of expression with *CDH1*. There were no differences in correlation between the gene groups.



**Figure C.5: Compare mtSLIPT and siRNA genes with siRNA viability.** Genes detected as candidate synthetic lethal partners by mtSLIPT (in TCGA breast cancer) expression analysis against *CDH1* mutation and experimental screening (with siRNA) were compared against the viability ratio of *CDH1* mutant and wild-type cells in the primary siRNA screen. There were clear no differences in viability between genes detected by mtSLIPT and those not with the differences being primarily due to viability thresholds that were used to detect synthetic lethality by Telford *et al.* (2015).

## C.5 Metagene Analysis

Metagene analysis was performed for synthetic lethal pathways against *CDH1* mutation. These were described and compared to expression analysis in Section 4.3.3.

Table C.7: Candidate synthetic lethal metagenes against *CDH1* from mtSLIPT

Pathway	ID	Observed	Expected	$\chi^2$ value	p-value	p-value (FDR)
Neurotoxicity of clostridium toxins	168799	8	36.7	79.4	$5.71 \times 10^{-18}$	$3.14 \times 10^{-15}$
Aquaporin-mediated transport	445717	8	36.7	76.3	$2.73 \times 10^{-17}$	$9.01 \times 10^{-15}$
Toxicity of botulinum toxin type G (BoNT/G)	5250989	8	36.7	76.3	$2.73 \times 10^{-17}$	$9.01 \times 10^{-15}$
ABC-family proteins mediated transport	382556	10	36.7	68.2	$1.58 \times 10^{-15}$	$1.86 \times 10^{-13}$
G <sub>αz</sub> signalling events	418597	10	36.7	59.9	$9.97 \times 10^{-14}$	$5.48 \times 10^{-12}$
Regulation of IGF transport and uptake by IGFBPs	381426	9	36.7	56.3	$5.88 \times 10^{-13}$	$2.11 \times 10^{-11}$
GP1b-IX-V activation signalling	430116	8	36.7	55.7	$8.20 \times 10^{-13}$	$2.76 \times 10^{-11}$
GABA receptor activation	977443	12	36.7	55.1	$1.07 \times 10^{-12}$	$3.26 \times 10^{-11}$
Vasopressin regulates renal water homeostasis via Aquaporins	432040	9	36.7	54.1	$1.77 \times 10^{-12}$	$4.88 \times 10^{-11}$
Toxicity of botulinum toxin type D (BoNT/D)	5250955	14	36.7	53.4	$2.54 \times 10^{-12}$	$6.64 \times 10^{-11}$
Toxicity of botulinum toxin type F (BoNT/F)	5250981	14	36.7	53.4	$2.54 \times 10^{-12}$	$6.64 \times 10^{-11}$
STAT6-mediated induction of chemokines	3249367	16	36.7	52.2	$4.72 \times 10^{-12}$	$1.13 \times 10^{-10}$
Toxicity of botulinum toxin type B (BoNT/B)	5250958	14	36.7	50.8	$9.5 \times 10^{-12}$	$1.98 \times 10^{-10}$
S6K1 signalling	165720	12	36.7	50.2	$1.24 \times 10^{-11}$	$2.5 \times 10^{-10}$
G <sub>αs</sub> signalling events	418555	11	36.7	49.2	$2.08 \times 10^{-11}$	$3.85 \times 10^{-10}$
RHO GTPases activate CIT	5625900	14	36.7	48.2	$3.34 \times 10^{-11}$	$5.9 \times 10^{-10}$
NADE modulates death signalling	205025	15	36.7	47.4	$5.00 \times 10^{-11}$	$8.32 \times 10^{-10}$
Keratan sulfate degradation	2022857	10	36.7	46.6	$7.5 \times 10^{-11}$	$1.15 \times 10^{-9}$
Signalling by Retinoic Acid	5362517	10	36.7	46.6	$7.5 \times 10^{-11}$	$1.15 \times 10^{-9}$
Adenylate cyclase inhibitory pathway	170670	14	36.7	45.9	$1.11 \times 10^{-10}$	$1.59 \times 10^{-9}$
Inhibition of adenylate cyclase pathway	997269	14	36.7	45.9	$1.11 \times 10^{-10}$	$1.59 \times 10^{-9}$
Fatty acids	211935	6	36.7	45.7	$1.21 \times 10^{-10}$	$1.72 \times 10^{-9}$
Ionotropic activity of Kainate Receptors	451306	13	36.7	44.6	$2.03 \times 10^{-10}$	$2.58 \times 10^{-9}$
Activation of Ca-permeable Kainate Receptor	451308	13	36.7	44.6	$2.03 \times 10^{-10}$	$2.58 \times 10^{-9}$
RA biosynthesis pathway	5365859	13	36.7	44.6	$2.03 \times 10^{-10}$	$2.58 \times 10^{-9}$

Strongest candidate synthetic lethal partners for *CDH1* by mtSLIPT with observed and expected numbers of mutant *CDH1* TCGA breast cancer tumours with low expression of partner metagenes.

## C.6 Expression of Somatic Mutations

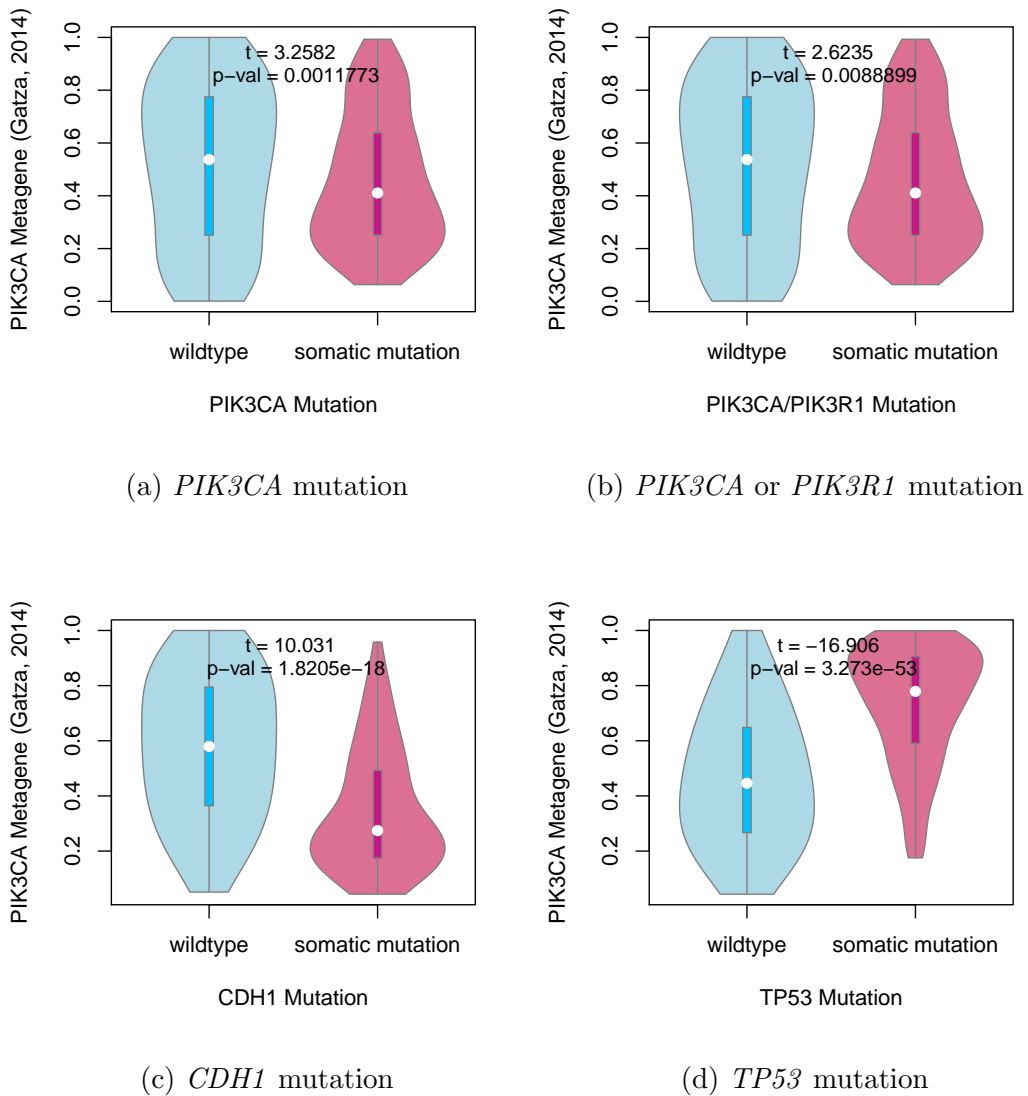
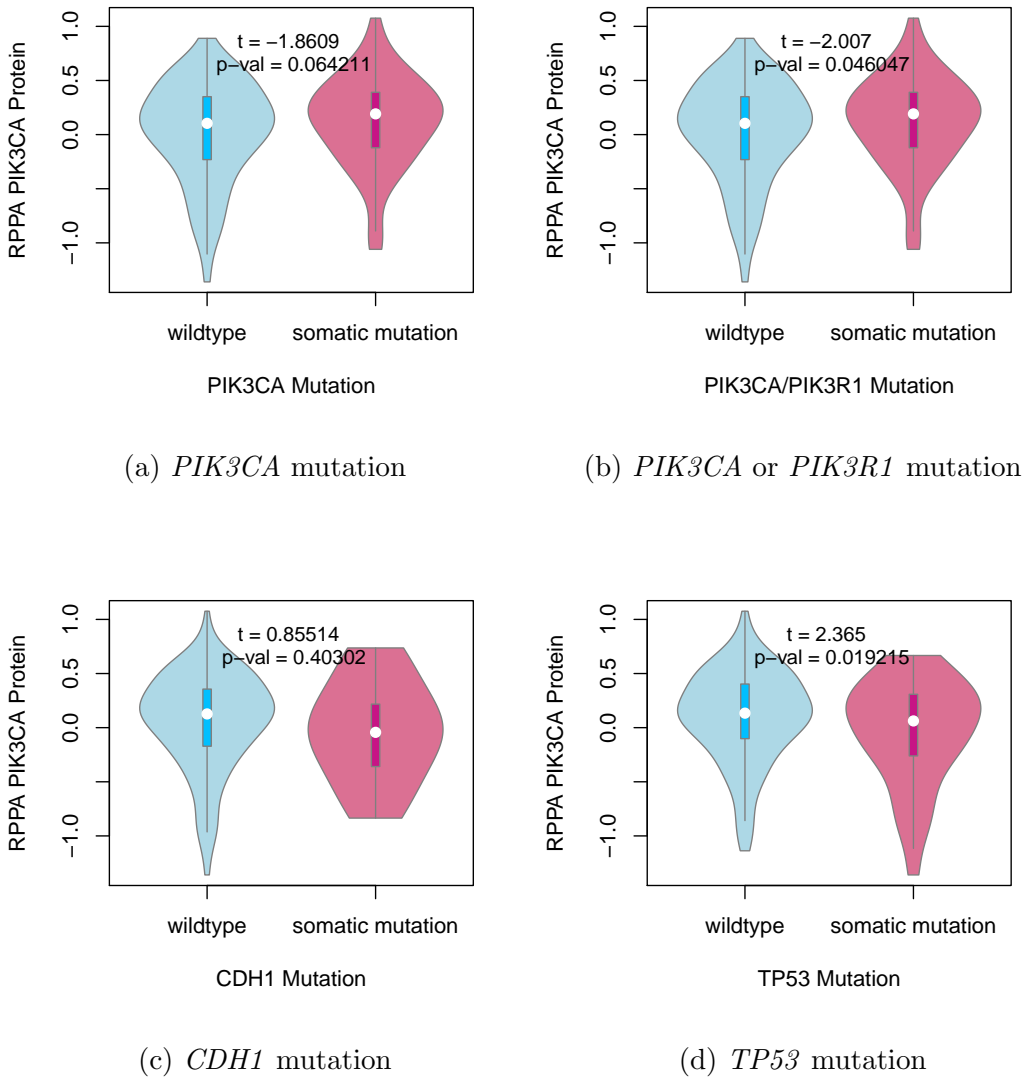
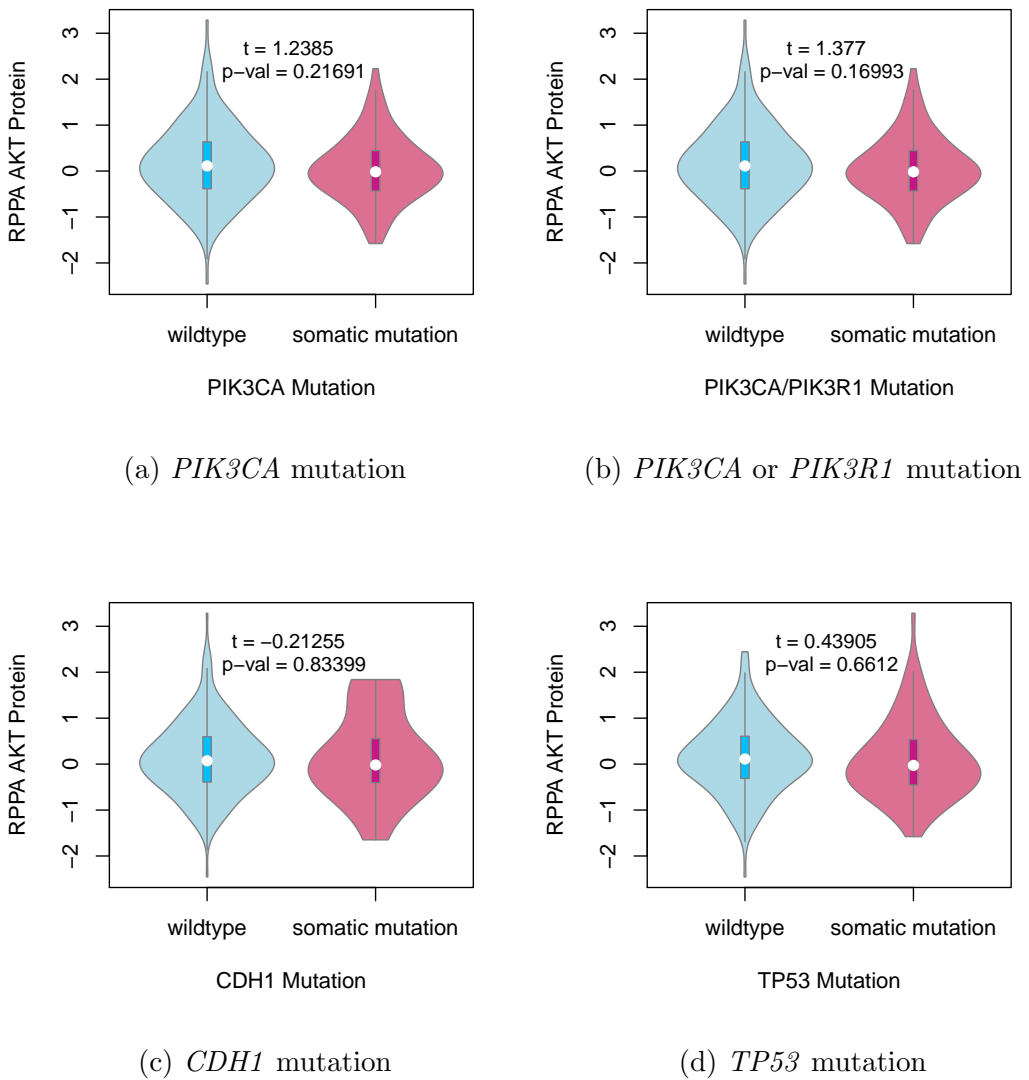


Figure C.6: **Somatic mutation against PIK3CA metagene.** Mutations in *PIK3CA*, *PIK3R1*, *CDH1*, and *TP53* were examined in [TCGA](#) breast cancer for their effect on the PIK3CA (Gatza *et al.*, 2014) pathway metagene. The tumour suppressors *CDH1* and *TP53* showed an increase and decrease in the metagene respectively, whereas *PIK3CA* and *PIK3R1* mutations weaker evidence of decrease in metagene levels.



**Figure C.7: Somatic mutation against PI3K protein.** Mutations in *PIK3CA*, *PIK3R1*, *CDH1*, and *TP53* were examined in TCGA breast cancer for their effect on the expression of the p110 $\alpha$  protein (encoded by *PIK3CA*). Protein levels were significantly elevated in samples with *PIK3CA* or *PIK3R1* mutations and lower in samples with *TP53* mutations.



**Figure C.8: Somatic mutation against AKT protein.** Mutations in *PIK3CA*, *PIK3R1*, *CDH1*, and *TP53* were examined in TCGA breast cancer for their effect on the expression of the AKT protein (a downstream target of *PIK3CA*). Protein levels were not significantly different in samples mutations in any of these cancer genes.

## C.7 Metagene Expression Profiles

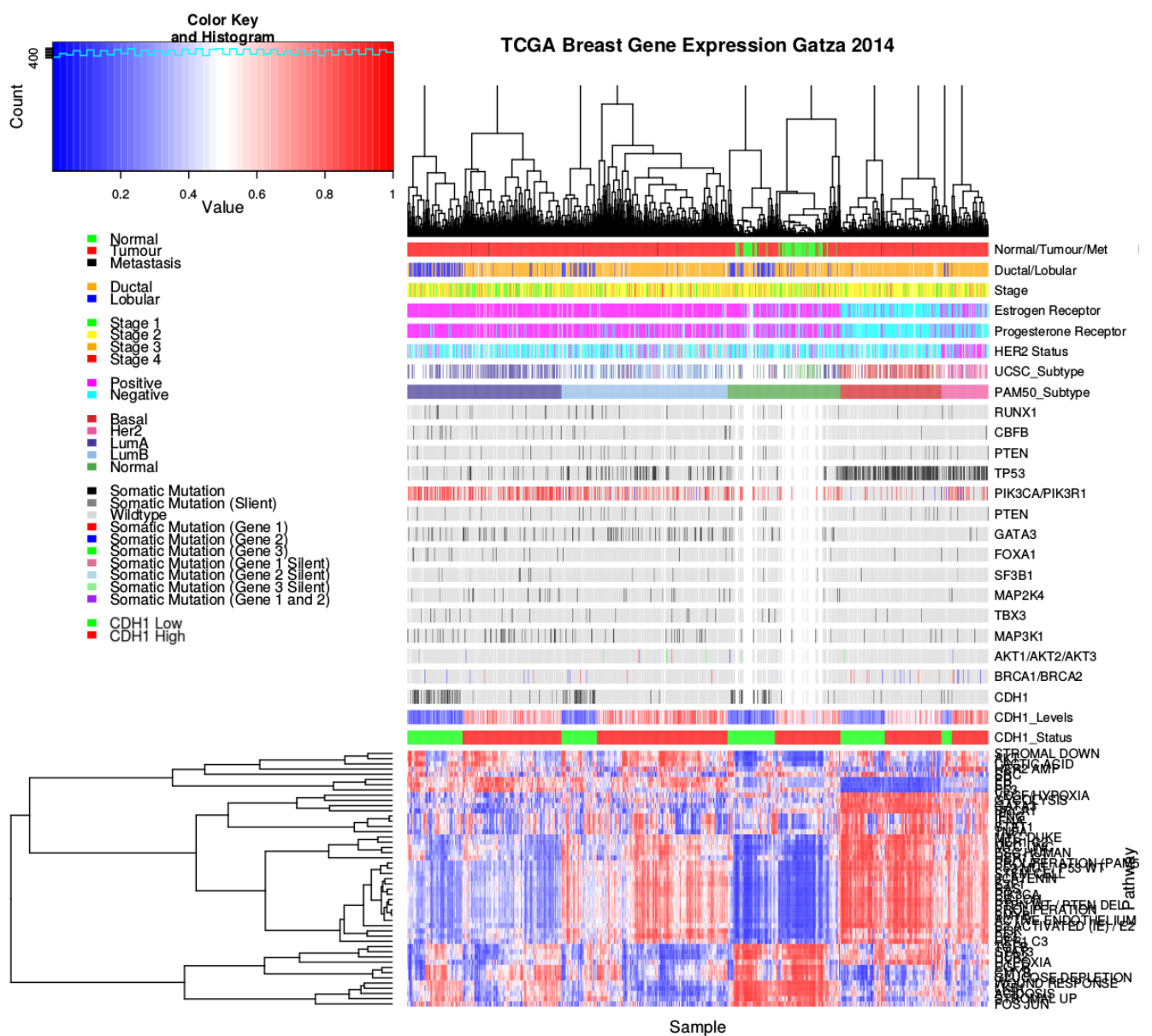
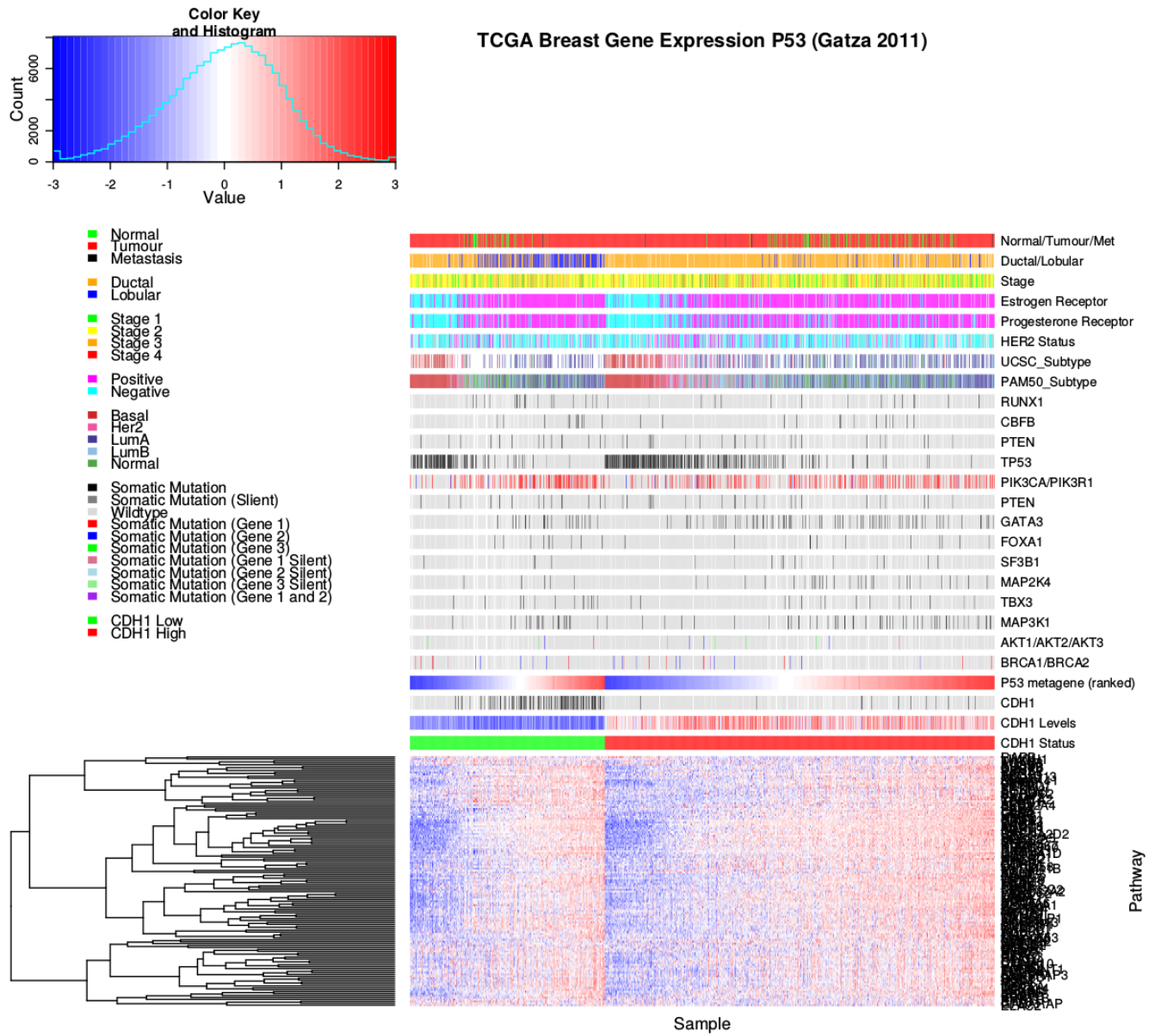


Figure C.9: **Pathway metagene expression profiles.** Expression profiles for metagene signatures from [Gatza et al. \(2014\)](#) in [TCGA](#) breast data, annotated for clinical factors and cancer gene mutations.



**Figure C.10: Expression profiles for p53 related genes.** Expression profiles the genes contained in the *TP53* gene signature from [Gatza et al. \(2011\)](#) in TCGA breast data, annotated for clinical factors and cancer gene mutations. Samples were separated by *CDH1* expression status and sorted by the metagene. In both cases, the majority of genes were consistent with the direction of the metagene, with few very exceptions. *TP53* mutant samples had low metagene expression, consistent with loss of tumour suppressor functions, and were less likely to have *CDH1* or *PIK3CA* mutations.

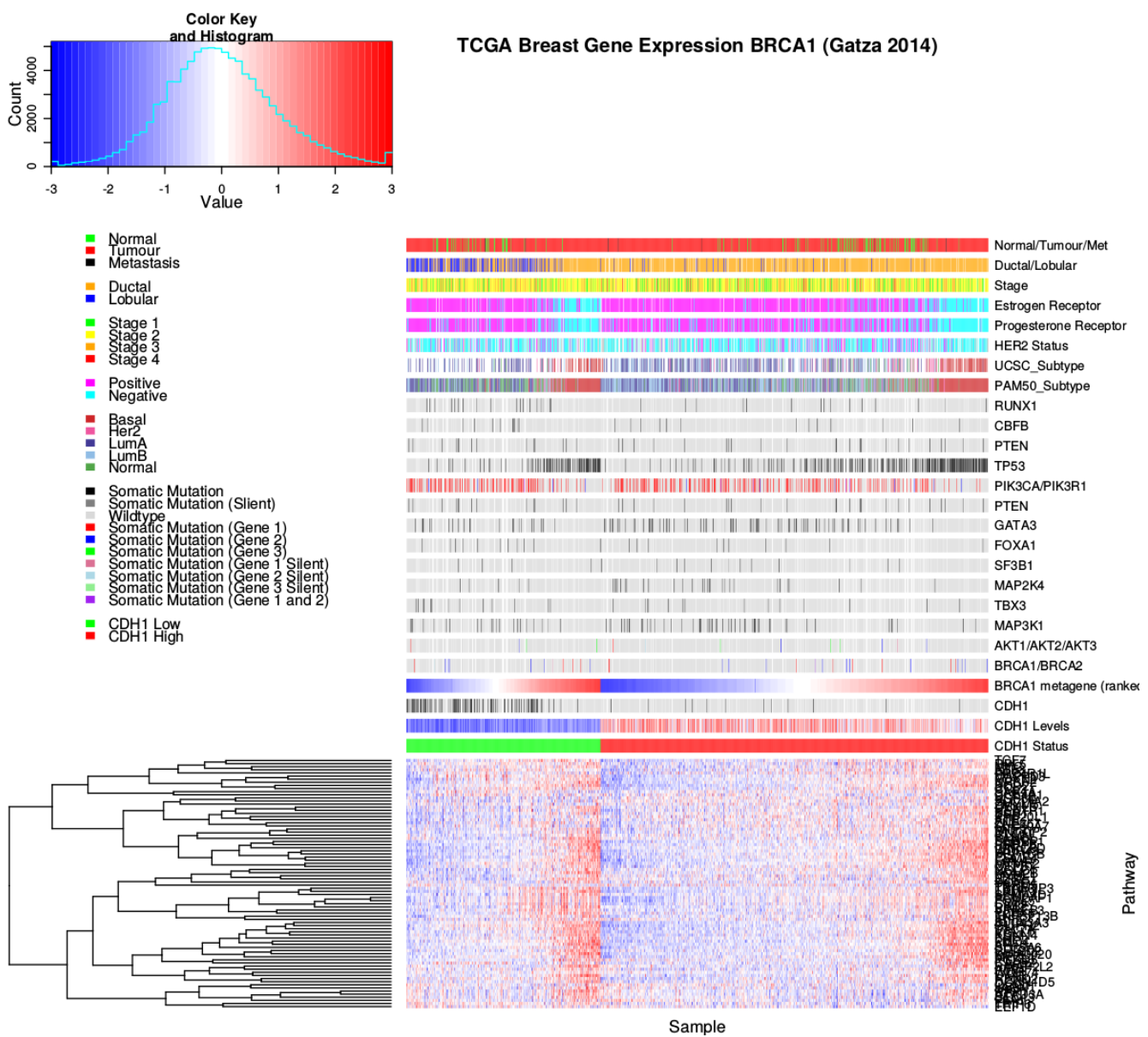


Figure C.11: **Expression profiles for BRCA related genes.** Expression profiles the genes contained in the gene signature related to *BRCA1* and *BRCA2* functions from [Gatza et al. \(2014\)](#) in **TCGA** breast data, annotated for clinical factors and cancer gene mutations. Samples were separated by *CDH1* expression status and sorted by the metagene. In both cases, the majority of genes were consistent with the direction of the metagene, with few very exceptions. *BRCA1* and *BRCA2* mutant samples had higher metagene expression than most samples for the ductal subtype, although this was not the case (for the lobular samples for which the metagene was lower). However, the metagene was higher for basal subtype and **ER** negative samples.

# Appendix D

## Intrinsic Subtyping

The intrinsic subtypes for [TCGA](#) breast cancer samples provided by [UCSC](#) ([Koboldt et al., 2012](#); [UCSC, 2012](#)) that were derived from microarray analysis have been compared to the [PAM50](#) results for performing subtyping from [RNA-Seq](#) data ([Parker et al., 2009](#)). As shown in Table D.1, these subtypes were highly concordant for samples which had both procedures performed upon them ( $\chi^2 = 1305.9, p = 2.73 \times 10^{-268}$ ). The main exception were the luminal A samples some of which were reclassified as luminal B or “normal-like”.

Table D.1: Comparison of intrinsic subtypes

UCSC Subtype					
	Basal-like	HER2-enriched	Luminal A	Luminal B	Normal-like
	100	58	232	128	30

PAM50 Subtype					
	Basal-like	HER2-enriched	Luminal A	Luminal B	Normal-like
	208	94	314	334	227

UCSC Subtype					
PAM50 Subtype	Basal-like	HER2-enriched	Luminal A	Luminal B	Normal-like
Basal-like	96	4	2	2	1
HER2-enriched	0	47	5	3	0
Luminal A	1	0	141	1	0
Luminal B	2	7	49	121	0
Normal-like	1	0	35	1	29

The intrinsic subtypes of [TCGA](#) breast samples were compared between those provided by [UCSC](#) ([Koboldt et al., 2012](#)) from microarray expression to those derived from [RNA-Seq](#) data ([Parker et al., 2009](#)). Comparisons between these were limited to samples for which both data types were available.

The PAM50 subtypes could be more accurate given similarity of these subtypes and

that the remainder of the subtypes were accurately recapitulated with **RNA-Seq** data. Furthermore, **UCSC** subtypes correctly identified 22/22 normal samples as “normal-like” and **PAM50** subtyping in **RNA-Seq** data had a success rate of 112/113 (including all of those identified from microarrays). Therefore the **PAM50** subtypes (performed on a larger cohort of samples) are appropriate to use for further interpretation, superseding the **UCSC** subtypes available for a limited set of samples.

# Appendix E

## Stomach Expression Analysis

The following results are a replication of the [TCGA](#) results (in Chapter 4) with stomach cancer data, using synthetic lethality (SLIPT) against *CDH1*.

### E.1 Synthetic Lethal Genes and Pathways

Table E.1: Synthetic lethal gene partners of *CDH1* from SLIPT in stomach cancer

Gene	Observed*	Expected*	$\chi^2$ value	p-value	p-value ( <a href="#">FDR</a> )
<i>PRAF2</i>	17	50.4	121	$3.54 \times 10^{-25}$	$1.45 \times 10^{-21}$
<i>EMP3</i>	17	50.4	115	$5.06 \times 10^{-24}$	$1.48 \times 10^{-20}$
<i>PLEKHO1</i>	22	50.4	112	$2.14 \times 10^{-23}$	$4.75 \times 10^{-20}$
<i>SELM</i>	20	50.4	111	$5.13 \times 10^{-23}$	$8.09 \times 10^{-20}$
<i>GYPC</i>	20	50.4	110	$5.77 \times 10^{-23}$	$8.45 \times 10^{-20}$
<i>COX7A1</i>	18	50.4	109	$1.15 \times 10^{-22}$	$1.39 \times 10^{-19}$
<i>TNFSF12</i>	20	50.4	106	$4.06 \times 10^{-22}$	$4.38 \times 10^{-19}$
<i>SEPT4</i>	17	50.4	106	$6.58 \times 10^{-22}$	$5.91 \times 10^{-19}$
<i>LGALS1</i>	19	50.4	105	$6.64 \times 10^{-22}$	$5.91 \times 10^{-19}$
<i>RARRES2</i>	27	50.4	105	$8.02 \times 10^{-22}$	$6.85 \times 10^{-19}$
<i>VEGFB</i>	16	50.4	104	$1.19 \times 10^{-21}$	$9.74 \times 10^{-19}$
<i>PRR24</i>	22	50.4	102	$2.96 \times 10^{-21}$	$2.02 \times 10^{-18}$
<i>SYNC</i>	19	50.4	102	$3.73 \times 10^{-21}$	$2.39 \times 10^{-18}$
<i>MAGEH1</i>	17	50.4	100	$9.52 \times 10^{-21}$	$5.01 \times 10^{-18}$
<i>HSPB2</i>	23	50.4	99.6	$1.19 \times 10^{-20}$	$5.82 \times 10^{-18}$
<i>SMARCD3</i>	19	50.4	99	$1.59 \times 10^{-20}$	$7.57 \times 10^{-18}$
<i>CREM</i>	13	50.4	98.1	$2.48 \times 10^{-20}$	$1.13 \times 10^{-17}$
<i>GNG11</i>	20	50.4	97.3	$3.68 \times 10^{-20}$	$1.59 \times 10^{-17}$
<i>GNAI2</i>	17	50.4	96.4	$5.75 \times 10^{-20}$	$2.36 \times 10^{-17}$
<i>FUNDC2</i>	22	50.4	95.9	$7.39 \times 10^{-20}$	$2.91 \times 10^{-17}$
<i>CNRIP1</i>	21	50.4	95.3	$1.0 \times 10^{-19}$	$3.66 \times 10^{-17}$
<i>CALHM2</i>	22	50.4	93.1	$2.94 \times 10^{-19}$	$1.06 \times 10^{-16}$
<i>ARID5A</i>	18	50.4	92.7	$3.47 \times 10^{-19}$	$1.22 \times 10^{-16}$
<i>ST3GAL3</i>	27	50.4	92.2	$4.49 \times 10^{-19}$	$1.56 \times 10^{-16}$
<i>LOC339524</i>	21	50.4	92.1	$4.8 \times 10^{-19}$	$1.59 \times 10^{-16}$

Strongest candidate [synthetic lethal](#) partners for *CDH1* by [SLIPT](#) in [TCGA](#) stomach cancer expression data

\* Observed and expected numbers of samples which had low [expression](#) of both genes

Table E.2: Pathways for *CDH1* partners from SLIPT in stomach cancer

Pathways Over-represented	Pathway Size	SL Genes	p-value (FDR)
Extracellular matrix organization	241	104	$7.5 \times 10^{-140}$
Hemostasis	445	138	$1.8 \times 10^{-121}$
Developmental Biology	432	125	$9.2 \times 10^{-107}$
Axon guidance	289	94	$1.5 \times 10^{-102}$
Eukaryotic Translation Termination	84	49	$1.9 \times 10^{-99}$
GPCR ligand binding	373	108	$3.8 \times 10^{-99}$
Viral mRNA Translation	82	48	$3.3 \times 10^{-98}$
Formation of a pool of free 40S subunits	94	51	$3.3 \times 10^{-98}$
Eukaryotic Translation Elongation	87	49	$1.6 \times 10^{-97}$
Peptide chain elongation	84	48	$7.2 \times 10^{-97}$
Class A/1 (Rhodopsin-like receptors)	289	90	$2.7 \times 10^{-96}$
Nonsense Mediated Decay independent of the Exon Junction Complex	89	49	$3.0 \times 10^{-96}$
Infectious disease	349	100	$2.6 \times 10^{-94}$
GTP hydrolysis and joining of the 60S ribosomal subunit	105	52	$3.4 \times 10^{-94}$
L13a-mediated translational silencing of Ceruloplasmin expression	104	51	$2.8 \times 10^{-92}$
3' -UTR-mediated translational regulation	104	51	$2.8 \times 10^{-92}$
Neuronal System	272	84	$8.4 \times 10^{-92}$
SRP-dependent cotranslational protein targeting to membrane	105	51	$9.5 \times 10^{-92}$
Eukaryotic Translation Initiation	112	52	$2.0 \times 10^{-90}$
Cap-dependent Translation Initiation	112	52	$2.0 \times 10^{-90}$

Gene set over-representation analysis (hypergeometric test) for Reactome pathways in [SLIPT](#) partners for *CDH1*.

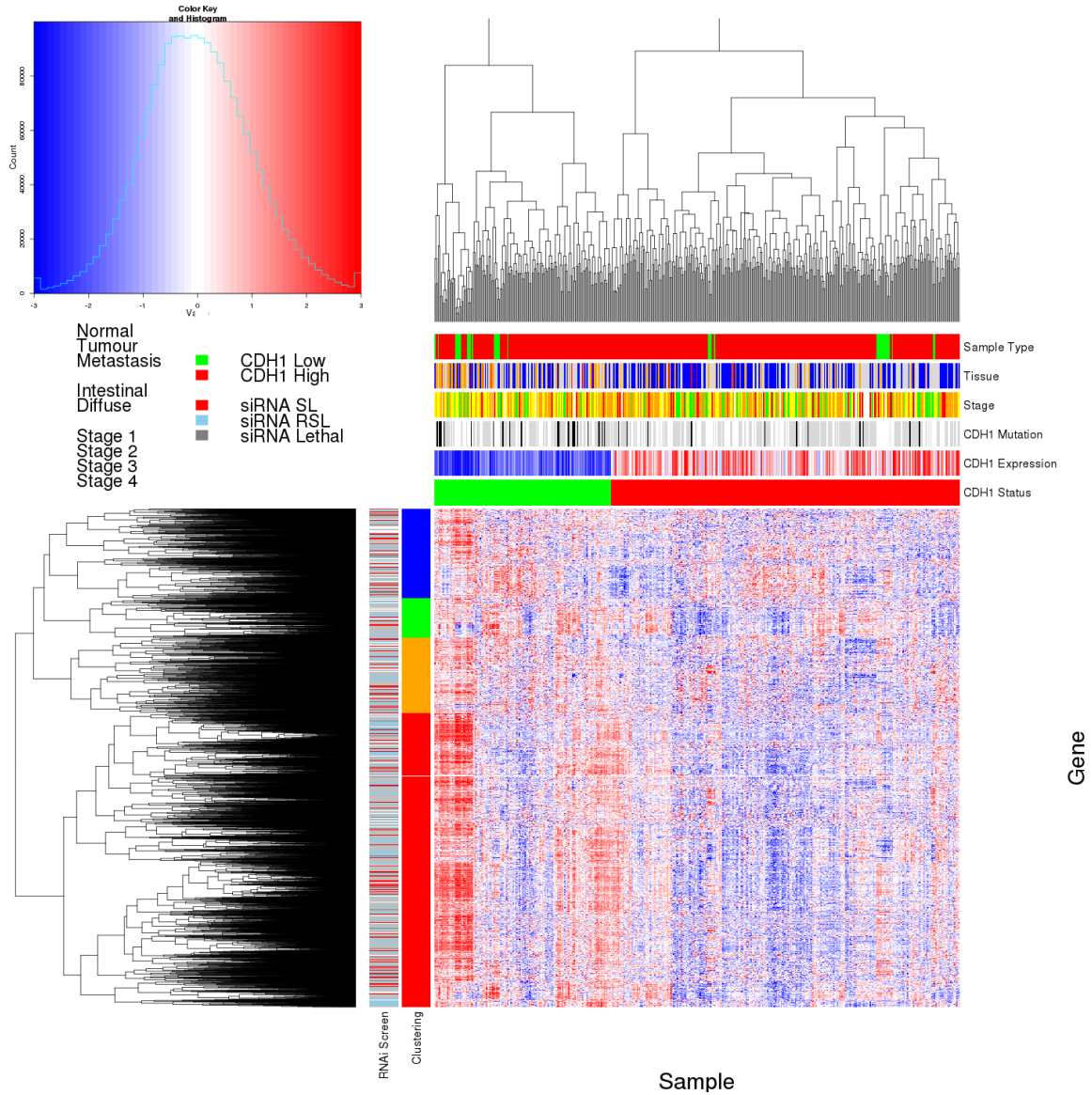


**Figure E.1: Synthetic lethal expression profiles of analysed samples.** Gene expression profile heatmap (correlation distance) of all samples (separated by the  $1/3$  quantile of *CDH1* expression) analysed in [TCGA](#) stomach cancer dataset for gene expression of 4365 candidate partners of [E-cadherin](#) (*CDH1*) from [SLIPT](#) prediction (with significant [FDR](#) adjusted  $p < 0.05$ ). Deeply clustered, inter-correlated genes form several main groups, each containing genes that were SL candidates or toxic in an [siRNA](#) screen [Telford et al. \(2015\)](#). Clusters had different sample groups highly expressing the synthetic lethal candidates in *CDH1* low samples. Notably, diffuse and *CDH1* mutant samples had elevated expression in one or more distinct clusters, although there was less complexity and variation among candidate synthetic lethal partners than in breast data. *CDH1* low samples also contained most of samples with *CDH1* mutations.

Table E.3: Pathways for clusters of *CDH1* partners in stomach SLIPT

Pathways Over-represented in Cluster 1	Pathway Size	Cluster Genes	p-value (FDR)
Viral mRNA Translation	82	48	$1.3 \times 10^{-97}$
Formation of a pool of free 40S subunits	94	51	$1.3 \times 10^{-97}$
Eukaryotic Translation Elongation	87	49	$4.8 \times 10^{-97}$
Peptide chain elongation	84	48	$1.4 \times 10^{-96}$
Eukaryotic Translation Termination	84	48	$1.4 \times 10^{-96}$
GTP hydrolysis and joining of the 60S ribosomal subunit	105	52	$7.9 \times 10^{-94}$
Nonsense Mediated Decay independent of the Exon Junction Complex	89	48	$3.1 \times 10^{-93}$
L13a-mediated translational silencing of Ceruloplasmin expression	104	51	$5.1 \times 10^{-92}$
3' -UTR-mediated translational regulation	104	51	$5.1 \times 10^{-92}$
SRP-dependent cotranslational protein targeting to membrane	105	51	$1.7 \times 10^{-91}$
Eukaryotic Translation Initiation	112	52	$3.3 \times 10^{-90}$
Cap-dependent Translation Initiation	112	52	$3.3 \times 10^{-90}$
Translation	142	56	$3.6 \times 10^{-85}$
Nonsense-Mediated Decay	104	48	$1.2 \times 10^{-84}$
Nonsense Mediated Decay enhanced by the Exon Junction Complex	104	48	$1.2 \times 10^{-84}$
Influenza Viral RNA Transcription and Replication	109	48	$4.1 \times 10^{-82}$
Influenza Life Cycle	113	48	$3.4 \times 10^{-80}$
Influenza Infection	118	48	$6.4 \times 10^{-78}$
Pathways Over-represented in Cluster 2	Pathway Size	Cluster Genes	p-value (FDR)
Immunoregulatory interactions between a Lymphoid and a non-Lymphoid cell	65	12	$1.3 \times 10^{-15}$
Phosphorylation of CD3 and TCR zeta chains	18	6	$1.7 \times 10^{-12}$
Generation of second messenger molecules	29	7	$2.7 \times 10^{-12}$
PD-1 signalling	21	6	$7.4 \times 10^{-12}$
TCR signalling	62	9	$4.3 \times 10^{-11}$
Translocation of ZAP-70 to Immunological synapse	16	5	$1.1 \times 10^{-10}$
Interferon alpha/beta signalling	68	9	$1.6 \times 10^{-10}$
Initial triggering of complement	17	5	$1.6 \times 10^{-10}$
IKK complex recruitment mediated by RIP1	19	5	$5.1 \times 10^{-10}$
TRIF-mediated programmed cell death	10	4	$6.2 \times 10^{-10}$
Creation of C4 and C2 activators	11	4	$1.3 \times 10^{-9}$
RHO GTPases Activate NADPH Oxidases	11	4	$1.3 \times 10^{-9}$
Interferon Signalling	175	15	$2.3 \times 10^{-9}$
Chemokine receptors bind chemokines	52	7	$4.0 \times 10^{-9}$
Interferon gamma signalling	74	8	$1.6 \times 10^{-8}$
TRAF6 mediated induction of TAK1 complex	15	4	$1.6 \times 10^{-8}$
Activation of IRF3/IRF7 mediated by TBK1/IKK epsilon	16	4	$2.7 \times 10^{-8}$
Downstream TCR signalling	45	6	$3.5 \times 10^{-8}$
Pathways Over-represented in Cluster 3	Pathway Size	Cluster Genes	p-value (FDR)
Uptake and actions of bacterial toxins	22	4	$3.5 \times 10^{-6}$
Neurotoxicity of clostridium toxins	10	3	$3.5 \times 10^{-6}$
Activation of PPARGC1A (PGC-1alpha) by phosphorylation	10	3	$3.5 \times 10^{-6}$
SMAD2/SMAD3:SMAD4 heterotrimer regulates transcription	28	4	$1.4 \times 10^{-5}$
Assembly of the primary cilium	149	10	$2.5 \times 10^{-5}$
Serotonin Neurotransmitter Release Cycle	15	3	$2.5 \times 10^{-5}$
Glycosaminoglycan metabolism	114	8	$3.3 \times 10^{-5}$
Platelet homeostasis	54	5	$3.3 \times 10^{-5}$
Norepinephrine Neurotransmitter Release Cycle	17	3	$3.3 \times 10^{-5}$
Acetylcholine Neurotransmitter Release Cycle	17	3	$3.3 \times 10^{-5}$
G <sub>αs</sub> signalling events	100	7	$5.5 \times 10^{-5}$
GABA synthesis, release, reuptake and degradation	19	3	$5.6 \times 10^{-5}$
deactivation of the beta-catenin transactivating complex	39	4	$6.7 \times 10^{-5}$
Dopamine Neurotransmitter Release Cycle	20	3	$6.7 \times 10^{-5}$
IRS-related events triggered by IGF1R	83	6	$7.1 \times 10^{-5}$
Generic Transcription Pathway	186	11	$7.1 \times 10^{-5}$
Termination of O-glycan biosynthesis	21	3	$7.4 \times 10^{-5}$
Kinesins	22	3	$8.5 \times 10^{-5}$
Pathways Over-represented in Cluster 4	Pathway Size	Cluster Genes	p-value (FDR)
Extracellular matrix organization	241	97	$8.8 \times 10^{-126}$
Axon guidance	289	75	$8.3 \times 10^{-72}$
Hemostasis	445	101	$8.3 \times 10^{-72}$
Developmental Biology	432	95	$3.0 \times 10^{-67}$
Response to elevated platelet cytosolic Ca <sup>2+</sup>	84	37	$5.8 \times 10^{-67}$
Platelet degranulation	79	36	$5.8 \times 10^{-67}$
Degradation of the extracellular matrix	104	39	$6.7 \times 10^{-63}$
Platelet activation, signalling and aggregation	186	52	$6.6 \times 10^{-62}$
ECM proteoglycans	66	31	$8.1 \times 10^{-61}$
Neuronal System	272	64	$5.1 \times 10^{-60}$
Signalling by PDGF	173	47	$9.7 \times 10^{-57}$
Integrin cell surface interactions	82	31	$1.9 \times 10^{-53}$
Collagen biosynthesis and modifying enzymes	56	26	$1.1 \times 10^{-52}$
Collagen formation	67	28	$1.4 \times 10^{-52}$
Class A/1 (Rhodopsin-like receptors)	289	61	$2.3 \times 10^{-52}$
GPCR ligand binding	373	73	$2.8 \times 10^{-52}$
Elastic fibre formation	38	22	$4.7 \times 10^{-52}$
Non-integrin membrane-ECM interactions	53	24	$7.0 \times 10^{-49}$

Pathway over-representation analysis for Reactome pathways with the number of genes in each pathway (Pathway Size), number of genes within the pathway identified (Cluster Genes), and the pathway over-representation p-value (adjusted by FDR) from the hypergeometric test.

## E.2 Comparison to Primary Screen

The synthetic lethal partners with *CDH1* expression in stomach cancers were also compared to [siRNA](#) primary screen data (Telford *et al.*, 2015), as performed in Section 4.2.1. These were expected to be more concordant with the experimental results performed on a null mutant, however this was not the case at the gene level: less genes overlapped with experimental candidates in Figure E.2. This may be due to lower sample size for mutations in [TCGA](#) data or lower frequency (expected value) of *CDH1* mutations compared to low expression.

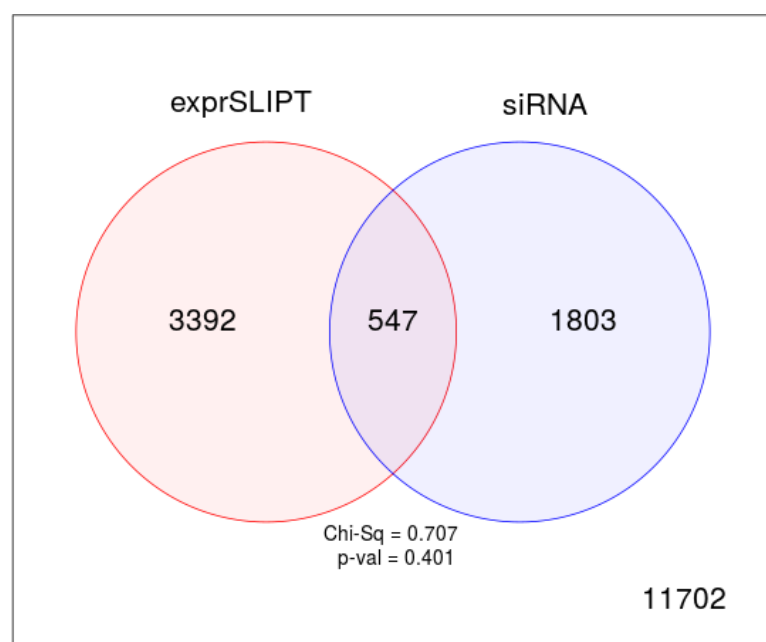


Figure E.2: **Comparison of SLIPT in stomach to siRNA.** The overlap of gene candidates for [E-cadherin](#) synthetic lethal partners between computational (SLIPT) and experimental screening (siRNA) approaches. The  $\chi^2$  test suggests that the overlap is no more than would be expected by chance ( $p = 0.281$ ).

Table E.4: Pathways for *CDH1* partners from SLIPT and siRNA

Predicted only by SLIPT (3392 genes)	Pathway Size	Genes Identified	p-value (FDR)
Extracellular matrix organization	238	90	$3.4 \times 10^{-107}$
Eukaryotic Translation Termination	79	46	$7.6 \times 10^{-91}$
Viral mRNA Translation	77	45	$1.2 \times 10^{-89}$
Eukaryotic Translation Elongation	82	46	$5.8 \times 10^{-89}$
Peptide chain elongation	79	45	$2.1 \times 10^{-88}$
Nonsense Mediated Decay independent of the Exon Junction Complex	84	46	$9.4 \times 10^{-88}$
Formation of a pool of free 40S subunits	89	47	$3.3 \times 10^{-87}$
GTP hydrolysis and joining of the 60S ribosomal subunit	100	48	$3.2 \times 10^{-83}$
Axon guidance	284	84	$3.9 \times 10^{-82}$
Developmental Biology	426	111	$4.2 \times 10^{-82}$
L13a-mediated translational silencing of Ceruloplasmin expression	99	47	$1.4 \times 10^{-81}$
3' -UTR-mediated translational regulation	99	47	$1.4 \times 10^{-81}$
SRP-dependent cotranslational protein targeting to membrane	99	47	$1.4 \times 10^{-81}$
Nonsense-Mediated Decay	99	47	$1.4 \times 10^{-81}$
Nonsense Mediated Decay enhanced by the Exon Junction Complex	99	47	$1.4 \times 10^{-81}$
Hemostasis	438	112	$1.2 \times 10^{-80}$
Eukaryotic Translation Initiation	107	48	$8.0 \times 10^{-80}$
Cap-dependent Translation Initiation	107	48	$8.0 \times 10^{-80}$
Infectious disease	338	90	$1.6 \times 10^{-76}$
Neuronal System	267	77	$1.6 \times 10^{-76}$

Detected only by siRNA screen (1803 genes)	Pathway Size	Genes Identified	p-value (FDR)
Class A/1 (Rhodopsin-like receptors)	282	62	$8.1 \times 10^{-50}$
GPCR ligand binding	363	71	$4.9 \times 10^{-46}$
Peptide ligand-binding receptors	175	38	$7.9 \times 10^{-38}$
G <sub>αi</sub> signalling events	184	37	$1.1 \times 10^{-34}$
Gastrin-CREB signalling pathway via PKC and MAPK	180	35	$1.4 \times 10^{-32}$
G <sub>αq</sub> signalling events	159	32	$4.8 \times 10^{-32}$
DAP12 interactions	159	29	$1.4 \times 10^{-27}$
Downstream signal transduction	146	26	$2.4 \times 10^{-25}$
DAP12 signalling	149	26	$6.4 \times 10^{-25}$
VEGFA-VEGFR2 Pathway	91	19	$8.1 \times 10^{-24}$
Signalling by PDGF	172	27	$5.7 \times 10^{-23}$
Signalling by ERBB2	146	24	$1.4 \times 10^{-22}$
Signalling by VEGF	99	19	$2.0 \times 10^{-22}$
Visual phototransduction	85	17	$1.3 \times 10^{-21}$
Downstream signalling of activated FGFR1	134	22	$1.3 \times 10^{-21}$
Downstream signalling of activated FGFR2	134	22	$1.3 \times 10^{-21}$
Downstream signalling of activated FGFR3	134	22	$1.3 \times 10^{-21}$
Downstream signalling of activated FGFR4	134	22	$1.3 \times 10^{-21}$
Signalling by FGFR	146	23	$2.0 \times 10^{-21}$
Signalling by FGFR1	146	23	$2.0 \times 10^{-21}$

Intersection of SLIPT and siRNA screen (547 genes)	Pathway Size	Genes Identified	p-value (FDR)
Class A/1 (Rhodopsin-like receptors)	282	25	$3.9 \times 10^{-9}$
Platelet activation, signalling and aggregation	182	17	$3.9 \times 10^{-9}$
Response to elevated platelet cytosolic Ca <sup>2+</sup>	82	9	$5.5 \times 10^{-8}$
Platelet homeostasis	53	7	$5.7 \times 10^{-8}$
Nucleotide-like (purinergic) receptors	16	4	$1.8 \times 10^{-7}$
Platelet degranulation	77	8	$2.8 \times 10^{-7}$
Peptide ligand-binding receptors	175	14	$3.8 \times 10^{-7}$
Molecules associated with elastic fibres	34	5	$7.1 \times 10^{-7}$
Amine ligand-binding receptors	35	5	$8.6 \times 10^{-7}$
G <sub>αi</sub> signalling events	184	14	$9.8 \times 10^{-7}$
GPCR ligand binding	363	27	$1.1 \times 10^{-6}$
Elastic fibre formation	38	5	$1.5 \times 10^{-6}$
G <sub>αq</sub> signalling events	159	12	$1.9 \times 10^{-6}$
Serotonin receptors	12	3	$3.8 \times 10^{-6}$
P2Y receptors	12	3	$3.8 \times 10^{-6}$
Signal amplification	16	3	$2.3 \times 10^{-5}$
Gastrin-CREB signalling pathway via PKC and MAPK	180	12	$2.3 \times 10^{-5}$
Complement cascade	33	4	$2.4 \times 10^{-5}$
Glycosaminoglycan metabolism	110	8	$2.5 \times 10^{-5}$
Glycogen breakdown (glycogenolysis)	17	3	$2.7 \times 10^{-5}$

## E.2.1 Resampling Analysis

Table E.5: Pathways for *CDH1* partners from SLIPT in stomach cancer

Reactome Pathway	Over-representation	Permutation
<i>Extracellular matrix organization</i>	$7.5 \times 10^{-140}$	0.070215
Hemostasis	$1.8 \times 10^{-121}$	0.25804
Developmental Biology	$9.2 \times 10^{-107}$	0.53032
Axon guidance	$1.5 \times 10^{-102}$	0.6704
<b>Eukaryotic Translation Termination</b>	$1.9 \times 10^{-99}$	$> 1.031 \times 10^{-5}$
GPCR ligand binding	$3.8 \times 10^{-99}$	0.54914
<b>Viral mRNA Translation</b>	$3.3 \times 10^{-98}$	$> 1.031 \times 10^{-5}$
Formation of a pool of free 40S subunits	$3.3 \times 10^{-98}$	$> 1.031 \times 10^{-5}$
<b>Eukaryotic Translation Elongation</b>	$1.6 \times 10^{-97}$	$> 1.031 \times 10^{-5}$
Peptide chain elongation	$7.2 \times 10^{-97}$	$> 1.031 \times 10^{-5}$
Class A/1 (Rhodopsin-like receptors)	$2.7 \times 10^{-96}$	0.58174
<b>Nonsense Mediated Decay independent of the Exon Junction Complex</b>	$3 \times 10^{-96}$	$> 1.031 \times 10^{-5}$
Infectious disease	$2.6 \times 10^{-94}$	0.25484
GTP hydrolysis and joining of the 60S ribosomal subunit	$3.4 \times 10^{-94}$	$> 1.031 \times 10^{-5}$
L13a-mediated translational silencing of Ceruloplasmin expression	$2.8 \times 10^{-92}$	$> 1.031 \times 10^{-5}$
3' -UTR-mediated translational regulation	$2.8 \times 10^{-92}$	$> 1.031 \times 10^{-5}$
Neuronal System	$8.4 \times 10^{-92}$	0.53433
SRP-dependent cotranslational protein targeting to membrane	$9.5 \times 10^{-92}$	$> 1.031 \times 10^{-5}$
Eukaryotic Translation Initiation	$2.0 \times 10^{-90}$	$> 1.031 \times 10^{-5}$
Cap-dependent Translation Initiation	$2.0 \times 10^{-90}$	$> 1.031 \times 10^{-5}$
Nonsense-Mediated Decay	$7.4 \times 10^{-90}$	$> 1.031 \times 10^{-5}$
Nonsense Mediated Decay enhanced by the Exon Junction Complex	$7.4 \times 10^{-90}$	$> 1.031 \times 10^{-5}$
Adaptive Immune System	$8.1 \times 10^{-88}$	0.14116
<b>Translation</b>	$1.3 \times 10^{-87}$	$> 1.031 \times 10^{-5}$
Platelet activation, signalling and aggregation	$1.3 \times 10^{-86}$	0.28959
<b>Influenza Infection</b>	$1 \times 10^{-82}$	$> 1.031 \times 10^{-5}$
<b>Influenza Viral RNA Transcription and Replication</b>	$2.4 \times 10^{-82}$	$> 1.031 \times 10^{-5}$
<b>Influenza Life Cycle</b>	$2 \times 10^{-80}$	$> 1.031 \times 10^{-5}$
Response to elevated platelet cytosolic Ca2+	$4.9 \times 10^{-78}$	0.50817
Signalling by NGF	$1.6 \times 10^{-75}$	0.38518
Rho GTPase cycle	$5.1 \times 10^{-75}$	0.14864
Signalling by PDGF	$7.4 \times 10^{-74}$	0.40493
<i>Signalling by Rho GTPases</i>	$5.1 \times 10^{-73}$	0.077217
Glycosaminoglycan metabolism	$1.4 \times 10^{-68}$	0.52984
<i>G<sub>ai</sub> signalling events</i>	$1.8 \times 10^{-66}$	0.9254
Metabolism of carbohydrates	$1.1 \times 10^{-65}$	0.39501
<b>G<sub>as</sub> signalling events</b>	$2.7 \times 10^{-65}$	0.0050293
Potassium Channels	$2.7 \times 10^{-65}$	0.53359
Transmission across Chemical Synapses	$1.8 \times 10^{-64}$	0.81833
ECM proteoglycans	$3.4 \times 10^{-64}$	0.083482
Peptide ligand-binding receptors	$4.8 \times 10^{-64}$	0.62817
Degradation of the extracellular matrix	$1.1 \times 10^{-63}$	0.80879
Platelet homeostasis	$5.3 \times 10^{-63}$	0.53134
NGF signalling via TRKA from the plasma membrane	$6.1 \times 10^{-63}$	0.57117
Integration of energy metabolism	$4.5 \times 10^{-61}$	0.10889
Collagen formation	$5.4 \times 10^{-61}$	0.29896
Integrin cell surface interactions	$7 \times 10^{-59}$	0.18167
Collagen biosynthesis and modifying enzymes	$7 \times 10^{-59}$	0.30208
Neurotransmitter Receptor Binding And Downstream Transmission	$8.7 \times 10^{-57}$	0.82522
In The Postsynaptic Cell		
Signalling by Wnt	$8.7 \times 10^{-57}$	0.25468

Over-representation (hypergeometric test) and Permutation p-values adjusted for multiple tests across pathways (**FDR**). Significant pathways were marked in bold (**FDR** < 0.05) and italics (**FDR** < 0.1).

Table E.6: Pathways for *CDH1* partners from SLIPT in stomach and siRNA

Reactome Pathway	Over-representation	Permutation
Platelet activation, signalling and aggregation	$3.9 \times 10^{-9}$	0.49557
Class A/1 (Rhodopsin-like receptors)	$3.9 \times 10^{-9}$	0.98432
Response to elevated platelet cytosolic Ca <sup>2+</sup>	$5.5 \times 10^{-8}$	0.54349
Platelet homeostasis	$5.7 \times 10^{-8}$	0.45017
Nucleotide-like (purinergic) receptors	$1.8 \times 10^{-7}$	0.36966
Peptide ligand-binding receptors	$3.8 \times 10^{-7}$	0.91294
<b>Molecules associated with elastic fibres</b>	$7.1 \times 10^{-7}$	0.0025868
Amine ligand-binding receptors	$8.6 \times 10^{-7}$	0.43303
G <sub>ai</sub> signalling events	$9.8 \times 10^{-7}$	0.99626
GPCR ligand binding	$1.1 \times 10^{-6}$	0.97733
<b>Elastic fibre formation</b>	$1.5 \times 10^{-6}$	0.0025868
G <sub>aq</sub> signalling events	$1.9 \times 10^{-6}$	0.86089
P2Y receptors	$3.8 \times 10^{-6}$	0.18795
Serotonin receptors	$3.8 \times 10^{-6}$	0.37853
Signal amplification	$2.3 \times 10^{-5}$	0.47856
Gastrin-CREB signalling pathway via PKC and MAPK	$2.3 \times 10^{-5}$	0.98567
<b>Complement cascade</b>	$2.4 \times 10^{-5}$	$> 3.4628 \times 10^{-6}$
Glycosaminoglycan metabolism	$2.5 \times 10^{-5}$	0.38953
Glycogen breakdown (glycogenolysis)	$2.7 \times 10^{-5}$	0.83772
Defective B4GALT7 causes EDS, progeroid type	$4.9 \times 10^{-5}$	0.10792
Defective B3GAT3 causes JDSSDHD	$4.9 \times 10^{-5}$	0.10792
Role of LAT2/NTAL/LAB on calcium mobilization	$5.6 \times 10^{-5}$	0.35373
Cell surface interactions at the vascular wall	$5.6 \times 10^{-5}$	0.47642
<b>G<sub>as</sub> signalling events</b>	$6 \times 10^{-5}$	0.019858
Signalling by NOTCH	$6 \times 10^{-5}$	0.19008
A tetrasaccharide linker sequence is required for GAG synthesis	0.00017	0.47642
<b>Extracellular matrix organization</b>	0.00018	0.0047308
Collagen formation	0.00018	0.19245
Effects of PIP2 hydrolysis	0.0002	0.37779
Syndecan interactions	0.0002	0.37779
<b>Diseases associated with glycosaminoglycan metabolism</b>	0.00023	0.01028
<b>Diseases of glycosylation</b>	0.00023	0.01028
<i>Chondroitin sulfate/dermatan sulfate metabolism</i>	0.00023	0.085541
Integrin alphaIIb beta3 signalling	0.00028	0.76936
Keratan sulfate biosynthesis	0.00034	0.68744
Rho GTPase cycle	0.00034	0.15675
Creation of C4 and C2 activators	0.00035	0.12275
Abacavir transport and metabolism	0.00035	0.12443
Amine compound SLC transporters	0.00037	0.69773
FCER1 mediated NF-κB activation	0.00037	0.69846
Fc epsilon receptor (FCER1) signalling	0.00056	0.43303
Defective EXT2 causes exostoses 2	0.00067	0.16053
Defective EXT1 causes exostoses 1, TRPS2 and CHDS	0.00067	0.16053
<i>Collagen biosynthesis and modifying enzymes</i>	0.00071	0.052911
Keratan sulfate/keratin metabolism	0.00073	0.46533
G alpha (12/13) signalling events	0.00078	0.59164
<b>SEMA3A-Plexin repulsion signalling by inhibiting Integrin adhesion</b>	0.00084	0.038504
Signal attenuation	0.00084	0.37779
Eicosanoid ligand-binding receptors	0.0011	0.11117
SOS-mediated signalling	0.0011	0.25387

Over-representation (hypergeometric test) and Permutation p-values adjusted for multiple tests across pathways (**FDR**). Significant pathways were marked in bold (**FDR** < 0.05) and italics (**FDR** < 0.1).

### E.3 Metagene Analysis

Metagenes used to detect synthetic lethal pathways with *CDH1* in stomach cancer.

Table E.7: Synthetic lethal metagenes against *CDH1* in stomach cancer

Pathway	ID	Observed	Expected	$\chi^2$ value	p-value	p-value (FDR)
Cell-Cell communication	1500931	18	50.4	110	$7.43 \times 10^{-23}$	$1.53 \times 10^{-20}$
VEGFR2 mediated vascular permeability	5218920	19	50.4	109	$1.36 \times 10^{-22}$	$2.49 \times 10^{-20}$
Sema4D in semaphorin signalling	400685	20	50.4	104	$1.62 \times 10^{-21}$	$2.12 \times 10^{-19}$
Ion transport by P-type ATPases	936837	17	50.4	100	$8.29 \times 10^{-21}$	$8.06 \times 10^{-19}$
Sialic acid metabolism	4085001	19	50.4	95.3	$9.95 \times 10^{-20}$	$7.82 \times 10^{-18}$
Synthesis of pyrophosphates in the cytosol	1855167	26	50.4	94	$1.86 \times 10^{-19}$	$1.23 \times 10^{-17}$
Keratan sulfate/keratin metabolism	1638074	25	50.4	93.5	$2.36 \times 10^{-19}$	$1.44 \times 10^{-17}$
Ion channel transport	983712	19	50.4	92.8	$3.37 \times 10^{-19}$	$1.99 \times 10^{-17}$
Keratan sulfate biosynthesis	2022854	26	50.4	91.4	$6.79 \times 10^{-19}$	$3.62 \times 10^{-17}$
Arachidonic acid metabolism	2142753	22	50.4	90.6	$9.81 \times 10^{-19}$	$5.07 \times 10^{-17}$
RHO GTPases activate CIT	5625900	22	50.4	87	$5.80 \times 10^{-18}$	$2.66 \times 10^{-16}$
Stimuli-sensing channels	2672351	25	50.4	85.8	$1.03 \times 10^{-17}$	$4.58 \times 10^{-16}$
Synthesis of PI	1483226	19	50.4	85.6	$1.15 \times 10^{-17}$	$4.89 \times 10^{-16}$
G-protein activation	202040	19	50.4	85.3	$1.34 \times 10^{-17}$	$5.53 \times 10^{-16}$
NrCAM interactions	447038	22	50.4	84.3	$2.1 \times 10^{-17}$	$8.27 \times 10^{-16}$
Inwardly rectifying $K^+$ channels	1296065	24	50.4	83.5	$3.19 \times 10^{-17}$	$1.22 \times 10^{-15}$
Calcitonin-like ligand receptors	419812	20	50.4	82.2	$6.07 \times 10^{-17}$	$2.13 \times 10^{-15}$
Prostacyclin signalling through prostacyclin receptor	392851	24	50.4	81.8	$7.27 \times 10^{-17}$	$2.5 \times 10^{-15}$
Presynaptic function of Kainate receptors	500657	26	50.4	79.7	$2.00 \times 10^{-16}$	$6.34 \times 10^{-15}$
ADP signalling through P2Y purinoceptor 12	392170	23	50.4	79.2	$2.57 \times 10^{-16}$	$7.71 \times 10^{-15}$
regulation of FZD by ubiquitination	4641263	22	50.4	78.8	$3.15 \times 10^{-16}$	$9.3 \times 10^{-15}$
Toxicity of tetanus toxin (TeNT)	5250982	27	50.4	78.7	$3.36 \times 10^{-16}$	$9.75 \times 10^{-15}$
Gap junction degradation	190873	21	50.4	78.5	$3.66 \times 10^{-16}$	$1.04 \times 10^{-14}$
Nephrin interactions	373753	25	50.4	78.2	$4.21 \times 10^{-16}$	$1.14 \times 10^{-14}$
GABA synthesis, release, reuptake and degradation	888590	26	50.4	77	$7.69 \times 10^{-16}$	$1.95 \times 10^{-14}$

Strongest candidate *synthetic lethal* partners for *CDH1* by SLIPT with observed and expected numbers of [TCGA](#) stomach cancer samples with low expression of both genes.

## Appendix F

# Synthetic Lethal Genes in Pathways

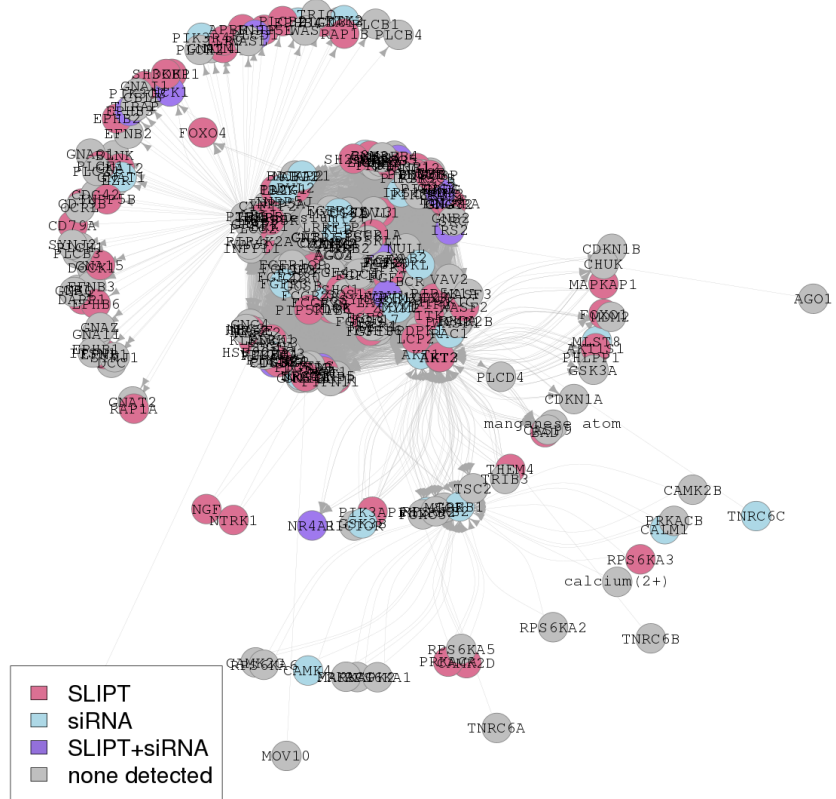
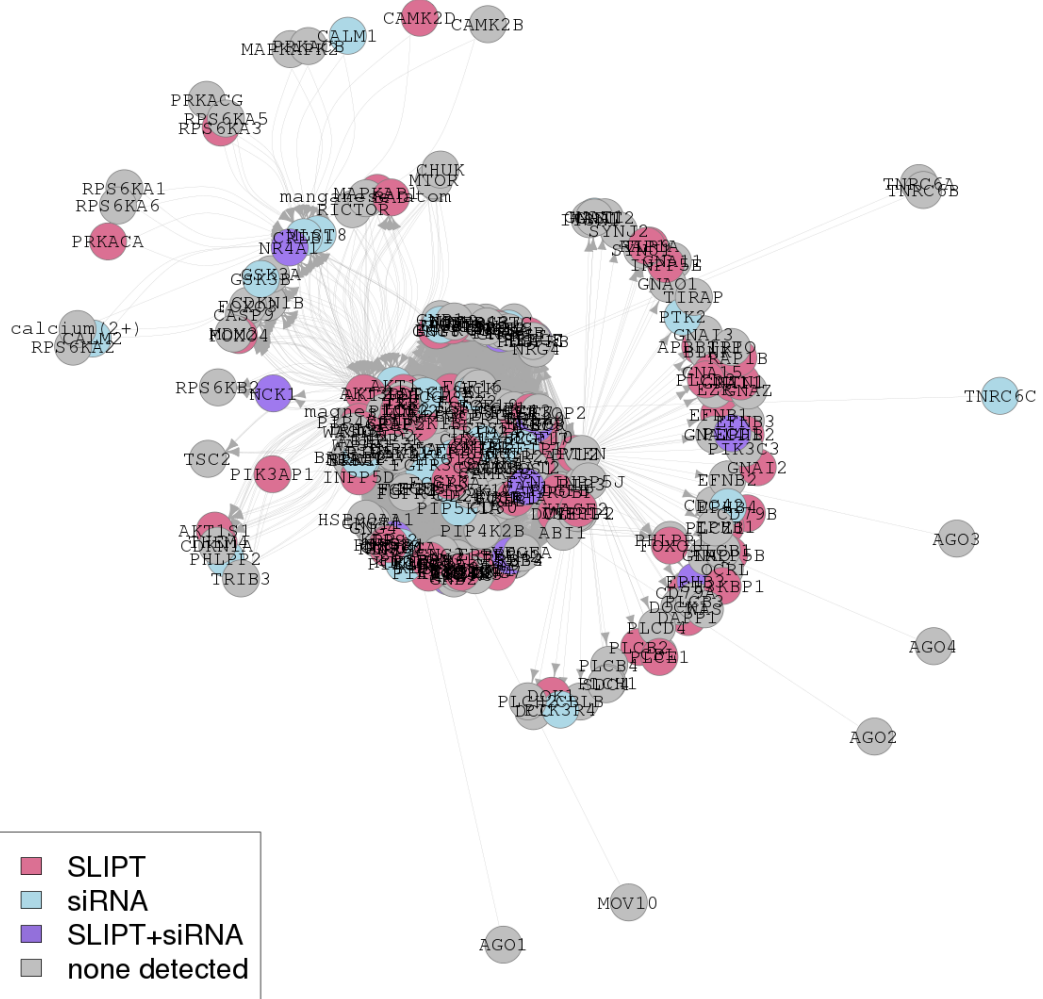
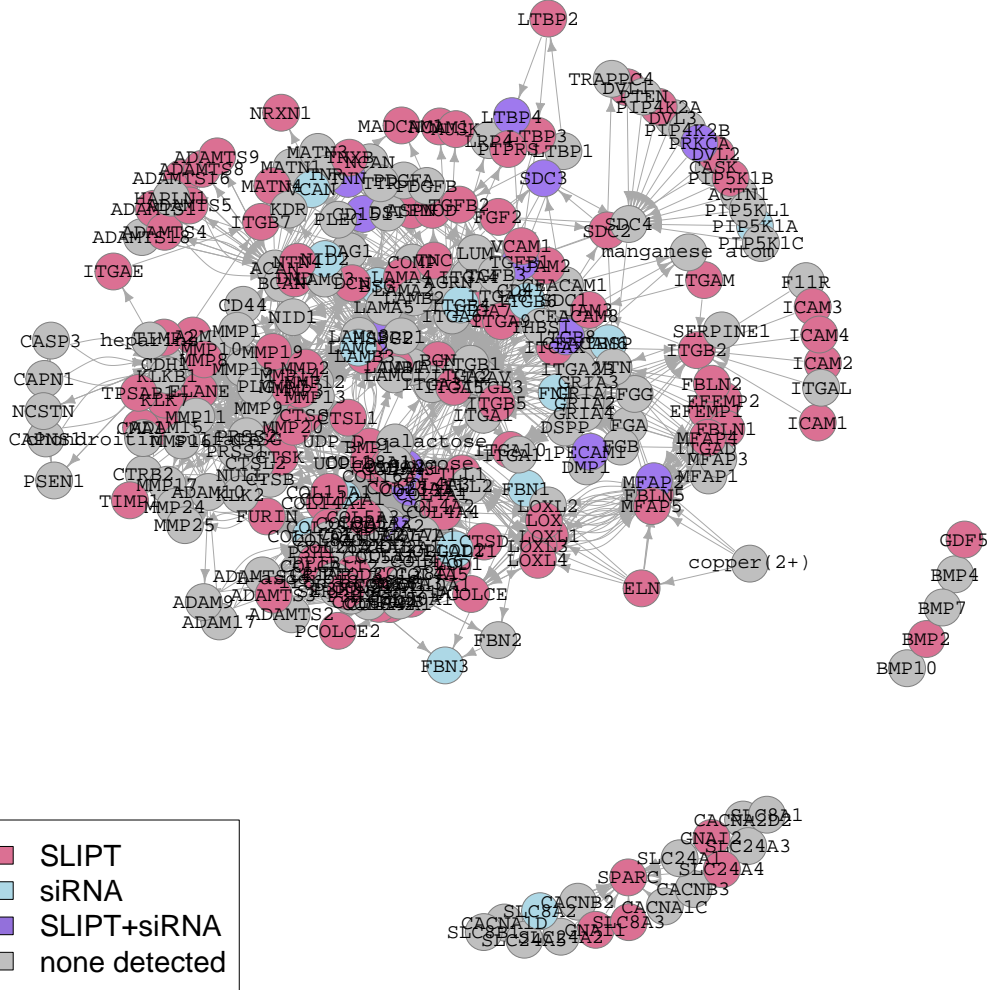


Figure F.1: Synthetic lethality in the PI3K/AKT pathway. The Reactome PI3K/AKT pathway with synthetic lethal candidates, coloured as shown in the legend.



**Figure F.2: Synthetic lethality in the PI3K/AKT pathway in cancer.** The Reactome PI3K/AKT in cancer pathway with synthetic lethal candidates, coloured as shown in the legend.



**Figure F.3: Synthetic lethality in the Extracellular Matrix.** The Reactome Extracellular Matrix pathway with synthetic lethal candidates, coloured as shown in the legend.

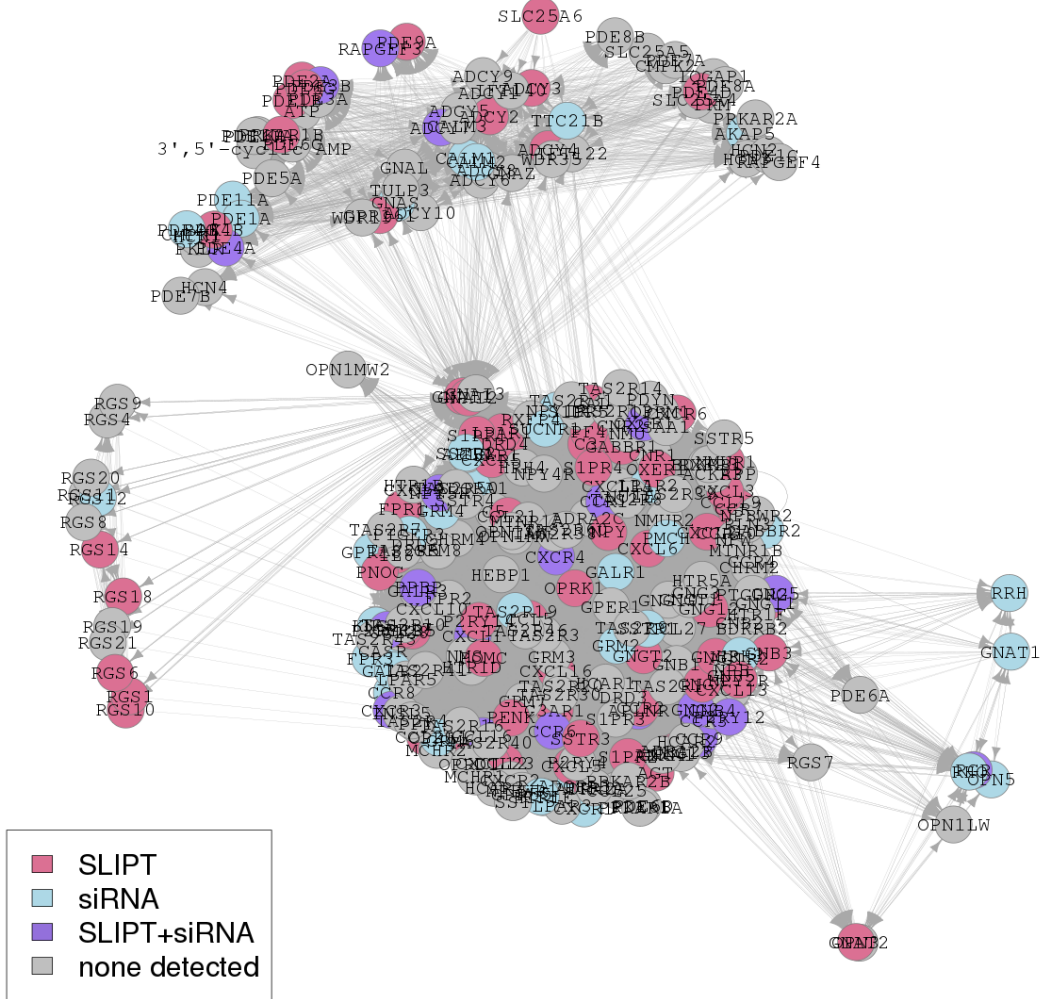


**Figure F.4: Synthetic lethality in the GPCRs.** The Reactome  $G_{\alpha i}$  pathway with synthetic lethal candidates, coloured as shown in the legend.

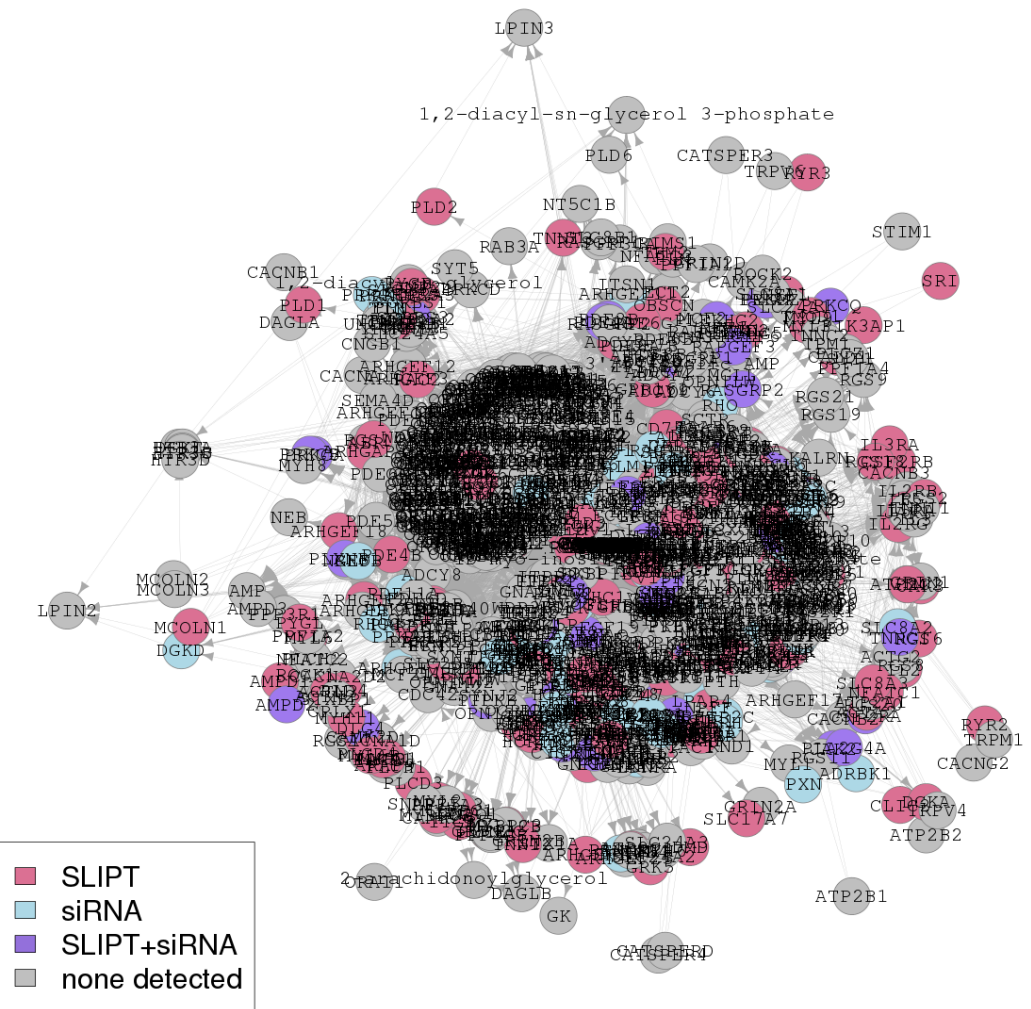


**Figure F.5: Synthetic lethality in the GPCR Downstream.** The Reactome GPCR Downstream pathway with synthetic lethal candidates, coloured as shown in the legend.

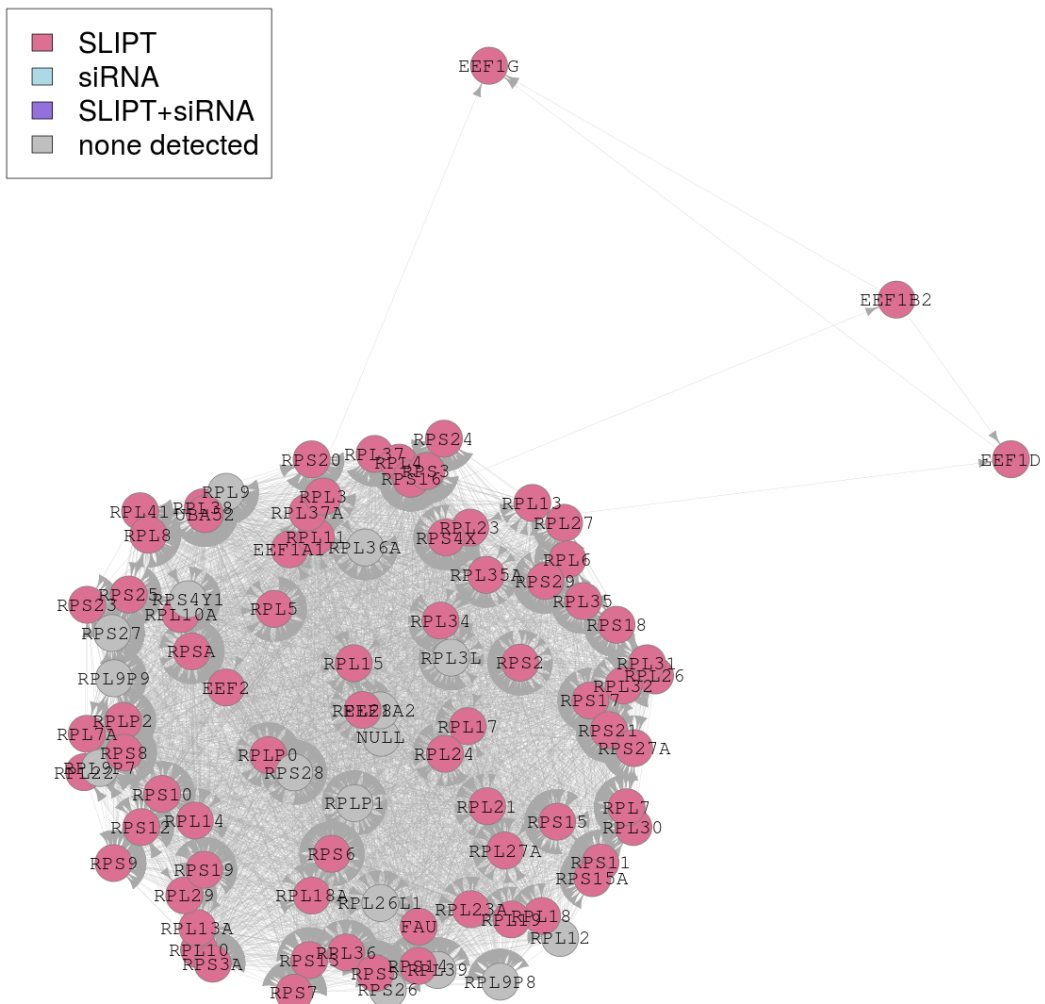


Figure F.6: **Synthetic lethality in the Translation Elongation.** The Reactome Translation Elongation pathway with synthetic lethal candidates, coloured as shown in the legend.

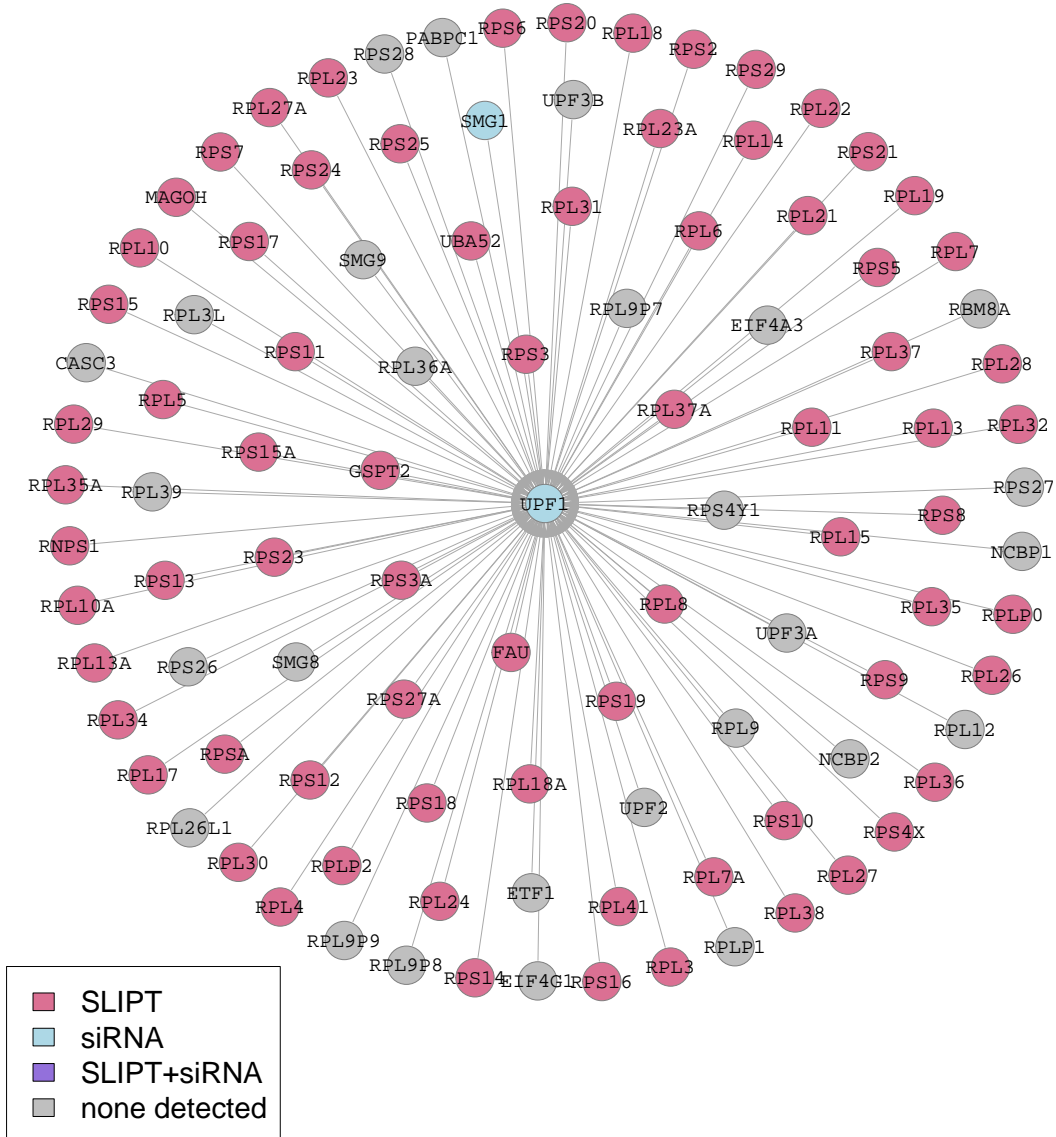


Figure F.7: **Synthetic lethality in the Nonsense-mediated Decay**. The Reactome NMD pathway with synthetic lethal candidates, coloured as shown in the legend.

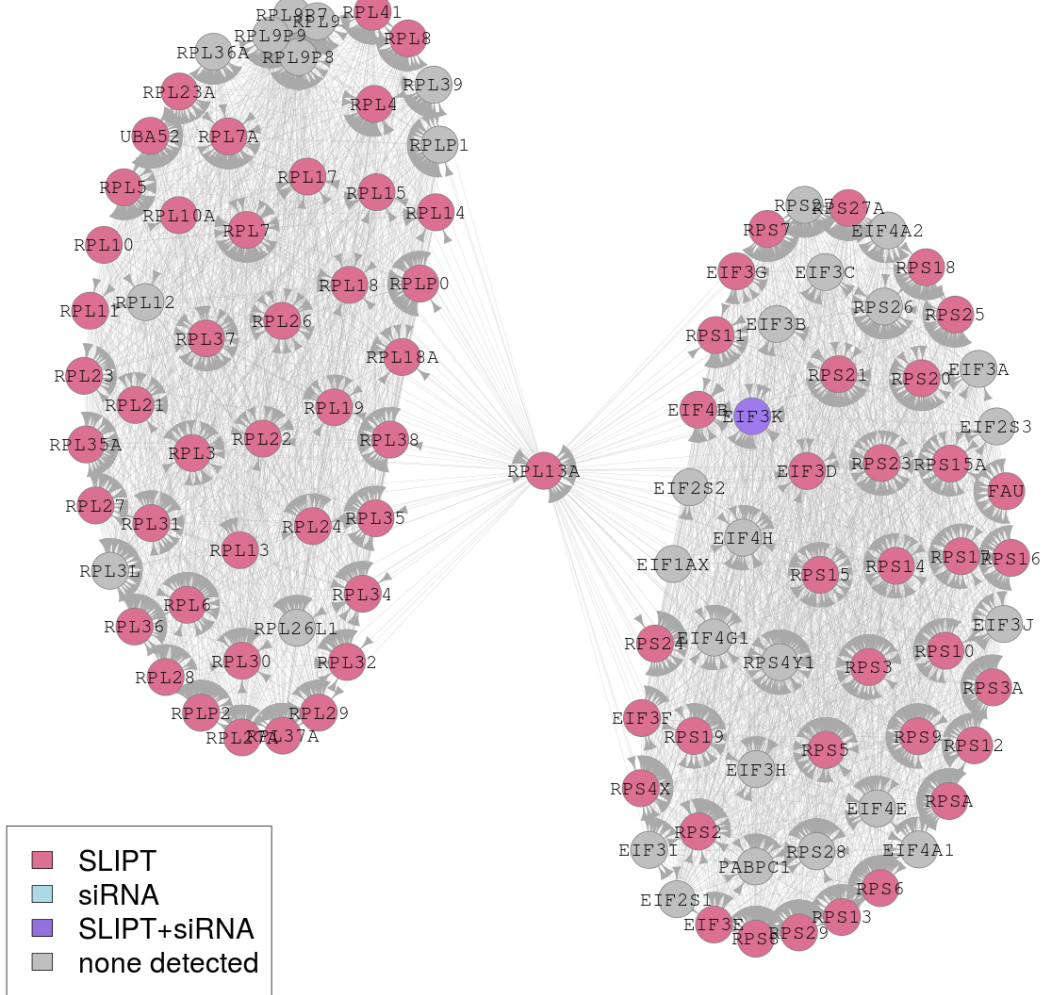


Figure F.8: **Synthetic lethality in the 3' UTR.** The Reactome 3' UTR pathway with synthetic lethal candidates, coloured as shown in the legend.

## Appendix G

# Pathway Connectivity for Mutation SLIPT

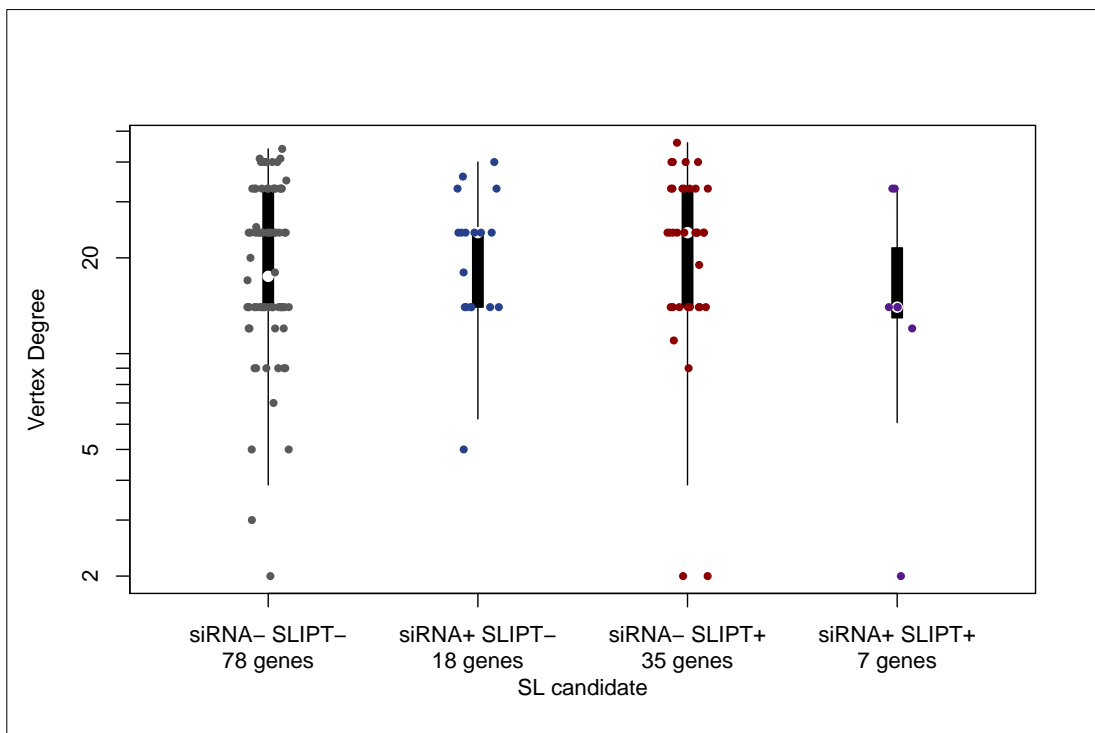


Figure G.1: **Synthetic lethality and vertex degree.** The number of connected genes (vertex degree) was compared (on a log-scale across genes detected by mtSLIPT and siRNA screening in the Reactome PI3K cascade pathway. There were very few differences in vertex degree between the groups, although genes detected by siRNA included those with the fewest connections.

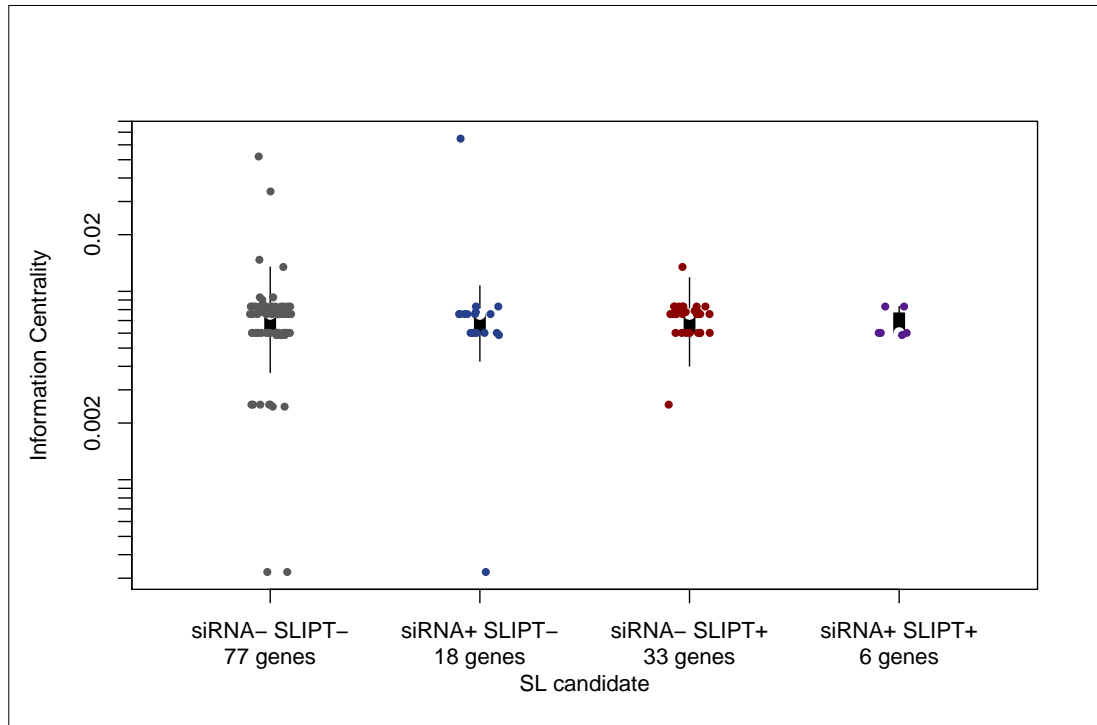
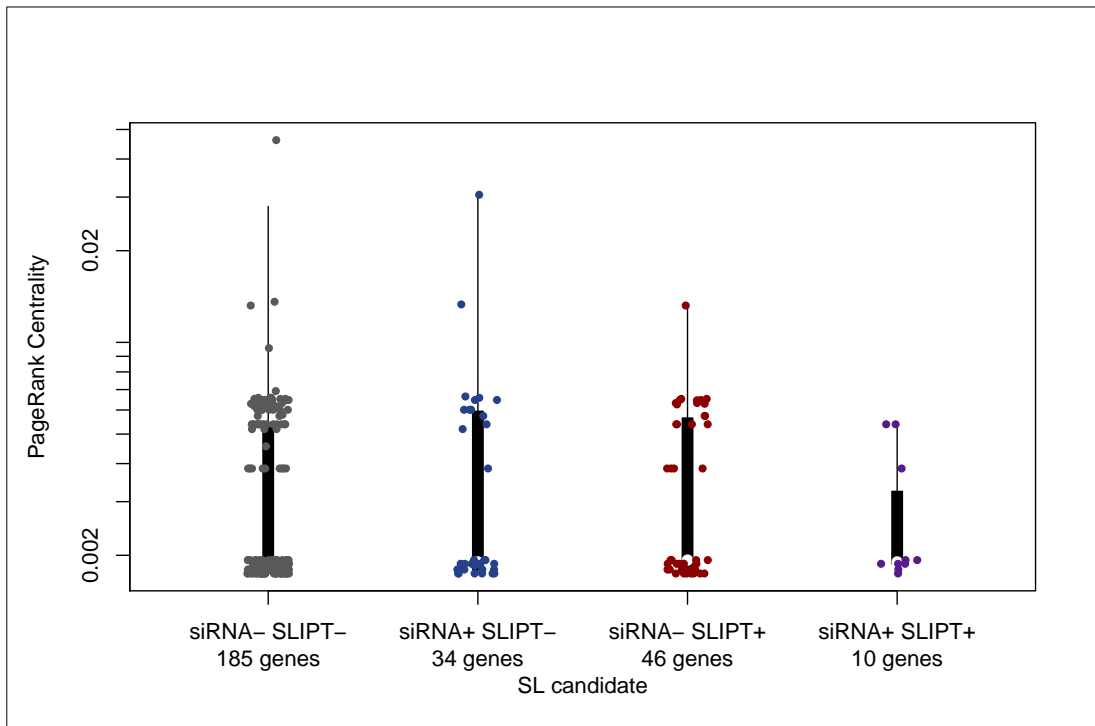


Figure G.2: **Synthetic lethality and centrality.** The information centrality was compared (on a log-scale across genes detected by [mtSLIPT](#) and [siRNA](#) screening in the Reactome PI3K cascade pathway. Genes detected by [mtSLIPT](#) or [siRNA](#) did not have higher connectivity than genes not detected by either approach. The gene with the highest centrality was detected by [siRNA](#).



**Figure G.3: Synthetic lethality and PageRank.** The PageRank centrality was compared (on a log-scale across genes detected by [mtSLIPT](#) and [siRNA](#) screening in the Reactome PI3K cascade pathway. Genes detected by [siRNA](#) had a more restricted range of centrality values than other genes not detected by either approach, although these groups also had fewer genes.

Table G.1: ANOVA for synthetic lethality and vertex degree

	DF	Sum Squares	Mean Squares	F-value	p-value
siRNA	1	15	15.50	0.0134	0.9084
mtSLIPT	1	196	195.94	0.1689	0.6825
siRNA×mtSLIPT	1	9	9.17	0.0079	0.9294

Analysis of variance for [vertex degree](#) against [synthetic lethal](#) detection approaches (with an interaction term)

Table G.2: ANOVA for synthetic lethality and information centrality

	DF	Sum Squares	Mean Squares	F-value	p-value
siRNA	1	0.000256	0.0002561	0.1851	0.6685
mtSLIPT	1	0.003225	0.0032247	2.3308	0.1318
siRNA×mtSLIPT	1	0.001238	0.0012385	0.8952	0.3476

Analysis of variance for [information centrality](#) against [synthetic lethal](#) detection approaches (with an interaction term)

Table G.3: ANOVA for synthetic lethality and PageRank centrality

	DF	Sum Squares	Mean Squares	F-value	p-value
siRNA	1	0.0002038	$2.0385 \times 10^{-4}$	1.1423	0.2892
mtSLIPT	1	0.0000208	$2.0752 \times 10^{-5}$	0.1163	0.7342
siRNA×mtSLIPT	1	0.0000137	$1.3743 \times 10^{-5}$	0.0770	0.7823

Analysis of variance for [PageRank centrality](#) against [synthetic lethal](#) detection approaches (with an interaction term)

## Appendix H

# Information Centrality for Gene Essentiality

Network structure could be used to analyse gene function. This has been performed to investigate network properties of a network constructed from Reactome pathways ([Croft et al., 2014](#)) imported via Pathway Commons with Paxtools ([Cerami et al., 2011](#); [Demir et al., 2013](#)). [Information centrality](#), which has been proposed as a measure of gene [essentiality](#), was calculated as performed by [Kranthi et al. \(2013\)](#) using the efficiency and shortest path between each pair of nodes in the network before and after a node of interest is removed to test the importance of a node to network connectivity. Reactome contains substrates and cofactors in addition to genes or proteins. In support of centrality as a measure of essentiality, a number of nodes with the highest centrality (shown in Table H.1) were essential nutrients including Mg<sup>2+</sup>, Ca<sup>2+</sup>, Zn<sup>2+</sup>, and Fe. In addition, there were genes important in development of epithelial tissues and breast cancer such as *IL8*, *GATA3*, and *CTNNB1* detected with relatively high [information centrality](#).

Table H.1: Information centrality for genes and molecules in the Reactome network

<b>Node</b>	<b>Centrality</b>
<i>ZNF473</i>	0.0510
Magnesium ( $Mg^{2+}$ )	0.0082
<i>XBP1</i>	0.0053
Calcium ( $Ca^{2+}$ )	0.0050
Zinc ( $Zn^{2+}$ )	0.0048
Iron atom (Fe)	0.0041
<i>FMN</i>	0.0040
<i>AGT</i>	0.0037
<i>HSP90AA1</i>	0.0029
Phosphatidyl-L-serine	0.0029
<i>P2RX7</i>	0.0026
<i>PANX1</i>	0.0024
<i>NCAM1</i>	0.0022
<i>NUDT1</i>	0.0021
<i>PLAUR</i>	0.0020
<i>IL8</i>	0.0020
<i>HSPA8</i>	0.0019
<i>TYROBP</i>	0.0019
<i>CASP3</i>	0.0017
<i>GNAL</i>	0.0015
<i>CBLB</i>	0.0015
<i>HBB</i>	0.0014
<i>GATA4</i>	0.0013
<i>TGS1</i>	0.0013
<i>CTNNB1</i>	0.0012

Highest information centrality for genes (proteins), cofactors, and minerals in the Reactome network

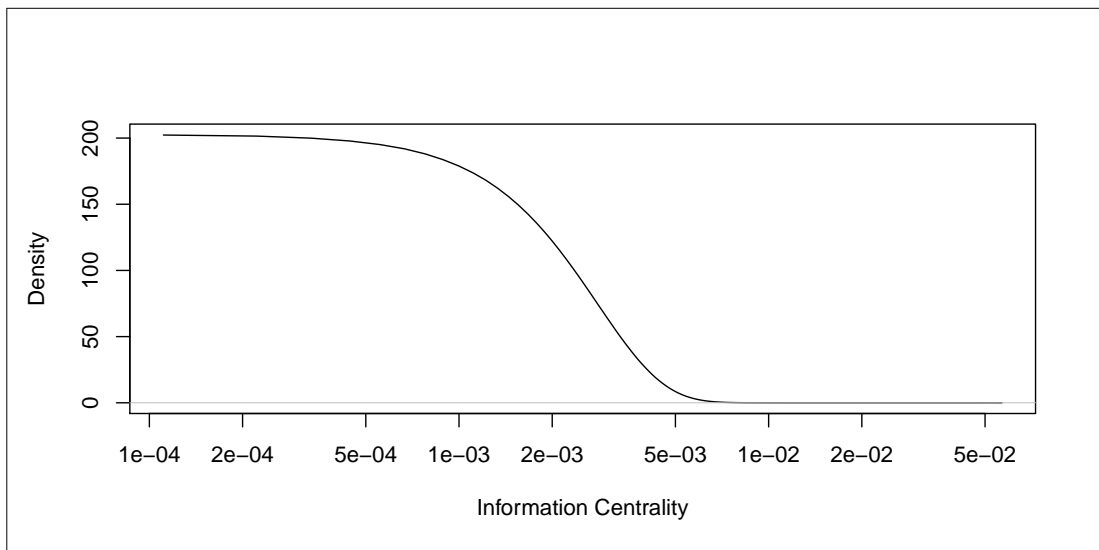


Figure H.1: **Information centrality distribution.** [Information centrality](#) in the Reactome network for nodes, including genes/proteins and other biomolecules.

# Appendix I

## Pathway Structure for Mutation SLIPT

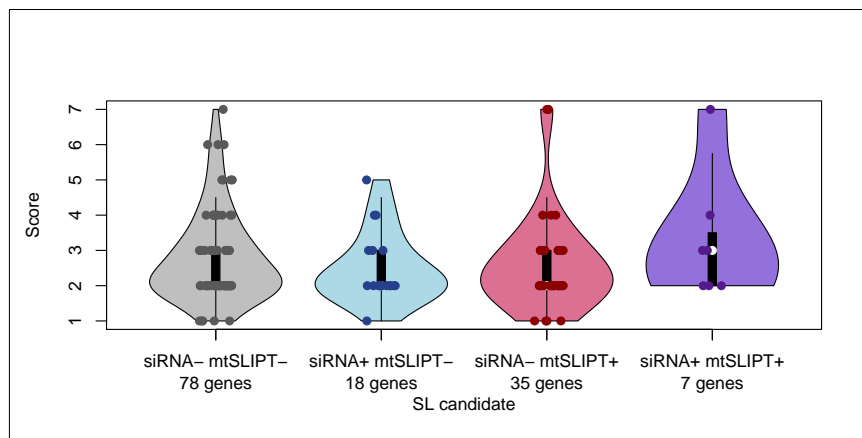
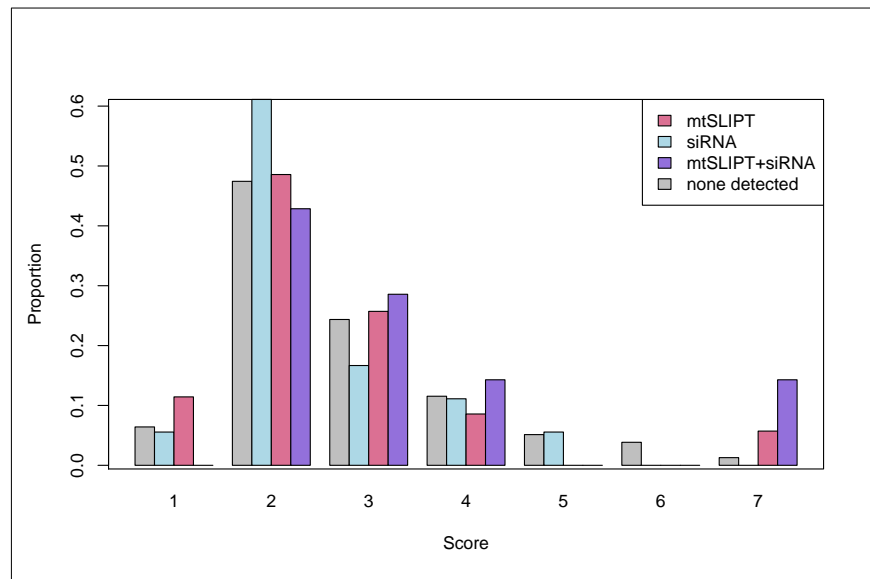


Figure I.1: Synthetic lethality and heirarchy score in PI3K. The hierarchical distance scores were similarly distributed across mtSLIPT and siRNA genes. Genes detected by both methods had a higher (downstream) median than either group.

Table I.1: ANOVA for synthetic lethality and PI3K hierarchy

	DF	Sum Squares	Mean Squares	F-value	p-value
siRNA	1	0.001	0.00070	0.0004	0.9841
mtSLIPT	1	0.007	0.0066	0.0040	0.9496
siRNA×mtSLIPT	1	3.906	3.9056	2.3829	0.1250

Analysis of variance for PI3K hierarchy score against synthetic lethal detection approaches (with an interaction term)



**Figure I.2: Hierarchy score in PI3K against synthetic lethality in PI3K.** The number of mtSLIPT and siRNA genes against the hierarchical distance scores showing no significant tendency for either method to either of the pathway upstream or downstream extremities.

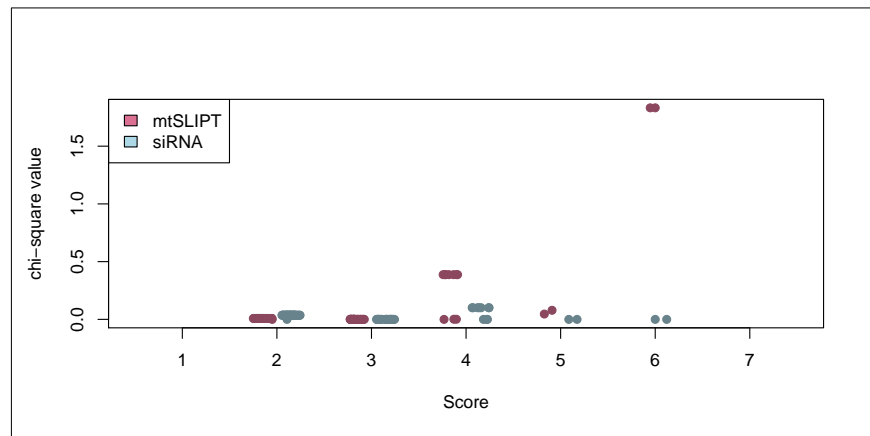


**Figure I.3: Structure of synthetic lethality in PI3K.** The number of mtSLIPT and siRNA genes against the hierarchical distance scores showing no significant tendency for either method to either of the pathway upstream or downstream extremities. The number of mtSLIPT and siRNA genes upstream or downstream of each gene in the Reactome PI3K pathway were tested (by the  $\chi^2$ -test). These were plotted as a split jitter stripchart against the hierarchical distance scores showing no significant tendency for either method to either of the pathway upstream or downstream extremities.

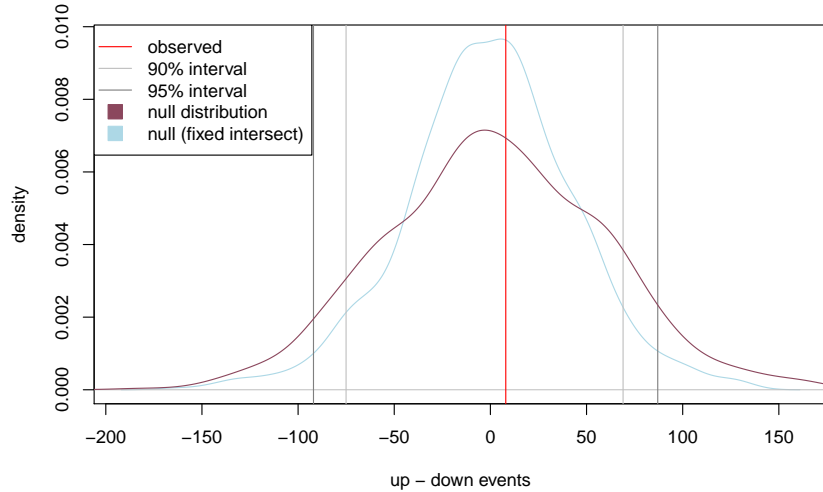


**Figure I.4: Structure of synthetic lethality resampling.** A null distribution (10,000 iterations) of the siRNA genes upstream or downstream of mtSLIPT genes (shown by the difference) in the PI3K pathway. The observed events (red) were compared to the the distribution (violet) and were not significant. Genes detected by both methods were fixed for the distribution (blue). The genes detected by both approaches were used.

Table I.2: Resampling for pathway structure of synthetic lethal detection methods

Pathway	Graph		States		Observed				Permutation p-value	
	Nodes	Edges	mtSL	siRNA	Up	Down	Up-Down	Up/Down	Up-Down	Down-Up
PI3K Cascade	138	1495	42	25	131	123	8	1.065	0.4473	0.5466
PI3K/AKT Signalling in Cancer	275	12882	56	44	478	440	38	1.086	0.4163	0.5810
<b>G<sub>αi</sub> Signalling</b>	292	22003	57	58	543	866	-323	0.627	0.9507	0.0488
GPCR downstream	1270	142071	218	160	7632	6500	1132	1.174	0.1707	0.8291
Elastic fibre formation	42	175	16	7	6	7	-1	0.857	0.5512	0.3681
Extracellular matrix	299	3677	81	29	313	347	-34	0.902	0.5762	0.4215
Formation of Fibrin	52	243	11	5	8	19	-11	0.421	0.7993	0.1800
Nonsense-Mediated Decay	103	102	56	2	0	0	0		0.197	0.1373
3'-UTR-mediated translational regulation	107	2860	56	1	52	1	51	52	0.1210	0.8751
Eukaryotic Translation Elongation	92	3746	57	0	0	0	0		0.4952	0.4892

Pathways in the Reactome network tested for structural relationships between mtSLIPT and siRNA genes by resampling. The raw p-value (computed without adjusting for multiple comparisons over pathways) is given for the difference in upstream and downstream paths from mtSLIPT to siRNA gene candidate partners of CDH1 with significant pathways highlighted in bold. Sampling was performed only in the target pathway and shortest paths were computed within it. Loops or paths in either direction that could not be resolved were excluded from the analysis. The gene detected by both mtSLIPT and siRNA (or resampling for them) were included in the analysis and the number of these were fixed to the number observed.

## Appendix J

# Performance of SLIPT and $\chi^2$

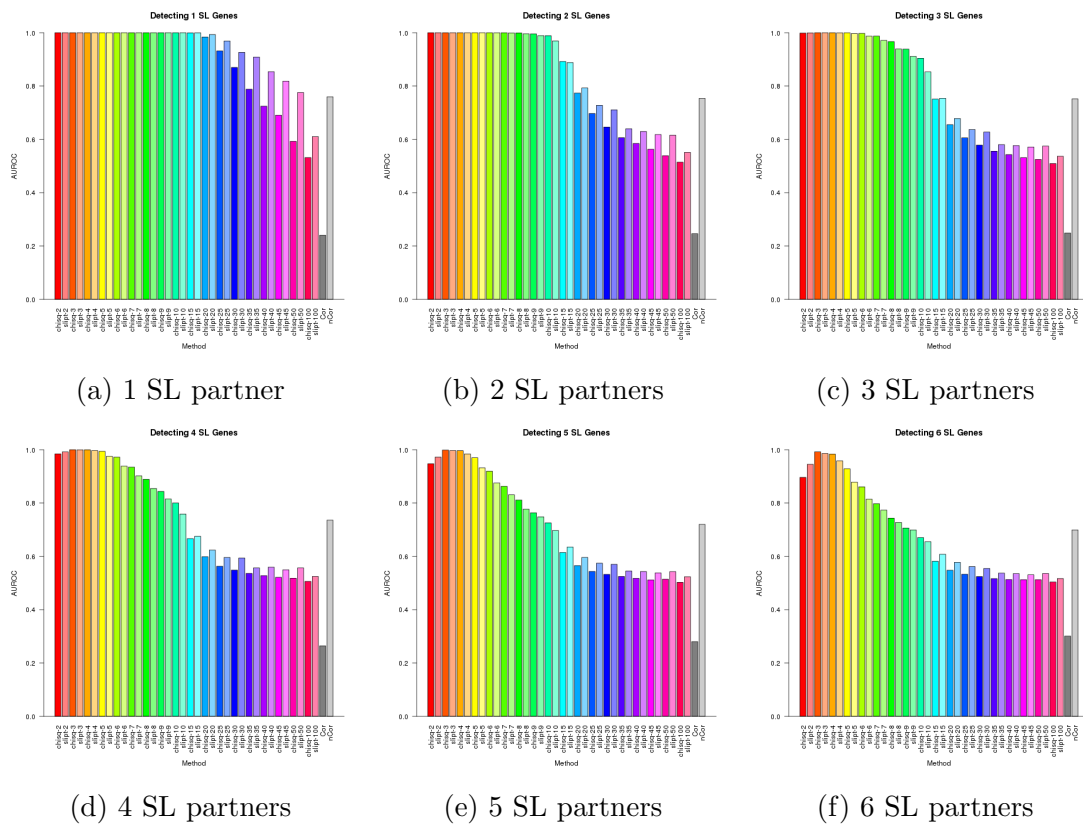
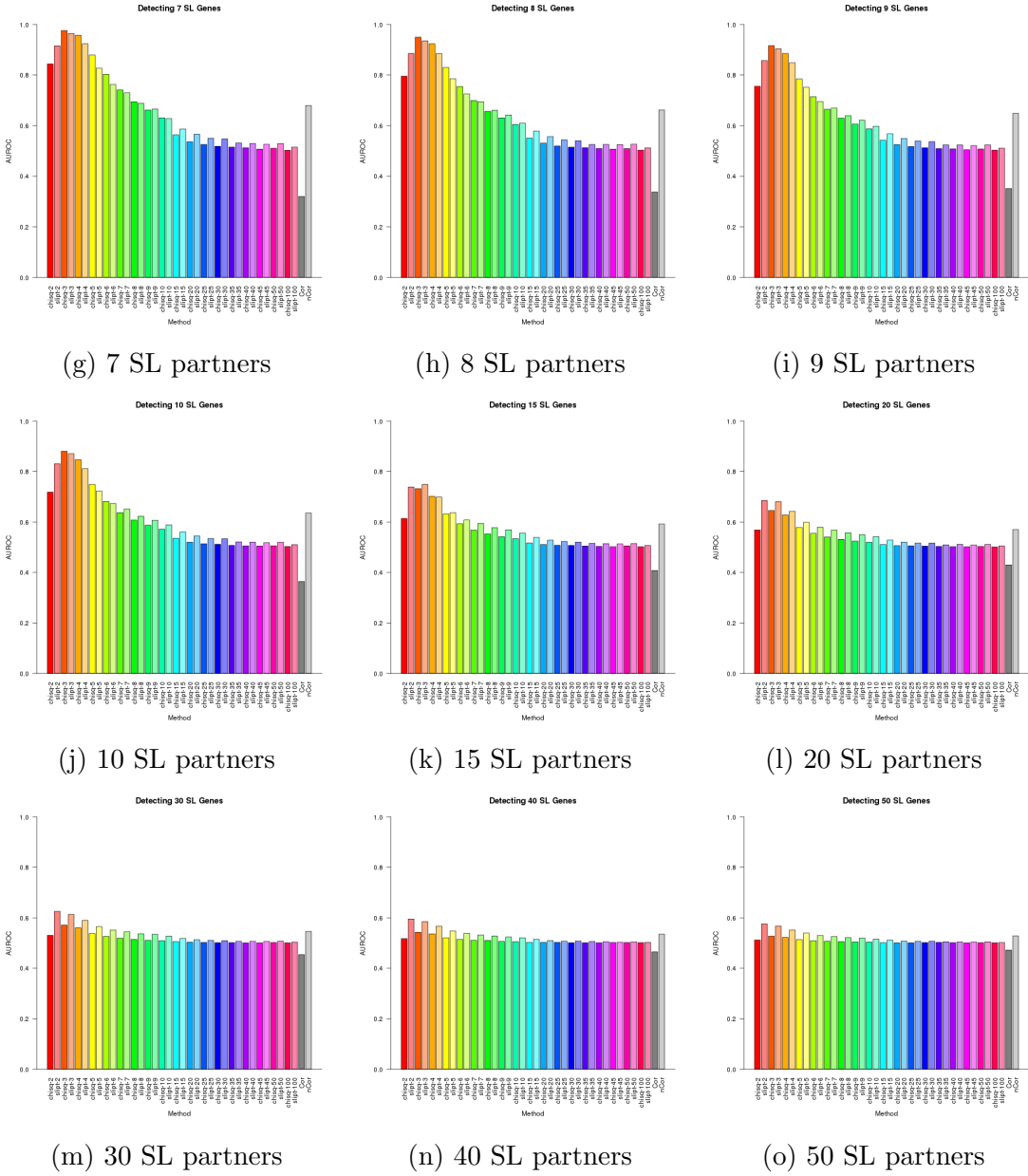


Figure J.1: **Performance of  $\chi^2$  and SLIPT across quantiles.** (continued on next page)



**Figure J.1: Performance of  $\chi^2$  and SLIPT across quantiles.** Synthetic lethal detection with quantiles as in axis labels. The barplots have the same hue for each quantile (grey for correlation) and darker for  $\chi^2$  (and positive correlation). SLIPT and  $\chi^2$  performed similarly, peaking at  $1/3$ -quantiles and converging to random (0.5). Negative correlation was higher than positive but not optimal quantiles for SLIPT or  $\chi^2$ . These findings were robust across different numbers of underlying synthetic lethal genes in 10,000 simulations of 100 genes and 1000 samples. SLIPT performed better than  $\chi^2$  for higher numbers of synthetic lethal genes and finer quantiles.

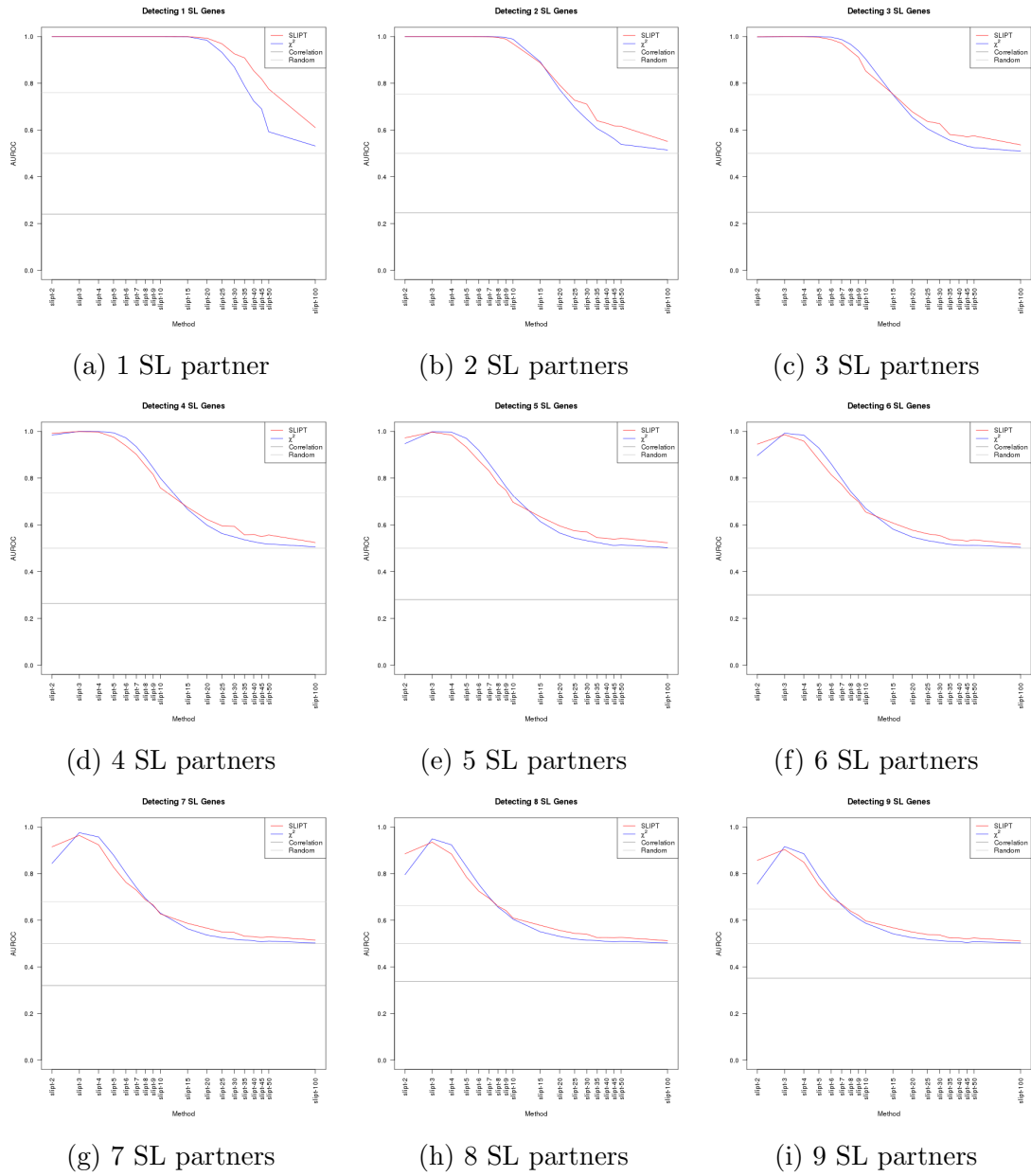
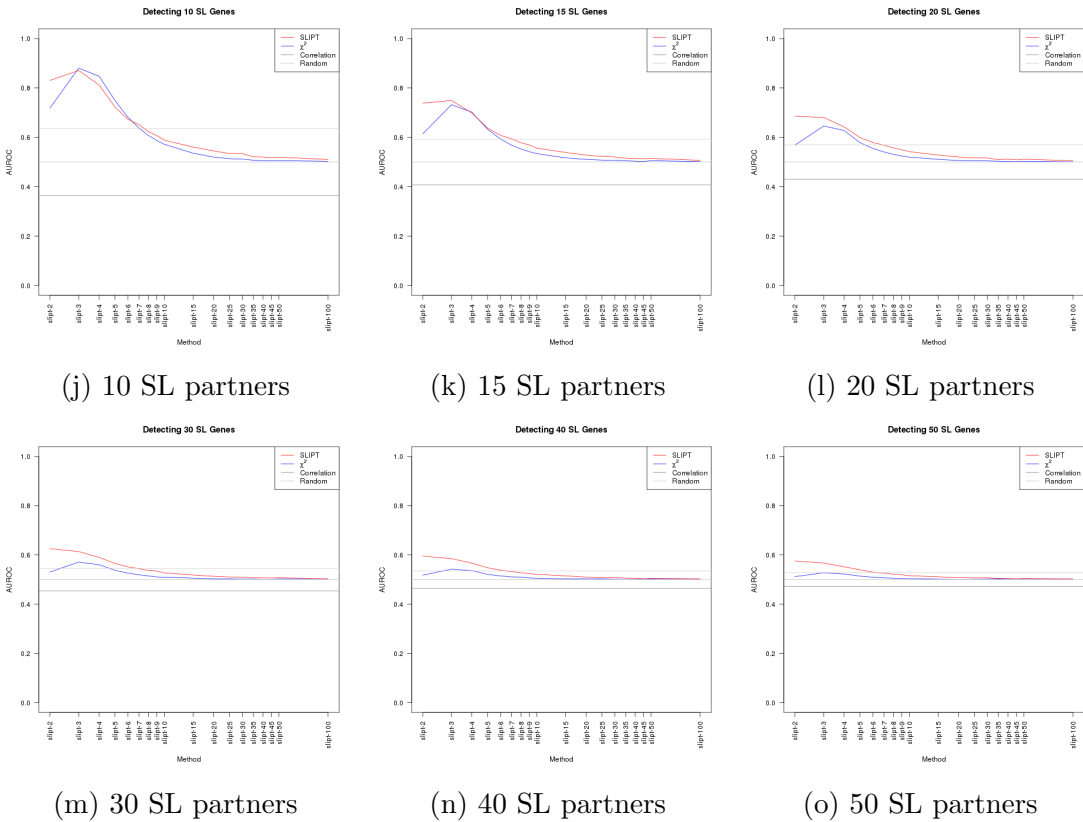


Figure J.2: **Performance of  $\chi^2$  and SLIPT across quantiles.** (continued on next page)



**Figure J.2: Performance of  $\chi^2$  and SLIPT across quantiles.** Synthetic lethal detection with quantiles as in axis labels. The line plots are coloured for SLIPT (red),  $\chi^2$  (blue) and correlation (grey), according to the legend. SLIPT and  $\chi^2$  performed similarly, peaking at  $1/3$ -quantiles and converging to random (0.5). Negative correlation was higher than positive but not optimal quantiles for SLIPT or  $\chi^2$ . These findings were robust across different numbers of underlying synthetic lethal genes in 10,000 simulations of 100 genes and 1000 samples. SLIPT performed better than  $\chi^2$  for higher numbers of synthetic lethal genes and finer quantiles.

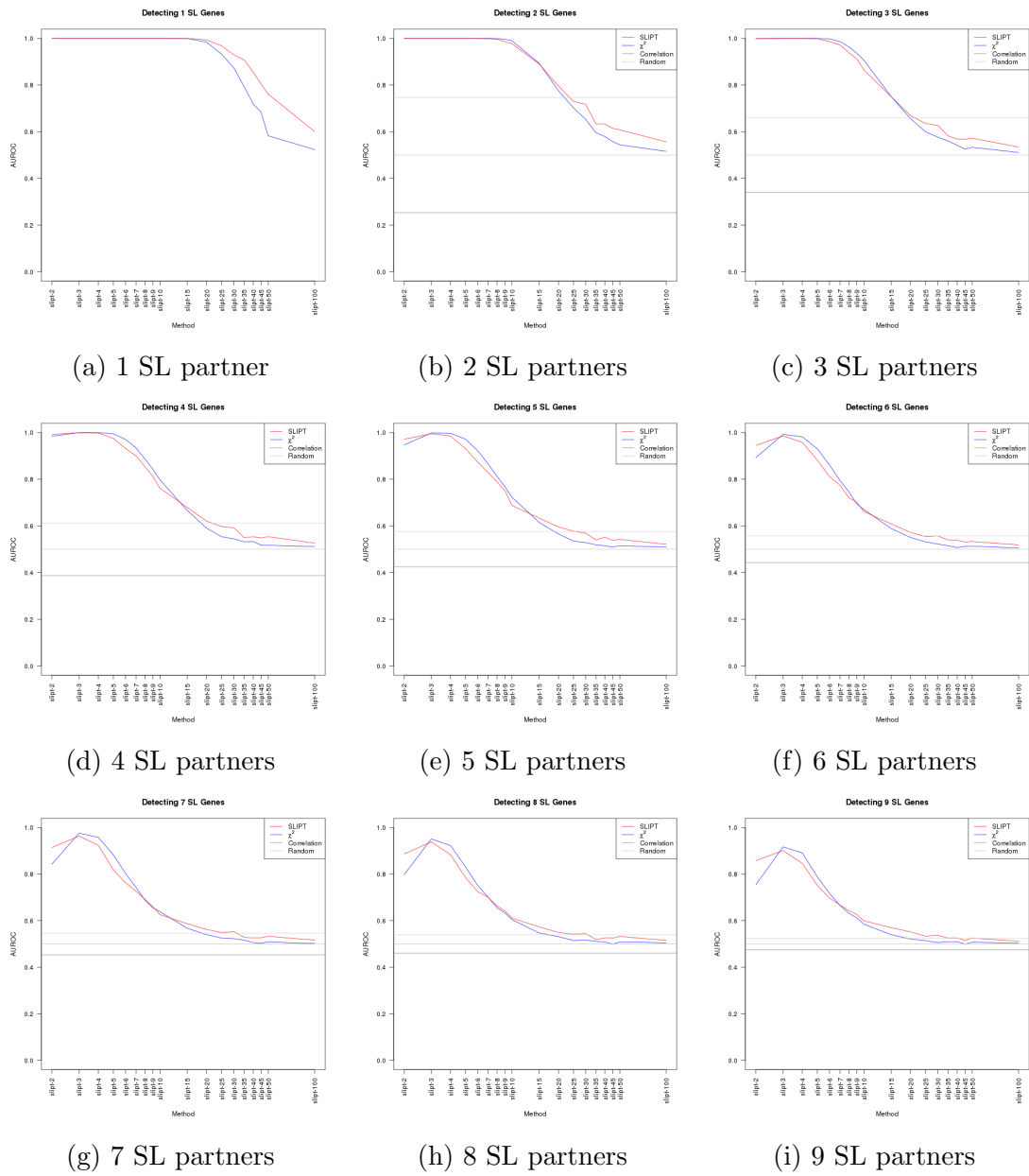
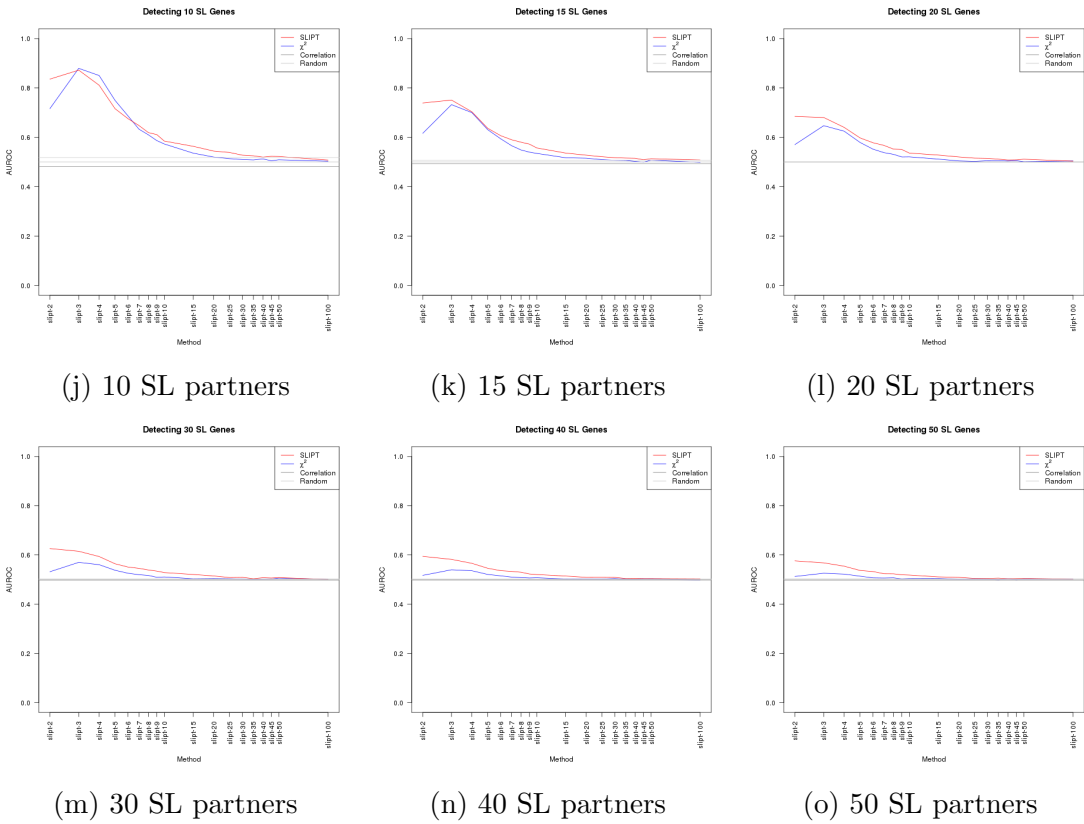


Figure J.3: **Performance of  $\chi^2$  and SLIPT across quantiles with more genes.**  
 (continued on next page)



**Figure J.3: Performance of  $\chi^2$  and SLIPT across quantiles with more genes.**  
 Synthetic lethal detection with quantiles as in axis labels. The line plots are coloured for SLIPT (red),  $\chi^2$  (blue) and correlation (grey), according to the legend. SLIPT and  $\chi^2$  performed similarly, peaking at  $1/3$ -quantiles and converging to random (0.5). Negative correlation was higher than positive but not optimal quantiles for SLIPT or  $\chi^2$ . These findings were robust across different numbers of underlying synthetic lethal genes in 1000 simulations of 20,000 genes and 1000 samples. SLIPT performed better than  $\chi^2$  for higher numbers of synthetic lethal genes and finer quantiles.

## J.1 Correlated Query Genes affects Specificity

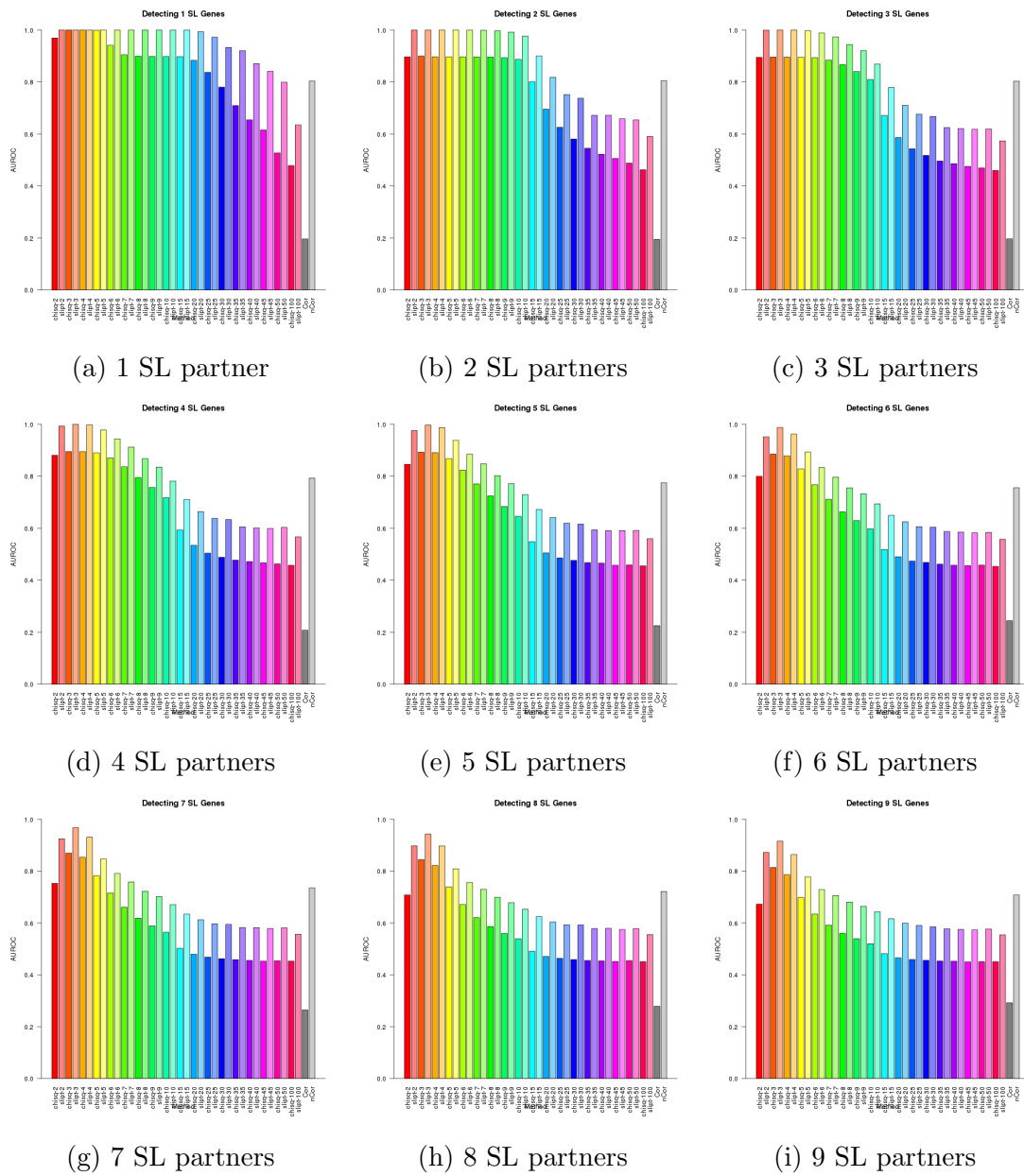
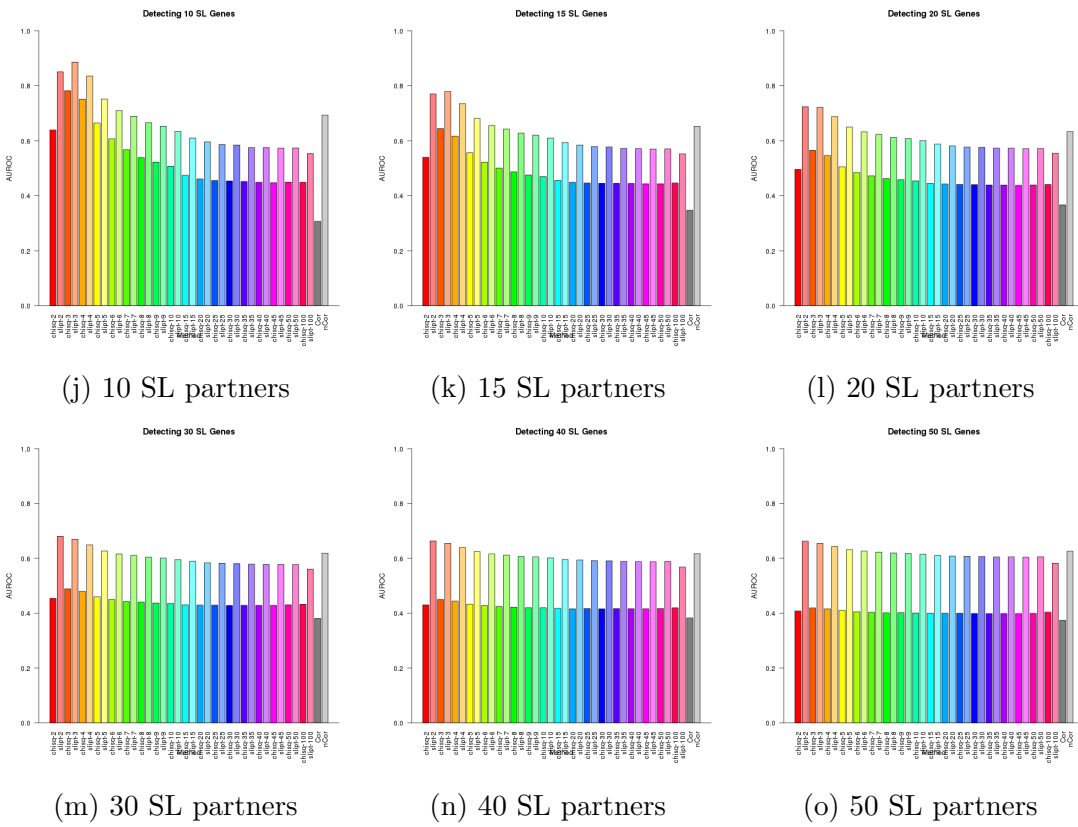


Figure J.4: **Performance of  $\chi^2$  and SLIPT across quantiles with query correlation.** (continued on next page)



**Figure J.4: Performance of  $\chi^2$  and SLIPT across quantiles with query correlation.** Synthetic lethal detection with quantiles as in axis labels. The barplots have the same hue for each quantile (grey for correlation) and darker for  $\chi^2$  (and positive correlation). SLIPT and  $\chi^2$  performed similarly, peaking at  $1/3$ -quantiles and converging to random (0.5). Negative correlation was higher than positive but not optimal quantiles for SLIPT or  $\chi^2$ . These findings were robust across different numbers of underlying synthetic lethal genes in 10,000 simulations of 100 genes (including 10 correlated with the query) and 1000 samples. SLIPT performed consistently better than  $\chi^2$  with positively correlated genes.

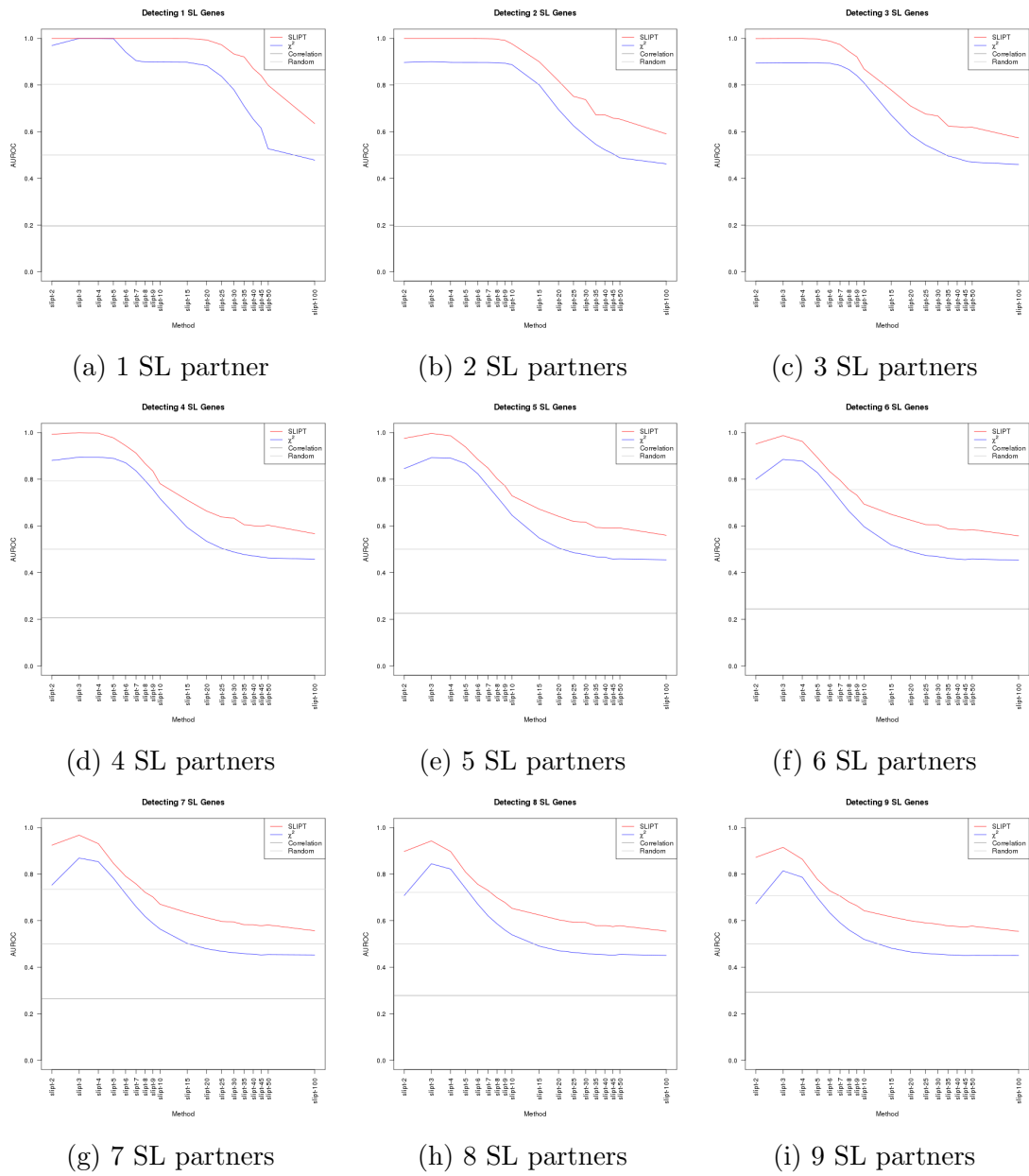
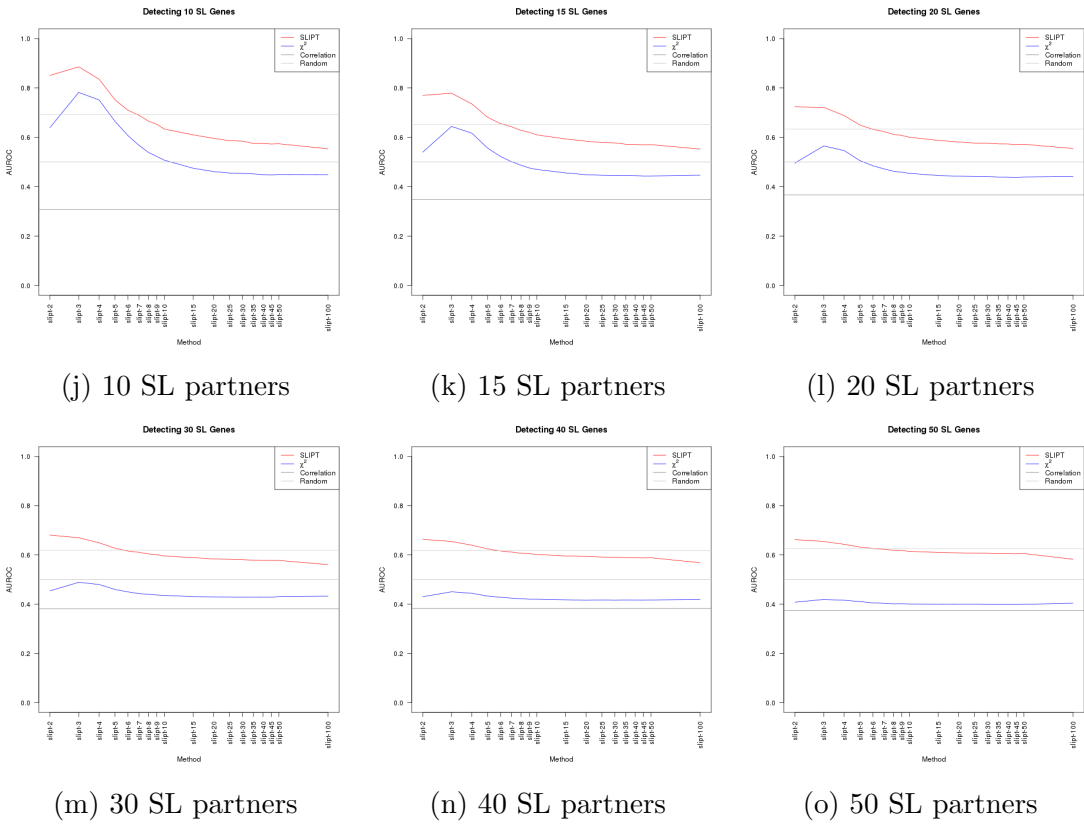


Figure J.5: **Performance of  $\chi^2$  and SLIPT across quantiles with query correlation.** (continued on next page)



**Figure J.5: Performance of  $\chi^2$  and SLIPT across quantiles with query correlation.** Synthetic lethal detection with quantiles as in axis labels. The line plots are coloured for SLIPT (red),  $\chi^2$  (blue) and correlation (grey), according to the legend. SLIPT and  $\chi^2$  performed similarly, peaking at  $1/3$ -quantiles and converging to random (0.5). Negative correlation was higher than positive but not optimal quantiles for SLIPT or  $\chi^2$ . These findings were robust across different numbers of underlying synthetic lethal genes in 10,000 simulations of 100 genes (including 10 correlated with the query) and 1000 samples. SLIPT performed consistently better than  $\chi^2$  with positively correlated genes.

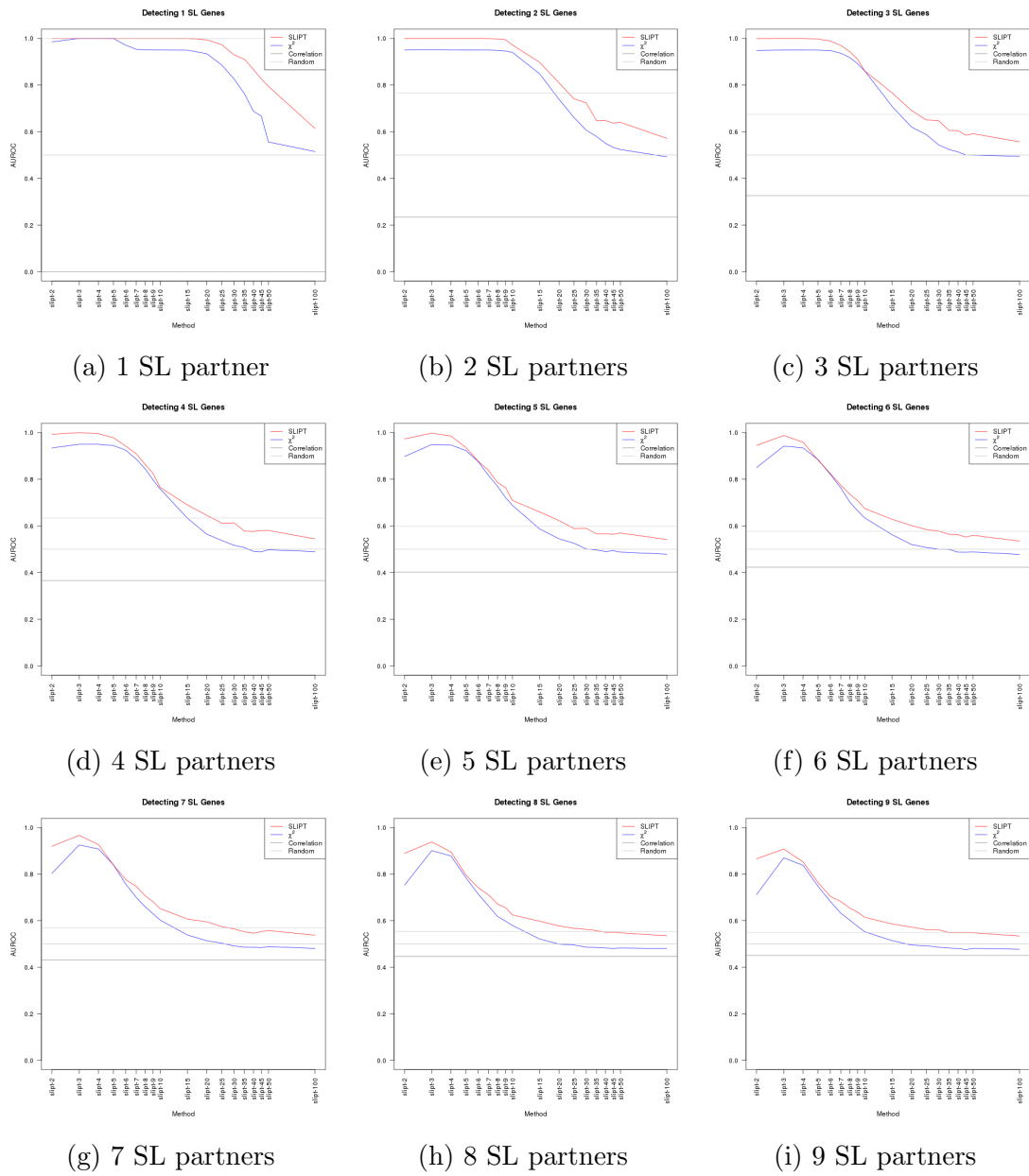
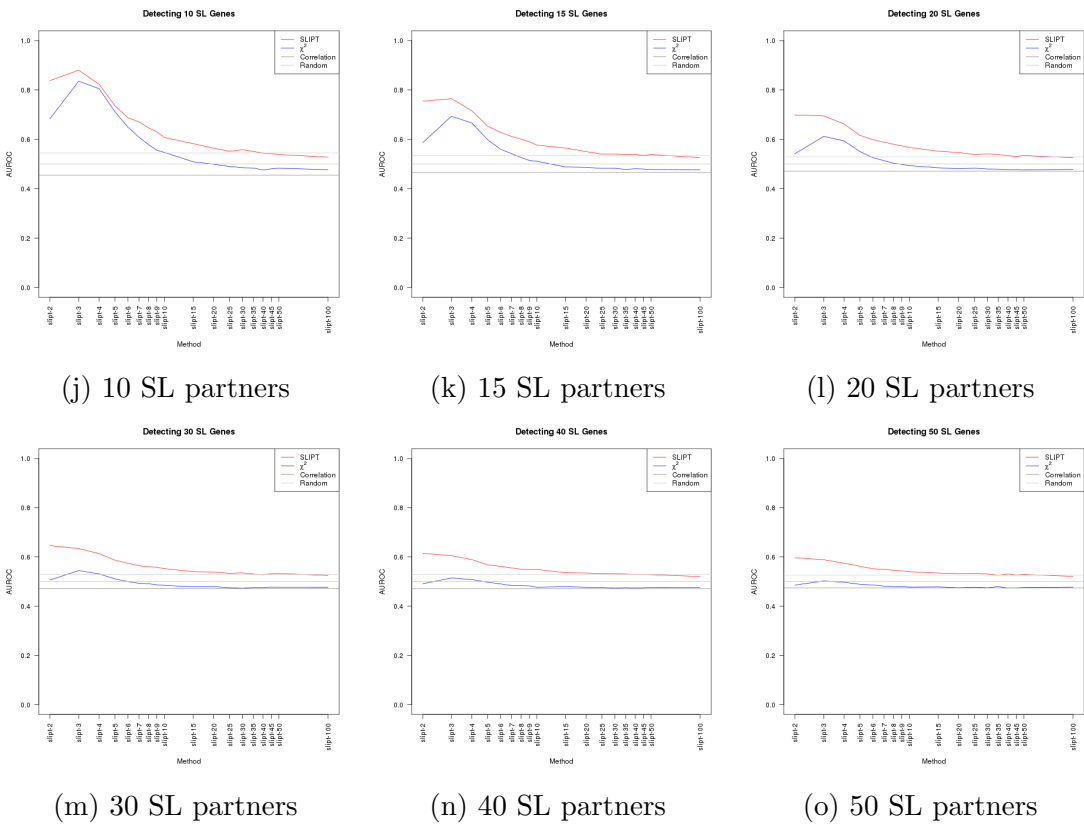


Figure J.6: **Performance of  $\chi^2$  and SLIPT across quantiles with query correlation and more genes.** (continued on next page)



**Figure J.6: Performance of  $\chi^2$  and SLIPT across quantiles with query correlation and more genes.** Synthetic lethal detection with quantiles as in axis labels. The line plots are coloured for SLIPT (red),  $\chi^2$  (blue) and correlation (grey), according to the legend. SLIPT and  $\chi^2$  performed similarly, peaking at  $1/3$ -quantiles and converging to random (0.5). Negative correlation was higher than positive but not optimal quantiles for SLIPT or  $\chi^2$ . These findings were robust across different numbers of underlying synthetic lethal genes in 1000 simulations of 20,000 genes (including 1000 correlated with the query) and 1000 samples. SLIPT performed consistently better than  $\chi^2$  with positively correlated genes.

# Appendix K

## Simulations on Graph Structures

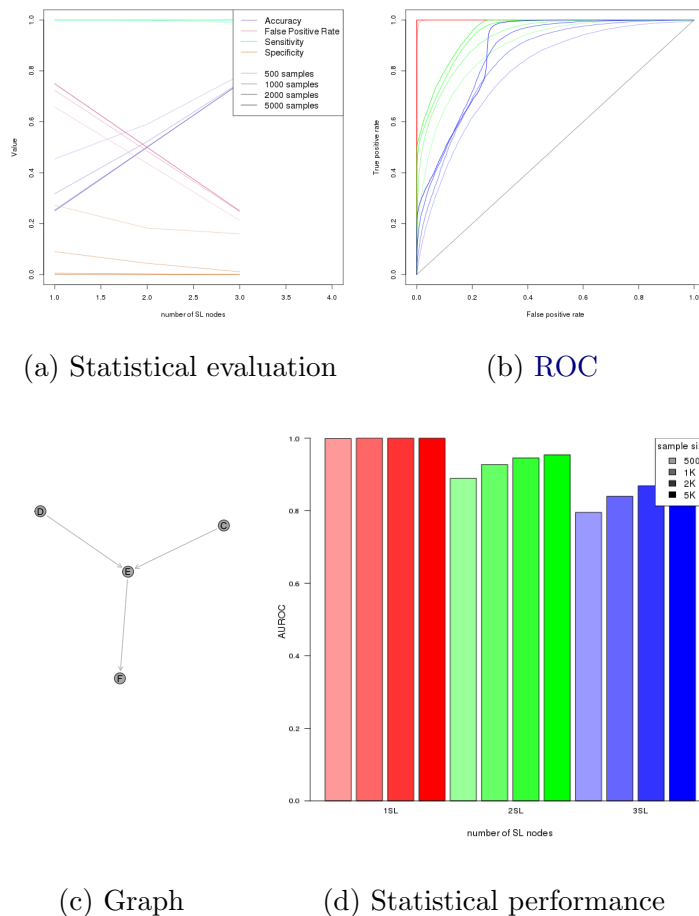


Figure K.1: **Performance of simulations on a simple graph.** Simulation of synthetic lethality was performed using a multivariate normal distribution from a converging graph. For each parameter, 10,000 simulations were used. Colours in Figure K.1b match Figure K.1d.

### K.0.1 Simulations from Inhibiting Graph Structures

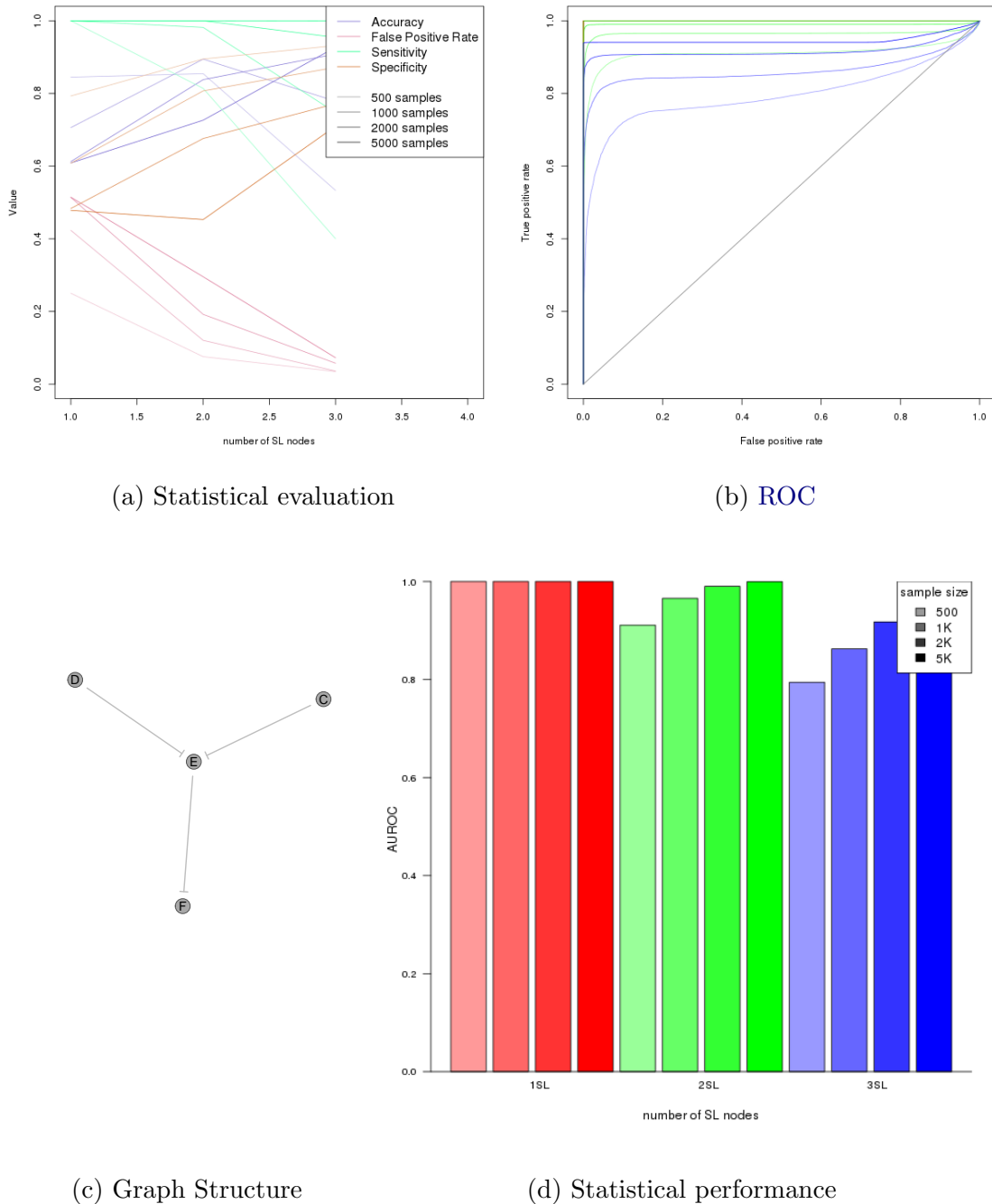
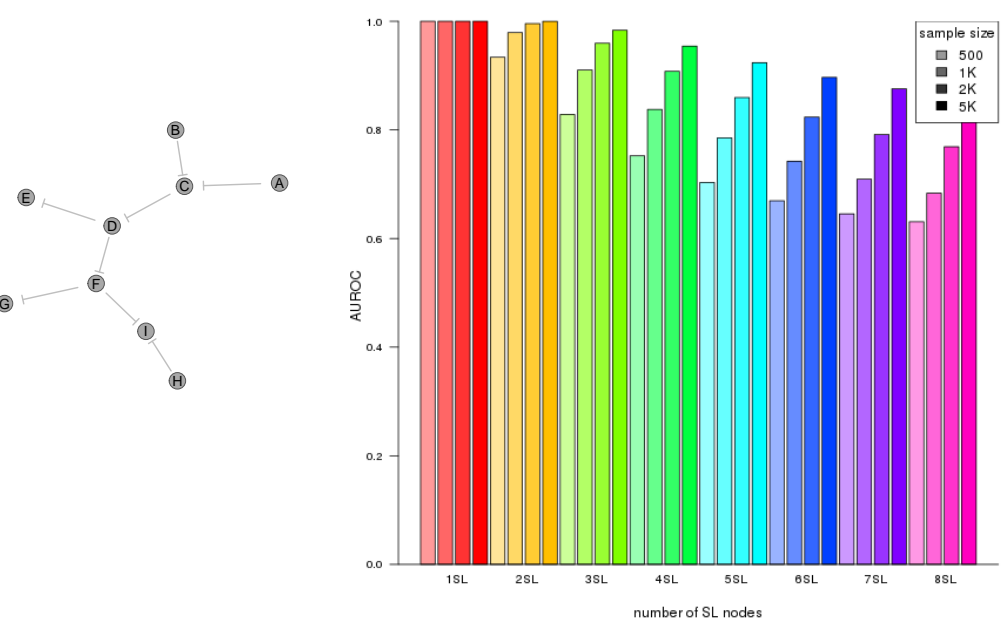
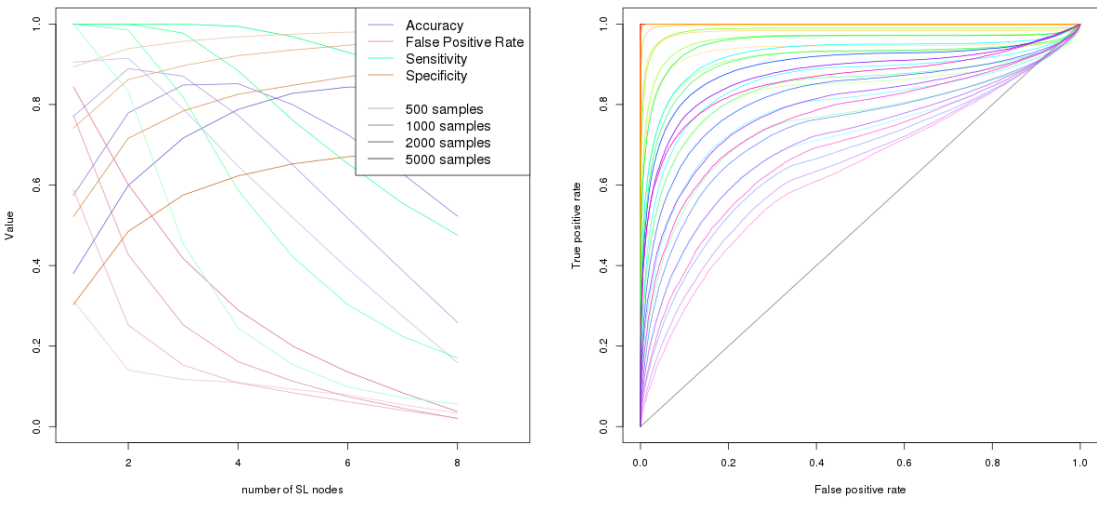
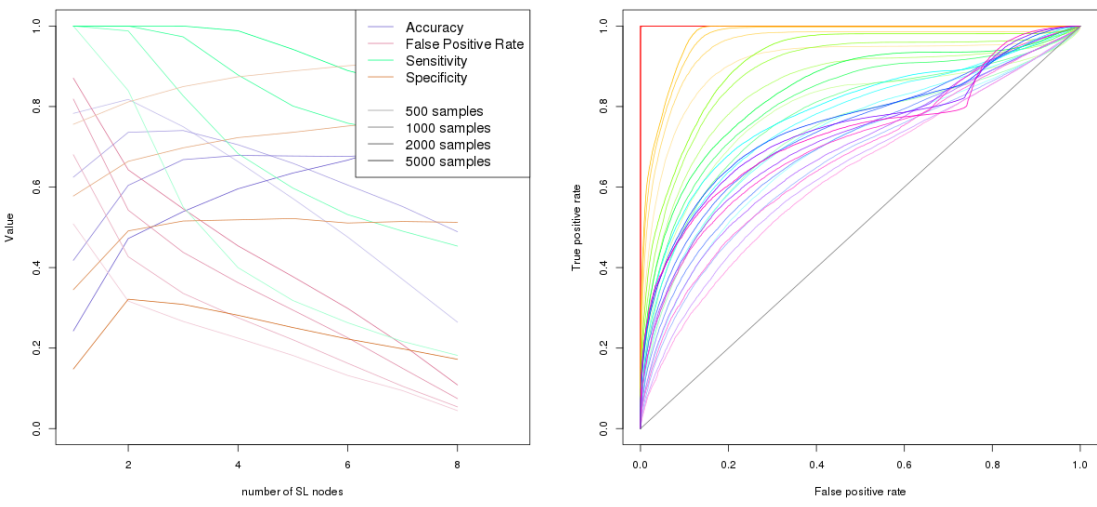


Figure K.2: **Performance of simulations on an inhibiting graph.** Simulation of synthetic lethality used a multivariate normal distribution from a converging graph. For each parameter, 10,000 simulations were used. Colours in Figure K.2b match Figure K.2d.

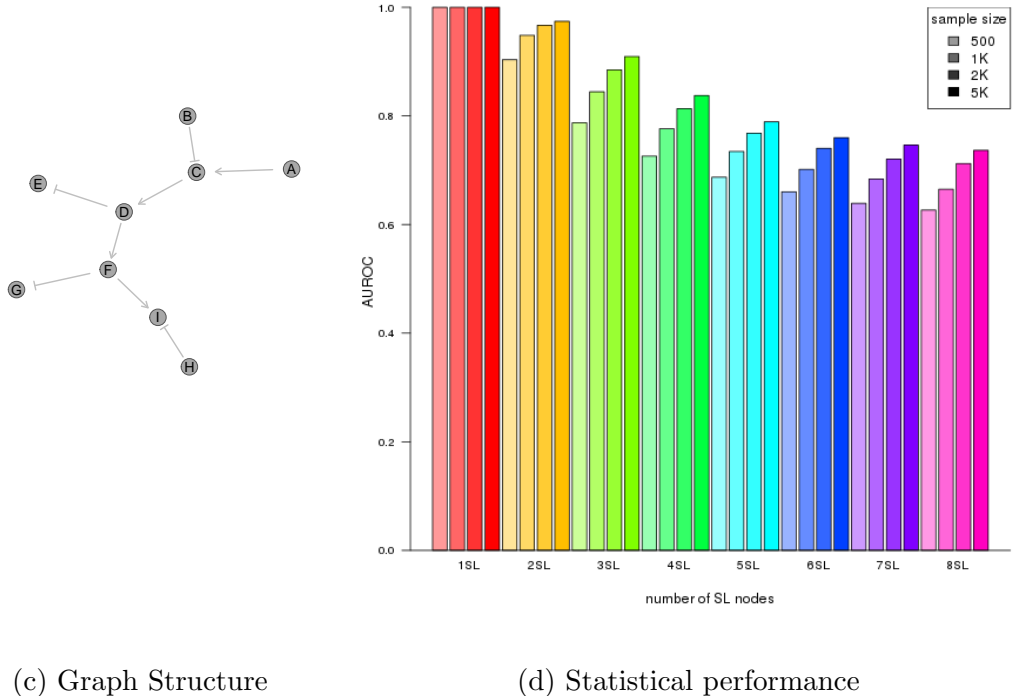


**Figure K.3: Performance of simulations on a constructed graph with inhibition.**  
 Simulation of synthetic lethality used a multivariate normal distribution from a pathway with only inhibitions. For each parameter, 10,000 simulations were used. Colours in Figure K.3b match Figure K.3d.



(a) Statistical evaluation

(b) ROC

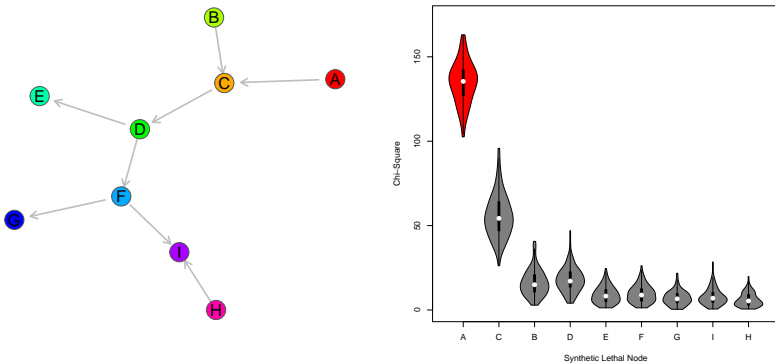


(c) Graph Structure

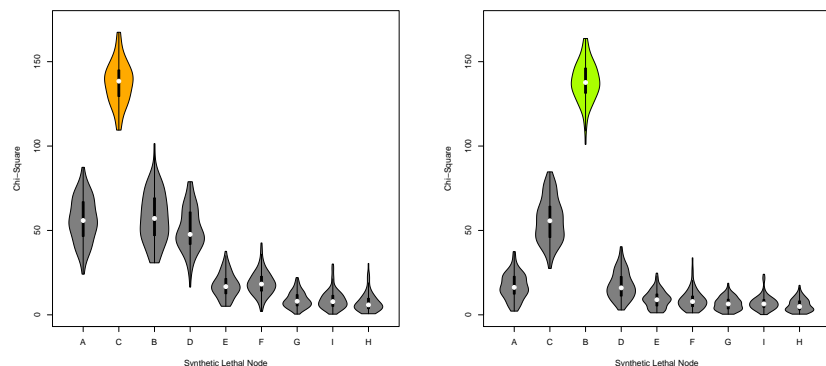
(d) Statistical performance

**Figure K.4: Performance of simulations on a constructed graph with inhibition.**  
 Simulation of synthetic lethality used a multivariate normal distribution from a pathway with a combination of inhibitions. For each parameter, 10,000 simulations were used. Colours in Figure K.4b match Figure K.4d.

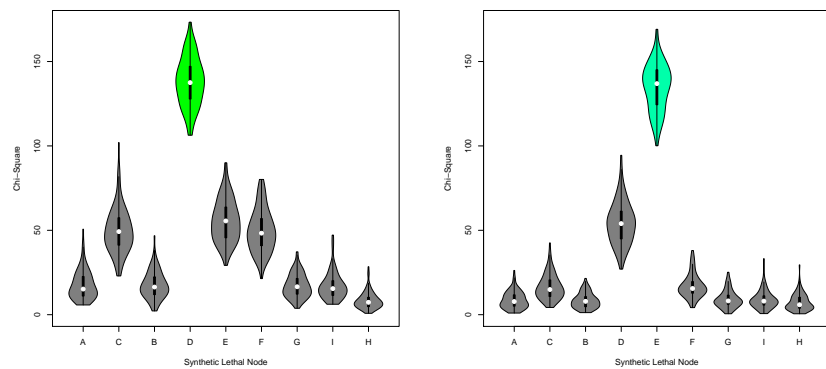
## K.1 Simulation across Graph Structures



(a) Activating Graph Structure      (b)  $\chi^2$  distribution for “A” SL



(c) Gene “B” SL      (d) Gene “C” SL



(e) Gene “D” SL      (f) Gene “E” SL

Figure K.5: **Detection of synthetic lethality within a graph Structure.** (continued on next page)

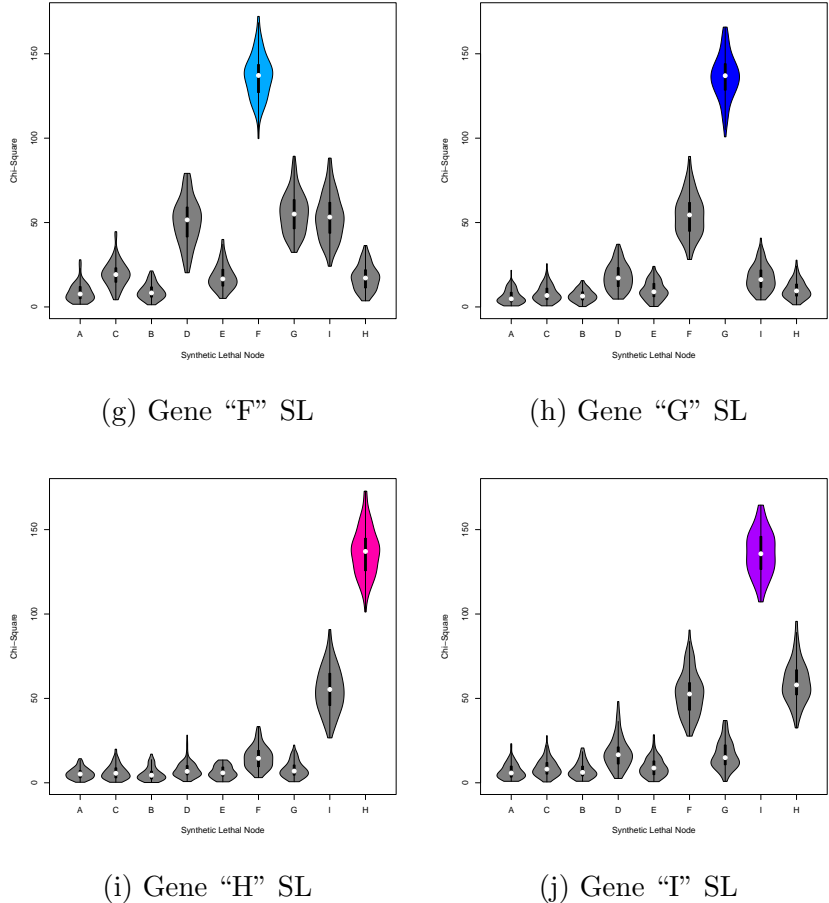
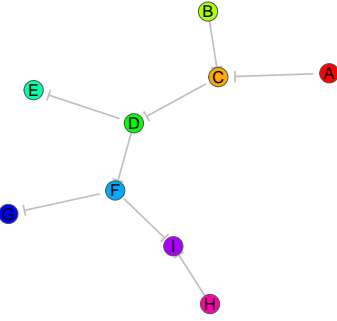
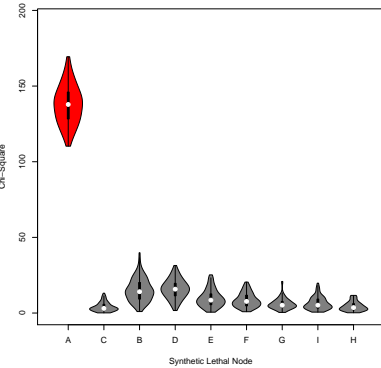


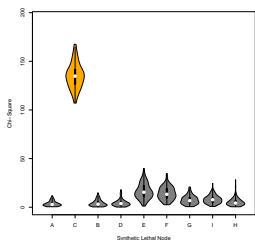
**Figure K.5: Detection of synthetic lethality within a graph structure.** Each gene was designated to be synthetic lethal separately and the  $\chi^2$  value from [SLIPT](#) was computed for each gene across the graph. For each synthetic lethal gene (highlighted in the respective colours), the  $\chi^2$  values were computed in 100 simulations of datasets of 20,000 genes including the graph structure and 1000 samples. For each synthetic lethal gene, the adjacent genes in the network also had elevated test statistics.



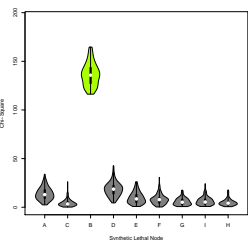
(a) Inhibiting Graph Structure



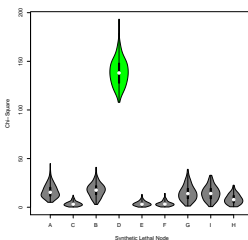
(b)  $\chi^2$  distribution for "A" SL



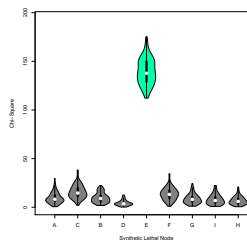
(c) Gene "B" SL



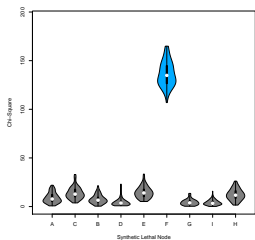
(d) Gene "C" SL



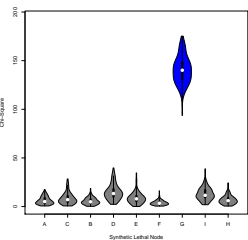
(e) Gene "D" SL



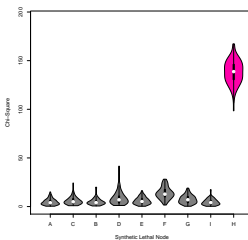
(f) Gene "E" SL



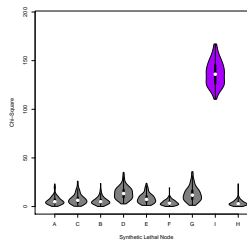
(g) Gene "F" SL



(h) Gene "G" SL

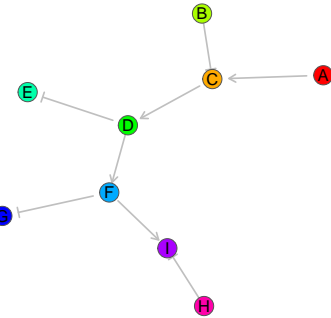


(i) Gene "H" SL

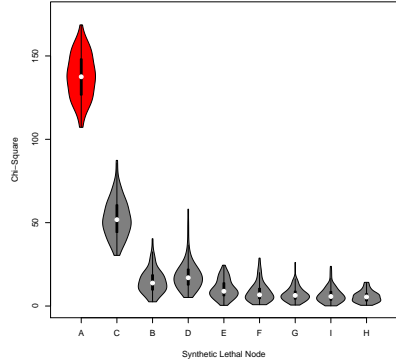


(j) Gene "I" SL

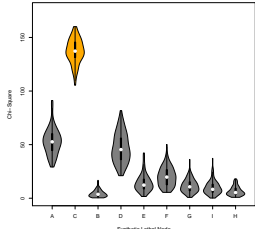
**Figure K.6: Detection of synthetic lethality within an inhibiting graph.** Each gene was designated to be synthetic lethal separately and the  $\chi^2$  value from [SLIPT](#) was computed for each gene across the graph structure with inhibiting relationships. For each synthetic lethal gene (highlighted in the respective colours), the  $\chi^2$  values were computed in 100 simulations of datasets of 20,000 genes including the graph structure and 1000 samples. For each synthetic lethal gene, the adjacent genes exhibited lower  $\chi^2$  values with inhibiting relationships.



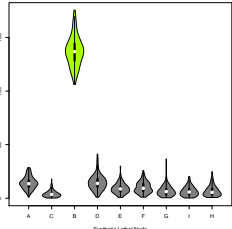
(a) Inhibiting Graph Structure



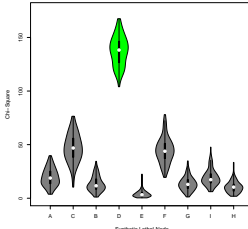
(b)  $\chi^2$  distribution for "A" SL



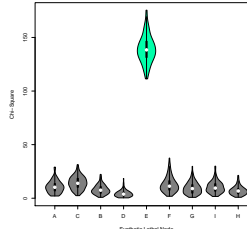
(c) Gene "B" SL



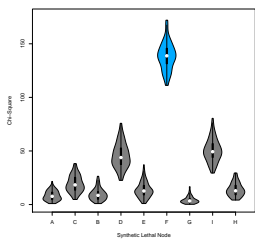
(d) Gene "C" SL



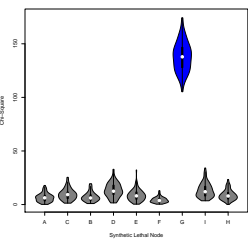
(e) Gene "D" SL



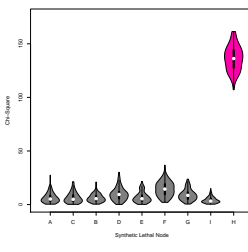
(f) Gene "E" SL



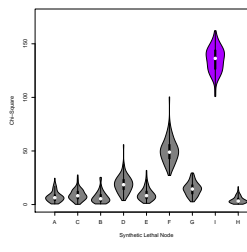
(g) Gene "F" SL



(h) Gene "G" SL



(i) Gene "H" SL



(j) Gene "I" SL

**Figure K.7: Detection of synthetic lethality within an inhibiting graph.** Each gene was designated to be synthetic lethal separately and the  $\chi^2$  value from **SLIPT** was computed for each gene across the graph structure with inhibiting and relationships. For each synthetic lethal gene (highlighted in the respective colours), the  $\chi^2$  values were computed in 100 simulations of datasets of 20,000 genes including the graph structure and 1000 samples.

## K.2 Simulations from Complex Graph Structures

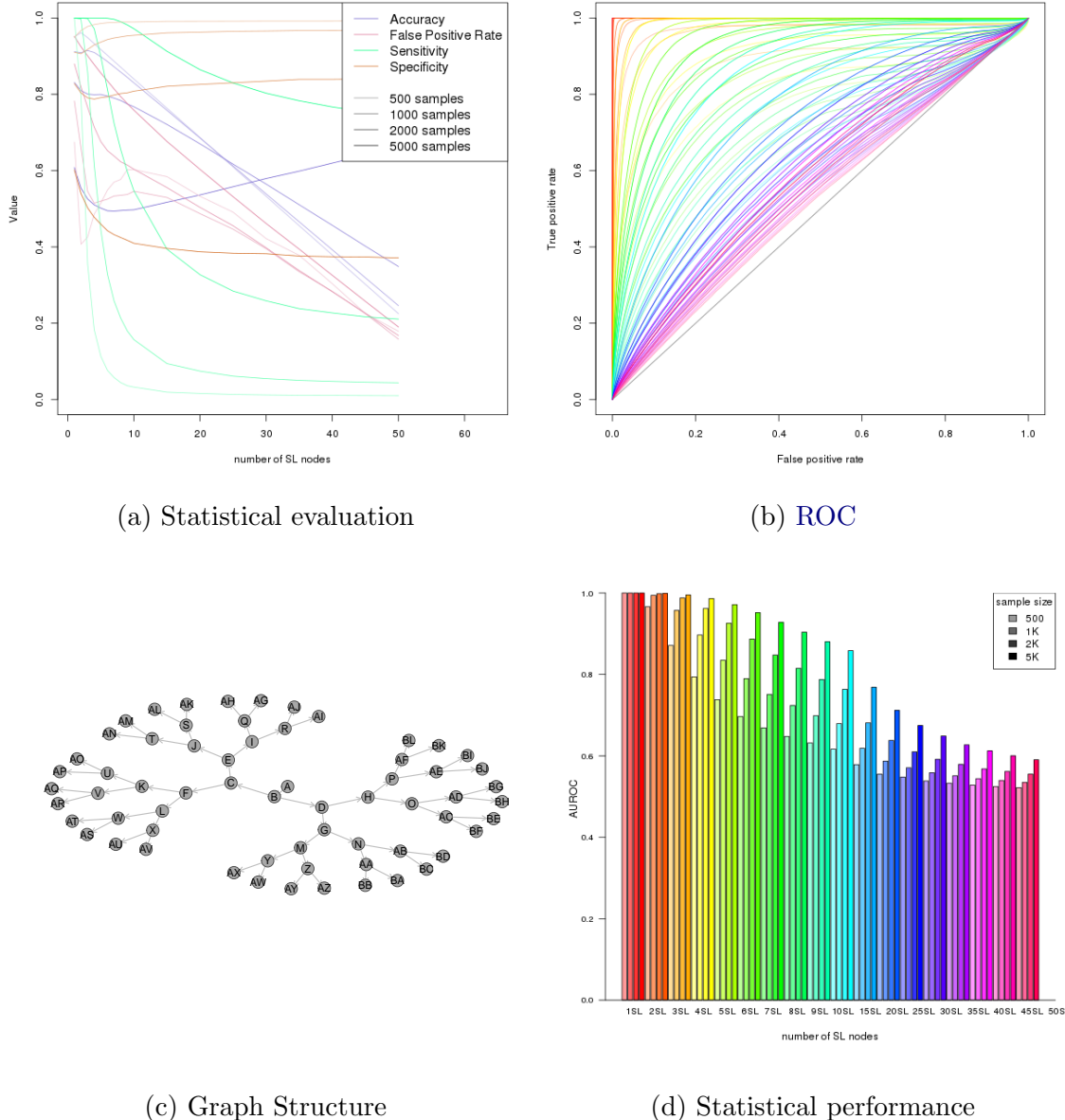
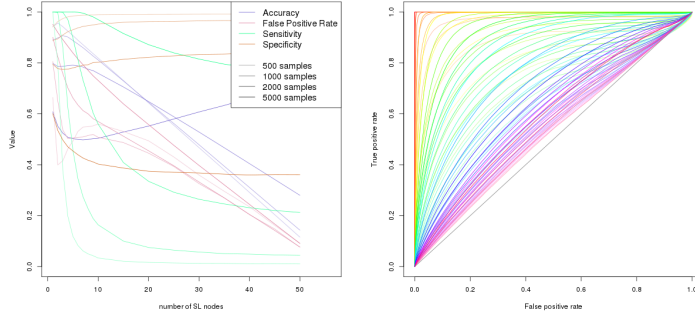
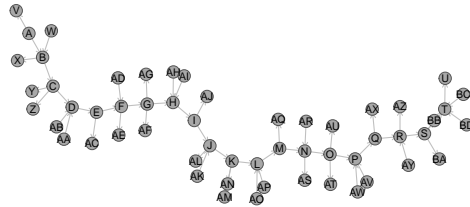


Figure K.8: **Performance of simulations on a branching graph.** Simulation of synthetic lethality used a multivariate normal distribution from a branching graph. For each parameter, 10,000 simulations were used. Colours in Figure K.8b match Figure K.8d.

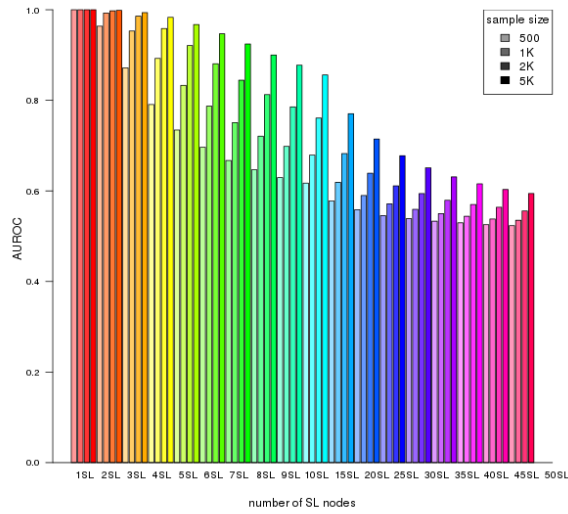


(a) Statistical evaluation

(b) ROC

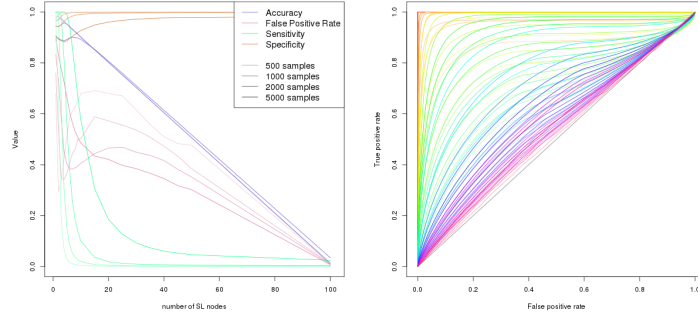


(c) Graph Structure

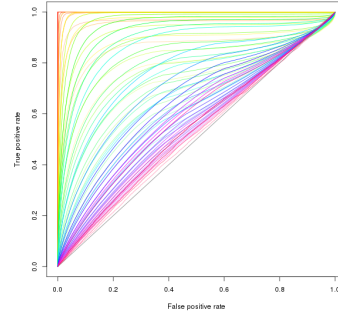


(d) Statistical performance

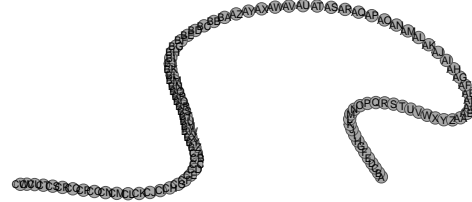
**Figure K.9: Performance of simulations on a complex graph.** Simulation of synthetic lethality used a multivariate normal distribution from a complex graph. For each parameter, 10,000 simulations were used. Colours in Figure K.9b match Figure K.9d.



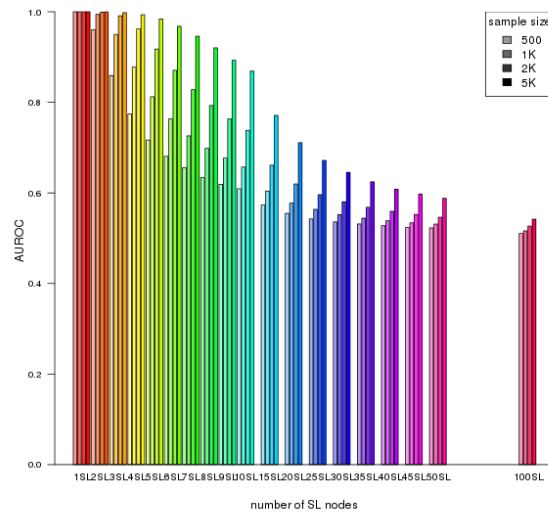
(a) Statistical evaluation



(b) ROC



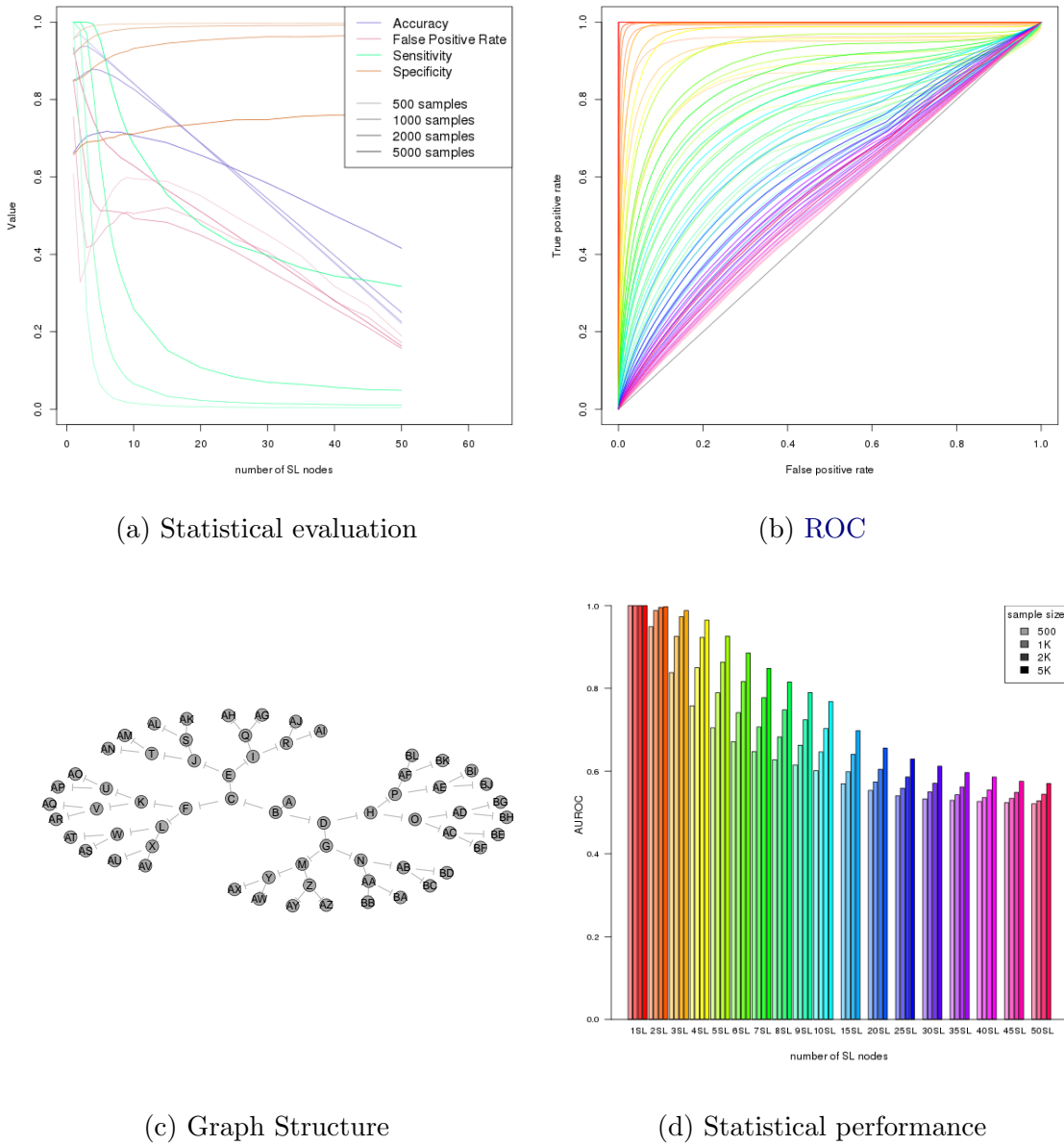
(c) Graph Structure



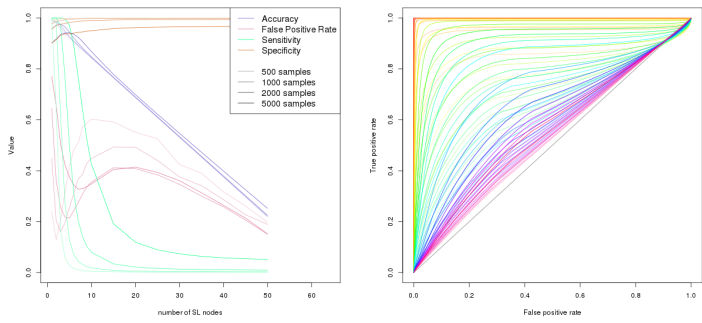
(d) Statistical performance

Figure K.10: **Performance of simulations on a large graph.** Simulation of synthetic lethality used a multivariate normal distribution from a large graph. For each parameter, 10,000 simulations were used. Colours in Figure K.10b match Figure K.10d.

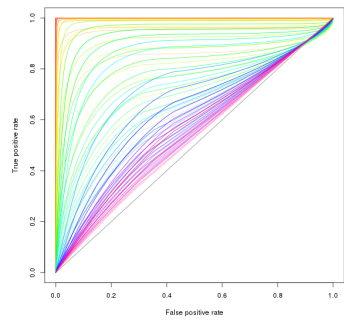
### K.2.1 Simulations from Complex Inhibiting Graphs



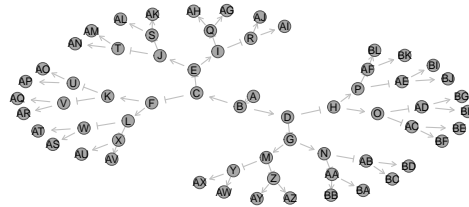
**Figure K.11: Performance of simulations on a branching graph with inhibition.**  
 Simulation of synthetic lethality used a multivariate normal distribution from a branching graph with only inhibitions. For each parameter, 10,000 simulations were used. Colours in Figure K.11b match Figure K.11d.



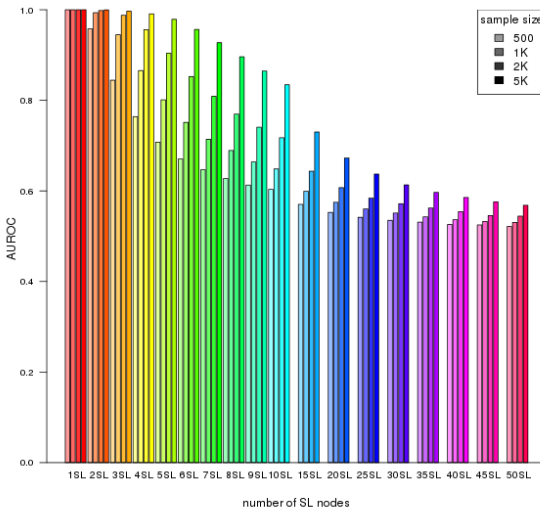
(a) Statistical evaluation



(b) ROC

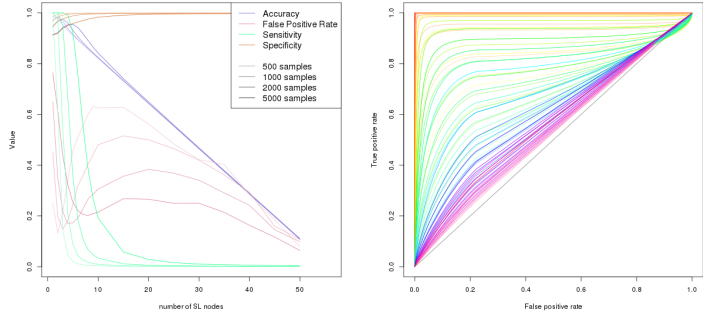


(c) Graph Structure



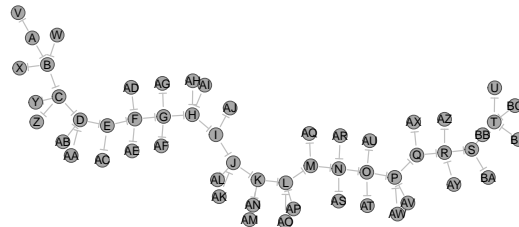
(d) Statistical performance

**Figure K.12: Performance of simulations on a branching graph with inhibition.**  
 Simulation of synthetic lethality used a multivariate normal distribution from a branching graph with alternating inhibitions. For each parameter, 10,000 simulations were used. Colours in Figure K.12b match Figure K.12d.

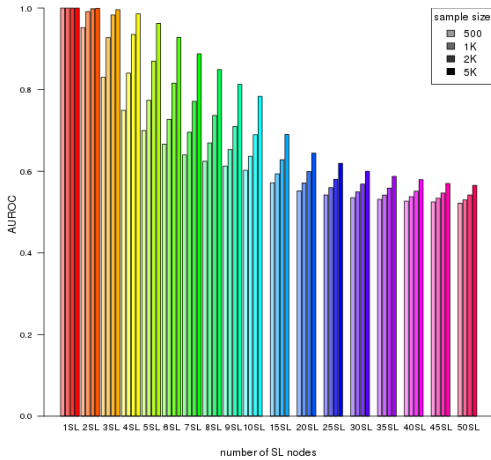


(a) Statistical evaluation

(b) ROC

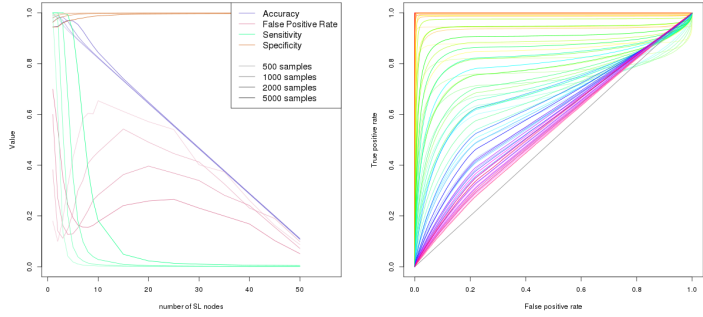


(c) Graph Structure



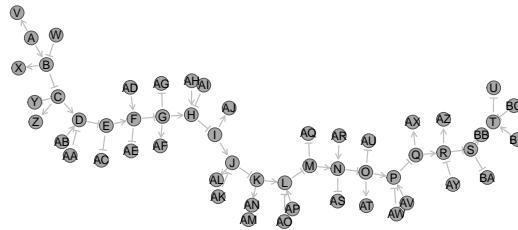
(d) Statistical performance

**Figure K.13: Performance of simulations on a complex graph with inhibition.**  
 Simulation of synthetic lethality used a multivariate normal distribution from a complex graph with only inhibitions. For each parameter, 10,000 simulations were used. Colours in Figure K.13b match Figure K.13d.

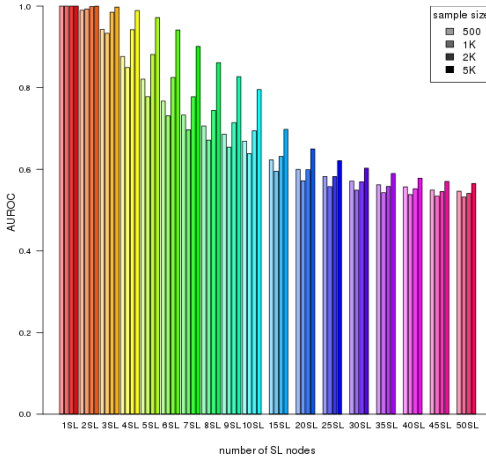


(a) Statistical evaluation

(b) ROC

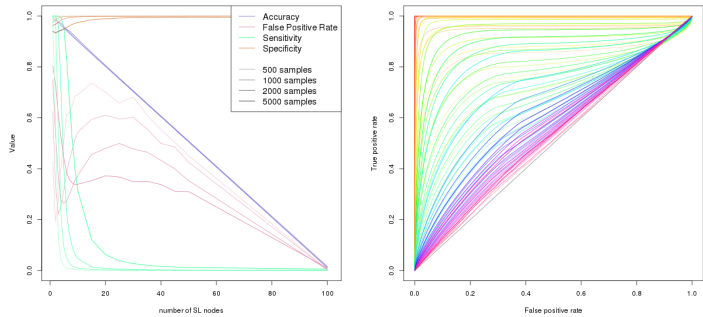


(c) Graph Structure



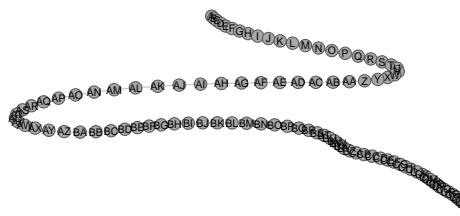
(d) Statistical performance

**Figure K.14: Performance of simulations on a complex graph with inhibition.**  
 Simulation of synthetic lethality used a multivariate normal distribution from a complex graph with a combination of relationships. For each parameter, 10,000 simulations were used. Colours in Figure K.14b match Figure K.14d.

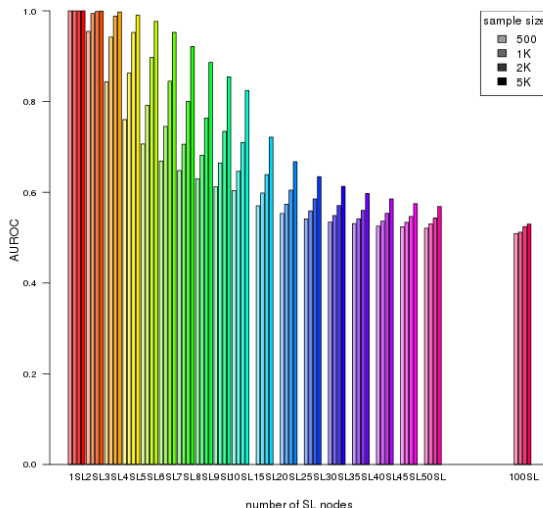


(a) Statistical evaluation

(b) ROC

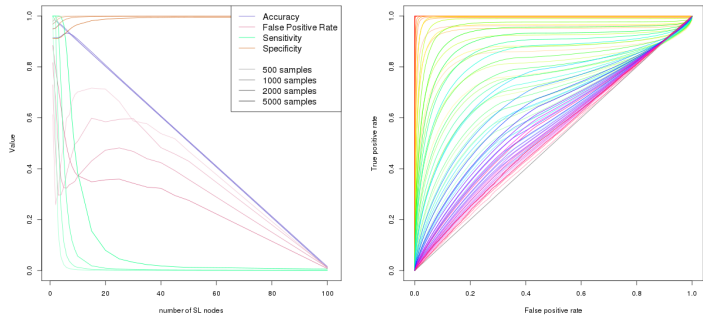


(c) Graph Structure



(d) Statistical performance

**Figure K.15: Performance of simulations on a large constructed graph with inhibition.** Simulation of synthetic lethality used a multivariate normal distribution from a large graph with only inhibitions. For each parameter, 10,000 simulations were used. Colours in Figure K.15b match Figure K.15d.

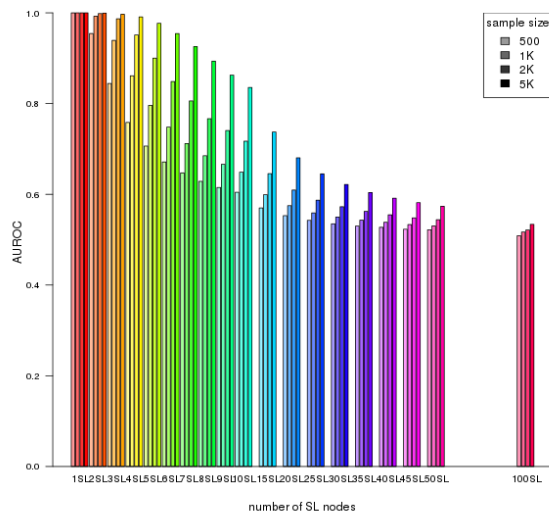


(a) Statistical evaluation

(b) ROC



(c) Graph Structure



(d) Statistical performance

**Figure K.16: Performance of simulations on a large constructed graph with inhibition.** Simulation of synthetic lethality used a multivariate normal distribution from a large graph with alternating inhibitions. For each parameter, 10,000 simulations were used. Colours in Figure K.16b match Figure K.16d.

### K.3 Simulations from Pathway Graph Structures

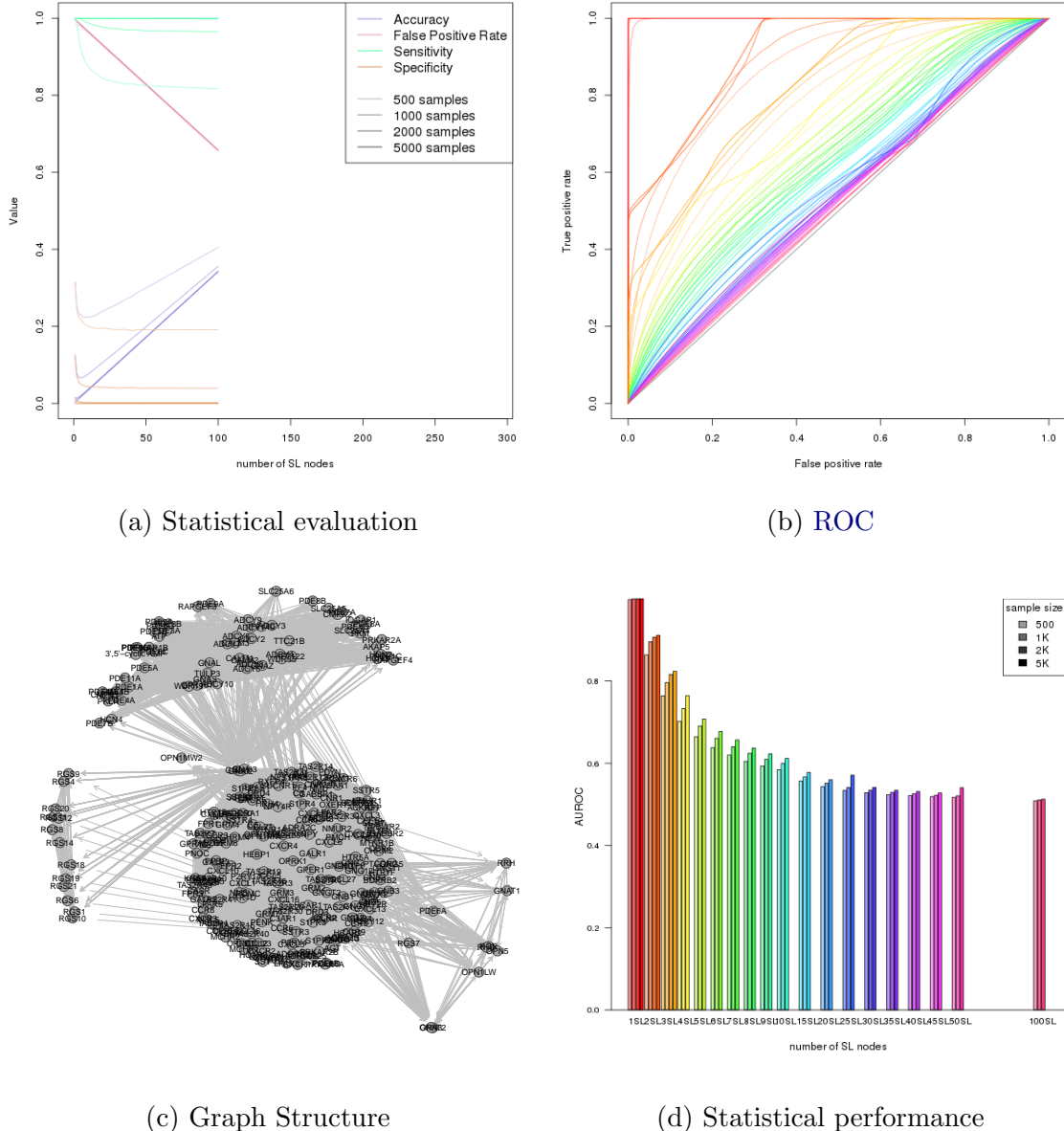


**Figure K.17: Performance of simulations on the  $G_{\alpha i}$  signalling pathway.** Simulation of synthetic lethality used a multivariate normal distribution based on the Reactome  $G_{\alpha i}$  signalling pathway. Performance of [SLIPT](#) was high across parameters for detecting synthetic lethality in the graph structure within a larger dataset. The performance decreased for a greater number of true positives to detect but the accuracy increased with a low false positive rate.

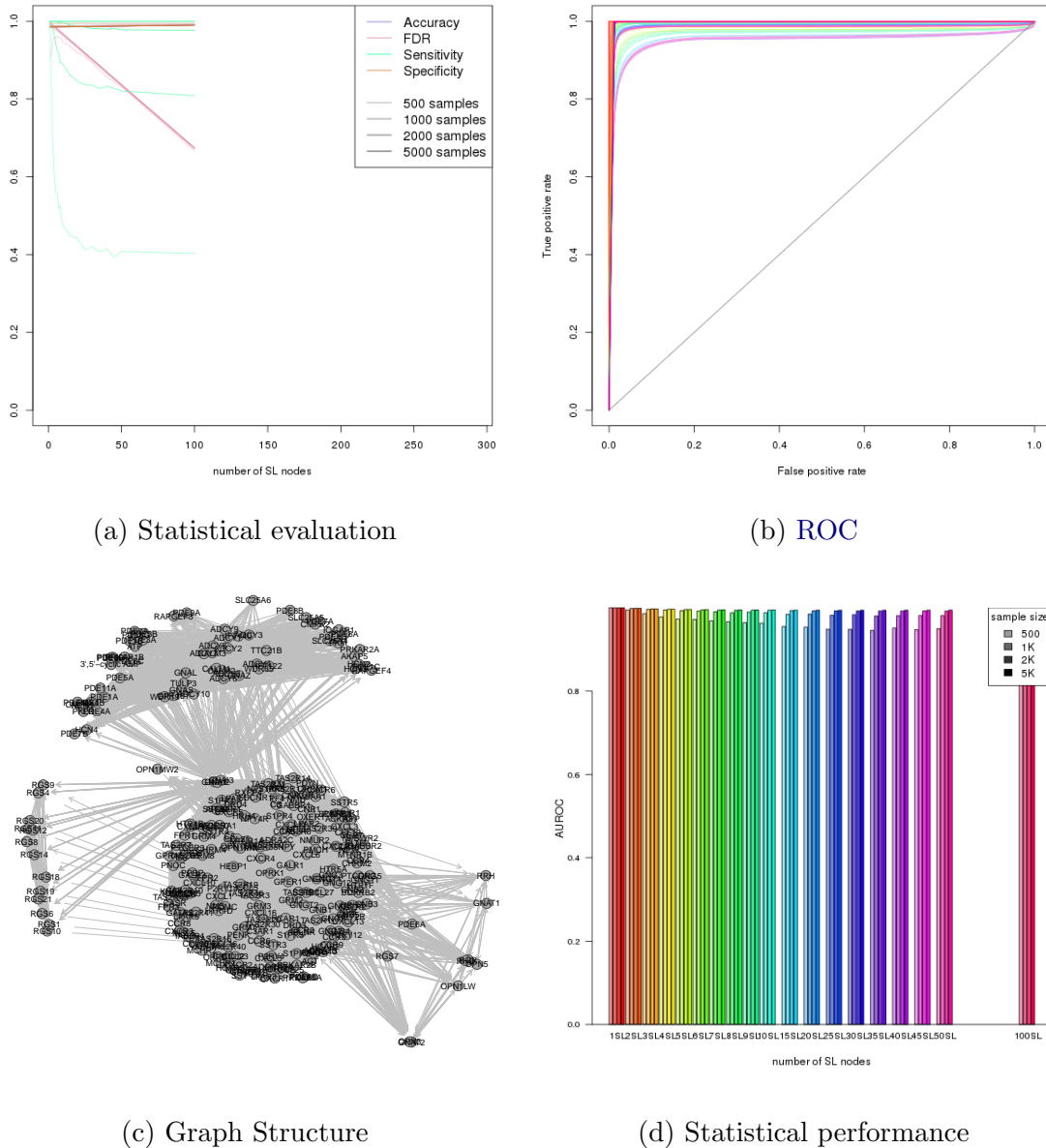


**Figure K.18: Performance of simulations including the  $G_{\alpha i}$  signalling pathway.** Simulation of synthetic lethality used a multivariate normal distribution (without correlation structure apart from the Reactome  $G_{\alpha i}$  signalling pathway. Performance of **SLIPT** was high across parameters for detecting synthetic lethality in the graph structure within a larger dataset. The sensitivity decreased for a greater number of true positives to detect but the specificity remained high with a low false positive rate.